

Inhibiting IL-17 Production by Blocking Endogenous ROR γ t Agonists for the Treatment of Autoimmune Diseases

Daphne Lynda Davies

Submitted to Swansea University in fulfilment of the
requirements for the Degree of Doctor of Philosophy

Swansea University

2021

Summary

The expression of pro-inflammatory cytokine IL-17 has been implicated in the pathogenesis of various autoimmune diseases. This project investigates the role of the cholesterol metabolising enzyme, CYP7B1 in the generation of the endogenous ligand of the master transcription factor, ROR γ t, driving the production of pro-inflammatory cytokine, IL-17 in Th17 cells. Oxysterols are oxidised derivatives of cholesterol which are intermediates in bile acid synthesis and have more recently been shown to have biological activity including roles in lipid homeostasis and immunity.

This study uses an enzyme assisted derivatization method with HPLC-ESI-MSⁿ for free and total sterol analysis of CD4⁺ T cells from cell cultures isolated from healthy human donors. Inhibition of CYP7B1 activity with azole compounds is confirmed *in vitro* with Th17 differentiated cells isolated from healthy human donors and LC-MS analysis of oxysterols 24(S),25-diHC and 7 α ,24,25-triHC, upstream and downstream of CYP7B1 activity respectively. The activity of potent LXR agonist 24(S),25-EC, which is produced abundantly in CD4⁺ T cells, and downstream metabolites towards ROR γ t is investigated *in vitro* with CD4⁺ T cells from healthy human donors. The pathway in which 24(S),25-EC is deactivated in CD4⁺ T cells through CYP7B1 and HSD3B7 is revealed and the mechanism which determines agonists or inverse agonists activity of oxysterols towards ROR γ t is demonstrated through *in silico* molecular modelling.

This study provides the foundations to progress the understanding of the role of oxysterols as ROR γ t ligands in Th17 cells. Further investigation may reveal a potential new target for the treatment of autoimmune diseases in which elevated Th17 cells and IL-17 production are observed.

DECLARATION

This work has not previously been accepted in substance for any degree and is not being concurrently submitted in candidature for any degree.

Signed .. . (candidate)

Date 27/09/2021

STATEMENT 1

This thesis is the result of my own investigations, except where otherwise stated. Where correction services have been used, the extent and nature of the correction is clearly marked in a footnote(s).

Other sources are acknowledged by footnotes giving explicit references. A bibliography is appended.

Signed . . (candidate)

Date 27/09/2021

STATEMENT 2

I hereby give consent for my thesis, if accepted, to be available for photocopying and for inter-library loan, and for the title and summary to be made available to outside organisations.

Signed . ..... (candidate)

Date 27/09/2021

Table of Contents

Summary	ii
Declaration and statements.....	iii
Acknowledgements.....	xiv
List of Tables.....	xv
List of Figures.....	xviii
Abbreviations.....	xxix
Chapter 1. General Introduction.....	1
1.1 The Immune System.....	1
1.1.1 Innate Immunity.....	1
1.1.2 Adaptive Immunity.....	2
1.2 T Cell Biology.....	5
1.2.1 T cell development.....	5
1.2.2 T cell subsets.....	8
1.2.3 Th17 cells.....	10
1.2.4 Retinoic acid receptor-related orphan receptor gamma t, ROR γ t.....	11
1.2.5 The role of Th17 cells in autoimmune diseases.....	12
1.3 Cholesterol.....	14
1.3.1 Structure and nomenclature.....	14
1.3.2 Cholesterol synthesis.....	15
1.4 Oxysterols.....	22
1.4.1 Nomenclature.....	22
1.4.2 Oxysterol synthesis.....	24
1.4.2.1 Enzymatic production of oxysterols.....	24
1.4.2.2 Autoxidation of cholesterol.....	27
1.4.3 The role of oxysterols in cholesterol homeostasis.....	27

1.4.4 Oxysterol ligands of nuclear receptor (NR) transcription factors and G-protein coupled receptors (GPCR)	27
1.4.5 Oxysterols and the immune system	30
1.5 Mass spectrometry	32
1.5.1 Ionisation sources	32
1.5.2 Mass Analyser	34
1.5.2.1 Linear Quadrupole Ion Trap (LIT)	34
1.5.2.2 Orbitrap	35
1.5.3 Tandem mass spectrometry (MS ⁿ)	37
1.5.4 Analysis of Sterols through Chromatography MS coupling	37
1.5.4.1 Gas Chromatography-Mass Spectrometry (GC-MS)	37
1.5.4.2 Liquid Chromatography-Mass Spectrometry (LC-MS)	38
1.6 General Thesis Aim	43
1.7 References	44
Chapter 2. Materials and Methods	65
2.1 Cell Culture	65
2.1.1 Cell culture materials	65
2.1.1.1 Cell line	65
2.1.1.2 Culture media	65
2.1.1.3 Cell isolation kits and buffers	65
2.1.1.4 Culture cytokines, activators and inhibitors	66
2.1.2 Preparation of Oxysterols for Cell Culture Treatments	67
2.1.2.1 7 α ,24(<i>S</i>),25-EC sample preparation for HPLC UV purification	68
2.1.2.2 HPLC purification of 7 α ,24(<i>S</i>),25-EC	68
2.1.2.3 Synthesis of downstream metabolites of 7 α ,24(<i>S</i>),25-EC	68
2.1.2.3.1 7 α ,24(<i>S</i>),25-EC cholesterol oxidase enzyme reaction	69
2.1.2.3.2 Hydrolysis of oxysterols	70

2.1.3 Human Blood Donors and Ethical Approval for Human Studies.....	72
2.1.4 Human Peripheral Blood Mononuclear Cell Isolation.....	72
2.1.5 Human T Lymphocyte Isolation by MACs.....	73
2.1.5.1 MACs Depletion protocol for isolating human naïve CD4 ⁺ T cells.....	73
2.1.5.2 MACs Depletion protocol for isolating human total CD4 ⁺ T cells.....	74
2.1.6 Human T Lymphocyte Culture Conditions.....	74
2.1.6.1 Cell culture concentrations and density.....	74
2.1.6.2 Activation of CD4 ⁺ T cells.....	75
2.1.6.2.1 Antibody loading of iMACs Beads.....	75
2.1.6.2.2 Activation of CD4 ⁺ T cells with iMACs Beads.....	75
2.1.6.2.3 Activation of CD4 ⁺ T cells with LEAF TM Purified anti-human CD3 coated culture plates.....	76
2.1.7 Mouse CD4 ⁺ T Lymphocyte Isolation by MACs.....	76
2.1.7.1 MACs Depletion protocol for isolating mouse naïve CD4 ⁺ T cells.....	76
2.1.8 Mouse T Lymphocyte Culture Conditions.....	77
2.1.8.1 Cell culture concentration and density.....	77
2.1.8.2 Antibody loading of iMACs Beads.....	77
2.1.8.3 Activation of mouse CD4 ⁺ T cells with iMACs Beads.....	77
2.1.9 EL4 Cell Culture Conditions.....	78
2.1.9.1 Cell culture concentration and density.....	78
2.1.9.2 Activation of EL4 cells.....	78
2.1.10 Cell Cryopreservation, Storage and Recovery.....	78
2.1.11 Cell Counting and Cell Viability Assay.....	79
2.1.11.1 Cell counting and Trypan blue exclusion by microscopy.....	79
2.1.11.2 7-Amino actinomycin D cell viability assay by flow cytometry.....	79

2.1.12 T Lymphocyte Flow Cytometry Assay.....	80
2.1.12.1 Instrumentation and software packages.....	80
2.1.12.2 Flow cytometry staining reagents and buffers.....	80
2.1.12.3 Flow cytometry fluorochrome conjugated antibodies.....	81
2.1.12.4 Surface staining for flow cytometry analysis.....	81
2.2 Analysis of T Lymphocyte Gene and Protein Expression.....	82
2.2.1 Molecular Biology Materials.....	82
2.2.1.1 Reagents, instruments and kits.....	82
2.2.1.2 Oligonucleotide Primers.....	82
2.2.2 Relative Gene Expression Analysis by qRT-PCR.....	84
2.2.2.1 Isolation of total mRNA.....	84
2.2.2.2 Elimination of genomic DNA by DNase digestion.....	84
2.2.2.3 Complementary DNA synthesis.....	85
2.2.2.3.1 cDNA synthesis from RNA.....	85
2.2.2.3.2 cDNA synthesis from TURBO DNase treated RNA.....	85
2.2.2.4 Primer reconstitution.....	86
2.2.2.5 Real time Quantitative Reverse Transcription Polymerase Chain Reaction.....	86
2.2.2.6 Quantitative PCR analysis.....	87
2.2.3 Soluble IL-17 Detection and Quantification by Immunoassay.....	88
2.2.3.1 Measurement of soluble IL-17 produced by CD4 ⁺ T cells by sandwich ELISA.....	88
2.2.3.2 Data analysis for sandwich ELISA.....	89
2.3 Sterol Analysis by Liquid Chromatography Mass Spectrometry.....	90
2.3.1 Sterol Analysis Materials.....	90
2.3.1.1 Sample preparation, chromatographic separation materials and solvents.....	90
2.3.1.2 Sterol standards and preparation.....	91

2.3.2 Sample processing using Enzyme-Assisted Derivatisation for Sterol Analysis (EADSA).....	91
2.3.2.1 Extraction of endogenous free sterols from cell fractions.....	91
2.3.2.2 Alkali hydrolysis and extraction of total sterols from cell fractions.....	92
2.3.2.3 Extraction of endogenous free sterols from media fractions.....	92
2.3.2.4 Alkali hydrolysis and extraction of total sterols from media fractions.....	92
2.3.2.5 First Solid Phase Extraction (SPE1) to separate cholesterol and oxysterols.....	93
2.3.2.6 Cholesterol oxidase treatment and charge-tagging with Girard's Reagent P.....	94
2.3.2.7 Second Solid Phase Extraction (SPE2) to remove excess derivatisation reagent and sample clean up.....	97
2.3.3 Sample preparation prior to LC-ESI-MS ⁿ analysis.....	97
2.3.3.1 Oxysterol fraction sample preparation for LC-MS.....	98
2.3.3.2 Cholesterol fraction sample preparation for LC-MS.....	98
2.3.4 Sterol separation, Analysis and Quantification by HPLC-ESI-MS ⁿ	98
2.3.4.1 Orbitrap Elite and ID-X calibration.....	98
2.3.4.2 HPLC-ESI-MS ⁿ sterol analysis.....	98
2.3.4.3 Scan events and parameters for MS and MS ³	101
2.3.4.4 Identification and quantification of chromatographically separated sterols.....	101
2.3.4.5 Normalisation of relative endogenous sterol quantities.....	102
2.4 In silico Modelling and Docking Simulations.....	109
2.4.1 Modelling protein and ligand structures.....	109
2.4.1.1 Modeller homology modelling of protein structure.....	109
2.4.1.2 Modelling ligand structure.....	109
2.4.2 Protein-ligand docking simulations.....	109
2.4.2.1 FKCOMBU pre-docking preparations.....	109

2.4.2.2 Protein-ligand docking simulations with PLANTS	109
2.5 References	111
Chapter 3. Method Development of Sterol Analysis	115
3.1 Introduction	115
3.2 Materials and Methods	116
3.2.1 Plasma preparation, total sterol extraction and LC-MS ⁿ analysis	116
3.2.2 Isolation of neonatal naïve CD4 ⁺ T cells from neonatal cord blood	116
3.2.2.1 Isolation of mononuclear cells from neonatal cord blood	116
3.2.2.2 Isolation of naïve CD4 ⁺ T cells from total neonatal CD4 ⁺ T cells	117
3.2.3 Purity and activation analysis of naïve CD4 ⁺ T cells by flow cytometry	117
3.2.4 Culture conditions for CD3 and CD28 activated naïve CD4 ⁺ T cells under non-polarising, Th0 conditions	117
3.2.5 Flow cytometry analysis of CD25 activation and cell viability of neonatal naïve CD4 ⁺ T cell cultures	119
3.2.6 Cell pellet and supernatant preparation, Sterol extraction and LC-MS ⁿ analysis	119
3.3 Results	119
3.3.1 Precise oxysterol quantification is achievable with reduced sample volume	119
3.3.2 Comparison of esterified and non-esterified sterols in human plasma	120
3.3.3 Total sterol analysis of activated and non-activated neonatal naïve CD4 ⁺ T cells	125
3.3.3.1 Isolation of neonatal naïve CD4 ⁺ T cells by MACs showed >61% purity	126
3.3.3.2 CD25 expression increased following activation and culture of isolated neonatal naïve CD4 ⁺ T cells under non-polarising conditions	126
3.3.3.3 Comparison of free and esterified sterols in activated and non-activated neonatal naïve CD4 ⁺ T cells	130
3.4 Discussion	147

3.5 References.....	149
Chapter 4. Investigating the effect of azole inhibition of CYP7B1 on Th17 polarised nCD4 ⁺ T cells.....	152
4.1 Introduction.....	152
4.2 Materials and Methods.....	153
4.2.1 Isolation of human naïve CD4 ⁺ T cells from peripheral blood.....	153
4.2.2 Monitoring cell proliferation by flow cytometry	153
4.2.3 Purity and activation analysis of naïve CD4 ⁺ T cells by flow cytometry	153
4.2.4 Culture conditions for CD3/CD28 activated naïve CD4 ⁺ T cells in X-Vivo-20 media with azole treatment on the third day of culture.....	154
4.2.5 Culture conditions for CD3/CD28 activated naïve CD4 ⁺ T cells in X-Vivo-20 media with azole treatment on the first day of culture.....	156
4.2.6 Gene expression and protein secretion analysis	157
4.2.7 Sterol analysis	158
4.2.8 Statistical analysis	158
4.3 Results.....	158
4.3.1 Naïve CD4 ⁺ T cells isolated from human PBMCs by MACs showed >88% CD4 ⁺ purity.....	158
4.3.2 Variation in CD25 expression, cell viability and proliferation of polarised cells was observed between Donors with day 3 azole treatments..	161
4.3.3 Variation in CD25 expression, cell viability and proliferation of polarised cells was observed between Donors with day 0 azole treatments ..	169
4.3.4 Azole treatment of Th17-polarised cells on day 3 of cell culture revealed variable effects on the mRNA expression of Th17 signature genes.....	173
4.3.5 Azole treatment of Th17-polarised cells on the first day of cell culture inhibits <i>IL17A</i> expression in a dose dependant manner.....	187
4.3.6 Azole treatment inhibits CYP7B1 activity in activated Th17 polarised naïve CD4 ⁺ T cells.....	194
4.4 Discussion.....	219

4.5 References	221
Chapter 5. Investigating the role of CYP7B1 in the expression of IL17 in primary murine CD4 ⁺ T cells and the potential of murine cell line EL4 for the study of IL-17 production	224
5.1 Introduction	224
5.2 Materials and Methods	225
5.2.1 Isolation of naïve CD4 ⁺ T cells from murine splenocytes	225
5.2.2 Purity and activation analysis of naïve CD4 ⁺ T cells by flow cytometry	226
5.2.3 Culture conditions for unstimulated murine naïve CD4 ⁺ T cells in X-Vivo-20 media	226
5.2.4 Culture conditions for CD3 and CD28 activated Th17 or Treg polarised naïve CD4 ⁺ T cells in X-Vivo-20 media	226
5.2.5 Culture conditions for PMA and ionomycin stimulated EL4 cell line ..	227
5.2.6 Oxysterol treatment and inhibition of EL4 cell line	227
5.2.7 Flow cytometry analysis of CD25 activation and cell viability of EL4 cell line	229
5.2.8 Sample processing for qRT-PCR analysis	229
5.2.9 Sample processing for oxysterol analysis	229
5.3 Results	231
5.3.1 Naïve CD4 ⁺ T cells isolated from murine splenocytes by MACs showed >98% CD4 ⁺ purity	231
5.3.2 <i>Cyp7b1</i> KO in murine CD4 ⁺ T cells has little effect on CD25 expression and cell viability of activated naïve CD4 ⁺ T cells	234
5.3.3 <i>Il17a</i> mRNA expression was downregulated in <i>Cyp7b1</i> KO mice	237
5.3.4 Oxysterol profiling of murine CD4 ⁺ T cells	238
5.3.5 Stimulation of murine cell line EL4 induces <i>Il17a</i> mRNA expression	244
5.3.6 Stimulation of murine cell line EL4 induces <i>Ifng</i> and <i>Il4</i> mRNA expression	245

5.3.7 EL4 cell experiments with oxysterols and known inhibitor treatments.....	246
5.3.8 Oxysterol profile of EL4 cells.....	259
5.4 Discussion.....	267
5.5 References.....	270
Chapter 6. Investigating oxysterol pathways in total CD4 ⁺ T helper cells....	273
6.1 Introduction.....	273
6.2 Materials and Methods.....	274
6.2.1 Preparation of oxysterols for cell culture treatments.....	274
6.2.2 Isolation of human CD4 ⁺ T cells from peripheral blood.....	274
6.2.3 Purity and activation analysis of CD4 ⁺ T cells by flow cytometry.....	274
6.2.4 Culture conditions for CD3/CD28 activated CD4 ⁺ T cells in X-Vivo-20 media.....	274
6.2.5 Gene expression analysis.....	276
6.2.6 Statistical analysis.....	276
6.3 Results.....	277
6.3.1 CD4 ⁺ T cells isolated from human PBMCs by MACs showed >96% CD4 ⁺ purity.....	277
6.3.2 Oxysterol treatments showed little effect on CD25 expression and cell viability of activated CD4 ⁺ T helper cells after 24 hrs.....	280
6.3.3 Downstream metabolites of 24(<i>S</i>),25-EC reveal a potential pathway of deactivation in CD4 ⁺ T cells.....	287
6.4 Discussion.....	291
6.5 References.....	292
Chapter 7. <i>In silico</i> Modelling of the interaction between potential endogenous oxysterol ligands and nuclear hormone transcription factors ROR γ t and LXR β	294
7.1 Introduction.....	294
7.2 Methods.....	295
7.2.1 <i>In silico</i> modelling of protein and ligand structures.....	295

7.2.1.1 Homology modelling of protein structures with Modeller.....	295
7.2.1.2 Modelling ligand structures.....	295
7.2.2 Protein-ligand docking simulations.....	298
7.2.2.1 Pre-docking preparation.....	298
7.2.2.2 FKCOMBU pre-docking preparations.....	298
7.2.2.3 Protein-ligand docking simulations with PLANTS.....	298
7.3 Results.....	302
7.3.1 ROR γ t protein-ligand docking simulations.....	302
7.3.2 LXR β protein-ligand docking simulations.....	315
7.4 Discussion.....	326
7.5 References.....	329
Chapter 8. General Discussion.....	332

Acknowledgements

I would like to thank my supervisors Professor Yuqin Wang, Professor William J. Griffiths, Professor Cathy Thornton and Dr Jonathan Mullins for the opportunity and privilege to study and work with experts in their fields. Collaboration with the Human Immunology Group and Genome and Structural Bioinformatics Research Group has truly enhanced my PhD study. Specifically, I would like to express my gratitude to Professor Yuqin Wang for her mentoring throughout my PhD study.

I would like to thank Griffiths-Wang group members, past and present, Dr Eylan Yutuc, Dr Alison Dickson and Dr Roberto Angelini for their advice, encouragement and contributions. Specifically, I am thankful for the assistance and guidance of Dr Tom Hearn with the T cell studies in the initial stages of my PhD. I would like to thank Dr Karl Austin-Muttitt for his friendly welcome to the world of molecular modelling and his invaluable help and advice with the *in silico* study of transcription factors ROR γ t and LXR β .

Finally, I would like thank my family who have been a great support throughout my PhD especially through the challenges we have faced over the past year.

List of Tables

Table 2.1 List of cell culture reagents, kits and cytokines.....	66
Table 2.2 Cell culture plate sizes according to cell density for seeding CD4 ⁺ T cells.....	75
Table 2.3 Reagents and buffers required for flow cytometry analysis.....	80
Table 2.4 Monoclonal antibodies used for flow cytometry assays.....	81
Table 2.5 Reagents and kits used for qPCR and ELISA analysis.....	82
Table 2.6 Human and mouse primers for qRT-PCR.....	83
Table 2.7 Materials and solvents required for sterol analysis by mass spectrometry.....	90
Table 2.8 List of sterols monitored and identified with EADSA.....	104
Table 3.1 Culture conditions for neonatal naïve CD4 ⁺ T cell experiments...	118
Table 3.2 Quantification of sterols detected in human plasma with and without hydrolysis in KOH representing total and free sterols respectively..	121
Table 3.3 Percentage of free sterols in human plasma.....	122
Table 3.4 MACs isolation method summary for neonatal naïve CD4 ⁺ T cell experiments.....	125
Table 3.5 Free sterol analysis of cell pellets from non-polarised neonatal naïve CD4 ⁺ T cells activated for 24 to 48 hrs.....	131
Table 3.6 Total sterol analysis of cell pellets from non-polarised neonatal naïve CD4 ⁺ T cells activated for 24 to 48 hrs.....	131
Table 3.7 Total sterol analysis of cell culture media from non-polarised neonatal naïve CD4 ⁺ T cells activated for 24 to 48 hrs.....	133
Table 3.8 Free sterol analysis of cell pellets from non-polarised neonatal naïve CD4 ⁺ T cells activated or non-activated for 24 to 72 hrs.....	135
Table 3.9 Total sterol analysis of cell pellets from non-polarised neonatal naïve CD4 ⁺ T cells activated or non-activated for 24 to 72 hrs.....	136
Table 3.10 Total sterol analysis of cell culture media from non-polarised neonatal naïve CD4 ⁺ T cells activated or non-activated for 24 to 72 hrs.....	139
Table 3.11 Free sterol analysis of cell pellets from non-polarised neonatal naïve CD4 ⁺ T cells activated or non-activated for 24 hrs.....	141
Table 3.12 Total sterol analysis of cell pellets from non-polarised neonatal naïve CD4 ⁺ T cells activated or non-activated for 24 hrs.....	142

Table 3.13 Total sterol analysis of cell culture media from non-polarised neonatal naïve CD4 ⁺ T cells activated or non-activated for 24 hrs	144
Table 4.1 Activated non-polarised (Th0), Th17-polarised and Treg-polarised naïve CD4 ⁺ T cell culture conditions in X-Vivo-20 media	155
Table 4.2 Experiment conditions and end point analysis for naïve CD4 ⁺ T cell cultures in X-Vivo-20 with azole treatments on day 3	156
Table 4.3 Experiment conditions and end point analysis for naïve CD4 ⁺ T cell cultures in X-Vivo-20 with azole treatments on day 0	157
Table 4.4 Surface marker expression of isolated nCD4 ⁺ cells from healthy human donors	161
Table 4.5 Quantified oxysterols in media fraction of Donor 1 activated naïve CD4 ⁺ T cells cultured under Th17 polarising conditions with and without clotrimazole treatment after 6 days	195
Table 4.6 Quantified oxysterols in media fraction of Donor 2 activated naïve CD4 ⁺ T cells cultured under Th17 or Treg polarised conditions with and without azole treatments	199
Table 4.7 Quantified oxysterols in media fraction of Donor 3 activated naïve CD4 ⁺ T cells cultured under Th17 or Treg polarised conditions with and without azole treatments	203
Table 4.8 Quantified oxysterols in the media fraction of Donor 4 activated naïve CD4 ⁺ T cells cultured under non-polarised, Th0 or Th17 polarised conditions with and without 0.5 µM clotrimazole treatments	206
Table 4.9 Quantified oxysterols in media fraction of Donor 5 activated naïve CD4 ⁺ T cells cultured under non-polarised, Th0 or Th17 polarised conditions with and without 0.0625 to 0.5 µM clotrimazole treatments	208

Table 4.10 Quantified oxysterols in media fraction of Donor 6 activated naïve CD4 ⁺ T cells cultured under non-polarised, Th0 or Th17 polarised conditions with and without 0.5 µM clotrimazole treatments.....	210
Table 4.11 Quantified oxysterols in media fraction of Donor 7 activated naïve CD4 ⁺ T cells cultured under Th17 polarised conditions with and without day 0 clotrimazole treatments.....	212
Table 4.12 Quantified oxysterols in media fraction of Donor 8 activated naïve CD4 ⁺ T cells cultured under Th17 polarised conditions with and without day 0 0.125 to 0.5 µM clotrimazole treatments.....	214
Table 4.13 Quantified oxysterols in media fraction of Donor 9 activated naïve CD4 ⁺ T cells cultured under non-polarised, Th0 or Th17 polarised conditions with and without day 0 0.125 to 0.25 µM clotrimazole treatments.....	216
Table 5.1 Th17, Treg and non-polarising cell culture conditions for murine naïve CD4 ⁺ T cells in X-Vivo-20 media.....	227
Table 6.1 Experiment conditions and end point analysis for CD4 ⁺ T cell cultures in X-Vivo-20 with oxysterol treatments.....	275
Table 7.1 PLANTS scoring functions.....	301
Table 7.2 25-HC in the RORγ control model ‘HC3’.....	305
Table 7.3 Binding affinities of sterol ligands for RORγ.....	308
Table 7.4 Binding affinities of sterol ligands for LXRβ LBD.....	325

List of Figures

Figure 1.1 Lymphocyte cell lineages.....	4
Figure 1.2 Simplified schematic of CD4 ⁺ and CD8 ⁺ T cell development.....	7
Figure 1.3 Simplified differentiation of CD4 ⁺ T helper cell subsets.....	10
Figure 1.4 Nuclear receptor domain regions.....	11
Figure 1.5 Structure of Cholesterol.....	14
Figure 1.6 3D structure of Cholesterol.....	15
Figure 1.7 Simplified schematic of the SCAP-SREBP regulatory pathway of cholesterol.....	18
Figure 1.8 The mevalonate pathway.....	20
Figure 1.9 Cholesterol biosynthesis pathways from squalene.....	21
Figure 1.10 Nomenclature of oxysterol stereoisomers.....	23
Figure 1.11 Cholesterol metabolism and primary bile acid biosynthesis pathway.....	26
Figure 1.12 The components of mass spectrometry analysis.....	32
Figure 1.13 Electrospray Ionisation (ESI) source.....	34
Figure 1.14 Schematic of a 2D linear ion trap (LIT).....	35
Figure 1.15 Orbitrap Elite and ID-X mass spectrometer schematics.....	36
Figure 1.16 Solid Phase Extraction (SPE) technique.....	41
Figure 1.17 Schematic of sample preparation process for sterol analysis by LC-MS.....	42
Figure 1.18 Schematic of 24(<i>S</i>),25-EC metabolism through CYP7B1 and HSD3B7 in the kandutsch-russell pathway.....	43
Figure 2.1 7 α ,24(<i>S</i>),25-EC HPLC purification.....	68
Figure 2.2 Reaction scheme for the conversion of 7 α ,24(<i>S</i>),25-EC to the downstream metabolite 7 α ,24(<i>S</i>),25-EC-3-one with cholesterol oxidase.....	69
Figure 2.3 Hydrolysis reaction scheme for 24(<i>S</i>),25-EC and downstream metabolites using glacial acetic acid.....	71
Figure 2.4 Charge-tagging of sterols with Girard Reagent P using cholesterol oxidase.....	95
Figure 2.5 Sterols derivatised with Girard Reagent P (GP).....	96
Figure 2.6 Multi-step gradients for separation of derivatised sterols by Liquid chromatography.....	100

Figure 2.7 MS ⁿ fragmentation of precursor [M] ⁺ ions.....	103
Figure 2.8 Isolation, identification and quantification of sterols by LC-MS with Xcalibur Qual Browser.....	103
Figure 2.9 Sterol structure.....	110
Figure 3.1 Representative reconstructed ion chromatograms for monohydroxycholesterols present in human plasma at 539.4368 <i>m/z</i> ± 10 ppm with a 17 minute gradient.....	123
Figure 3.2 Representative reconstructed ion chromatogram for dihydroxycholesterols present in human plasma at 555.4317 <i>m/z</i> ± 10 ppm with a 17 minute gradient.....	123
Figure 3.3 Representative reconstructed ion chromatogram for trihydroxycholesterols present in human plasma at 571.4266 <i>m/z</i> ± 10 ppm with a 17 minute gradient.....	124
Figure 3.4 Neonatal naïve CD4 ⁺ T cells stimulated with anti-CD3 and anti- CD28 and cultured for 24 hrs under Th0 conditions.....	125
Figure 3.5 Gating strategy applied to isolated neonatal naïve CD4 ⁺ T cells to identify live cells and exclude dead cells using 7AAD Viability dye staining.....	127
Figure 3.6 Representative flow cytometry analysis of isolated neonatal naïve CD4 ⁺ T cells prior to cell culture.....	128
Figure 3.7 Flow cytometry analysis of CD25 expression of neonatal naïve CD4 ⁺ T cells after 24, 48 or 72 hrs of culture under non-polarising conditions.....	129
Figure 3.8 Comparison of free and total sterols present in cell pellets from non-polarised neonatal naïve CD4 ⁺ T cell activated for 24 to 48 hrs.....	132
Figure 3.9 Total sterol analysis of cell culture media for non-polarised neonatal naïve CD4 ⁺ T cells activated for 24 to 48 hrs.....	133
Figure 3.10 Comparison of free and total sterols present in cell pellets of non-polarised neonatal naïve CD4 ⁺ T cells activated or non-activated for 24 to 72 hrs.....	138
Figure 3.11 Total sterol analysis of cell culture media from non-polarised neonatal naïve CD4 ⁺ T cells activated or non-activated for 24 to 72 hrs.....	140

Figure 3.12 Comparison of free and total sterols present in cell pellets from non-polarised neonatal naïve CD4 ⁺ T cells activated or non-activated for 24hrs.....	143
Figure 3.13 Total sterol analysis of cell culture media from non-polarised neonatal naïve CD4 ⁺ T cells activated or non-activated for 24 hrs.....	145
Figure 3.14 Representative reconstructed ion chromatogram at 532.3898 m/z \pm 10ppm with a 26 minute gradient for 24(S),25-EC and 24-KC present in human neonatal naïve CD4 ⁺ T cells.....	146
Figure 4.1 Representative Gating strategy applied to isolated naïve CD4 ⁺ T cells to identify live cells and exclude dead cells using 7AAD Viability dye staining.....	159
Figure 4.2 Representative flow cytometry analysis of isolated naïve CD4 ⁺ T cells prior to cell culture.....	160
Figure 4.3 Flow cytometry analysis of naïve CD4 ⁺ T cells from Donor 3 cultured under Th17 polarising conditions with or without treatment with azole inhibitors clotrimazole and tebuconazole at 0.5 μ M and 1.0 μ M concentrations harvested after 6 days of cell culture.....	163
Figure 4.4 Flow cytometry analysis of naïve CD4 ⁺ T cells from Donor 3 cultured under Treg polarising conditions with or without treatment with azole inhibitors clotrimazole and tebuconazole at 0.5 μ M and 1.0 μ M concentrations harvested after 6 days of cell culture.....	164
Figure 4.5 Flow cytometry analysis of naïve CD4 ⁺ T cells from Donor 4 cultured under non-polarising Th0 or Th17 polarising conditions with or without 0.5 μ M clotrimazole treatment harvested after 6 days of cell culture.....	166
Figure 4.6 Flow cytometry analysis of naïve CD4 ⁺ T cells from Donor 5 cultured under non-polarising Th0 or Th17 polarising conditions with or without 0.0625 to 0.5 μ M clotrimazole treatments harvested after 6 days of cell culture.....	167
Figure 4.7 Flow cytometry analysis of naïve CD4 ⁺ T cells from Donor 6 cultured under non-polarising Th0 or Th17 polarising conditions with or without 0.5 μ M clotrimazole treatment harvested after 6 days of cell culture.....	168

Figure 4.8 Flow cytometry analysis of naïve CD4 ⁺ T cells from Donor 7 cultured under Th17 polarising conditions with or without 0.0625 µM clotrimazole treatment harvested after 6 days of cell culture.....	170
Figure 4.9 Flow cytometry analysis of naïve CD4 ⁺ T cells from Donor 8 cultured under Th17 polarising conditions with or without 0.125 or 0.5µM clotrimazole treatment harvested after 6 days of cell culture.....	171
Figure 4.10 Flow cytometry analysis of naïve CD4 ⁺ T cells from Donor 9 cultured under non-polarising Th0 or Th17 polarising conditions with or without 0.125 and 0.25 µM clotrimazole treatments harvested after 6 days of cell culture.....	172
Figure 4.11 qRT-PCR analysis of mRNA expression of Th17 polarised nCD4 ⁺ cells from Donor 1.....	175
Figure 4.12 qRT-PCR analysis of mRNA expression of Th17 and Treg polarised nCD4 ⁺ cells from Donor 2.....	176
Figure 4.13 qRT-PCR analysis of mRNA expression of Th17 and Treg polarised nCD4 ⁺ cells from Donor 3.....	178
Figure 4.14 qRT-PCR analysis of mRNA expression of Th17 polarised naïve CD4 ⁺ cells from Donor 4.....	180
Figure 4.15 IL-17A production of non-polarised Th0 or Th17 polarised naïve CD4 ⁺ T cells of Donor 4 quantified by sandwich ELISA.....	181
Figure 4.16 qRT-PCR analysis of mRNA expression of Th0 or Th17 polarised naïve CD4 ⁺ cells from Donor 5.....	182
Figure 4.17 IL-17A production of non-polarised Th0 or Th17 polarised naïve CD4 ⁺ T cells of Donor 5.....	183
Figure 4.18 qRT-PCR analysis of mRNA expression of Th0 or Th17 polarised naïve CD4 ⁺ cells from Donor 6.....	184
Figure 4.19 IL-17A concentration of non-polarised Th0 or Th17 polarised naïve CD4 ⁺ T cell culture media from Donor 6 quantified by sandwich ELISA.....	185
Figure 4.20 qRT-PCR analysis of mRNA expression of Th17 polarised naïve CD4 ⁺ cells with day 3 clotrimazole treatments.....	186
Figure 4.21 qRT-PCR analysis of mRNA expression of Th17 polarised naïve CD4 ⁺ cells from Donor 7 with clotrimazole treatment on day 0.....	188

Figure 4.22 IL-17A production in Th17 polarised naïve CD4 ⁺ T cells of Donor 7 with clotrimazole treatment on the first day of culture quantified by sandwich ELISA.....	189
Figure 4.23 qRT-PCR analysis of mRNA expression of Th17 polarised naïve CD4 ⁺ cells from Donor 8 with clotrimazole treatment on day 0.....	190
Figure 4.24 IL-17A production of Th17 polarised naïve CD4 ⁺ T cells of Donor 8.....	191
Figure 4.25 qRT-PCR analysis of mRNA expression of non-polarised Th0 or Th17 polarised naïve CD4 ⁺ cells from Donor 9 with clotrimazole treatment on day 0.....	192
Figure 4.26 IL-17A production of non-polarising Th0 or Th17 polarised naïve CD4 ⁺ T cells of Donor 9.....	193
Figure 4.27 Representative reconstructive ion chromatograms for monohydroxycholesterols present in cell culture media, detected at 534.5054 m/z \pm 10 ppm.....	196
Figure 4.28 Representative reconstructive ion chromatograms for dihydroxycholesterols present in cell culture media, detected at 550.4003 m/z \pm 10 ppm.....	197
Figure 4.29 Representative reconstructive ion chromatograms for trihydroxycholesterols present in cell culture media, detected at 566.3952 m/z \pm 10 ppm.....	198
Figure 4.30 Normalised LC-MS ⁿ quantification of upstream and downstream oxysterols of CYP7B1 activity reveal inhibition of CYP7B1 with clotrimazole treatment from Donor 1 activated Th17-polarised naïve CD4 ⁺ T cell culture media.....	199
Figure 4.31 Normalised LC-MS ⁿ quantification of upstream and downstream oxysterols of CYP7B1 activity reveal inhibition of CYP7B1 with clotrimazole and tebuconazole treatment from Donor 2 activated Th17 and Treg polarised naïve CD4 ⁺ T cell culture media.....	200
Figure 4.32 Normalised GC-MS quantification of upstream and downstream sterols of CYP51 in Donor 2 activated Th17 and Treg polarised naïve CD4 ⁺ T cells.....	201

Figure 4.33 Normalised LC-MS ⁿ quantification of upstream and downstream oxysterols of CYP7B1 activity in Donor 3 activated Th17 and Treg polarised naïve CD4 ⁺ T cell culture media.....	204
Figure 4.34 Normalised GC-MS quantification of upstream and downstream sterols of CYP51 in Donor 3 activated Th17 and Treg polarised naïve CD4 ⁺ T cells	205
Figure 4.35 Normalised LC-MS ⁿ quantification of upstream and downstream oxysterols of CYP7B1 activity in Donor 4 activated non-polarised Th0 and Th17 polarised naïve CD4 ⁺ T cell culture media.....	207
Figure 4.36 Normalised LC-MS ⁿ quantification of upstream and downstream oxysterols of CYP7B1 activity in Donor 5 activated non-polarised Th0 and Th17 polarised naïve CD4 ⁺ T cell culture media.....	209
Figure 4.37 Normalised LC-MS ⁿ quantification of upstream and downstream oxysterols of CYP7B1 activity in Donor 6 activated non-polarised Th0 and Th17 polarised naïve CD4 ⁺ T cell culture media.....	211
Figure 4.38 Normalised LC-MS ⁿ quantification of upstream and downstream oxysterols of CYP7B1 activity in Donor 7 activated Th17 polarised naïve CD4 ⁺ T cell culture media with day 0 clotrimazole treatment.....	213
Figure 4.39 Normalised LC-MS ⁿ quantification of upstream and downstream oxysterols of CYP7B1 activity in Donor 8 activated Th17 polarised naïve CD4 ⁺ T cell culture media with day 0 clotrimazole treatments.....	215
Figure 4.40 Normalised LC-MS ⁿ quantification of upstream and downstream oxysterols of CYP7B1 activity in Donor 9 activated non-polarised Th0 or Th17 polarised naïve CD4 ⁺ T cell culture media with day 0 clotrimazole treatments.....	217
Figure 4.41 Normalised LC-MS ⁿ quantification of upstream and downstream oxysterols of CYP7B1 activity in activated Th17 polarised naïve CD4 ⁺ T cell culture media with day 3 clotrimazole treatments.....	218
Figure 5.1 Gating strategy applied to <i>Cyp7b1</i> KO and WT isolated naïve CD4 ⁺ T cells to identify live cells and exclude dead cells using 7AAD Viability dye staining.....	232
Figure 5.2 Representative flow cytometry analysis of isolated murine naïve CD4 ⁺ T cells from the splenocytes of set 1 <i>Cyp7b1</i> KO and WT littermate.....	233

Figure 5.3 Flow cytometry analysis of CD25 expression of murine naïve CD4 ⁺ T cells after 6 days of culture under Th0, Th17 or Treg polarising conditions.....	235
Figure 5.4 Flow cytometry analysis of incorporated 7AAD staining, gated from all isolated murine naïve CD4 ⁺ T cells after 6 days of culture under Th0, Th17 or Treg polarising conditions.....	236
Figure 5.5 qRT-PCR analysis of <i>Il17a</i> mRNA expression of murine <i>Cyp7b1</i> KO and WT naïve CD4 ⁺ non-polarised Th0, Th17 polarised or Treg polarised cells.....	237
Figure 5.6 Oxysterol analysis of polarised primary murine naïve CD4 ⁺ T cell culture media.....	240
Figure 5.7 Reconstructed ion chromatogram (RIC) of monohydroxycholesterols at 534.4054 ± 10 ppm detected in Fraction 1A non-activated and activated polarised WT or <i>Cyp7b1</i> KO murine CD4 ⁺ T cell culture supernatants after 6 days.....	241
Figure 5.8 Reconstructed ion chromatogram (RIC) of dihydroxycholesterols at 550.4003 ± 10 ppm detected in Fraction 1A non-activated and activated polarised WT or <i>Cyp7b1</i> KO murine CD4 ⁺ T cell culture supernatants after 6 days.....	242
Figure 5.9 Reconstructed ion chromatogram (RIC) at 534.4054 ± 10 ppm of reference mock X-Vivo-20 media.....	243
Figure 5.10 Reconstructed ion chromatogram (RIC) at 550.4003 ± 10 ppm of reference mock X-Vivo-20 media.....	243
Figure 5.11 qRT-PCR analysis of <i>Il17a</i> mRNA expression of murine cell line EL4 cells stimulated in DMEM 10% FBS (blue), serum-free DMEM (purple) or serum-free X-Vivo-20 (green).....	244
Figure 5.12 qRT-PCR analysis of cytokine mRNA expression of murine EL4 cells in DMEM 10% FBS (blue) and serum-free X-Vivo-20 (green)....	245
Figure 5.13 EL4 cells.....	246
Figure 5.14 qRT-PCR analysis of activated murine EL4 cells cultured in X-Vivo-20 media with 24(S),25-EC and 25-HC or ursolic acid (UA) treatments for 24 or 6 hrs.....	248
Figure 5.15 qRT-PCR analysis of murine EL4 cells with ursolic acid (UA) or T0901317 treatments for 24 or 6 hrs in X-Vivo-20 media.....	249

Figure 5.16 qRT-PCR analysis of murine EL4 cells with ursolic acid (UA) or T0901317 treatments for 24 or 6 hrs in DMEM 10% FBS media.....	250
Figure 5.17 Flow cytometry analysis of CD25 expression and 7AAD viability dyes staining of stimulated EL4 cells after 24 hr or 6 hr treatments with T0901317 or ursolic acid in X-Vivo-20 media.....	252
Figure 5.18 Flow cytometry analysis of CD25 and 7AAD viability dye staining of stimulated EL4 cells after 24 hr or 6 hr treatments with T0901317 or ursolic acid in DMEM 10% FBS.....	253
Figure 5.19 qRT-PCR analysis of <i>Il17a</i> mRNA expression in stimulated EL4 cells with 3µM clotrimazole treatment after 6 hrs in DMEM 10% FBS or serum-free X-Vivo-20 media.....	254
Figure 5.20 qRT-PCR analysis of <i>Il17a</i> mRNA expression in stimulated EL4 cells with 1 to 30µM clotrimazole treatment after 6 hrs in DMEM 10% FBS media.....	255
Figure 5.21 Flow cytometry analysis of CD25 expression and 7AAD viability dye staining of stimulated EL4 cells after 6 hr treatments with 3 µM clotrimazole in DMEM 10% FBS.....	256
Figure 5.22 Flow cytometry analysis of CD25 expression and 7AAD viability dye staining of stimulated EL4 cell after 6 hrs clotrimazole treatments in DMEM 10% FBS, experiment 1.....	257
Figure 5.23 Flow cytometry analysis of CD25 expression and 7AAD viability dye staining of stimulated EL4 cell after 6 hrs clotrimazole treatments in DMEM 10% FBS, experiment 2.....	258
Figure 5.24 Reconstructed ion chromatogram (RIC) of monohydroxycholesterols at 534.4054 ± 10 ppm in Fraction 1A of (A) non-activated and (B) activated EL4 cell pellets following cell culture.....	260
Figure 5.25 Reconstructed ion chromatogram (RIC) of monohydroxycholesterols at 534.4054 ± 10 ppm in Fraction 1A of (A) non-activated and (B) activated EL4 cell culture supernatant.....	261
Figure 5.26 Reconstructed ion chromatogram (RIC) of hydroxycholesterols at 534.4054 ± 10 ppm in Fraction 1A of X-Vivo-20 mock media.....	262
Figure 5.27 Reconstructed ion chromatogram (RIC) of dihydroxycholesterols at 550.4003 ± 10 ppm in Fraction 1A of (A) non-activated and (B) activated EL4 cell pellets following cell culture.....	263

Figure 5.28 Reconstructed ion chromatogram (RIC) of dihydroxycholesterols at 550.4003 ± 10 ppm in Fraction 1A of (A) non-activated and (B) activated EL4 cell culture media.....	264
Figure 5.29 Oxysterols detected in cell pellets of non-activated and activated EL4 cells after cell culture.....	265
Figure 5.30 Oxysterols detected in cell culture media of non-activated and activated EL4 cells after cell culture.....	266
Figure 6.1 Representative Gating strategy applied to isolated CD4 ⁺ T cells to identify live cells and exclude dead cells using 7AAD Viability dye staining.....	278
Figure 6.2 Representative flow cytometry analysis of isolated CD4 ⁺ T cells from Donor 1 prior to cell culture.....	279
Figure 6.3 Flow cytometry analysis of activated CD4 ⁺ T cells from Donor 1,3 and 5 cultured with 24(S),25-EC or 7 α ,24,25-EC treatment at 0.1 μ M, 0.5 μ M and 1.0 μ M concentrations harvested after 24hrs of cell culture.....	281
Figure 6.4 Flow cytometry analysis of activated CD4 ⁺ T cells from Donor 3 and 5 cultured with 7 α ,24,25-EC-3-one or 24,25-diHC treatment at 0.1 μ M, 0.5 μ M and 1.0 μ M concentrations harvested after 24hrs of cell culture.....	283
Figure 6.5 Flow cytometry analysis of activated CD4 ⁺ T cells from Donors 6 to 9 cultured with 7 α ,24,25-triHC or 7 α ,24,25-triHC-3-one treatment at 0.5 μ M or 1.0 μ M concentrations harvested after 24hrs of cell culture.....	285
Figure 6.6 Flow cytometry analysis of activated CD4 ⁺ T cells from Donors 6 to 9 cultured with 24(S),25-EC and 24,25-diHC treatment at 1.0 μ M concentrations harvested after 24hrs of cell culture.....	286
Figure 6.7 Schematic of 24(S),25-EC metabolism through CYP7B1 and HSD3B7 activity in the Kandutsch-Russell pathway and their hydroxyl equivalents.....	288
Figure 6.8 qRT-PCR analysis of mRNA expression of activated CD4 ⁺ cells with 1 μ M 24(S),25-EC and downstream metabolites treatments.....	289
Figure 6.9 qRT-PCR analysis of <i>ABCG1</i> mRNA expression in activated CD4 ⁺ T cells with increasing concentration of 24(S),25-EC and downstream metabolites.....	290
Figure 7.1 Initial oxysterol structures for <i>in silico</i> study.....	296

Figure 7.2 Further sterol structures for <i>in silico</i> study.....	297
Figure 7.3 Initial HIS479 rotomer, tautomer poses for protein-ligand docking simulations with PLANTS.....	299
Figure 7.4 Initial HIS435 rotomer, tautomer poses for protein-ligand docking simulations with PLANTS.....	300
Figure 7.5 A network of three hydrogen bonds (black) including a solvent bridge fixes TYR502 in the active conformation with 25-HC (cyan) bound ROR γ	302
Figure 7.6 Hydrogen bonding (black) between HIS479 and TYR502 hold H12 in the active conformation with 22(R)-HC (blue) bound ROR γ	303
Figure 7.7 25-HC docking simulations with HC3 model reproduces binding seen in co-crystallised structure PDB:3L0L.....	305
Figure 7.8 25-HC ROR γ docking simulation with HC9 model.....	307
Figure 7.9 24(S),25-EC-ROR γ docking simulation with HC9 model.....	309
Figure 7.10 7 α ,24(S),25-EC-ROR γ docking simulation with HC9 model....	309
Figure 7.11 7 α ,24(S),25-EC-3-one-ROR γ docking simulation with HC9 model.....	310
Figure 7.12 24,25-diHC-ROR γ docking simulation with HC9 model.....	311
Figure 7.13 7 α ,24,25-triHC-ROR γ docking simulation with HC9 model....	312
Figure 7.14 7 α ,24,25-triHC-3-one-ROR γ docking simulation with HC9 model.....	312
Figure 7.15 7 α ,25-diHC-ROR γ docking simulation with HC9 model.....	313
Figure 7.16 7 α ,27-diHC-ROR γ docking simulation with HC9 model.....	313
Figure 7.17 Desmosterol-ROR γ docking simulation with HC9 model.....	314
Figure 7.18 Desmosterol-ROR γ docking simulations show the Desmosterol side-chain tail is orientated in close proximity towards HIS479 and electrostatic forces positions HIS479 in a favourable pose for H12 stabilisation.....	314
Figure 7.19 LXR β is fixed in an active conformation with 24(S),25-EC (green) by stabilisation of the HIS-TRP switch.....	315
Figure 7.20 25-HC-LXR β docking simulation with CO1 model.....	317
Figure 7.21 24(S),25-EC-LXR β docking simulation with CO1 model.....	317
Figure 7.22 7 α ,24(S),25-EC-LXR β docking simulation with CO1 model....	318

Figure 7.23 7 α ,24(<i>S</i>),25-EC-3-one-LXR β docking simulation with CO1 model.....	318
Figure 7.24 24,25-diHC-LXR β docking simulation with CO1 model.....	320
Figure 7.25 7 α ,24,25-triHC-LXR β docking simulation with CO1 model.....	321
Figure 7.26 7 α ,24,25-triHC-3-one-LXR β docking simulation with CO1 model.....	321
Figure 7.27 7 α ,25-diHC-LXR β docking simulation with CO1 model.....	322
Figure 7.28 7 α ,27-diHC-LXR β docking simulation with CO1 model.....	323
Figure 7.29 Desmosterol-LXR β docking simulation with CO1 model.....	324

Abbreviations

20(<i>S</i>)-HC	20(<i>S</i>)-Hydroxycholesterol
20(<i>R</i>),22(<i>R</i>)-diHC	20(<i>R</i>),22(<i>R</i>)-dihydroxycholesterol
22(<i>R</i>)-HC	22(<i>R</i>)-Hydroxycholesterol
24-HC	24-Hydroxycholesterol
24(<i>S</i>),25-EC	24(<i>S</i>),25-Epoxycholesterol
25-HC	25-Hydroxycholesterol
27-HC	27-Hydroxycholesterol
5,6-EC	5,6-Epoxycholesterol
6-HC	6-Hydroxycholesterol
7AAD	7-Aminoactinomycin D
7 α -HC	7 α -Hydroxycholesterol
7 α ,25-diHC	7 α ,25-diHydroxycholesterol
7-KC	7-Ketocholesterol
ABCA1	ATP-binding cassette transporter isoform A1
ABCG1	ATP-binding cassette transporter isoform G1
AC	Alternating current
ACN	Acetonitrile
ACO	Ant colony optimisation
ACATA	Acyl coenzyme A cholesterol acyltransferase
ACK	Ammonium-Chloride-Potassium
AF1	Activation function 1
AF2	Activation function 2
Akt	RAC-alpha serine/threonine-protein kinase
AP-1	Activator protein 1
APCs	Antigen presenting cells

APIC	Atmospheric pressure chemical ionisation
Apo A	Apolipoprotein A
Apo B	Apolipoprotein B
Apo E	Apolipoprotein E
ARDS	Acute respiratory distress syndrome
ARNTL	Aryl hydrocarbon receptor nuclear translocator-like 1
7AAD	7-Aminoactinomycin D
BBB	Blood-brain barrier
BSA	Bovine Serum Albumin
CAM	Cell adhesion molecules
cAMP	Cyclic adenosine monophosphate
cDNA	complementary Deoxyribonucleic acid
CH25H	Cholesterol 25-Hydroxylase
CI	Chemical ionisation
CID	Collision induced dissociation
CNS	Central nervous system
COPII	Coat protein complex II
CREBH	Cyclic adenosine monophosphate (cAMP)-response element binding protein H
CTE	C-terminal extension
CTLA4	Cytotoxic T-lymphocyte antigen-4
CYP11A1	Cytochrome P450 11A1
CYP27A1	Cytochrome P450 27A1
CYP39A1	Cytochrome P450 39A1
CYP46A1	Cytochrome P450 46A1
CYP7A1	Cytochrome P450 7A1
CYP7B1	Cytochrome P450 7B1

CYP8B1	Cytochrome P450 8B1
CXCR2	C-X-C Motif chemokine receptor-2
DAG	Diacylglycerol
DC	Direct current
DHCR24	24-Dehydrocholesterol reductase
DMAPP	Dimethylallyl pyrophosphate
DMG	N,N-dimethylglycine
DMSO	Dimethyl sulfoxide
DN	Double negative cells
DNA	Deoxyribonucleic acid
DP	Double positive cells
DR	Dorsal raphé
EAE	Experimental autoimmune encephalomyelitis
EADSA	Enzyme assisted derivatisation for sterol analysis
EBI2	Epstein-Barr virus-induced G-protein coupled receptor 2
EDTA	Ethylenediaminetetraacetic acid disodium salt
EI	Electron ionisation
ELISA	Enzyme-linked immunosorbent assay
ER	Endoplasmic reticulum
ERK	Extracellular-signal-regulated kinase
ESI	Electrospray ionisation
EtOH	Ethanol
ETP	Early thymocyte precursors
FAB	Fast atom bombardment
FKCOMBU	Flexible ‘K’emical structure comparison using build up algorithm
FBS	Fetal Bovine Serum

FFT	Fast Fourier-transformation
FoxP3	Forkhead box P3
FPP	Farnesyl pyrophosphate
GC-MS	Gas chromatography-mass spectrometry
GP	Girard Reagent P
GPP	Geranyl pyrophosphate
GR	Glucocorticoid receptor
H ₃ PO ₄	Phosphoric acid
HClO	Hypochlorous acid
HDL	High density lipoproteins
HMG-CoA	Hydroxymethylglutaryl CoA
HMGCR	Hydroxymethylglutaryl CoA reductase
HLB	Hydrophilic-lipophilic balance
HOAc	Acetic acid
HPLC	High performance liquid chromatography
HRP	Horseradish peroxidase
HSP	Heat shock protein
HSCs	Haematopoietic stem cells
HSD3B7	3 β -hydroxy- Δ 5-C27 steroid oxidoreductase
IgA	Immunoglobulin A
INSIG	Insulin-induced gene 1 protein
IFN γ	Interferon gamma
IL-1 β	Interleukin 1 beta
IL-17	Interleukin 17
IL-2	Interleukin 2
IL-21	Interleukin 21
IL-23	Interleukin 23

IL-6	Interleukin 6
IP3	Inositol 1,4,5-triphosphate
IPA	Isopropyl alcohol
IPP	Isopenteyl pyrophosphate
ISG	IFN-stimulated genes
ITAMS	Immunoreceptor tyrosine-based activation motifs
KH ₂ PO ₄	Potassium Phosphate
KO	Knock out
KOH	Potassium hydroxide
LAT	Linker for activation of T cells
LBD	Ligand binding domain
Lck	Lymphocyte-specific protein tyrosine kinase
LCMS	Liquid Chromatography Mass Spectrometry
LDL	Low density lipoproteins
LIT	Linear ion trap
LXR	Liver X receptor
LXRE	LXR response elements
M ⁺	Monoisotopic precursor ion
MAb	Monoclonal antibody
MALDI	Matrix-assisted laser desorption ionisation
MAMPs	Microbe associated molecular patterns
MBP	Major basic protein
MeCN	Acetonitrile
MeOH	Methanol
MHCI	Major histocompatibility complex class I
MHCII	Major histocompatibility complex class II
MMP1	matrix metalloproteinases-1

MNC	Mononuclear cells
mRNA	messenger ribonucleic acid
MS	Multiple sclerosis
m/z	mass-to-charge ratio
NFAT	Nuclear factor of activated T-cells
NaN ₃	Sodium Azide
NF- κ B	Nuclear factor kappa-B
NK	Natural killer cells
NO	Nitrogen oxide
OCDO	Oxysterol 6-oxo-cholesten-3 β ,5 α -diol
OD	Optical density
PAMPs	Pathogen associated molecular patterns
PAK	p21-activated kinase
PBMCs	Peripheral Blood Mononuclear Cells
PBS	Phosphate Buffered Saline
PDB	Protein Data Bank
PKC	Protein kinase C
PLANTS	Protein-ligand ANT system
PLTP	Phospholipid transfer protein
PMA	Phorbol 12-myristate 13-acetate
ppm	Part per million
PRR	Pattern recognition receptors
PSG	Penicillin-streptomycin-glutamine
PTCH1	Patched-1
PVDF	Polyvinylidene fluoride
qRT-PCR	quantitative reverse transcription polymerase chain reaction
RAC	Ras-related C3 botulinum toxin substrate

RAG1	Recombination activating gene 1
RAG2	Recombination activating gene 2
RA	Rheumatoid arthritis
RANKL	Receptor activator of nuclear factor kappa-B ligand
RE	Response elements
RF	Radio frequency
RIC	Reconstructed ion chromatogram
RNA	Ribonucleic acid
ROR	Retinoic acid-related orphan receptor
RORE	ROR response elements
ROR γ t	thymus retinoic acid-related orphan receptor gamma
ROS	Reactive oxygen species
RP	Reverse phase
RT	Room temperature
RXR	Retinoid X receptor
S1P	Site-1 protease
S2P	Site-2 protease
SCAP	SREBP cleavage-activating protein
Src	Proto-oncogene tyrosine-protein kinase
SREBP-1	Sterol regulatory element binding protein-1
SREBP-2	Sterol regulatory element binding protein-2
SERMs	Selective oestrogen receptor modulators
SHH	Sonic hedgehog
SLP-76	SH2-domain containing leukocyte protein of 76 kDa
SMO	Smoothened
SP	Single positive cells
SPE	Solid phase extraction

SRC-1	Sterol receptor co-activator-1
SRE	Sterol regulatory elements
SSD	Sterol sensing domain
TBDMS	Tert-butyldimethylsilyl
TCR	T cell receptor
TE	Tris-EDTA
TGF- β	Transforming growth factor beta
TIC	Total ion chromatogram
TLR	Toll-like receptors
TMB	Tetramethylbenzidine
TME	Tumour microenvironment
TMS	Trimethylsilyl
UA	Ursolic acid
VLDL	Very low density lipoproteins
WT	Wild type
ZAP-70	Zeta chain of T cell receptor associated protein kinase 70

Chapter 1. Introduction

1.1 The Immune System

All living organisms are continuously exposed to pathogenic organisms and evolutionary pressure has ensured adaptation and development of effective characteristics and processes to identify and destroy invading pathogens. The immune system is a highly connected and interactive network of lymphoid organs, cells, humoral factors and cytokines which work as the primary defence mechanism against invading pathogens. Innate immunity is a universal immune response present in bacteria, fungi, plants and animals. Bacteria use restriction modification to recognise and modify specific sequence motifs in viral genomes as a marker for cleavage and DNA degradation by restriction endonucleases ^(1,2). Plants have cell surface pattern-recognition receptors (PRRs) which recognise microbe-associated molecular patterns (MAMPs) disease resistance (R) proteins which respond to pathogen secreted effector molecules ^(3,4). Innate immunity in animals depends on germline-encoded receptors that recognise highly conserved pathogen-associated molecular patterns (PAMPs) conserved in many microbes and damage-associated molecular patterns (DAMPs) such as S100 proteins and heat shock proteins (HSP) released from damaged cells^(5,6). Vertebrates also have an adaptive immune system in which antigen specific lymphocytes are produced in response to specific antigens (Figure 1.1) ⁽⁷⁾.

1.1.1 Innate Immunity

As the first line of defence against infection the innate immune system acts rapidly and non-specifically to clear infections. Physical barriers including epithelial cell layers and mucosal membranes provide innate protection against pathogens entering the body. Enzymes such as lysozymes and antimicrobial peptides such as defensins are secreted in the mucosal layer with the ability to destroy or inactivate pathogens ⁽⁸⁾. The innate immune cells, primarily derived from myeloid progenitor cells in the bone marrow, recognise pathogen-associated molecules which are found in a wide-range of pathogens through Toll-like receptors (TLRs). This initiates an inflammatory response and phagocytosis by neutrophils and macrophages (Figure 1.1) leading to the production of reactive oxygen species (ROS) and nitrogen oxide (NO) ⁽⁹⁾. Other innate immune cells including natural killer (NK) cells induce apoptosis of infected cells and regulate the activation of further immune cells

through cytokine production. Eosinophils, mediated by major basic protein (MBP) production, target parasitic infections by producing enzymes and proteins including histaminase, eosinophil cationic protein and eosinophil peroxidase ⁽¹⁰⁾. Basophils mediate allergic reactions through synthesis and release of histamine and leukotrienes ⁽¹¹⁾. Following phagocytosis of antigens, innate cells including neutrophils and dendritic cells act as a functional bridge between the innate and adaptive immune system by presenting digested foreign antigens on their membrane surface activating the adaptive immune cells.

1.1.2 Adaptive Immunity

The innate immune system is not always sufficient in clearing infections and can become overwhelmed or circumvented allowing pathogens to thrive and cause further damage. This leads to induction of the more efficient and highly specific adaptive immune system ⁽¹²⁾. The adaptive immune cells are derived from lymphoid progenitor cells in the bone marrow and mature into B or T lymphocytes ⁽¹³⁾. T cells migrate to the thymus where they develop and mature while B cells remain in the bone marrow and progressively develop into progenitor B (pro-B) cells, precursor B (pre-B) cells and immature B cells. Cell adhesion molecules (CAMs) on stromal cells and cytokine interactions initiate growth and differentiation of developing B cells to immature B cells which migrate and fully mature in the secondary peripheral lymphoid tissues comprised of mucosal tissue, lymph nodes and the spleen. Following activation, B cells differentiate into plasma cells which produce and secrete antibodies or memory B cells which respond rapidly upon re-exposure to the same antigen.

B and T cells achieve specificity through VDJ gene recombination of the variable regions of their respective receptors during differentiation ⁽¹⁴⁾. B cells have membrane bound immunoglobulins (Igs) which act as B cell receptors. Immunoglobulins are composed of a heavy polypeptide chain and a light polypeptide chain forming an antigen binding region. Alternative splicing of the variable (V), diversity (D) and joining (J) gene segments of the light chain results in novel antigen binding regions and high diversity of Ig receptors.

The ability to distinguish self from non-self is an important requirement of the adaptive immune system. Both B and T cells undergo negative selection in the

peripheral lymphoid organs to destroy any cells which bind 'self-antigens'. Failure to discriminate non-self from self results in damage to cells leading to autoimmune diseases ⁽¹⁵⁾.

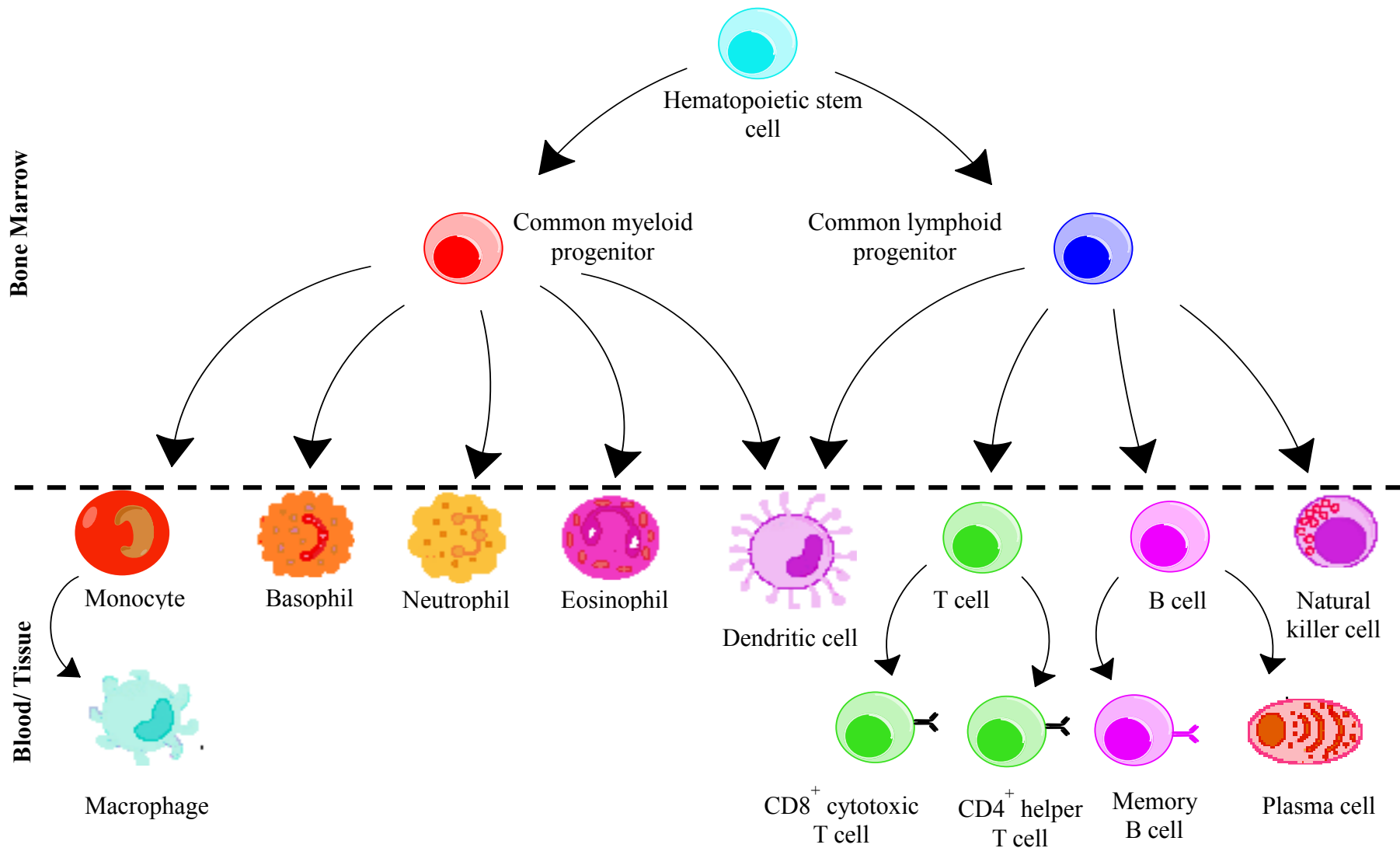


Figure 1.1 Lymphocyte cell lineages. Self-renewing haematopoietic stem cells (HSCs) in the bone marrow develop into non-self-renewing progenitor myeloid or lymphoid cells. The myeloid lineage differentiates into innate immune cells; macrophages, basophils and eosinophils. The lymphoid lineage differentiates into innate immune cells; natural killer (NK) cells and adaptive immune T cells and B cells. Dendritic cells can be derived from both myeloid and lymphoid progenitor cells.

1.2 T Cell Biology

T cells have an important role in adaptive immunity regulating and coordinating immune responses of other immune cells. Immature T cells migrate from the bone marrow to the thymus where they differentiate and mature into naïve CD8⁺ cytotoxic T cells or naïve CD4⁺ T helper cells ⁽¹⁶⁾. Following differentiation mature naïve T cells are released into the blood to recirculate and interact with antigen presenting cells (APCs). Activation by APCs leads to clonal expansion and differentiation into effector T cells providing targeted immune responses specific to the pathogen present.

1.2.1 T cell development

Bone marrow lymphoid progenitor cells destined for T cell lineage migrate to the thymus where they undergo a series of intermediate stages of development illustrated in Figure 1.2. Notch signalling has a crucial role in the developmental stages of T cell production and inhibition of notch signalling results in the loss of T cell production and precursor cell differentiation to B cells or NK cells ^(17, 18).

Rearrangement of antigen receptor genes occurs through the intermediate development stages distinguished through the expression of cell surface markers. The location of the progenitor cells within the thymus (thymocytes) correlates with their stage of development.

T cell precursor cells from the bone marrow, known as early thymocyte precursors (ETP), enter the thymus at the cortico-medullar junction ⁽¹⁷⁾. These are double negative (DN) cells as they lack expression of CD4, CD8 and other markers of committed T cell lineage. DN cells diverge into two distinct T cell lineages with different T cell receptors (TCRs), $\alpha\beta$ T cells and $\gamma\delta$ T cells. A small minority become $\gamma\delta$ T cells while the majority follow the $\alpha\beta$ T cell lineage. DN cells are subdivided by the expression of cell surface marker CD44 and IL-2 receptor α chain, CD25. DN1 cells (CD44⁺, CD25⁻) are further subdivided into subsets DN1a-e depending on the expression of CD117 and CD24. DN1a and DN1b cells expressing CD117 typically generates T cells.

Rearrangement of the TCR variable region (V) through VDJ recombination provides diversity of T cell antigen receptors as with B cells. The β chain of the TCR is the

first rearrangement to take place when DN2 cells expressing both CD44 and CD25 migrate to the cortex and undergo TCR β , TCR γ and TCR δ rearrangement mediated by RAG1 and RAG2 ⁽¹⁹⁾. Following TCR β rearrangement, CD44 expression is downregulated and cells (CD44⁻, CD25⁺) are fully committed to the T cell lineage. DN3 cells undergoes surrogate α chain pairing with a pre-T cell α (pT α) to form a pre-T cell receptor. The pre-T cell receptor is expressed on the cell surface and forms a complex with CD3 for successful β chain selection. Expression of CD25 is downregulated following successful β chain selection leading to DN4 cells which upregulate CD4 and CD8 expression resulting in double positive (DP) cells and subsequent rearrangement of the α chain. DP cells undergo positive selection in the cortex when cells bind with thymic cortical epithelial cells expressing MHC I or MHC II and self peptide ⁽²⁰⁾. DP cells with efficiency to receive a survival signal undergo CD4⁺ or CD8⁺ differentiation to become single positive (SP) cells and move to the cortico-medullar junction. Negative selection occurs in the medulla when SP cells bind bone marrow derived APCs expressing MHC I or MHC II and self peptide with efficiency to receive an apoptosis signal. Following positive and negative selection naïve CD4⁺ and CD8⁺ cells leave the thymus and enter circulation.

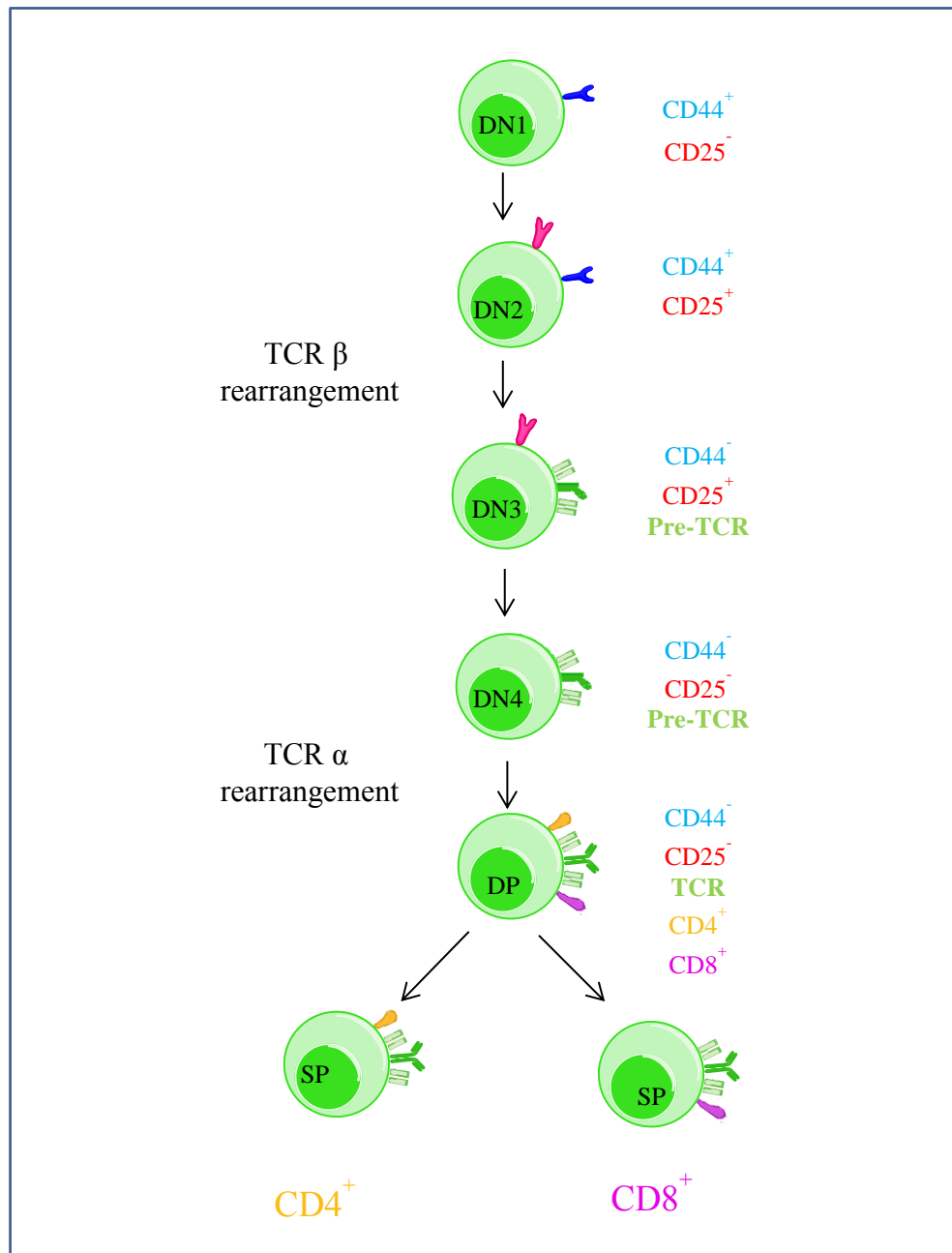


Figure 1.2 Simplified schematic of CD4⁺ and CD8⁺ T cell development. Double negative (CD4⁻, CD8⁻) early thymocyte precursors expressing CD44 cell surface marker differentiate into DN2 cells expressing CD44 and CD25. DN2 cells undergo T cell receptor β chain rearrangement, CD44 is downregulated and cells differentiate into DN3 cells with a pre-T cell receptor. DN3 cells downregulate CD25 expression differentiating into DN4 cells undergoing T cell receptor α chain rearrangement and upregulation of CD4 and CD8 into double positive (DP) cells which undergo positive selection producing CD4⁺ and CD8⁺ T cells.

1.2.2 T cell subsets

Naïve T cells leave the thymus and circulate through the blood and lymphatic system in readiness for an encounter with their specific antigen. Naïve T cells remain in a quiescent state until activated by a primary signal through the TCR and antigens presented on major histocompatibility complexes MHCI or MHCII of APCs and co-stimulatory signals provided by the interactions of co-receptors. Once activated T helper cells further differentiate into effector T helper cells depending on the cytokine environment present. Upon recognition of antigens on the MHC II complex a signal cascade is induced involving cytokines, costimulatory molecules, chemokines, integrins and metabolites which drives the differentiation of T cells into specific effector cell subsets ⁽²¹⁾.

Co-receptor protein CD28 recognise B7 co-stimulatory proteins on APCs which induces production of IL-2 and IL-2 cell surface receptor activating intracellular signalling pathways and increasing T cell proliferation ⁽²¹⁾. This leads to a positive feedback loop of effector T cells which promote the expression of B7 proteins on APCs amplifying the T cell response. Negative regulation occurs through natural inhibitor CTLA4 (cytotoxic T-lymphocyte antigen-4) which binds to B7 proteins on APCs competing with CD28 reducing the activation signal ⁽²²⁾.

TCR ligation leads to activation of Src family protein tyrosine kinases Lck which mediate the phosphorylation of immunoreceptor tyrosine-based activation motifs (ITAMs) of the CD3 chains ⁽²³⁾. The CD45 receptor tyrosine phosphatase modulates Lck phosphorylation of ITAMs in the TCR/CD3 complex inhibiting signal initiation ⁽²⁴⁾. Phosphorylated ITAMs recruit tyrosine kinase ZAP-70 which facilitates interactions of the TCR with other effector molecules ⁽²⁵⁾. ZAP-70 phosphorylates tyrosine residues of scaffold protein LAT which associates with SLP-76 providing additional binding sites for downstream signalling molecules including PLC- γ 1 ⁽²⁶⁾. Activated PCL- γ 1 produces second messengers diacylglycerol (DAG) and Inositol 1,4,5-triphosphate) IP3 which activate transcription factors involved in the T cell signalling pathway including NFAT, NF- κ B, and AP-1 ⁽²⁷⁻²⁹⁾. DAG activates protein kinase C (PKC) which subsequently activates the NF- κ B pathway. IP3 stimulates efflux of Ca²⁺ from the ER to the cytosol leading to the activation of calcineurin which dephosphorylates transcription factor NFAT enabling translocation to the

nucleus. TCR activation also causes cytoskeletal rearrangement through the activation of GTP-binding proteins Rac and PAK ⁽³⁰⁾.

There are several effector T cells with specific roles in the immune response. Naïve CD8⁺ T cells differentiate into cytotoxic T cells that recognise and destroy infected cells. CD8⁺ effector T cells which remain after an infection become memory T cells which respond quickly upon reinfection.

Upon activation by APCs, naïve CD4⁺ T helper cells proliferate, requiring upregulation of the cholesterol biosynthesis pathway, and differentiate into effector cell lineages Th1, Th2, Th17 or immunosuppressive regulatory T cell (Treg) in Figure 1.3 ⁽³¹⁾.

The Th17 subset of T helper cells was distinguished from Th1 and Th2 cells due to its specific cytokine expression profile of IL-17A, IL-17F, IL-22 and GM-CSF ⁽³²⁻³⁴⁾. Th1, Th2 and Th17 cells stimulate an inflammatory immune response to pathogens whereas Treg cells, regulated by transcription factor forkhead box P3 (FoxP3) are crucial for negative control of the immune system ⁽³⁵⁾.

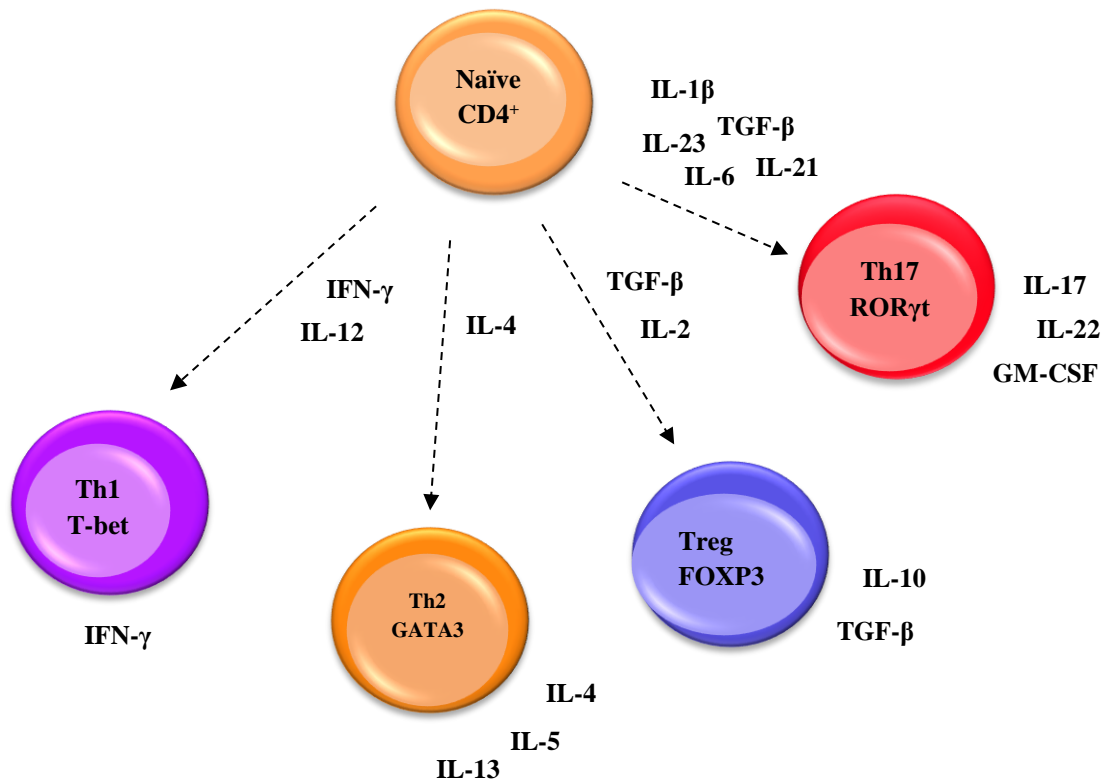


Figure 1.3 Simplified differentiation of CD4⁺ T helper cell subsets. The cytokine environment during naïve CD4⁺ T cell activation determines the lineage of CD4⁺ T helper cells.

1.2.3 Th17 cells

CD4⁺ T helper lymphocytes (T helper cells) are an important component of the adaptive immune system with an essential role in the regulation of the immune response. Characterised by the pro-inflammatory cytokine interleukin-17 (IL-17), Th17 cells mediate the recruitment of neutrophils and macrophages to infected tissues providing a crucial defence against extracellular pathogens such as *Klebsiella pneumonia* ⁽³⁶⁻³⁸⁾. The differentiation of human Th17 cells is driven by cytokines TGF- β , IL-6, IL-1 β and IL-23 and the master transcription factor regulating Th17 cell differentiation is the ligand-activated transcription factor thymus retinoic acid-related orphan receptor gamma (ROR γ t) an isoform of ROR γ from the nuclear receptor family of transcription factors ⁽³⁹⁻⁴³⁾. Th17 cells specifically produce IL-17

homologues IL-17A and IL-17F, which induce the inflammatory responses ⁽⁴⁴⁻⁴⁵⁾. Elevated Th17 cells and IL-17 production has been implicated in the pathogenesis of various autoimmune diseases including rheumatoid arthritis (RA), multiple sclerosis (MS) and psoriasis ⁽⁴⁶⁻⁵¹⁾.

While IL-17 expression is characteristic of Th17 cells it is also produced by several other cells including CD8⁺ T cells, CD3⁺ CD4⁻CD8⁻ T cells, $\gamma\delta$ -T cells, natural killer cells and neutrophils ⁽⁴⁴⁾.

1.2.4 Retinoic acid receptor-related orphan receptor gamma t, ROR γ t

Retinoic acid receptor-related orphan receptor gamma t, ROR γ t, is the master transcription factor required for the differentiation of Th17 cells and IL-17 production ⁽⁵²⁾. Aberrant expression of Th17 cells and excess secretion of IL-17 has been associated with various autoimmune diseases therefore ROR γ t is a key target for treatment ^(44,46-50).

The superfamily of nuclear receptors, of which ROR γ t is a member, have a modular structure comprised of four main domain regions, the N-terminal A/B domain, The DNA binding domain (DBD), a flexible hinge and the C-terminal ligand binding domain (LBD) illustrated in Figure 1.4 ⁽⁵³⁾. The most divergent N-terminal A/B domain contains the AF1 (activation function 1) region responsible for corepressor and coactivator interactions. The DBD is the most conserved region of nuclear receptors and is responsible for binding response elements (REs) within regulatory regions of target genes. The LBD contains the AF2 (activation function 2) region, which acts in a ligand-dependent manner.



Figure 1.4 Nuclear receptor domain regions. The N-terminal A/B domain contains the activation function 1 (AF1) region responsible for corepressor and coactivator interactions. The DNA binding domain (DBD) is responsible for binding response elements (REs) while the activation function 2 (AF2) region is located in the C-terminal ligand binding domain (LBD).

ROR γ t belongs to the retinoic acid-related orphan receptor (ROR) subgroups of nuclear receptors, which includes ROR α , ROR β and ROR γ ⁽⁵⁴⁻⁵⁶⁾. ROR β is not expressed in immune cells and although there is high expression of ROR α in Th17 cells, partial redundancy has been seen in mouse Th17 cell differentiation ⁽⁵⁷⁾.

ROR γ t is an isoform of ROR γ encoded by *RORC* gene on chromosome 1q21 that differs by 21 amino acids in the N-terminal domain ⁽⁵⁸⁾. In contrast to ROR γ which is expressed widely, ROR γ t is expressed almost exclusively in immune thymocytes ⁽⁵⁹⁻⁶⁰⁾.

The DBD of ROR γ contains two highly-conserved zinc finger motifs involved in the recognition of DNA elements ^(53,61). RORs recognise common ROR response elements (ROREs) with the consensus sequence WWCWAGGTCA (W = A or T) ⁽⁶²⁻⁶³⁾. The P-box in the DBD loops between the last two cysteines within the first zinc finger and recognises the core motif in the major groove of the DNA ⁽⁶³⁻⁶⁴⁾. The DNA binding specificity is further determined by the C-terminal extension (CTE) immediately downstream of the second zinc finger which interacts with the 50-AT-rich segment of the RORE in the adjacent groove of the DNA. The LBD of ROR γ is comprised of a conserved three-layered fold of 12 α -helices (H1-H12) with two short β -strands forming a shorter sheet structure ⁽⁶⁵⁾. Co-activators and co-repressors interact with the AF2 region also known as Helix 12 (H12) in the LBD which contains three additional helices, H2, H3 and H11 and the ligand –binding pocket forming part of the hydrophobic core ^(61,66).

Recent studies have implicated the cholesterol metabolic pathways as key regulators of ROR γ t activity ^(67, 68). The activation of CD4⁺ T cells involves cell membrane expansion and proliferation requiring the cholesterol biosynthesis pathway. During Th17 differentiation cholesterol biosynthesis and uptake pathways are induced and the metabolism and efflux pathways suppressed. Cholesterol derivatives including oxysterols and cholesterol precursors have been associated with ROR γ t but the endogenous ligand of ROR γ t is yet to be determined.

1.2.5 The role of Th17 cells in autoimmune diseases

Autoimmunity was initially thought to be through the uncontrolled response of Th1 cells; however, mice studies of experimental autoimmune encephalomyelitis (EAE), the animal model of multiple sclerosis, revealed mice deficient in the Th1 cytokine

IFN γ actually show worsened symptoms ⁽⁵⁰⁾. In contrast, mice deficient in the Th17 cytokine IL-17 did not induce EAE efficiently suggesting IL-17 has an important role in the activation of encephalitogenic T cells ^(51, 69).

Psoriasis is predominantly mediated by Th17 cells following cytokine IL-23 secretion from dendritic cells driving pathogenic Th17 cell differentiation from naïve CD4⁺ T cells ⁽⁶⁹⁻⁷⁴⁾. IL-17 production activates keratinocytes proliferation, promotes epidermal hyperplasia, antimicrobial peptides production and recruits pro-inflammatory cells creating a positive pro-inflammatory feedback loop accelerating lesion formation ⁽⁷⁵⁾.

Elevated circulating Th17 cells are also observed in rheumatoid arthritis (RA) patients ⁽⁷⁶⁾. Expression of IL-17 by Th17 cells promotes osteoclastogenesis via the NF- κ B ligand, receptor activator of nuclear factor kappa-B ligand (RANKL) and induces pro-inflammatory cytokine and chemokine production in synovial fibroblast resulting in cartilage loss ⁽⁷⁶⁾. Upregulation of matrix metalloproteinases-1 (MMP1) in chondrocytes and synoviocytes is also induced by IL-17 leading to further cartilage damage.

Prolonged Th17 response has also been implicated in the pathogenesis of acute respiratory distress syndrome (ARDS) associated with infections of which influenza is an example ⁽⁷⁷⁾. Recently Th17 has been linked to severe ARDS associated with SARS-CoV-2 (COVID-19) by mediating an aggressive hyperactive inflammatory response through neutrophil recruitment and excessive pro-inflammatory cytokines expression leading to a 'cytokine storm' ⁽⁷⁸⁻⁸¹⁾.

Current treatments for autoimmune diseases include antibodies targeting Th17 cytokines or IL-23 and their receptors and more recently a recombinant human monoclonal antibody (mAb) targeting IL-17 specifically has shown clinical efficacy in psoriasis, rheumatoid arthritis, uveitis and ankylosing spondylitis ⁽⁸²⁻⁸³⁾. However there are limitations with biological treatments such as biological fatigue in which the efficiency of treatment is reduced with long term use as the immune system develops antibodies to the drugs. Alternative research focuses on the development of small molecule inhibitors to compete with endogenous agonist at the ligand-binding domain to suppress the activity of ROR γ t ⁽⁸⁴⁻⁸⁵⁾. Digoxin and its derivatives have

been shown to inhibit IL-17 induction in human CD4⁺ T cells and delay the onset of autoimmune diseases in mouse models.

1.3 Cholesterol

Cholesterol has an integral role in the structure of the cell membrane of eukaryotic cells by moderating membrane fluidity and maintaining the integrity of lipid rafts within the cell plasma membranes. Cholesterol also functions as a precursor of bile acids and a substrate for synthesis of vitamin D and steroid hormones.

1.3.1 Structure and nomenclature

Cholesterol was discovered in 1815 by lipid chemist Michel Chevreul when Chevreul isolated cholesterol from human gallstones ⁽⁸⁶⁾. The structure was later established by chemists Adolf Windaus and Heinrich Wieland ⁽⁸⁷⁾. Typical of steroid compounds, cholesterol has a central four-ring structure with three cyclohexane rings and a 1,2-cyclopentanoperhydrophenanthrene ring shown in Figure 1.5. Cholesterol is an amphipathic compound, the carbon frame is 3 β -hydroxylated and methylated at C10 and C13 positions with a Δ^5 double bond in the B ring and hydrocarbon side-chain attached at the C17 position (Figure 1.6) ^(88, 89). Cholesterol is composed of a polar 3 β hydroxyl group and non-polar hydrocarbon ring and side-chain. It has the molecular formula C₂₇H₄₆O and the systematic name given is Cholest-5en-3 β -ol.

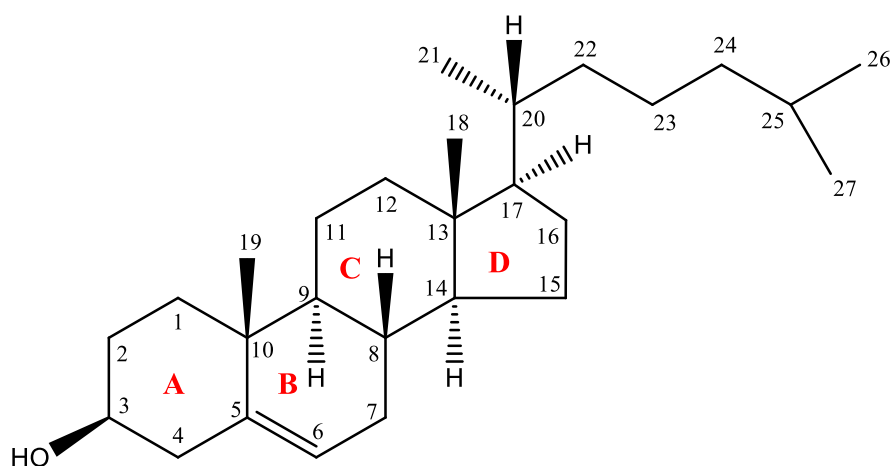


Figure 1.5 Structure of Cholesterol. Cholesterol has three cyclohexane rings (A-C) and a 1,2 cyclopentanperhydrophenanthrene ring (D). The carbon ring is methylated at C10 and C13. Cyclohexane ring A is 3 β -hydroxylated and ring B has a Δ^5 double bond. A hydrocarbon side-chain is attached at C17 on ring D.

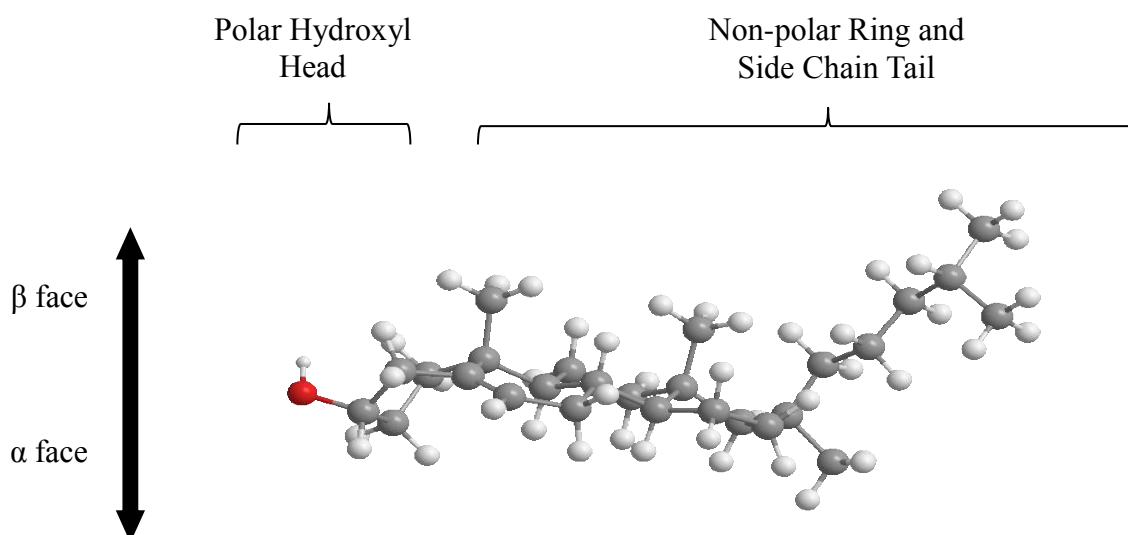


Figure 1.6 3D structure of Cholesterol. Cholesterol is comprised of a polar hydroxyl head and a non-polar ring and side chain tail. Groups which extend in front of the plane are β groups and groups which extend below the plane are α groups.

1.3.2 Cholesterol synthesis

The main sources of cholesterol in humans are through the diet (~30%) and de novo synthesis in cells (~70%). Cholesterol biosynthesis occurs in the liver and circulates to the rest of the body however as cholesterol is unable to cross the blood-brain barrier (BBB) cholesterol in the brain and nervous system is locally synthesised.

Due to the insoluble nature of cholesterol it is packaged with apolipoproteins to be transported as water-soluble lipoproteins, the most abundant of which are apolipoprotein A (Apo A) and apolipoprotein B (Apo B) ⁽⁹⁰⁾. Lipids such as fatty acids, triglycerides and cholesterol are transported to and from the liver by lipoproteins. There are several classes of lipoproteins based on their lipid composition, apolipoproteins and size. Chylomicrons are triglyceride rich lipoproteins made in the intestine that transport absorbed dietary lipids including cholesterol from the intestine to the liver. Lipids in the liver are packaged as very low density lipoproteins (VLDL) to transport fatty acids and triglycerides to the rest of the body. Low density lipoproteins (LDL) derived from triglyceride and fatty acid depleted VLDLs have an increased protein-to-lipid ratio and act as the main

cholesterol transporters from the liver and deliver cholesterol to LDL receptors of target cells through endocytosis.

Reverse cholesterol transport is the mechanism by which excess cholesterol is removed from peripheral tissue to the liver ⁽⁹⁰⁾. High density lipoproteins (HDL) circulate the periphery tissues and take up any excess cholesterol and deliver it to the liver for redistribution, removal or metabolism. In the endoplasmic reticulum (ER) excess cholesterol may be esterified by acyl coenzyme A cholesterol acyltransferase (ACAT) with the addition of fatty acids forming cholesteryl esters deposited as cytosolic lipid droplets ⁽⁹¹⁾.

Cholesterol is synthesised by over 30 enzymatic reactions beginning with the mevalonate pathway and the conversion of acetyl CoA to hydroxymethylglutaryl CoA (HMG-CoA) in the cytosol (Figure 1.8). In the ER HMG-CoA is reduced to mevalonate by the rate limiting enzyme of this pathway hydroxymethylglutaryl CoA reductase (HMGCR). HMGCoA contains a conserved sterol sensing domain (SSD) consisting of 5 α -helices which span the ER membrane, required for interaction with ER bound protein Insig ⁽⁹²⁾.

Mevalonate undergoes a series of phosphorylation reactions to isopentenyl pyrophosphate (IPP) and isomerisation to dimethylallyl pyrophosphate (DMAPP). Successive condensation reactions with enzyme prenyl transferase convert DMAPP to geranyl pyrophosphate (GPP) followed by farnesyl pyrophosphate (FPP). A subsequent condensation reaction with squalene synthase converts FPP to squalene. Squalene is oxidised to 2,3-epoxysqualene by monooxygenase which undergoes a cyclisation step and oxidosqualene monooxygenase catalyses lanosterol production, the first sterol in cholesterol synthesis. Lanosterol can follow two alternative pathways, the Bloch pathway or Kandutsch-Russell pathway both involving multiple enzyme reactions to produce cholesterol (Figure 1.9). Reduction of the double bond at C24 by 24-dehydrocholesterol reductase (DHCR24) converts lanosterol to saturated dihydrolanosterol which follows the Kandutsch-Russell pathway. Unsaturated intermediates in the Bloch pathway can also be converted to the Kandutsch-Russell pathway by DHCR24 reduction. Both pathways undergo oxidation, demethylation, decarboxylation and isomerisation and reduction reaction steps shown in Figure 1.8. Parallel to cholesterol synthesis 24(*S*),25-EC is

synthesised in a shunt pathway when 2,3-epoxycholesterol is converted to 2,3,22,23-diepoxyqualene with the introduction of a side chain epoxy group which is retained in the shunt pathway ⁽⁹⁰⁾.

Cholesterol homeostasis is regulated through the SCAP-SREBP-2 complex in which cholesterol interacts with SREBP cleavage activating protein (SCAP) and insulin induced gene (INSIG) on the ER to control sterol regulatory element binding protein-2 (SREBP-2) transcription factor ⁽⁹³⁾. When cholesterol concentrations are sufficient cholesterol binds to SCAP causing a conformational change that enables SCAP to bind to INSIG illustrated in Figure 1.7. When the SCAP-SREBP-2 complex is bound to INSIG, SREBP-2 remains anchored to the ER membrane and cannot induce HMGCR or LDL receptor genes. When cholesterol levels are reduced the level of cholesterol bound to SCAP is reduced and INSIG dissociates from the SCAP-SREBP-2 complex to be degraded by the proteasome ⁽⁹⁴⁾. In the absence of INSIG the complex translocate to the Golgi apparatus through coat protein complex II (COPII) coated vesicles where proteolytic cleavage by site-1 protease (S1P) and site-2 protease (S2P) releases the active N-terminal SREBP-2 transcription factor domain ⁽⁹⁵⁻⁹⁸⁾. The active domain of SREBP-2 migrates to the nucleus and binds to the sterol regulatory elements (SRE) in the promoter region of cholesterol synthesis and uptake target genes including HMGCR and LDL receptors inducing gene expression. Oxysterols, oxidised derivatives of cholesterol, also have a role in the regulation of cholesterol synthesis by binding to INSIG which subsequently binds to the SCAP-SREBP complex anchoring the complex to the ER ⁽⁹⁹⁾.

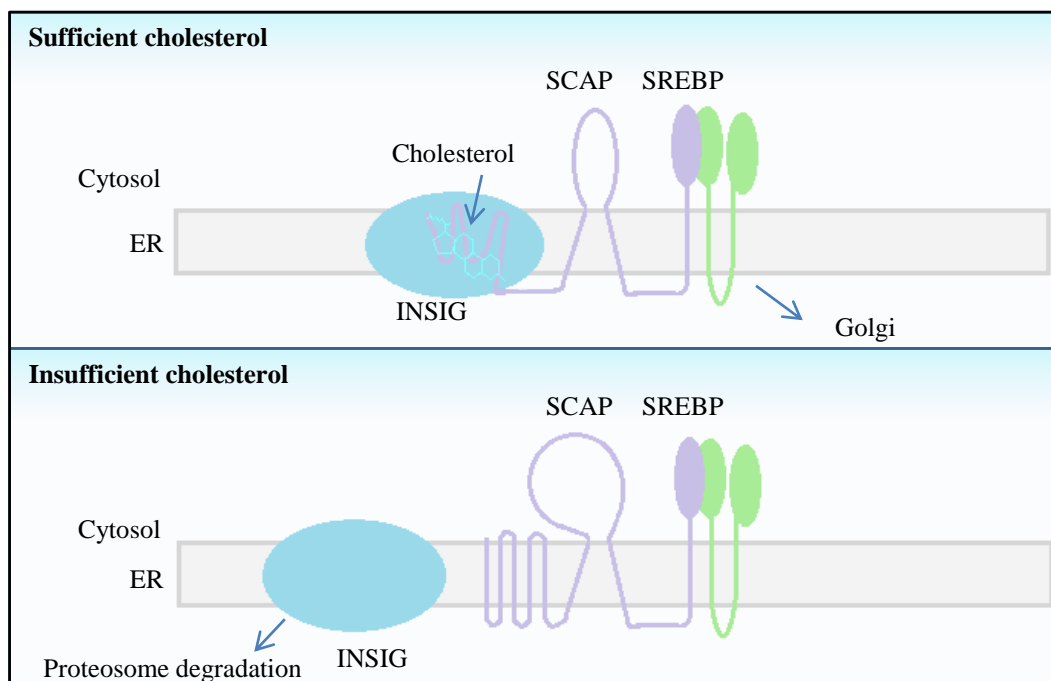


Figure 1.7 Simplified schematic of the SCAP-SREBP regulatory pathway of cholesterol. When there is sufficient cholesterol present cholesterol binds to the ER bound SCAP-SREBP complex with INSIG. When there is insufficient cholesterol present INSIG dissociates from the SCAP-SREBP complex causing a conformational change enabling the SCAP-SREBP complex to move to the glogi apparatus for proteolytic cleavage of the SREBP active domain. Adapted from Ye & Debose-boyd (2011) ⁽⁹⁶⁾.

Transcriptional regulation of cholesterol is achieved through liver X receptor (LXR) transcription factors. Accumulation of oxysterols leads to LXR activation increasing cholesterol efflux from peripheral tissues. LXR isomers LXR α (NR1H3) and LXR β (NR1H2) form heterodimers with retinoid X receptors (RXR) and in the presence of agonists bind to LXR response elements (LXREs) of target genes involved in reverse cholesterol transport such as ATP-binding cassette transport isoforms A1 (ABCA1) and G1 (ABCG1), Apolipoprotein E (ApoE) and phospholipid transfer protein (PLTP) upregulating gene expression ⁽¹⁰⁰⁾. Agonist bound LXR heterodimers bind to LXREs in SREBP-1 promoter region initiating a conformational change that enables coactivators to bind to the heterodimer such as sterol receptor coactivator-1 (SRC-1) inducing SREBP transcription to promote triglyceride synthesis ⁽¹⁰¹⁾.

Cholesterol homeostasis is also regulated through endocrine signalling of insulin and glucagon. It has been proposed that insulin and glucagon regulate HMGCR gene expression with opposing action through the phosphorylation state of HMGCR ⁽¹⁰²⁾.

It has also been suggested that the inhibitory effect of glucagon is mediated by cyclic adenosine monophosphate (cAMP)/protein kinase A pathway with cyclic AMP-responsive element binding protein H (CREBH) ⁽¹⁰³⁾. Glucagon is proposed to activate CREBH which inhibits cholesterol synthesis by upregulating mRNA and protein expression of INSIG-2.

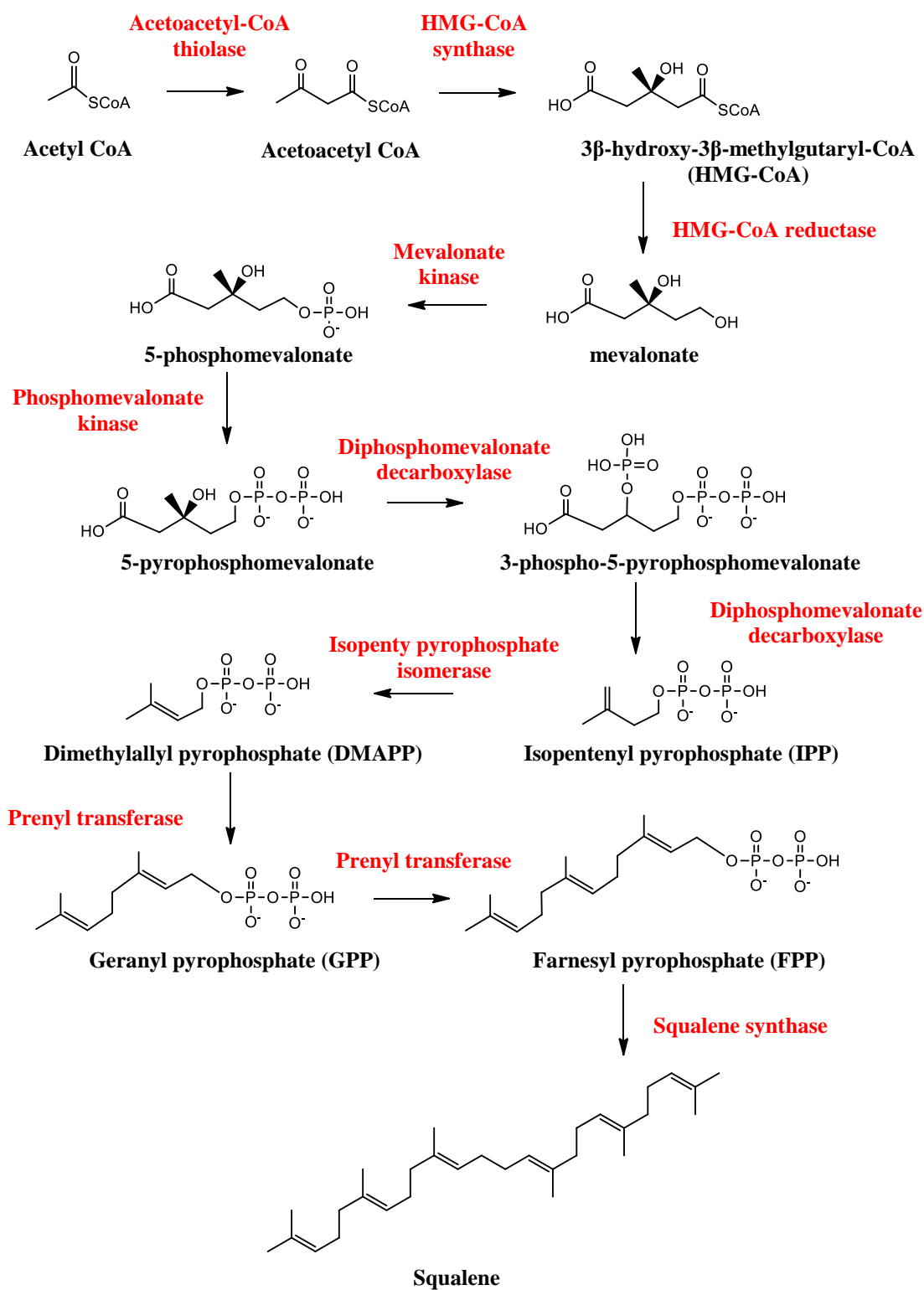


Figure 1.8 The mevalonate pathway. Cholesterol biosynthesis begins with the conversion of acetyl CoA to squalene. Key enzymes are indicated in red.

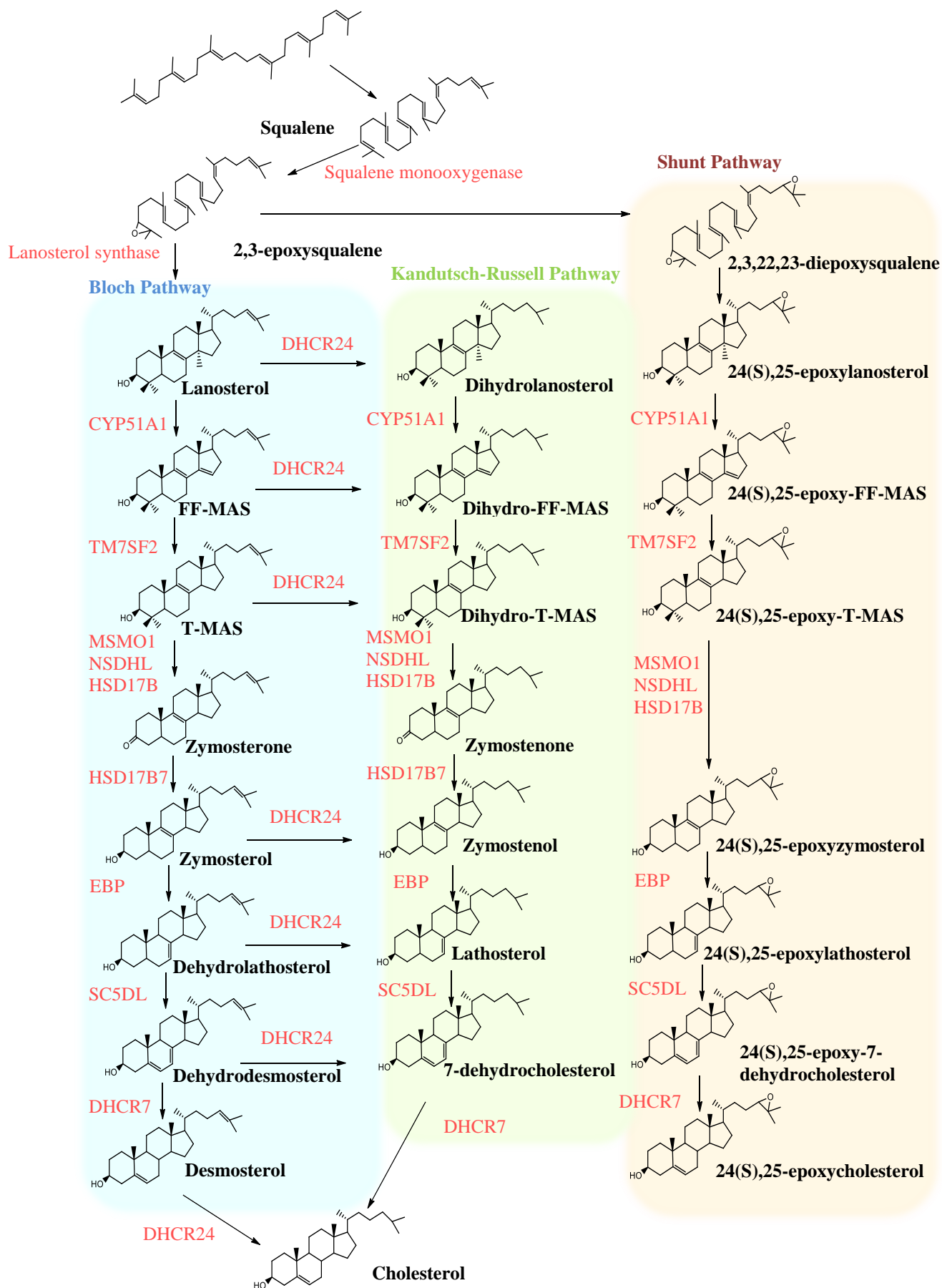


Figure 1.9 Cholesterol biosynthesis pathways from squalene. Lanosterol is converted into cholesterol through the Bloch pathway (blue). Lanosterol and intermediates in the Bloch pathway can be converted to saturated equivalents through DHCR24 and are converted to cholesterol through the Kandutsch-Russell pathway (green). 24(S),25-EC is synthesised parallel to cholesterol through a shunt pathway (orange). Key enzymes are indicated in red.

1.4 Oxysterols

Oxysterols are oxidised metabolites of cholesterol which act as intermediates in the cholesterol metabolism and bile acid synthesis pathway with a feedback role in cholesterol homeostasis. Oxysterols have more recently been shown to have their own biological functions with roles as nuclear transcription factor and G-protein coupled receptor ligands.

1.4.1 Nomenclature

Oxysterols are named from the 27-carbon cholestane as with cholesterol (cholest-5en-3 β -ol)^(88, 104). Modifications including hydroxylation and unsaturated bonds follow the cholesterol numbering system^(88, 103, 104). Orientation and chirality of additional functional groups in relation to sterol stereochemistry is identified by α/β anomers and R/S axial chirality. Below the steroid plane are α anomers denoted by broken lines ($\overline{}$) and above the plane are β anomers denoted by a solid line (\blacktriangledown). Substitutions in the steroid side chain use R/S chirality nomenclature in which the side chain hydroxyl group orientation is based on a chiral centre with four groups attached as shown in Figure 1.10. The groups attached to the chiral centre are arranged based on atomic numbers with the lowest atomic number positioned away from the observer. The remaining groups are in front of the observer positioned from the highest to the lowest atomic number. Isomers with a clockwise direction are R isomers while isomers with an anticlockwise direction are S isomers.

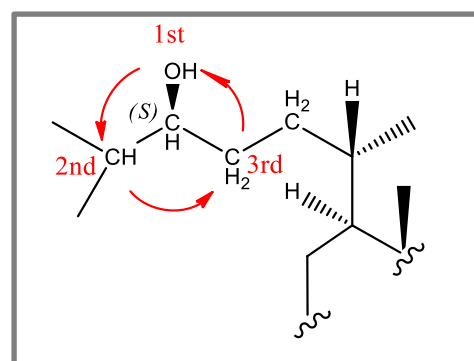
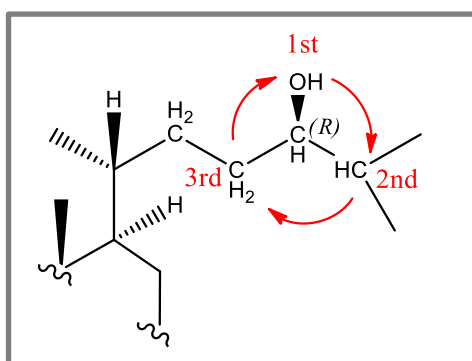
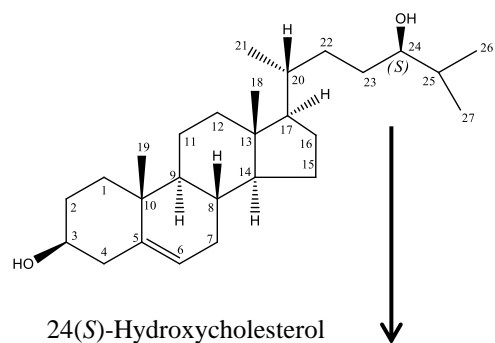
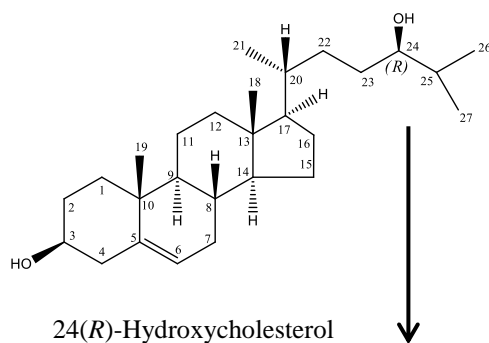


Figure 1.10 Nomenclature of oxysterol stereoisomers. The orientation of the oxysterol sidechain hydroxyl group around the chiral carbon centre determines *R/S* stereoisomers. For example 24-hydroxycholesterol exist as 24(*R*)-hydroxycholesterol with clockwise orientation of the hydroxyl group at C24 or 24(*S*)-hydroxycholesterol with anti-clockwise orientation of the hydroxyl group.

1.4.2 Oxysterol synthesis

Although cholesterol is an essential component of eukaryotic cells the cellular concentration of cholesterol must be strictly regulated. High cholesterol levels can be toxic and lead to a build-up of plaques in blood vessels leading to atherosclerosis⁽⁹¹⁾. Approximately 90% of cholesterol is metabolised and converted to bile acids in the liver through two multiple-enzyme pathways, the classic and alternate bile acid synthesis pathways depicted in Figure 1.11. Cholesterol metabolising enzymes in the bile acid synthesis and steroid biosynthesis pathways collectively convert cholesterol into oxysterol compounds. Oxysterols are present at 1,000 -10,000 fold lower concentrations than cholesterol and may also be synthesised non-enzymatically through autooxidation.

1.4.2.1 Enzymatic production of oxysterol

Initiation of bile acid synthesis through 7 α -hydroxylation produces trihydroxycholesterols. In the classic pathway cholesterol is converted to 7 α -hydroxycholesterol (7 α -HC) through microsomal cytochrome P450 7A1 (CYP7A1), expression of which is limited to the liver. Hydroxylation of the cholesterol side chain at positions 24, 25 and 27 through cytochrome P450 46A1 (CYP46A1), cholesterol 25-hydroxylase (CH25H) and cytochrome P450 27A1 (CYP27A1) produces oxysterols 24-hydroxycholesterol (24-HC), 25-hydroxycholesterol (25-HC) and 27-hydroxycholesterol (27-HC) respectively which act as substrates for bile acids in the alternate pathway⁽¹⁰⁶⁻¹⁰⁷⁾. Cytochrome P450 39A1 (CYP39A1) hydroxylates 24-HC at the 7 α position while cholesterol metabolising enzyme cytochrome P450 7B1 (CYP7B1) is an oxysterol 7 α -hydroxylase enzyme abundantly expressed in the liver, which hydrolyses oxysterols 25-HC and 27-HC at the 7 α position in the cholesterol metabolism pathway⁽¹⁰⁷⁻¹⁰⁸⁾. Following 7 α -hydroxylation the ring structure of these oxysterols are further modified to 3-oxo, Δ^4 intermediates by a microsomal 3 β -hydroxy- Δ^5 -C27 steroid oxidoreductase (HSD3B7)⁽¹⁰⁸⁾. HSD3B7 catalyses isomerisation of the double bond from the 5 to the 4 position and oxidation of the 3 β -hydroxyl group to a 3-oxo group in 7 α -hydroxycholesterols⁽¹⁰⁹⁾. These oxysterols undergo further oxidation through a sterol 12 α -hydroxylase cytochrome P450 8B1 (CYP8B1) and side chain shortening through CYP27A1 to produce aldehydes which are further metabolised to a carboxylic acid and subsequently the primary bile acid cholic acid. Oxysterols which are not oxidised at

the 12 α position are further metabolised to the primary bile acid chonodeoxycholic acid.

Oxysterol 22(*R*)-hydroxycholesterol (22(*R*)-HC) is synthesised through the steroid biosynthesis pathway and converted to 20(*R*),22(*R*)-dihydroxycholesterol (20(*R*),22(*R*)-diHC) and ultimately pregnenalone through cytochrome P450 11A1 (CYP11A1) ⁽¹⁰⁹⁾.

While oxysterols act as precursors to bile acids and steroid hormones, hydroxylation of cholesterol precursor 7-dehydrocholesterol produces the sterol precursor of vitamin D, previtamin D₃ ⁽¹¹¹⁾. Further hydroxylation of previtamin D₃ in the liver and kidneys produces the active form of vitamin D (1,25-dihydroxyvitamin D).

1.4.2.2 Autoxidation of cholesterol

Cholesterol can be oxidised by autoxidation which can occur upon exposure to light, heat and initiation by free radicals such as those from superoxide, hydrogen peroxide and hydroxyl radical systems or reactive oxygen species (ROS) including single oxygen, hypochlorous acid (HOCl) and ozone ⁽¹¹²⁻¹¹³⁾. Autoxidation can occur during sample collection, preparation, analysis and storage producing oxysterols 7-hydroxycholesterol (7-HC), 7-ketocholesterol (7-KC), 5,6-epoxycholesterol (5,6-EC) and 6-hydroxycholesterol (6-HC) ⁽¹¹²⁻¹¹³⁾.

1.4.3 The role of oxysterols in cholesterol homeostasis

Oxysterols have a short half-life, this can be less than an hour depending on the position of oxidation ^(114, 115). They have a role in the regulation of cholesterol homeostasis through SREBP and LXR ⁽¹¹⁶⁾. Excess cholesterol induces a negative feedback loop in which 25-HC and 27-HC activate LXR and inhibit SREBP suppressing cholesterol synthesis. Nuclear receptor transcription factors LXR α and LXR β regulate cholesterol homeostasis through gene expression of lipid transport proteins *ABCA1*, *ABCG1* and *APOE* in a ligand dependent manner. While LXR α expression is limited to the liver, intestines and adipose tissues, LXR β is ubiquitously expressed.

1.4.4 Oxysterol ligands of nuclear receptor (NR) transcription factor and G-protein coupled receptors (GPCR)

In addition to their roles as intermediates in the bile acid synthesis pathway and regulators of cholesterol homeostasis, oxysterols also have a role in the immune response through ligand-activated receptors. Oxysterols have been identified as endogenous ligands for ligand-dependent nuclear receptor transcription factors which bind to specific DNA response elements of target genes to mediate transcription. 20(*S*)-hydroxycholesterol (20(*S*)-HC), 22(*R*)-HC, 24(*S*)-HC, 25-HC, 27-HC and 24(*S*),25-epoxycholesterol (24(*S*),25-EC) are oxysterols which activate nuclear receptor transcription factor LXR ⁽¹¹⁷⁻¹¹⁹⁾. Binding of these oxysterols to the ligand binding domain (LBD) of LXR-RXR heterodimers causes a conformational change enabling the heterodimer to bind to the DNA response element of target genes including *SREBP-1c* releasing corepressor and recruiting coactivators ⁽¹²⁰⁾. Oxysterols activation of LXR helps maintain cholesterol homeostasis by reducing the cellular cholesterol content by upregulating the expression of genes involved in

cholesterol efflux including *ABCA1*, *ABCG1* and *APOE* ^(117-119, 121-123). LXR activation has also been shown to negatively regulate the inflammatory response in the innate immune system and lymphocyte proliferation in the adaptive immune system ⁽¹²⁴⁾.

Oxysterols are also ligands of the ROR family of nuclear receptor transcription factors comprised of ROR α , ROR β and ROR γ ^(125, 21). RORs have been shown to play a role in circadian rhythm regulating cyclic expression of aryl hydrocarbon receptor nuclear translocator-like 1 (*ARNTL*) also referred to as *BMAL1*. *ARNTL* is a core clock gene with an important role in the transcription-translation feedback loop (TTFL) ⁽¹²⁶⁾. ROR α is expressed in the brain and is important for the development of cerebellum and differentiation of Purkinje cells ⁽¹²⁷⁾.

ROR β expression is restricted with the highest expression in the neurophotoendocrine system, the pineal gland, retina and brain. Expression of ROR γ is highest in the thymus with a development role in lymphoid tissues through lymphoid tissue inducer cells. Oxysterols which are oxygenated at the C7 position including 7 α -HC and 7-KC bind to the LBD of ROR α and ROR γ while 24(*S*)-HC has been reported to bind to ROR α and ROR γ and acts as an inverse agonist suppressing the activity of target genes ⁽¹²⁸⁻¹²⁹⁾. 24(*S*)-HC binds to ROR α and suppresses BMAL1 transcription inhibiting recruitment of coactivator SRC-2. Potent LXR agonist 24(*S*),25-EC has also been reported to have selective inverse agonist activity towards ROR γ t, an isoform of ROR γ essential for Th17 cell differentiation, while 25-HC is proposed to have agonist activity towards ROR γ t ⁽¹³⁰⁾.

Oxysterols have also been reported to bind to the oestrogen receptor (ER) family of nuclear receptors comprised of ER α (NR3A1) and ER β (NR3A2) that form a multiprotein complex with heat shock proteins (HSPs) ⁽¹³¹⁻¹³²⁾. ER β is expressed in the ovaries, cardiovascular system, prostate and serotonergic neurons of the dorsal raphe (DR) in the central nervous system (CNS) while ER α is predominantly expressed in the uterus, ovaries and breasts but it is also expressed in the heart, liver and spinal cord motor neurons ⁽¹³³⁾. Oxysterols including 20(*S*)-HC, 22(*R*)-HC, and 24(*S*)-HC bind to ERs initiating a conformational change which causes HSPs to subsequently dissociate from the receptor. Ligand bound ER monomers combine to

form homodimers or heterodimers which bind to the oestrogen response elements of target genes enabling transcription. Oxysterols 27-HC and 25-HC have been identified as selective oestrogen receptor modulators (SERMs), the activity of which may be agonistic or antagonistic depending on the cell type and ability to recruit coactivators or corepressors ⁽¹³⁴⁻¹³⁶⁾.

The oxysterol 6-oxo-cholesten-3 β ,5 α -diol (OCDO) derived from 5,6-epoxycholesterol (5,6-EC) binds to the glucocorticoid receptor (GR) nuclear receptor (NR3C1) which is ubiquitously expressed and has a regulatory role of genes involved in development, metabolism and the immune response ⁽¹³⁷⁾. OCDO bind with GRs to form dimers that translocate to the nucleus and promote transcription of selective target genes including MMP1.

G-protein coupled receptors (GPCRs) are cell membrane receptors that upon ligand binding activate signal transduction pathways within cells. Epstein-Barr virus-induced G-protein coupled receptor 2 (EBI2) also known as GP183 is a chemoattractant receptor expressed on the surface of immune cells including monocytes, B lymphocytes and T lymphocytes. Oxysterol 7 α ,25-dihydroxycholesterol (7 α ,25-diHC) synthesised from cholesterol by enzymes CH25H and CYP7B1 has been identified as an endogenous ligand of EBI2 ⁽¹³⁸⁾. Expression of 7 α ,25-diHC synthesising enzymes CH25H, CYP7B1 and metabolising enzyme HSD3B7 is important for the regulation of oxysterol production in lymphoid tissues. The differential expression of these enzymes in stromal cells is suggested to create a 7 α ,25-diHC gradient required for B cell responses ⁽¹³⁸⁻¹⁴¹⁾. EBI2 is also expressed in Th17 cells during inflammation and infiltrating cells of multiple sclerosis lesions ⁽¹⁴²⁾. Furthermore, expression of CH25H is upregulated in the spinal cord, while CYP7B1 expression is upregulated in monocytes and lymphocytes which has led to the proposed role for EBI2 and 7 α ,25-diHC in the migration of inflammatory CD4⁺ T cells to the CNS ⁽¹⁴²⁾.

It has also been proposed that oxysterols can activate the hedgehog pathway involved in normal embryonic development and tissue redevelopment ⁽¹⁴³⁾. Oxysterols bind to the cysteine rich domain of the class F GPCR smoothened (SMO) which transmits hedgehog signal ⁽¹⁴⁴⁾. In the absence of a ligand patched-1 (PTCH1) is bound to

SMO and inhibits hedgehog signalling, when hedgehog ligands such as sonic hedgehog (SHH) bind to PTCH1 the inhibition of SMO is released and the hedgehog signal is transmitted across the plasma membrane. Inactivation of PTCH1 with hedgehog ligands can lead to accumulation of sterols and oxysterols which activate SMO ⁽¹⁴⁵⁻¹⁴⁶⁾.

1.4.5 Oxysterols and the immune system

In addition to their role in the immune system through ligand-activated receptors, oxysterols are also produced during immune responses. Activation of the innate immune system through Toll-like receptors (TLR) of macrophages induces expression of *CH25H* and synthesis of 25-HC which has been reported to modulate Ig isotype expression in B cells ⁽¹⁴⁷⁻¹⁴⁸⁾. Macrophage derived 25-HC regulates immune response through inhibition of B cell proliferation which results in reduced immunoglobulin A (IgA) ⁽¹⁴⁷⁾. *CH25H* is also a member of the family of IFN-stimulated genes (ISGs) which have a role in inflammation, innate and adaptive immunity through interferon (IFN) signalling ⁽¹⁴⁹⁾. A role in viral resistance has been shown for 25-HC, upon viral infections *CH25H* is upregulated and 25-HC synthesis induced ⁽¹⁵⁰⁾. Modification of cell membranes through 25-HC including reducing cellular cholesterol altering the lipid composition of cell membranes prevents viral entry ⁽¹⁵¹⁾. A further function of 25-HC may also be inhibiting viral replication through integrated stress response and suppression of protein synthesis ^(110,152-153).

A dual role in the inflammatory response has been identified for 25-HC with pro-inflammatory and anti-inflammatory activity. Downstream of type-1 IFN, 25-HC has an anti-inflammatory role through suppression of SREBP and preventing activation of the Akt and NF κ B signalling pathway ⁽¹⁵⁴⁾. Conversely, 25-HC may also amplify an inflammatory response by promoting the production of pro-inflammatory cytokines through the NF κ B and ERK pathways and recruitment of transcription factor activator protein-1 (AP-1) ⁽¹⁵⁵⁻¹⁵⁷⁾.

Oxysterols have also been implicated in the pathology of tumour development by suppressing the immune response and promoting tumour growth ⁽¹⁵⁸⁾. 22(*R*)-HC recruits immunosuppressive neutrophils to the tumour microenvironment (TME) promoting angiogenesis through CXC chemokine receptor 2 (CXCR2) ⁽¹⁵⁹⁾. The

predominant oxysterol found in circulation, 27-HC, has also been linked to the recruitment of tumour promoting immune cells to the TME by attracting neutrophils and $\gamma\delta$ T cells promoting metastasis ⁽¹⁶⁰⁾.

1.5 Mass spectrometry

Mass spectrometry (MS) is an analytical technique used to accurately determine the chemical compositions of a sample based on the mass to charge ratio (m/z) of ions. There are four main stages in the mass spectrometry process; sample introduction, ionisation, mass analysis and detection represented in Figure 1.12. Samples are ionised and accelerated towards a mass analyser which sorts ions by their mass and charge which is measured by a detector and single ion currents are converted into amplified electrical signals and processed creating a mass spectrum.

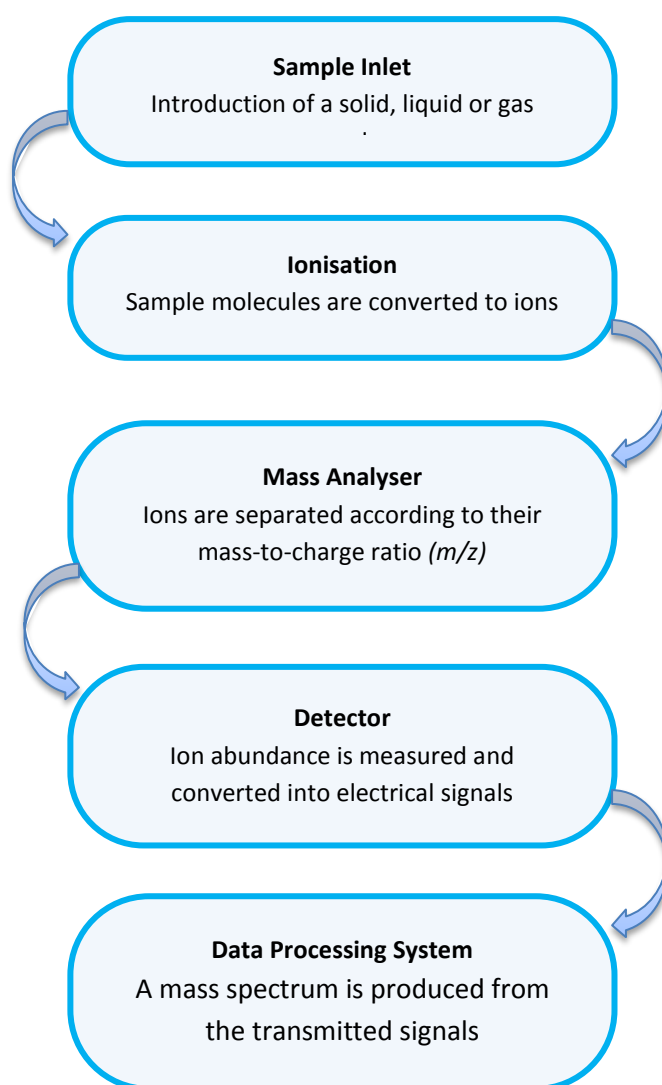


Figure 1.12 The components of mass spectrometry analysis.

1.5.1 Ionisation sources

A variety of ionisation sources are utilised in mass spectrometry analysis. Earlier methods include hard ionisation techniques such as electron ionisation (EI) in which volatile analytes presented as gas phase molecules are bombarded by a beam of

electrons leading to high fragmentation of ions ⁽¹⁶¹⁻¹⁶⁴⁾. Complementary to EI, chemical ionisation (CI) is a soft ionisation technique which produces ions with less fragmentation through collision of analyte molecules with reagent gases pre-ionised by EI present in the source. A significant ionisation technique developed for non-volatile compounds was fast atom bombardment (FAB) in which samples in a matrix are bombarded with a beam of atoms in a vacuum causing low fragmentation. More recently, ionisation sources such as matrix-assisted laser desorption ionisation (MALDI), atmospheric pressure chemical ionisation (APCI) and electrospray ionisation (ESI) have been established. The optimum ionisation source for mass spectrometry analysis is dependent on the chemical nature of the analyte of interest. MALDI is a solid-phase ionisation source often used in imaging mass spectrometry, in which analytes, introduced as involatile deposits prepared with a matrix, are bombarded by laser pulses under vacuum conditions. APCI is a gas-phase ionisation source similar to CI suitable for thermally stable, neutral compounds, in which samples are introduced through a heated nebuliser needle to form an aerosol of sample and solvent molecules. Molecules pass by a charged corona discharge electrode needle becoming ionised and proton transfer between reactant ions and sample molecules leads to ionisation of sample molecules.

ESI is a liquid-phase soft ionisation source which provides high sensitivity, a strong electric field is applied to analytes presented in a solvent and streamed through a charged heated capillary at atmospheric pressure with a high potential difference as illustrated in Figure 1.13 ⁽¹⁶³⁾. This induces charge accumulation at the end of the capillary which leads to a spray of charged droplets, the solvent is lost from the droplets through desolvation and as the solvent evaporates the droplet size is reduced. The charged droplets dissociate through coulombic fission into gas phase ions accelerating to the negatively charged electrode and continue to the mass analyser.

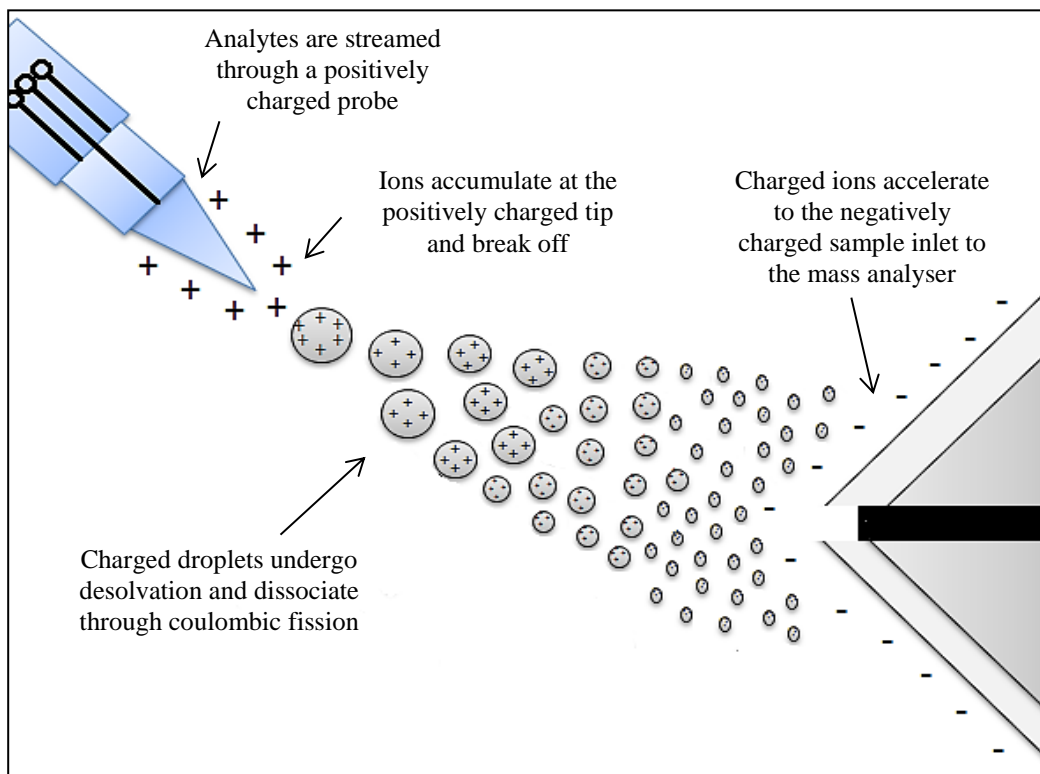


Figure 1.13 Electrospray Ionisation (ESI) source. Analytes are heated and nebulised to form a fine spray of charged droplets. Solvent evaporates from the droplets which divide by coulombic fission forming gas-phase ions. Ions accelerate towards the mass spectrometer sample inlet. Adapted and modified from Thermo Scientific API source manual ⁽¹⁶⁵⁾.

1.5.2 Mass Analysers

Many mass analysers exist which differ in mechanisms by which ions are sorted prior to detection but all mass analysers use static or dynamic electric and magnetic fields to sort ions based on their mass-to-charge ratio. Mass analysers used in this study are described below.

1.5.2.1 Linear Quadrupole Ion Trap (LIT)

The quadrupole ion trap was designed to enable ion storage and selective ejection of ions depending on their m/z using electric fields to trap and sort charged ions ^(166, 167). Four cylindrical segmented electrodes are symmetrically arranged in pairs as depicted in Figure 1.14. Radio frequency (RF) and direct current (DC) voltages applied to opposing electrodes in the z plane under vacuum induce oscillation of ions in the x, y -plane. Ions are trapped radially between the four electrodes by the RF and axially by three DC voltages applied to each section of the electrodes. Stable oscillation of ions allows ions to continue their trajectory through the analyser.

towards the detector. Ions trapped within the LIT can undergo activation, isolation and mass-selective ejection through slots in two opposing rods with an appropriate alternating current (AC) voltage applied.

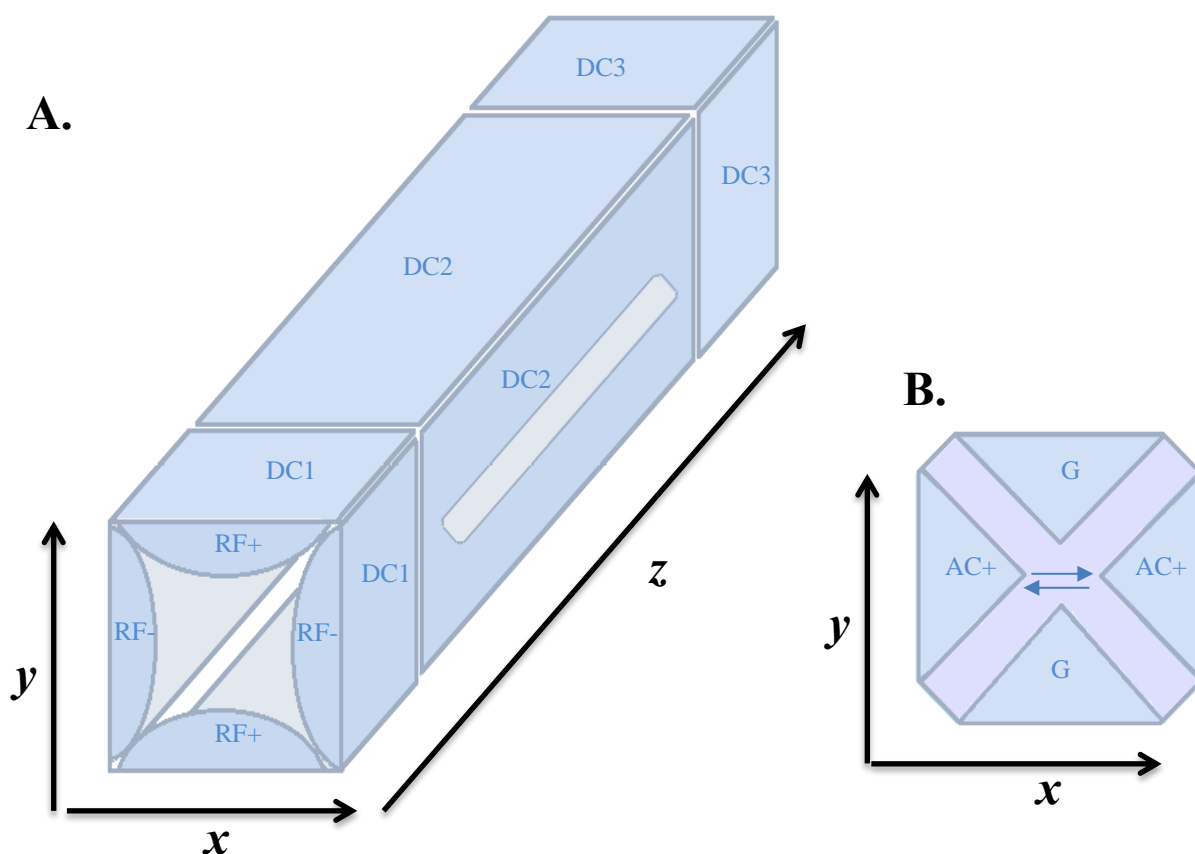


Figure 1.14 Schematic of a 2D linear ion trap (LIT). Four hyperbolic rods are symmetrically arranged in pairs with opposing RF voltages applied to each pair. Axial and radial trapping contain ion clusters in the quadrupole LIT. A) Ions are contained axially using three DC voltages applied to each segment of the quadrupoles. B) An AC voltage can activate or excite trapped ions acting as a mass filter to selectively eject ions radially through slots in opposing rods or eject ions to the detector.

1.5.2.2 Orbitrap

The Orbitrap is an electrostatic ion trap comprised of an external barrel-like electrode divided into two equal parts at ground potential and a central spindle-like electrode with an electrostatic voltage applied illustrated in Figure 1.15⁽¹⁶⁸⁻¹⁶⁹⁾. Prior to injection into the Orbitrap ions first undergo pulsation through a dual-pressure LIT into a curved linear trap (C-Trap) filled with nitrogen gas. The C-Trap stores and cools ions prior to injection into the Orbitrap through collision of ions with the nitrogen gas causing a loss of kinetic energy and concentration of ions. A RF

voltage is applied to the ions which pushes ions out of the C-Trap in short packets and into the Orbitrap. Ions are injected tangentially through the space between the outer electrode segments. Ions oscillate harmonically in the trap in intricate spirals around the central electrode along the z axis under an electrostatic field obtained by a DC voltage. The outer electrode acts as a receiver for image current detection of axial oscillations and a mass spectrum is produced through fast fourier-transformation (FFT).

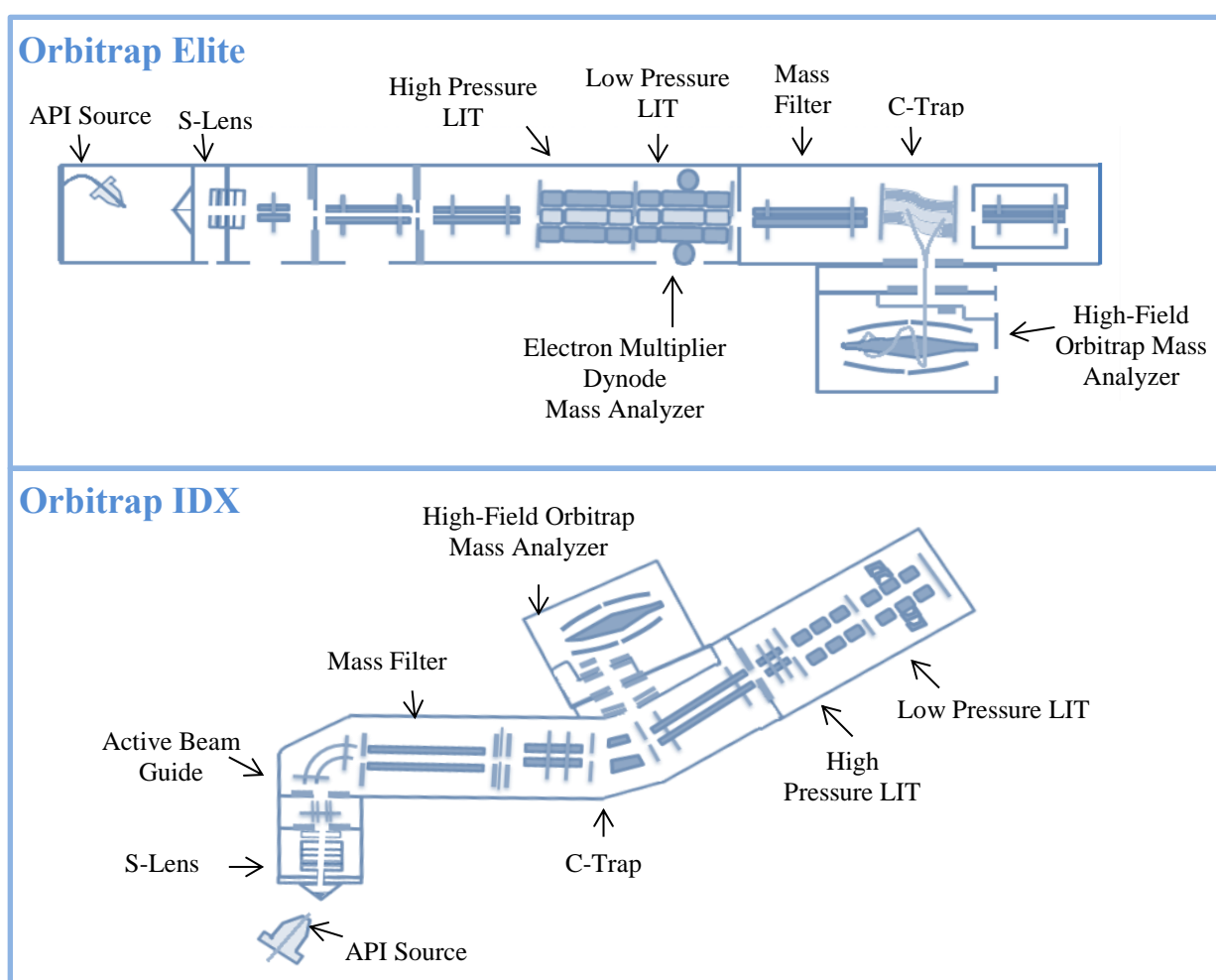


Figure 1.15 Orbitrap Elite and ID-X mass spectrometer schematics. Analytes introduced in a liquid-phase are converted to gas-phase ions in the atmospheric pressure ionisation (API) source. Ions are accelerated and focussed towards a dual-pressure linear ion trap (LIT). Ions can be stored and concentrated in the C-Trap before ejection into the Orbitrap. Adapted from Michalski et al. (2012) ⁽¹⁶⁹⁾ and <https://planetorbitrap.com/orbitrap-id-x>

1.5.3 Tandem Mass Spectrometry (MSⁿ)

Tandem mass spectrometry (MSⁿ) is the technique in which coupled mass analysis is used to fragment ions of a particular m/z ratio ⁽¹⁶¹⁾. The simplest form of tandem mass spectrometry separates and fragments ions in space using two physically coupled mass spectrometers connected by a collision cell. Alternatively, tandem mass spectrometry in time use ion traps to store precursor ions which are then fragmented through collision-induced dissociation (CID) and daughter ions are analysed.

This study uses targeted tandem mass spectrometry with Orbitrap dual-pressure LIT in three stages (MS³). An initial scan event performed filters and isolates precursor ions of specific m/z ratio and CID fragmentation produces daughter ions. A subsequent scan event selects a particular daughter ion which is fragmented to produce granddaughter ions which are then detected. In this study a combination of LIT MS³ analysis and Orbitrap MS¹ high mass accuracy detection was used to identify and quantify oxysterols.

1.5.4 Analysis of Sterols through Chromatography MS coupling

Chromatography coupling with MS is used to separate analytes prior to presentation to the mass spectrometer. Samples are introduced in a gaseous state for gas chromatography mass spectrometry (GC-MS) or in solution for liquid-chromatography mass spectrometry (LC-MS).

1.5.4.1 Gas Chromatography-Mass Spectrometry (GC-MS)

The traditional method of oxysterol analysis is through GC-MS ^(170, 171, 43). GC-MS is an analytical technique used with liquid, gaseous or solid samples. Samples are vaporised in gas chromatography and a capillary column with a stationary phase is used to separate molecules in the sample. The molecules are propelled in an inert carrier gas such as helium, hydrogen or nitrogen and molecular separation is determined by the dimensions of the column and the phase properties. The boiling point of molecules and their relative affinity for the stationary phase of the column promote separation of the molecules in the sample as they travel along the column. Molecules are retained by the column and elute at different times before entering the ionisation stage in the mass spectrometer.

Several methods for oxysterol analysis have been established which have been expanded to further metabolites including cholestenoic acids and vitamin D derivatives ⁽¹⁷²⁻¹⁷⁵⁾. Due to the low abundance and the chemical nature of oxysterols, prior to GC-MS analysis sample preparation including conjugate cleavage, solid phase extraction (SPE) and derivatisation is performed to increase sensitivity, ionisation and stability of analytes. Oxysterols can exist as free sterol or as ester conjugates in samples such as plasma and cell culture supernatants. In order to analyse the total oxysterols present including these esters, hydrolysis by saponification with ethanoic potassium hydroxide (KOH) is performed and samples are subsequently neutralised by the addition of phosphoric acid before extraction. As the abundance of cholesterol is much greater than oxysterols SPE is performed to separate the more polar oxysterols from cholesterol with a silica-based cartridge (Figure 1.16). This also avoids any contamination from cholesterol autoxidation in subsequent sample processing steps. SPE is used to concentrate and purify analytes of interest in an aqueous solution through absorption of a cartridge in solid phase ⁽¹⁷⁶⁾. Following SPE the collected oxysterol fraction can be derivatised to increase volatility, thermal stability and MS sensitivity ⁽¹⁷⁷⁾. Derivatisation through silylation of hydroxyl groups (OH) is typically applied with trimethylsilylating reagents such as trimethylsilyl (TMS) and t-butyldimethylsilyl (TBDMS). In order to quantify oxysterols present in a sample stable isotope labelled standards can also be added to samples during sample preparation. Quantification is achieved by monitoring the retention times and the electron impact (EI) fragmentation patterns relative to a library of authentic standards. Although GC-MS analysis involves long sample preparation steps, this method is frequently used today as it provides high chromatography resolution and low running cost and the use of isotope labelled standards at the start of sample processing compensates for any loss of sample during the preparation steps.

1.5.4.2 Liquid Chromatography-Mass Spectrometry (LC-MS)

High performance liquid chromatography (HPLC) coupled mass spectrometry is used for analysis of a wide range of compounds including compounds with high polarity and molecular mass and removes the requirement for volatile and thermally stable samples ⁽¹⁷⁸⁻¹⁷⁹⁾. Compounds are separated based on functional groups and their relative interaction with the stationary phase column. The LC-MS analytical

column is packed with a solid or liquid stationary phase and liquid mobile phase. Analysis of oxysterols is commonly performed with reverse phase (RP) LC involving a non-polar hydrophobic stationary phase and polar mobile phase with an organic solvent and water composition. Samples are dissolved in a similar composition to the mobile phase and injected into the analytical column through isocratic or gradient elution. Analytes are separated in solution through retention interactions of analytes to the stationary phase such as Van der Waals forces and the eluting strength of the liquid mobile phase. In RP sterol analysis the more polar hydroxycholesterols elute early as they are weakly retained in the non-polar stationary phase. Less polar hydroxycholesterols and cholesterol have stronger interactions with the column and elute later. The elution of hydroxycholesterols is reversed with normal phase chromatography.

As with GC-MS, sample preparation is required for HPLC-MS analysis of oxysterols, this is summarised in Figure 1.17 ⁽¹⁸⁰⁾. The first step of sample preparation is the separation of sterols from oxysterols to minimise cholesterol autoxidation artefacts, drying steps may be performed under vacuum. SPE involves the separation of sample components through interactions of components with the silica based, non-polar, C18 column stationary phase shown in Figure 1.16. Columns are conditioned with a low polarity solvent prior to sample loading in order to organise C18 chains in the column to increase the surface area and improve binding and recovery of compounds. Compounds with no affinity pass through and impurities are removed through subsequent washing steps. Retained components are subsequently eluted with solvents typically ethanol or methanol.

As oxysterols are neutral lipids they are not readily ionised and without chemical modification a low ionisation signal is attained, derivatisation is used to improve sensitivity of MS analysis through the addition of a more polar group or charged moiety which may also be used to provide structural information. Various derivatisation methods have been utilised for the analysis of oxysterols with ESI or APCI targeting the 3 β hydroxyl group of sterols including derivatisation to trimethylsilyl esters, phenyl-isothiocyanates, picolinyl/ nicotinyl esters, N,N-dimethylglycine (DMG) esters and Girard hydrazones ⁽¹⁸¹⁻¹⁸⁶⁾. Two Girard reagents routinely used for oxysterol derivatisation are Girard T and Girard P hydrazines ⁽¹⁸⁷⁻¹⁸⁸⁾. High throughput LC-MS methods have previously been developed with no

derivatisation step which relies on chromatographic separation of isomeric oxysterols and authentic standards ⁽¹⁸⁹⁻¹⁹³⁾.

Derivatisation of oxysterols with Girard P hydrazine through the enzyme-assisted derivatisation for sterol analysis (EADSA) charge tagging technique has been used in the studies for this thesis ⁽¹⁹⁴⁻¹⁹⁶⁾. Girard hydrazones have a positively charged quaternary amine group which tag sterol molecules containing oxo groups to form hydrazones. For oxysterols in which there is no oxo group present an oxo group is introduced with cholesterol oxidase enzyme converting 3 β -hydroxy-5-ene sterols to the 3-oxo-4-ene equivalents. Derivatisation of sterols with naturally occurring oxo groups is performed separately excluding the cholesterol oxidase step. Oxysterols are separated from excess reagent by a subsequent SPE step with an Oasis hydrophilic-lipophilic balance (HLB) column. EADSA enhances solubility of solvents for RP chromatography and introduces specificity for 3-oxo oxysterols. GP-derived sterols in solution are separated by an LC analytical column and directed to the ion source. HPLC-ESI-MS/MS with Orbitrap Elite/IDX was used for oxysterol analysis in this thesis. Following LC separation the column effluent enters the ESI source passing through the heated electrospray ionisation (HESI-II) probe maintained at approximately 5kV undergoing desolvation. Samples are nebulised at the tip of the capillary forming a spray of electrically charged droplets that dissociate into charged gas-phase ions through coulombic fission and accelerate towards the sample inlet of the mass spectrometer. The GP hydrazone charge tag increases sensitivity of ESI through improved gas ion formation.

Tandem LIT MS³ and high mass accuracy Orbitrap analysis enables precise and efficient identification and quantification of sterol species. In the mass spectrometer ions are focussed to the LIT and undergo fragmentation and mass scanning for sterol identification. Derivatised endogenous oxysterols and internal standards are observed as [M]⁺ ions and stored in the LIT. [M]⁺ ions are selected for MS² CID in the LIT producing a neutral loss of the 79Da pyridine ring. [M-79]⁺ daughter ions undergo further MS³ CID fragmentation producing distinct fragmentation patterns providing structural information for sterol fingerprinting. For a high mass accuracy scan, ion clusters passing through the LIT are slowed and stored in C-trap where [M]⁺ ions are ejected from the C-trap and focussed into the high field Orbitrap for high mass accuracy scanning events. Ions are subjected to an electrostatic potential inducing

axial, radical and rotational oscillations. Axial oscillations relative to ion m/z are detected as an image current frequency and processed via fourier transformation through the Orbitrap electrodes.

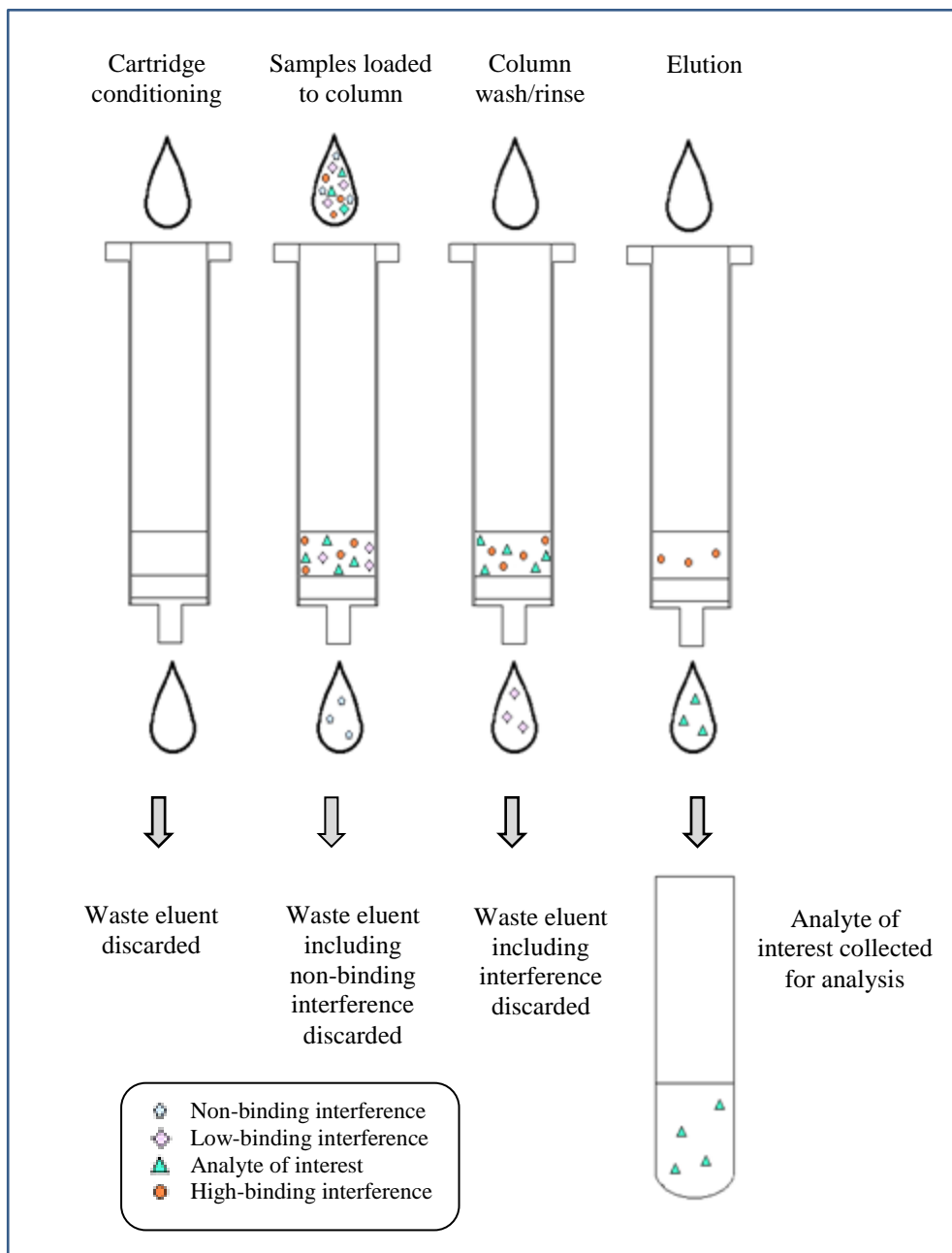


Figure 1.16 Solid Phase Extraction (SPE) technique. C18 silica cartridges are conditioned and samples are loaded onto the column and eluent containing interference is discarded. Following the column wash the analyte of interest is eluted and collected in an appropriate eluent.

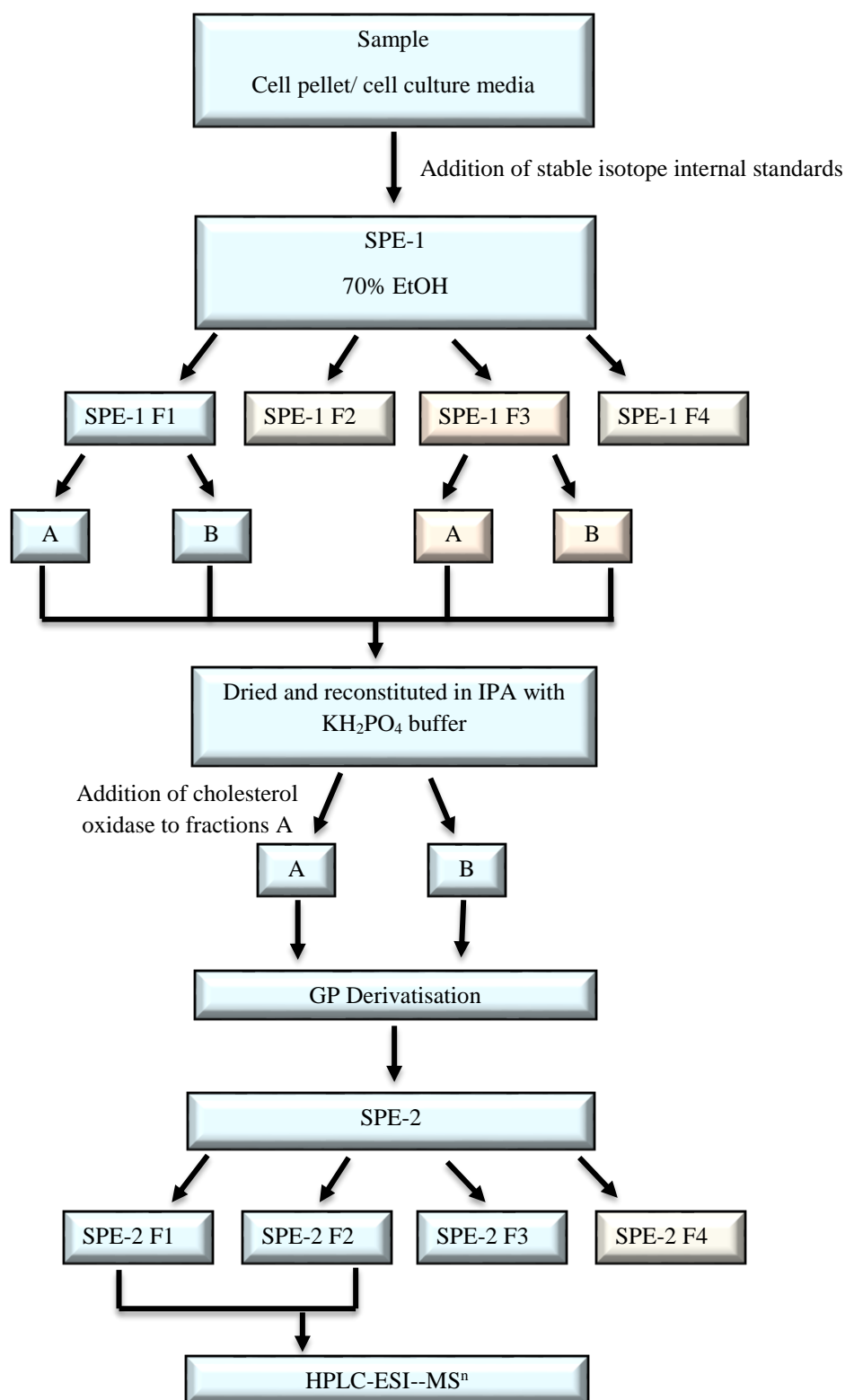


Figure 1.17 Schematic of sample preparation process for sterol analysis by LC-MS. Sterols are extracted from samples in an ultrasonic bath with EtOH containing stable isotope internal standards and diluted to 70% EtOH. Cholesterol and oxysterols within samples are separated by solid phase extraction (SPE-1) as Fractions 1 and 3 respectively and divided equally into A and B fractions. Fractions are dried and reconstituted in IPA and KH₂PO₄ buffer. Cholesterol oxidase is added to Fractions A and samples are incubated at 37°C for 1 hour. Oxidation reactions are terminated with the addition of MeOH and samples are derivatised with Girard Reagent P with 5% acetic acid overnight at room temperature. Excess derivatisation reagent is removed by a second solid phase extraction (SPE-2) and sterols are eluted in four fractions. Fractions 1 to 3 are then analysed by HPLC-ESI-MSⁿ.

1.6 General Thesis Aim

The overall aim of this study was to investigate the role of oxysterols upstream and downstream of CYP7B1 in Th17 cell differentiation and function specifically focussing on 24(S),25-EC and downstream metabolites (Figure 1.18). The objective for Chapter 3 is the development of a method for total sterol analysis by LC-MS which can be applied to cell culture supernatants and cell pellets. Chapter 4 aims to investigate the effect of CYP7B1 inhibition by azole compounds in differentiated Th17 cells. The objectives for Chapter 5 was to determine whether the EL4 cell line is a suitable cell line for the study of Th17 differentiated CD4⁺ T cells and CYP7B1 inhibition is investigated in *Cyp7b1*^{-/-} murine Th17 polarised CD4⁺ T cells. Chapter 6 investigates the effect of oxysterols upstream and downstream of CYP7B1 on CD4⁺ T cell cytokine expression and LXR activity. Lastly, Chapter 7 uses *in silico* modelling and protein-docking simulation to investigate the mechanism by which oxysterols upstream and downstream of CYP7B1 interact with Th17 master transcription factor ROR γ t.

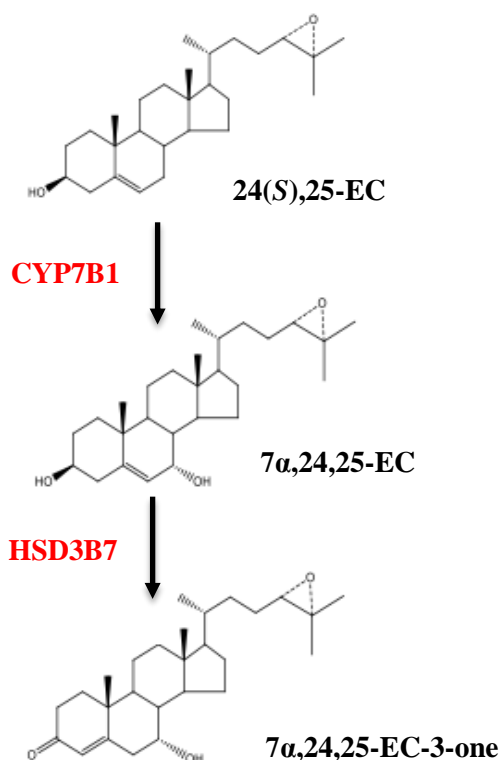


Figure 1.18 Schematic of 24(S),25-EC metabolism through CYP7B1 and HSD3B7 activity in the Kandutsch-Russell pathway.

1.7 References

1. Tock, M. R., & Dryden, D. T. F. (2005). The biology of restriction and anti-restriction. *Current Opinion in Microbiology*, 8, 466–472.
<https://doi.org/10.1016/j.mib.2005.06.003>
2. Pingoud, A., & Jeltsch, A. (2001). Structure and function of type II restriction endonucleases. *Nucleic Acids Research*, 29(18), 3705–3727.
3. Boller, T., & Felix, G. (2009). A Renaissance of Elicitors : Perception of Microbe-Associated Molecular Patterns and Danger Signals by Pattern-Recognition Receptors. *Annual Review of Plant Biology*, 60, 379–406.
<https://doi.org/10.1146/annurev.arplant.57.032905.105346>
4. Upson, J. L., Zess, E. K., Bialas, A., Wu, C., & Kamoun, S. (2018). The coming of age of EvoMPMI : evolutionary molecular plant – microbe interactions across multiple timescales. *Current Opinion in Plant Biology*, 44, 108–116. <https://doi.org/10.1016/j.pbi.2018.03.003>
5. Mogensen, T. H. (2009). Pathogen Recognition and Inflammatory Signaling in Innate Immune Defenses. *Clinical Microbiology Reviews*, 22(2), 240–273.
<https://doi.org/10.1128/CMR.00046-08>
6. Roh, J. S., & Sohn, D. H. (2018). Damage-Associated Molecular Patterns in Inflammatory Diseases. *Immune Network*, 18(4), 1–14.
doi.org/10.4110/in.2018.18.e27
7. Nicholson, L. B. (2016). The immune system. *Essays in Biochemistry*, 60, 275–301. <https://doi.org/10.1042/EBC20160017>
8. Hazlett, L., & Wu, M. (2011). Defensins in innate immunity. *Cell Tissue Res*, 343, 175–188. <https://doi.org/10.1007/s00441-010-1022-4>
9. Takeda, K., & Akira, S. (2005). Toll-like receptors in innate immunity. *International Immunology*, 17(1), 1–14.
<https://doi.org/10.1093/intimm/dxh186>
10. Hazlett, L., & Wu, M. (2011). Defensins in innate immunity. *Cell Tissue Res*, 343, 175–188. <https://doi.org/10.1007/s00441-010-1022-4>
11. Chirumbolo, S. (2018). The role of basophils as innate immune regulatory cells in allergy and immunotherapy. *Human Vaccines & Immunotherapeutics*, 14(4), 815–831. <https://doi.org/10.1080/21645515.2017.1417711>

12. Iwasaki, A., & Medzhitov, R. (2015). Control of adaptive immunity by the innate immune system. *Nature Immunology*, 16(4), 343–353.
<https://doi.org/10.1038/ni.3123>
13. Rajewsky, K., & Von Boehmer, H. (2008). Lymphocyte development. Overview. *Curr Opin Immunol*, 20(2), 127–130.
14. Market, E., & Papavasiliou, F. N. (2003). V(D)J Recombination and the Immune System. *PLOS Biology*, 1(1), 24–27.
<https://doi.org/10.1371/journal.pbio.0000016>
15. Rosenblum, M. D., Remedios, K. A., Abbas, A. K., Rosenblum, M. D., Remedios, K. A., & Abbas, A. K. (2015). Mechanisms of human autoimmunity. *Journal of Clinical Investigation*, 125(6), 2228–2233.
<https://doi.org/10.1172/JCI78088.disease>.
16. Kumar, B. V, Connors, T., & Farber, D. L. (201AD). Human T cell development, localization, and function throughout life. *Immunity*, 48(2), 202–213. <https://doi.org/10.1016/j.immuni.2018.01.007.Human>
17. Shah, D. K., & Zúñiga-Pflücker, J. C. (2014). An Overview of the Intrathymic Intricacies of T Cell Development. *The Journal of Immunology*, 192(9), 4017–4023. <https://doi.org/10.4049/jimmunol.1302259>
18. Deftos, M. L., & Bevan, M. J. (2000). Notch signaling in T cell development. *Current Opinion in Immunology*, 12, 166–172.
19. Yannoutsos, N., Wilson, P., Yu, W., Chen, H. T., Nussenzweig, A., Petrie, H., & Nussenzweig, M. C. (2001). The Role of Recombination Activating Gene (RAG) Reinduction in Thymocyte Development In Vivo. *J. Exp. Med*, 194(4), 471–480.
20. Werner, J. M., & Freund, C. (2017). Major Histocompatibility Complex (MHC) Class I and MHC Class II Proteins : Conformational Plasticity in Antigen Presentation. *Frontiers in Immunology*, 8(March), 1–16.
<https://doi.org/10.3389/fimmu.2017.00292>
21. Smith-Garvin, J. E., Koretzky, G. A., & Jordan, M. S. (2009). T cell activation. In *Annual Review of Immunology* (Vol. 27, pp. 591–619).
<https://doi.org/10.1146/annurev.immunol.021908.132706>
22. Rudd, C. E., Taylor, A., & Schneider, H. (2009). CD28 and CTLA-4 coreceptor expression and signal transduction. In *Immunological Reviews*

- (Vol. 229, Issue 1, pp. 12–26). <https://doi.org/10.1111/j.1600-065X.2009.00770.x>
23. Letourneur, F., & Klausner, R. D. (1992). *Activation of T Cells by a Tyrosine Kinase Activation Domain in the Cytoplasmic Tail of CD3 epsilon*. <https://www.science.or>
 24. McNeill, L., Salmond, R. J., Cooper, J. C., Carret, C. K., Cassady-Cain, R. L., Roche-Molina, M., Tandon, P., Holmes, N., & Alexander, D. R. (2007). The Differential Regulation of Lck Kinase Phosphorylation Sites by CD45 Is Critical for T Cell Receptor Signaling Responses. *Immunity*, 27(3), 425–437. <https://doi.org/10.1016/j.immuni.2007.07.015>
 25. Zhang, W., Sloan-Lancaster, J., Kitchen, J., Tribble, R. P. & Samelson, L. E. LAT: the ZAP-70 tyrosine kinase substrate that links T cell receptor to cellular activation. *Cell* **92**, 83–92 (1998).
 26. Bubeck Wardenburg J, Fu C, Jackman JK, Flotow H, Wilkinson SE, Williams DH, Johnson R, Kong G, Chan AC, Findell PR. Phosphorylation of SLP-76 by the ZAP-70 protein-tyrosine kinase is required for T-cell receptor function. *J Biol Chem*. 1996;271:19641–4.
 27. Oh-hora, M. & Rao, A. The calcium/NFAT pathway: role in development and function of regulatory T cells. *Microbes Infect.* **11**, 612–619 (2009)
 28. Schulze-Luehrmann, J., & Ghosh, S. (2006). Antigen-Receptor Signaling to Nuclear Factor κ B. In *Immunity* (Vol. 25, Issue 5, pp. 701–715). <https://doi.org/10.1016/j.immuni.2006.10.010>
 29. Yukawa, M., Jagannathan, S., Vallabh, S., Kartashov, A. v., Chen, X., Weirauch, M. T., & Barski, A. (2020). AP-1 activity induced by co-stimulation is required for chromatin opening during T cell activation. *Journal of Experimental Medicine*, 217(1). <https://doi.org/10.1084/jem.20182009>
 30. Burkhardt JK, Carrizosa E, Shaffer MH. The actin cytoskeleton in T cell activation. *Annu Rev Immunol*. 2008;26:233–59.

31. Spann, N. J., & Glass, C. K. (2013). Sterols and oxysterols in immune cell function. *Nature Immunology*, 14(9), 893–900.
<https://doi.org/10.1038/ni.2681>
32. Harrington L. E., Hatton R. D., Mangan P. R., et al. (2005) Interleukin 17-producing CD4⁺ effector T cells develop via a lineage distinct from the T helper type 1 and 2 lineages. *Nature Immunology*. 6(11):1123–1132
33. Park H., Li Z., Yang X. O., et al. (2005) A distinct lineage of CD4 T cells regulates tissue inflammation by producing interleukin 17. *Nature Immunology*. 6(11):1133–1141
34. Bettelli E, Korn T, Oukka M, Kuchroo VK. (2008) Induction and effector functions of T(H)17 cells. *Nature*. 453(7198):1051–7. pmid:18563156.
35. Sakaguchi, S. (2004) Naturally arising CD4⁺ regulatory T cells for immunologic self-tolerance and negative control of immune responses, *Annu. Rev. Immunol* , 22 pg.531
36. Ouyang, W., Kolls, J. K., Zheng, Y. (2008). The biological functions of T helper 17 cell effector cytokines in inflammation. *Immunity*, 28(4), 454-467
37. Ye, P., F. H. Rodriguez, S. Kanaly, K. L. Stocking, J. Schurr, P. Schwarzenberger, P. Oliver, W. Huang, P. Zhang, J. Zhang, et al. (2001) Requirement of interleukin 17 receptor signaling for lung CXC chemokine and granulocyte colony-stimulating factor expression, neutrophil recruitment, and host defense. *J. Exp. Med.*194: 519-527
38. Conti, H.R., F. Shen, et al. (2009) Th17 cells and IL-17 receptor signaling are essential for mucosal host defense against oral candidiasis. *J Exp Med*. 206(2): p. 299-311
39. Langrish C. L., Chen Y., Blumenschein W. M., et al. (2005) IL-23 drives a pathogenic T cell population that induces autoimmune inflammation. *The Journal of Experimental Medicine*. 201(2):233-240
40. Ivanov I.I., McKenzie B. S., Zhou L., Tadokoro C. E., Lepelley A., Lafaille J. J., et al., (2006) The Orphan Nuclear Receptor ROR γ t Directs the Differentiation Program of Proinflammatory IL-17⁺ T Helper Cells, *Cell*. 126 1121–1133

41. Manel, N., Unutmaz, D., & Littman, D. R. (2008). The differentiation of human TH-17 cells requires transforming growth factor-beta and induction of the nuclear receptor RORgamma. *Nature Immunology*, 9(6), 641-9.
42. Ghilardi N, Ouyang W (2007) Targeting the development and effector functions of TH17 cells. *Semin Immunol* 19:383–393
43. Acosta-Rodriguez, E.V., G. Napolitani, et al. (2007) Interleukins 1beta and 6 but not transforming growth factor-beta are essential for the differentiation of interleukin 17-producing human T helper cells. *Nat Immunol*. 8(9): p. 942-9.
44. Kolls, J. K., Lindén, A. (2004). Interleukin-17 family members and inflammation. *Immunity*, 21(4), 467-476
45. Korn T., Oukka M., Kuchroo V., Bettelli E. (2007) Th17 cells: Effector T cells with inflammatory properties. *Seminars in immunology*. 19(6):362-371.
46. Hot A., Miossec P. (2011) Effects of Interleukin (IL)-17A and IL-17F in human rheumatoid arthritis synoviocytes. *Ann Rheum Dis* 70:727-732
47. Adami, S., Cavani, A., Rossi, F., Girolomoni, G. (2014). The role of interleukin-17A in psoriatic disease. *BioDrugs*, 28(6), 487-97.
48. Tabarkiewicz, J., Pogoda, K., Karczmarczyk, A., Pozarowski, P., Giannopoulos, K. (2015). The role of IL-17 and Th17 lymphocytes in autoimmune diseases. *Archivum Immunologiae Et Therapiae Experimentalis*, 63(6), 435-449
49. Hemdan, N.Y.A., G. Birkenmeier, et al. (2010) Interleukin-17-producing T helper cells in autoimmunity. *Autoimmunity Reviews*. 9(11): p. 785-792.
50. Ferber, I. A., Brocke, S., Taylor-Edwards, C., Ridgway, W., Dinisco, C., Steinman, L., Dalton, D., Farhman, C. G. (1996). Mice with a disrupted IFN-gamma gene are susceptible to the induction of experimental autoimmune encephalomyelitis (EAE). *J Immunol*. 156(1): 5-7
51. Komiyama Y., Nakae S., Matsuki T., et al. (2006) IL-17 plays an important role in the development of experimental autoimmune encephalomyelitis. *Journal of Immunology*. 177(1):566–573
52. Ivanov I. I., McKenzie B. S., Zhou L., Tadokoro C. E., Lepelley A., Laflaille J. J., et al. (2006). The orphan nuclear receptor RORγt directs the differentiation program of proinflammatory IL-17+ T helper cells. *Cell* 126, 1121–1133. doi: 10.1016/j.cell.2006.07.035

53. Robinson-Rechavi M., Escriva Garcia H., Laudet V. (2003) The nuclear receptor superfamily, *J. Cell Sci.* 116, 585–586. Doi:10.1242/jcs.00247
54. Becker-André M., André E., DeLamarter J.F. (1993) Identification of nuclear receptor mRNAs by RT-PCR amplification of conserved zinc-finger motif sequences, *Biochem. Biophys. Res. Commun.* 194: 1371–1379
55. Carlberg C., Hooft van Huijsduijnen R., Staple J.K., DeLamarter J.F., Becker- André M. (1994). RZR_s, a new family of retinoid-related orphan receptors that function as both monomers and homodimers, *Mol. Endocrinol.* 8:757–770. Doi:10.1210/mend.8.6.7935491
56. Hirose T., Smith R.J., Jetten A.M. (1994). ROR γ : the third member of ROR/RZR orphan receptor subfamily that is highly expressed in skeletal muscle, *Biochem. Biophys. Res. Commun.* 205: 1976–1983. Doi:10.1006/bbrc.1994.2902
57. Yang XO, Pappu BP, Nurieva R, Akimzhanov A, Kang HS, Chung Y, Ma L, Shah B, Panopoulos AD, Schluns KS, Watowich SS, Tian Q, Jetten AM, Dong C. (2008) T helper 17 lineage differentiation is programmed by orphan nuclear receptors ROR α and ROR γ . *Immunity.* 28:29–39.
58. He Y.W., Deftos M.L., Ojala E.W., Bevan M.J. (1998). ROR γ _t, a novel isoform of an orphan receptor, negatively regulates Fas ligand expression and IL-2 production in T cells. *Immunity* 9:797–806
59. Hirose, T., R.J. Smith, and A.M. Jetten (1994) ROR γ : the third member of ROR/RZR orphan receptor subfamily that is highly expressed in skeletal muscle. *Biochem Biophys Res Commun.* 205(3): p. 1976-83. 30.
60. Villey, I., R. de Chasseval, and J.P. de Villartay (1999) ROR γ _T, a thymus-specific isoform of the orphan nuclear receptor ROR γ / TOR, is up-regulated by signaling through the pre-T cell receptor and binds to the TEA promoter. *Eur J Immunol.* 29(12): p. 4072-80.
61. Rutz S., Eidenschenk C., Kiefer J.R., Ouyang W. (2016) Post-translational regulation of ROR γ _t-A therapeutic target for the modulation of interleukin-17-mediated responses in autoimmune diseases. *Cytokine and Growth Factor Reviews.* Doi:10.1016/j.cytogfr.2016.07.004
62. Medvedev A., Yan Z.H., Hirose T., Giguère V., Jetten A.M. (1996) Cloning of a cDNA encoding the murine orphan receptor RZR/ROR γ and characterization of its response element, *Gene* 181, 199–206

63. Giguère V., Beatty B., Squire J., Copeland N.G., Jenkins N.A. (1995) The orphan nuclear receptor ROR alpha (RORA) maps to a conserved region of homology on human chromosome 15q21-q22 and mouse chromosome 9, *Genomics* 28, 596–598. Doi:<http://dx.doi.org/10.1006/geno.1995.1197>
64. McBroom L.D., Flock G., Giguère V. (1995) The nonconserved hinge region and distinct amino-terminal domains of the ROR alpha orphan nuclear receptor isoforms are required for proper DNA bending and ROR alpha-DNA interactions, *Mol. Cell. Biol.* 15, 796–808
65. McEwan I.J. (2009) Nuclear receptors: one big family, *Methods Mol. Biol.* 505: 3–18, doi:http://dx.doi.org/10.1007/978-1-60327-575-0_1
66. Solt L. A.; Griffin P. R., Burris T. P. (2010) Ligand Regulation of Retinoic Acid Receptor-Related Orphan Receptors: Implications for Development of Novel Therapeutics. *Curr. Opin. Lipidol.* 21, 204–211
67. Santori, F. R., Huang, P., van de Pavert, S. A., Douglass, E. F., Leaver, D. J., Haubrich, B. A., ... Littman, D. R. (2015). Identification of Natural ROR γ Ligands that Regulate the Development of Lymphoid Cells. *Cell Metabolism*, 21(2), 286–297. <https://doi.org/10.1016/j.cmet.2015.01.004>
68. Wang, Y., Kumar, N., Solt, L. A., Richardson, T. I., Helvering, L. M., Crumbley, C., ... Burris, T. P. (2010). Modulation of Retinoic Acid Receptor-related Orphan Receptor α and γ Activity by 7-Oxygenated Sterol Ligands. *Journal of Biological Chemistry*, 285(7), 5013–5025. <https://doi.org/10.1074/jbc.M109.080614>
69. Nakae, S., Y. Komiyama, et al. (2002) Antigen specific T cell sensitization is impaired in IL-17deficient mice, causing suppression of allergic cellular and humoral responses. *Immunity*. 17(3): p. 375-87
70. Tang, L., Yang, X., Liang, Y., Xie, H., Dai, Z., & Zheng, G. (2018). Transcription factor retinoid-related orphan receptor γ t: A promising target for the treatment of psoriasis. *Frontiers in Immunology*, 9(MAY). <https://doi.org/10.3389/fimmu.2018.01210>
71. Ogawa, E. (2018). Pathogenesis of psoriasis and development of treatment. *Journal of Dermatology*, 45, 264–272. <https://doi.org/10.1111/1346-8138.14139>

72. Marinoni, B., Ceribelli, A., Massarotti, M. S., & Selmi, C. (2014). The Th17 axis in psoriatic disease : pathogenetic and therapeutic implications. *Autoimmun Highlights*, 5, 9–19. <https://doi.org/10.1007/s13317-013-0057-4>
73. Aggarwal, S., Ghilardi, N., Xie, M., Sauvage, F. J. De, & Gurney, A. L. (2003). Interleukin-23 Promotes a Distinct CD4 T Cell Activation State Characterized by the Production of Interleukin-17. *Journal of Biological Chemistry*, 278(3), 1910–1914. <https://doi.org/10.1074/jbc.M207577200>
74. Aggarwal, S., Ghilardi, N., Xie, M., Sauvage, F. J. De, & Gurney, A. L. (2003). Interleukin-23 Promotes a Distinct CD4 T Cell Activation State Characterized by the Production of Interleukin-17. *Journal of Biological Chemistry*, 278(3), 1910–1914. <https://doi.org/10.1074/jbc.M207577200>
75. Nasef, N., Elnagdy, M., Younis, W., Badr, R., El-bussiouni, S., Akef, A., & Rashwan, M. (2019). T helper 17 cells and interleukin-17 in patients with rheumatoid arthritis. *International Journal of Clinical Rheumatology*, 14, 113–119.
76. Kotake, S., Udagawa, N., Takahashi, N., Matsuzaki, K., Itoh, K., Ishiyama, S., ... Suda, T. (1999). IL-17 in synovial fluids from patients with rheumatoid arthritis is a potent stimulator of osteoclastogenesis. *Journal of Clinical Investigation*, 103(9), 1345–1352.
77. Crowe, C. R., Chen, K., Pociask, D. A., Alcorn, J. F., Krivich, C., Enelow, R. I., ... Kolls, J. K. (2009). Critical Role of IL-17RA in Immunopathology of Influenza Infection. *The Journal of Immunology*, 183(8), 5301–5310. <https://doi.org/10.4049/jimmunol.0900995>
78. Sarmiento-monroy, J. C., & Parra-medina, R. (2021). T Helper 17 Response to Severe Acute Respiratory Syndrome Coronavirus 2 : A Type of Immune Response with Possible Therapeutic Implications. *Viral Immunology*, 34(3), 190–200. <https://doi.org/10.1089/vim.2020.0177>
79. Wu, D., & Yang, X. O. (2020). TH17 responses in cytokine storm of COVID-19 : An emerging target of JAK2 inhibitor Fedratinib. *Journal of Microbiology, Immunology and Infection*, 53, 368–371.
80. Pacha, O., Sallman, M. A., & Evans, S. E. (2020). COVID-19 : a case for inhibiting IL-17? *Nature Reviews Immunology*, 20, 345–346. <https://doi.org/10.1038/s41577-020-0328-z>

81. Orlov, M., Wander, P. L., Morrell, E. D., Mikacenic, C., & Wurfel, M. M. (2020). A Case for Targeting Th17 Cells and IL-17A in SARS-CoV-2 Infections. *The Journal of Immunology*, 205(4), 892–898.
<https://doi.org/10.4049/jimmunol.2000554>
82. Baeten D, Baraliakos X, Braun J, Sieper J, Emery P, van der Heijde D, et al. (2013) Anti-interleukin-17A monoclonal antibody secukinumab in treatment of ankylosing spondylitis: a randomised, double-blind, placebo-controlled trial. *Lancet*. 382(9906):1705–13. pmid:24035250.
83. Hueber W, Patel DD, Dryja T, Wright AM, Koroleva I, Bruin G, et al. (2010) Effects of AIN457, a fully human antibody to interleukin-17A, on psoriasis, rheumatoid arthritis, and uveitis. *Sci Transl Med*.2(52):52ra72. pmid:20926833.
84. Huh JR, Leung MW, Huang P, Ryan DA, Krout MR, Malapaka RR, Chow J, Manel N, Ciofani M, Kim SV, Cuesta A, Santori FR, Lafaille JJ, Xu HE, Gin DY, Rastinejad F, Littman DR. (2011) Digoxin and its derivatives suppress TH17 cell differentiation by antagonizing ROR γ activity. *Nature*. 472:486–490.
85. Huh J.R. and Littman D. R. (2012) Small molecule inhibitors of ROR γ T: Targeting Th17 cells and other applications. *Eur. J. Immunol*. 42: 2232-2237
86. M.E. Chevreul, (1816) Examen des graisses d’homme, de mouton, de boeuf, de jaguar et d’oie, *Ann. Chim. Phys.* 2 339–372.
87. Vance, D. E. (2000). Cholesterol in the year 2000, *1529*, 1–8
88. Fahy, E., Subramaniam, S., Brown, H. A., Glass, C. K., Merrill, A. H., Murphy, R. C., ... Dennis, E. A. (2005). A comprehensive classification system for lipids. *Journal of Lipid Research*, 46, 839–861.
<https://doi.org/10.1194/jlr.E400004-JLR200>
89. Cerqueira, N. M. F. S. A., Oliveira, E. F., Gesto, D. S., Santos-martins, D., Moorthy, H. N., Ramos, M. J., & Fernandes, P. A. (2016). Cholesterol Biosynthesis: A Mechanistic Overview. *Biochemistry*, 55, 5483–5506.
<https://doi.org/10.1021/acs.biochem.6b00342>
90. Marques, L. R., Diniz, T. A., Antunes, B. M., Rossi, F. E., Caperuto, E. C., Lira, F. S., & Gonçalves, D. C. (2018). Reverse Cholesterol Transport : Molecular Mechanisms and the Non-medical Approach to Enhance HDL

- Cholesterol. *Frontiers in Physiology*, 9, 1–11.
<https://doi.org/10.3389/fphys.2018.00526>
91. Simons, K., & Ikonen, E. (2000). How Cells Handle Cholesterol. *Cell Biology*, 290, 1721–1727
 92. Ikonen, E. (2006). Mechanisms for Cellular Cholesterol Transport : Defects and Human Disease. *Physiol Rev*, 86, 1237–1261.
<https://doi.org/10.1152/physrev.00022.2005>.
 93. Murphy, R. C., & Johnson, K. M. (2008). Cholesterol , Reactive Oxygen Species , and the Formation of Biologically Active Mediators. *The Journal of Biological Chemistry*, 283(23), 15521–15525.
<https://doi.org/10.1074/jbc.R700049200>
 94. Nohturfft, A., Yabe, D., Goldstein, J. L., Brown, M. S., & Espenshade, P. J. (2000). Regulated Step in Cholesterol Feedback Localized to Budding of SCAP from ER Membranes. *Cell*, 102, 315–323.
 95. Hua, X., Sakai, J., Brown, M. S., & Goldstein, J. L. (1996). Regulated Cleavage of Sterol Regulatory Element Binding Proteins Requires Sequences on Both Sides of the Endoplasmic Reticulum Membrane *. *Journal of Biological Chemistry*, 271(17), 10379–10384.
<https://doi.org/10.1074/jbc.271.17.10379>
 96. Ye, J., & Debose-boyd, R. A. (2011). Regulation of Cholesterol and Fatty Acid Synthesis. *Cold Spring Harb Perspect Biol*, 1–13.
 97. Nohturfft, A., Debose-boyd, R. A., Scheek, S., Goldstein, J. L., & Brown, M. S. (1999). Sterols regulate cycling of SREBP cleavage-activating protein (SCAP) between endoplasmic reticulum and Golgi. *Proc. Natl. Acad. Sci. USA*, 96(September), 11235–11240
 98. Sun, L., Li, L., Goldstein, J. L., & Brown, M. S. (2005). Insig Required for Sterol-mediated Inhibition of Scap / SREBP Binding to COPII Proteins in Vitro. *Journal of Biological Chemistry*, 280(28), 26483–26490.
<https://doi.org/10.1074/jbc.M504041200>
 99. Horton, J. D., Goldstein, J. L., & Brown, M. S. (2002). SREBPs : activators of the complete program of cholesterol and fatty acid synthesis in the liver. *Journal of Clinical Investigation*, 109(9), 1125–1131.
<https://doi.org/10.1172/JCI200215593>.Lipid

100. Zhao, C., & Dahlman-wright, K. (2009). Liver X receptor in cholesterol metabolism. *Journal of Endocrinology*, 204, 233–240.
<https://doi.org/10.1677/JOE-09-0271>
101. Eberlé, D., Hegarty, B., Bossard, P., Ferré, P., & Foufelle, F. (2004). SREBP transcription factors : master regulators of lipid homeostasis. *Biochimie*, 86, 839–848. <https://doi.org/10.1016/j.biochi.2004.09.018>
102. Ness, G. C., & Chambers, C. M. (2000). Feedback and Hormonal Regulation of Cholesterol Buffering Capacity. *Proceedings of the Society for Experimental Biology and Medicine*, (224), 8–19.
103. Wang, H., Zhao, M., Sud, N., Christian, P., Shen, J., Song, Y., ... Su, Q. (2016). Glucagon regulates hepatic lipid metabolism via cAMP and Insig-2 signaling : implication for the pathogenesis of hypertriglyceridemia and hepatic steatosis. *Nature Scientific Reports*, (January), 1–11.
<https://doi.org/10.1038/srep32246>
104. IUPAC-IUB Joint Commission on Biochemical Nomenclature (JCBN) Nomenclature of Steroids. Recommendations 1989. *Eur J Biochem* 1989;61:1783–822
105. Fakheri, R. J., & Javitt, N. B. (2012). 27-Hydroxycholesterol , does it exist ? On the nomenclature and stereochemistry of 26-hydroxylated sterols. *Steroids*, 77(6), 575–577. <https://doi.org/10.1016/j.steroids.2012.02.006>
106. Russell, D. W., Halfors, R. W., Ramirez, D. M. O., Shah, R., & Kotti, T. (2009). Cholesterol 24-Hydroxylase: An Enzyme of Cholesterol Turnover in the Brain. *Annual Review of Biochemistry*, 78, 1017–1040.
<https://doi.org/10.1146/annurev.biochem.78.072407.103859>
107. Javitt, N. B. (2002). Cholesterol , Hydroxycholesterols , and Bile Acids. *Biochemical and Biophysical Research Communications*, 292, 1147–1153. <https://doi.org/10.1006/bbrc.2001.2013>
108. Li-hawkins, J., Lund, E. G., Bronson, A. D., & Russell, D. W. (2000). Expression Cloning of an Oxysterol 7 α -Hydroxylase Selective for 24-Hydroxycholesterol. *Journal of Biological Chemistry*, 275(22), 16543–16549. <https://doi.org/10.1074/jbc.M001810200>
109. Russell, D. W. (2003). The Enzymes, Regulation, and Genetics of Bile Acid Synthesis. *Annual Review of Biochemistry*, 72(1), 137–174.
<https://doi.org/10.1146/annurev.biochem.72.121801.161712>

110. Blanc, M., Hsieh, W. Y., Robertson, K. A., Kropp, K. A., Forster, T., Shui, G., ... Ghazal, P. (2013). The Transcription Factor STAT-1 Couples Macrophage Synthesis of 25-Hydroxycholesterol to the Interferon Antiviral Response. *Immunity*, 38, 106–118. <https://doi.org/10.1016/j.immuni.2012.11.004>
111. Wolf, G. (2004). History of Nutrition The Discovery of Vitamin D : The Contribution of Adolf Windaus. *American Society for Nutritional Sciences*, 134, 1299–1302.
112. Murphy, R. C., & Johnson, K. M. (2008). Cholesterol , Reactive Oxygen Species , and the Formation of Biologically Active Mediators. *The Journal of Biological Chemistry*, 283(23), 15521–15525. <https://doi.org/10.1074/jbc.R700049200>
113. Zerbinati, C., & Iuliano, L. (2017). Free Radical Biology and Medicine Cholesterol and related sterols autoxidation. *Free Radical Biology and Medicine*, 111(April), 151–155. <https://doi.org/10.1016/j.freeradbiomed.2017.04.013>
114. Meaney, S., Hassan, M., Sakinis, A., Lütjohann, D., von Bergmann, K., Wennmalm, Å., Diczfalusy, U., & Björkhem, I. (2001). Evidence that the major oxysterols in human circulation originate from distinct pools of cholesterol: A stable isotope study. *Journal of Lipid Research*, 42(1), 70–78. [https://doi.org/10.1016/s0022-2275\(20\)32337-3](https://doi.org/10.1016/s0022-2275(20)32337-3)
115. Meaney, S., Bodin, K., Diczfalusy, U., & Björkhem, I. (2002). On the rate of translocation in vitro and kinetics in vivo of the major oxysterols in human circulation: Critical importance of the position of the oxygen function. *Journal of Lipid Research*, 43(12), 2130–2135. <https://doi.org/10.1194/jlr.M200293-JLR200>
116. Griffiths, W. J., & Wang, Y. (2019). Oxysterol research: A brief review. *Biochemical Society Transactions*, 47(2), 517–526. <https://doi.org/10.1042/BST20180135>
117. Yang, C., McDonald, J. G., Patel, A., Zhang, Y., Umetani, M., Xu, F., ... Hobbs, H. H. (2006). Sterol Intermediates from Cholesterol Biosynthetic Pathway as Liver X Receptor Ligands. *Journal of Biological Chemistry*, 281(38), 27816–27826. <https://doi.org/10.1074/jbc.M603781200>
118. Lehmann, M., Kliewer, S. A., Moore, L. B., Smith-oliver, T. A., Oliver, B. B., Su, J., ... Willson, T. M. (1996). Activation of the Nuclear Receptor LXR by Oxysterols Defines a New Hormone Response Pathway. *Journal of Biological Chemistry*, 272(6), 3137–3140. <https://doi.org/10.1074/jbc.272.6.3137>

119. Janowski, B. A., Grogan, M. J., Jones, S. A., Wisely, G. B., Kliewer, S. A., Corey, E. J., Mangelsdorf, D. J. (1999). Structural requirements of ligands for the oxysterol liver X receptors LXR alpha and LXR beta. *Proc. Natl. Acad. Sci. USA*, 96, 266–271. Retrieved from papers://b266c7f0-8dfd-47e2-9d28-64397eb23d54/Paper/p2357
120. Yoshikawa, T., Shimano, H., Amemiya-kudo, M., Yahagi, N., Hasty, A. H., Matsuzaka, T., ... Ishibashi, S. (2001). Identification of Liver X Receptor-Retinoid X Receptor as an Activator of the Sterol Regulatory Element-Binding Protein 1c Gene Promoter. *Molecular and Cellular Biology*, 21(9), 2991–3000. <https://doi.org/10.1128/MCB.21.9.2991>
121. Morello, F., Saglio, E., Noghero, A., Schiavone, D., Ann, T., Verhovez, A., ... Mulatero, P. (2009). LXR-activating oxysterols induce the expression of inflammatory markers in endothelial cells through LXR-independent mechanisms. *Atherosclerosis*, 207, 38–44. <https://doi.org/10.1016/j.atherosclerosis.2009.04.001>
122. Chen, W., Chen, G., Head, D. L., Mangelsdorf, D. J., & David, W. (2011). Enzymatic Reduction of Oxysterols Impairs LXR Signaling in Cultured Cells and the Livers of Mice. *Cell Metabolism*, 5(1), 73–79. <https://doi.org/10.1016/j.cmet.2006.11.012>.
123. Fu, X., Menke, J. G., Chen, Y., Zhou, G., Macnaul, K. L., Wright, S. D., ... Lund, E. G. (2001). 27-Hydroxycholesterol Is an Endogenous Ligand for Liver X Receptor in Cholesterol-loaded Cells. *Journal of Biological Chemistry*, 276(42), 38378–38387. <https://doi.org/10.1074/jbc.M105805200>
124. Bensinger, S. J., Bradley, M. N., Joseph, S. B., Zelcer, N., Edith, M., Hausner, M. A., ... Tontonoz, P. (2008). LXR signaling couples sterol metabolism to proliferation in the acquired immune response. *Cell*, 134(1), 97–111
125. Jetten, A. M., Kurebayashi, S., & Ueda, E. (2001). The ROR nuclear orphan receptor subfamily: Critical regulators of multiple biological processes. *Progress in Nucleic Acid Research and Molecular Biology*, 69, 205–247.
126. Shearman, L. P., Sriram, S., Weaver, D. R., Maywood, E. S., Chaves, I. I., Zheng, B., Kume, K., Lee, C. C., van der Horst, G. T. J., Hastings, M. H., & Reppert, S. M. (2000). Interacting Molecular Loops in the Mammalian Circadian Clock. *Science*, 288, 1013–1019. <https://www.science.org>

127. Gold, D. A., Baek, S. H., Schork, N. J., Rose, D. W., Delaine, D., Sachs, B. D., ... Hamilton, B. A. (2009). ROR α coordinates reciprocal signaling in cerebellar development through Sonic hedgehog and calcium-dependent pathways. *Neuron*, 40(6), 1119–1131.
128. Wang, Y., Kumar, N., Solt, L. A., Richardson, T. I., Helvering, L. M., Crumbley, C., ... Burris, T. P. (2010). Modulation of Retinoic Acid Receptor-related Orphan Receptor α and γ Activity by 7-Oxygenated Sterol Ligands. *Journal of Biological Chemistry*, 285(7), 5013–5025.
<https://doi.org/10.1074/jbc.M109.080614>
129. Wang, Y., Kumar, N., Crumbley, C., Griffin, P. R., & Burris, T. P. (2010). A second class of nuclear receptors for oxysterols: Regulation of ROR α and ROR γ activity by 24S-hydroxycholesterol (cerebrosterol). *Biochimica et Biophysica Acta - Molecular and Cell Biology of Lipids*, 917–923.
<https://doi.org/10.1016/j.bbalip.2010.02.012>
130. Jin, L., Martynowski, D., Zheng, S., Wada, T., Xie, W., & Li, Y. (2010). Structural Basis for Hydroxycholesterols as Natural Ligands of Orphan Nuclear Receptor ROR γ . *Molecular Endocrinology*, 24(5), 923–929.
<https://doi.org/10.1210/me.2009-0507>
131. Fuentes, N., Silveyra, P., States, U., & Hill, C. (2019). Estrogen receptor signaling mechanisms. *Adv Protein Chem Struct Biol*, (116), 135–170.
<https://doi.org/10.1016/bs.apcsb.2019.01.001.Estrogen>
132. Dhamad, A. E., Zhou, Z., Zhou, J., & Du, Y. (2016). Systematic Proteomic Identification of the Heat Shock Proteins (Hsp) that Interact with Estrogen Receptor Alpha (ER α) and Biochemical Characterization of the ER α - Hsp70 Interaction. *PLOS ONE*, 1–19. <https://doi.org/10.1371/journal.pone.0160312>
133. Suzuki, H., Barros, R. P. A., Sugiyama, N., Krishnan, V., Yaden, B. C., Kim, H., ... Gustafsson, J.-å. (2013). Involvement of estrogen receptor b in maintenance of serotonergic neurons of the dorsal raphe. *Molecular Psychiatry*, 18, 674–680. <https://doi.org/10.1038/mp.2012.62>
134. DuSell, C. D., Umetani, M., Shaul, P. W., Mangelsdorf, D. J., & McDonnell, D. P. (2008). 27-Hydroxycholesterol is an endogenous selective estrogen receptor modulator. *Molecular Endocrinology*, 22(1), 65–77.
<https://doi.org/10.1210/me.2007-0383>

135. Meljon, A., Crick, P. J., Yutuc, E., Yau, J. L., Seckl, J. R., Theofilopoulos, S., ... Gri, W. J. (2019). Mining for Oxysterols in Cyp7b1 – / – Mouse Brain and Plasma : Relevance to Spastic Paraplegia Type 5. *Biomolecules*, 9(149), 1–22.
136. Hiramitsu, S., Ishikawa, T., Lee, W. R., Khan, T., Crumbley, C., Khwaja, N., ... Umetani, M. (2018). Estrogen receptor beta-mediated modulation of lung cancer cell proliferation by 27-hydroxycholesterol. *Frontiers in Endocrinology*, 9(AUG), 1–9. <https://doi.org/10.3389/fendo.2018.00470>
137. Voisin, M., Medina, P. De, Mallinger, A., Dalenc, F., & Huc-claustre, E. (2017). Identification of a tumor-promoter cholesterol metabolite in human breast cancers acting through the glucocorticoid receptor. *Proc. Natl. Acad. Sci. USA*, 114(44), 9346–9355. <https://doi.org/10.1073/pnas.1707965114>
138. Liu, C., Yang, X. V, Wu, J., Kuei, C., Mani, N. S., Zhang, L., ... Lovenberg, T. W. (2011). Oxysterols direct B-cell migration through EBI2. *Nature*, 3–9. <https://doi.org/10.1038/nature10226>
139. Hannedouche, S., Zhang, J., Yi, T., Shen, W., Nguyen, D., Pereira, J. P., ... Sailer, A. W. (2011). Oxysterols direct immune cell migration via EBI2. *Nature*, 475(7357), 524–527. <https://doi.org/10.1038/nature10280>
140. Yi, T., Wang, X., Kelly, L. M., An, J., Xu, Y., Saller, A. W., ... Cyster, J. G. (2012). Oxysterol gradient generation by lymphoid stromal cells guides activated B cell movement during humoral responses. *Immunity*, 37(21), 535–548. <https://doi.org/10.1038/jid.2014.371>
141. Gatto, D., & Brink, R. (2013). B cell localization : regulation by EBI2 and its oxysterol ligand. *Trends in Immunology*, 34(7), 336–341. <https://doi.org/10.1016/j.it.2013.01.007>
142. Wanke, F., Moos, S., Croxford, A. L., Heinen, A. P., Gräf, S., Kalt, B., ... Kurschus, F. C. (2017). EBI2 Is Highly Expressed in Multiple Sclerosis Lesions and Promotes Early CNS Migration of Encephalitogenic CD4 T Cells. *Cell Reports*, 18(5), 1270–1284. <https://doi.org/10.1016/j.celrep.2017.01.020>
143. Nedelcu, D., Liu, J., Xu, Y., Jao, C., & Salic, A. (2013). Oxysterol binding to the extracellular domain of Smoothened in Hedgehog signaling. *Nat Chem Biol*, 9(9), 557–564. <https://doi.org/10.1038/nchembio.1290>. Oxysterol
144. Dwyer, J. R., Sever, N., Carlson, M., Nelson, S. F., Beachy, P. A., & Parhami, F. (2007). Oxysterols Are Novel Activators of the Hedgehog Signaling

- Pathway in Pluripotent Mesenchymal Cells. *Journal of Biological Chemistry*, 282(12), 8959–8968. <https://doi.org/10.1074/jbc.M611741200>
145. Raleigh, D. R., Sever, N., Choksi, P. K., Sigg, M. A., Garcia-gonzalo, F. R., Krup, A. L., ... Sunny, Y. (2019). Cilia-associated oxysterols activate Smoothed. *Mol Cell*, 72(2), 316–327. <https://doi.org/10.1016/j.molcel.2018.08.034>. Cilia-associated
 146. Deshpande, I., Liang, J., Hedeem, D., Roberts, K. J., Zhang, Y., Ha, B., & Latorraca, N. R. (2019). Smoothed stimulation by membrane sterols drives Hedgehog pathway activity. *Nature*, 571, 284–288. <https://doi.org/10.1038/s41586-019-1355-4>
 147. Bauman, D., Bitmansour, A., McDonald, J., Thompson, B., Liang, G., & Russell, D. (2009). 25-Hydroxycholesterol secreted by macrophages in response to Toll-like receptor activation suppresses immunoglobulin A production. *Proceedings of the National Academy of Sciences of the United States of America*, 106(39), 16764–16769. <https://doi.org/10.1073/pnas.0909142106>
 148. Cyster, J. G., Dang, E. V., Reboldi, A., & Yi, T. (2014). 25-Hydroxycholesterol in innate and adaptive immunity. *Nature Reviews Immunology*, 14, 731–743. <https://doi.org/10.1038/nri3755>
 149. Schneider, W. M., Chevillotte, M. D., & Rice, C. M. (2014). Interferon-Stimulated Genes: A Complex Web of Host Defenses. *Annu Re Immunol*, 32, 513–545. <https://doi.org/10.1146/annurev-immunol-032713-120231>. Interferon-Stimulated
 150. Cyster, J. G., Dang, E. V., Reboldi, A., & Yi, T. (2014). 25-Hydroxycholesterol in innate and adaptive immunity. *Nature Reviews Immunology*, 14, 731–743. <https://doi.org/10.1038/nri3755>
 151. Liu, S., Aliyari, R., Chikere, K., Li, G., Matthew, D., Smith, J. K., ... Cheng, G. (2013). Interferon-Inducible Cholesterol-25-Hydroxylase Broadly Inhibits Viral Entry by Production of 25-Hydroxycholesterol. *Immunity*, 38(1), 92–105. <https://doi.org/10.1016/j.immuni.2012.11.005>. Interferon-Inducible
 152. Cagno, V., Civra, A., Rossin, D., Calfapietra, S., Caccia, C., Leoni, V., ... Lembo, D. (2017). Redox Biology Inhibition of herpes simplex-1 virus replication by 25-hydroxycholesterol and 27-hydroxycholesterol. *Redox Biology*, 12(March), 522–527. <https://doi.org/10.1016/j.redox.2017.03.016>

153. Shawli, G. T., Adeyemi, O. O., & Stonehouse, N. J. (2019). The Oxysterol 25-Hydroxycholesterol Inhibits Replication of Murine Norovirus. *Viruses*, 11(97), 1–16. <https://doi.org/10.3390/v11020097>
154. Ouyang, W., Zhou, H., Liu, C., Wang, S., Han, Y., & Xia, J. (2018). 25 - Hydroxycholesterol protects against acute lung injury via targeting MD-2. *J Cell Mol Med*, 22, 5494–5503. <https://doi.org/10.1111/jcmm.13820>
155. Koarai, A., Yanagisawa, S., Sugiura, H., Ichikawa, T., Kikuchi, T., Furukawa, K., ... Minakata, Y. (2012). 25-hydroxycholesterol enhances cytokine release and toll-like receptor 3 response in airway epithelial cells. *Respiratory Research*, 13(63), 1–11.
156. Aye, I. L. M. H., Waddell, B. J., Mark, P. J., & Keelan, J. A. (2012). Oxysterols exert proinflammatory effects in placental trophoblasts via activation of NF- k B. *Molecular Human Reproduction*, 18(7), 341–353. <https://doi.org/10.1093/molehr/gas001>
157. Aye, I. L. M. H., Waddell, B. J., Mark, P. J., & Keelan, J. A. (2012). Oxysterols exert proinflammatory effects in placental trophoblasts via activation of NF- k B. *Molecular Human Reproduction*, 18(7), 341–353. <https://doi.org/10.1093/molehr/gas001>
158. Kloudova, A., Guengerich, F. P., Soucek, P., Republic, C., & States, U. (2017). The role of oxysterols in human cancer. *Trends Endocrinol Metab*, 28(7), 485–496. <https://doi.org/10.1016/j.tem.2017.03.002>.The
159. Raccosta, L., Fontana, R., Maggioni, D., Lanterna, C., Villablanca, E. J., Paniccia, A., ... Traversari, C. (2013). The oxysterol – CXCR2 axis plays a key role in the recruitment of tumor-promoting neutrophils. *J. Exp. Med.*, 210(9), 1711–1728. <https://doi.org/10.1084/jem.20130440>
160. Baek, A. E., Yu, Y. A., He, S., Wardell, S. E., Chang, C., Kwon, S., ... Nelson, E. R. (2017). The cholesterol metabolite 27 hydroxycholesterol facilitates breast cancer metastasis through its actions on immune cells. *Nature Communications*, 8(864), 1–10. <https://doi.org/10.1038/s41467-017-00910-z>
161. E. de. Hoffmann, V. Stroobant, Mass spectrometry : principles and applications, J. Wiley, Chichester, West Sussex, England; Hoboken, NJ, 2007.
162. Banerjee, S., & Mazumdar, S. (2012). Electrospray Ionization Mass Spectrometry : A Technique to Access the Information beyond the Molecular

- Weight of the Analyte. *International Journal of Analytical Chemistry*, 1–40.
<https://doi.org/10.1155/2012/282574>
163. Ho, C. S., Lam, C. W. K., Chan, M. H. M., Cheung, R. C. K., Law, L. K., Lit, L. C. W., ... Tai, H. L. (2003). Electrospray Ionisation Mass Spectrometry : Principles and Clinical Applications. *Clin Biochem Rev*, 3–12.
 164. Berkel, G. J. Van. (2003). An overview of some recent developments in ionization methods for mass spectrometry. *Eur. J. Mass Spectrom.*, 9, 539–562.
<https://doi.org/10.1255/ejms.586>
 165. Thermo Scientific. (2009). Ion Max and Ion Max-S API Source Hardware Manual. <http://tools.thermofisher.com/content/sfs/manuals/Ion-Max-Ion-Max-S-Hardware.pdf>
 166. Schwartz, J. C., & Senko, M. W. (2002). A Two-Dimensional Quadrupole Ion Trap Mass Spectrometer. *Journal of the American Society for Mass Spectrometry*, 13, 659–669.
 167. Douglas, D. J., Frank, A. J., & Mao, D. (n.d.). LINEAR ION TRAPS IN MASS SPECTROMETRY. <https://doi.org/10.1002/mas.20004>
 168. Zubarev, R. A., & Makarov, A. (2013). Orbitrap Mass Spectrometry. *Analytical Chemistry*, 85, 5288–5296.
 169. Michalski, A., Damoc, E., Lange, O., Denisov, E., Nolting, D., Mu, M., ... Makarov, A. (2012). Ultra High Resolution Linear Ion Trap Orbitrap Mass Spectrometer (Orbitrap Elite) Facilitates Top Down LC MS / MS and Versatile Peptide Fragmentation Modes. *Molecular and Cellular Proteomics*, 11(3), 1–11.
<https://doi.org/10.1074/mcp.O111.013698>
 170. Griffiths, W. J., & Wang, Y. (2011). Analysis of oxysterol metabolomes. *Biochimica et Biophysica Acta - Molecular and Cell Biology of Lipids*, 1811, 784–799. <https://doi.org/10.1016/j.bbalip.2011.05.012>
 171. Dias, I. H. K., Wilson, S. R., & Roberg-larsen, H. (2018). Chromatography of Oxysterols. *Biochimie*. <https://doi.org/10.1016/j.biochi.2018.05.004>
 172. Lütjohann, D., Breuer, O., Ahlborg, G., Nennesmo, I., Sidén, Å., Diczfalusy, U., & Björkhem, I. (1996). Cholesterol homeostasis in human brain: Evidence for an age-dependent flux of 24S-hydroxycholesterol from the brain into the circulation. *Proceedings of the National Academy of Sciences of the United States of America*, 93(18), 9799–9804. <https://doi.org/10.1073/pnas.93.18.9799>

173. Dzeletovic, S., Breuer, O., Lund, E., & Diczfalusy, U. (1995). Determination of Cholesterol oxidation products in human plasma by isotope dilution mass spectrometry. *Analytical Biochemistry*, 225, 73–80.
174. Dzeletovic, S., Breuer, O., Lund, E., & Diczfalusy, U. (1995). Determination of Cholesterol oxidation products in human plasma by isotope dilution mass spectrometry. *Analytical Biochemistry*, 225, 73–80.
175. Pedersen, J. I., Hagenfeldt, Y., & Bjorkhem, I. (1988). Assay and properties of 25-hydroxyvitamin D3 23-hydroxylase. Evidence that 23,25-dihydroxyvitamin D3-treated or fasted guinea pigs. *Biochem. J*, 250, 527–532.
176. E.M. Thurman, M.S. Mills, (1998) Solid-phase extraction : principles and practice
177. Halket, J. M., & Zaikin, V. G. (2003). Derivatization in mass spectrometry — 1 . Silylation. *Journal. Mass Spectrom.*, 21, 1–21.
<https://doi.org/10.1255/ejms.527>
178. Bird, I. M., Peter, D., & Hayes, J. (1989). High performance liquid chromatography : principles and clinical applications VPL. *BMJ*, 299, 783–787.
179. Pitt, J. J. (2009). Principles and Applications of Liquid Chromatography-Mass Spectrometry in Clinical Biochemistry. *Clin Biochem Rev*, 30(February), 19–34.
180. Griffiths, W. J., Crick, P. J., & Wang, Y. (2013). Methods for oxysterol analysis : Past , present and future. *Biochemical Pharmacology*, 86(1), 3–14.
<https://doi.org/10.1016/j.bcp.2013.01.027>
181. DeBarber, A. E., Lutjohann, D., Merckens, L., & Steiner, R. D. (2008). Liquid Chromatography-Tandem Mass Spectrometry Determination of Plasma 24S-Hydroxycholesterol with Chromatographic Separation of 25-Hydroxycholesterol. *Analytical Chemistry*, 381(1), 151–153.
<https://doi.org/10.1016/j.ab.2008.05.037>
182. Ola, D., Solberg, R., Enot, D., Deigner, H., Koal, T., Scholl-bu, S., & Keller, M. (2010). Metabolomic Analyses of Plasma Reveals New Insights into Asphyxia and Resuscitation in Pigs. *PLOS ONE*, 5(3), 1–12.
<https://doi.org/10.1371/journal.pone.0009606>
183. Honda, A., Yamashita, K., Hara, T., Ikegami, T., & Miyazaki, T. (2009). Highly sensitive quantification of key regulatory oxysterols in biological samples

- by LC-ESI-MS / MS. *Journal Lipid Research*, 50(2), 350–357.
<https://doi.org/10.1194/jlr.D800040-JLR200>
184. Jiang, X., Ory, D. S., & Han, X. (2007). Characterization of oxysterols by electrospray ionization tandem mass spectrometry after one-step derivatization with dimethylglycine. *Rapid Commun Mass Spectrom*, 21(2), 141–152
 185. Girard A, Sandulesco G (1936). Sur une nouvelle serie de r actif du groupe carbonyle, leurs utilisation ~. l'extraction des substances cetoniques et 5. la caracterisation microchimique des aldehydes et cetones. *Heh' Chim Acta* 19:1095-1107.
 186. Jiang, X., Ory, D. S., & Han, X. (2007). Characterization of oxysterols by electrospray ionization tandem mass spectrometry after one-step derivatization with dimethylglycine. *Rapid Commun Mass Spectrom*, 21(2), 141–152.
 187. DeBarber, A. E., Sandlers, Y., Pappu, A. S., Merckens, L. S., Duell, B., Lear, S. R., ... Steiner, R. D. (2011). Profiling Sterols in Cerebrotendinous Xanthomatosis: Utility of Girard Derivatization and High Resolution Exact Mass LC-ESI-MSⁿ Analysis. *Journal Chromatogr B Ana Technol Biomed Life Scil*, 1–18. <https://doi.org/10.1016/j.jchromb.2010.11.019>.
 188. Roberg-larsen, H., Frank, M., Grimsmo, A., Angell, P., Dembinski, J. L., Rise, F., ... Ray, S. (2012). High sensitivity measurements of active oxysterols with automated filtration / filter backflush-solid phase extraction-liquid chromatography – mass spectrometry. *Journal of Chromatography A*, 1255, 291–297. <https://doi.org/10.1016/j.chroma.2012.02.002>
 189. Burkard, I., Rentsch, K. M., & Eckardstein, A. Von. (2004). Determination of 24S- and 27-hydroxycholesterol in plasma by high-performance liquid chromatography-mass spectrometry. *Journal Lipid Research*, 45(4), 776–781. <https://doi.org/10.1194/jlr.D300036-JLR200>
 190. Anita, L., Heverin, M., Larsson, H., Lundstr, E., Wahren, J., Diczfalusy, U., & Bj, I. (2007). Novel LC – MS / MS method for assay of 7 -hydroxy-4-cholesten-3-one in human plasma Evidence for a significant extrahepatic metabolism. *Journal of Chromatography B*, 856, 15–19. <https://doi.org/10.1016/j.jchromb.2007.05.019>
 191. McDonald, J. G., Smith, D. D., Stiles, A. R., & Russell, D. W. (2012). A comprehensive method for extraction and quantitative analysis of sterols and

- secosteroids from human plasma. *The Journal of Lipid Research*, 53(7), 1399–1409. <https://doi.org/10.1194/jlr.D022285>
192. Quehenberger, O., Armando, A. M., Brown, A. H., Milne, S. B., Myers, D. S., Merrill, A. H., ... Dennis, E. A. (2010). Lipidomics reveals a remarkable diversity of lipids in human plasma. *Journal of Lipid Research*, 51, 3299–3305. <https://doi.org/10.1194/jlr.M009449>
 193. McDonald, J. G., Thompson, B. M., McCrum, E. C., & Russell, D. W. (2007). Extraction and Analysis of Sterols in Biological Matrices by High Performance Liquid Chromatography Electrospray Ionization Mass Spectrometry. *Methods in Enzymology*, 432, 145–170. [https://doi.org/10.1016/S0076-6879\(07\)32006-5](https://doi.org/10.1016/S0076-6879(07)32006-5)
 194. Griffiths, W. J., Wang, Y., Alvelius, G., Liu, S., Bodin, K., & Sjövall, J. (2006). Analysis of Oxysterols by Electrospray Tandem Mass Spectrometry. *American Society for Mass Spectrometry*, 17, 341–362. <https://doi.org/10.1016/j.jasms.2005.10.012>
 195. Griffiths, W. J., Crick, P. J., Wang, Y., Ogundare, M., Tuschl, K., Morris, A. A., ... Wang, Y. (2013). Analytical strategies for characterization of oxysterol lipidomes: Liver X receptor ligands in plasma. *Free Radical Biology and Medicine*, 59, 69–84. <https://doi.org/10.1016/j.freeradbiomed.2012.07.027>
 196. Crick, P. J., Bentley, T. W., Wang, Y., & Griffiths, W. J. (2015). Revised sample preparation for the analysis of oxysterols by enzyme-assisted derivatisation for sterol analysis (EADSA). *Anal Bioanal Chem*, 407, 5235–5239. <https://doi.org/10.1007/s00216-015-8609-2>

Chapter 2. Materials and Methods

2.1 Cell Culture

2.1.1 Cell Culture Materials

2.1.1.1 Cell Line

The Murine lymphoblast EL4 cell line was obtained from Sigma-Aldrich (Cat. no. 85023105, ECACC).

2.1.1.2 Culture Media

Human and Mouse CD4⁺ T cell cultures were cultured in X-Vivo-20 Serum Free Hematopoietic Cell Medium from Lonza (Cat. no. LZBE04-448Q, Scientific Laboratory Supplies, Nottingham, UK) supplemented with 2mM Glutamine, 10 Units/mL Penicillin and 0.1 mg/mL Streptomycin from Sigma-Aldrich (Cat. no. G1146, Dorset, UK) unless otherwise stated.

The murine lymphoblast EL4 cell line was maintained in Gibco DMEM medium with glutamine (Cat. no. 41966-029) supplemented with 10% FBS from Invitrogen (Cat. no. 10106-169, Thermo Fisher Scientific). The majority of EL4 experiments were cultured with Lonza X-Vivo-20 Serum Free Hematopoietic Cell Medium (Scientific Laboratory Supplies) unless otherwise stated.

2.1.1.3 Cell isolation kits and buffers

T lymphocytes were isolated from peripheral blood mononuclear cells (PBMCs) by immunomagnetic bead separation using magnetic-activated cell sorting (MACS[®]) technology devised by Miltenyi Biotec with an autoMACS[®] separator. Human naïve CD4⁺ T cells were isolated with Miltenyi Biotec Naïve CD4⁺ T cell Isolation Kit II, human (Cat. no. 130-094-131, Surrey, UK). Human CD4⁺ T cells were isolated with CD4⁺ T cell Isolation kit, human (Cat. no. 130-096-533). Murine naïve CD4⁺ T cells were isolated with Naïve CD4⁺ T cell Isolation kit, Mouse (Cat. no. 130-104-453). Consumables for the autoMACS[®] separator including columns (Cat no. 130-021-101), Running Buffer (Cat. no. 130-091-221) and Rinsing Solutions (Cat. no. 130-091-222) were purchased from Miltenyi Biotec. Sterile-filtered 0.5% BSA in PBS buffer required for isolation was prepared in house. Syringe PVDF membrane 0.22 µm filters were obtained from Sartorius (Surrey, UK), Bovine Serum Albumin (BSA) was purchased from Labtech (Cat. no. PM-T1725, Sussex, UK) and Lonza

Phosphate Buffered Saline (PBS) 1X without $\text{Ca}^{2+}/\text{Mg}^{2+}$ was procured from Scientific Laboratory Supplies (Cat. no. LZBE17-516F).

2.1.1.4 Culture cytokines, activators and inhibitors

T cells were studied *in vitro* under several culture conditions. Reagents and kits used for T cell studies are listed in Table 2.1.

Table 2.1 List of cell culture reagents, kits and cytokines

Reagent	Manufacturer	Catalogue Number	Additional information
T cell Activation/Expansion Kit, human	Miltenyi Biotec	130-091-441	Prepared with anti-CD3 and anti-CD28 loaded beads
T cell Activation/Expansion Kit, mouse	Miltenyi Biotec	130-093-627	Prepared with anti-CD3 and anti-CD28 loaded beads
Phorbol 12-myristate 13-acetate (PMA)	Sigma-Aldrich	P1585	Reconstituted in sterile DMSO
Ionomycin	Sigma-Aldrich	10634	Reconstituted in sterile DMSO
Clotrimazole	Sigma-Aldrich	C6019	Reconstituted in EtOH
Tebuconazole	Sigma-Aldrich	32013	Reconstituted in DMSO
Ursolic acid	Sigma-Aldrich	89797	Reconstituted in DMSO
TO901317	Sigma-Aldrich	T2320	Reconstituted in DMSO
GW3965	Sigma-Aldrich	G6295	Reconstituted in DMSO
24(S),25-EC	Avanti	700039P	Reconstituted in EtOH
7α,24(S),25-EC			Reconstituted in EtOH
7α,24(S),25-EC-3-one	In house		Reconstituted in EtOH
24(S),25-diHC	In house		Reconstituted in EtOH
7α,24(S),25-triHC	In house		Reconstituted in EtOH
7α,24(S),25-triHC-3-one	In house		Reconstituted in EtOH
25-HC	Avanti	700019P	Reconstituted in EtOH
Anti-human Interferon-γ	Thermo Fisher Scientific	16-7318-85	PBS buffer
Anti-human Interleukin-4	Thermo Fisher Scientific	16-7048-85	PBS buffer
Human Interleukin-2	Thermo Fisher Scientific	14-8029-63	40 mM Sodium Acetate, 0.2 M NaCl, pH 5.0, 1% BSA sterile-filtered buffer

Human Interleukin-1β	Thermo Fisher Scientific	14-8018-80	150 mM NaCl, 1% BSA in PBS sterile-filtered buffer
Human Interleukin-6	R&D Systems	206-IL-010	PBS buffer
Human Interleukin-21	Thermo Fisher Scientific	14-8219-62	20 mM Sodium Phosphate, 0.6 M NaCl, pH 7.2, 1% BSA sterile-filtered buffer
Human Interleukin-23	Thermo Fisher Scientific	14-8239-63	20 mM Sodium Phosphate, 0.2M NaCl , pH 6.0, 1% BSA sterile-filtered buffer
Transforming Growth Factor-β	R&D Systems	240-B-002	4 mM HCl, 1 mg/mL BSA sterile-filtered buffer
Anti-mouse Interferon-γ	Thermo Fisher Scientific	16-7311-85	PBS buffer
Anti-mouse Interleukin-4	Thermo Fisher Scientific	16-7041-85	PBS buffer
Mouse Interleukin-2	Thermo Fisher Scientific	14-8021-64	0.1 mM TCEP, 5 mM Sodium Citrate in PBS, pH 4.0, 1% BSA sterile-filtered buffer
Mouse Transforming Growth Factor β1	R&D Systems	7666-MB-005	4 mM HCl, 0.1% BSA sterile-filtered buffer
Mouse Interleukin-23	R&D Systems	1887-ML-10	0.1% BSA PBS sterile-filtered buffer
Cell Proliferation Dye eFluor® 450	Thermo Fisher Scientific	65-0842	Reconstituted in sterile DMSO
Phosphate Buffered Saline 1X without Ca²⁺/Mg²⁺ (PBS)	Lonza Scientific Laboratory Supplies	LZBE17-516F	Sterile for cell culture
Dimethyl Sulphoxide, DMSO (Hybri-Max®)	Sigma-Aldrich	D2650	Sterile for cell culture

2.1.2 Preparation of Oxysterols for Cell Culture Treatment

Oxysterols 24(S),25-EC (Cat. no. 700039P) and 25-HC (700019P) were purchased from Avanti (Polar Lipids Inc. Alabaster, Alabama, USA) and 7 α ,24(S),25-EC was kindly provided by collaborators. Downstream metabolites and hydrolysed oxysterols were synthesised in house.

2.1.2.1 7 α ,24(S),25-EC sample preparation for HPLC UV purification

7 α ,24(S),25-EC was purified by HPLC UV purification. 7 α ,24(S),25-EC stock was firstly diluted to 70% EtOH from absolute EtOH with HPLC water. Sample injections were prepared by diluting 10 μ L 7 α ,24(S),25-EC to 70% EtOH and combining with 50 μ L 70% EtOH.

2.1.2.2 HPLC Purification of 7 α ,24(S),25-EC

7 α ,24(S),25-EC was purified by HPLC UV purification with an Ultimate 3000 HPLC system and UV detector. Samples injections were loaded manually by syringe. A two phased gradient was used for separation consisting of 70% Acetonitrile for mobile phase A and 50% IPA, 50% ACN for mobile phase B. An 18 minute experimental method was maintained at 1000 μ L/minute starting at 50% B and samples detected at 210 nm wavelength. The peak for 7 α ,24(S),25-EC was detected after 7 minutes shown in Figure 2.1, and the purified fraction was collected in EppendorfTM LoBind polypropylene tubes (Cat. no. 10051232, Thermo Fisher Scientific). Subsequently, samples were dried overnight in a Scanspeed Vacuum Concentrator (Labogene Lynge DK). Dried samples were reconstituted and combined in EtOH.

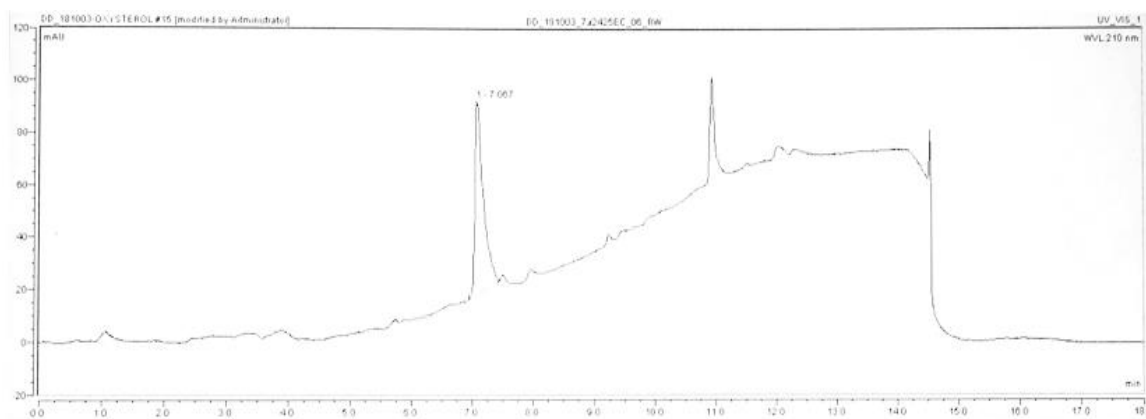


Figure 2.1 7 α ,24(S),25-EC HPLC purification. 7 α ,24(S),25-EC was manually injected through an Ultimate 3000 HPLC system with UV detector using 210 nm wavelength. Fractions were collected at 7 minutes when the 7 α ,24(S),25-EC peak was seen.

2.1.2.3 Synthesis of downstream metabolites of 7 α ,24(S),25-EC

Downstream metabolites of 7 α ,24(S),25-EC and hydrolysed oxysterols were synthesised in house since they are not commercially available.

2.1.2.3.1 7 α ,24(S),25-EC cholesterol oxidase enzyme reaction

7 α ,24(S),25-EC was treated with cholesterol oxidase for the conversion to downstream metabolite 7 α ,24(S),25-EC-3-one (Figure 2.2). Aliquots of 7 α ,24(S),25EC stock were transferred to two 1.5ml Eppendorf tubes labelled A and B with 1 mL 50 mM KH₂PO₄ pH 7 buffer and mixed well by vortex. To tube A only, 3 μ L of Cholesterol oxidase (containing 2 μ g/ μ L protein) was added while tube B was left untreated. Both tubes were mixed well and incubated at 37°C in a water bath for 1 hour to oxidise the sterol 3 β -OH-5-ene group to a 3-oxo-4-ene group. Afterwards, tubes were dried overnight in a Scanspeed Vacuum Concentrator (Labogene). Dried samples were reconstituted in EtOH and sonicated for 30 minutes at RT before centrifuging at 17000 x g at 4°C for 30 minutes and supernatants transferred to fresh tubes. Purity of 7 α ,24(S),25-EC and 7 α ,24(S),25-EC-3-one was confirmed by LC-MS analysis described in *section 2.3*.

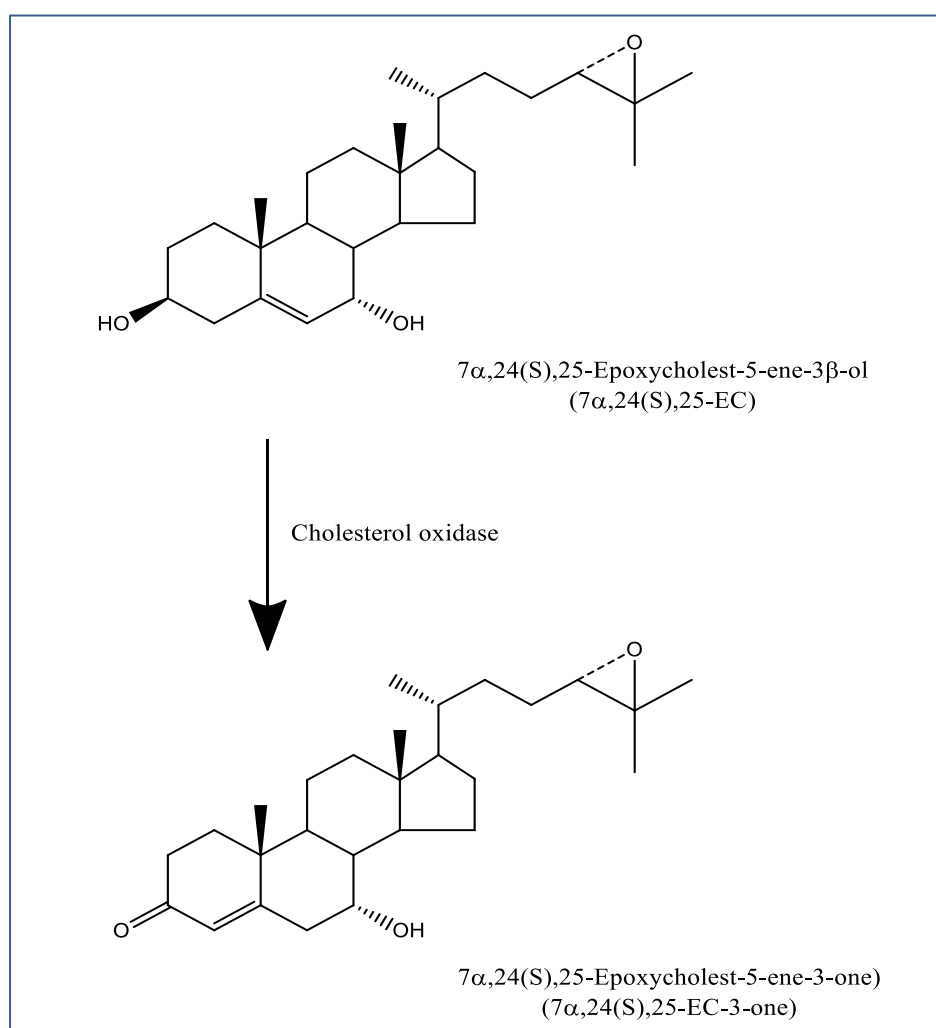


Figure 2.2 Reaction scheme for the conversion of 7 α ,24(S),25-EC to the downstream metabolite 7 α ,24(S),25,EC-3-one with cholesterol oxidase.

2.1.2.3.2 Hydrolysis of oxysterols

24(*S*),25-EC and downstream metabolites in the pathway were hydrolysed with glacial Acetic acid to hydroxycholesterols (Figure 2.3) which are detected during LC-MS sterol analysis of T cell cultures. Aliquots of 24(*S*),25-EC, HPLC purified 7 α ,24(*S*),25-EC and 7 α ,24(*S*),25-EC-3-one stocks were transferred to Eppendorf™ LoBind polypropylene tubes and dried in a Scanspeed Vacuum Concentrator (Labogene) for 1 hour. Samples were then reconstituted in 1 mL 70% Acetonitrile by sonication for 1 minute and vortexed well. 50 uL glacial acetic acid was added to each tube, mixed well and incubated in the dark for 24 hours at RT. Afterwards, samples were dried overnight in a Scanspeed Vacuum Concentrator (Labogene). Samples were reconstituted in EtOH.

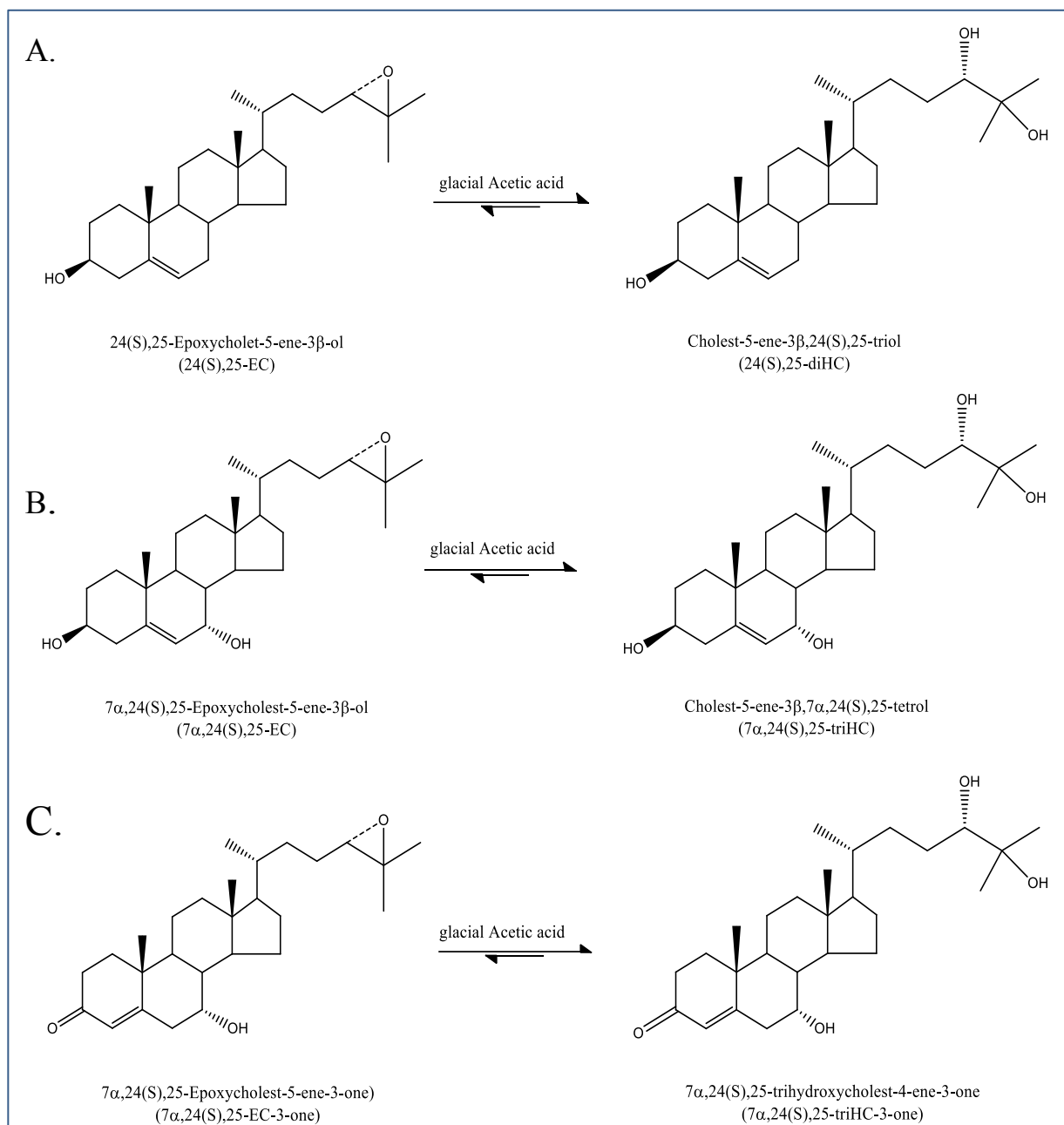


Figure 2.3 Hydrolysis reaction scheme for 24(S),25-EC and downstream metabolites using glacial Acetic acid. A. 24(S),25-EC was converted to 24(S),25-diHC, B. 7 α ,24(S),25-EC was converted to 7 α ,24(S),25-triHC, C. 7 α ,24(S),25-EC-3-one was converted to 7 α ,24(S),25-triHC-3-one.

2.1.3 Human Blood Donors and Ethical Approval for Human Studies

For human CD4⁺ T cell studies, peripheral venous blood was taken from healthy human donors recruited into the study “Regulation of immune function by oxysterols” by the Clinical Research Facility at Swansea University. Informed written consent was received from all donors and ethical approval obtained from Wales Research Ethics Committee 6 (13/WA/0190). Donors were aged between 21 to 60 years old. A maximum volume of 108 mL of drawn blood was collected per donor in 9 mL Lithium Heparin tubes (Cat. no. 455084, Greiner Bio-One, Stonehouse, UK) and taken to the laboratory for processing within 1 hour.

For neonatal naïve CD4⁺ T cells studies, blood samples from the umbilical cords of healthy women delivering by elective Caesarean section, were collected into heparinated VacuettesTM and immediately taken to the laboratory for processing. All samples were collected with informed written consent and ethical approval was obtained from Wales Research Committee 6 (11/WA/0140).

2.1.4 Human Peripheral Blood Mononuclear Cell Isolation

Peripheral blood collected from healthy human donors was processed in a class 2 Biosafety cabinet under sterile conditions at the primary tissue culture laboratory, 2nd floor Institute of Life Science 1, Swansea University. Peripheral blood mononuclear cells were isolated from whole blood by density gradient centrifugation in 50 mL LeucosepTM tubes (Cat. no. 227290, Greiner Bio-One) with Histopaque®-1077 Hybri-maxTM (Cat. no. H889, Sigma-Aldrich). Then, 15 mL of pre-warmed Histopaque was pipetted into a 50 mL LeucosepTM tube and centrifuged at 1000 x g for 30 seconds in order for the Histopaque to move to the bottom of the porous filter ready for separation. Subsequently, 12 mL of anti-coagulated blood was diluted in 20 mL pre-warmed PBS and gently mixed. Diluted blood was then carefully layered on top of the porous membrane of the LecosepTM tube. This process was repeated for all blood collected. Lecosep tubes were centrifuged at 800 x g for 15 minutes at RT with no brake to separate the blood components depending on their relative density to Histopaque. The top plasma layer was then removed by pipette to 0.5 cm above the buffy coat layer and discarded. The buffy coat lymphocyte layer containing mostly peripheral blood mononuclear cells (PBMCs) was transferred by pipette to a new 50 mL Corning® tube and the cell suspension washed with pre-warmed PBS (Lonza) up to 50 mL, gently mixed and centrifuged at 250 x g for 10 minutes at RT.

PBMCs were washed twice more by resuspending cells with 25 mL PBS and repeating the centrifugation step. Cells from all tubes were then combined and resuspended in 0.5% BSA in PBS, mixed well by pipette and volume recorded. An aliquot of 10 μ L was taken for cell counting. Typically, 10×10^7 to 30×10^7 PBMCs were isolated from donors.

2.1.5 Human T Lymphocyte Isolation by MACs

Human CD4⁺ T cells and naïve CD4⁺ T cells were isolated from washed PBMCs in 0.5% BSA in PBS buffer using the appropriate MACS[®] isolation kit and an AutoMACs Pro separator following the manufacturer's instruction. Pre-cooled buffers and beads volumes added were for the maximum 10^7 cells, for higher cell numbers volumes were scaled up. Cells were incubated and maintained at 2 to 8°C in a refrigerator or ice bath.

2.1.5.1 MACs Depletion protocol for isolating human naïve CD4⁺ T cells

Naïve CD4⁺ T cell isolation kit II, human (Cat. no. 130-094-131, Miltenyi Biotec) was used to negatively select naïve CD4⁺ T cells following the manufacturer's instructions. PBMCs suspension in 0.5% BSA in PBS buffer was pelleted by centrifugation at 515 x g at 4°C for 10 minutes then resuspended in 40 μ L buffer per 10^7 cells. Afterwards, 10 μ L of Naïve CD4⁺ T Cell Biotin-Antibody Cocktail II was added per 10^7 cells, mixed well by pipette and incubated in the refrigerator for 5 minutes. Afterwards, 30 μ L of buffer was added per 10^7 cells followed by 20 μ L of Naïve CD4⁺ T Cell MicroBead Cocktail II per 10^7 cells and mixed well by pipette. The suspension was incubated in the refrigerator for a further 10 minutes. Subsequently, cells were separated by magnetic cell separation with an AutoMAC[®] Pro separator with the "Depletes" program. The procedure magnetically labels CD8⁺, CD14⁺, CD15⁺, CD16⁺, CD19⁺, CD25⁺, CD34⁺, CD36⁺, CD45RO⁺, CD123⁺, TCR γ / δ ⁺, HLA-DR⁺ and CD23a⁺ cells and immobilises labelled cells in a magnetic column leaving unlabelled CD4⁺ and CD45RA⁺ cells to flow through the column. This provides a population of high purity unbound naïve CD4⁺ T cells. The unlabelled naïve CD4⁺ T cells were collected in the neg1 port while positive fractions were collected in the pos1 port. Cell fractions were pelleted by centrifugation at 515 x g at 4°C for 10 minutes and resuspended in X-Vivo-20 culture

media at the desired concentration. Typically, between 5×10^6 and 25×10^6 naïve CD4⁺ T cells were isolated from PBMCs.

2.1.5.2 MACs Depletion protocol for isolating human total CD4⁺ T cells

CD4⁺ T cell isolation kit, human (Cat. no. 130-096-533, Miltenyi Biotec) was used to negatively select total CD4⁺ T cells following the manufacturer's instructions. Naïve CD4⁺ T cells are T helper cells which have not yet encountered their corresponding antigen, total CD4⁺ T cells also include memory CD4⁺ T cells which are produced during a primary immune challenge. Memory CD4⁺ T cells persist and can be re-activated upon further antigen exposure. PBMCs suspension in 0.5% BSA in PBS buffer was pelleted by centrifugation at $515 \times g$ at 4°C for 10 minutes then resuspended in 40 µL buffer per 10^7 cells. Then, 10 µL of CD4⁺ T Cell Biotin-Antibody Cocktail was added per 10^7 cells, mixed well by pipette and incubated in the refrigerator for 5 minutes. Afterwards, 30 µL of buffer was added per 10^7 cells followed by 20 µL of CD4⁺ T Cell MicroBead Cocktail per 10^7 cells and mixed well by pipette. The suspension was incubated in the refrigerator for a further 10 minutes. Subsequently, cells were separated by magnetic cell separation with an AutoMAC[®] Pro separator with the “Depletes” program. The procedure magnetically labels CD8⁺, CD14⁺, CD15⁺, CD16⁺, CD19⁺, CD36⁺, CD56⁺, CD123⁺, TCRγ/δ⁺ and CD23a⁺ cells and immobilises labelled cells in a magnetic column leaving unlabelled CD4⁺ cells to flow through the column. The unlabelled CD4⁺ T cells were collected in the neg1 port while positive fractions were collected in the pos1 port. Cell fractions were pelleted by centrifugation at $515 \times g$ at 4°C for 10 minutes and resuspended in X-Vivo-20 culture media at the desired concentration.

2.1.6 Human T Lymphocyte Culture Conditions

2.1.6.1 Cell culture concentration and density

All studies with human CD4⁺ and naïve CD4⁺ T cells were performed *in vitro* in a humidified 37°C incubator maintained at 5% CO₂. Cell cultures were predominantly seeded at 2.5×10^6 cells per mL per cm² in CELLSTAR[®] tissue culture plates (Greiner Bio-One) following the seed volumes in Table 2.2 unless otherwise stated.

Table 2.2 Cell culture plate sizes according to cell density for seeding CD4⁺ T cells.

Cells seeded	Total media volume	Culture plate	Catalogue number
0.75 x 10 ⁶	0.3 mL	96 well plate	655180
2.5 x 10 ⁶	1.0 mL	48 well plate	677180
5.0 x 10 ⁶	2.0 mL	24 well plate	662160
10 x 10 ⁶	4.0 mL	12 well plate	665180

2.1.6.2 Activation of CD4⁺ T cells

Activation of human CD4⁺ T cells was achieved by stimulation with anti-human CD3 and anti-human CD28 loaded MACSiBeads (Miltenyi Biotec) or alternatively with LEAF™ Purified anti-human CD3 and anti-human CD28 Antibodies (BioLegend, London, UK).

2.1.6.2.1 Antibody loading of iMACS Beads

Human CD4⁺ T cells were stimulated with anti-human CD3 and anti-human CD28 loaded MACSiBeads from Miltenyi Biotec T cell Activation/ Expansion kit, human, unless otherwise stated. Firstly, 100 µL anti- CD3-Biotin and 100 µL anti-CD28-Biotin were combined in a 2 mL centrifuge tube and mixed well. Anti-Biotin MACSiBeads were thoroughly resuspended and 500 µL added to the antibody mix. The final volume was adjusted to 1 mL with the addition of 300 µL loading buffer comprising 0.5% BSA in PBS, 2 mM EDTA-Na₂ (Cat. no. E4844, Sigma-Aldrich).

2.1.6.2.2 Activation of CD4⁺ T cells with iMACs beads

CD4⁺ T cells were activated *in vitro* using anti-CD3 and anti-CD28 loaded MACSiBeads, unless otherwise stated. Loaded beads were added to cell cultures at a 1:1.5 bead-to-cell ratio where 7 µL of loaded beads were used per million cells. The number of cells to be activated was determined and cells seeded in the appropriate tissue culture plate. MACSiBeads were thoroughly resuspended by vortex and the required volume of MACSiBeads were transferred to a centrifuge tube with 300 µL of X-Vivo-20 media and mixed well. MACSiBeads were centrifuged at 300 x g for 5 minutes and the supernatant discarded. The pelleted beads were resuspended in 50 µL X-Vivo-20 media and then added to the seeded cells to be activated and mixed well. For non-activated control samples, cells were cultured in X-Vivo-20 media without beads.

2.1.6.2.3 Activation of CD4⁺ T cells with LEAFTM Purified anti-human CD3 coated culture plates

LEAFTM Purified anti-human CD3 and CD28 antibodies were used as an alternative method of CD4⁺ T cell activation. Briefly, 10 µg/mL LEAFTM anti-human CD3 antibodies were prepared in sterile PBS (Lonza) and 300 µL added to CELLSTAR[®] tissue culture well plates. Plates were sealed and incubated at 4°C overnight or alternatively where indicate plates were incubated at 37°C for 2 hours. Afterwards, the supernatant was removed and the anti-CD3 coated wells were washed with sterile PBS. This was repeated a further two times. Subsequently, isolated cells were seeded at the required density in the anti-CD3 coated plate. 200 µg/mL LEAFTM anti-human CD28 was prepared in X-Vivo-20 media and 100 µL added to the seeded cells and mixed well by pipette.

2.1.7 Mouse CD4⁺ T Lymphocyte Isolation by MACs

Mouse naïve CD4⁺ T cells were isolated from washed splenocytes in 0.5% BSA in PBS buffer with MACS[®] Naïve CD4⁺ T cell isolation kit, mouse (Miltenyi Biotec , Cat. no. 130-104-453) and an AutoMACs Pro separator following the manufacturer's instruction. Pre-cooled buffers and bead volumes added were for the maximum 10⁷ cells, for higher cell numbers volumes were scaled up. Cells were incubated and maintained at 2 to 8°C in a refrigerator or ice bath.

2.1.7.1 MACs Depletion protocol for isolating mouse naïve CD4⁺ T cells

Naïve CD4⁺ T cell isolation kit II, mouse (Cat. no. 130-104-453, Miltenyi Biotec) was used to negatively select naïve CD4⁺ T cells from splenocytes harvested by collaborator Tina Raselli, University Hospital Zurich following the manufacturer's instructions. A Splenocyte suspension in 0.5% BSA in PBS buffer was pelleted by centrifugation at 515 x g at 4°C for 10 minutes then resuspended in 40 µL buffer per 10⁷ cells. Then, 10 µL of Biotin-Antibody Cocktail was added per 10⁷ cells, mixed well by pipette and incubated in the refrigerator for 5 minutes. Afterwards, 20 µL of buffer and 20 µL Anti-Biotin MicroBeads was added per 10⁷ cells followed by 10 µL of CD44 MicroBeads per 10⁷ cells and mixed well by pipette. The suspension was incubated in the refrigerator for a further 10 minutes. Afterwards, cells were washed by adding 2 mL buffer per 10⁸ cells and centrifuged at 300 x g for 10 minutes. Supernatant was discarded and cells resuspended in 500 µL buffer for up to 10⁸ cells. Subsequently, cells were separated by magnetic cell separation with an AutoMAC[®]

Pro separator with the “Depletes” program. The procedure magnetically labels CD8⁺, CD11b⁺, CD11c⁺, CD19⁺, CD25⁺, CD45R⁺, CD49b⁺, CD105⁺, Anti-MHC class II, Ter-119⁺ and TCR γ/δ ⁺ cells and immobilises labelled cells in a magnetic column leaving unlabelled naïve CD4⁺ cells to flow through the column. The unlabelled naïve CD4⁺ T cells were collected in the neg1 port while positive fractions were collected in the pos1 port. Cell fractions were pelleted by centrifugation at 515 x g at 4°C for 10 minutes and resuspended in X-Vivo-20 culture media at the desired concentration.

2.1.8 Mouse T Lymphocyte Culture Conditions

2.1.8.1 Cell culture concentration and density

Studies of mouse naïve CD4⁺T cells were performed *in vitro* in a humidified 37°C incubator maintained at 5% CO₂. Cell cultures were seeded at 1.5 x 10⁶ cells per mL per cm² in CELLSTAR[®] tissue culture plates (Greiner Bio-One).

2.1.8.2 Antibody loading of iMACs Beads

Mouse naïve CD4⁺ T cells were stimulated with anti-mouse CD3 and anti-mouse CD28 loaded MACSiBeads from Miltenyi Biotec T cell Activation/ Expansion kit, mouse (Cat. no. 130-093-627). Firstly, 100 μ L anti- CD3-Biotin and 100 μ L anti-CD28-Biotin were combined in a 2 mL centrifuge tube and mixed well. Anti-Biotin MACSiBeads were thoroughly resuspended and 500 μ L added to the antibody mix. The final volume was adjusted to 1 mL with the addition of 300 μ L loading buffer comprising 0.5% BSA in PBS, 2 mM EDTA (Cat. no. E4844, Sigma-Aldrich).

2.1.8.3 Activation of mouse CD4⁺ T cells with iMACs Beads

Naïve CD4⁺ T cells were activated *in vitro* using anti-CD3 and anti-CD28 loaded MACSiBeads. Loaded beads were added to cell cultures at a 1.5:1 bead-to-cell ratio where 15 μ L of loaded beads were used per million cells. The number of cells to be activated was determined and cells seeded in the appropriate tissue culture plate. MACSiBeads were thoroughly resuspended by vortex and the required volume of MACSiBeads were transferred to a centrifuge tube with 500 μ L of X-Vivo-20 media and mixed well. MACSiBeads were centrifuged at 300 x g for 5 minutes and the supernatant discarded. The pelleted beads were resuspended in 50 μ L X-Vivo-20 media and then added to the seeded cells to be activated and mixed well. For non-activated control samples, cells were cultured in X-Vivo-20 media without beads.

2.1.9 EL4 Cell Culture Conditions

Murine Lymphoblast cell line EL4 was obtained from Sigma-Aldrich (Cat.no. 85023105). Cells were maintained in DMEM (Gibco, Cat.no. 41966-029) with 10% FBS (Invitrogen, Cat. no. 10106-169) media at 2×10^5 - 1×10^6 cells per mL in Corning® T-25 flasks in a humidified 37°C incubator maintained at 5% CO₂.

2.1.9.1 Cell culture concentration and density

Studies with EL4 cells were performed in a humidified 37°C incubator maintained at 5% CO₂. Cell cultures were predominantly seeded at 0.5×10^6 cells per mL in X-Vivo-20 media in CELLSTAR® tissue culture plates (Greiner Bio-One), unless otherwise stated.

2.1.9.2 Activation of EL4 cells

EL4 cells were stimulated with 50 ng/mL PMA (Sigma-Aldrich, Cat. no. P1585) and 1 µg/mL ionomycin (Sigma-Aldrich, Cat. no. 10634). Briefly, PMA and ionomycin was prepared at 20X in culture media. EL4 cells were seeded at 0.5×10^6 cells per mL in CELLSTAR® tissue culture plates unless otherwise stated. 100 µL of 20X PMA and ionomycin was added to seeded cells to give a total volume of 2 mL and mixed well by pipette. Non-activated control samples were cultured in culture media without the addition of PMA and ionomycin.

2.1.10 Cell Cryopreservation, Storage and Recovery

Cells to be preserved for long term storage were washed and pelleted by centrifuging at 125 x g at RT for 10 minutes. Afterwards, cells were resuspended in FBS with 10% DMSO (Sigma-Aldrich, Cat. no. D2650) at 3×10^6 cells per mL and transferred to 2 mL Cryo. S™ cryovials (Greiner Bio-One, Cat. no. 122263). Vials were incubated overnight in a Nalgene® Mr. Frosty isopropanol-lined freezing container (Sigma-Aldrich, Cat. no. C1562) in a -80°C freezer to achieve the cooling rate of -1°C/min. Subsequently, vials were transferred to the liquid phase of a nitrogen cryogenic Dewar.

To recover cells, cryovials were thawed by submerging in a 37°C water bath for approximately 2 minutes before transferring to pre-warmed culture media. Cells were pelleted by centrifuging at 125 x g at RT for 10 minutes and further washed in pre warmed media. The cell number was determined and cells were resuspended at the appropriate concentration prior to seeding.

2.1.11 Cell Counting and Cell Viability Assay

Cell Viability was determined with Trypan Blue exclusion by microscopy or 7-AAD staining by flow cytometry.

2.1.11.1 Cell counting and Trypan blue exclusion by microscopy

Cell concentration was determined by manual counting with a C-Chip disposable haemocytometer (Labtech International Ltd. Cat. no. DHC-N01). To determine cell viability, a Trypan blue assay was performed. An aliquot of cells was diluted with Trypan blue solution (Sigma-Aldrich, Cat. no. 93595) and mixed well. A 10 μ L aliquot was pipetted into a C-Chip haemocytometer chamber and cells counted under a microscope. Cells inside a 5x5 square of the chamber grid, measuring 1mm x 1mm x 0.1mm, were counted including any cells touching the bottom and right border. This square represented $\times 10^4$ cells per mL which was then multiplied by the dilution factor to give the cell concentration. The percentage of non-viable cells was determined by dividing the number of trypan blue stained cells by the total number of cells and multiplying by 100.

2.1.11.2 7-Amino actinomycin D cell viability assay by flow cytometry

A 7AAD viability assay was used to determine the viability of cells prior to and after cell culture. To ascertain the proportion of non-viable cells, 5 μ L 7-AAD stain solution (eBioscience, Thermo Fisher Scientific, Cat. no. 00-6993-50) was added to 0.1×10^6 cells in 100 μ L FACs buffer comprised of 0.2% BSA, 0.05% (w/v) NaN_3 in PBS. Cells were incubated at 4°C for 5 minutes before analysis. The 7AAD dye was excited by a 488 nm blue laser and emission detected with the PerCP channel of a Novocyte flow cytometer (ACEA Biosciences), or alternatively, the PerCP-Cy5.5 channel on a BD FACS Aria flow cytometer (BD Biosciences) when indicated. Flow cytometry analysis was performed using FlowJo™ software (FlowJo LLC, Ashland, Oregon, USA).

2.1.12 T Lymphocyte Flow Cytometry Assay

2.1.12.1 Instrumentation and software packages

Flow cytometry analysis was primarily performed on a regularly calibrated ACEA Novocyte flow cytometer running NovoExpress 1.2.4 software (ACEA Biosciences) unless otherwise stated. Raw data was exported as FCS files and analysis was performed with FlowJo™ software version 10 (FlowJo LLC) kindly provided by Swansea University Medical School.

2.1.12.2 Flow cytometry staining reagents and buffers

Flow cytometry assays were performed using the required reagents listed in Table 2.3.

Table 2.3 Reagents and buffers required for flow cytometry analysis.

Reagent	Manufacturer	Catalogue number	Additional information
FACS Buffer	In house		0.2 µM sterile filtered 0.2% BSA, 0.05% NaN ₃ (w/v) in PBS
Ethylenediaminetetraacetic acid disodium salt (EDTA-Na₂)	Sigma-Aldrich	E4844	
7-Amino actinomycin D (7AAD)	Thermo Fisher Scientific	00-6993-50	5 µL per 100 µL cells
Cell Proliferation Dye eFlour® 450	Thermo Fisher Scientific	65-0842-85	Reconstituted in DMSO
FACS Tubes	VWR	391-0000	12 x 75 mm polypropylene 5 mL tubes

2.1.12.3 Flow cytometry fluorochrome conjugated antibodies

Monoclonal antibodies used for flow cytometry staining are listed in Table 2.4.

Table 2.4 Monoclonal antibodies used for flow cytometry assays

Antibody	Clone	Fluorochrome	Manufacturer	Catalogue number	Additional information
Anti-human CD4	OKT4	FITC	Thermo Fisher Scientific	11-0048-42	5 μ L per 100 μ L cells
Anti-human CD25	BC96	APC	Thermo Fisher Scientific	17-0259-42	5 μ L per 100 μ L cells
Anti-human CD45RA	HI100	PerCP-Cy5.5	Thermo Fisher Scientific	45-0458-42	5 μ L per 100 μ L cells
Anti-human CD45RA	HI100	eFluor [®] 450	Thermo Fisher Scientific	48-0458-42	5 μ L per 100 μ L cells
Anti-human CD45RO	UCHL1	PE-Cy7	Thermo Fisher Scientific	25-0457-42	5 μ L per 100 μ L cells
Anti-mouse CD4	GK1.5	eFluor [®] 450	Thermo Fisher Scientific	48-0041-80	1.2 μ L per 100 μ L cells
Anti-mouse CD25	PC61.5	APC	Thermo Fisher Scientific	17-0251-81	0.6 μ L per 100 μ L cells
Anti-mouse CD44	IM7	FITC	Thermo Fisher Scientific	11-0441-81	1 μ L per 100 μ L cells
Anti-mouse CD62L	MEL-14	APC	Thermo Fisher Scientific	17-0621-81	0.3 μ L per 100 μ L cells

2.1.12.4 Surface staining for flow cytometry analysis

Surface markers of isolated T cells were stained with monoclonal antibodies and analysed by flow cytometry to determine the surface expression of isolated cells, prior to and after cell culture. An aliquot of 0.1×10^6 cells washed in PBS was taken per stain and transferred to 5 mL polypropylene FACS tubes. Ice cold FACS buffer was added to tubes and samples incubated in the dark on ice for 30 minutes together with an unstained sample. Subsequently, samples were washed with 3 mL FACS buffer and centrifuged at $515 \times g$ at 4°C for 7 minutes. The supernatant was discarded and stained cells were resuspended in 100 μ L FACS buffer and kept on ice away from light before flow cytometry analysis.

2.2 Analysis of T Lymphocyte Gene and Protein Expression

2.2.1 Molecular Biology Materials

2.2.1.1 Reagents, instruments and kits

The reagents and kits used for qPCR and ELISA analysis are listed in Table 2.5.

Table 2.5 Reagent and kits used for qPCR and ELISA analysis

Reagent/ kit	Manufacturer	Catalogue number
RNeasy Mini Kit	Qiagen	74104
QuantiTect Reverse Transcription Kit	Qiagen	205313
QuantiFast SYBR Green	Qiagen	204056
TURBO DNA-<i>free</i>TM Kit	Thermo Fisher Scientific	AM1907
Tris-EDTA buffer	Sigma-Aldrich	93283
0.2 mL Flat Cap PCR Tubes	VWR	732-0548
96-Well Plates	Bio-Rad	MLL9601
Micoseal[®] B sealing film	Bio-Rad	MSB1001
21G 1.5” Needles	Fisher Scientific	12339299
1 mL Luer Syringe	Fisher Scientific	15489199
Tween[®] 20	Sigma-Aldrich	P7949
InvitrogenTM IL-17A Human Uncoated ELISA Kit	Fisher Scientific	15591067

2.2.1.2 Oligonucleotide Primers

The oligonucleotide primers used to determine mRNA expression are listed in Table 2.6.

Table 2.6 Human and mouse primers used for qRT-PCR.

Target Gene	Forward and Reverse Sequence 5' - 3'	Manufacturer	Reference
Human <i>RP18S</i>	GGACAGGATTGACAGATTGAT AGTCTCGTTCGTTATCGGAAT	Sigma-Aldrich	Studer et al. 2012 ⁽¹⁾
Human <i>ACTB</i>	GATGGCCACGGCTGCTTC TGCCTCAGGGCAGCGGAA	Sigma-Aldrich	Cronin et al. 2011 ⁽²⁾
Human <i>ABCA1</i>	GCACTGAGGAAGATGCTGAAA AGTTCCTGGAAGGTCTTGTTTCAC	Sigma-Aldrich	Kielar et al. 2001 ⁽³⁾
Human <i>ABCG1</i>	TGTTTCGCGGCCCTCAT CCTTCAGGCTGTACCAAGTAGTTC	Sigma-Aldrich	Antonson et al. 2008 ⁽⁴⁾
Human <i>CD25</i>	GGACTGCTCACGTTTCATCATGG GCTTTGAATGTGGCGTGTGG	Sigma-Aldrich	Herrmann et al. 2014 ⁽⁵⁾
Human <i>CYP7B1</i>	GTCCTACATGGTGACCCTGA CATTTGCTGGTTCCAGTTCC	Sigma-Aldrich	Steckelbroek et al. 2002 ⁽⁶⁾
Human <i>FOXP3</i>	TGACCAAGGCTTCATCTGTG GAGGAACTCTGGGAATGTGC	Sigma-Aldrich	Huang et al. 2013 ⁽⁷⁾
Human <i>HMGCR</i>	GACGTGAACCTATGCTGGTCAG GGTATCTGTTTCAGCCACTAAGG	Sigma-Aldrich	Cai et al. 2014 ⁽⁸⁾
Human <i>IL4</i>	AACAGCCTCACAGAGCAGAAGAC GCCCTGCAGAAGGTTTCCTT	Sigma-Aldrich	Boeuf et al. 2005 ⁽⁹⁾
Human <i>IL10</i>	GGCGCTGTCATCGATTTCTT GGCTTTGTAGATGCCTTTCTCTTG	Sigma-Aldrich	François et al. 2012 ⁽¹⁰⁾
Human <i>IL17A</i>	ACCAATCCCAAAGGTCCTC GGGGACAGAGTTCATGTGGT	Sigma-Aldrich	Manel et al. 2008 ⁽¹¹⁾
Human <i>IL22</i>	GAGCGCTGCTATCTGATGAA GCACCACCTCCTGCATATAA	Sigma-Aldrich	Chellan et al. 2014 ⁽¹²⁾
Human <i>IL23R</i>	CATGACTTGACCTGGAATG GCTTGGACCCAAACCAAGTA	Sigma-Aldrich	Manel et al. 2008 ⁽¹¹⁾
Human <i>IFNG</i>	GGCTTTTCAGCTCTGCATCG TCTGTCACTCTCCTCTTTCCAA	Sigma-Aldrich	Shi et al. 2014 ⁽¹³⁾
Human <i>RORC</i>	TTTTCCGAGGATGAGATTGC CTTTCCACATGCTGGCTACA	Sigma-Aldrich	Manel et al. 2008 ⁽¹¹⁾
Mouse <i>Rp18s</i>	GTAACCCGTTGAACCCATT CCATCCAATCGGTAGTAGCG	Sigma-Aldrich	Chang et al. 2009 ⁽¹⁴⁾
Mouse <i>Cyp7b1</i>	TTCCTCCACTCATAACAATG CGTGCTTTTCTTCTTACCATC	Sigma-Aldrich	Yi et al. 2012 ⁽¹⁵⁾

Mouse <i>Il17a</i>	CTCCAGAAGGCCCTCAGACTAC AGCTTTCCTCCGCATTGACACAG	Sigma-Aldrich	Ivanov et al. 2006 ⁽¹⁶⁾
------------------------------	---	---------------	---------------------------------------

2.2.2 Relative Gene Expression Analysis by qRT-PCR

2.2.2.1 Isolation of total mRNA

Following T cell culture, cells were washed in PBS and counted before centrifuging at 300 x g for 10 minutes. mRNA was isolated from cell pellets using RNase-free consumables and Qiagen RNeasy kit following the manufacturers guidelines, 350 µL of Lysis buffer RLT was added to cell pellets and mixed well. Lysates were homogenised with a 21 gauge needle and 1 mL syringe, drawing the lysate through the needle 10 times. Then, 350 µL of 70% EtOH was added to the homogenised lysate and mixed well. The total volume was transferred to an RNeasy spin column placed in a 2 mL collection tube and centrifuged at 11,000 x g for 15 seconds. The flow through was discarded, 700 µL of wash buffer RW1 was added to the spin column and the centrifugation step was repeated. The spin column was then washed with 500 µL of buffer RPE and centrifuged at 11,000 x g for 15 seconds. A further 500 µL of buffer RPE was added to the spin column and samples were centrifuged at 11,000 x g for 2 minutes. Afterwards, the spin column was transferred to a new 2 mL collection tube and centrifuged at 13,000 x g for 1 minute removing the remaining RPE buffer. The spin column was transferred to a 1.5 mL collection tube and RNA was eluted by pipetting 40 µL of RNase-free water directly onto the spin column membrane and centrifuging at 11,000 x g for 1 minute. The eluate was collected and the elution step was repeated. The eluted RNA was kept on ice or stored at -80°C.

The nucleic acid concentration and quality of the eluted RNA was determined with a NanoDropTM 8000 Spectrophotometer (Thermo Fisher Scientific).

2.2.2.2 Elimination of genomic DNA by DNase digestion

When indicated, prior to cDNA synthesis, RNA was purified by removing any DNA contamination with a TURBO DNA-freeTM kit following the manufacturer's guidelines. RNA was diluted to 20 µL with RNase-free water in PCR tubes and 2 µL TURBO DNase buffer was added to tubes with 1 µL TURBO DNase. Samples were

gently mixed and incubated at 37°C for 30 minutes. DNase inactivation reagent was resuspended and 2 µL was added to tubes and mixed well and incubated at RT for 5 minutes. Tubes were periodically mixed during the incubation to disperse the DNase inactivation reagent. Afterwards, tubes were centrifuged at 10,000 x g for 1.5 minutes to pellet the DNase inactivation reagent and the RNA was transferred to a new PCR tube. The TURBO DNase treated RNA was kept on ice or stored at -80°C

2.2.2.3 Complementary DNA synthesis

When indicated, either mRNA from *section 2.2.2.1* or TURBO™ treated mRNA from *section 2.2.2.2* was used to synthesis cDNA. TURBO™ DNase treatment was used to eliminate any possible DNA contaminants.

2.2.2.3.1 cDNA synthesis from RNA

cDNA was synthesised from RNA using Qiagen QuantiTect Reverse Transcription Kit following the manufacturer's guidelines. Firstly, samples which did not undergo TURBO™ DNase treatment a genomic DNA elimination reaction was prepared on ice with 1000 µg of template RNA in 200 µL PCR tubes. Template RNA was diluted to a final volume of 12 µL with RNA-free water and 2 µL of 7X gDNA Wipeout buffer was added. Tubes were gently mixed and incubated at 42°C for 5 minutes in a T100™ Thermal cycler (Cat. no. 1861096, Bio-Rad, Hemel Hempstead, UK). In parallel, a second set of tubes was set up for control samples in which no reverse transcriptase enzyme was added to tubes, referred to as 'no RT' when required. A master mix was prepared on ice with 4 µL 5X Quantiscript RT buffer, 1 µL Primer mix and 1 µL Quantiscript Reverse Transcriptase per sample and mixed well. A second no RT master mix was prepared in which the Quantiscript Reserve Transcriptase was replaced with 1 µL RNase-free water per sample. Then, 6 µL of the master mix was added to sample tubes and mixed well to give a total volume of 20 µL. All reaction tubes were incubated at 42°C for 15 minutes followed by 3 minutes at 95°C on a T100™ Thermal cycler. cDNA synthesised was stored at -20°C.

2.2.2.3.2 cDNA synthesis from TURBO DNase treated RNA

cDNA was synthesised from TURBO DNase treated RNA using Qiagen QuantiTect Reverse Transcription Kit following the manufacturer's guidelines. Firstly, the genomic DNA elimination reaction was prepared on ice with 4 µL of template RNA

in 200 μ L PCR tubes. Then, 8 μ L of RNase-free water was added to template RNA to give a final volume of 12 μ L. Afterwards, 2 μ L of 7X gDNA Wipeout buffer was added and PCR tubes were gently mixed and incubated at 42°C for 5 minutes in a T100™ Thermal cycler (Cat. no. 1861096, Bio-Rad, Hemel Hempstead, UK). In parallel, a second set of tubes was set up for control samples in which no reverse transcriptase enzyme was added to the tubes, referred to as 'no RT' when required. A master mix was prepared on ice with 4 μ L 5x Quantiscript RT buffer, 1 μ L Primer mix and 1 μ L Quantiscript Reverse Transcriptase per sample and mixed well. A second no RT master mix was prepared in which the Quantiscript Reserve Transcriptase was replaced with 1 μ L RNase-free water per sample. Then, 6 μ L of the master mix was added to sample tubes and mixed well to give a total volume of 20 μ L. All reaction tubes were incubated at 42°C for 15 minutes followed by 3 minutes at 95°C on a T100™ Thermal cycler. cDNA synthesised was stored at -20°C.

2.2.2.4 Primer reconstitution and preparation

Oligonucleotides purchased from Sigma-Aldrich were reconstituted in Tris-EDTA (TE) buffer at 100 μ M following suppliers instructions. Aliquots of forward and reverse were diluted 1:1 for a combined forward and reverse primer mix. Reconstituted primers were stored at -20°C in DNase and RNase-free tubes.

2.2.2.5 Real time Quantitative Reverse Transcription Polymerase Chain Reaction

Relative mRNA expression of cell cultures was determined by qRT-PCR using QuantiFast SYBR Green Kit. Synthesised cDNA was diluted 1:10 in RNase-free water. A reaction master mix was prepared for each gene of interested with 12.5 μ L of 2X QuantiFast SYBR green, 0.25 μ L 50 μ M combined forward and reverse primers and 7.25 μ L RNase-free water per PCR reaction and mixed well. Then, 5 μ L diluted cDNA was added to 96-well PCR plates in triplicates followed by 20 μ L of the gene of interest master mix to give a total volume of 25 μ L per well. Plates were seal with Microseal® B sealing film and centrifuges at 1000 x g for 1 minute. The qPCR reaction was performed on a CFX Connect™ Real-Time PCR Detection System (Cat. no. 1855200, Bio-Rad). The protocol followed was: A PCR initial activation step at 95°C for 5 minutes followed by a two-step cycling of denaturing at

95°C for 10 seconds and combined annealing and extension step at 60°C for 30 seconds. Fluorescence data was collected and the denaturing and annealing/extension steps were repeated 44 times. Melt curve analysis was performed by cooling to 55°C for 5 seconds and increasing the temperature to 95°C at increments of 0.5°C every 5 seconds.

2.2.2.6 Quantitative PCR analysis

Data acquired from the CFX Connect™ Real-Time PCR Detection System was analysed with version 3.1 Bio-Rad CRF Manager software. Alternatively, data was exported to Microsoft Excel 2013 and manually analysed with the $2^{-\Delta\Delta Ct}$ method⁽¹⁷⁾. The mean value (\bar{x}) for the cycle threshold (Ct) was calculated from replicate wells. Equation 2.1 was used to calculate the difference in cycle threshold (ΔCt) between the target gene and housekeeping gene. The difference between the control sample ΔCt and the experimental sample ΔCt was measured as $\Delta\Delta Ct$ as shown in Equation 2.2. The relative expression level of a gene for the control and experimental samples was determined using Equation 2.3. Comparison of gene expression between control and experimental samples was expressed as the relative fold change to the control sample. Any outliers were identified using the melt curve analysis using the CFX Manager software and omitted from analysis.

Equation 2.1 Formula for calculation of the cycle threshold difference (ΔCt) of the target gene from the housekeeping gene

$$\Delta Ct = \bar{x} \text{ target gene } Ct - \bar{x} \text{ housekeeping gene } Ct$$

Equation 2.2 Formula for the calculation of the cycle threshold difference between experimental sample ΔCt and control sample ΔCt

$$\Delta\Delta Ct = \text{experimental sample } \Delta Ct - \text{control sample } \Delta Ct$$

Equation 2.3 Formula for the calculation of relative expression of target genes expressed as fold change

$$\text{fold change} = 2^{-(\Delta\Delta Ct)}$$

2.2.3 Soluble IL-17 Detection and Quantification by Immunoassay

Protein expression of T cell cultures was measured by plate bound sandwich enzyme-linked immunosorbent assay (ELISA) of cell culture media.

2.2.3.1 Measurement of soluble IL-17 produced by CD4⁺ T cells by sandwich ELISA

IL-17A cytokine expression of Human T cell cultures was determined by sandwich ELISA of cell culture media with Invitrogen™ IL-17A (homodimer) Human Uncoated ELISA Kit following the manufacturers guidelines. Firstly, 1X coating buffer was prepared by diluting 10X PBS 1:10 in deionised water. The capture antibody was diluted 1:250 with 1X coating buffer and 100 µL was added to each well of a Corning Costar 96-well plate. The plate was sealed with Microseal® B sealing film and incubated at 4°C overnight. The 96-well plate was aspirated and washed three times with ≥ 250 µL 1X PBS, 0.05% Tween®-20 wash buffer. Then, 1X ELISA diluent was prepared by diluting 1:5 in deionised water and 200 µL was added to block wells. Plates were incubated at RT for 1 hour. During incubation, IL-17A standard was reconstituted with ELISA diluent to give 500 pg/mL and an 8-point 2-fold serial dilution was performed with ELISA diluent to give 250, 125, 62.5, 31.25, 15.6, 7.8 ng/mL and blank. When required media samples were also diluted 1:2 with ELISA diluent. Following incubation wells were aspirated and washed three times with ≥ 250 µL wash buffer. Plates were blot dried with absorbent paper and 100 µL of standard or sample was added to wells in duplicates. Plates were sealed and incubated at RT for 2 hours. During incubation, 1X detection antibody was prepared by diluting 1:250 with ELISA diluent. Following incubation, plates were washed 5 times with wash buffer and blot dried. 100 µL of 1X detection antibody was added to wells and plates were sealed and incubated at RT for 1 hour. During incubation, Avidin-HRP was prepared at 1X from 250X by 1:250 dilution with ELISA diluent. Following incubation, plates were washed 5 times with wash buffer and blot dried. Then, 100 µL of Avidin-HRP was added to wells and plates were sealed and incubated at RT for 30 minutes. Following incubation, plates were washed 7 times with wash buffer and blot dried. Afterwards, 100 µL of TMB substrate was added to wells and plates were incubated at RT for 15 minutes in the dark. The reaction was stopped by adding 50 µL 1M H₃PO₄ to wells and plates were

read on a POLARstar OMEGA plate reader (BMG-LABTECH, Aylesbury, UK) at 450 nm and 570 nm.

2.2.3.2 Data analysis for sandwich ELISA

Optical density (OD) values at 450 nm and 570 nm were analysed using MARS data analysis software from BMG-LABTECH. Alternatively, raw data was exported to Microsoft Excel for manual analysis. The 570 nm OD values were subtracted from the 450 nm OD values. The average OD value of blank wells was subtracted from average sample and standard OD values and then fitted on a linear regression curve against standard concentration to generate a linear equation. The slope and intercept point of the equation was used to calculate the concentration of IL-17A in the sample expressed as ng/mL.

2.3 Sterol Analysis by Liquid Chromatography Mass Spectrometry

2.3.1 Sterol Analysis Materials

2.3.1.1 Sample preparation, chromatographic separation materials and solvents

Solvents and materials required for sterol analysis are listed in Table 2.7.

Table 2.7 Materials and solvents required for sterol analysis by mass spectrometry

Reagent	Manufacturer	Catalogue number	Additional information
Methanol (MeOH)	Fisher Scientific	10675112	HPLC grade
Acetonitrile (MeCN)	Fisher Scientific	10407440	HPLC grade
Isopropanol (IPA)	Fisher Scientific	10674732	HPLC grade
Ethanol (EtOH)	Fisher Scientific	10437341	Absolute, analytical grade
Water	Fisher Scientific	10449380	HPLC grade
Glacial Acetic acid	VWR	20104.334	AnalaR [®] NORMAPUR [®] grade
Formic acid	VWR	20318.297	AnalaR [®] NORMAPUR [®] grade
Hydrochloric acid	Sigma-Aldrich	H1758	
Sodium Hydroxide	Sigma-Aldrich	S5881	
Potassium Hydroxide	Sigma-Aldrich	P5958	
Potassium phosphate, monobasic (KH₂PO₄)	Sigma-Aldrich	P9791	
Cholesterol oxidase	Sigma-Aldrich	C8649	From <i>Streptomyces sp.</i> Lyophilized powder ≥20 units/mg protein
Girard's Reagent P	Tokyo Chemical Industry (TCI) Europe	G0030	[1-(Carboxymethyl)-pyridinium chloride hydrazide]
Sep-Pak[®] Cert tC18 200 mg 3cc	Waters	186004618	For SPE1
OASIS[®] HLB 60 mg 3cc	Waters	WAT094226	For SPE2
Hypersil GoldTM RP column	Thermo Fisher Scientific	25002-052130	1.9 μM particle size 50 x 2.1 mm
1.5 mL centrifuge tubes	STARLAB	S1615-5500	
2.0 mL EppendorfTM centrifuge tubes	Fisher Scientific	10038760	
12 mL Round-bottom polypropylene tubes	Greiner Bio-One	163270	
15 mL CorningTM polypropylene tubes	Fisher Scientific	10431013	
50 mL CorningTM polypropylene tubes	Fisher Scientific	10038980	
5 mL Luer-Lock syringe	Fisher Scientific	10038980	
300μL HPLC vials	Waters	186002639	
LTQ ESI Positive calibration solution	Fisher Scientific	11340360	
FlexMixTM calibration solution	Fisher Scientific	15988796	

2.3.1.2 Sterol standards and preparation

The relative quantities of endogenous sterols were established using stable isotope dilutions with LC-MS. Authentic deuterium labelled sterol standards including 24 (*R/S*)-[26,26,26,27,27,27-²H₆] Hydroxycholesterol (Cat. no. 700049P), 22*R*-[25,26,26,26,27,27,27] Hydroxycholesterol (Cat. no. 700052P) and [25,26,26,26,27,27,27-²H₇] Cholesterol (Cat. no. 700041P) were obtained from Avanti Polar Lipids, Inc. (Alabaster, Alabama, USA). A combined standard stock was prepared in EtOH from 24 (*R/S*)-[26,26,26,27,27,27-²H₆] Hydroxycholesterol, [25,26,26,26,27,27,27-²H₇] Cholesterol and [²H₇]-Cholest-4-ene-3-oxo,22(*R*)-ol, an oxidised derivative of [²H₇]-Cholest-5-ene-3β,22(*R*)-diol from an in house stock, unless otherwise stated. Prior to sterol extraction, the combined stock of 1 µg/mL 24(*R/S*)-HC(D6), 1 µg/mL 22(*R*)-3-oxo-HC(D7) and 200 µg/mL Cholesterol-D7 was diluted 1:500 with EtOH and 1 mL added to samples. Alternatively, for hydrolysed cell culture samples the combined stock was diluted 1:100 with MeOH and 200 µL added to samples.

2.3.2 Sample processing using Enzyme-Assisted Derivatisation for Sterol Analysis (EADSA)

After cell culture, cells were harvested by resuspending cells in culture media and transferring to centrifuge tubes. Cell suspensions were centrifuged at 300 x g for 10 minutes and the supernatant was transferred to 2 mL EppendorfTM tubes. Cell pellets were washed with PBS and counted before centrifuging at 300 x g for 10 minutes and supernatant discarded. Media was stored at -20°C and cell pellets at -80°C.

2.3.2.1 Extraction of endogenous free sterols from cell fractions

Cell pellets were loosened by gently flicking the tubes and placed in an ultrasonic bath. Then, 1 mL of sterol standard mix containing 2 ng 24(*R/S*)-HC(D6), 2 ng 22(*R*)-3-oxo-HC(D7) and 400 ng Cholesterol(D7) was added to samples drop-wise. Afterwards, 50 µL of EtOH was added to samples and samples were sonicated for a further 5 minutes. Following sonication, samples were centrifuged at 17,000 x g at 4°C for 30 minutes. The EtOH supernatant was transferred to a new tube and diluted to 70% EtOH with the addition of 400 µL of water for solid phase extraction.

2.3.2.2 Alkali hydrolysis and extraction of total sterols from cell fractions

Alkali hydrolysis with ethanolic 0.35 M KOH was performed in order to cleave any oxysterols with ester modifications. Cell pellets were loosened by gently flicking the tubes and placed in an ultrasonic bath. Then, 200 µL of sterol standard mix containing 2 ng 24(*R/S*)-HC(D6), 2 ng 22(*R*)-3-oxo-HC(D7) and 400 ng Cholesterol(D7) was added to samples drop-wise followed by 850 µL of 0.4324 M ethanolic KOH. Samples were sonicated for a further 5 minutes. Following sonication, samples were incubated at RT for 2 hours in the dark. In parallel, non-hydrolysed samples were processed by adding 200 µL of sterol standard mix containing 2 ng 24(*R/S*)-HC(D6), 2 ng 22(*R*)-3-oxo-HC(D7) and 400 ng Cholesterol(D7) to samples drop-wise followed by 850 µL of EtOH. After incubation, hydrolysed samples were neutralised by adding 400 µL of 6% HOAc in water while 400 µL of water was added to non-hydrolysed samples. Samples were placed in an ultrasonic bath and sonicated for 5 minutes. Following sonication samples were centrifuged at 17,000 x g at 4°C for 30 minutes. The EtOH supernatant was transferred to a new tube for solid phase extraction.

2.3.2.3 Extraction of endogenous free sterols from media fractions

Sterols were extracted from cell culture media at varying volumes up to 3 mL, 15 mL Corning® tubes containing 1 mL of sterol standard mix with 2 ng 24(*R/S*)-HC(D6), 2 ng 22(*R*)-3-oxo-HC(D7) and 400 ng Cholesterol(D7) were placed in an ultrasonic bath. An appropriate volume of EtOH, determined by the media volume, was added to tubes to give a final EtOH concentration of 70%. Media supernatant was added to the standard/ EtOH mix drop-wise and sonicated for a further 5 minutes. Following sonication, samples were centrifuged at 4,500 x g at 4°C for 1 hour. The supernatant was transferred to a new tube for solid phase extraction.

2.3.2.4 Alkali hydrolysis and extraction of total sterols from media fractions

Alkali hydrolysis with ethanolic 0.35 M KOH was performed in order to cleave any oxysterols with ester modifications, 2 mL Eppendorf™ tubes containing 200 µL of sterol standard mix containing 2 ng 24(*R/S*)-HC(D6), 2 ng 22(*R*)-3-oxo-HC(D7) and 400 ng Cholesterol(D7) were placed in an ultrasonic bath. Subsequently, 350 µL of cell culture media supernatant was added to tubes drop-wise followed by 850 µL of 0.4324 M ethanolic KOH. Samples were sonicated for a further 5 minutes. Following sonication, samples were incubated at RT for 2 hours in the dark. In

parallel, non-hydrolysed samples were processed by adding 350 μ L of cell culture media supernatant to 2 mL EppendorfTM tube containing 200 μ L of sterol standard mix with 2 ng 24(*R/S*)-HC(D6), 2 ng 22(*R*)-3-oxo-HC(D7) and 400 ng Cholesterol(D7) to samples drop-wise followed by 850 μ L of EtOH. After incubation, hydrolysed samples were neutralised by adding 100 μ L of 6% HOAc in water while 100 μ L of water was added to non-hydrolysed samples. Samples were placed in an ultrasonic bath and sonicated for 5 minutes. Following sonication samples were centrifuged at 17,000 x g at 4°C for 30 minutes. The supernatant was transferred to a new tube for solid phase extraction.

2.3.2.5 First Solid Phase Extraction (SPE1) to separate cholesterol and oxysterols

Cholesterol is liable to autoxidation and is typically found at 1000-fold higher concentrations to oxysterols. An initial reversed phase solid phase extraction (SPE1) was performed to separate cholesterol and oxysterol fractions to avoid any further cholesterol autoxidation which could misrepresent oxysterol levels and to obtain an enriched oxysterol sample for analysis. Firstly, Sep-Pak Cert tC18 200 mg 3cc cartridges were placed in a vacuum manifold (Agilent, Cheshire, UK, Cat. no. 5982-9120) and the sorbent beds were conditioned and solvated with 4 mL of absolute EtOH followed by 6 mL of 70% EtOH at ~0.25 mL/min or 1-2 drops per second. The flow rate was maintained with a vacuum pump through the manifold or positive pressure was applied using a 5 mL Luer-Lock syringe. The flow through was collected in 12 mL Greiner tubes and discarded. New 12 mL tubes were placed in the manifold and conditioned cartridges were loaded with samples at 70% EtOH. For cell pellet and hydrolysed extractions, the polar oxysterols were collected in the first flow through and column wash of 5.5 mL 70% EtOH referred to as Fraction 1 (Fr1). For the cell media extractions, the polar oxysterols were collected in the first flow through and column wash of 1 mL 70% EtOH. The columns were washed with a further 4 mL of 70% EtOH and collected as fraction 2 (Fr2). Cholesterol was eluted from the columns with 2 mL of absolute EtOH in fraction 3 (Fr3). A final 2 mL of absolute EtOH was added to the columns and collected as Fraction 4 (Fr4). Fr1 and Fr3 were then split equally into two new 12 mL Greiner tubes referred to as Fraction 1A (Fr1A), Fraction 1B (Fr1B), Fraction 3A (Fr3A) and Fraction 3B (Fr3B).

F2 and F4 were stored at -20°C while F1A, F1B, F3A and F3B were dried overnight in a Scanspeed vacuum Concentrator (Labgene).

2.3.2.6 Cholesterol oxidase treatment and charge-tagging with Girard's

Reagent P

In order to increase the ionisation efficiency and sensitivity for mass spectrometry analysis, a positive charge was introduced to oxysterols by the addition of GP hydrazine (Figure 2.5). The 3 β -OH group of A fractions was converted to a 3-oxo group with cholesterol oxidase ^(18,19). This enabled the reaction at the sterol 3C position with Girard Reagent P (GP) to form sterol-GP-hydrazones (Figure 2.4). Dried fractions from SPE1 in *section 2.3.2.5* were reconstituted in 100 μ L IPA and 1 mL of 50 mM KH₂PO₄, pH 7.0 was added to tubes and mixed well. Subsequently, 3 μ L of 2 μ g/ μ L cholesterol oxidase was added to the set 'A' fractions, while set 'B' fractions were left untreated. All tubes were mixed well and incubated in a water bath at 37°C for 1 hour to oxidise the 3 β -OH-5-ene group to a 3-oxo-4-ene group. Following incubation, 2 mL of 100% MeOH was added to all fractions to stop the reaction. Afterwards, 150 μ L of glacial acetic acid was added to tubes followed by 150mg of Girard Reagent P (GP) and mixed well. Tubes were incubated at RT overnight in the dark. Following incubation, 'A' fractions contained derivatised sterols from endogenous 3 β -OH and 3-oxo sterols, while 'B' fractions contained only derivatised sterols which were endogenous 3-oxo and underivatised 3 β -OH sterols.

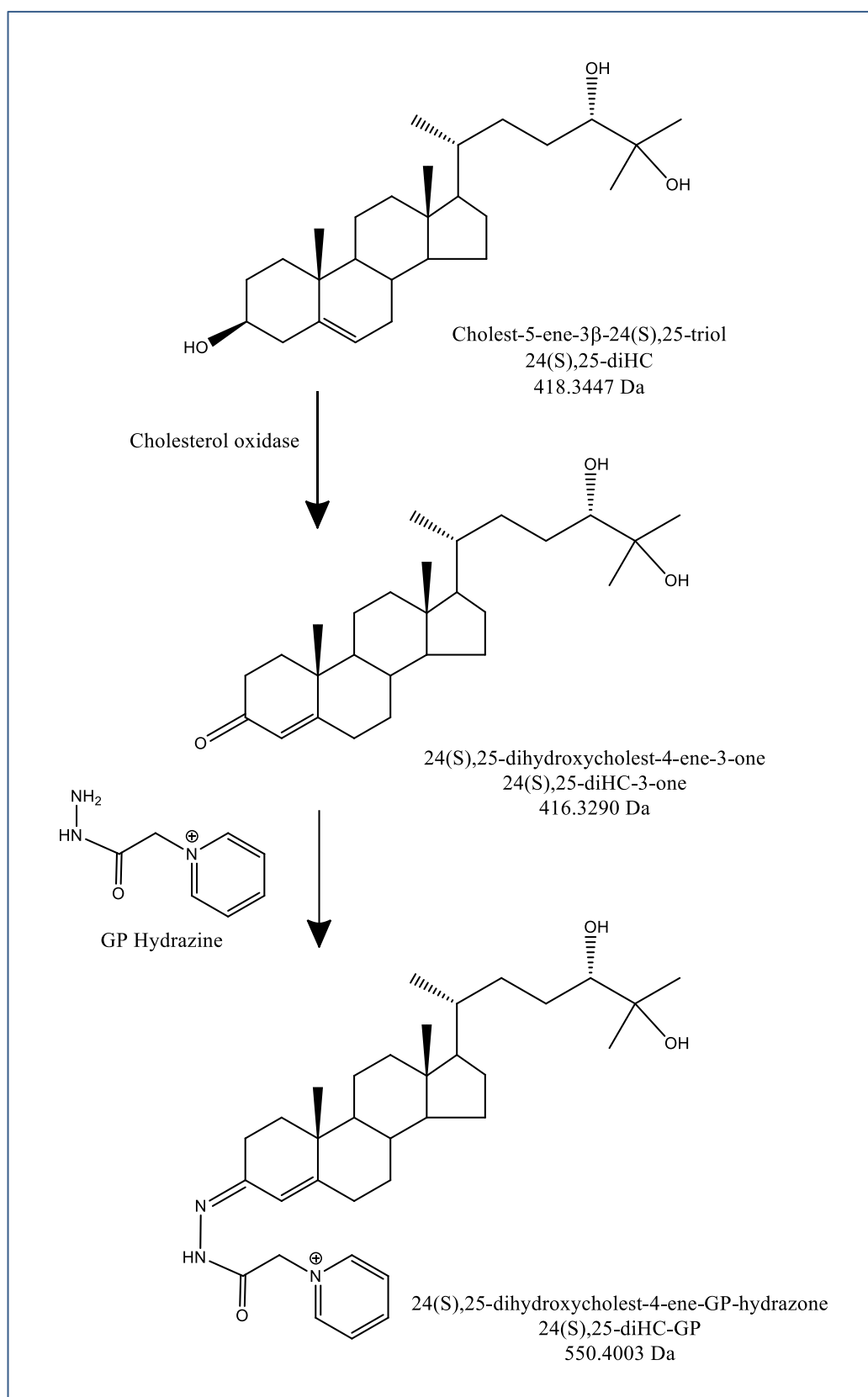


Figure 2.4 Charge-tagging of sterols with Girard Reagent P using cholesterol oxidase. Sterols from fractions 'A', here 24(*S*),25-diHC, were treated with cholesterol oxidase to convert the 3 β -hydroxy-5-ene group to a 3-oxo-4-ene group. The 3-oxo group was then derivatised with Girard Reagents P hydrazine to form a GP hydrazone. Sterols in fractions 'B' which endogenously contain a 3-oxo group were derivatised with GP without Cholesterol oxidase treatment.

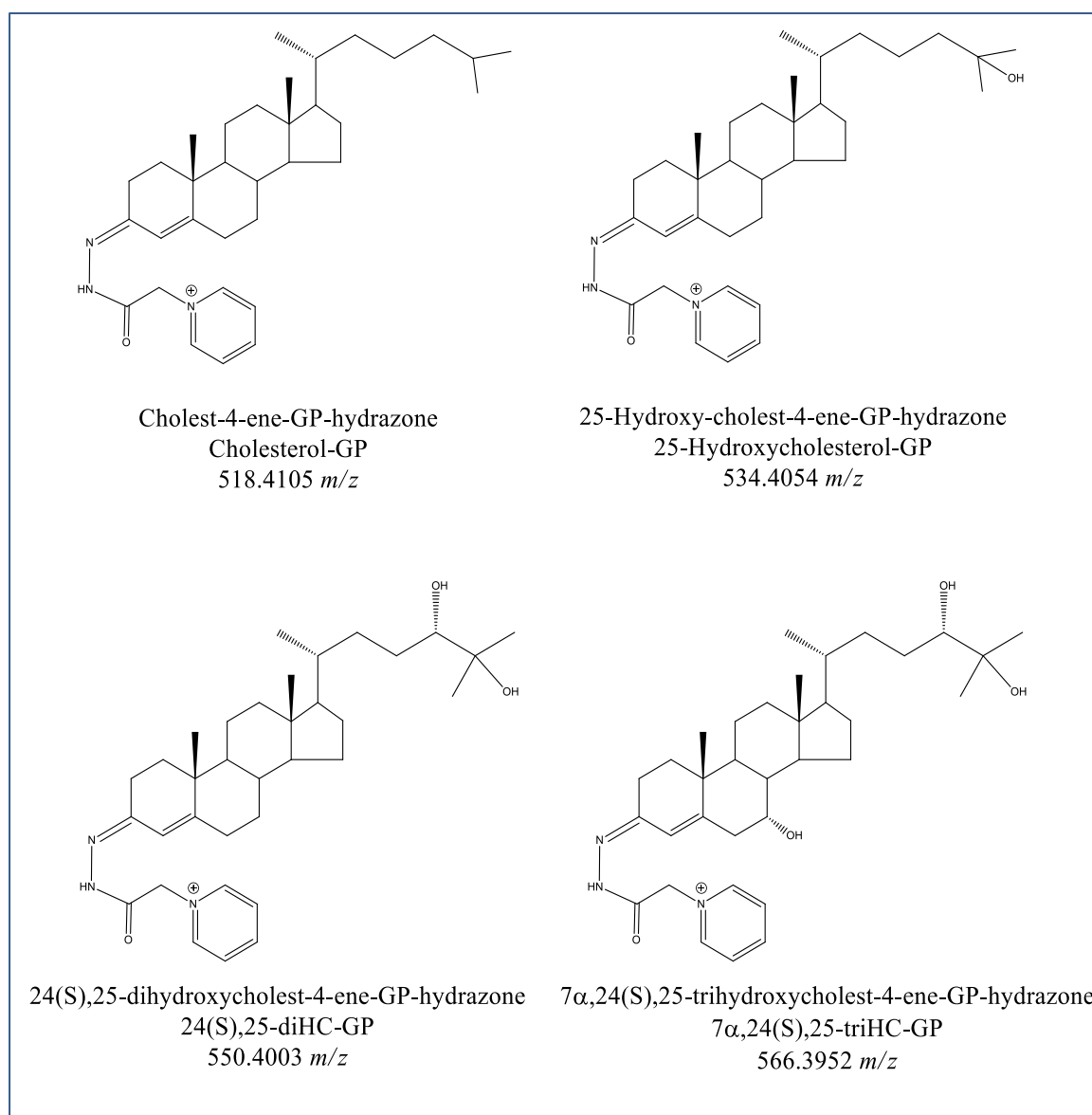


Figure 2.5 Sterols derivatised with Girard Reagent P (GP). A quaternary nitrogen is introduced by the GP which increased the ionisation efficiency and sensitivity for mass spectrometry analysis.

2.3.2.7 Second Solid Phase Extraction (SPE2) to remove excess derivatisation reagent and sample clean up

An excess of derivatisation reagent is required for the charge-tagging of sterols to drive a forward reaction. To remove the excess GP and any other impurities from charge-tagged sterols in *section 2.3.2.6*, a second reverse phased SPE was performed (SPE2). Firstly, Oasis[®] HLB 60 mg 3cc cartridges were placed in a vacuum manifold (Agilent). Cartridges were conditioned and solvated with 6 mL of 100% MeOH followed by 6 mL 10% MeOH and 4 mL 70% MeOH. Flow rate was maintained at ~0.25 mL/min or 1-2 drops per second with a vacuum pump through the manifold or positive pressure was applied using a 5 mL Luer-Lock syringe. Flow through was collected in a 12 mL Greiner tube and discarded. New 12 mL Greiner tubes were placed in the manifold and derivatised fractions of ~3.25 mL were loaded onto the HLB columns. For hydrolysed samples, prior to loading column, fractions were centrifuged at 4,500 x g at RT for 30 minutes and supernatant transferred to new tubes. Columns were washed with 1 mL of 70% MeOH followed by 1 mL 35% MeOH and collected with sample flow through. Subsequently, 4 mL of water was added to the collected flow through (~5mL) and mixed well before recycling back through the columns. The columns were washed with 1 mL 17% MeOH and flow through collected. The collected flow through (~10 mL) was diluted with 9 mL of water in a 50 mL Corning[®] tube and mixed well. A second recycling step was performed by applying the ~19 mL to the columns and flow through was discarded. Columns were washed with 6 mL of 10% MeOH and flow through was discarded. Subsequently, bound oxysterols were eluted in 4 fractions. FrA1, FrA2, and FrA3 were each eluted with 1 mL of 100% MeOH in 1.5 mL centrifuge tubes. Fr1A4 was eluted with 1 mL of absolute EtOH. This method was also applied to Fr1B, Fr3A and Fr3B. Samples were stored at -20°C.

2.3.3 Sample preparation prior to LC-ESI-MSⁿ analysis

Prior to LC-MSⁿ analysis of samples in *section 2.3.2.7* fractions were combined and diluted to 60% MeOH. Analysis of oxysterols was performed on Fr1A and Fr1B, while cholesterol and cholesterol precursor analysis was performed on Fr3A and Fr3B. Endogenous oxysterols with 3 β -hydroxy-5-ene or 3-oxo-4-ene groups were analysed in 'A' fractions, while only endogenous oxysterols which contained a 3-oxo-4-ene group could be analysed in 'B' fractions. In order to establish the amount

of sterols which originally contained a 3 β -hydroxy-5-ene group the measured sterol in 'B' was subtracted from 'A'.

2.3.3.1 Oxysterol fraction sample preparation for LC-MS

Oxysterol analysis was performed on 'A' fractions Fr1A1 and Fr1A2 and when indicated 'B' fractions Fr1B1 and Fr1B2, from SPE2 fractions in *section 2.3.2.7*. Fractions were centrifuged at 17,000 x g at 4°C for 30 minutes. Then, 90 μ L of F1A1 and 90 μ L of F1A2 were transferred from the top of fraction tubes into a 1.5 mL centrifuge tube and mixed well. Afterwards, 120 μ L of HPLC water was added to tubes to dilute samples to 60% MeOH with a total volume of 300 μ L. Samples were mixed well and 270 μ L was transferred to 300 μ L HPLC vials.

2.3.3.2 Cholesterol fraction sample preparation for LC-MS

Cholesterol analysis was performed on 'A' fractions F3A1, F3A2 and F3A3 from SPE fractions in *section 2.3.2.7*. Firstly, Fractions were centrifuged at 17,000 x g at 4°C for 30 minutes. Then, 7 μ L was taken from the top of Fr3A1, Fr3A2 and Fr3A3 and transferred to a 1.5 mL centrifuge tube, mixing well. The combined fractions were diluted 1:10 with 189 μ L of 100% MeOH and mixed well. Afterwards, 180 μ L of the diluted samples was transfer to a new 1.5 mL centrifuge tube and diluted to 60% MeOH with the addition of 120 μ L of HPLC water to give a total volume of 300 μ L. Samples were mixed well and 270 μ L was transferred to 300 μ L HPLC vials.

2.3.4 Sterol separation, Analysis and Quantification by HPLC-ESI-MSⁿ

2.3.4.1 Orbitrap Elite and ID-X calibration

Orbitrap Elite and Orbitrap ID-X were regularly maintained and calibrated to a mass accuracy of <5ppm using LTQ ESI positive calibration solution and FlexMixTM calibration solution respectively with semi-automatic calibration using Thermo TunePlus software.

2.3.4.2 HPLC-ESI-MSⁿ sterol analysis

Samples prepared in HPLC vials in *section 2.3.3.1 or 2.3.3.2* were loaded onto an autosampler maintained at 4°C and 90 μ L was injected to a Hypersil GOLD RP column through an UltiMate 3000 HPLC system for chromatographic separation. Two mobile phases were used for the separation gradient, phase A was composed of

33.3% MeOH, 16.7% MeCN, 50% Water, 0.1% formic acid, while phase B was 63.3% MeOH, 31.7% MeCN, 5% Water, 0.1% formic acid. Two experimental LC methods were used to achieve separation, a 17-minute LC method or 26-minute LC method; both were maintained at 200 $\mu\text{L}/\text{min}$ ⁽²⁰⁾. The 17-minute LC method started at 20% B for 1 minute before linearly increasing for 7 minutes to 80% B and was sustained at 80% B for 5 minutes. This was equilibrated back to 20% B in 6 seconds and sustained for 3.9 minutes (Figure 2.6A). The 26-minute LC method started at 20% B before linearly increasing for 10 minutes to 50% B and sustained at 50% B for 6 minutes. Then, 50% B was linearly increased for 3 minutes to 80% B which was sustained for 3 minutes before the gradient was equilibrated back to 20% B in 6 seconds and sustained for 3.9 minutes (Figure 2.6B). Eluate from the column was then directed to the electrospray ionisation source of an Orbitrap Elite or alternatively Orbitrap ID-X mass spectrometer running in positive ion mode. Samples were injected 2-3 times as technical replicates and a set of scan events performed for each injection.

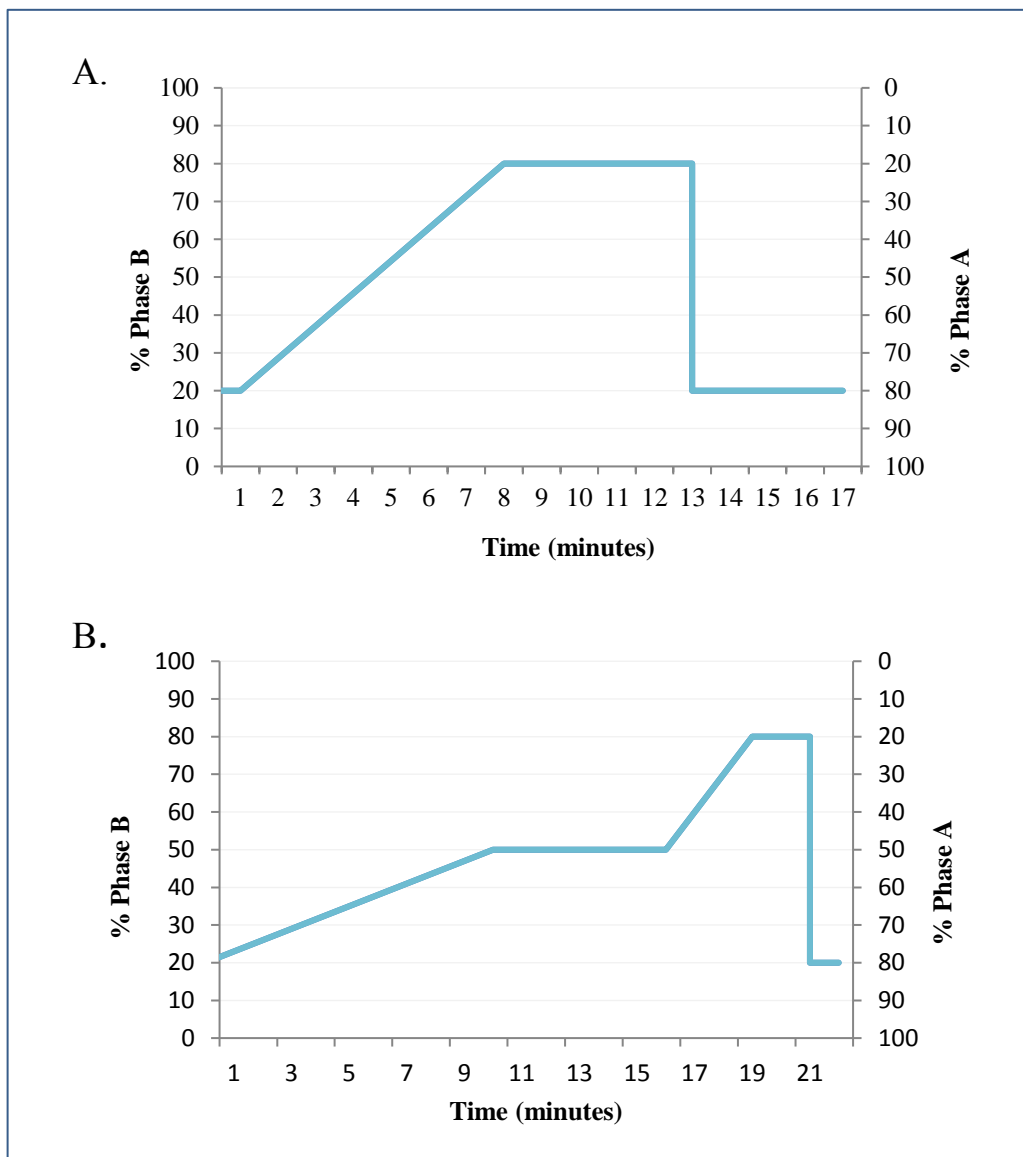


Figure 2.6 Multi-step gradients for separation of derivatised sterols by Liquid chromatography. Two LC experimental methods were used to separate derivatised sterols of the same m/z by liquid chromatography with two mobile phases. Mobile phases were maintained at 200 $\mu\text{L}/\text{min}$ and separation performed at multi-step gradients. (A) The 17-minute LC method. (B) The 26-minute LC method. The extended 26-minute gradient provided greater separation of structurally similar monohydroxycholesterols.

2.3.4.3 Scan events and parameters for MS and MS³

A full MS scan in profile mode was recorded on the Orbitrap analyser with the range of 400-610 m/z at 120,000 resolution. Subsequent multi-stage fragmentation scans in centroid mode were performed on the linear ion trap (LIT) to isolate monoisotopic precursor ions $[M]^+$ specific to the mass of GP-derivatised sterols (Figure 2.7). Precursor ions were fragmented at 30 eV CID collision energy for the first fragmentation event, MS². Daughter ions containing a predicted neutral loss of a pyridine ring at 79 m/z , $[M-79]^+$ were isolated in the LIT and fragmented a second time, MS³ at 35 eV CID collision energy for each precursor ⁽¹⁹⁾. MS³ fragments were detected and recorded using the LIT dynodes. For each cycle two to six fragmentation scans were performed while the Orbitrap recorded a full accurate mass scan.

2.3.4.4 Identification and quantification of chromatographically separated sterols

Selective analysis of GP-derivatised sterols was possible using MS³ fragmentation with the linear ion trap (LIT) which provides a distinct fragmentation pattern used to distinguish sterols. Authentic sterol standards subjected to EADSA and HPLC-ESI-MSⁿ have previously been analysed by former group members and a library compiled with expected chromatographic retention times and specific MS³ spectra for each authentic sterol. This library was used together with the full mass scan of the Orbitrap analyser to isolate, identify and integrate peak areas using Thermo Xcalibur Qual Browser software version 3.0. Sterols monitored and identified in these studies are listed in Table 2.8. To isolate the $[M]^+$ ion detected on the Orbitrap, a reconstructed ion chromatogram (RIC) with a 10 ppm mass window was applied to the full MS scan (Figure 2.8A). All ions with the same accurate mass as the sterol of interest are isolated with the RIC. A total ion chromatogram (TIC) for the MS³ fragmentation was also applied on a second panel to isolate the $[M]^+$ ions which have lost 79 m/z , $[M-79]^+$ (Figure 2.8B). The distinct MS³ fragmentation pattern from the TIC was cross-referenced with the authentic sterol standard library for identification. Once identification was confirmed, the full MS peak was integrated and the peak area was exported to Microsoft Excel. Deuterated internal standards were also identified and peak area extracted. The quantities of endogenous sterols were calculated relative to the deuterated internal standards as shown in Equation 2.4.

2.3.4.5 Normalisation of relative endogenous sterol quantities

Sterols from media extractions were quantified with stable isotope mass spectrometry and normalised to the number of T cells initially seeded for cell culture. Sterols from cell pellet extractions were normalised to the number of T cells when cells were harvested. Quantifications were expressed as pictograms per million cells (pg/millions cells), unless otherwise stated.

Equation 2.4 Formula for the calculation of relative sterol quantity by stable isotope dilution.

[Q_E] relative quantity, [A_E] peak area of endogenous sterol, [A_{ISTD}] peak area of internal standard,

[Q_{ISTD}] quantity of internal standard added

$$[Q_E] = \frac{[A_E]}{[A_{ISTD}]} \times [Q_{ISTD}]$$

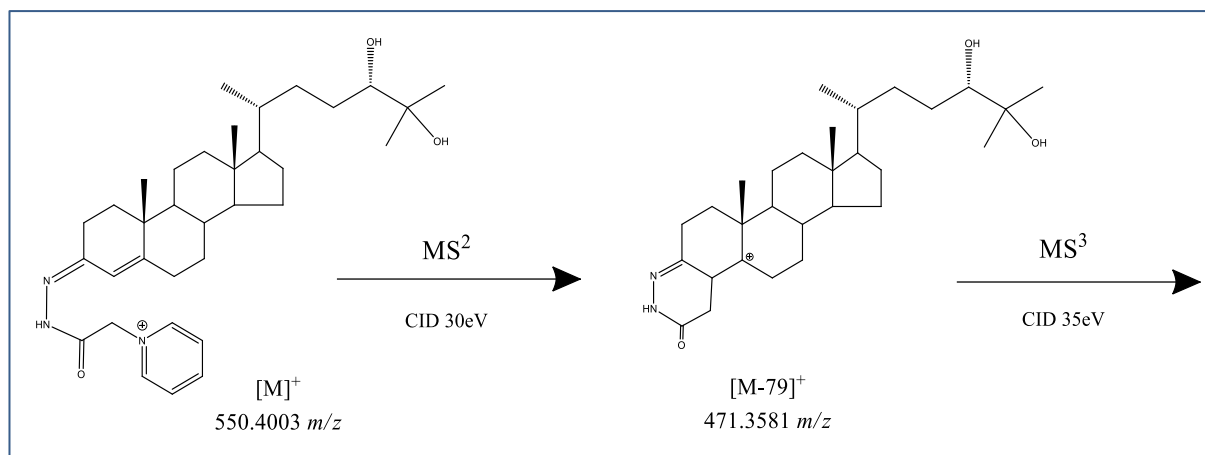


Figure 2.7 MSⁿ fragmentation of precursor $[M]^+$ ions. Precursor ions $[M]^+$ were selected for fragmentation in the linear ion trap (LIT) and MS³ fragmentation was performed on daughter ions $[M-79]^+$ to obtain unique MS³ spectra.

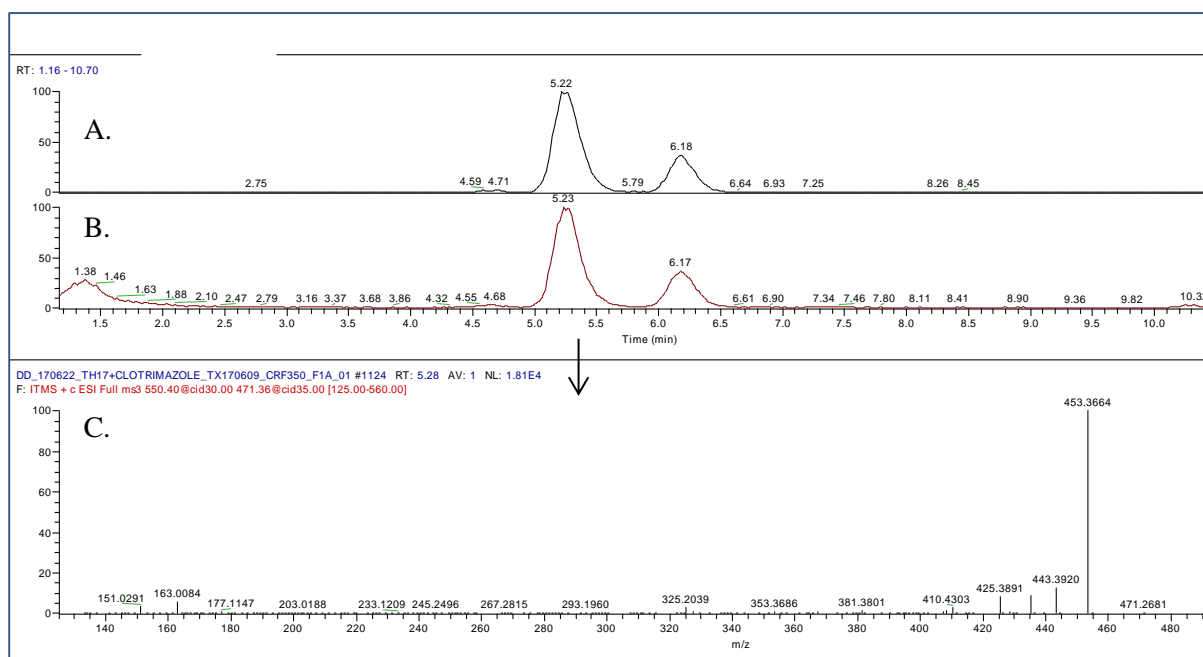
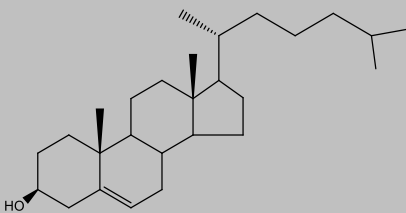
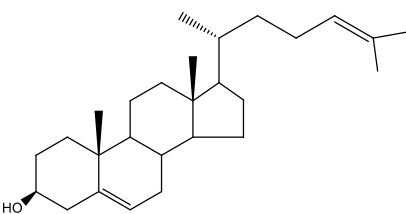
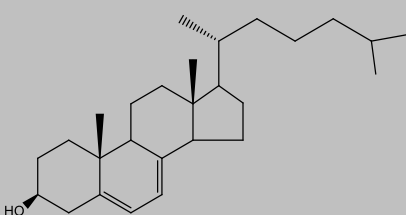
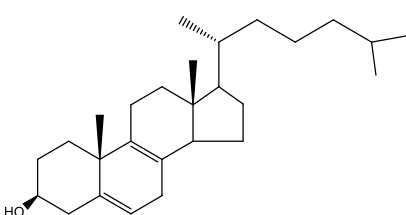
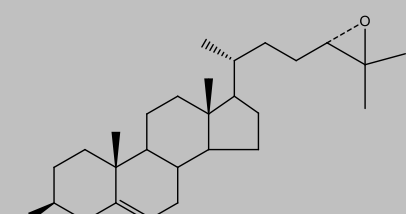
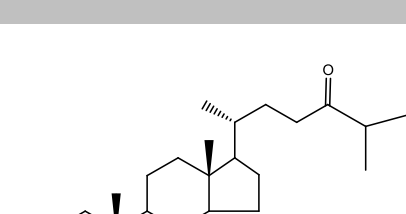
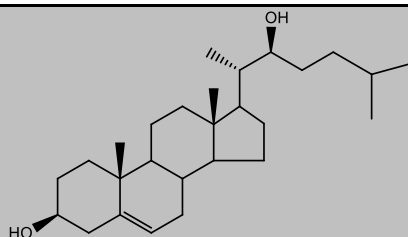


Figure 2.8 Isolation, identification and quantification of sterols by LCMS with Xcalibur Qual Browser. (A) Reconstructed ion chromatogram (RIC) of full MS to isolate $[M]^+$ ion with 24(S),25-diHC, 550.4003 m/z in this example, detected on the Orbitrap analyser. (B) A total ion chromatograph (TIC) in the linear ion trap (LIT) showed the MS³ spectra 550→471→. (C) The peaks of the TIC were used to confirm the fragmentation pattern with the authentic standard. Once identified, the full MS scan peaks were integrated and peak area exported to Microsoft Excel. Internal standards were integrated and sterol quantities quantified.

Table 2.8 List of sterols monitored and identified with EADSA.

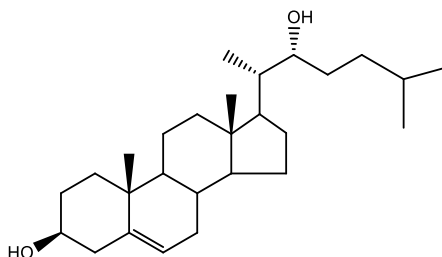
Sterol	Structure	Mass before derivatisation (m/z)	Mass after derivatisation (m/z)
Cholesterol Cholest-5-ene-3β-ol		386.3549	518.4105
Desmosterol Cholest-5,24-dien-3β-ol		384.3392	516.3948
7-Dehydrocholesterol Cholest-5,7-dien-3β-ol		384.3392	516.3948
8(9)-Dehydrocholesterol		384.3392	516.3948
24(S),25-Epoxycholesterol “24(S),25-EC” 24(S),25-Epoxycholest-5-ene-3β-ol		400.3341	532.3898
24-Ketocholesterol “24-KC” 24-Ketocholest-5-ene-3β-ol		400.3341	532.3898

**22(*S*)-
Hydroxycholest
erol
“22(*S*)-HC”
Cholest-5-ene-
3 β ,22*S*-diol**



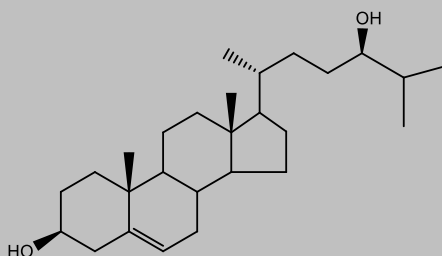
402.3498 534.4054

**22(*R*)-
Hydroxycholest
erol
“22(*R*)-HC”
Cholest-5-ene-
3 β ,22*R*-diol**



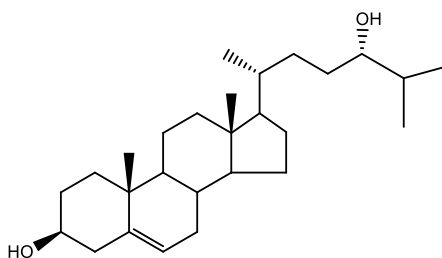
402.3498 534.4054

**24(*S*)-
Hydroxycholest
erol
“24(*S*)-HC”
Cholest-5-ene-
3 β ,24*S*-diol**



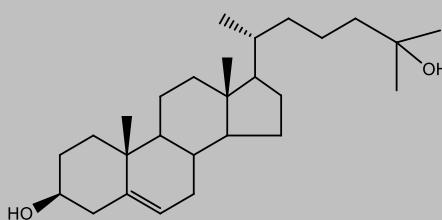
402.3498 534.4054

**24(*R*)-
Hydroxycholest
erol
“24(*R*)-HC”
Cholest-5-ene-
3 β ,24*R*-diol**



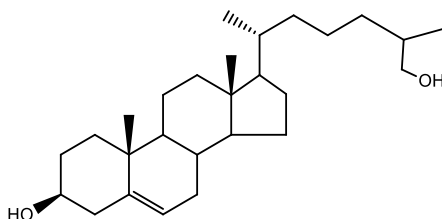
402.3498 534.4054

**25-
Hydroxycholest
erol
“25-HC”
Cholest-5-ene-
3 β ,25-diols**

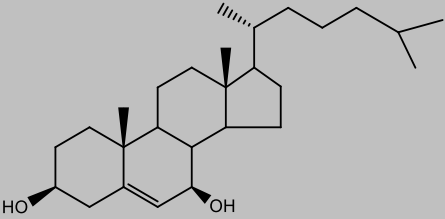
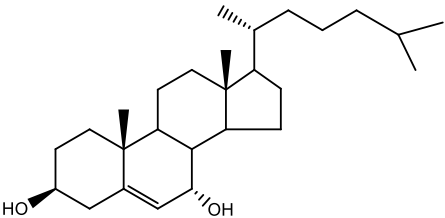
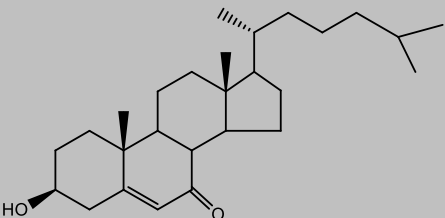
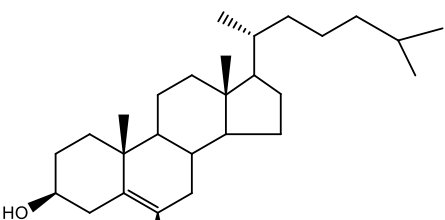
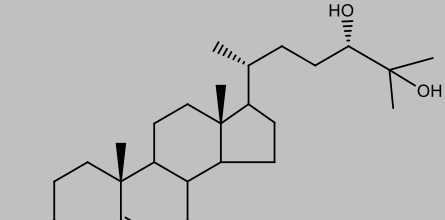
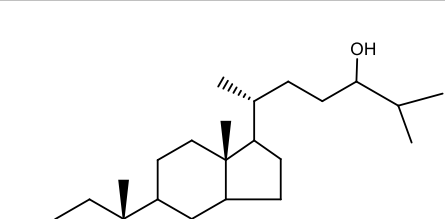


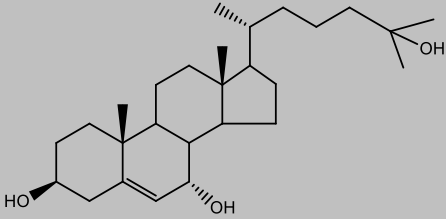
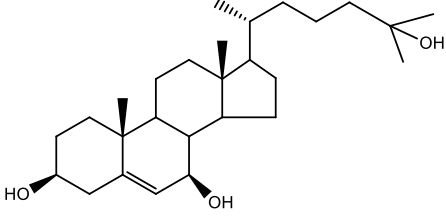
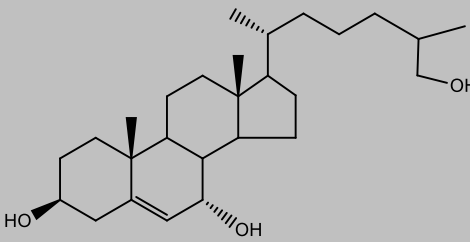
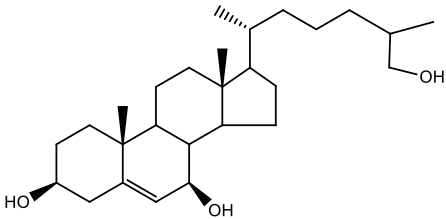
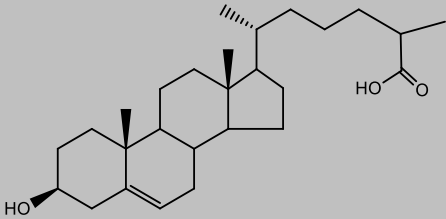
402.3498 534.4054

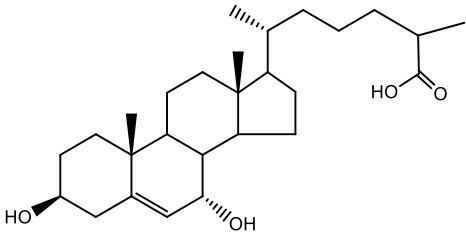
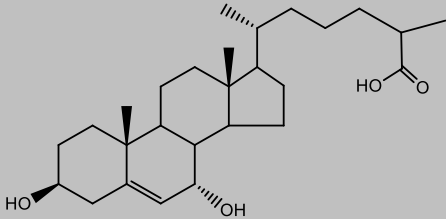
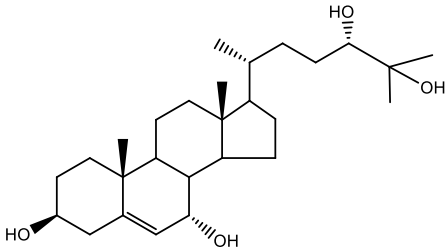
**27-
Hydroxycholest
erol
“27-HC”
Cholest-5-ene-
3 β ,27-diols**



402.3498 534.4054

7β- Hydroxycholest erol “7β-HC” Cholest-5-ene- 3β,7β-diol		402.3498	534.4054
7α- Hydroxycholest erol “7α-HC” Cholest-5-ene- 3$\beta$$\alpha$-diol		402.3498	534.4054
7- Ketocholesterol “7-KC” 3β- Hydroxycholest -5-en-7-one		402.3498	534.4054
6β- Hydroxycholest erol “6β-HC” Cholest-5-ene- 3β,6β-diol		402.3498	534.4054
24(S),25- dihydroxychole sterol “24(S),25- diHC” Cholest-5-ene- 3β,24S,25-triol		418.3447	550.4003
7α,24- dihydroxychole sterol “7α,24-diHC” Cholest-5-ene- 3β,7α,24-triol		418.3447	550.4003

7α,25- dihydroxychole sterol “7α,25-diHC” Cholest-5-ene- 3β,7α,25-triol		418.3447	550.4003
7β,25- dihydroxychole sterol “7β,25-diHC” Cholest-5-ene- 3β,7β,25-diol		418.3447	550.4003
7α,27- dihydroxychole sterol “7α,27-diHC” Cholest-5-ene- 3β,7α,27-triol		418.3447	550.4003
7β,27- dihydroxychole sterol “7β,27-diHC” Cholest-5-ene- 3β,7β,27-triol		418.3447	550.4003
Cholestenoic acid “CA” 3β- Hydroxycholest -5-en-27-oic acid		416.3290	548.3847

7α- Cholesteniolic acid “7α-CA” 3β, 7α- dihydroxychole- st-5-en-27-oic acid		432.3240	564.3796
7β- Cholestenolic acid “7β-CA” 3β, 7β- dihydroxychole- st-5-en-27-oic acid		432.3240	564.3796
7α,24(S),25- trihydroxychol esterol “7α,24(S),25- triHC” Cholest-5-ene- 3β,7α,24S,25- tetrol		434.3396	566.3952

2.4 In silico Modelling and Docking Simulations

2.4.1 Modelling protein and ligand structures

2.4.1.1 Modeller homology modelling of protein structures

Homology models of protein of interest were built with the relevant mouse amino acid sequence obtained from UniProt with appropriate x-ray crystal structures with bound agonists from the RCSB Protein Data Bank (PDB) ^(21,22). Modeller software was used to produce homology models of the proteins ligand binding domain (LBD) in their active conformation ⁽²³⁾. Modeller produces 3D protein models through satisfaction of spatial restraints and optimisation of molecular probability density functions.

2.4.1.2 Modelling ligand structures

The 3D structures of ligands were produced in Chem3D software (PerkinElmer). It was observed that bound sterols in x-ray crystal structures have unusual ring geometries *in vitro* therefore the structures of ligands were created with Chem3D using 25-Hydroxycholesterol (25-HC) extracted from an x-ray crystal structure, PDB:3I0I to obtain the ring structure base⁽²⁴⁾. Ligands were then relaxed in a full-atom molecular mechanics simulation to correct any inaccuracies from x-ray crystallisation or Chem3D modifications.

2.4.2 Protein-ligand docking simulations

2.4.2.1 FKCOMBU pre-docking preparations

The FKCOMBU (Flexible 'K' emical structure 'COM' parison using Build Up algorithm) program was used for pairwise comparison and flexible molecular alignment superposition of ligands with an example binding from the reference ligands to create an initial ligand fit in the ligand binding domain (LBD) ⁽²⁵⁾.

2.4.2.2 Protein-ligand docking simulations with PLANTS

Initial predicted docking complexes produced with FKCOMBU in *section 2.4.2.1* were refined with a flexible protein-ligand docking algorithm PLANTS (Protein-Ligand ANT System) ⁽²⁶⁾. PLANTS is a swarm based docking method that uses Ant Colony Optimisation (ACO) to generate the lowest energy conformations ⁽²⁷⁾. ACO is a class of stochastic optimisation algorithms, which uses the analogy of the behaviour of ants, which find the shortest path between their nest and a food source

using pheromone trails to mark paths between their nests and a food source. PLANTS employs an artificial ant colony to find the minimum energy conformation of the ligand in the binding site by marking low energy ligand conformations with an artificial pheromone trail which is modified in subsequent iterations to generate low energy conformations with a higher probability. The most energetically favourable pose of the ligand in the binding site is determined using PLANTS scoring functions to determine the strongest binding affinity ⁽²⁸⁾. In the PLANTS simulations the sterol B and C rings (Figure 2.9) were fixed in their pre-docked position while the remaining ligand structure was able to flex freely. The protein sidechain residues were also able to flex freely during docking simulations to obtain the optimum sidechain residue pose which gave the greatest probability. A library of initial states of significant residues was used to provide initial poses for optimisation. PLANTS software was initially designed with kinase structures which have numerous CHO (carbon-oxygen hydrogen) interactions involved in ligand binding, CHO interactions are of less significance in the protein structures studied therefore CHO interactions were disabled. Simulation search parameters were increased, $N = 80$, $\sigma = 64$, to account for the high degrees of freedom in a system with side-chain flexibility, ligand flexibility and added water molecules. Molecular graphics and analyses were performed with UCSF Chimera ⁽²⁹⁾.

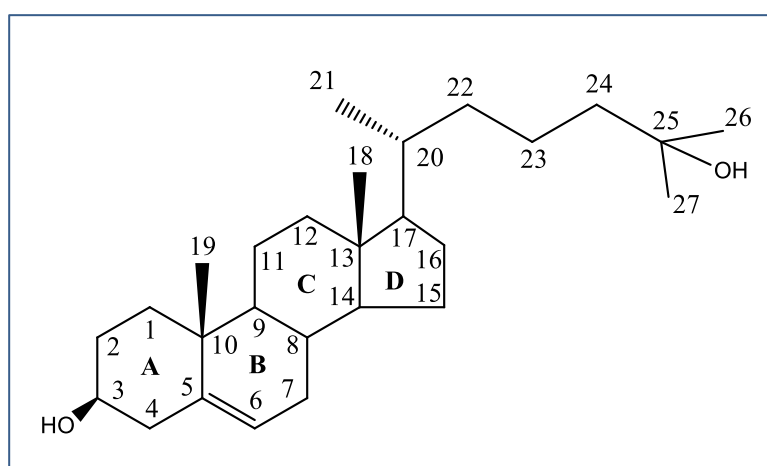


Figure 2.9 Sterol structure. The four-ring cyclopentanono-perhydrophenanthrene backbone and sidechain of Cholesterol. The Band C rings of the steroid backbones was fixed for protein-ligand docking simulations. The remaining structure was free to flex.

2.5 References

1. Studer, D., Lischer, S., Jochum, W., Ehrbar, M., Zenobi-Wong, M., & Maniura-Weber, K. (2012). Ribosomal protein L13a as a reference gene for human bone marrow-derived mesenchymal stromal cells during expansion, adipo-, chondro-, and osteogenesis. *Tissue Engineering - Part C: Methods*, 18(10), 761–771. <https://doi.org/10.1089/ten.tec.2012.0081>
2. Cronin J, McAdam E, Danikas A, et al. (2011). Epidermal growth factor receptor (EGFR) is overexpressed in high-grade dysplasia and adenocarcinoma of the esophagus and may represent a biomarker of histological progression in Barrett's esophagus (BE). *Am J Gastroenterol.* 106(1):46-56. doi:10.1038/ajg.2010.433
3. Kielar, D., Dietmaier, W., Langmann, T., Aslanidis, C., Probst, M., Naruszewicz, M., & Schmitz, G. (2001). Rapid quantification of human ABCA1 mRNA in various cell types and tissues by real-time reverse transcription-PCR. *Clinical Chemistry*, 47(12), 2089–2097. <https://doi.org/10.1093/clinchem/47.12.2089>
4. Antonson, P., Jakobsson, T., Almlöf, T., Guldevall, K., Steffensen, K. R., & Gustafsson, J. Å. (2008). RAP250 is a coactivator in the transforming growth factor β signaling pathway that interacts with Smad2 and Smad3. *Journal of Biological Chemistry*, 283(14), 8995–9001. <https://doi.org/10.1074/jbc.M707203200>
5. Herrmann, H., Sadovnik, I., Cerny-Reiterer, S., Rüllicke, T., Stefanzi, G., Willmann, M., ... Valent, P. (2014). Dipeptidylpeptidase IV (CD26) defines leukemic stem cells (LSC) in chronic myeloid leukemia. *Blood*, 123(25), 3951–3962. <https://doi.org/10.1182/blood-2013-10-536078>
6. Steckelbroeck, S., Watzka, M., Lütjohann, D., Makiola, P., Nassen, A., Hans, V. H. J., ... Klingmüller, D. (2002). Characterization of the dehydroepiandrosterone (DHEA) metabolism via oxysterol 7 α -hydroxylase and 17-ketosteroid reductase activity in the human brain. *Journal of Neurochemistry*, 83(3), 713–726. <https://doi.org/10.1046/j.1471-4159.2002.01187.x>
7. Huang, C., Martin, S., Pfleger, C., Du, J., Buckner, J. H., Bluestone, J. A., ... Ziegler, S. F. (2013). A Novel, Human-Specific Interacting Protein Couples

- FOXP3 to a Chromatin Remodeling Complex that Contains KAP1/TRIM28. *NIH Public Access*, 190(9), 4470–4473. <https://doi.org/10.1038/jid.2014.371>
8. Cai, K., Lucki, N. C., & Sewer, M. B. (2014). Silencing diacylglycerol kinase- θ expression reduces steroid hormone biosynthesis and cholesterol metabolism in human adrenocortical cells. *Biochimica et Biophysica Acta - Molecular and Cell Biology of Lipids*, 1841(4), 552–562. <https://doi.org/10.1016/j.bbalip.2013.12.005>
 9. Boeuf, P., Vigan-Womas, I., Jublot, D., Loizon, S., Barale, J. C., Akanmori, B. D., ... Behr, C. (2005). CyProQuant-PCR: A real time RT-PCR technique for profiling human cytokines, based on external RNA standards, readily automatable for clinical use. *BMC Immunology*, 6. <https://doi.org/10.1186/1471-2172-6-5>
 10. François, M., Romieu-Mourez, R., Li, M., & Galipeau, J. (2012). Human MSC suppression correlates with cytokine induction of indoleamine 2,3-dioxygenase and bystander M2 macrophage differentiation. *Molecular Therapy*, 20(1), 187–195. <https://doi.org/10.1038/mt.2011.189>
 11. Manel, N., Unutmaz, D., & Littman, D. R. (2008). The differentiation of human TH-17 cells requires transforming growth factor- β and induction of the nuclear receptor ROR γ t. *Nature Immunology*, 9(6), 641–649. <https://doi.org/10.1038/ni.1610>
 12. Chellan, B., Yan, L., Sontag, T. J., Reardon, C. A., & Hofmann Bowman, M. A. (2014). IL-22 is induced by S100/calgranulin and impairs cholesterol efflux in macrophages by downregulating ABCG1. *Journal of Lipid Research*, 55(3), 443–454. <https://doi.org/10.1194/jlr.M044305>
 13. Shi, Y., Fan, X., Meng, W., Deng, H., Zhang, N., & An, Z. (2014). Engagement of immune effector cells by trastuzumab induces HER2/ERBB2 downregulation in cancer cells through STAT1 activation. *Breast Cancer Research*, 16(2), 1–11. <https://doi.org/10.1186/bcr3637>
 14. Chang, T. C., Zeitels, L. R., Hwang, H. W., Chivukula, R. R., Wentzel, E. A., Dews, M., ... Mendella, J. T. (2009). Lin-28B transactivation is necessary for Myc-mediated let-7 repression and proliferation. *Proceedings of the National Academy of Sciences of the United States of America*, 106(9), 3384–3389. <https://doi.org/10.1073/pnas.0808300106>

15. Yi, T., Wang, X., Kelly, L. M., An, J., Xu, Y., Saller, A. W., ... Cyster, J. G. (2012). Oxysterol gradient generation by lymphoid stromal cells guides activated B cell movement during humoral responses. *Immunity*, 37(21), 535–548. <https://doi.org/10.1038/jid.2014.371>
16. Ivanov, I. I., McKenzie, B. S., Zhou, L., Tadokoro, C. E., Lepelley, A., Lafaille, J. J., ... Littman, D. R. (2006). The Orphan Nuclear Receptor ROR γ t Directs the Differentiation Program of Proinflammatory IL-17+ T Helper Cells. *Cell*, 126(6), 1121–1133. <https://doi.org/10.1016/j.cell.2006.07.035>
17. Livak, K. J., & Schmittgen, T. D. (2001). Analysis of Relative Gene Expression Data Using Real-Time Quantitative PCR and the 2 $^{-\Delta\Delta CT}$ Method. *Methods*, 25(4), 402–408. <https://doi.org/10.1006/meth.2001.1262>
18. Griffiths, W. J., Abdel-Khalik, J., Crick, P. J., Yutuc, E., & Wang, Y. (2016). New methods for analysis of oxysterols and related compounds by LC-MS. *Journal of Steroid Biochemistry and Molecular Biology*, 162, 4–26. <https://doi.org/10.1016/j.jsbmb.2015.11.017>
19. Karu, K., Hornshaw, M., Woffendin, G., Bodin, K., Hamberg, M., Sjövall, J., ... Griffiths, W. J. (2008). UKPMC Funders Group Author Manuscript Liquid Chromatography Combined with Mass Spectrometry Utilising High-Resolution , Exact Mass , and Multi-Stage Fragmentation for the Identification of Oxysterols in Rat Brain. *Medical Biochemistry*, 48(4), 976–987.
20. Griffiths, W. J., Hornshaw, M., Woffendin, G., Baker, S. F., Lockhart, A., Heidelberger, S., ... Wang, Y. (2008). Discovering Oxysterols in Plasma : A Window on the Metabolome, 3602–3612. <https://doi.org/10.1021/pr8001639>
21. Consortium, T. U. (2019). UniProt : a worldwide hub of protein knowledge, 47(November 2018), 506–515. <https://doi.org/10.1093/nar/gky1049>
22. Berman, H. M., Westbrook, J., Feng, Z., Gilliland, G., Bhat, T. N., Weissig, H., ... Bourne, P. E. (2000). The Protein Data Bank Helen. *Nucleic Acids Research*, 28(1), 235–242. <https://doi.org/10.1093/nar/28.1.235>
23. B. Webb, A. Sali. Comparative Protein Structure Modeling Using Modeller. Current Protocols in Bioinformatics 54, John Wiley & Sons, Inc., 5.6.1-5.6.37, 2016

24. Jin, L., Martynowski, D., Zheng, S., Wada, T., Xie, W., & Li, Y. (2010). Structural Basis for Hydroxycholesterols as Natural Ligands of Orphan Nuclear Receptor ROR γ . *Molecular Endocrinology*, 24(5), 923–929. <https://doi.org/10.1210/me.2009-0507>
25. Kawabata, T., & Nakamura, H. (2014). 3D Flexible Alignment Using 2D Maximum Common Substructure: Dependence of Prediction Accuracy on Target-Reference Chemical Similarity. <https://doi.org/10.1021/ci500006d>
26. Korb O., Stützle T., Exner T.E. (2006) PLANTS: Application of Ant Colony Optimization to Structure-Based Drug Design. In: Dorigo M., Gambardella L.M., Birattari M., Martinoli A., Poli R., Stützle T. (eds) Ant Colony Optimization and Swarm Intelligence. ANTS 2006. Lecture Notes in Computer Science, vol 4150. Springer, Berlin, Heidelberg
27. Korb, O., Stützle, T., & Exner, T. E. (2009). Empirical scoring functions for advanced Protein-Ligand docking with PLANTS. *Journal of Chemical Information and Modeling*, 49(1), 84–96. <https://doi.org/10.1021/ci800298z>
28. Korb, O., Stützle, T., & Exner, T. E. (2009). Empirical scoring functions for advanced Protein-Ligand docking with PLANTS. *Journal of Chemical Information and Modeling*, 49(1), 84–96. <https://doi.org/10.1021/ci800298z>
29. Pettersen, E. F., Goddard, T. D., Huang, C. C., Couch, G. S., Greenblatt, D. M., Meng, E. C., & Ferrin, T. E. (2004). UCSF Chimera - A visualization system for exploratory research and analysis. *Journal of Computational Chemistry*, 25(13), 1605–1612. <https://doi.org/10.1002/jcc.20084>

Chapter 3. Method Development of Sterol Analysis

3.1 Introduction

Oxysterols analysis can be challenging due to the low abundance of oxysterols in biological systems in comparison to cholesterol and often only small sample volumes are attainable. Endogenous sterols are present as ‘free’ sterols or may be esterified with the addition of a fatty acid at the 3C position. Generally, oxysterol analysis is performed on free sterols which are biologically active with roles as ligands for nuclear receptors including LXR, ERs and G-protein coupled receptor EBI2 and also have roles in immunity and viral resistance ⁽¹⁻⁸⁾. Previously, classical sterol analysis was performed by GC-MS which measured both free and esterified sterol to give the total sterols present in samples ⁽⁹⁾. More recently, GC-MS analysis measuring total sterols in SARS-CoV-2 patient plasma revealed a possible role of 27-HC in viral resistance of SARS-CoV-2 ⁽¹⁰⁾.

This chapter investigates the method of alkaline hydrolysis with LC-MS for analysis of free and esterified oxysterols which can be applied to small sample volumes to provide an accurate quantification of total oxysterols. Free and esterified sterols were analysed in human plasma sample, human neonatal nCD4⁺ T cell pellets and cell culture supernatant in collaboration with Cathy Thornton’s human immunology group.

Aims:

1. Investigate total sterol analysis by LC-MS with alkaline hydrolysis.
2. Compare the levels of free and esterified sterols present in human plasma and neonatal CD4⁺ T cells.

3.2 Materials and Methods

3.2.1 Plasma preparation, total sterol extraction and LC-MSⁿ analysis

Sterols were extracted from 100 μ L, 50 μ L and 10 μ L plasma aliquots in ethanolic 0.35M potassium hydroxide (KOH) containing 10ng 22(*R*),3-oxo-HC(D7), 20ng 24(*R/S*)-HC(D6) and 40 μ g Cholesterol(D7) internal sterol standards. Samples were ultrasonicated for 5 minutes followed by 2 hour incubation at room temperature protected from light. Afterwards, samples were ultrasonicated for 5 minutes and neutralised to pH 7 with glacial acetic acid. Further aliquots of 100 μ L, 50 μ L and 10 μ L of plasma were extracted in parallel in ethanol only, excluding KOH and acetic acid neutralisation to represent the free sterols. Samples were further processed by EADSA as described in *section 2.3.2* however in order to analyse Fractions (A) and (B) simultaneously, Fraction (A) aliquots were derivatised with [²H₅]GP and [²H₀]GP was used to derivatise Fraction (B) aliquots. Sterols derivatised with [²H₅]GP have a mass 5.0314 Da heavier than [²H₀]GP derived sterols. The two aliquots were subsequently combined immediately before HPLC-ESI-MSⁿ analysis. Identification and quantification of enzymatically derived oxysterols was achieved with the method described in *section 2.3.4.4*.

3.2.2 Isolation of neonatal naive CD4⁺ T cells from neonatal cord blood

Mononuclear cells (MNCs) from the cord blood of healthy women were isolated by collaborator Sean Holm. Blood samples from the umbilical cord of healthy women delivering by elective Caesarean section, were collected into heparinated VacuettesTM and immediately processed *ex vivo*. All samples were collected with informed written consent and ethical approval was obtained from Wales Research Ethics Committee 6 (11/WA/0140).

3.2.2.1 Isolation of mononuclear cells from neonatal cord blood

MNCs isolated by collaborator Sean Holm were isolated by diluting whole blood 1:4 with phosphate buffered saline (PBS). Approximately 25 to 35 mL of the diluted whole blood was layered onto 15 mL sterile LymphoprepTM (STEMCELL Technologies, Cambridge, UK) and separated by density centrifugation at 400 x g for 40 minutes at room temperature. The Plasma was removed with a sterile plastic Pasteur pipette prior to carefully removing the MNC layer. MNCs were washed twice with RPMI 1640 GlutaMAXTM (ThermoFisher Scientific, Massachusetts,

USA) by centrifugation at 515 x g at room temperature. The resulting MNC pellet was resuspended in RPMI 1640 media and cell density determined using the Countess® automated cell counter (Life Technologies).

Total CD4⁺ T cells were isolated from MNCs by negative selection with CD4⁺ T cell isolation kit, human (Cat. no. 130-096-533, Miltenyi Biotec) and an autoMACS Pro separator as described in *section 2.1.5* and *2.1.5.2* or manual separation by loading cells onto a MACs LC column on a MACs separator and eluted with MACs buffer. CD4⁺ T cells were washed twice with RPMI 1640 GlutaMAX™ by centrifugation at 515 x g at room temperature. The resulting cell pellet was resuspended in RPMI 1640 media and cell density determined using the Countess® automated cell counter (Life Technologies).

3.2.2.2 Isolation of naïve CD4⁺ T cells from total neonatal CD4⁺ T cells

Naïve CD4⁺ T cells were isolated from aliquots of MNCs or total CD4⁺ neonatal cells provided by collaborator Sean Holm. Naïve CD4⁺ T cells were isolated by negative selection with MACS® technology with an AutoMAC® Pro separator as described in *section 2.1.5* and *2.1.5.1* or by manual separation by loading cells onto a MACs LC column on a MACs separator and eluted with MACs buffer. The cell number was determined with a C-chip haemocytometer as described in *section 2.1.11.1*.

3.2.3 Purity and activation analysis of naïve CD4⁺ T cells by flow cytometry

Following isolation of naïve CD4⁺ T cells, aliquots of cells were stained with anti-CD4, anti-CD45RA and anti-CD45RO antibodies and analysed by flow cytometry as described in *section 2.1.12.4*. The activation of cells following cell culture was determined by staining an aliquot of cells with anti-CD25 antibodies and analysed by flow cytometry.

3.2.4 Culture conditions for CD3 and CD28 activated naïve CD4⁺ T cells under non-polarising, Th0 conditions

Cells were resuspended in X-Vivo-20 (Lonza) media supplemented with penicillin-streptomycin-glutamine (PSG) (Sigma) and 2.5 x 10⁶ nCD4⁺ cells were seeded in 48

well-plates coated with anti-CD3 antibodies (Biolegend) at 2 µg/ml or non-coated wells for non-activated samples. Anti-CD28 antibodies (Biolegend) were added to cell cultures at 20µg/ml to aid stimulation of activated samples. Cells were cultured in non-polarising conditions (Th0) with the addition of recombinant human IL-2 cytokine and anti-IL-4 and anti-IFN γ antibodies (eBiosciences, R&D Systems) at 37°C and 5% CO₂ for 24 to 72 hours summarised in Table 3.1.

Table 3.1 Culture conditions for neonatal naïve CD4⁺ T cell experiments. Isolated nCD4⁺ were cultured under non-polarising non-activated and anti-CD3, anti-CD28 activated conditions for 24, 48 or 72 hrs.

	24 hrs		48 hrs		72 hrs	
	Activated	Non-Activated	Activated	Non-Activated	Activated	Non-Activated
Experiment 1	X		X			
Experiment 2	X	X	X	X	X	X
Experiment 3	X	X				

After 24, 48 or 72 hours cells were harvested by re-suspended cells in culture media and centrifugation at 500 x g for 10 minutes. Supernatants were transferred to 2 mL collection tubes and stored at -20°C. Cell pellets were re-suspended in 1mL PBS and 300,000 cells were taken for flow cytometry analysis. The remaining cells were divided between two 1 mL Eppendorf tubes and centrifuged at 300 x g for 10 minutes. The supernatant was removed and cell pellets were stored at -80°C for further analysis.

3.2.5 Flow cytometry analysis of CD25 activation and cell viability of neonatal naïve CD4⁺ T cell cultures

CD25 and 7AAD staining and flow cytometry analysis of cell aliquots taken during harvesting of cell cultures was performed as described in *section 2.1.12.4* and *2.1.11.2* respectively.

3.2.6 Cell pellet and supernatant preparation, sterol extraction and LC-MSⁿ analysis

Oxysterols were extracted from cell pellets of 1×10^6 cells and cell culture supernatant in ethanoic 0.35M KOH containing deuterated internal sterol standards 2ng 24(*R/S*)-HC(D6), 2ng 22(*R*),3-oxo-HC(D7) and 40ng Cholesterol(D7) as described in *section 2.3.1.2*. Extracts were subjected to EADSA processing and oxysterol analysis was performed by LC-ESI-MSⁿ on an Orbitrap Elite mass spectrometer. Identification and quantification of enzymatically derived oxysterols was achieved with the method described in *section 2.3.4.4*. Autoxidation products of the cholesterol B-ring which can be produced during sample preparation and sterols in the mock media were considered artefacts and were not included in the analysis.

3.3 Results

3.3.1 Precise oxysterol quantification is achievable with reduced sample volume

Table 3.2 lists the total and free sterols detected from 100 μ L 50 μ L and 10 μ L plasma extraction methods with and without alkaline hydrolysis in KOH. Target monohydroxycholesterols 24(*S*)-HC, 25-HC, 27-HC, 7 α -HC and 7 β -HC were detectable at 539.4368 *m/z* (Figure 3.1), dihydroxycholesterols 7 α ,25-diHC and 7 α ,27-diHC were detectable at 555.4317 *m/z* (Figure 3.2) and trihydroxycholesterol 7 α ,24,25-triHC was detectable at 571.4266 *m/z* (Figure 3.3). Overall, the reproducibility of estimated oxysterol concentration between the varying volumes for extractions was good. Target oxysterol concentrations showed strong agreement between extraction methods with the exception of those that can be generated through *ex vivo* autoxidation of cholesterol during sample processing. The greatest variation for the monohydroxycholesterols was observed with 24(*S*)-HC with concentrations between 61.66 ng/mL and 96.7 ng/mL detected with free sterol analysis.

3.3.2 Comparison of esterified and non-esterified sterols in human plasma

In concurrence with previous studies approximately 25% of cholesterol is present in its non-esterified form, while side-chain monohydroxycholesterols account for 10 to 28% of their total quantified concentrations (Table 3.2 and Table 3.3) ^(9,11-13). The percentage of non-esterified 7 α ring-oxidised sterols was greater and showed a much wider range of variation from 50 to 80% for 7 α -HC and 7 β -HC, 30 to 50% for dihydroxycholesterol 7 α ,25-diHC and 17 to 78% for 7 α ,27-diHC, while the percentage of free sterols was in excess of 100% for 7 α ,24,25-triHC with 50 μ L and 10 μ L extraction methods. Similarly, CA and 7 α / β -CA also showed a percentage in excess of 100% for free sterols. 7-hydroxy-5-ene and 7-hydroxy-4-en-3-one structures are chemically labile and during alkaline hydrolysis in KOH they may undergo dehydration of the labile hydroxyl groups ⁽¹⁴⁾. There was no authentic isotope labelled standard for the 7-hydroxy structures to compensate for the loss of these 7-hydroxy structures which may explain the high percentages observed.

Table 3.2 Quantification of sterols detected in human plasma with and without hydrolysis in KOH representing total and free sterols respectively. (n=3)

Sterol	Quantification (ng/mL \pm SD)					
	Non-hydrolysed 100 μ L plasma extraction	Hydrolysed 100 μ L plasma extraction	Non-hydrolysed 50 μ L plasma extraction	Hydrolysed 50 μ L plasma extraction	Non-hydrolysed 10 μ L plasma extraction	Hydrolysed 10 μ L plasma extraction
24(S)-HC	19.21 \pm 0.17	96.7 \pm 13.1	19.18 \pm 0.05	68.51 \pm 2.0	16.98 \pm 0.31	61.66 \pm 1.69
25-HC	1.46 \pm 0.09	10.7 \pm 1.22	1.57 \pm 0.28	8.62 \pm 0.68	1.46 \pm 0.15	7.44 \pm 0.39
27-HC	36.1 \pm 0.39	352.18 \pm 48.5	37.14 \pm 0.82	261.48 \pm 10.88	32.7 \pm 1.65	269.06 \pm 20.36
7α-HC	10.12 \pm 0.81	19.9 \pm 2.75	9.02 \pm 0.95	11.03 \pm 0.71	11.29 \pm 3.64	23.41 \pm 4.43
7β-HC	1.0 \pm 0.03	2.09 \pm 0.23	0.92 \pm 0.26	1.46 \pm 0.16	2.79 \pm 2.31	4.47 \pm 2.09
7α,25-diHC	1.59 \pm 0.54	5.3 \pm 1.12	2.08 \pm 0.34	4.32 \pm 0.17	4.24 \pm 0.22	8.33 \pm 1.08
7α,27-diHC	3.37 \pm 1.29	18.87 \pm 6.81	5.05 \pm 0.68	14.13 \pm 0.59	14.54 \pm 0.49	18.43 \pm 4.73
7α,24,25-triHC	1.35 \pm 0.77	1.63 \pm 0.91	2.02 \pm 0.46	0.86 \pm 0.07	5.4 \pm 0.54	0.95 \pm 0.54
CA	119.43 \pm 10.98	158.89 \pm 18.32	147.07 \pm 4.47	119.33 \pm 5.57	195.67 \pm 18.47	146.06 \pm 10.55
7α-CA	7.10 \pm 3.6	0.23 \pm 0.48	70.84 \pm 7.83	42.19 \pm 1.42	126.48 \pm 7.06	64.68 \pm 20.72
7β-CA	0.24 \pm 0.03	0.43 \pm 0.11	7.38 \pm 0.7	9.1 \pm 0.9	8.15 \pm 0.47	8.85 \pm 2.14
Cholesterol	657768.81 \pm 14490.7	2636580.34 \pm 118612.72	697134.18 \pm 14468.17	2597309.41 \pm 90792.63	589469.25 \pm 40512.92	2185688.98 \pm 331388.87

Table 3.3 Percentage of free sterols in human plasma.

Sterol	% free sterol		
	100 μ L plasma extraction	50 μ L plasma extraction	10 μ L plasma extraction
24(S)-HC	19.87	28.0	27.54
25-HC	13.64	18.21	19.62
27-HC	10.25	14.20	12.15
7 α -HC	50.85	81.78	48.23
7 β -HC	47.85	63.01	62.42
7 α ,25-diHC	30.0	48.15	50.9
7 α ,27-diHC	17.86	35.74	78.89
7 α ,24,25- triHC	82.82	234.88	568.42
CA	75.17	123.25	133.97
7 α -CA	3086.96	167.91	195.55
7 β -CA	55.81	81.1	92.09
Cholesterol	24.95	26.84	26.97

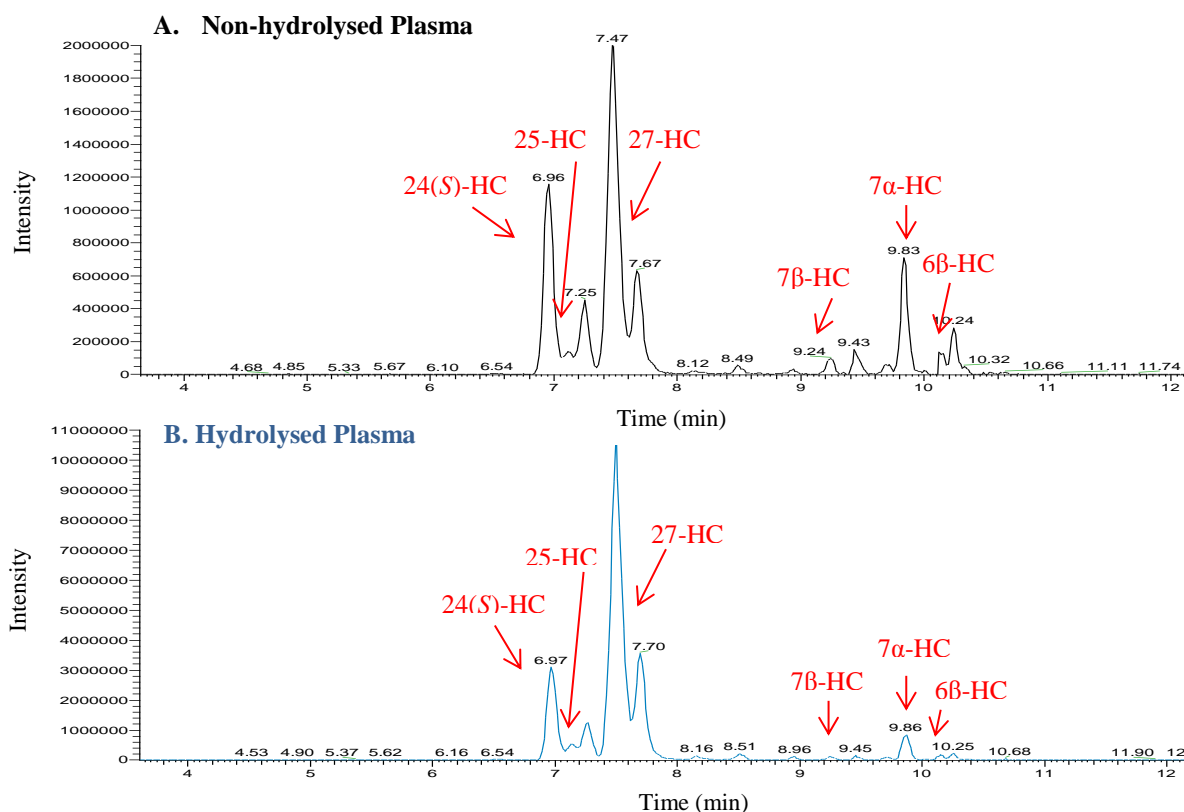


Figure 3.1 Representative reconstructed ion chromatograms for monohydroxycholesterols present in human plasma at $539.4368\text{ m/z} \pm 10\text{ppm}$ with a 17 minute gradient. (A) Free sterols detected in non-hydrolysed plasma. (B) Total sterols detected in hydrolysed plasma.

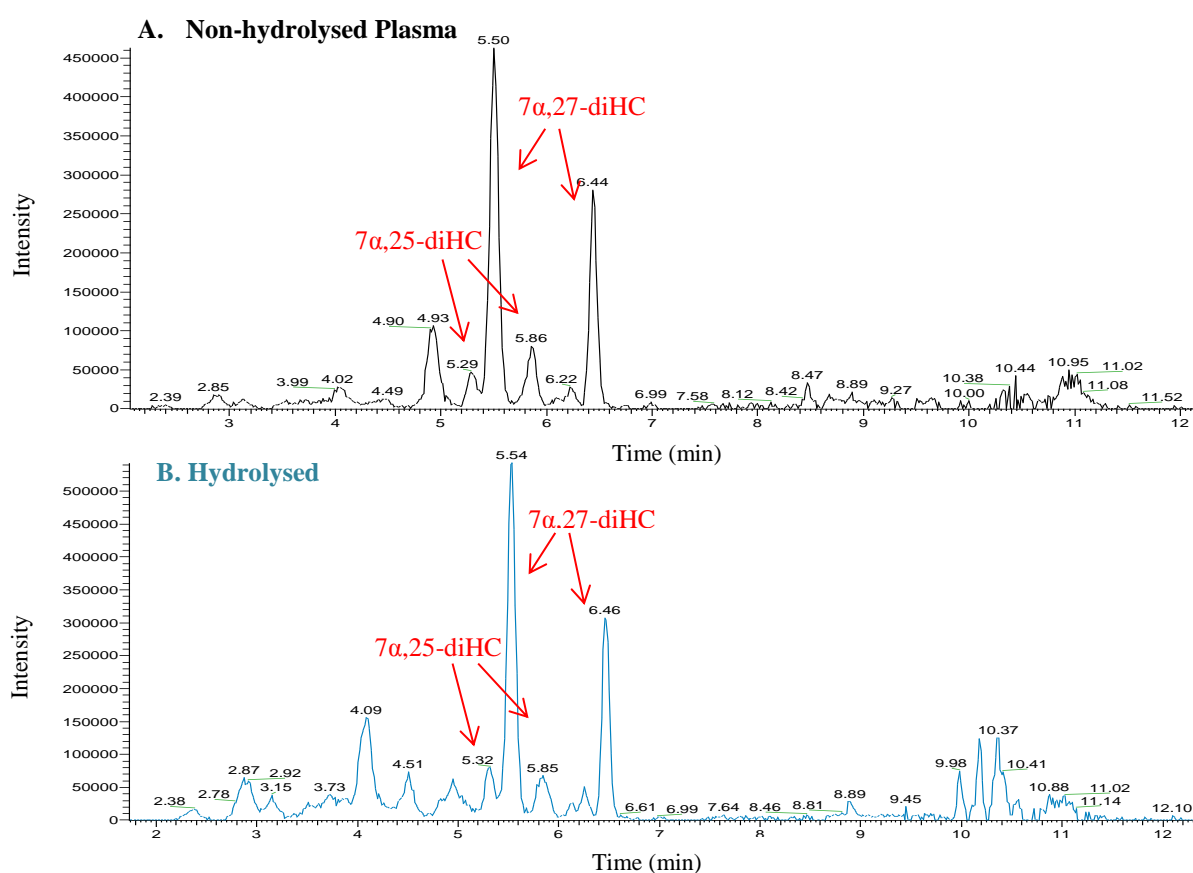
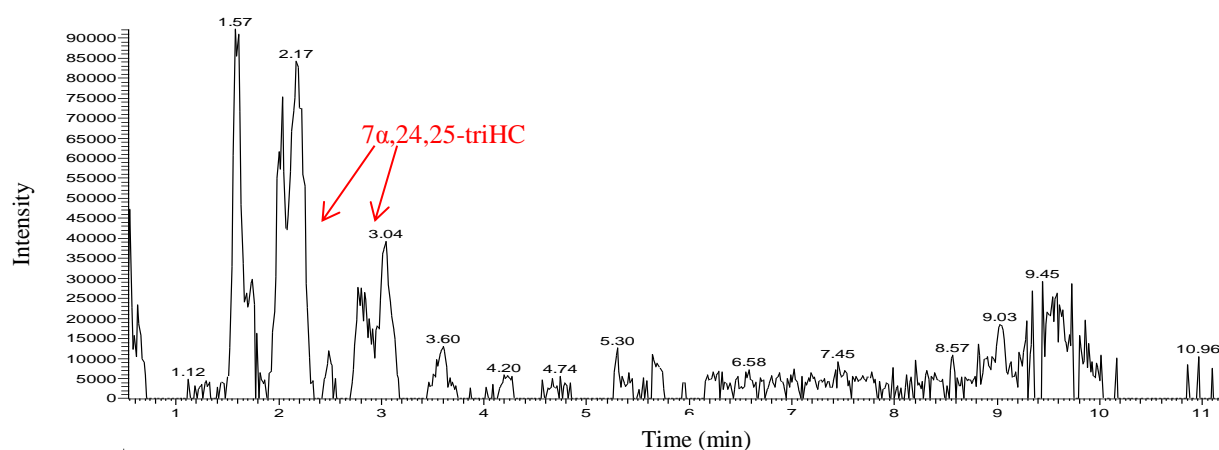


Figure 3.2 Representative reconstructed ion chromatograms for dihydroxycholesterols present in human plasma at $555.4317\text{ m/z} \pm 10\text{ppm}$ with a 17 minute gradient. (A) Free sterols detected in non-hydrolysed plasma. (B) Total sterols detected in hydrolysed plasma.

A. Non-hydrolysed Plasma



B. Hydrolysed Plasma

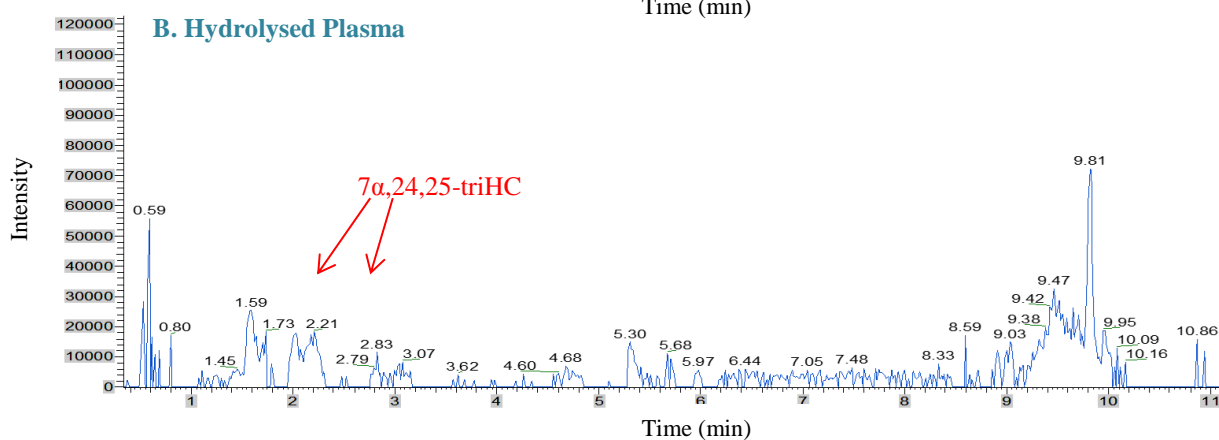


Figure 3.3 Representative reconstructed ion chromatograms for trihydroxycholesterols present in human plasma at $571.4266 \text{ m/z} \pm 10 \text{ ppm}$ with a 17 minute gradient. (A) Free sterols detected in non-hydrolysed plasma. (B) Total sterols detected in hydrolysed plasma.

3.3.3 Total sterol analysis of activated and non-activated neonatal naïve CD4⁺ T cells

nCD4⁺ T cells for the following experiments were isolated from cord blood representing neonatal nCD4⁺ T cells. Isolation of neonatal nCD4⁺ T cells was achieved by manual or automated MACs isolation summaries in Table 3.4. Isolated cells cultured under non-polarising activated and non-activated conditions were harvested after 24 to 72 hrs. After 24hrs the uniformity of cells was lost and cells could be seen to be enlarged and elongated with aggregation of cells. Figure 3.4 represents non-polarising anti-CD3, anti-CD28 simulated cells harvested after 24 hrs.

Table 3.4 MACs isolation method summary for neonatal naïve CD4⁺ T cell experiments.

	Manual MACs isolation of nCD4 ⁺ T cells	automated MACs isolation of nCD4 ⁺ T cells
Experiment 1	X	
Experiment 2	X	
Experiment 3		X

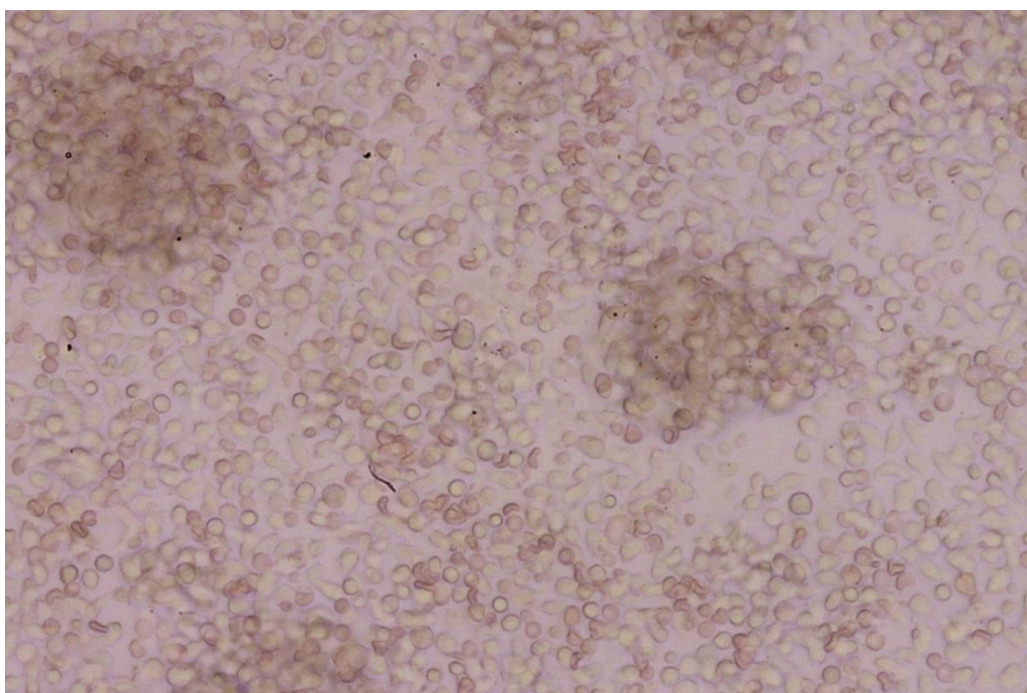


Figure 3.4 Neonatal naïve CD4⁺ T cells stimulated with anti-CD3 and anti-CD28 and cultured for 24 hrs under Th0 conditions. X20 magnification

3.3.3.1 Isolation of neonatal naïve CD4⁺ T cells by MACs showed > 61% purity

Single stain flow cytometry analysis of MACs manual and automated isolated cells showed 61 to 86 % CD4⁺ purity with the greatest purity achieved through autoMACs isolation. Surface staining of marker CD45RA⁺ showed purity >61% however CD45RO⁺ surface staining also showed approximately 52% CD45RO⁺ cells. Aliquots were also stained for activation marker CD25 (IL-2 receptor α) expression with 12 to 15% CD25⁺ cells. Figure 3.5 shows a representation of the gating strategy used to identify live cells. The purity of isolated nCD4⁺ cells analysed by flow cytometry prior to culture is represented in Figure 3.6.

3.3.3.2 CD25 expression increased following activation and culture of isolated neonatal naïve CD4⁺ T cells under non-polarising conditions

Cells harvested after 24, 48 or 72 hours under non-polarising conditions stimulated by anti-CD3 and anti-CD28 showed increased activation monitored by CD25⁺ surface marker expression shown in Figure 3.7. Flow cytometry analysis of harvested cells showed an increased expression of CD25 after 24 hrs to approximately 68% which further increased after 48 and 72 hrs whilst non-activated cells showed little variation in CD25 expression after 24 to 72 hrs.

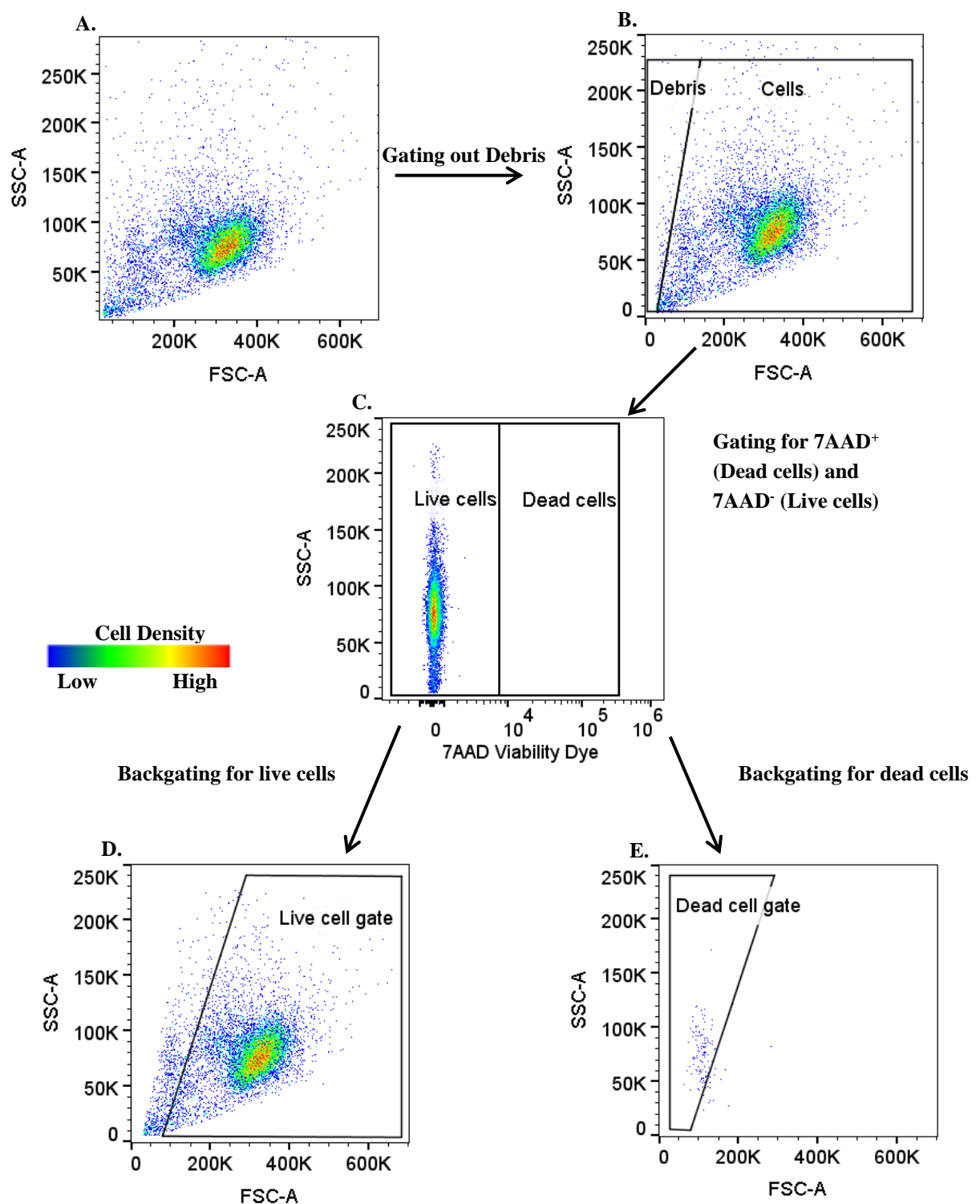


Figure 3.5 Gating strategy applied to isolated neonatal naïve CD4⁺ T cells to identify live cells and exclude dead cells using 7AAD Viability dye staining. Sample aliquots were single stained with 7AAD viability stain and not fixed prior to processing with ACEA Bioscience Novocyte. Analysis was performed with FlowJo software. Events were plotted on FSC/SSC for (A) isolated cells to gate only cells and exclude debris (B) Cells were plotted with 7AAD/SSC to identify the dead/ apoptotic cells which have incorporated the 7AAD stain that was able to penetrate compromised cell membranes and bind to the double stranded DNA (C) An FSC/SSC plot was applied to the identified cells to create the Live cell gate and Dead cell gates respectively (D, E). The Live cell gate was then applied to other single stained aliquots of the same sample.

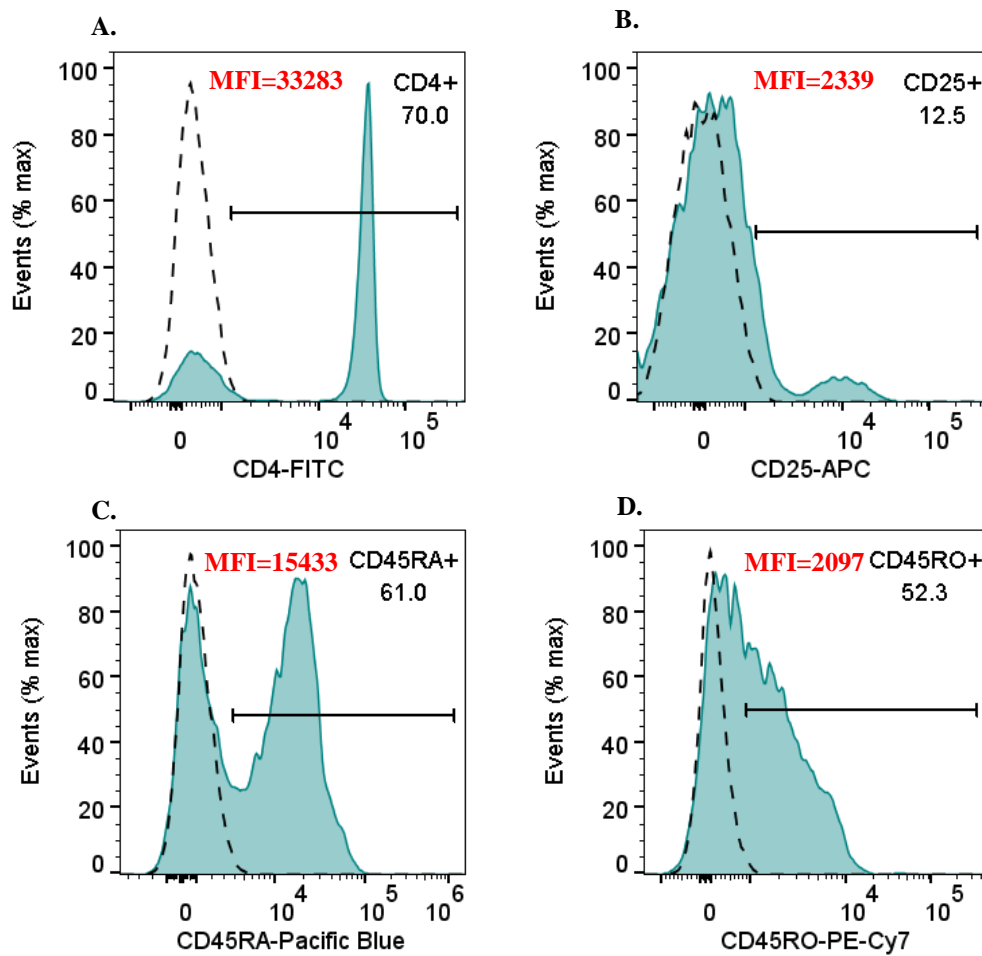


Figure 3.6 Representative flow cytometry analysis of isolated neonatal naïve CD4⁺ T cells prior to cell culture. (A) 70% CD4⁺ purity was achieved with manual MACs separation. (B) Low CD25 expression was observed with 12.5% of isolated cells CD25⁺. (C) 61% of isolated cells were CD45RA⁺. (D) 52.3% of isolated cells were CD45RO⁺. Filled histograms represent the fluorochrome conjugated antibody stained cells. Gates were determined using background fluorescence of unstained samples (1%) indicated by the dashed histogram. The Median Fluorescence intensities (MFI) are indicated in red.

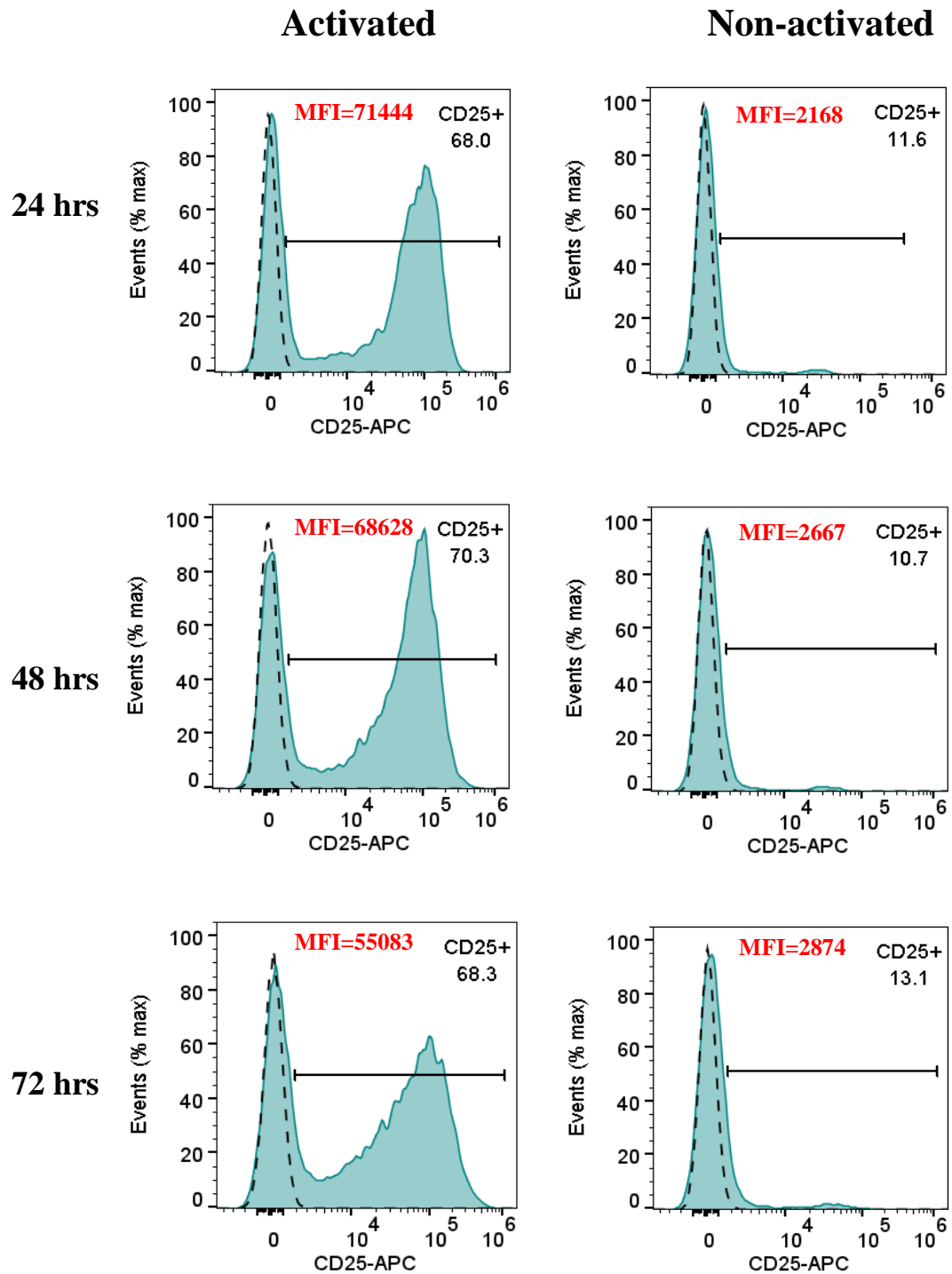


Figure 3.7 Flow cytometry analysis of CD25 expression of neonatal naïve CD4⁺ T cells after 24, 48 or 72 hrs of culture under non-polarising conditions. Filled blue histograms represent the fluorochrome conjugated antibody stained cells. Gates were determined using background fluorescence of unstained samples (1%) indicated by the dashed histogram. The Median Fluorescence intensities (MFI) are indicated in red.

3.3.3.3 Comparison of free and esterified sterols in activated and non-activated neonatal naïve CD4⁺ T cells

In order to analyse both free and esterified sterols present in activated and non-activated neonatal nCD4⁺ cells alkaline hydrolysis was performed prior to sterol extraction of cell pellets.

In a preliminary experiment in which cells were activated with anti-CD3 and anti-CD28 and cultured in non-polarising conditions for 24 to 48 hrs, oxysterols detected as free sterols in cell pellets included 24(*S*)-HC, 7 α / β -HC, 24-KC and 7 α ,24,25-triHC summarised in Table 3.5. 25-HC and 24,25-diHC were also detected in the total sterol analysis of cell pellets which includes esterified sterols summarised in Table 3.6. Increased concentrations of 24(*S*)-HC, 25-HC, 24,25-diHC and 7 α ,24,25-triHC were observed with increased incubation shown in Figure 3.8 and approximately 33% of 24(*S*)-HC was found to be present as free sterols.

Table 3.7 summaries the total oxysterols present in the supernatant harvested from cell cultures following 24 to 48 hrs activation. In addition to the oxysterols detected in total sterol analysis of the cell pellet, total sterol analysis of the supernatant also detected 24,25-diHC, 24(*S*),25-EC and the most abundant oxysterol present in plasma 27-HC. Increased concentrations were detected in a time dependant manner with the exception of 27-HC (Figure 3.9).

As mentioned in previous chapters, due to the labile nature of the 24(*S*),25-EC epoxide group 24(*S*),25-EC can be detected as isomer 24-KC, hydrolysed to 24,25-diHC or methanolysed to 24-hydroxycholesterol-25-methylether and 25-hydroxycholesterol-24-methylether⁽¹⁵⁾. Although in previous chapters only hydrolysed 24(*S*),25-diHC was detected, it is possible 24-KC detected in these cell pellets represents 24(*S*),25-EC concentrations in cells.

Table 3.5 Free sterol analysis of cell pellets from non-polarised neonatal naïve CD4⁺ T cells activated for 24 to 48 hrs. \pm SD of three individual LC-MS injections, ND = not detected, n=1

Experiment 1	Non activated day 0 (pg/10 ⁶ cells)	Activated 24hrs (pg /10 ⁶ cells)	Activated 48hrs (pg /10 ⁶ cells)
24(S)-HC	ND	4.45 \pm 0.93	21.72 \pm 1.04
25-HC	4.23 \pm 1.83	ND	27.16 \pm 1.6
24(R)-HC	ND	ND	ND
27-HC	ND	ND	ND
7 β -HC	573.69 \pm 1.14	106.05 \pm 2.4	214.79 \pm 0.26
7 α -HC	506.95 \pm 18.13	308.92 \pm 7.5	335.65 \pm 14.66
24,25-diHC	ND	ND	ND
7 α ,24,25-triHC	ND	ND	12.07 \pm 1.61
24(S),25-EC	ND	ND	ND
24-KC	267.23 \pm 2.19	203.10 \pm 1.78	224.39 \pm 1.26

Table 3.6 Total sterol analysis of cell pellets from non-polarised neonatal naïve CD4⁺ T cells activated for 24 to 48 hrs. \pm SD of three individual LCMS injections, ND = not detected, n=1

Experiment 1	Activated 24hrs (pg /10 ⁶ cells)	Activated 48hrs (pg /10 ⁶ cells)
24(S)-HC	12.99 \pm 1.96	32.93 \pm 1.46
25-HC	8.33 \pm 0.73	41.78 \pm 4.66
24(R)-HC	ND	29.66 \pm 2.32 (24R+27)
27-HC	7.34 \pm 1.63	29.66 \pm 2.32 (24R +27)
7 β -HC	153.09 \pm 3.9	133.17 \pm 5.49
7 α -HC	267.39 \pm 3.77	196.45 \pm 11.65
24,25-diHC	60.81 \pm 1.66	135.43 \pm 053
7 α ,24,25-triHC	14.16 \pm 0.93	35.99 \pm 1.71
24(S),25-EC	ND	5.14 \pm 2.76
24-KC	264.97 \pm 5.46	272.74 \pm 10.67

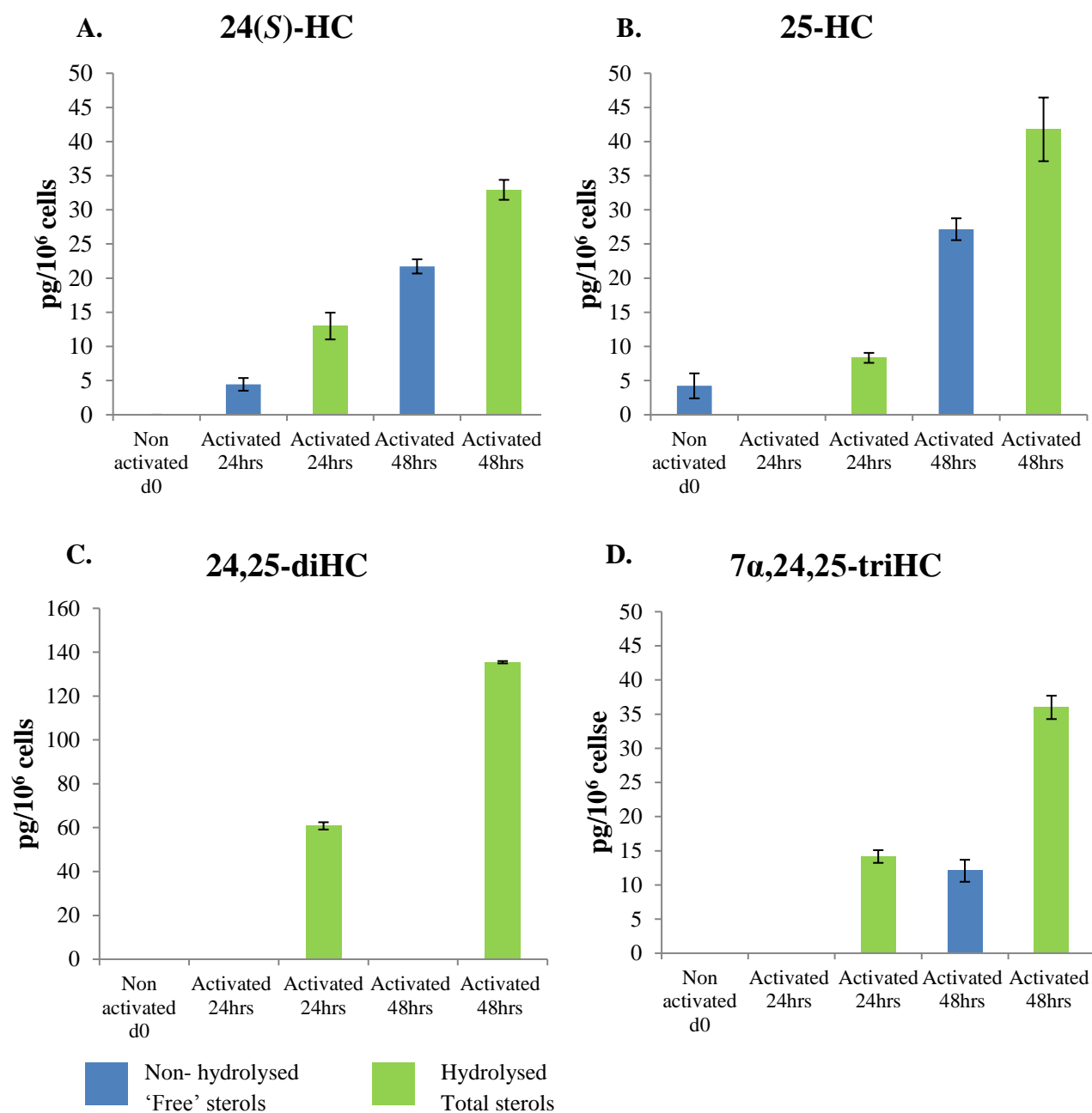


Figure 3.8 Comparison of free and total sterols present in cell pellets from non-polarised neonatal naïve CD4⁺ T cells activated for 24 to 48 hrs (A) 24-HC, (B), 25-HC, (C) 24,25-diHC, (D) 7 α ,24,25-triHC. \pm SD of three individual LC-MS injections, n=1

Table 3.7 Total sterol analysis of cell culture media from non-polarised neonatal naïve CD4⁺ T cells activated for 24 to 48 hrs. ND = not detected, n=1

Experiment 1	Activated 24hrs (pg/mL)	Activated 48hrs (pg /m L)
24(<i>S</i>)-HC	38.46	64.89
25-HC	60.05	133.56
24(<i>R</i>)-HC	ND	ND
27-HC	69.41	71.89
24,25-diHC	225.08	810.88
7 α ,24,25-triHC	16.34	120.08
24(<i>S</i>),25-EC	19.97	61.85
24-KC	734.28	809.13

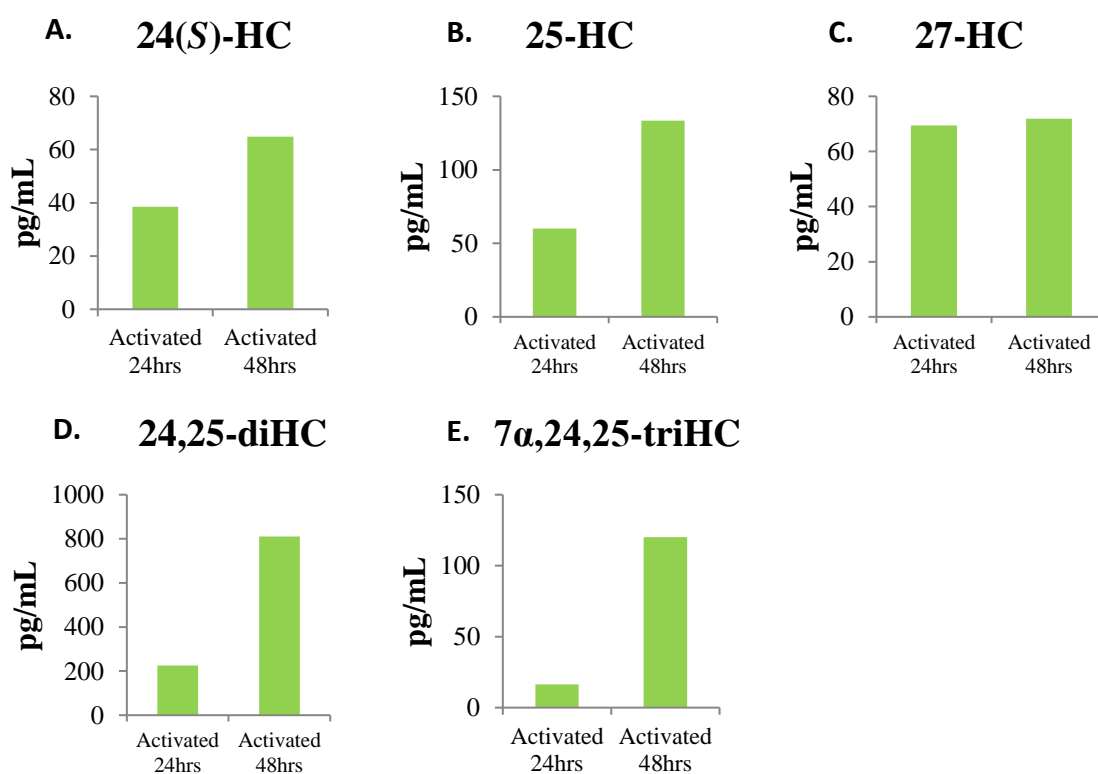


Figure 3.9 Total sterol analysis of cell culture media from non-polarised neonatal naïve CD4⁺ T cells activated for 24 to 48 hrs. (A) 24(*S*)-HC, (B), 25-HC, (C) 27-HC, (D) 24,25-diHC, (E) 7 α ,24,25-triHC. n=1

Subsequently, a further experiment was performed in which cells were cultured under non-activated non-polarising conditions or activated with anti-CD3 and anti-CD28 and cultured for 24 to 72 hrs. Oxysterols were detected as free sterols after 24 or 48 hrs in activated or non-activated conditions respectively summarised in Table 3.8. 24(*S*)-HC was quantified between 4.86 to 13.42 pg/10⁶ cells for cell pellets and 25-HC was quantified between 11.23 to 74.99 pg/10⁶ cells with the highest concentrations in activated samples. In contrast, the higher concentrations of oxysterols, 27-HC and 24,25-diHC were detected in non-activated cells. Table 3.9 summarises the total sterols quantified for cell pellets, 16 to 25% of 24(*S*)-HC was present as free sterols for activated samples and 13% for non-activated conditions (Figure 3.10). 25-HC was detected as free sterols at 38 to 60% in activated conditions or 28 to 41% in non-activated conditions. Similar total sterol concentrations of 27-HC were detected in activated and non-activating conditions with approximately 30% present as free sterols. Total sterol analysis of 24,25-diHC revealed approximately 30% of 24,25-diHC is present as free sterols with the highest concentrations in 48 to 72 hrs non-activated samples.

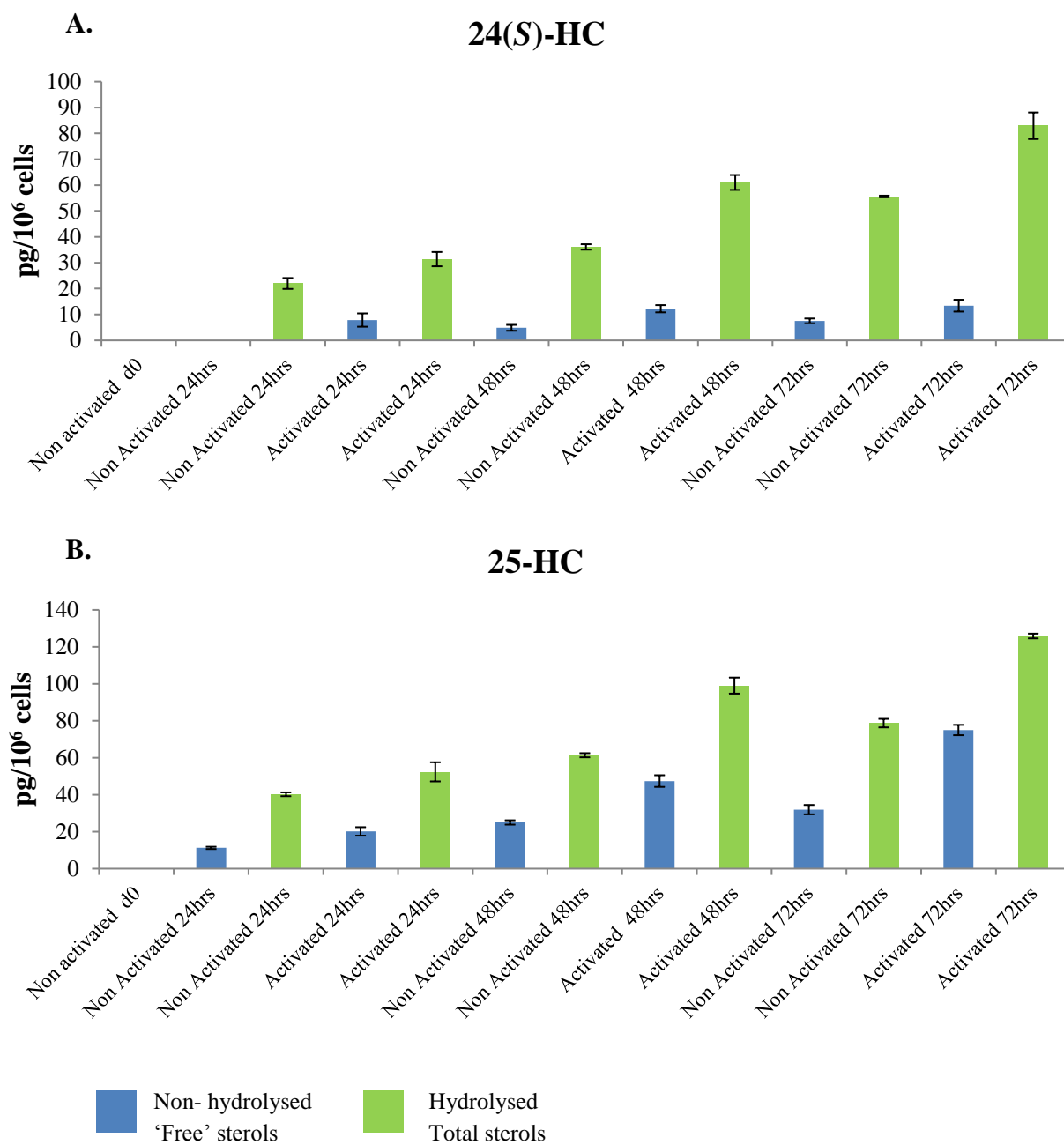
Total sterols analysis of cell culture supernatant is summarised in Table 3.10. The most abundant oxysterols present were 25-HC, 27-HC and 24,25-diHC (Figure 3.11). The greatest total sterol levels were detected in cell culture supernatant from cells activated for 72 hrs.

Table 3.8 Free sterol analysis of cell pellets from non-polarised neonatal naïve CD4⁺ T cells activated or non-activated for 24 to 72 hrs. \pm SD of three individual LC-MS injections, ND = not detected, n=1

Experiment 2	Non activated day 0 (pg/10 ⁶ cells)	Non Activated 24hrs (pg /10 ⁶ cells)	Activated 24hrs (pg /10 ⁶ cells)	Non Activated 48hrs (pg /10 ⁶ cells)	Activated 48hrs (pg /10 ⁶ cells)	Non Activated 72hrs (pg /10 ⁶ cells)	Activated 72hrs (pg /10 ⁶ cells)
24(S)-HC	ND	ND	7.86 \pm 2.57	4.86 \pm 1.14	12.24 \pm 1.4	7.54 \pm 0.92	13.42 \pm 2.28
25-HC	ND	11.23 \pm 0.61	20.13 \pm 2.3	24.99 \pm 1.18	47.38 \pm 3.15	31.92 \pm 2.54	74.99 \pm 2.79
24(R)-HC	ND	ND	ND	ND	ND	ND	ND
27-HC	ND	12.72 \pm 0.03	29.62 \pm 1.67	62.41 \pm 0.6	49.93 \pm 2.58	111.48 \pm 5.41	58.56 \pm 0.87
7 β -HC	93.76 \pm 3.89	164.54 \pm 8.03	171.42 \pm 3.33	90.74 \pm 0.88	167.66 \pm 15.74	160.40 \pm 9.81	1006.67 \pm 9.64
7 α -HC	136.54 \pm 11.16	157.57 \pm 8.36	194.62 \pm 15.96	81.99 \pm 4.74	200.34 \pm 15.59	141.69 \pm 13.36	930.37 \pm 44.99
24,25-diHC	ND	ND	68.53 \pm 6.3	115.15 \pm 4.41	57.59 \pm 1.16	160.75 \pm 4.25	92.38 \pm 3.77
7 α ,24,25- triHC	ND	ND	ND	9.87 \pm 1.3	13.21 \pm 2.47	18.62 \pm 2.54	26.71 \pm 0.81
24(S),25-EC	ND	ND	ND	ND	ND	119.70 \pm 2.48	44.71 \pm 3.59
24-KC	265.38 \pm 1.67	186.80 \pm 2.14	214.93 \pm 3.44	226.93 \pm 3.64	241.13 \pm 8.54	227.56 \pm 6.81	255.35 \pm 3.52

Table 3.9 Total sterol analysis of cell pellets from non-polarised neonatal naïve CD4⁺ T cells activated or non-activated for 24 to 72 hrs. \pm SD of three individual LC-MS injections, ND = not detected, n=1

Experiment 2	Non Activated 24hrs (pg /10⁶ cells)	Activated 24hrs (pg /10⁶ cells)	Non Activated 48hrs (pg /10⁶ cells)	Activated 48hrs (pg /10⁶ cells)	Non Activated 72hrs (pg /10⁶ cells)	Activated 72hrs (pg /10⁶ cells)
24(S)-HC	21.99 \pm 2.11	31.40 \pm 2.76	36.11 \pm 1.05	61.03 \pm 2.88	55.61 \pm 0.33	82.93 \pm 5.13
25-HC	40.24 \pm 1.02	52.37 \pm 5.17	61.36 \pm 1.12	99.03 \pm 4.34	78.73 \pm 2.3	125.87 \pm 1.27
24(R)-HC	ND	ND	ND	ND	ND	ND
27-HC	49.21 \pm 3.15	100.24 \pm 1.8	209.20 \pm 3.38	221.46 \pm 4.29	448.73 \pm 3.3	268.21 \pm 6.98
7 β -HC	185.79 \pm 4.66	94.13 \pm 3.79	80.35 \pm 3.23	163.82 \pm 5.58	113.19 \pm 1.04	139.47 \pm 4.82
7 α -HC	169.83 \pm 11.79	88.93 \pm 8.26	62.43 \pm 1.78	159.16 \pm 5.03	85.16 \pm 5.34	119.83 \pm 6.07
24,25-diHC	81.17 \pm 1.78	191.53 \pm 4.39	422.19 \pm 4.6	192.58 \pm 6.02	838.35 \pm 7.44	340.08 \pm 6.8
7 α ,24,25- triHC	ND	ND	10.72 \pm 0.58	7.09 \pm 2.64	28.69 \pm 4.58	8.26 \pm 3.21
24(S),25-EC	ND	ND	ND	ND	26.49 \pm 0.84	ND
24-KC	231.79 \pm 5.28	242.96 \pm 10.8	343.21 \pm 6.35	203.84 \pm 8.72	324.05 \pm 3.58	190.06 \pm 21.67



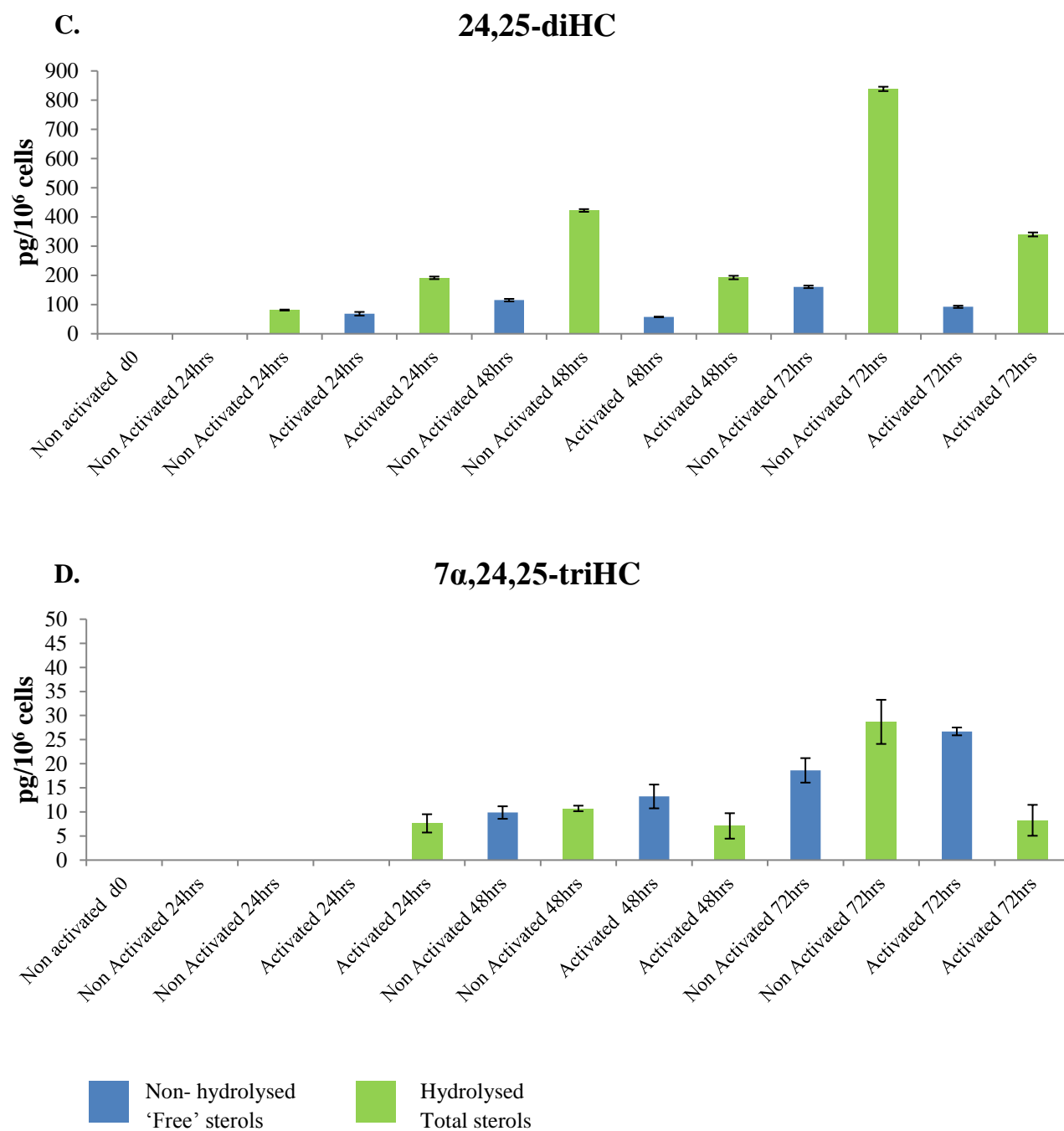


Figure 3.10 Comparison of free and total sterols present in cell pellets of non-polarised neonatal naïve CD4⁺ T cells activated or non-activated for 24 to 72 hrs. (A) 24(*S*)-HC, (B), 25-HC, (C) 24,25-diHC, (D) 7 α ,24,25-triHC. \pm SD of three individual LC-MS injections. n=1

Table 3.10 Total sterol analysis of cell culture media from non-polarised neonatal naïve CD4⁺ T cells activated or non-activated for 24 to 72 hrs. ND = not detected, n=1

Experiment 2	Non Activated 24hrs (pg /mL)	Activated 24hrs (pg /mL)	Non Activated 48hrs (pg /mL)	Activated 48hrs (pg /mL)	Non Activated 72hrs (pg /mL)	Activated 72hrs (pg /mL)
24(<i>S</i>)-HC	120.31	83.78	122.81	71.8	81.590	148.71
25-HC	331.86	341.13	528.0	372.56	366.46	793.47
24(<i>R</i>)-HC	ND	ND	ND	ND	ND	ND
27-HC	502.94	842.33	1987.31	770.41	655.68	5070.03
24,25-diHC	259.45	533.29	3661.13	1224.91	1371.98	6592.59
7 α ,24,25-triHC	ND	10.02	151.04	21.57	45.58	281.94
24(<i>S</i>),25-EC	61.85	56.88	951.02	802.24	159.46	412.63
24-KC	809.13	850.7	4888.49	2119.42	899.14	1051.79

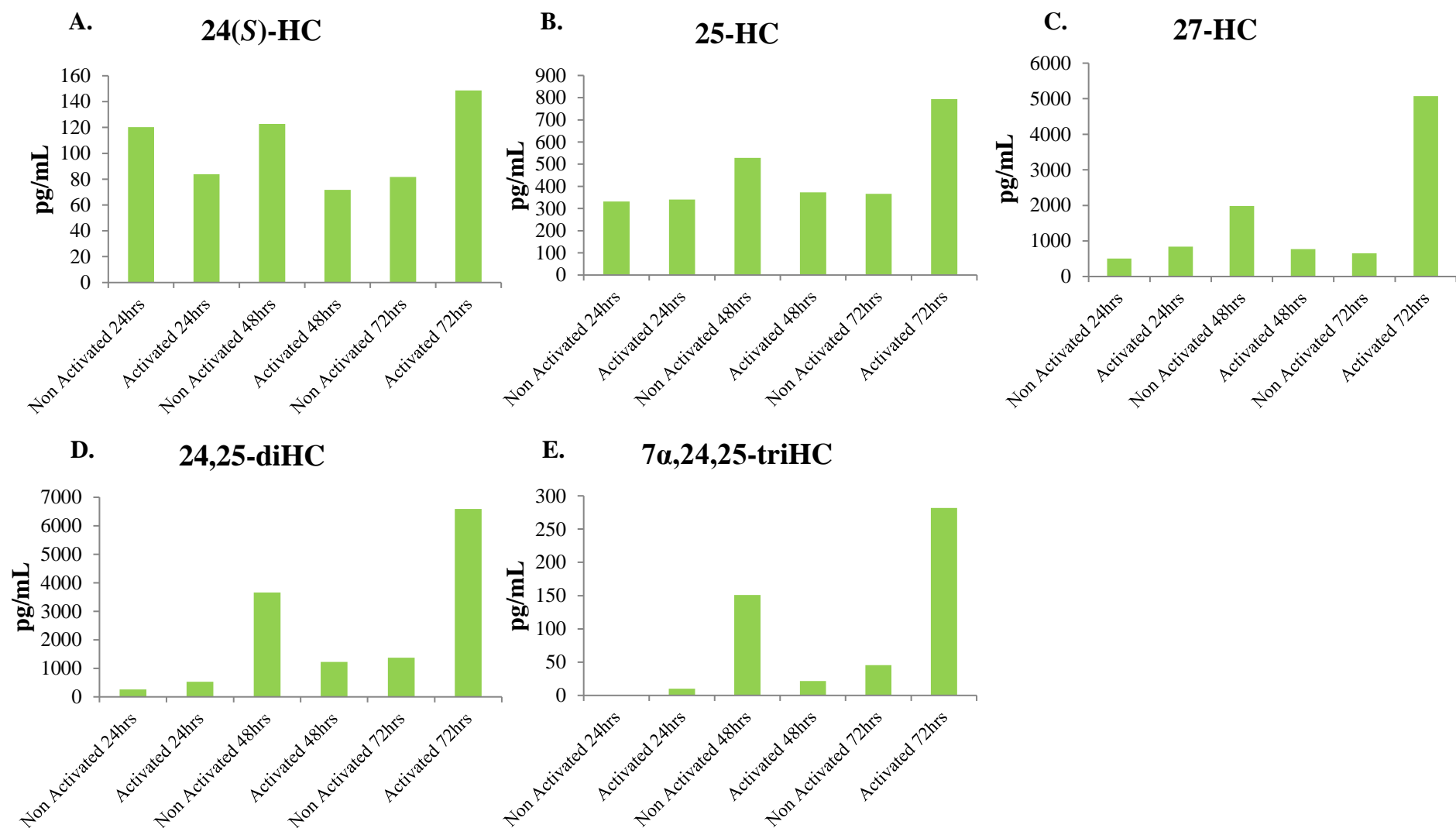


Figure 3.11 Total sterol analysis of cell culture media from non-polarised neonatal naïve CD4⁺ T cells activated or non-activated for 24 to 72 hrs. (A) 24(*S*)-HC, (B), 25-HC, (C) 27-HC, (D) 24,25-diHC, (E) 7α,24,25-triHC. n=1

Free sterol analysis of a third experiment performed in which neonatal nCD4⁺ T cells were incubated under non-activated or activated non-polarising conditions for 24hrs is summarised in Table 3.11. In contrast to the two previously experiments, no detectable levels of 24(*S*)-HC, 25-HC, 27-HC or 24,25-diHC free sterols were observed however these oxysterols were detected as esterified sterols in the total sterol analysis shown in Figure 3.12 and summarised in Table 3.12. Table 3.13 summaries the total sterols present in the cell culture media. Similar concentrations of 24(*S*)-HC, 25-HC and 27-HC were detected in non-activated and activated conditions while a slight increase in 24,25-diHC was detected in activated conditions (Figure 3.13).

Table 3.11 Free sterol analysis of cell pellets from non-polarised neonatal naïve CD4⁺ T cells activated or non-activated for 24 hrs. \pm SD of three individual LC-MS injections, ND = not detected, n=1

Experiment 3	Non Activated 24hrs (pg /10⁶ cells)	Activated 24hrs (pg /10⁶ cells)
24(<i>S</i>)-HC	ND	ND
25-HC	ND	ND
24(<i>R</i>)-HC	ND	ND
27-HC	ND	ND
7 β -HC	198.65 \pm 8.35	168.14 \pm 1.21
7 α -HC	186.92 \pm 12.59	278.25 \pm 9.88
24,25-diHC	ND	ND
7 α ,24,25-triHC	ND	ND
24(<i>S</i>),25-EC	ND	ND
24-KC	188.0 \pm 4.28	207.98 \pm 7.04

Table 3.12 Total sterol analysis of cell pellets from non-polarised neonatal naïve CD4⁺ T cells activated or non-activated for 24 hrs. \pm SD of three individual LC-MS injections, ND = not detected, n=1

Experiment 3	Non Activated 24hrs (pg /10 ⁶ cells)	Activated 24hrs (pg /10 ⁶ cells)
24(<i>S</i>)-HC	8.16 \pm 0.56	9.51 \pm 0.6
25-HC	3.45 \pm 0.59	2.04 \pm 0.77
24(<i>R</i>)-HC	ND	ND
27-HC	2.81 \pm 0.91	4.37 \pm 0.77
7 β -HC	329.07 \pm 1.38	111.92 \pm 5.59
7 α -HC	280.68 \pm 3.49	159.06 \pm 4.0
24,25-diHC	13.43 \pm 1.48	56.78 \pm 2.14
7 α ,24,25-triHC	ND	1.55 \pm 1.34
24(<i>S</i>),25-EC	195.91 \pm 3.98	ND
24-KC	233.76 \pm 2.41	221.5 \pm 5.94

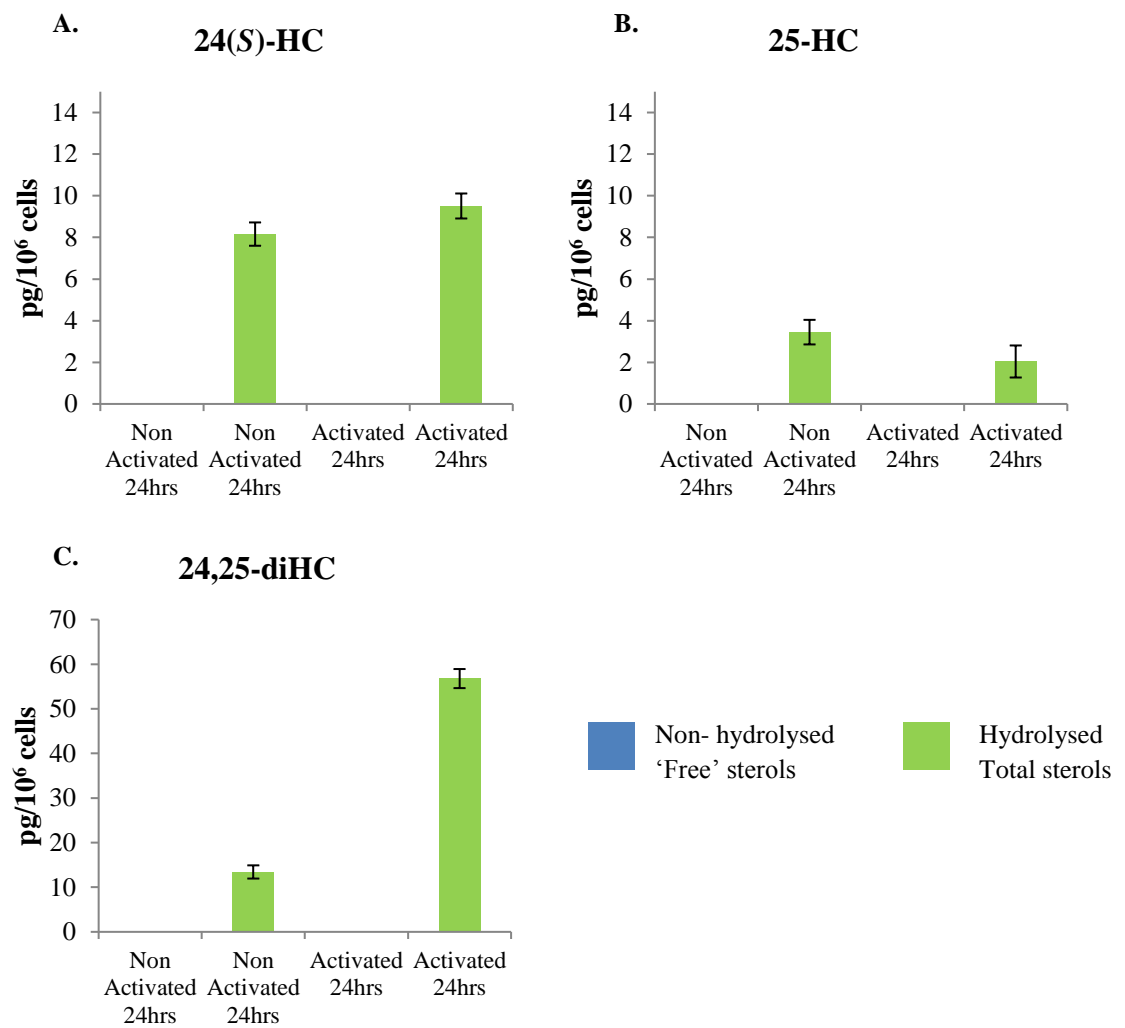


Figure 3.12 Comparison of free and total sterols present in cell pellets from non-polarised neonatal naïve CD4⁺ T cells activated or non-activated for 24 hrs. (A) 24(S)-HC, (B), 25-HC, (C) 24,25-diHC. \pm SD of three individual LCMS injections, n=1

Table 3.13 Total sterol analysis of cell culture media from non-polarised neonatal naïve CD4⁺T cells activated or non-activated for 24 hrs. ND = not detected, n=1

Experiment 3	Non Activated 24hrs (pg /mL)	Activated 24hrs (pg /mL)
24(S)-HC	18.97	27.58
25-HC	9.57	18.99
24(R)-HC	ND	ND
27-HC	66.44	75.51
24,25-diHC	ND	225.28
7 α ,24,25-triHC	ND	ND
24(S),25-EC	ND	ND
24-KC	839.82	788.28

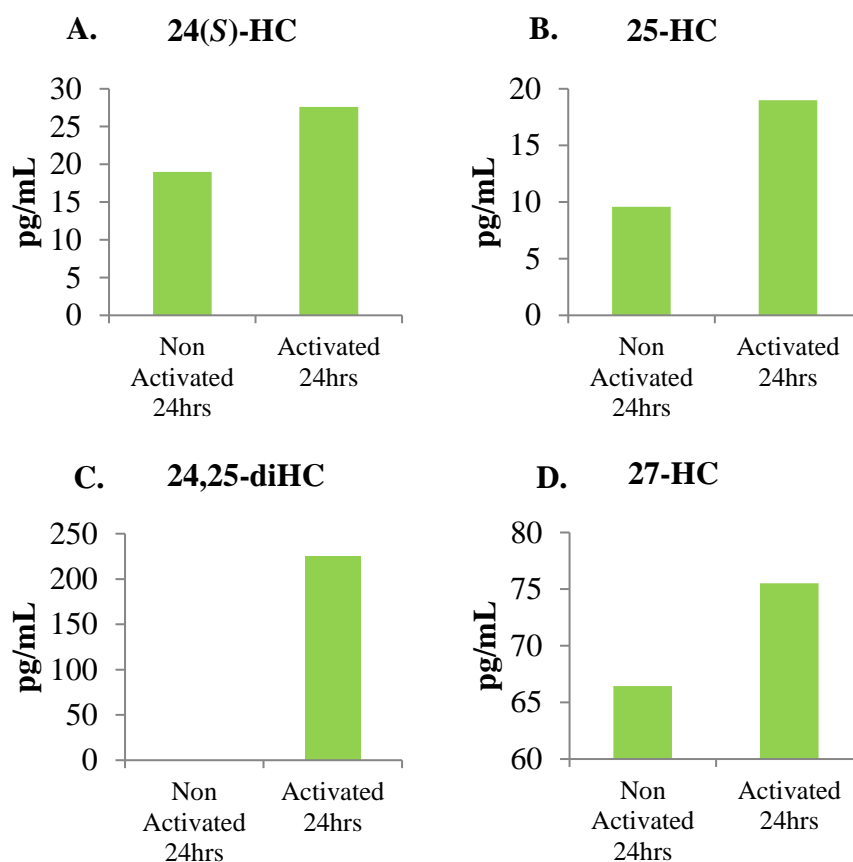


Figure 3.13 Total sterol analysis of cell culture media from non-polarised neonatal naïve CD4⁺ T cells activated or non-activated for 24 hrs. (A) 24(*S*)-HC, (B), 25-HC, (C) 24,25-diHC, (D) 7 α ,24,25-triHC. n=1

Notably, a peak was also detected at 532.3898 m/z in both cell pellets and to a lesser extent in cell culture supernatants shown in Figure 3.14. Increasing concentrations were detected in a time-dependent manner between 24 to 72 hrs incubation; however it was not possible to identify this peak with no authentic labelled standard available. Further investigation of this peak may reveal a possible sterol of interest.

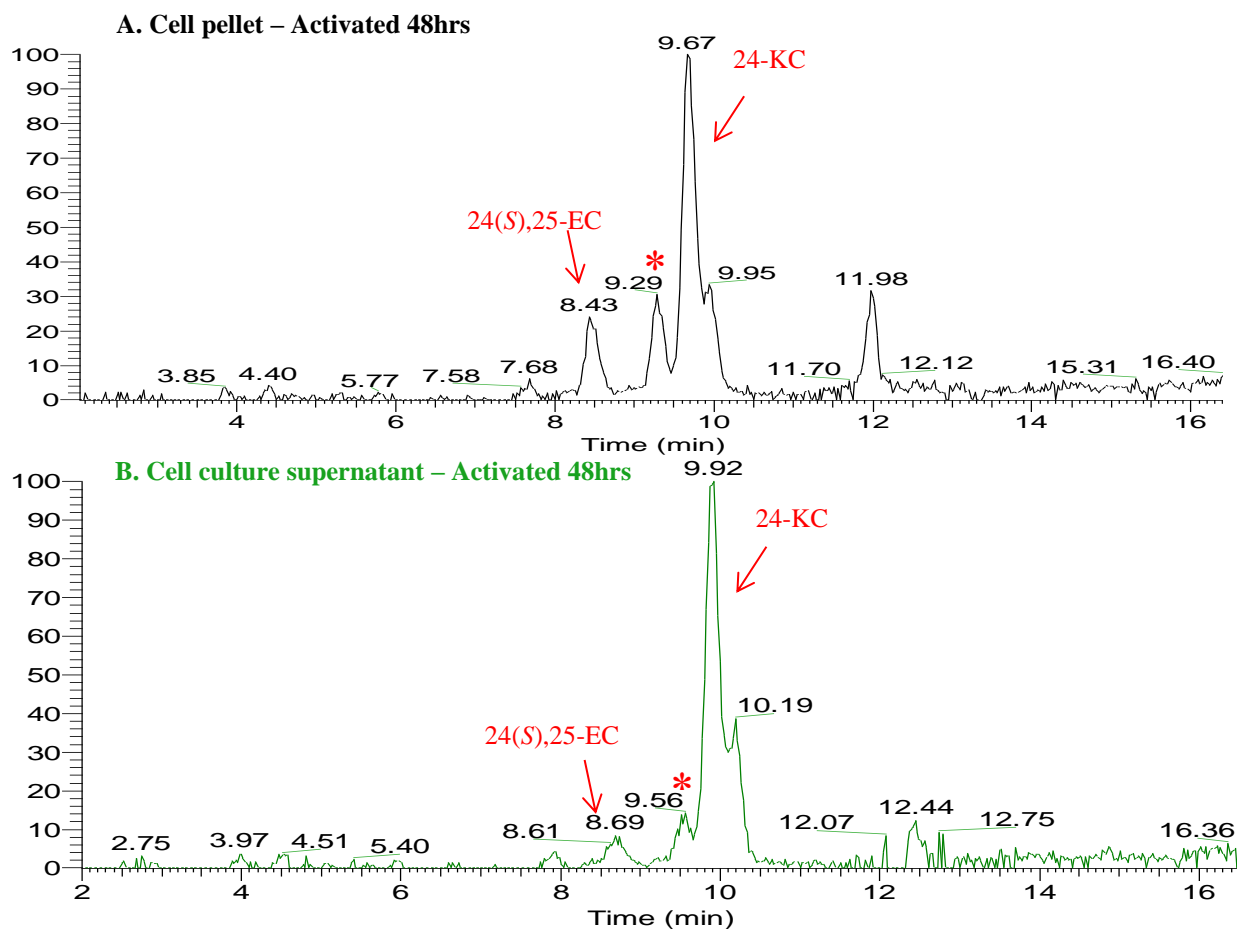


Figure 3.14 Representative reconstructed ion chromatogram at $532.3898 \text{ m/z} \pm 10\text{ppm}$ with a 26 minute gradient for 24(S),25-EC and 24-KC present in human neonatal naïve CD4^+ T cells. (A) Cell pellet of non-polarised 48 hr activated cells. (B) Cell culture media of non-polarised 48 hr activated cells. * indicates unidentified peak of interest detected between peaks for 24(S),25-EC and 24-K seen in both cell pellet and cell culture media analysis.

3.4 Discussion

This chapter explored total sterol analysis with an alkaline hydrolysis LC-MS method with extraction volumes of 10 μ L, 50 μ L and 100 μ L for plasma analysis. Strong agreement of quantified sterol levels was shown between extraction methods with 10 to 28% of detected side-chain monohydroxycholesterols present as free sterols while 7 α ring oxidised sterols accounted for up to 80% of the total sterol levels.

Sterol analysis of cell pellets and cell culture media was extended to include esterified sterols through alkaline hydrolysis prior to extraction providing an estimate of total sterols present. By applying an alkaline hydrolysis method to human neonatal nCD4⁺ T cell pellets and cell culture media samples it was possible to analyse both the free sterols and esterified sterols present.

Stimulation of the T cell receptor and coactivator receptors of neonatal nCD4⁺ T cells via anti-CD3 and anti-CD28 antibodies increased CD25 expression within 24 hrs enabling comparison of oxysterols in non-activated and activated neonatal nCD4⁺ T cells. As seen in previous chapters focussing on adult nCD4⁺ T cells, oxysterols 25-HC, 24(*S*)-HC, 24,25-diHC and 7 α ,24,25-triHC were detected in neonatal nCD4⁺ T cell pellets and cell culture media. 27-HC the most abundant oxysterol in human plasma was also present at quantifiable levels in neonatal nCD4⁺ T cell pellets and cell culture media. 27-HC has been reported to have an anti-viral role by inhibiting entry of viruses including herpes simplex virus (HSV), rotavirus and more recently it has been proposed that 27-HC inhibits SARS-CoV-2 ^(6,8,10).

The highest oxysterol concentrations were detected in the cell culture media with accumulation in a time-dependent manner which suggests exportation of the sterols from cells. As previously seen with adult nCD4⁺ T cell the most abundant oxysterol detected was 24,25-diHC representing 24(*S*),25-EC levels. Activation of T cells stimulates production of cholesterol through the mevalonate pathway in which 24(*S*),25-EC is produced in parallel to cholesterol through a shunt pathway ⁽¹⁶⁾. While a general trend could be seen in the oxysterol concentrations and activation in a time-dependant manner, variation in oxysterols detected and concentrations was seen between donor samples. This variation may also be due to the purity of isolated

cells prior to cell culture. Flow cytometry analysis for CD4 cell surface marker showed purity of 61 to 86% therefore it is possible that other mononuclear cells present during cell culture may contribute to the oxysterols detected during cell pellet and supernatant analysis.

Recently a study of neonatal oxysterols showed a developmental decline in detected urinary total oxysterols 4 β -HC, 22(*R*)-HC, 24(*S*)-HC and 27-HC in urine ⁽¹⁷⁾. Total oxysterols detected in serum including 4 β -HC, 24(*S*)-HC, 25-HC and 27-HC showed an opposite trend. A larger scale study of free and esterified oxysterols present in neonatal nCD4⁺ T cells would provide a greater indication of the normal oxysterols present in neonatal nCD4⁺ T cells and provide information on any developmental trends in concentrations.

3.5 References

1. Yang, C., McDonald, J. G., Patel, A., Zhang, Y., Umetani, M., Xu, F., ... Hobbs, H. H. (2006). Sterol Intermediates from Cholesterol Biosynthetic Pathway as Liver X Receptor Ligands. *Journal of Biological Chemistry*, 281(38), 27816–27826. <https://doi.org/10.1074/jbc.M603781200>
2. Lehmann, M., Kliewer, S. A., Moore, L. B., Smith-oliver, T. A., Oliver, B. B., Su, J., ... Willson, T. M. (1996). Activation of the Nuclear Receptor LXR by Oxysterols Defines a New Hormone Response Pathway. *Journal of Biological Chemistry*, 272(6), 3137–3140. <https://doi.org/10.1074/jbc.272.6.3137>
3. Janowski, B. A., Grogan, M. J., Jones, S. A., Wisely, G. B., Kliewer, S. A., Corey, E. J., Mangelsdorf, D. J. (1999). Structural requirements of ligands for the oxysterol liver X receptors LXR alpha and LXR beta. *Proc. Natl. Acad. Sci. USA*, 96, 266–271. Retrieved from [papers://b266c7f0-8dfd-47e2-9d28-64397eb23d54/Paper/p2357](https://pubmed.ncbi.nlm.nih.gov/10531211/)
4. DuSell, C. D., Umetani, M., Shaul, P. W., Mangelsdorf, D. J., & McDonnell, D. P. (2008). 27-Hydroxycholesterol is an endogenous selective estrogen receptor modulator. *Molecular Endocrinology*, 22(1), 65–77. <https://doi.org/10.1210/me.2007-0383>
5. Liu, S., Aliyari, R., Chikere, K., Li, G., Matthew, D., Smith, J. K., ... Cheng, G. (2013). Interferon-Inducible Cholesterol-25-Hydroxylase Broadly Inhibits Viral Entry by Production of 25-Hydroxycholesterol. *Immunity*, 38(1), 92–105. <https://doi.org/10.1016/j.immuni.2012.11.005>. Interferon-Inducible
6. Cagno, V., Civra, A., Rossin, D., Calfapietra, S., Caccia, C., Leoni, V., ... Lembo, D. (2017). Redox Biology Inhibition of herpes simplex-1 virus replication by 25-hydroxycholesterol and 27-hydroxycholesterol. *Redox Biology*, 12(March), 522–527. <https://doi.org/10.1016/j.redox.2017.03.016>
7. Liu, C., Yang, X. V., Wu, J., Kuei, C., Mani, N. S., Zhang, L., ... Lovenberg, T. W. (2011). Oxysterols direct B-cell migration through EBI2. *Nature*, 3–9. <https://doi.org/10.1038/nature10226>
8. Civra, A., Francese, R., Gamba, P., Testa, G., Cagno, V., Poli, G., & Lembo, D. (2018). Redox Biology 25-Hydroxycholesterol and 27-hydroxycholesterol inhibit human rotavirus infection by sequestering viral particles into late

- endosomes. *Redox Biology*, 19(September), 318–330.
<https://doi.org/10.1016/j.redox.2018.09.003>
9. Dzeletovic, S., Breuer, O., Lund, E., & Diczfalusy, U. (1995). Determination of Cholesterol oxidation products in human plasma by isotope dilution mass spectrometry. *Analytical Biochemistry*, 225, 73–80.
 10. Marcello, A., Civra, A., Milan, R., Nascimento, L., Rajasekharan, S., Giacobone, C., ... Leoni, V. (2020). The cholesterol metabolite 27-hydroxycholesterol inhibits SARS-CoV-2 and is markedly decreased in COVID-19 patients. *Redox Biology*, 36, 1–11.
<https://doi.org/10.1016/j.redox.2020.101682>
 11. Quehenberger, O., Armando, A. M., Brown, A. H., Milne, S. B., Myers, D. S., Merrill, A. H., ... Dennis, E. A. (2010). Lipidomics reveals a remarkable diversity of lipids in human plasma. *Journal of Lipid Research*, 51, 3299–3305. <https://doi.org/10.1194/jlr.M009449>
 12. Institutet, K. (2004). Analysis of Cholesterol Oxidation Products in Biological Samples. *Journal of AOAC International*, 87(2), 467–473.
 13. Yutuc, E., Dickson, A. L., Pacciarini, M., Grif, L., Forsgren, L., Trupp, M., ... Philip, H. (2021). Deep mining of oxysterols and cholestenoic acids in human plasma and cerebrospinal fluid : Quantification using isotope dilution mass spectrometry. *Analytica Chimica Acta*, 1154, 1–16.
<https://doi.org/10.1016/j.aca.2021.338259>
 14. Griffiths, W. J., & Sjövall, J. (2010). Bile acids : analysis in biological fluids and tissues. *Thematic Review*, 51, 23–41.
<https://doi.org/10.1194/jlr.R001941-JLR200>
 15. Griffiths, W. J., Crick, P. J., Wang, Y., Ogundare, M., Tuschl, K., Morris, A. A., ... Wang, Y. (2013). Analytical strategies for characterization of oxysterol lipidomes: Liver X receptor ligands in plasma. *Free Radical Biology and Medicine*, 59, 69–84.
<https://doi.org/10.1016/j.freeradbiomed.2012.07.027>.
 16. Englemans, E. G., & Chakrabarti, R. (1991). Interrelationships between Mevalonate Metabolism and the Mitogenic Signaling Pathway in T Lymphocyte Proliferation. *The Journal of Biological Chemistry*, 266(19), 12216–12222. [https://doi.org/10.1016/S0021-9258\(18\)98884-8](https://doi.org/10.1016/S0021-9258(18)98884-8)

17. Takaki, Y., Mizuochi, T., Takei, H., Eda, K., Konishi, K., Ishihara, J., ... Yamashita, Y. (2020). Urinary and serum oxysterols in children : developmental pattern and potential biomarker for pediatric liver disease. *Scientific Reports Nature Research*, 10, 20–26.
<https://doi.org/10.1038/s41598-020-63758-2>

Chapter 4. Investigating the effect of azole inhibition of CYP7B1 on Th17 polarised nCD4⁺ T cells

4.1 Introduction

Th17 cells mediate the recruitment of neutrophils and macrophages to infected tissues providing a crucial immune response against extracellular pathogens such as *Klebsiella pneumonia* ⁽¹⁻³⁾. Th17 cells have a specific cytokine expression profile of IL-17A, IL-17F, IL-22 and GM-CSF ⁽⁴⁻⁶⁾. The differentiation of human Th17 subset is driven by cytokines TGF- β , IL-6, IL-1 β and IL-23 and regulated by the transcription factor thymus retinoic acid-related orphan receptor gamma (ROR γ t) ⁽⁷⁻¹¹⁾. Treg cells, regulated by transcription factor forkhead box P3 (FoxP3), are crucial for negative regulation of the immune system ⁽¹²⁾. Activation of CD4⁺ T cells involves cell membrane expansion and proliferation requiring the cholesterol biosynthesis pathway. During Th17 differentiation cholesterol biosynthesis and uptake pathways are induced and the metabolism and efflux pathways suppressed. Cholesterol derivatives have previously been proposed to act as ROR γ t agonists but the endogenous ligand of ROR γ t is yet to be determined ⁽¹³⁻¹⁴⁾. Preliminary studies from the Griffiths-Wang group propose that cholesterol metabolising enzyme cytochrome P450 7B1 (CYP7B1) may be involved in the generation of endogenous agonists of ROR γ t (pending publication). Increased levels of cholesterol precursors are seen in all differentiated T helper cell subsets, however CYP7B1, induced by TGF- β , is specifically expressed in both Th17 and Treg cells ⁽¹⁵⁾. Treatment of Th17 cells with azole compounds have previously been reported to inhibit IL-17 expression which has been attributed to inhibition of cytochrome P450 enzyme CYP51, an enzyme in the cholesterol biosynthesis pathway ⁽¹⁶⁾. However the inhibition of azole compounds is non-specific towards CYP enzymes and azole compounds have also been reported to inhibit CYP7B1 ⁽¹⁶⁾. The focus of this chapter was to investigate the inhibitory effect of azole compounds clotrimazole and tebuconazole towards CYP7B1 and the effect on IL-17 expression in Th17 polarised naïve CD4⁺ T cells.

Aims:

- Investigate inhibition of CYP7B1 in Th17 cells with treatment with azole compounds

- Investigate the inhibition of IL-17 expression in Th17 cells with azole compound treatment

4.2 Materials and Methods

4.2.1 Isolation of human naïve CD4⁺ T cells from peripheral blood

Naïve CD4⁺ T cells were isolated from human peripheral blood by density gradient centrifugation with MACS[®] technology as described in *section 2.14* and *section 2.15* respectively.

4.2.2 Monitoring cell proliferation by flow cytometry

Naïve CD4⁺ T cell proliferation was monitored using cell proliferation dye eFluor[®]450 from eBiosciences (Hatfield, UK). The cell-permeable proliferation dye is non-fluorescent until covalently bound to cellular primary amines. As cells divide the dye is distributed equally between daughter cells halving the fluorescent intensity which can be measured by flow cytometry. Cell proliferation dye eFluor[®]450 was reconstituted with anhydrous dimethyl sulfoxide (DMSO) to 10 mM stock which was stored as 10 µL aliquots at -20°C and protected from light. Isolated cells were stained prior to cell culture following the manufacturer instructions. Briefly, 20 µM cell proliferation dye was prepared in phosphate buffered saline (PBS) from stock and added dropwise to equal volume of cells resuspended at 10 x 10⁶ cells per mL in PBS while being gently mixed by vortex. The cell-stain suspension was incubated at 37°C for 10 minutes protected from light. Labelling was stopped by the addition of 4X volume of complete media and cells were pelleted by centrifugation at 500 x g for 5 minutes at 4°C. A further three washes were performed with X-Vivo-20 media before seeding cells in X-Vivo-20 media for culture. Following cell culture, cells were harvested and aliquots were analysed with a BD FACS Aria or Novocyte. The violet fluorescent proliferation dye was excited with a 405nm violet laser and emission detected with 450/50nm band pass filter through Pacific Blue and eFluor450 channel. Data was analysed using FlowJo software.

4.2.3 Purity and activation analysis of naïve CD4⁺ T cells by flow cytometry

Following isolation, the purity of isolated cells from each donor was determined by flow cytometry. Aliquots of naïve CD4⁺ T cells were stained with anti-CD4, anti-CD45RA or anti-CD45RO antibodies and analysed by flow cytometry as described

in *section 2.1.12*. The activation of cells following cell culture was determined by staining 0an aliquot of cells with anti-CD25 antibodies and analysed by flow cytometry.

4.2.4 Culture conditions for CD3/CD28 activated naïve CD4⁺ T cells in X-Vivo-20 media with azole treatments on the third day of culture

Cell culture, activation and polarisation methods were adapted from Manel et al. 2008 ⁽⁹⁾. Naïve CD4⁺ T cells were isolated from healthy human donors and purity of isolated cells was assessed by flow cytometry prior to cell culture. Isolated CD4⁺ T cells were cultured at 1.0 to 2.5 x 10⁶ cells/mL/cm² and activated with anti-CD3 and anti-CD28 microbeads as described in *section 2.1.6*. Cells were cultured in X-Vivo-20 haematopoietic media under non-polarising, Treg-polarising or Th17-polarising conditions summarised in Table 4.1. On day three, cells were divided equally into fresh wells and topped up with fresh media with added azole treatments of clotrimazole or tebuconazole summarised in Table 4.2. Cells were stimulated with PMA and ionomycin for 6 hours prior to harvesting on day 6 for Donors 1 and 2, however as azole compounds also act on calcium channels this step was removed in further experiments ⁽¹⁷⁻¹⁸⁾.

Media fractions were extracted for EADSA processing and LC-MS analysis of oxysterols. When indicated cells were extracted for GC-MS sterol analysis by Alison Dickson. Cells were taken for RNA extraction and gene expression analysis.

Variable cell numbers obtained with different donors was a limiting factor on the polarising conditions and treatments possible in each experiment (Table 4.2). In the initial experiment performed nCD4⁺ T cells were cultured under Th17 polarising conditions with and without 1µM clotrimazole treatment on the third day of cell culture. The second experiment performed isolated enough cells from Donor 2 to compare 1µM clotrimazole and tebuconazole treatments in Th17 and Treg polarised nCD4⁺ T cells. In the subsequent experiment these treatments were repeated with the addition of 0.5µM clotrimazole and tebuconazole treatments. The next experiments focussed on comparison of non-polarised (Th0) and Th17 polarised nCD4⁺ cells treated with 0.0625 to 0.5µM treatments. Enough cells were isolated for donors 4 to 6 to perform duplicate sets of Th17 conditions for these experiments.

Table 4.1 Activated non-polarised (Th0), Th17-polarised and Treg-polarised naïve CD4⁺ T cell culture conditions in X-Vivo-20 media

Treatment	Time point	Th0 non-polarising	Th17 polarising	Treg polarising
Anti-CD3/CD28 MACS iBeads	Day 0	1:2 bead to cell ratio	1:2 bead to cell ratio	1:2 bead to cell ratio
Human IL-2 (Thermo Fisher Scientific 14-8029-63)	Day 0 and day 3	10U/mL	10U/mL	50U/mL
Human IL1-β (Thermo Fisher Scientific 14-8018-80)	Day 0 and day 3	-	10ng/mL	-
Human IL-6 (R&D Systems 206-IL-010)	Day 0 and day 3	-	10ng/mL	-
Human IL-21 (Thermo Fisher Scientific 14-8219-62)	Day 0 and day 3	-	10ng/mL	-
Human IL-23 (Thermo Fisher Scientific 14-8239-63)	Day 0 and day 3	-	10ng/mL	-
Human TGF-β1 (R&D Systems 240-B-002)	Day 0 and day 3	-	10ng/mL	5ng/mL
Anti-human IL-4 (Thermo Fisher Scientific clone:NIB42 16-7048-85)	Day 0 and day 3	10μg/mL	10μg/mL	10μg/mL
Anti-human IFN-γ (Thermo Fisher Scientific clone:MP4 25DC 16-7318-85)	Day 0 and day 3	10μg/mL	10μg/mL	10μg/mL
Clotrimazole (Sigma-Aldrich C6019)	Day 3	0.0625 - 1.0μM	0.0625 – 0.5μM	0.5 - 1.0μM
Tebuconazole (Sigma-Aldrich 32013)	Day 3	0.5 - 1.0μM	-	0.0625 - 1.0μM
Phorbol myristate acetate (PMA) (Sigma-Aldrich P1585)	Day 6	50ng/mL	50ng/mL	50ng/mL
Ionomycin (Sigma-Aldrich 10634)	Day 6	500ng/mL	500ng/mL	500ng/mL

Table 4.2 Experiment conditions and end point analysis for naïve CD4⁺ T cell cultures in X-Vivo-20 with azole treatments on day 3

Donor	Culture conditions	Number of cells seeded (10 ⁶)	Treatments	Analysis
1	Th17	2.5	1.0 µM clotrimazole	Cells for RNA extraction, Media for oxysterol analysis
2	Th17 Treg	1.5	1.0 µM clotrimazole 1.0 µM Tebuconazole	Cells for RNA extraction, Cells for GC-MS analysis Media for oxysterol analysis
3	Th17 Treg	1.5	0.5 µM clotrimazole 1.0 µM clotrimazole 0.5 µM Tebuconazole 1.0 µM Tebuconazole	Cells for RNA extraction, Cells for GC-MS analysis Media for oxysterol analysis
4	Th0 Th17	1.0	0.5 µM clotrimazole	Cells for RNA extraction, Media for oxysterol analysis, Media for ELISA
5	Th0 Th17	1.5	0.0625 µM clotrimazole 0.125 µM clotrimazole 0.5 µM clotrimazole	Cells for RNA extraction, Media for oxysterol analysis
6	Th0 Th17	1.3	0.5 µM clotrimazole	Cells for RNA extraction, Media for oxysterol analysis, Media for ELISA

4.2.5 Culture conditions for CD3/CD28 activated naïve CD4⁺ T cells in X-Vivo-20 media with azole treatments on the first day of culture

Naïve cells were isolated from healthy human donors and purity of isolated cells was assessed by flow cytometry prior to cell culture. Isolated nCD4⁺ T cells were cultured at 1.0 to 1.4 x 10⁶ cells/mL/cm² and activated with anti-CD3 and anti-CD28 microbeads as described in *section 2.1.6*. Cells were cultured in X-Vivo-20

haematopoietic media under non-polarising or Th17-polarising conditions (Table 4.1). For these experiments clotrimazole treatments were added to cell cultures on the first day of culture and on day three cells were divided equally into fresh wells and topped up with fresh media and harvested on day six summarised in Table 4.3. nCD4⁺ T cells isolated from Donor 7 were cultured under Th17 polarising conditions with and without 0.0625 μ M clotrimazole treatment. nCD4⁺ T cells isolated from Donor 8 were cultured under Th17 polarising conditions with and without 0.125 μ M and 0.5 μ M clotrimazole treatments. In the final experiment nCD4⁺ T cells isolated from Donor 9 were cultured under non-polarising or Th17 polarising conditions with 0.125 μ M and 0.25 μ M treatments. Media fractions were extracted for EADSA processing and LC-MS analysis of oxysterols and cells were taken for RNA extraction and gene expression analysis.

Table 4.3 Experiment conditions and end point analysis for naïve CD4⁺ T cell cultures in X-Vivo-20 with azole treatments on day 0

Donor	Culture conditions	Number of cells seeded (10^6)	Treatments	Analysis
7	Th17	1.0	0.0625 μ M clotrimazole	Cells for RNA extraction, Media for oxysterol analysis, Media for ELISA
8	Th17	1.4	0.125 μ M clotrimazole 0.5 μ M clotrimazole	Cells for RNA extraction, Media for oxysterol analysis, Media for ELISA
9	Th17 Th0	1.0	0.125 μ M clotrimazole 0.25 μ M clotrimazole	Cells for RNA extraction, Media for oxysterol analysis, Media for ELISA

4.2.6 Gene expression and protein secretion analysis

Messenger RNA expression of CD4⁺ T cell cytokines and transcription factors were analysed by qRT-PCR as described in *section 2.2.2*. Genomic DNA was removed with TURBO DNase treatment of extracted RNA as described in *section 2.2.2.2*.

Raw Ct values normalised against *RP18S* and *ACTB* were used to calculate the relative expression levels of cultured cells using the $2^{-\Delta\Delta C_t}$ method ⁽¹⁹⁾. IL-17 secreted by cells into the culture media was measured by sandwich ELISA as described in *section 2.2.3.1*.

4.2.7 Sterol analysis

Sterol content of either cell pellets or culture media of CD4⁺ T cells were subjected to EADSA processing as described in *section 2.3.2* and analysed by LC-MSⁿ as described in *section 2.3.4*. When indicated GC-MS sterol analysis was also performed on cell pellets by Alison Dickson.

4.2.8 Statistical analysis

When indicated, the statistical significance of differences in mean sterol quantities and mRNA expression were determined using a two tailed T test or Mann-Whitney rank test using Microsoft Excel for normal and non-normal distribution respectively, where p values ≤ 0.05 were considered statistically significant.

4.3 Results

4.3.1 Naïve CD4⁺ T cells isolated from human PBMCs by MACs showed > 88% CD4⁺ purity

Single stain flow cytometry analysis of MACs isolated cells from human PBMCs showed 88.5 to 98.6% CD4⁺ purity Table (4.4). Figure 4.1 shows a representation of the gating strategy used to identify cells. Surface staining of marker CD45RA showed between 98.3 to 99.7% CD45RA⁺ cells. Aliquots were also stained for memory T cell marker CD45RO, 12.0 to 31.3% of isolated cells were CD45RO⁺. The level of activation of isolated cells monitored by CD25 (IL-2 receptor α) expression revealed < 23% of isolated cells were CD25⁺. Figure 4.2 shows a representation of day 0 flow analysis of naïve CD4⁺ T cells isolated from Donor 3.

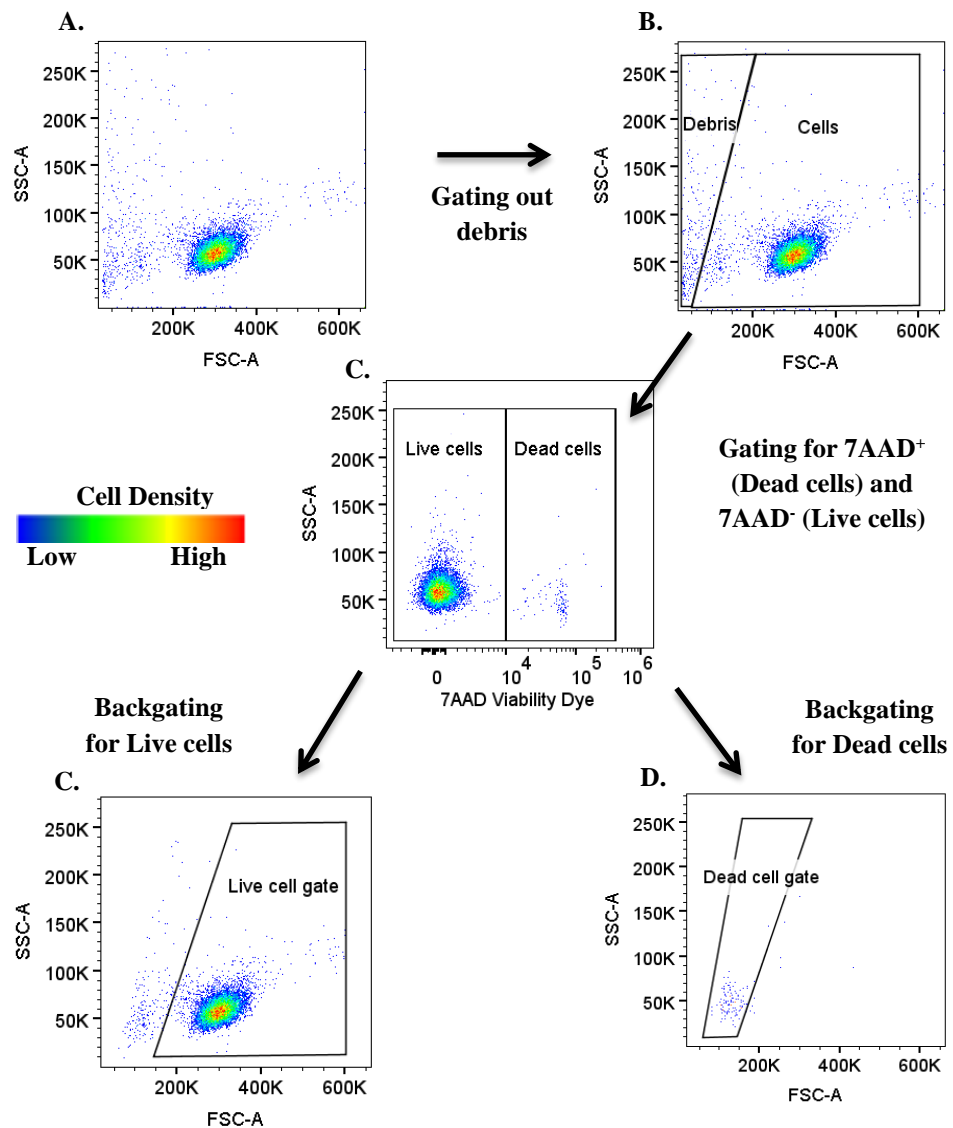


Figure 4.1 Representative Gating strategy applied to isolated naïve CD4⁺ T cells to identify live cells and exclude dead cells using 7AAD Viability dye staining. Sample aliquots were single stained with 7AAD viability stain and not fixed prior to processing with ACEA Bioscience Novocyte. Analysis was performed with FlowJo software. Events were plotted on FSC/SSC for (A) ungated, (B) isolated cells excluding debris. (C) Cells were plotted with 7AAD/SSC to identify the dead/ apoptotic cells which have incorporated the 7AAD stain that was able to penetrate compromised cell membranes and bind to the double stranded DNA. An FSC/SSC plot was applied to the identified cells to create the (D) live cell gate and (E) dead cell gate. The Live cell gate was then applied to other single stained aliquots of the same sample.

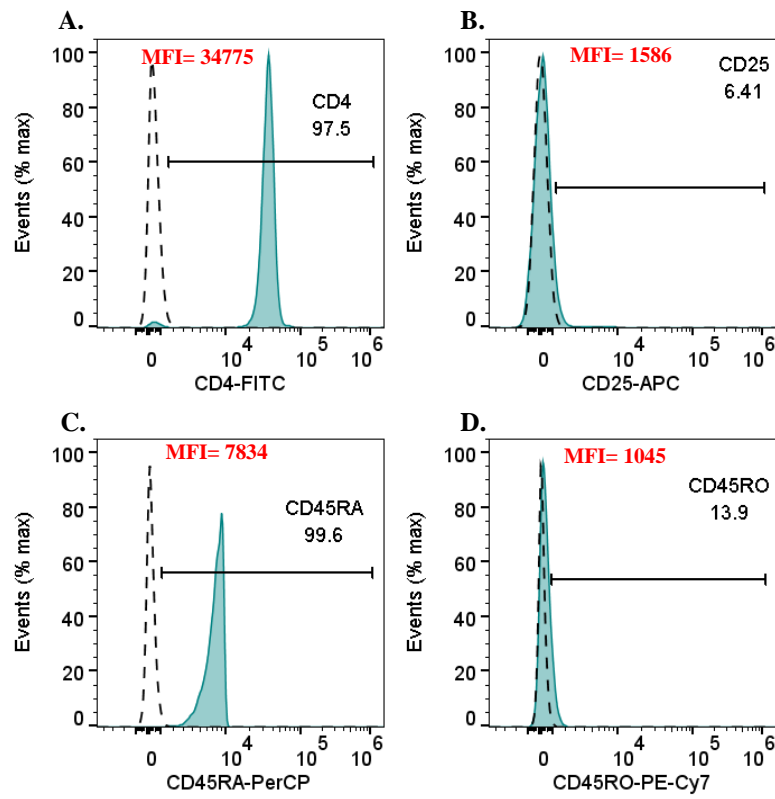


Figure 4.2 Representative flow cytometry analysis of isolated naïve CD4⁺ T cells prior to cell culture. (A) 97.5% CD4⁺ purity was achieved with MACs separation. (B) Low CD25 expression was observed with 6.41% CD25⁺ cells. (C) 99.6% CD45RA⁺ cells expression was seen (D) 13.9% of isolated cells were CD45RO⁺. Filled histograms represent the fluorochrome conjugated antibody stained cells. Gates were determined using background fluorescence of unstained samples (1%) indicated by the dashed histogram. The Median Fluorescence intensities (MFI) are indicated in red.

Table 4.4 Surface marker expression of isolated nCD4⁺ T cells from healthy human donors

Donor	% CD25	% CD4	% CD45RA	% CD45RO
1	11.9	97.6	-	-
2	1.4	94.3	-	-
3	15.3	98.6	99.7	31.3
4	13.4	98.4	98.6	19.4
5	11.1	97.6	99.3	25.9
6	6.41	97.5	99.6	13.9
7	3.22	88.11	89.73	1.07
8	22.2	88.5	99.4	12.0
9	11.7	92.2	99.0	13.0

4.3.2 Variation in CD25 expression, cell viability and proliferation of polarised cells was observed between Donors with day 3 azole treatments

An initial experiment performed in which isolated nCD4⁺ T cells from Donor 1 were cultured under Th17 polarising conditions with and without 1 μ M clotrimazole treatment on day 3 showed little effect on CD25 expression or cell proliferation on day 6. A slight increase in 7AAD viability staining was observed from 27.6% in untreated Th17 polarised cells to 36.5% in Th17 polarised cells with 1 μ M clotrimazole treatment. Isolated nCD4⁺ T cells from Donor 2 cultured under Th17 polarising conditions with 1 μ M clotrimazole or tebuconazole treatments on day 3 had no obvious impact on cell proliferation and no change in 7AAD viability staining. CD25 expression in Th17 polarised cells with 1 μ M clotrimazole or tebuconazole was < 5% lower than Th17 polarised cells with vehicle treatment. No change in proliferation of Treg polarised cells was observed with 1 μ M clotrimazole or tebuconazole treatments however cell viability was lower in comparison to Treg polarised cells with vehicle treatment. Generally, CD25 expression of Treg polarised cells was ~ 20% lower in comparison to Th17 polarised cells and slight reduction of CD25 expression was seen with azole treatments.

No change in cell viability or activation was observed with Th17 polarised cells of Donor 3 with clotrimazole or tebuconazole treatments at 0.5 μ M and 1 μ M shown in Figure 4.3. Proliferation of Th17 cells was also unaffected by azole treatments at 0.5 μ M and only slightly reduced with 1 μ M treatments. As with Donor 2 the activation of Donor 3 Treg polarised cells was ~20% lower compared to Th17 cells but no change in activation was seen with clotrimazole or tebuconazole treatments at 0.5

μM and 1 μM shown in Figure 4.4. Little difference in cell viability or cell proliferation was observed in Treg cells with clotrimazole or tebuconazole treatments.

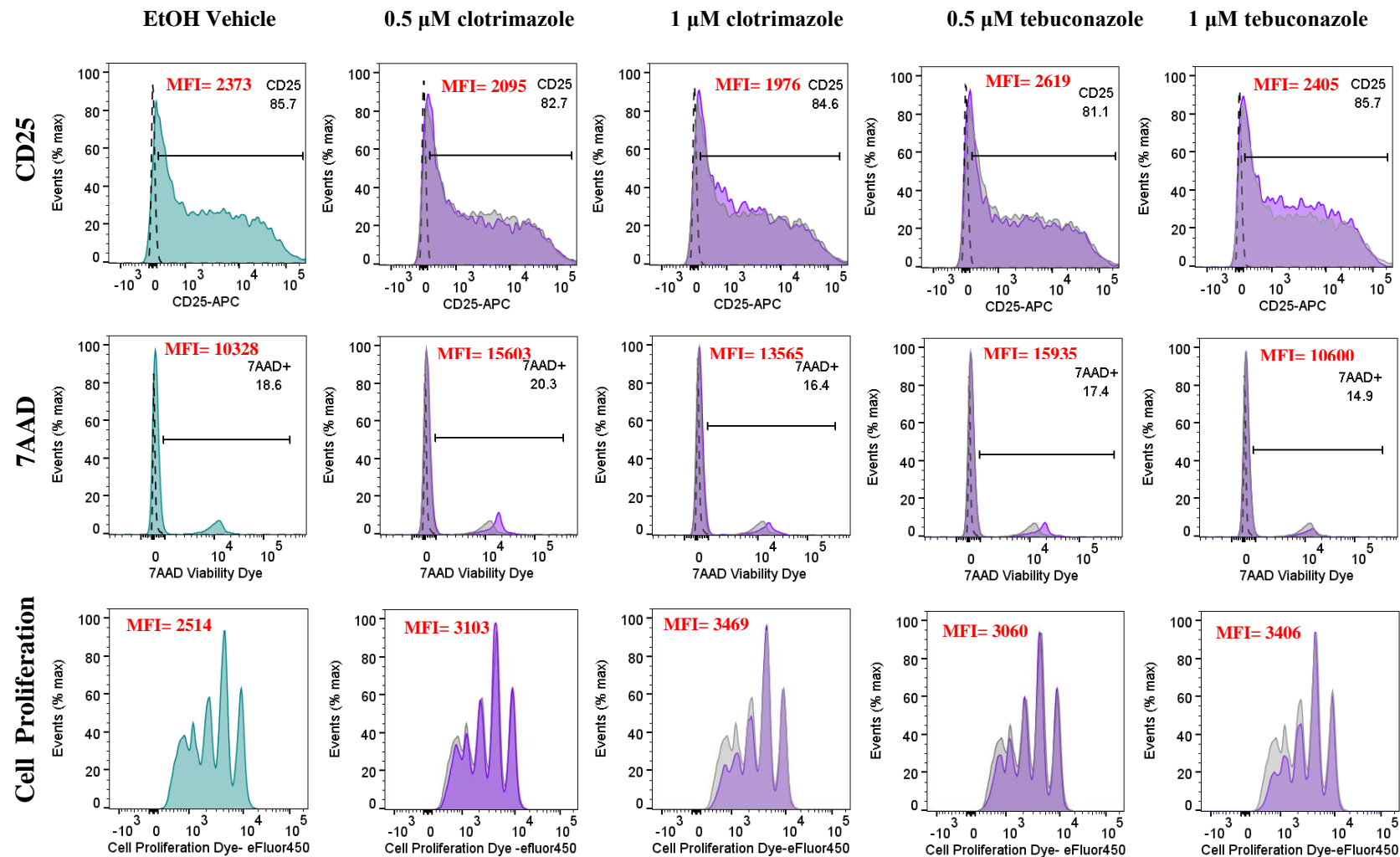


Figure 4.3 Flow cytometry analysis of naïve CD4⁺ T cells from Donor 3 cultured under Th17 polarising conditions with or without treatment with azole inhibitors clotrimazole and tebuconazole at 0.5µM and 1.0µM concentrations harvested after 6 days of cell culture. Top panel: CD25 expression Middle panel: 7AAD cell viability staining. Bottom panel: cell proliferation. Filled blue histograms represent the fluorochrome conjugated antibody stained Th17 polarised cells with vehicle control. Filled purple histograms represent the fluorochrome conjugated antibody stained Th17 polarised cells with azole treatments overlaid with vehicle control (grey). Gates were determined using background fluorescence of unstained samples (1%) indicated by the dashed histogram. The Median Fluorescence intensities (MFI) are indicated in red.

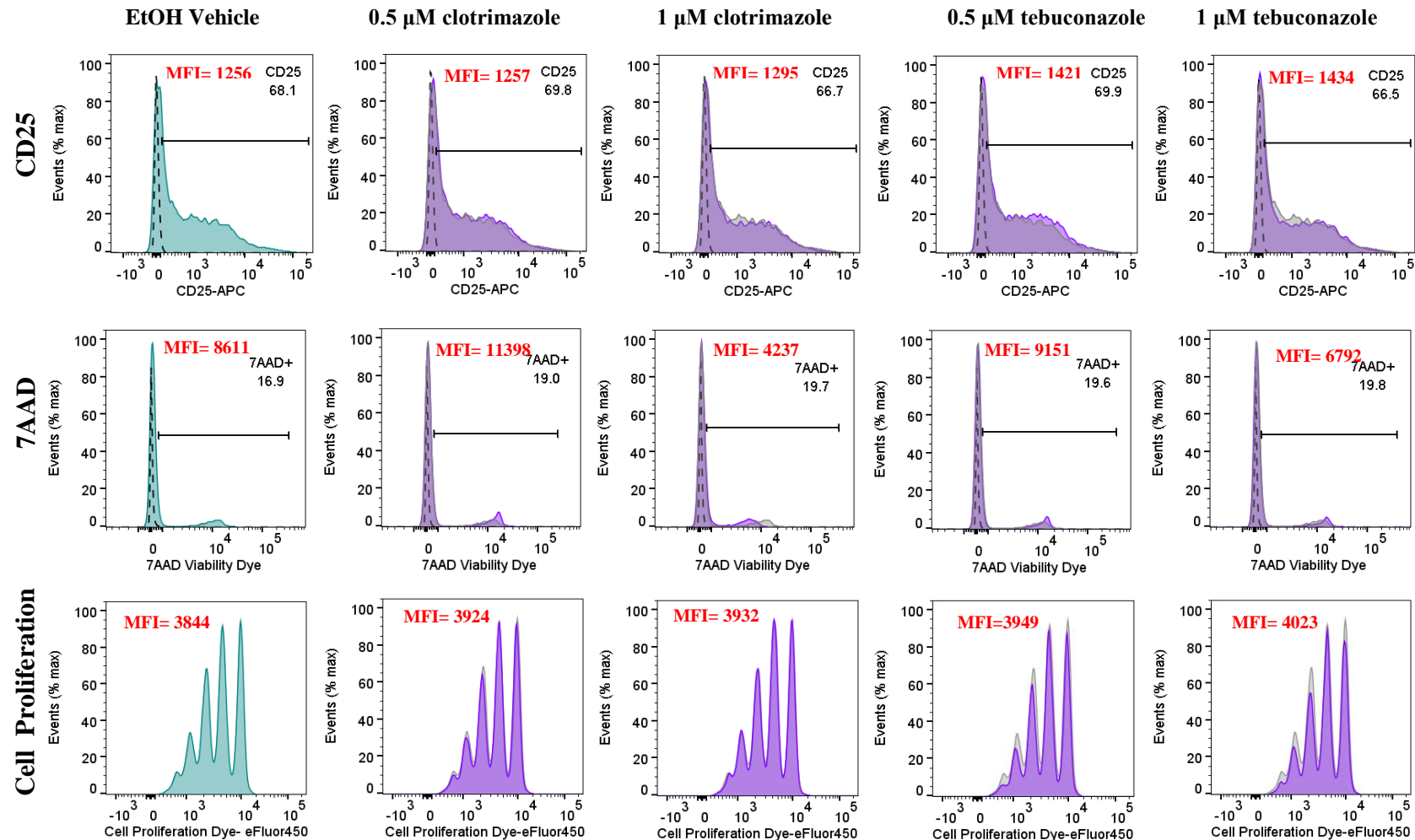


Figure 4.4 Flow cytometry analysis of naïve CD4⁺ T cells from Donor 3 cultured under Treg polarising conditions with or without treatment with azole inhibitors clotrimazole and tebuconazole at 0.5µM and 1.0µM concentrations harvested after 6 days of cell culture. Top panel: CD25 expression Middle panel: 7AAD cell viability staining. Bottom panel: cell proliferation. Filled blue histograms represent the fluorochrome conjugated antibody stained Treg polarised cells with vehicle control. Filled purple histograms represent the fluorochrome conjugated antibody stained Treg polarised cells with azole treatments overlaid with vehicle control (grey). Gates were determined using background fluorescence of unstained samples (1%) indicated by the dashed histogram. The Median Fluorescence intensities (MFI) are indicated in red.

Low activation and poor proliferation of non-polarised cells was achieved with nCD4⁺ T isolated from Donor 4 with both vehicle and 0.5 μ M clotrimazole treatments shown in Figure 4.5. In contrast with the previous experiments, an inhibitory effect on cell proliferation was seen in Th17 polarised cells with 0.5 μ M clotrimazole treatment and activation was reduced with 66.9% CD25⁺ cells with clotrimazole treatment compared to 77.4% CD25⁺ cells with the vehicle control. As inhibitory effects were seen with Th17 polarised cells cultured with 0.5 μ M clotrimazole treatments from Donor 4, lower concentrations were investigated in the following experiment. Isolated nCD4⁺ T cells from Donor 5 were cultured under non- polarised conditions with vehicle control or Th17 polarised conditions with vehicle control, 0.0625 μ M clotrimazole or 0.5 μ M clotrimazole. Low activation and poor proliferation of Th0 non-polarised cells was also seen with nCD4⁺ T isolated from Donor 5 with vehicle treatment presented in Figure 4.6. Donor 5 nCD4⁺ T cells cultured under Th17 polarised conditions with clotrimazole treatments showed similar activation, viability and proliferation to Donors 1 to 3 with a small decrease in CD25⁺ cells and proliferation with 0.5 μ M clotrimazole treatment.

The final experiment performed with day 3 azole treatments repeated culture of non-polarised Th0 cells or Th17 polarised cells with or without 0.5 μ M clotrimazole treatment for nCD4⁺ T cells isolated from Donor 6. Higher activation and proliferation of Th0 non-polarised cells was achieved with Donor 6 isolated cells than previously achieved with Donors 4 and 5, however Th17 polarised cells showed greater activation with vehicle control (Figure 4.7). Similarly to Donor 5, a small decrease in CD25⁺ cells and proliferation of cells was seen with 0.5 μ M clotrimazole treatment.

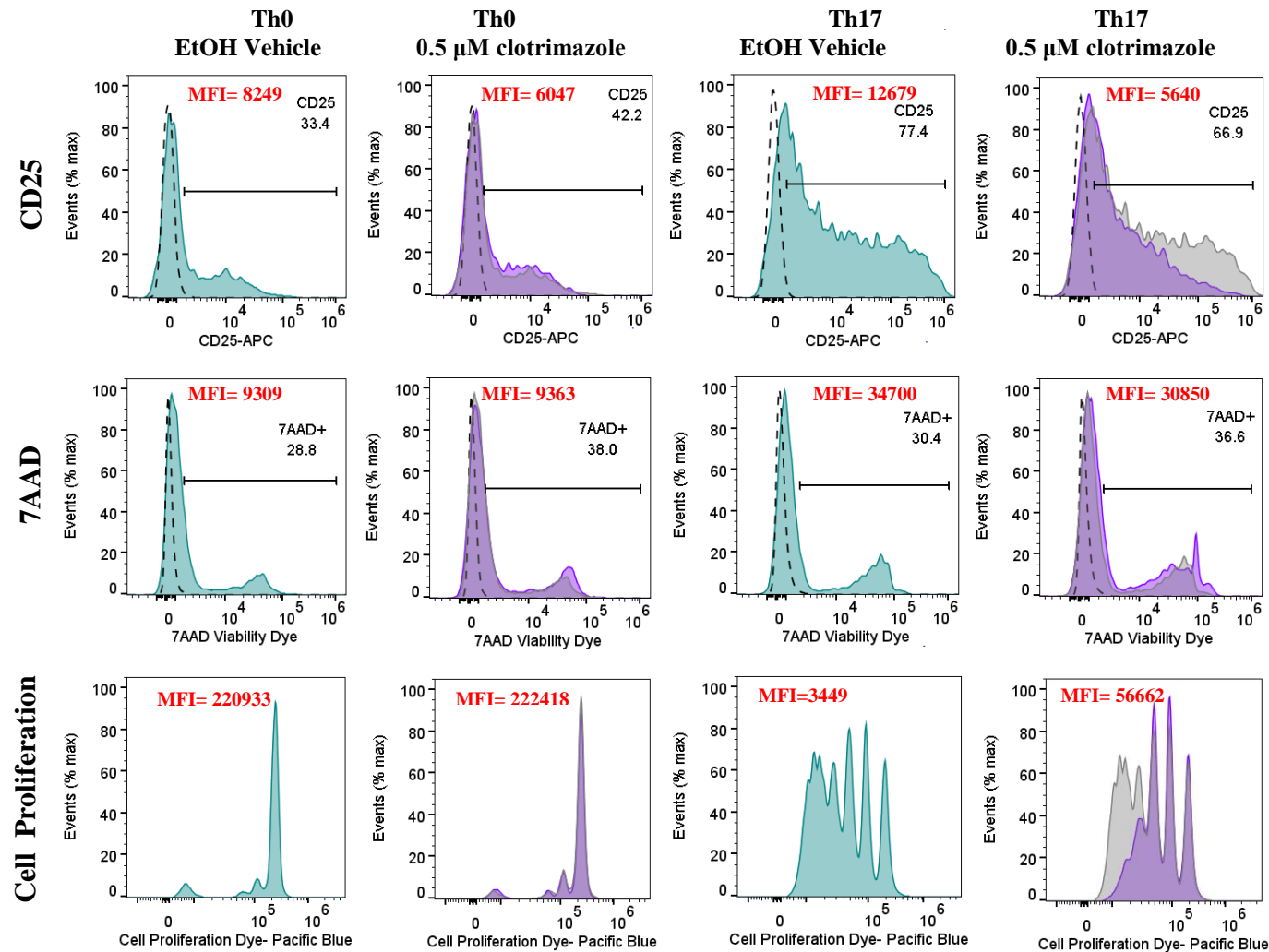


Figure 4.5 Flow cytometry analysis of naïve CD4⁺ T cells from Donor 4 cultured under non-polarising Th0 or Th17 polarising conditions with or without 0.5 µM clotrimazole treatment harvested after 6 days of cell culture. Top panel: CD25 expression Middle panel: 7AAD cell viability staining. Bottom panel: cell proliferation. Filled blue histograms represent the fluorochrome conjugated antibody stained Th0 and Th17 polarised cells with vehicle control. Filled purple histograms represent the fluorochrome conjugated antibody stained Th0 and Th17 polarised cells with clotrimazole treatment overlaid with vehicle control (grey). Gates were determined using background fluorescence of unstained samples (1%) indicated by the dashed histogram. The Median Fluorescence intensities (MFI) are indicated in red.

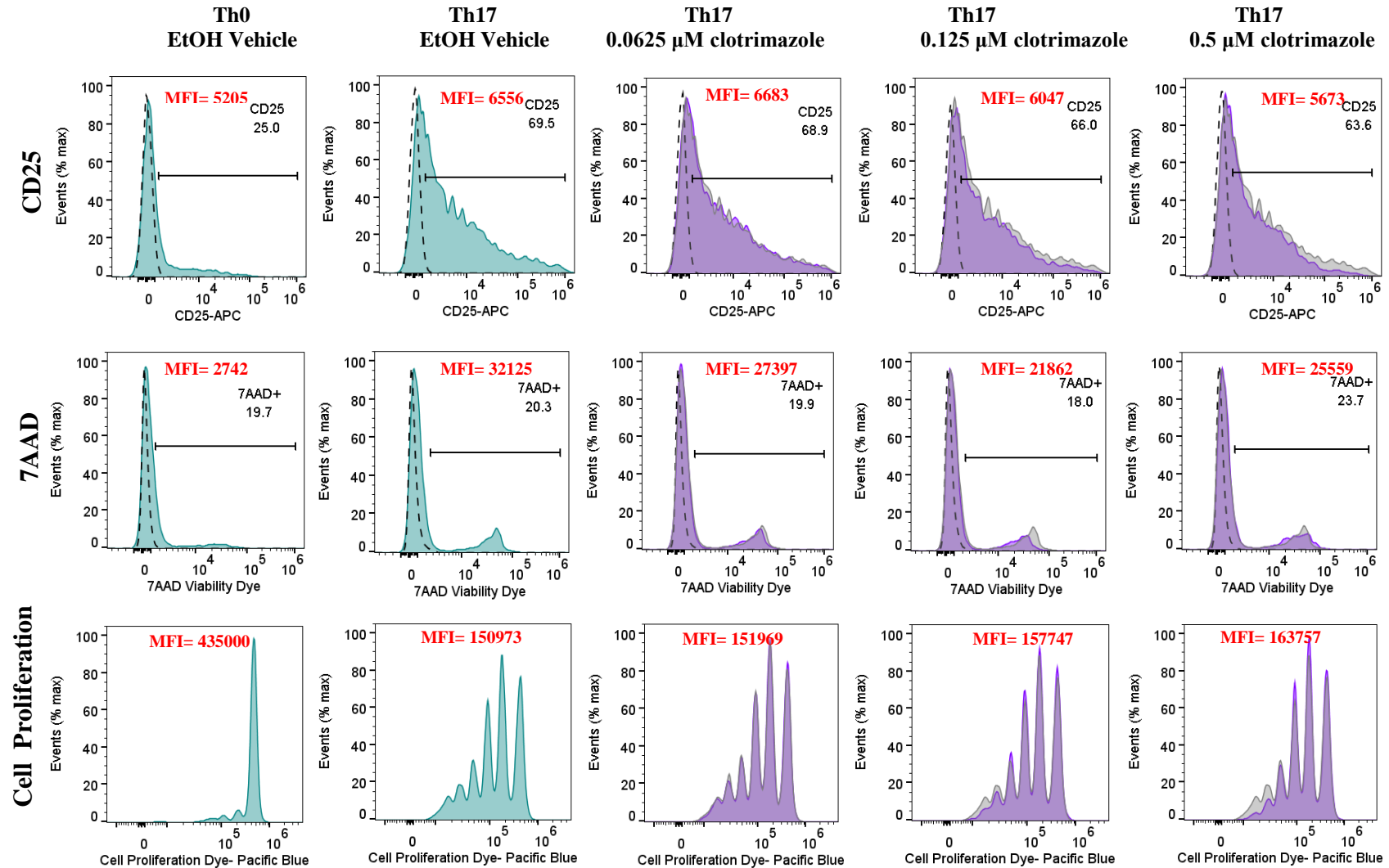


Figure 4.6 Flow cytometry analysis of naïve CD4⁺ T cells from Donor 5 cultured under non-polarising Th0 or Th17 polarising conditions with or without 0.0625 to 0.5 µM clotrimazole treatments harvested after 6 days of cell culture. Top panel: CD25 expression Middle panel: 7AAD cell viability staining. Bottom panel: cell proliferation. Filled blue histograms represent the fluorochrome conjugated antibody stained Th0 and Th17 polarised cells with vehicle control. Filled purple histograms represent the fluorochrome conjugated antibody stained Th17 polarised cells with clotrimazole treatment overlaid with vehicle control (grey). Gates were determined using background fluorescence of unstained samples (1%) indicated by the dashed histogram. The Median Fluorescence intensities (MFI) are indicated in red.

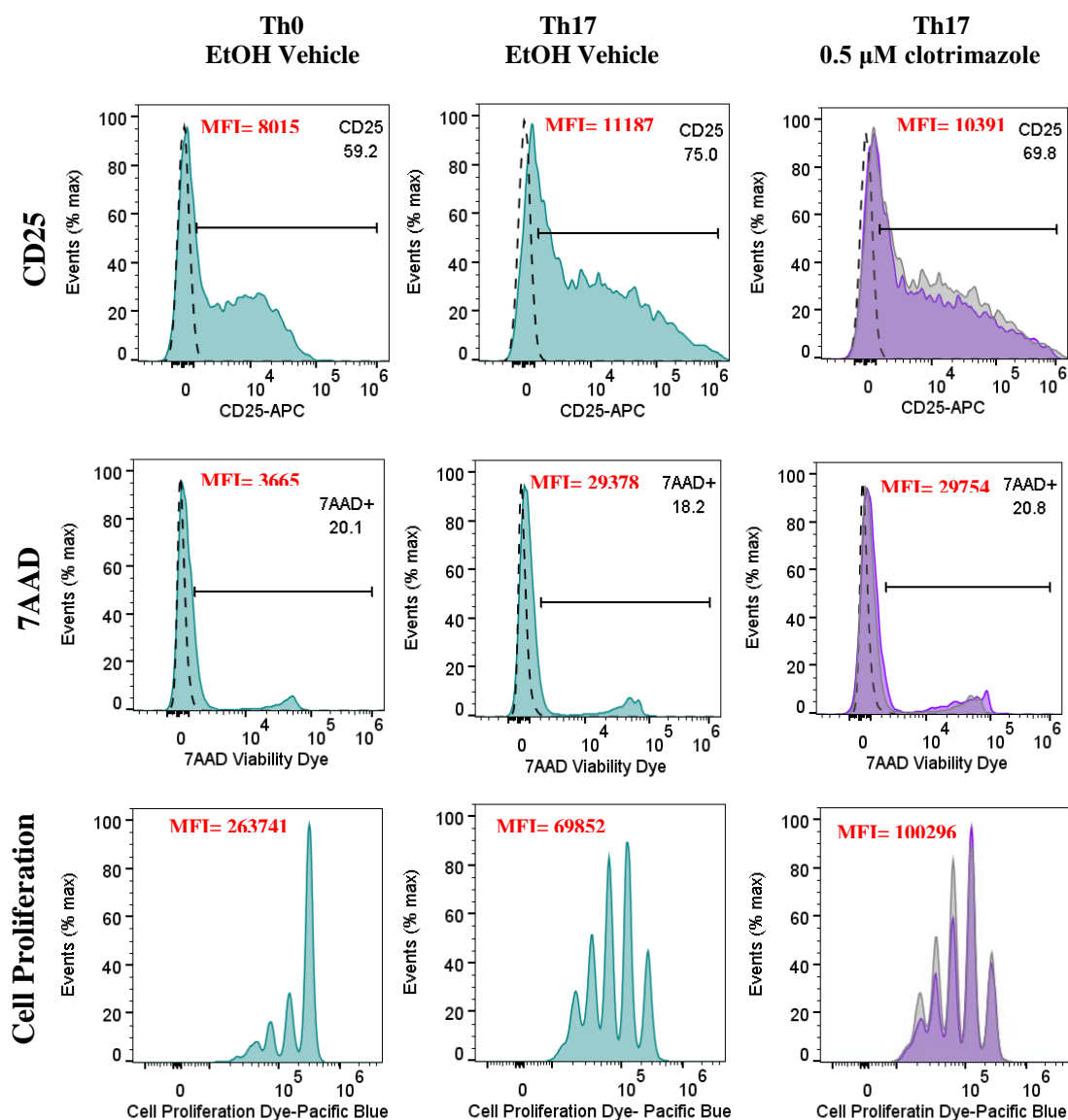


Figure 4.7 Flow cytometry analysis of naïve CD4⁺ T cells from Donor 6 cultured under non-polarising Th0 or Th17 polarising conditions with or without 0.5 µM clotrimazole treatment harvested after 6 days of cell culture. Top panel: CD25 expression Middle panel: 7AAD cell viability staining. Bottom panel: cell proliferation. Filled blue histograms represent the fluorochrome conjugated antibody stained Th0 and Th17 polarised cells with vehicle control. Filled purple histograms represent the fluorochrome conjugated antibody stained Th17 polarised cells with clotrimazole treatment overlaid with vehicle control (grey). Gates were determined using background fluorescence of unstained samples (1%) indicated by the dashed histogram. The Median Fluorescence intensities (MFI) are indicated in red.

4.3.3 Variation in CD25 expression, cell viability and proliferation of polarised cells was observed between Donors with day 0 azole treatments

Due to the variation seen with day 3 azole treatments at higher concentrations it was decided to investigate the effect of azole treatment from 0.0625 to 0.5 μM added on the first day of cell culture. Isolated nCD4^+ T cells from Donor 7 cultured under Th17 polarising conditions with and without 0.0625 μM clotrimazole treatment on day 0 showed no change in CD25 expression, cell viability or proliferation on day 6 with similar MFI for Th17 vehicle control and clotrimazole treated Th17 cells shown in Figure 4.8.

Isolated nCD4^+ T cells from Donor 8 cultured under Th17 polarising conditions showed lower activation and reduced proliferation with increasing clotrimazole treatments. CD25 expression was $\sim 10\%$ lower with 0.5 μM clotrimazole treatment although no clear effect on the viability of cells was seen, presented in Figure 4.9. In the final experiment from Donor 9, isolated nCD4^+ T cells were cultured under Th0 or Th17 polarising conditions with 0.125 or 0.25 μM clotrimazole treatments. As with previous experiments lower CD25 expression and poorer proliferation was achieved for Th0 cells shown in Figure 4.10. The expression of CD25 in Th17 polarised cells with 0.125 and 0.25 μM clotrimazole treatments did not differ from Th17 polarised cells with vehicle treatment and viability of cells was also unaffected.

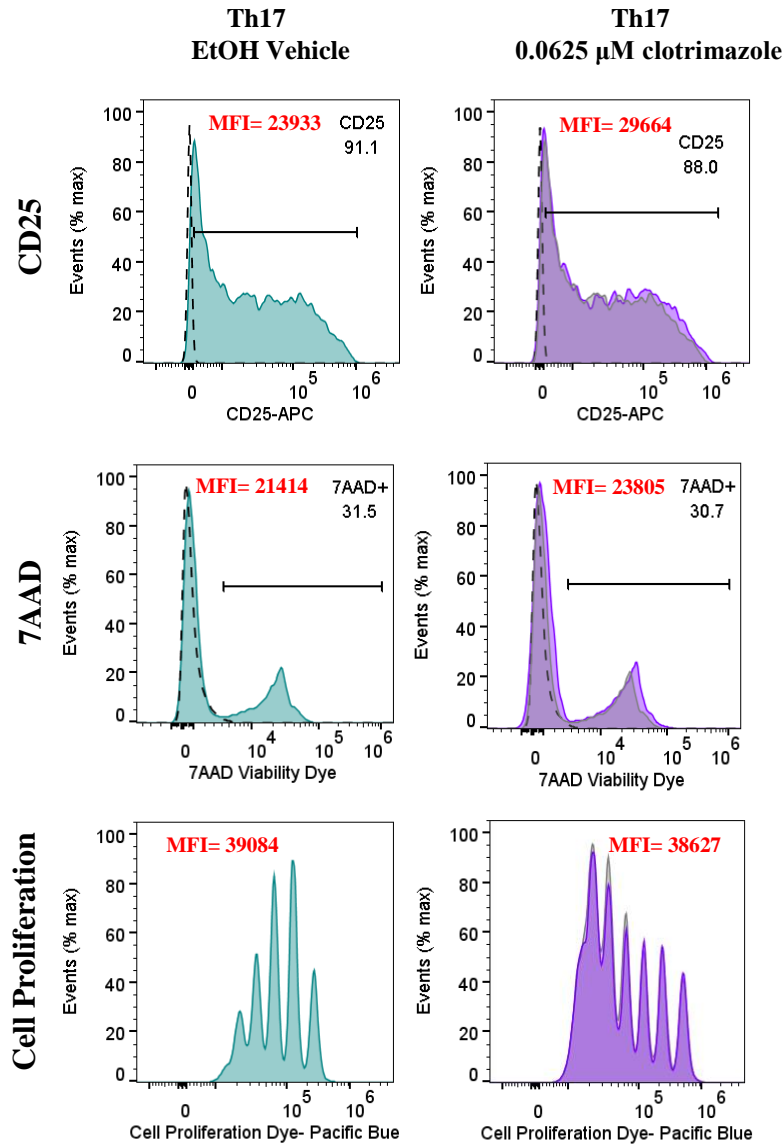


Figure 4.8 Flow cytometry analysis of naïve CD4⁺ T cells from Donor 7 cultured under Th17 polarising conditions with or without 0.0625 µM clotrimazole treatment harvested after 6 days of cell culture. Top panel: CD25 expression Middle panel: 7AAD cell viability staining. Bottom panel: cell proliferation. Filled blue histograms represent the fluorochrome conjugated antibody stained Th17 polarised cells with vehicle control. Filled purple histograms represent the fluorochrome conjugated antibody stained Th17 polarised cells with clotrimazole treatment overlaid with vehicle control (grey). Gates were determined using background fluorescence of unstained samples (1%) indicated by the dashed histogram. The Median Fluorescence intensities (MFI) are indicated in red.

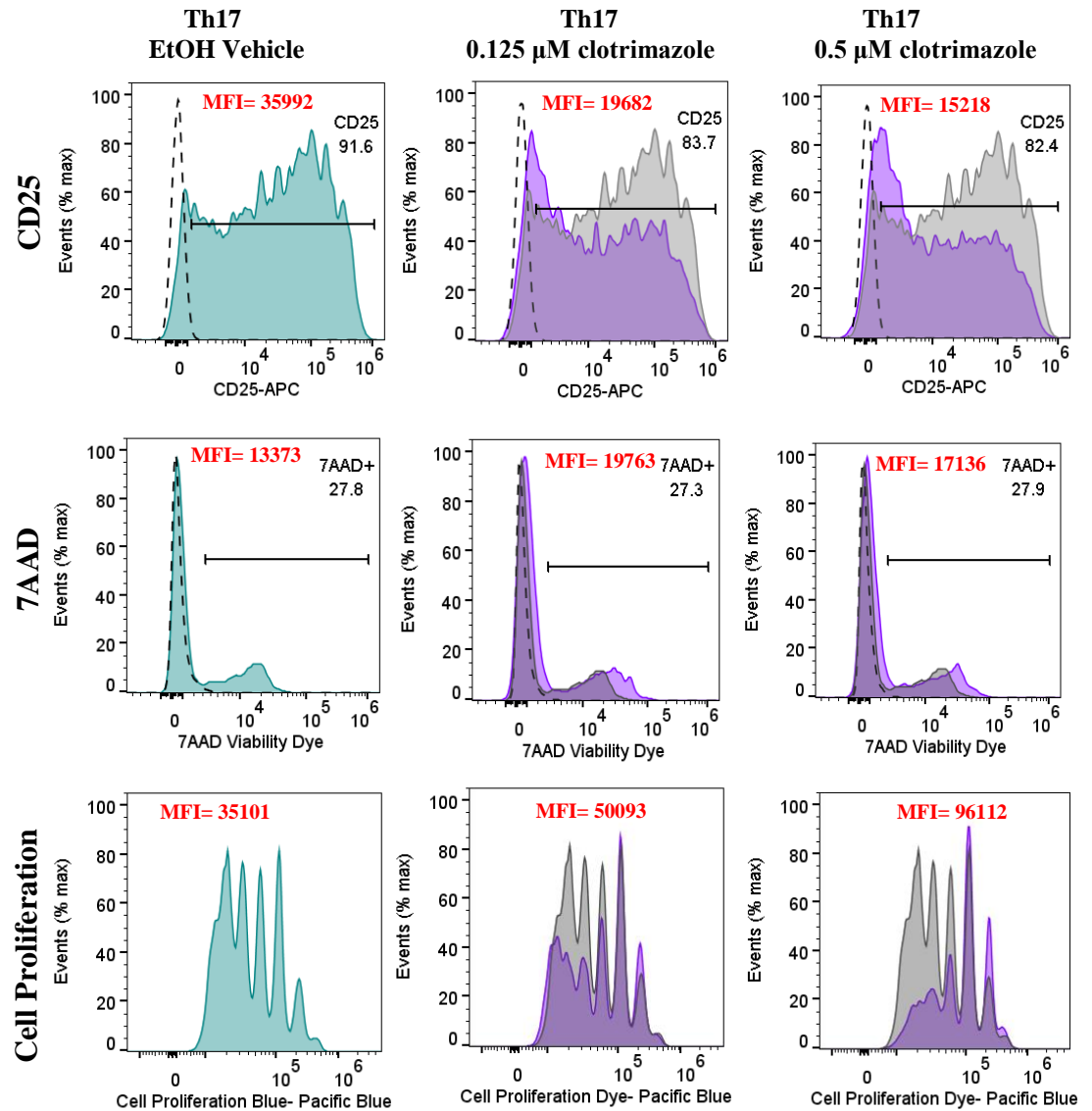


Figure 4.9 Flow cytometry analysis of naïve CD4⁺ T cells from Donor 8 cultured under Th17 polarising conditions with or without 0.125 or 0.5µM clotrimazole treatment harvested after 6 days of cell culture. Top panel: CD25 expression Middle panel: 7AAD cell viability staining. Bottom panel: cell proliferation. Filled blue histograms represent the fluorochrome conjugated antibody stained Th17 polarised cells with vehicle control. Filled purple histograms represent the fluorochrome conjugated antibody stained Th17 polarised cells with clotrimazole treatment overlaid with vehicle control (grey). Gates were determined using background fluorescence of unstained samples (1%) indicated by the dashed histogram. The Median Fluorescence intensities (MFI) are indicated in red.

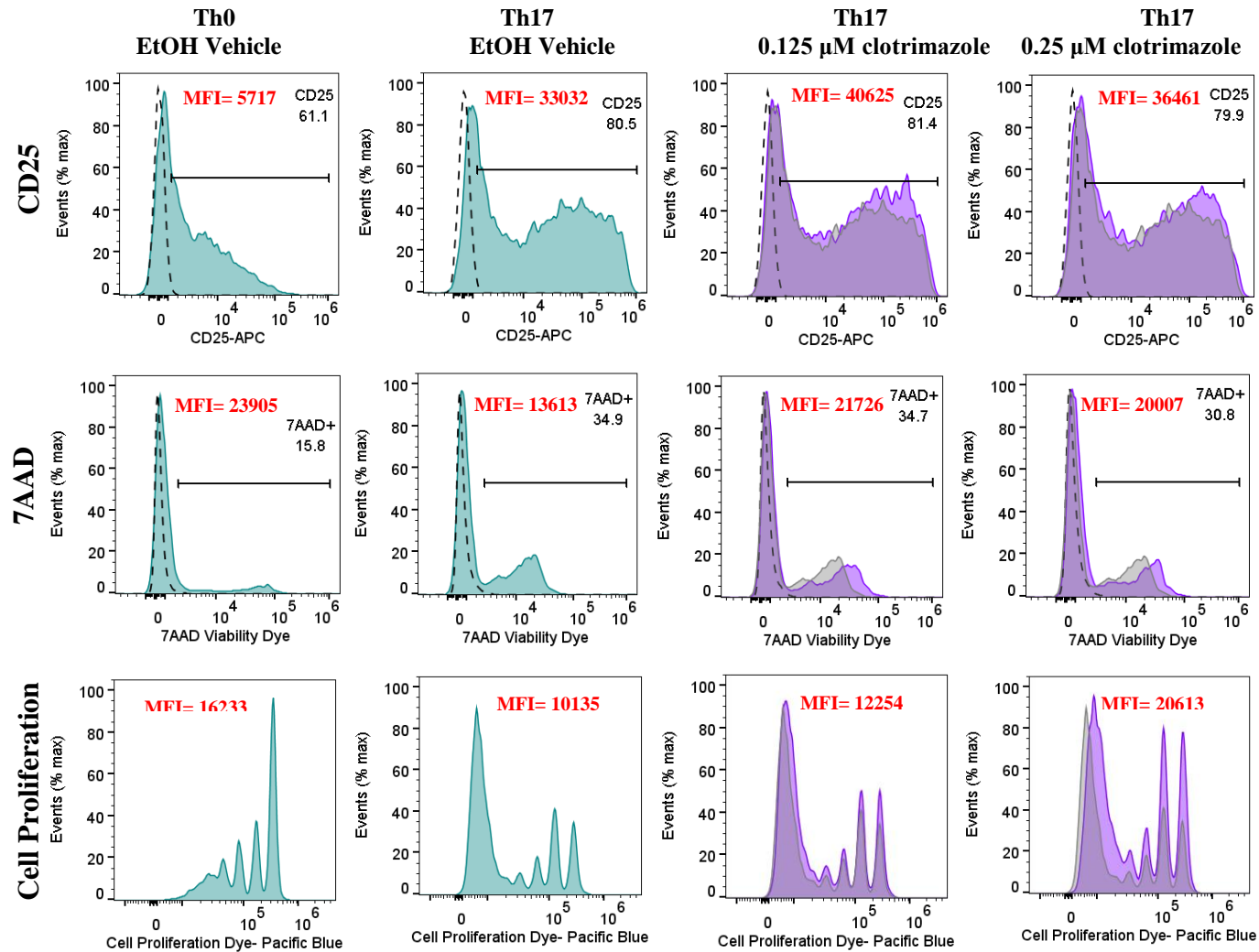


Figure 4.10 Flow cytometry analysis of naïve CD4⁺ T cells from Donor 9 cultured under non-polarising Th0 or Th17 polarising conditions with or without 0.125 and 0.25 µM clotrimazole treatments harvested after 6 days of cell culture. Top panel: CD25 expression Middle panel: 7AAD cell viability staining. Bottom panel: cell proliferation. Filled blue histograms represent the fluorochrome conjugated antibody stained Th0 and Th17 polarised cells with vehicle control. Filled purple histograms represent the fluorochrome conjugated antibody stained Th17 polarised cells with clotrimazole treatment overlaid with vehicle control (grey). Gates were determined using background fluorescence of unstained samples (1%) indicated by the dashed histogram. The Median Fluorescence intensities (MFI) are indicated in red.

4.3.4 Azole treatment of Th17-polarised cells on day 3 of cell culture revealed variable effects on the mRNA expression of Th17 signature genes

Quantitative reverse transcription PCR (qRT-PCR) analysis of mRNA expression of Th17 signature genes *IL17A*, *RORC* and *IL23R* confirmed successful Th17 polarisation. This is seen when comparing the expression of these genes under non-polarised conditions (Th0) and Th17 polarised conditions (Figures 4.14 – 4.19) respectively. The cytokine profile of T helper cells defines the T helper cell subset therefore the mRNA expression of *IL10*, *IFNG* was also monitored. The *IL17A* mRNA expression of Th17-polarised cells from Donor 1 with 1µM clotrimazole treatment was revealed to be downregulated by 0.43 relative to Th17-polarised cells with vehicle treatment shown in Figure 4.11A. *RORC* expression was also downregulated by 0.36 in treated Th17 polarised cells (Figure 4.11G) while *CYP7B1* mRNA expression showed only 10% reduction with clotrimazole treatment (Figure 4.11H). No change in *IL23R* or *IFNG* expression was revealed shown in Figure 4.11C and Figure 4.11E respectively. In contrast, *IL22* expression was two times higher with clotrimazole treatment (Figure 4.11B) while *FOXP3* expression increased by 0.56 shown in Figure 4.11F. The greatest expression change was seen with *IL10* which was upregulated three fold with clotrimazole treatment (Figure 4.11D).

The effect of 1µM clotrimazole and tebuconazole on Th17 and Treg polarisation and mRNA expression was investigated with nCD4⁺ T cells isolated from Donor 2. As with Donor 1 the mRNA expression of *IL17A* in Th17 polarised cells with 1 µM clotrimazole treatment was downregulated by 0.42, similarly with 1 µM tebuconazole treatment of Th17 polarised cells *IL17A* was also downregulated by 0.43 (Figure 4.12A). Figure 4.12G shows downregulation of *RORC* was not seen with 1 µM clotrimazole or tebuconazole treatment of Donor 2 Th17 polarised cells in contrast to Donor 1 Th17 polarised cells (Figure 4.11G). Th17 polarised cells showed greater expression of *CYP7B1* compared with Treg polarised cells which was one hundred fold lower with vehicle control showed in Figure 4.12H.

Downregulation of *CYP7B1* was seen in Th17 polarised cells with both 1µM clotrimazole and tebuconazole treatments. *IL22* expression of Th17 polarised cells showed a slight increase with clotrimazole, while expression of *IL22* in Treg polarised cells was twofold higher with clotrimazole treatment which was not seen

with tebuconazole treatment shown in Figure 4.12B. *IL23R* expression was slightly lower in Th17 polarised cells with both azole treatments shown in Figure 4.12C. *IL10* expression was upregulated with clotrimazole and tebuconazole treatment of Th17 polarised cells shown in Figure 4.12D as seen with Donor 1 Th17 polarised cells. In agreement with Donor 1, Th17 polarised cells with clotrimazole showed no change in *IFNG* expression while a slight reduction was observed with tebuconazole treatment. Figure 4.12E shows clotrimazole and tebuconazole treatment of Treg polarised cells increased *IFNG* expression. As expected high expression of *FOXP3* was revealed in Treg-polarised cells which was downregulated with both azole treatments shown in Figure 4.12F while increased expression of *FOXP3* was observed with azole treatments in Th17-polarised cells.

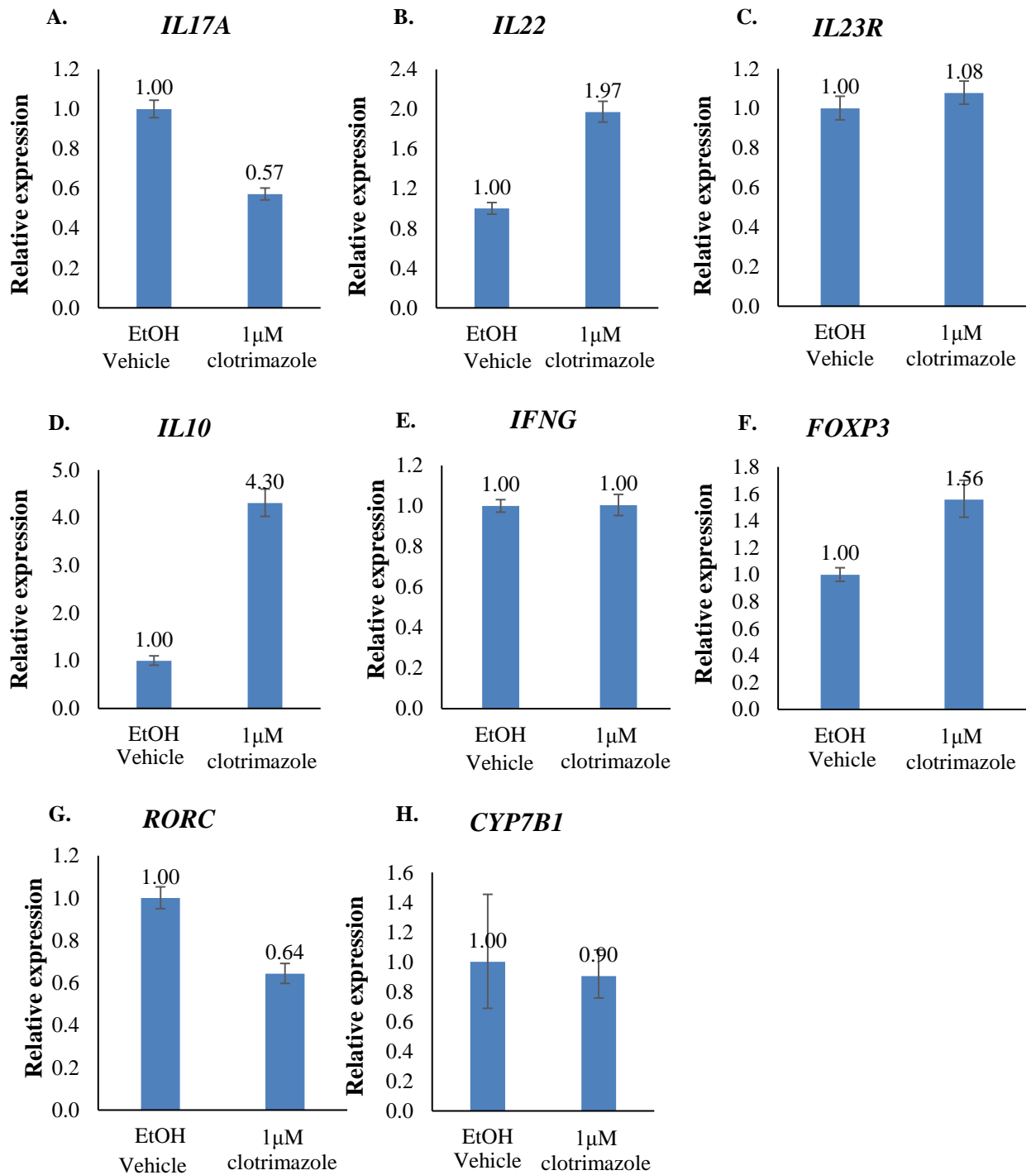


Figure 4.11 qRT-PCR analysis of mRNA expression of Th17 polarised nCD4⁺ cells from Donor 1. (A) *IL17A* was downregulated with 1µM clotrimazole treatment (B) *IL22* was upregulated with clotrimazole treatment (C) no change in *IL23R* expression was observed (D) *IL10* upregulation was seen with clotrimazole treatment (E) no change in *IFNG* expression was seen. (F) Increased *FOXP3* expression was seen with clotrimazole treatment (G) Downregulation of *RORC* expression clotrimazole was observed in clotrimazole treated cells (H) *CYP7B1* expression was lower in clotrimazole treated cells. mRNA expression was normalised to *RP18S* and *ACTB*. Fold change is relative to the Th17+ EtOH vehicle sample \pm SD of technical triplicates. n=1

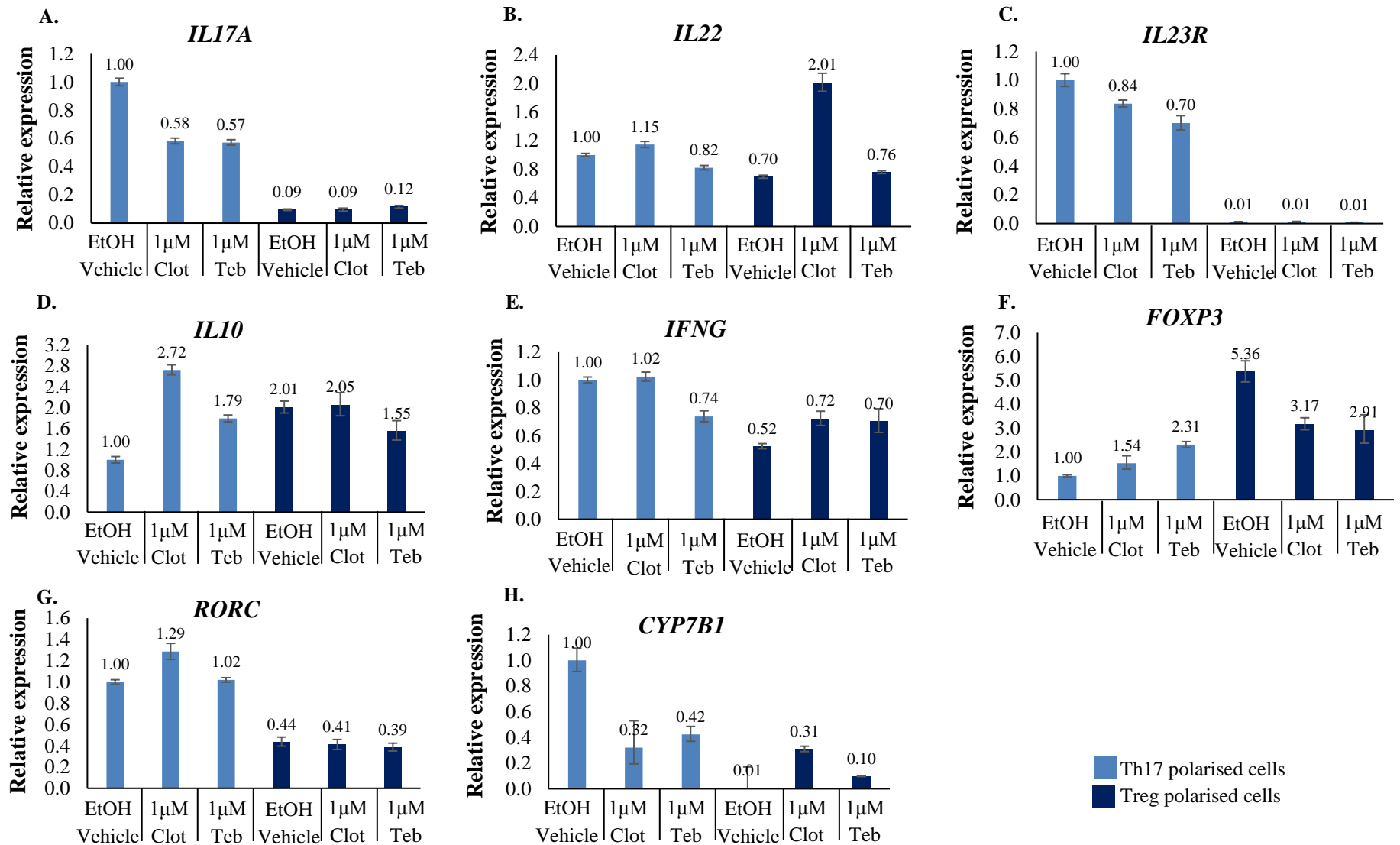


Figure 4.12 qRT-PCR analysis of mRNA expression of Th17 and Treg polarised nCD4⁺ cells from Donor 2. (A) *IL17A* was downregulated with 1µM clotrimazole and tebuconazole treatment (B) *IL22* was upregulated in Treg cells with 1 µM clotrimazole treatment (C) *IL23R* expression was downregulated with azole treatment (D) *IL10* upregulation was seen with clotrimazole treatment of Th17-polarised cells (E) no change in *IFNG* expression was seen with clotrimazole treated Th17 cells and upregulated in azole treated Treg-polarised cells. (F) Increased *FOXP3* expression was seen with azole treatment of Th17-polarised cells and downregulated in azole treated Treg-polarised cells (G) *RORC* expression was highest in Th17 polarised cells (H) *CYP7B1* expression was reduced in azole treated cells. mRNA expression was normalised to RP18S and ACTB. Fold change is relative to Th17+ EtOH vehicle sample. ±SD of technical triplicates. n=1

To further investigate the effect of azoles compounds on Th17 and Treg polarised cells and determine if an inhibitory effect on *IL-17* is seen with azole treatments at a reduced dosage without effecting the activation and viability of cells, nCD4⁺ T cells isolated from Donor 3 were cultured with 0.5 and 1.0 μ M clotrimazole and tebuconazole treatments added on the third day of cell culture. cDNA synthesised from RNA extracted from Treg polarised cells with 1 μ M clotrimazole treatment was of poor quality and was therefore excluded from analysis. Downregulation of *IL17A* in Th17 polarised cells was observed with clotrimazole treatment in a dose dependant manner shown in Figure 4.13A. Treatment of Th17 polarised cells with 0.5 μ M tebuconazole also showed downregulation of *IL17A* however this inhibitory effect was not seen at 1.0 μ M which correlates with the expression of *RORC* shown in Figure 4.13G. In contrast to the previous experiments, downregulation of *IL22* expression was seen in Th17 polarised cells with azole treatment and Treg polarised cells showed low *IL22* expression generally (Figure 4.13B). *IL23R* expression in Th17 polarised cells was lower with azole treatments with the exception of 1 μ M tebuconazole (Figure 4.13C). Upregulation of *IL10* in Th17 polarised cells was not seen with 0.5 μ M clotrimazole treatment and expression was only 13% higher with 1 μ M clotrimazole treatment (Figure 4.13D). No change in *IL10* expression was observed with Treg polarised cells with azole treatments.

As previously seen with Donor 2, expression of *CYP7B1* was greatest in Th17 polarised cells and both azole treatments reduced *CYP7B1* expression with little change from 0.5 μ M to 1 μ M treatments shown in Figure 4.13H. Figure 4.13F shows tebuconazole inhibition of *FOXP3* expression in Treg polarised cells in a dose dependant manner while upregulation of *FOXP3* was observed in Th17 polarised cells with both azole treatments at 0.5 μ M. Both Th17 and Treg polarised cells showed reduced *IFNG* expression with azole treatments shown in Figure 4.13E.

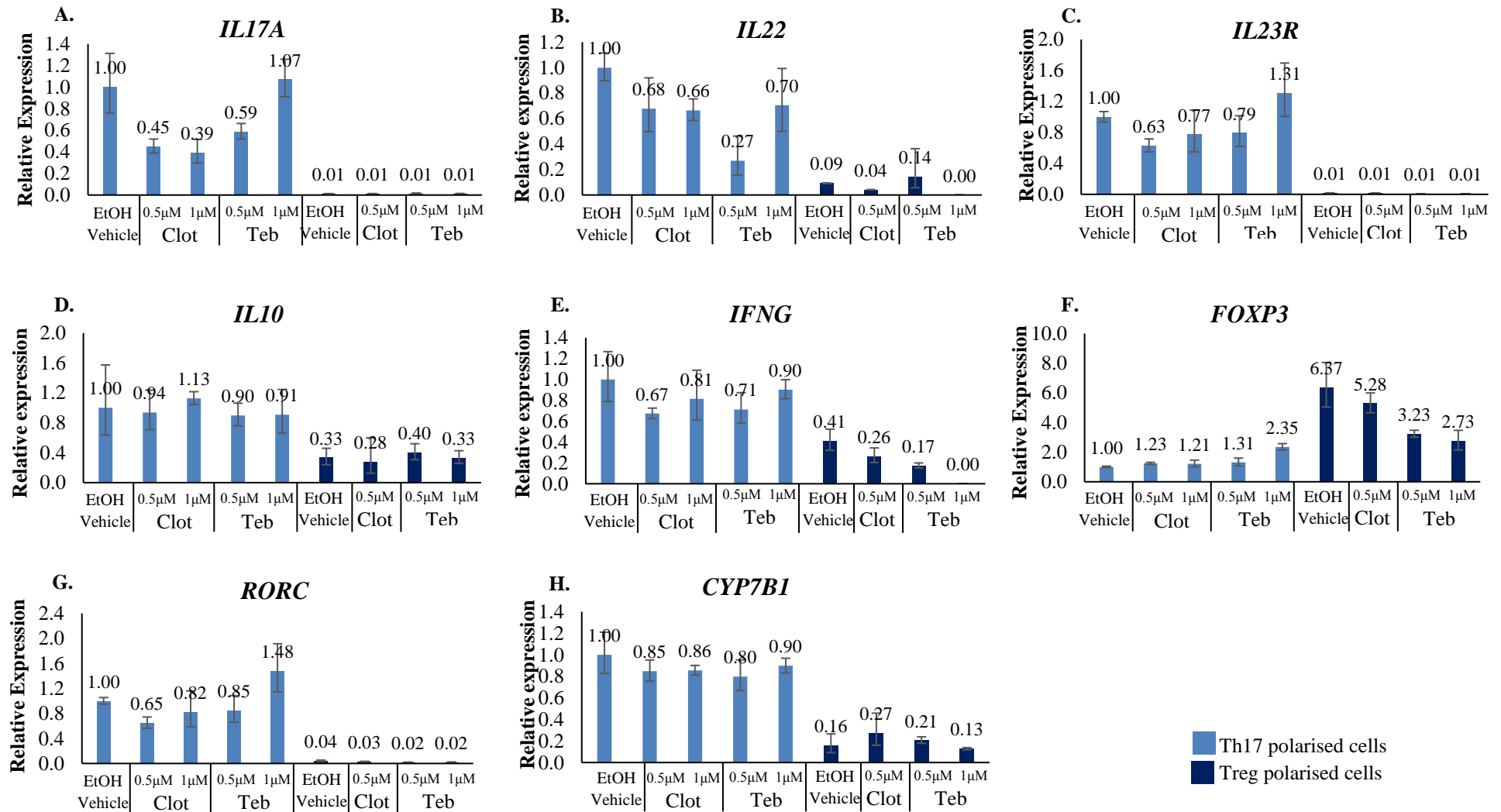


Figure 4.13 qRT-PCR analysis of mRNA expression of Th17 and Treg polarised naïve CD4⁺ cells from Donor 3. (A) *IL17A* was downregulated in Th17 cells with 0.5µM clotrimazole and tebuconazole treatment (B) *IL22* was downregulated with clotrimazole and tebuconazole treatment (C) *IL23R* expression was downregulated with azole treatment Th17 cells (D) *IL10* upregulation was not seen with azole treatment of Th17 or Treg polarised cells (E) *IFNG* expression was downregulated in Th17 and Treg cells with azole treatment (F) increased *FOXP3* expression was seen with azole treatment of Th17-polarised cells and downregulated in azole treated Treg-polarised cells (G) *RORC* expression was highest in Th17-polarised cells and downregulated with clotrimazole treatment (H) *CYP7B1* expression was reduced in azole treated cells. mRNA expression was normalised to *RP18S* and *ACTB*. Fold change is relative to Th17+ EtOH vehicle sample. ±SD of technical triplicates. n=1

In the following experiment, isolated nCD4⁺ T cells from Donor 4 were cultured under non-polarising Th0 and Th17 polarising conditions with 0.5 µM clotrimazole treatment. As expected *IL17* expression was specific to Th17 polarised cells and expression was downregulated with 0.5 µM clotrimazole treatment to 0.34 relative to Th17 polarised cells with vehicle treatment shown in Figure 4.14A. In concurrence with mRNA expression, secretion of IL-17A in the culture media of Th17 polarised cells was reduced fourfold with clotrimazole presented in Figure 4.15. As seen with the previous donors clotrimazole treatment increased *FOXP3* expression (Figure 4.14B). A slight reduction in *IFNG* and *IL23R* was also observed with 0.5 µM shown in Figure 4.14C and Figure 4.14D respectively. Expression of *RORC* in Th17 polarised cells with 0.5 µM clotrimazole treatment showed similar downregulation to Donor 1 Th17 polarised cells with 1 µM treatment (Figure 4.14E).

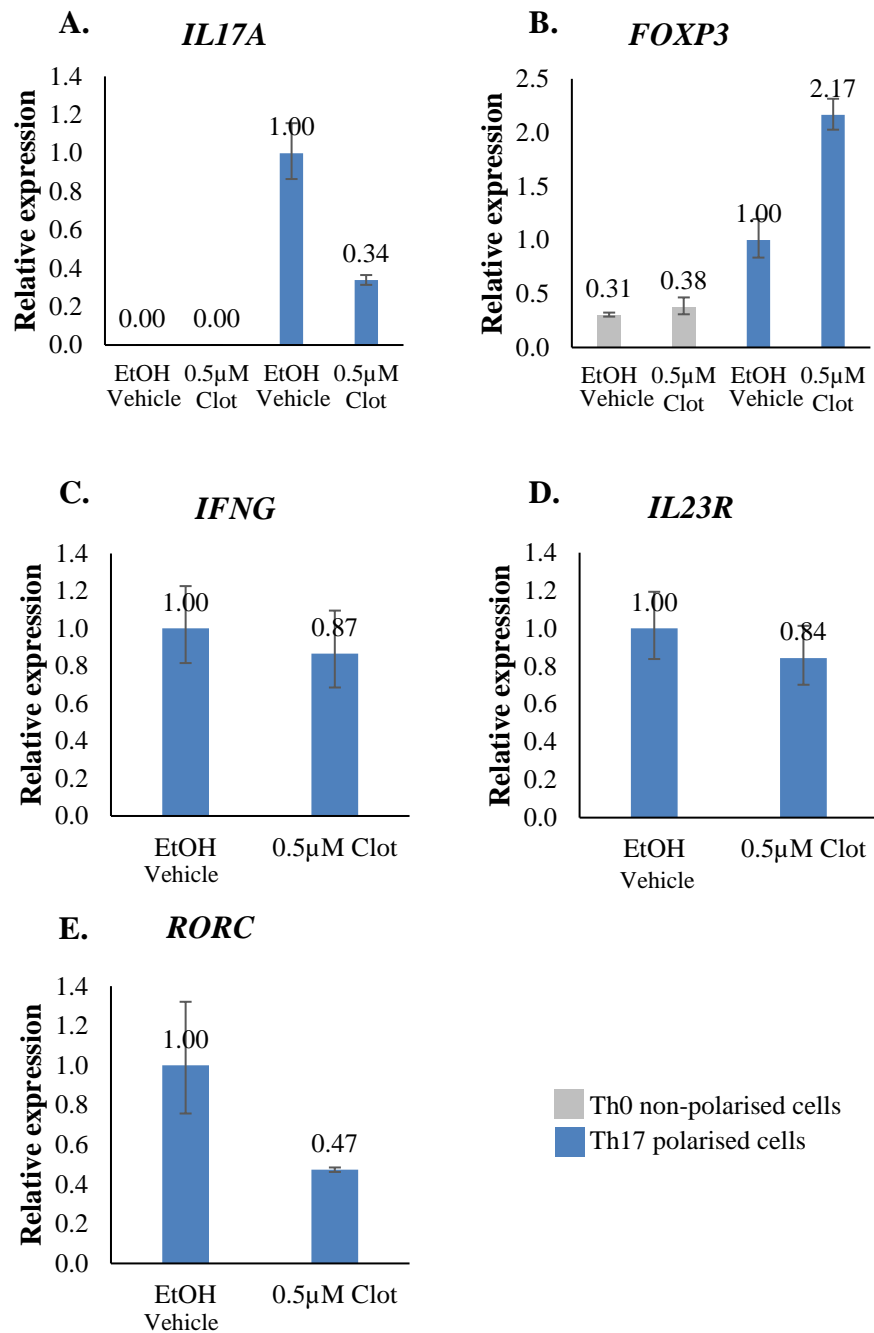


Figure 4.14 qRT-PCR analysis of mRNA expression of Th17 polarised naïve CD4⁺ cells from Donor 4. (A) *IL17A* was downregulated in Th17 polarised with 0.5 µM clotrimazole treatment (B) Increased *FOXP3* expression was seen with clotrimazole treatment (C) Reduced *IFNG* expression was seen with 0.5 µM clotrimazole (D) *IL23R* expression was lower in Th17 polarised cells with clotrimazole treatment. (E) Downregulation of *RORC* expression was observed in clotrimazole treated cells. mRNA expression was normalised to *RPI8S*. Fold change is relative to Th17+ EtOH vehicle sample. ±SD of technical triplicates for Th0 polarised samples and ± SD of duplicate culture of Th17 polarised samples from

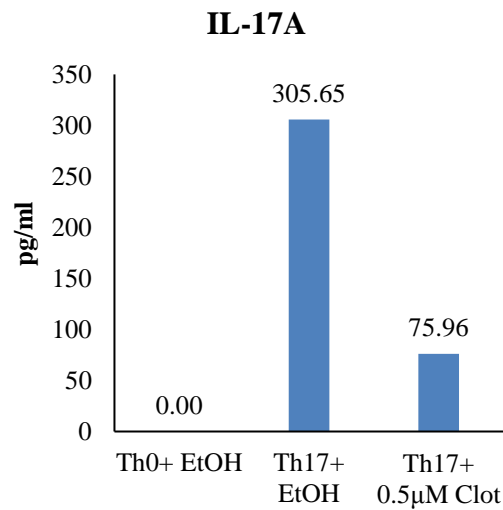


Figure 4.15 IL-17A production of non-polarised Th0 or Th17 polarised naïve CD4⁺ T cells of Donor 4 quantified by sandwich ELISA. IL-17A concentration in the media of Th17 polarised cells was reduced with clotrimazole treatment.n=1

Donor 5 isolated nCD4⁺ T cells were cultured under non-polarising Th0 or Th17 polarising conditions with 0.0625 to 0.5 µM clotrimazole treatments. Inhibition of *IL17A* expression in Th17 polarised cells with clotrimazole treatments was shown in a dose dependant manner (Figure 4.16A). Expression of *IL23R* and *RORC* was also downregulated to similar levels with 0.0625 to 0.5 µM clotrimazole treatments shown in Figure 4.16B and Figure 4.16C respectively. Similar expression of *IFNG* and *FOXP3* was seen with all clotrimazole treatments (Figure 4.16D and Figure 4.16E respectively) while 0.0625 µM clotrimazole treatment of Th17 polarised cells was shown to have no effect on *CYP7B1* expression and 0.125 to 0.5 µM treatments only reduced expression to 0.88 and 0.84 relatively to Th17 polarised cells with vehicle treatment shown in Figure 4.16F. In correlation with the dose dependent inhibition of *IL17A* mRNA expression, IL-17A concentrations in the media of Th17 polarised cells with clotrimazole treatment was also reduced in a dose dependent manner presented in Figure 4.17.

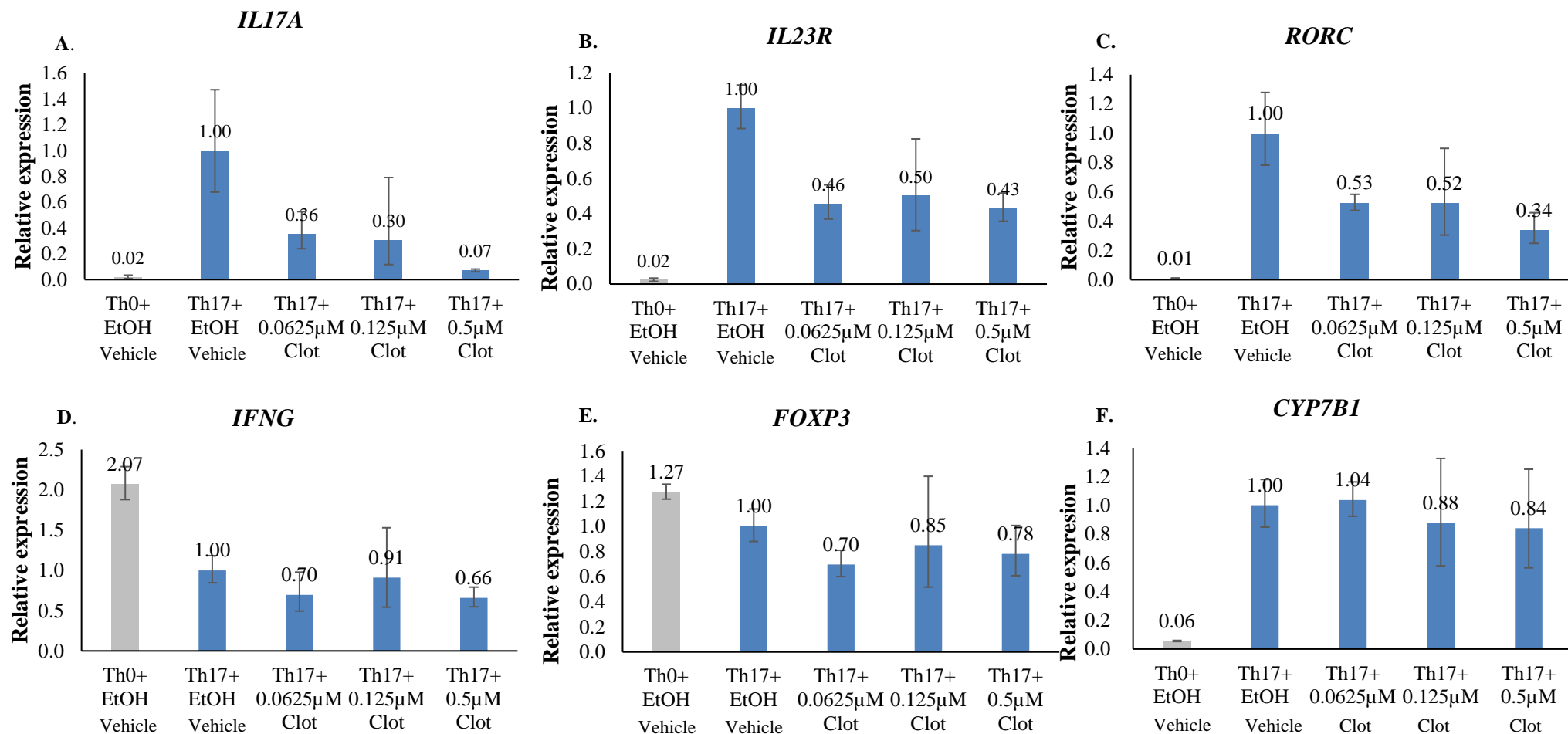


Figure 4.16 qRT-PCR analysis of mRNA expression of Th0 or Th17 polarised naïve CD4⁺ cells from Donor 5. (A) *IL17A* was downregulated in Th17 polarised with clotrimazole treatment in a dose dependant manner (B) *IL23R* expression was downregulated in Th17 polarised cells with similar expression levels seen with 0.0625 to 0.5 μM clotrimazole treatments (C) Downregulation of *RORC* expression was observed in clotrimazole treated cells (D) Reduced *IFNG* expression was seen with 0.0625 to 0.5 μM clotrimazole (E) Reduced *FOXP3* expression was seen with clotrimazole treatment (F) *CYP7B1* expression was downregulated with 0.125 and 0.5 μM clotrimazole treatments. mRNA expression was normalised to *RP18S*. Fold change is relative to Th17+ EtOH vehicle sample. ±SD of technical triplicates for Th0 polarised samples and ± SD of triplicate cultures of Th17 polarised samples from Donor 5. n=1

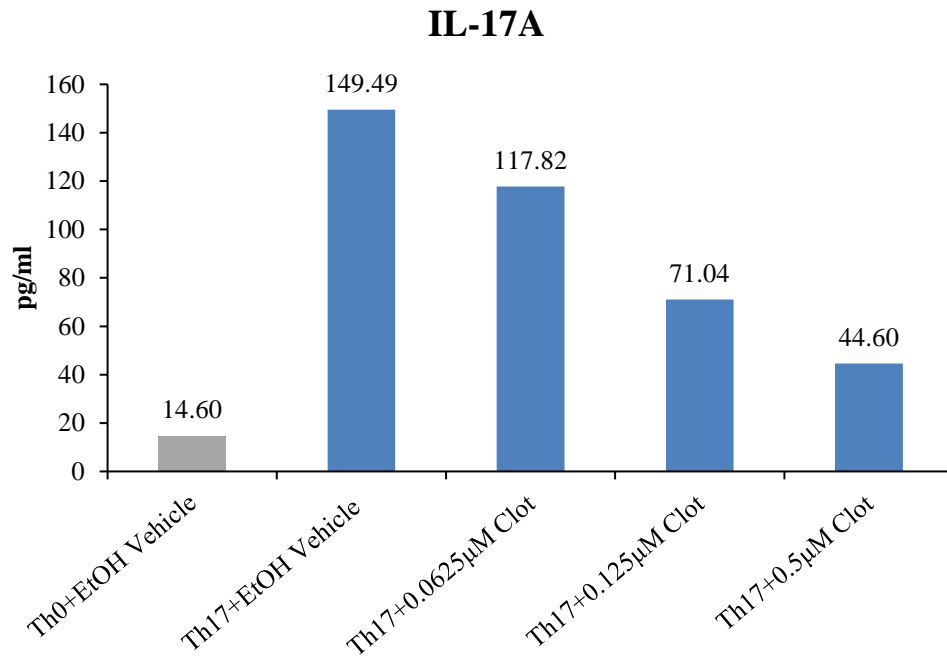


Figure 4.17 IL-17A production of non-polarised Th0 or Th17 polarised naïve CD4⁺ T cells of Donor 5. Reduced IL-17A concentration in the media of Th17 polarised cells with clotrimazole treatment was seen in a dose dependent manner, quantified by sandwich ELISA, \pm SD of technical duplicates, n=1

In the final experiment with clotrimazole treatments added on the third day of cell culture nCD4⁺ T cells from Donor 6 were cultured under non-polarising Th0 or Th17 polarising conditions with or without 0.5 μ M clotrimazole treatments. In contrast to Donors 3 to 5 *IL17A* expression was not inhibited by 0.5 μ M clotrimazole treatments shown in Figure 4.18A and similar concentrations of IL-17A was detected in the cell culture media with and without treatment (Figure 4.19). Increased *IFNG* and *FOXP3* expression was observed in Th17 polarised cells with clotrimazole treatments (Figure 4.18C and Figure 4.18D). Lower expression of *IL23R* and *RORC* was seen with clotrimazole treatments shown in Figure 4.18B and Figure 4.18E respectively while no inhibition of *CYP7B1* expression was observed (Figure 4.18F).

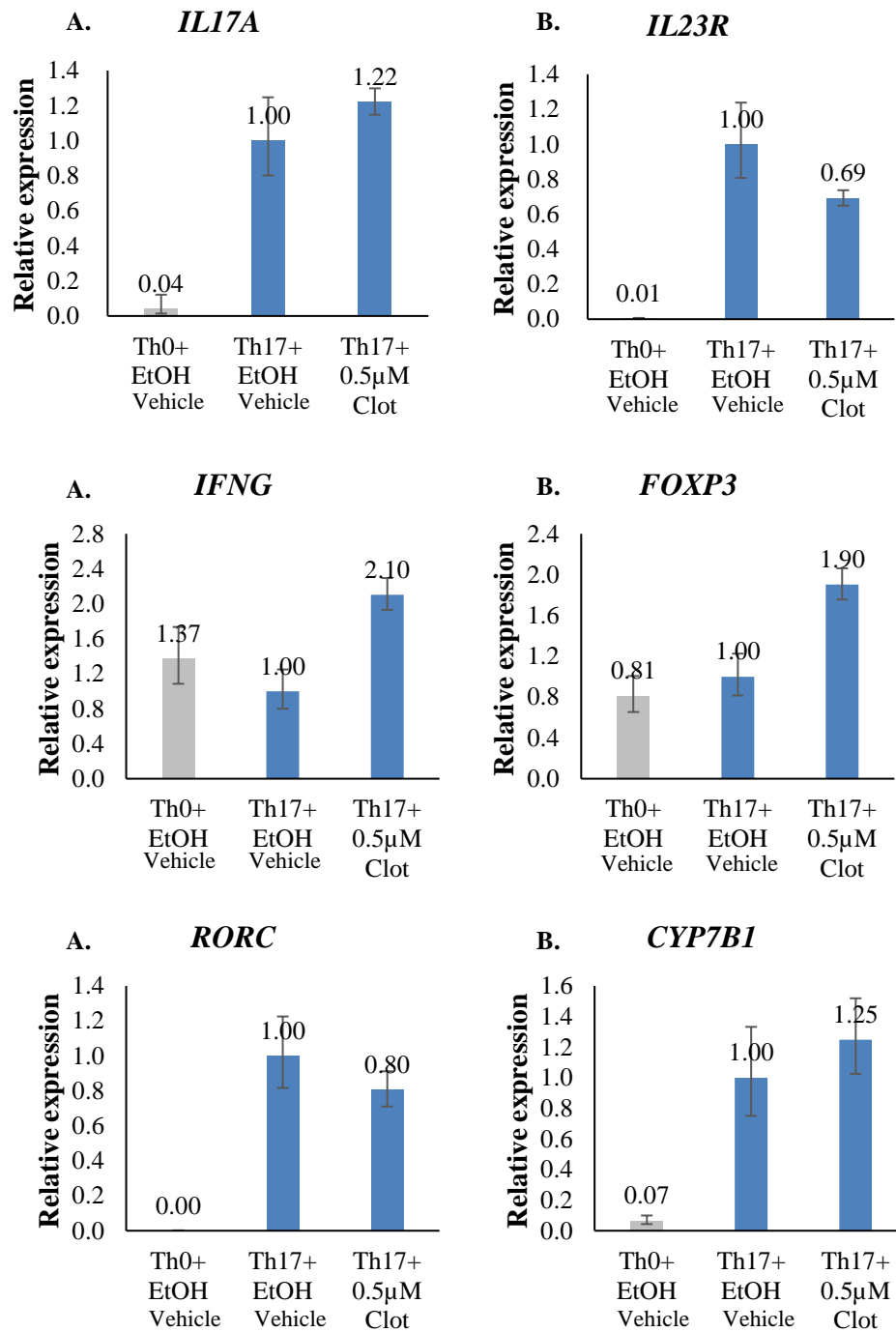


Figure 4.18 qRT-PCR analysis of mRNA expression of Th0 or Th17 polarised naïve CD4⁺ cells from Donor 6. (A) inhibition of *IL17A* was not seen in Th17 polarised with clotrimazole treatment (B) *IL23R* expression was downregulated in Th17 polarised cells with 0.5 µM clotrimazole treatments (C) Increased *IFNG* expression was seen with 0.5 µM clotrimazole (D) Upregulated *FOXP3* expression was seen with clotrimazole treatment (E) Downregulation of *RORC* expression was observed in clotrimazole treated cells (F) *CYP7B1* expression was not inhibited by 0.5 µM clotrimazole treatments. mRNA expression was normalised to *RP18S*. Fold change is relative to Th17+ EtOH vehicle sample. ±SD of technical triplicates for Th0 polarised samples and ± SD of duplicate cultures of Th17 polarised samples from Donor 6. n=1

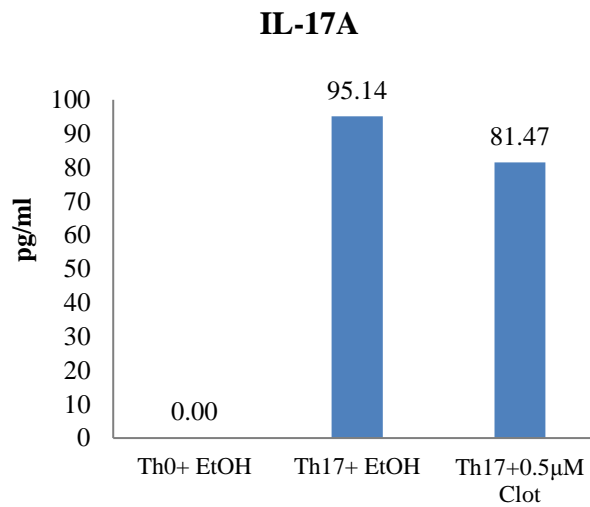


Figure 4.19 IL-17A concentration of non-polarised Th0 or Th17 polarised naïve CD4⁺ T cell culture media from Donor 6 quantified by sandwich ELISA. Th17 polarised cells were unaffected by the presence of 0.5 µM clotrimazole. n=1

Downregulation of *IL17A* expression and IL-17 production was demonstrated in all experiments with the addition of azole treatment on the third day of cell culture with the exception of Donor 6. Both azole treatments showed inhibitory abilities towards *IL17A*, with the greatest effect seen with clotrimazole treatment which was also shown to have a lesser effect on activation, proliferation and viability of cells. However there was donor variation of the level of *IL17A* downregulation seen and these experiments did not show a significant inhibitory effect (Figure 4.20). A Slight reduction in *RORC* and *IL23R* expression was also found with azole treatment although large variation was seen.

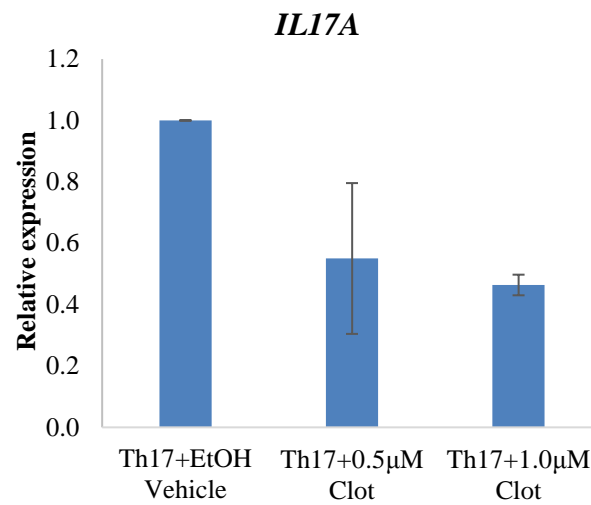


Figure 4.20 qRT-PCR analysis of *IL17A* mRNA expression of Th17 polarised naïve CD4⁺ cells with day 3 clotrimazole treatments. mRNA expression was normalised to *RP18S* and *ACTB*. Fold change is relative to the Th17+ EtOH vehicle sample. \pm SEM of biological replicates. $p = 0.149$ and 0.513 for $0.5 \mu\text{M}$ and $1.0 \mu\text{M}$ clotrimazole treatments respectively. $n \geq 3$

4.3.5 Azole treatment of Th17-polarised cells on the first day of cell culture inhibits *IL17A* expression in a dose dependent manner

Due to the donor variation of *IL17A* inhibition, CD25 activation and cell viability seen with clotrimazole treatment on the third day of cell culture further experiments were performed with clotrimazole treatment on the first day of cell culture (day 0). In the initial experiment with Donor 7 isolated nCD4⁺ T cells, 0.0625 μ M clotrimazole treatment was added to cultures of Th17 polarised cells. No change in *IL17A*, *IL23R*, *RORC* or *CYP7B1* expression was seen with 0.0625 μ M clotrimazole treatments shown in Figure 4.21. Treatment of Th17 polarised cells with 0.0625 μ M clotrimazole was also found to have little effect on IL-17 concentrations in culture media (Figure 4.22) therefore further experiments were performed with an increased clotrimazole dosage.

Isolated nCD4⁺ T cells from Donor 8 were cultured under Th17 polarising conditions with 0.125 μ M and 0.5 μ M clotrimazole treatments. Inhibition of *IL17A* expression was seen in a dose dependant manner shown in Figure 4.23A. In correlation with *IL17A* expression the concentration of IL-17A in the culture media was also reduced in a dose dependent manner shown in Figure 4.24. Downregulation of *IL23R* expression was observed with 0.125 μ M clotrimazole treatment however *IL23R* expression was higher with 0.5 μ M clotrimazole treatment presented in Figure 4.23B. *IFNG* expression was upregulated with increasing clotrimazole treatment while *FOXP3* expression upregulation was only achieved with 0.5 μ M clotrimazole treatment (Figure 4.23C and Figure 4.23D respectively). Reduced *RORC* expression was also seen in a dose dependent manner shown in Figure 4.23E while *CYP7B1* expression was unaffected by clotrimazole treatments shown in Figure 4.23F.

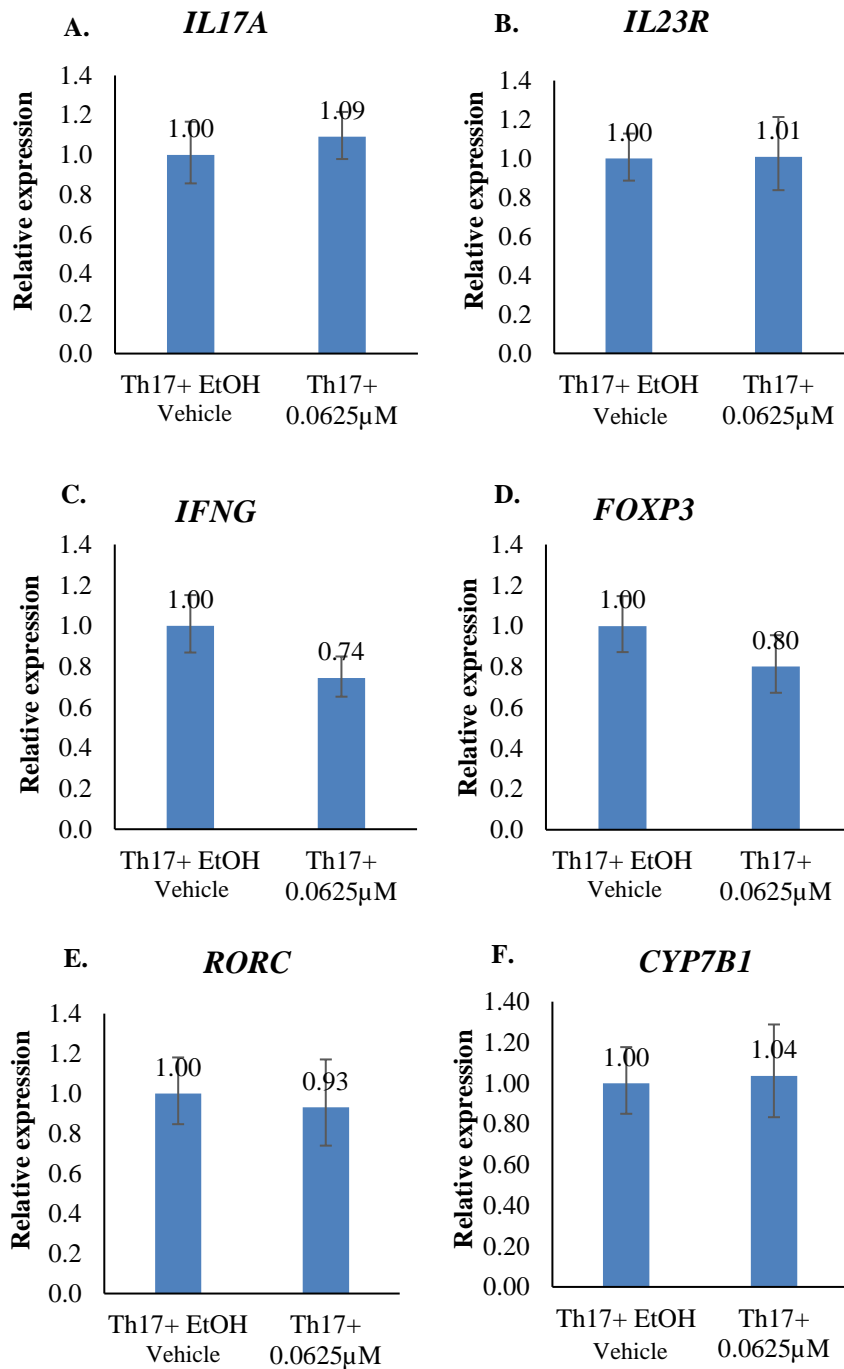


Figure 4.21 qRT-PCR analysis of mRNA expression of Th17 polarised naïve CD4⁺ cells from Donor 7 with clotrimazole treatment on day 0. (A) no change in *IL17A* expression was seen in Th17 polarised with 0.0625 µM clotrimazole treatment (B) *IL23R* expression was unaffected in Th17 polarised cells with 0.0625 µM clotrimazole treatments (C) *IFNG* expression was lower in 0.0625 µM clotrimazole treated cells (D) Decreased *FOXP3* expression was seen with clotrimazole treatment (E) No change in *RORC* expression was observed in clotrimazole treated cells (F) *CYP7B1* expression was not inhibited by 0.0625 µM clotrimazole treatments. mRNA expression was normalised to *RP18S* and *ACTB*. Fold change is relative to Th17+ EtOH vehicle sample. \pm SD of technical triplicates, n=1

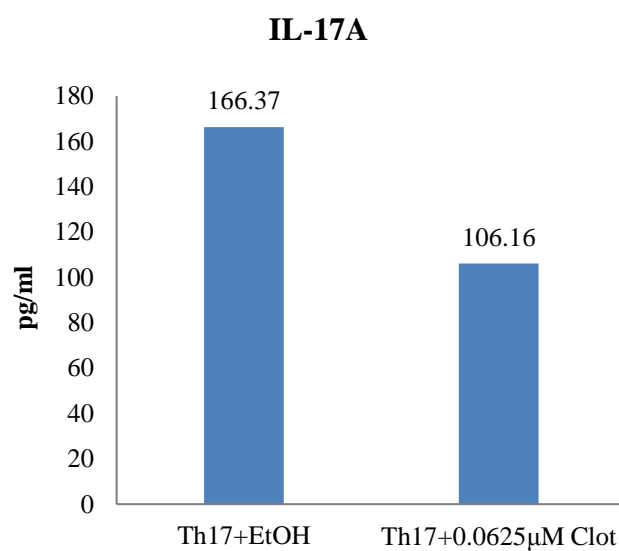


Figure 4.22 IL-17A production in Th17 polarised naïve CD4⁺ T cells of Donor 7 with clotrimazole treatment on the first day of culture quantified by sandwich ELISA. A small reduction of IL-17A concentration was seen in the media of Th17 polarised cells in the presence of 0.0625 µM clotrimazole. n=1

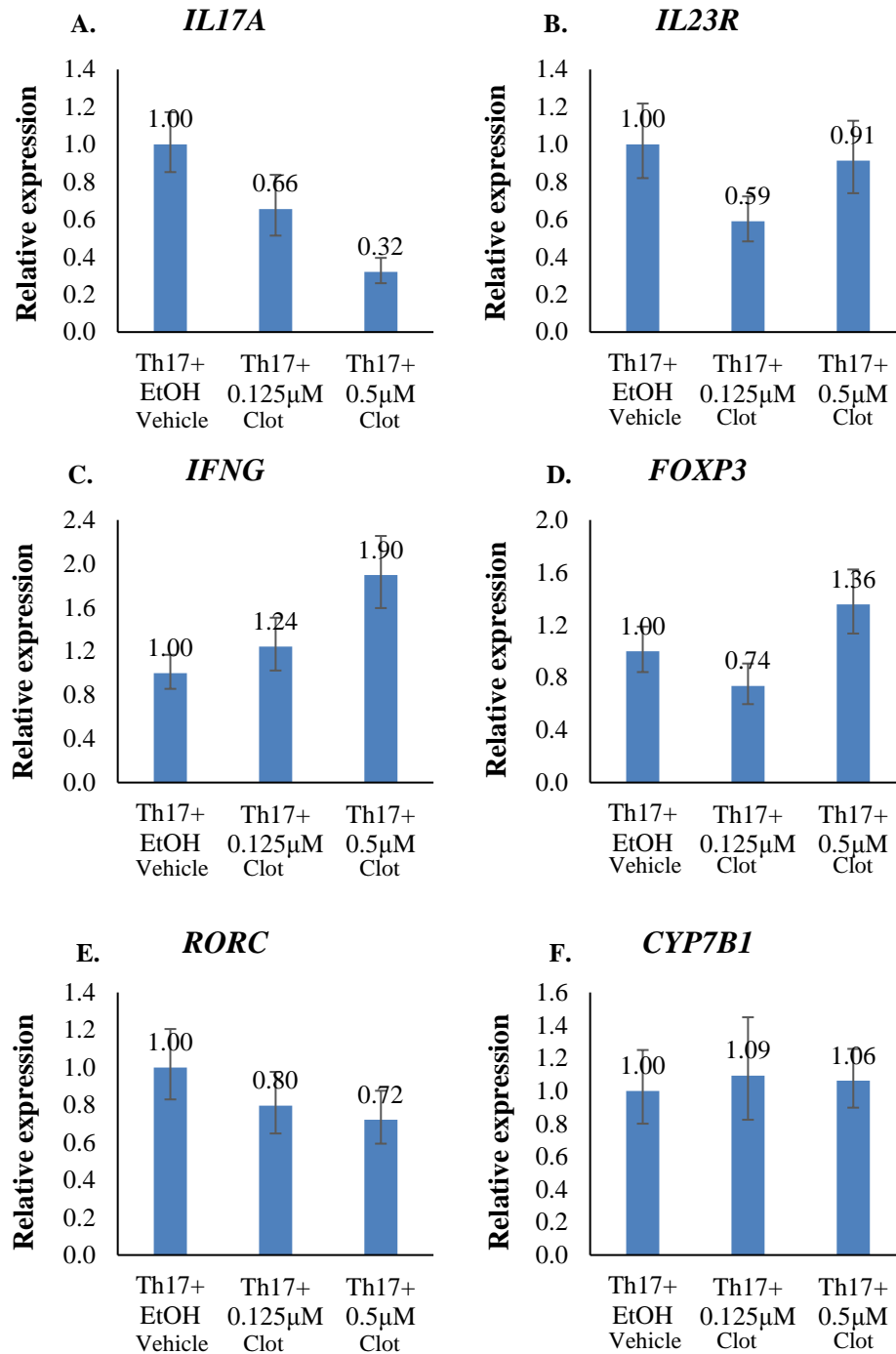


Figure 4.23 qRT-PCR analysis of mRNA expression of Th17 polarised naïve CD4⁺ cells from Donor 8 with clotrimazole treatment on day 0. (A) *IL17A* expression was inhibited in Th17 polarised with clotrimazole treatment in a dose dependent manner (B) *IL23R* expression was downregulated with 0.125 µM clotrimazole treatment (C) *IFNG* expression was increased in clotrimazole treated cells (D) Increased *FOXP3* expression was seen with 0.5 µM clotrimazole treatment (E) *RORC* expression was downregulated in 0.5 µM clotrimazole treated cells (F) *CYP7B1* expression was unaffected by clotrimazole treatments. mRNA expression was normalised to *RPI8S* and *ACTB*. Fold change is relative to Th17+ EtOH vehicle sample. ±SD of technical triplicates, n=1

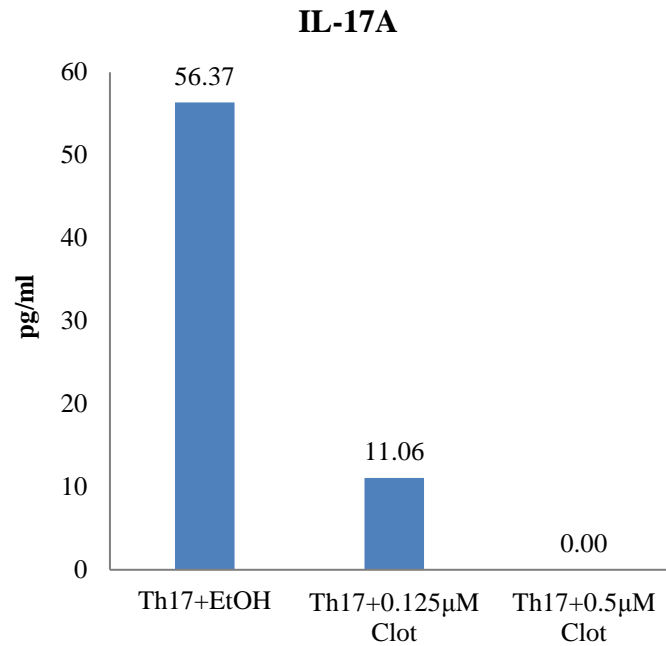


Figure 4.24 IL-17A production of Th17 polarised naïve CD4⁺ T cells of Donor 8. Reduced IL-17A concentration in the media of Th17 polarised cells with clotrimazole treatment was seen in a dose dependent manner, quantified by sandwich ELISA. n=1

In the final experiment with day 0 clotrimazole treatments Donor 9 nCD4⁺ T cells were cultured under Th0 or Th17 polarising conditions with 0.125 and 0.25 µM clotrimazole treatments. As previously seen with Donor 8, day 0 clotrimazole treatment inhibited *IL17A* expression in Th17 polarised cells in a dose dependent manner shown in Figure 4.25A. IL-17A concentrations in culture media was also reduced in a dose dependent manner with clotrimazole treatment presented in Figure 4.26. Downregulation of *IL23R* expression in Th17 polarised cells was downregulated with 0.125 µM clotrimazole treatment but this was not seen with 0.25 µM clotrimazole treatment shown in Figure 4.25B. Figure 4.25C shows the highest expression of *IFNG* was in non-polarised cells with expression of Th17 polarised cells four fold lower. In contrast with Donor 8, *RORC* expression was unaffected by clotrimazole treatment while *CYP7B1* expression was reduced (Figure 4.25E and Figure 4.25F respectively).

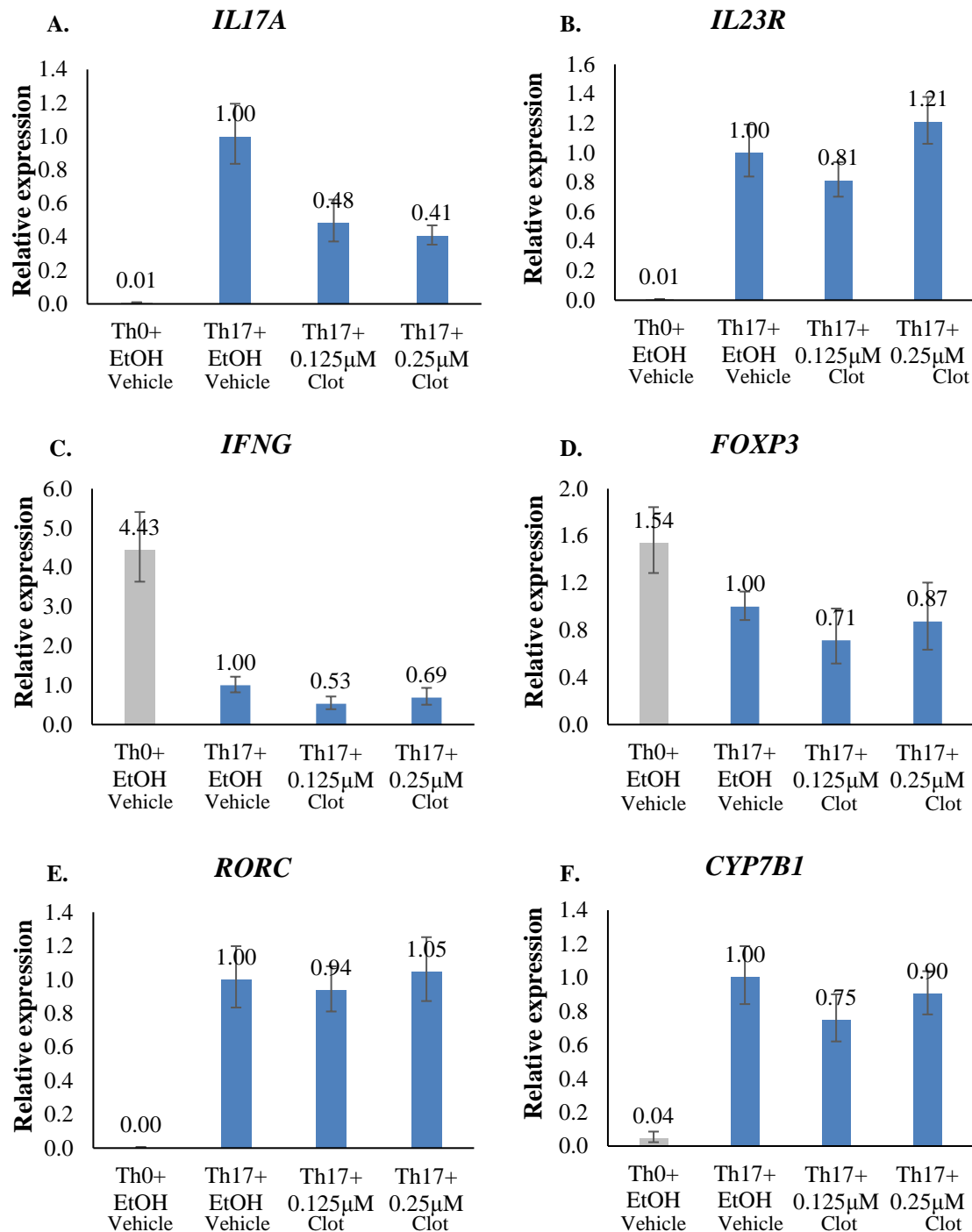


Figure 4.25 qRT-PCR analysis of mRNA expression of non-polarised Th0 or Th17 polarised naïve CD4⁺ cells from Donor 9 with clotrimazole treatment on day 0. (A) *IL17A* expression was inhibited in Th17 polarised with clotrimazole treatment in a dose dependent manner (B) *IL23R* expression was downregulated only with 0.125 μM clotrimazole treatment (C) Highest *IFNG* expression was seen in non-polarised cells (D) *FOXP3* expression was downregulated with clotrimazole treatment (E) *RORC* expression was unaffected by clotrimazole treatment (F) *CYP7B1* expression was reduced with clotrimazole treatments. mRNA expression was normalised to *RPI8S* and *ACTB*. Fold change is relative to Th17+ EtOH vehicle sample. ±SD of technical triplicates, n=1

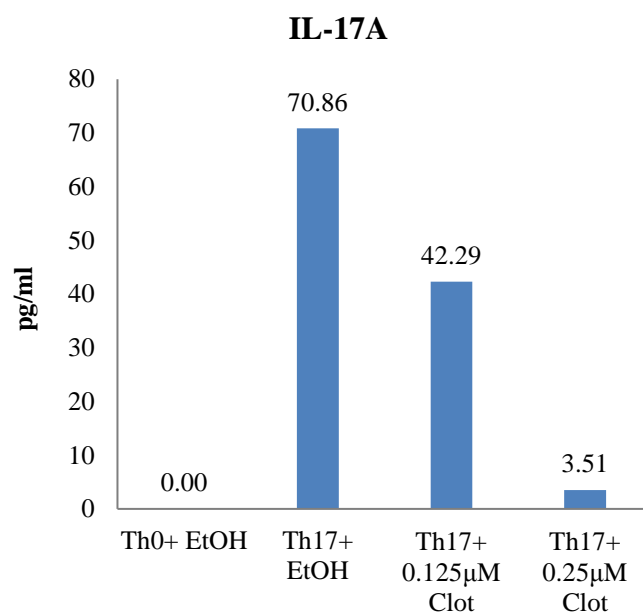


Figure 4.26 IL-17A production of non-polarising Th0 or Th17 polarised naïve CD4⁺ T cells of Donor 9. IL-17A concentration in the media of Th17 polarised cells with clotrimazole treatment was reduced in a dose dependent manner, quantified by sandwich ELISA. n=1

Experiments performed with 0.125 to 0.5 µM clotrimazole treatment on day 0 showed inhibition of *IL17A* expression in a dose dependent manner while no trend was found with other Th17 or alternate T helper cell subset related genes. The concentration of IL-17A in the culture media of Th17 polarised cells was also lower in the presence of clotrimazole and inhibition of IL-17A was seen in a dose dependent manner.

4.3.6 Azole treatment inhibits CYP7B1 activity in activated Th17 polarised naïve CD4⁺ T cells

Oxysterol analysis of cell culture media from Donor 1 Th17 polarised cells with and without 1 μ M clotrimazole is summarised in Table 4.5. Similar concentrations of enzymatically derived side-chain oxidised monohydroxycholesterols 24(*S*)-HC, 24(*R*)-HC and 25-HC were produced in Th17 polarised cells with or without clotrimazole treatment detected at 534.5054 m/z (Figure 4.27). Analysis of fraction B confirmed these monohydroxycholesterols detected were the 3 β hydroxyl forms. 27-HC, naturally present in X-Vivo-20 media, was also monitored and detected but no substantial change was observed between mock X-Vivo-20 media and nCD4⁺ T cell conditioned media. The most abundant oxysterol produced was 24(*S*),25-EC detected as the hydrolysed form 24,25-diHC at 550.4003 m/z (Figure 4.28). 24(*S*),25-EC concentrations can be determined through the combined values of 24,25-diHC, 24-KC and 24-hydroxycholesterol-25-methylether the isomerised, hydrolysed and methanolysed forms when detected. In these experiments only 24,25-diHC was detected. Downstream metabolite, 7 α ,24,25-triHC was also detected at 566.3952 m/z (Figure 4.29). The concentration of 7 α ,24,25-triHC in the media of Th17 polarised cells with 1 μ M clotrimazole treatment was forty fold lower than the Th17 polarised cells with no treatment confirming the inhibitory effect of clotrimazole towards CYP7B1 shown in Figure 4.30.

Quantification of oxysterols in culture media of Th17 and Treg polarised nCD4⁺ T cells of Donor 2 with and without 1 μ M clotrimazole or tebuconazole treatment is summarised in Table 4.6. Monohydroxycholesterols 24(*S*)-HC, 24(*R*)-HC and 25-HC were detected in both Th17 and Treg polarised cells with and without azole treatment. 24(*S*),25-EC was the most abundant oxysterol in both Th17 and Treg polarised cells although higher concentrations were quantified in Th17 polarised cells. As with Donor 1, 1 μ M clotrimazole treatment inhibited CYP7B1 activity with metabolite 7 α ,24,25-triHC not detected in Th17 polarised cells with clotrimazole treatment shown in Figure 4.31. Tebuconazole treatment of Th17 polarised cells was also shown to inhibit CYP7B1 activity to a lesser extent with a threefold decrease of 7 α ,24,25-triHC shown in Figure 4.31. Likewise, CYP7B1 activity in Treg polarised cells was inhibited with azole treatments.

The activity of azole compounds clotrimazole and tebuconazole towards their primary target enzyme CYP51 was monitored in Donor 2 Th17 and Treg polarised cells using GC-MS quantification. This GC-MS analysis work was performed by Alison Dickson. GC-MS analysis revealed increased concentrations of CYP51 upstream substrates lanosterol and lanostenol with clotrimazole and tebuconazole treatments in both Th17 and Treg polarised cells (Figure 4.32.A and Figure 4.32B respectively). Reduced concentrations of downstream products of CYP51 was also revealed confirming inhibition on CYP51 activity in both Th17 and T reg polarised cells although partial rescue was observed in further downstream metabolites (Figure 4.32).

Table 4.5 Quantified oxysterols in media fraction of Donor 1 activated naïve CD4⁺ T cells cultured under Th17 polarising conditions with and without clotrimazole treatment after 6 days.

Sterols in conditioned media	Activated naïve CD4 ⁺ T cells (pg/million cells)	
	Th17 polarised cells	Th17 polarised cells with 1µM clotrimazole
24(S)-HC	98.05	72.35
24(R)-HC	14.62	7.73
25-HC	22.71	26.38
27-HC	12.69	12.61
24(S),25-EC	2157.71	2039.30
7α,24,25-triHC	454.40	10.83

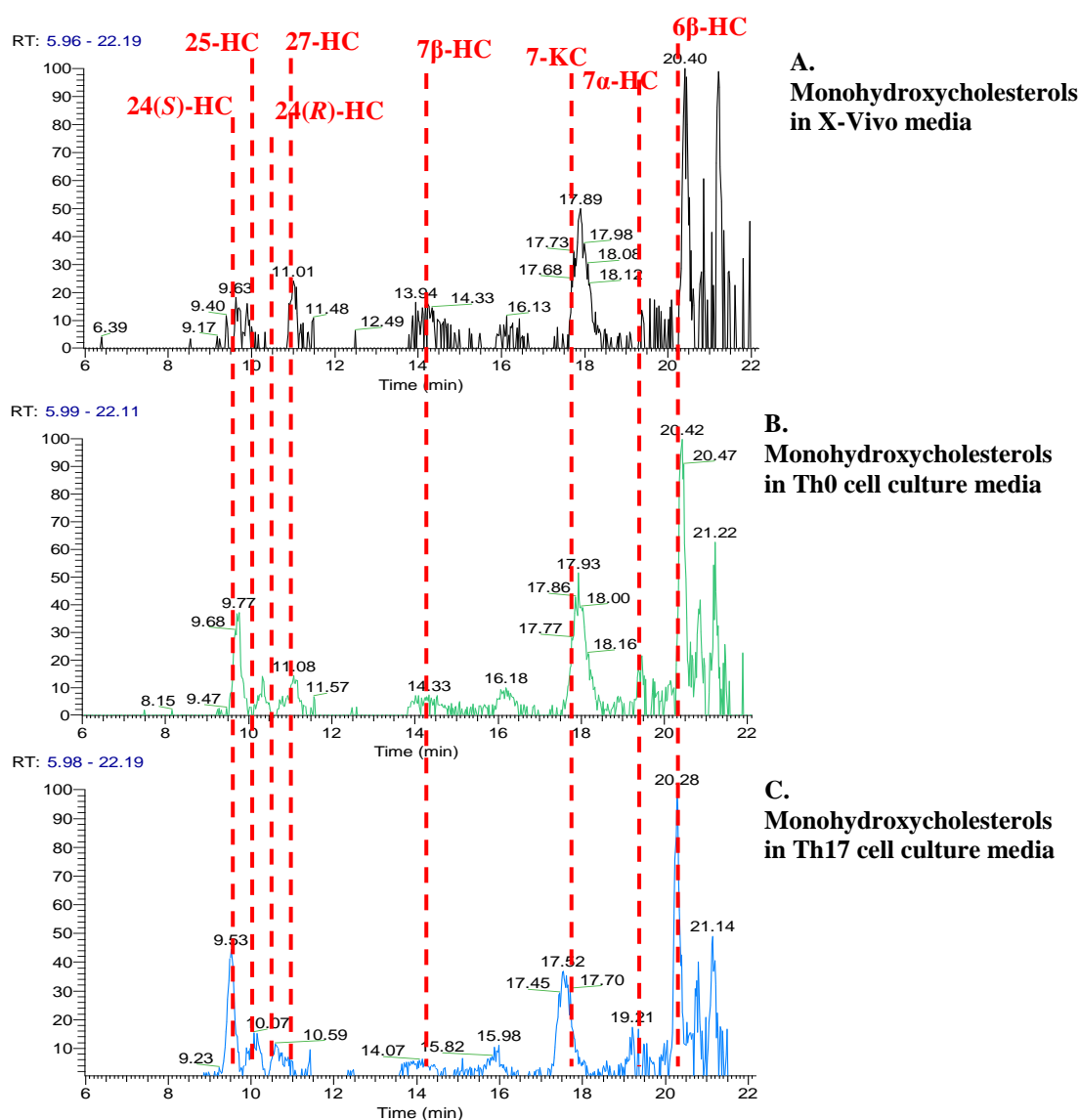


Figure 4.27 Representative reconstructive ion chromatograms for monohydroxycholesterols present in cell culture media, detected at $534.5054 \text{ m/z} \pm 10 \text{ ppm}$. Cholesterol autoxidation products 7β -HC, 7-KC , 7α -HC and 6β -HC were present in all chromatograms. Enzymatically-derived monohydroxycholesterols were identified by exact mass and MS^3 fragmentation patterns. (A) Mock X-Vivo-20 media showed a peak at 11.01 min for 27-HC , naturally present in X-Vivo-20 media. (B) Media extracted from activated non-polarised, Th0 naïve CD4^+ T cells showed peaks for $24(\text{S})\text{-HC}$ at 9.86 and 10.52 min, 25-HC at 10.25 min, $24(\text{R})\text{-HC}$ at 11.02 min, and 27-HC at 11.08 min. (C) Media extracted from activated Th17-polarised naïve CD4^+ T cells showed peaks for $24(\text{S})\text{-HC}$ at 9.53 and 10.16 min, 25-HC at 9.96 min, $24(\text{R})\text{-HC}$ at 10.59 min, and 27-HC at 10.98 min.

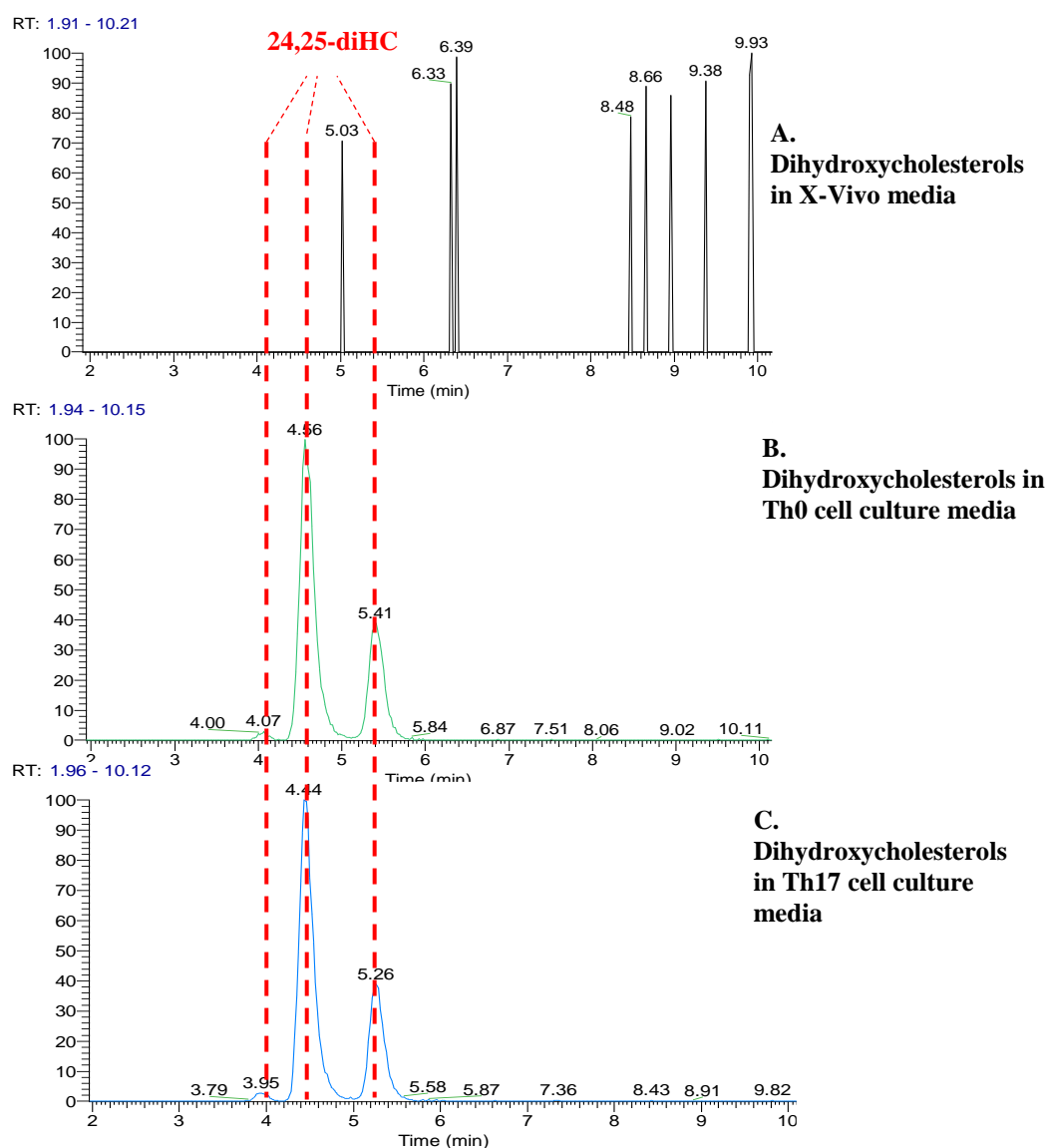


Figure 4.28 Representative reconstructive ion chromatograms for dihydroxycholesterols present in cell culture media, detected at $550.4003 \text{ m/z} \pm 10 \text{ ppm}$. Dihydroxycholesterols were identified by exact mass and MS^3 fragmentation patterns. (A) No identifiable dihydroxycholesterol peaks were detected in mock X-Vivo-20 media. (B) Peaks at 4.07, 4.56 and 5.41 min were identified as 24,25-diHC, eluting as pairs of peaks with the second pair eluting at the same time as the first pair in activated non-polarised, Th0 naïve CD4^+ T cell culture media. (C) 24,25-diHC peaks at 3.96, 4.44 and 5.26 min were also identified in activated Th17 polarised naïve CD4^+ T cell culture media.

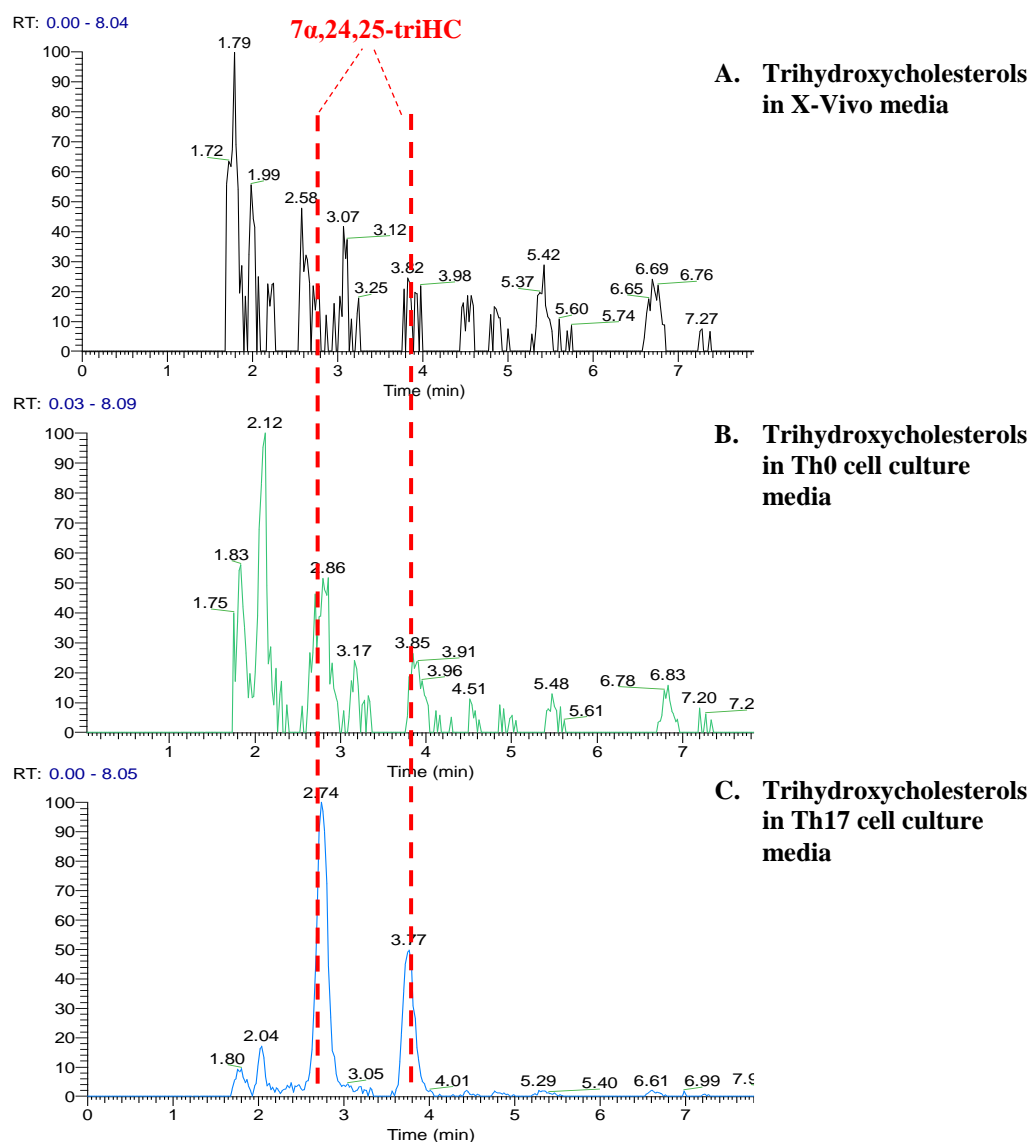


Figure 4.29 Representative reconstructive ion chromatograms for trihydroxycholesterols present in cell culture media, detected at $566.3952 \text{ m/z} \pm 10 \text{ ppm}$. Trihydroxycholesterols were identified by exact mass and MS^3 fragmentation patterns. (A) No identifiable trihydroxycholesterol peaks were detected in mock X-Vivo-20 media. (B) Peaks at 2.86 and 3.85min were identified as $7\alpha,24,25\text{-triHC}$ in activated non-polarised, Th0 naïve CD4^+ T cell culture media. (C) $7\alpha,24,25\text{-triHC}$ peaks at 2.74 and 3.77 min were identified with high abundance in activated Th17 polarised naïve CD4^+ T cell culture media.

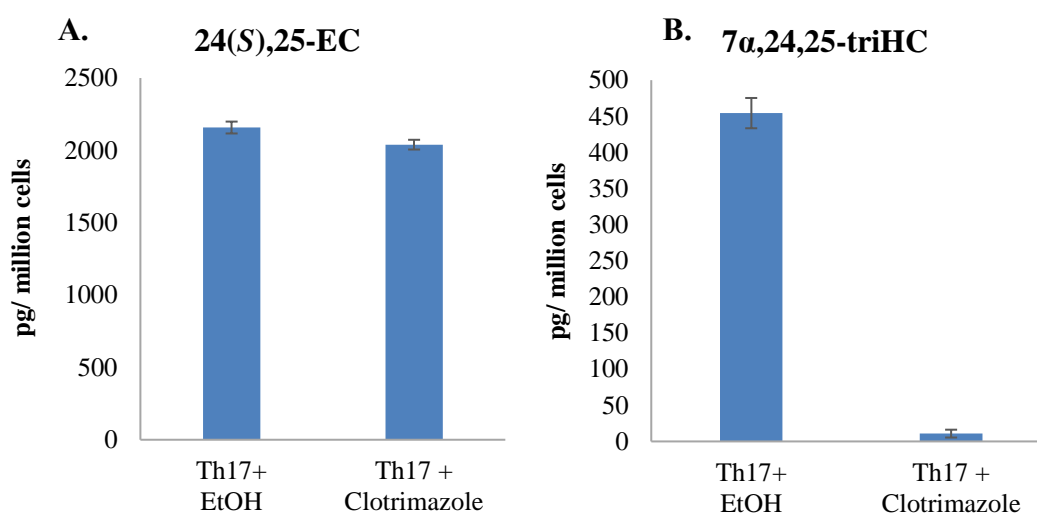


Figure 4.30 Normalised LC-MSⁿ quantification of upstream and downstream oxysterols of CYP7B1 activity reveal inhibition of CYP7B1 with clotrimazole treatment from Donor 1 activated Th17-polarised naïve CD4⁺ T cell culture media. (A) No considerable change in 24(S),25-EC concentration was detected in Th17-polarised cells with or without clotrimazole treatment. (B) 7α,24,25-triHC concentration in Th17 polarised cells with clotrimazole treatment was considerably lower than Th17 polarised cells without treatment. Data normalised to the number of cells initially seeded. Error bars represent S.D. of triplicate LC-MSⁿ injections, n=1.

Table 4.6 Quantified oxysterols in media fraction of Donor 2 activated naïve CD4⁺ T cells cultured under Th17 or Treg polarised conditions with and without azole treatments. ND = not detected

Sterols in conditioned media	Activated naïve CD4 ⁺ T cells (pg/million cells)					
	Th17 polarised cells	Th17 polarised cells with 1 µM Clotrimazole	Th17 polarised cells with 1 µM Tebuconazole	Treg polarised cells	Treg polarised cells with 1 µM Clotrimazole	Treg polarised cells with 1 µM Tebuconazole
24(S)-HC	126.22	113.54	85.91	82.25	57.08	62.75
24(R)-HC	24.17	17.0	9.36	19.67	7.64	8.04
25-HC	48.81	41.64	47.39	198.82	82.73	116.49
27-HC	27.80	25.88	24.58	31.60	21.34	29.20
24(S),25-EC	3690.99	30363.55	1964.19	2887.01	1569.76	1674.31
7α,24,25-triHC	472.25	ND	130.22	180.78	ND	ND

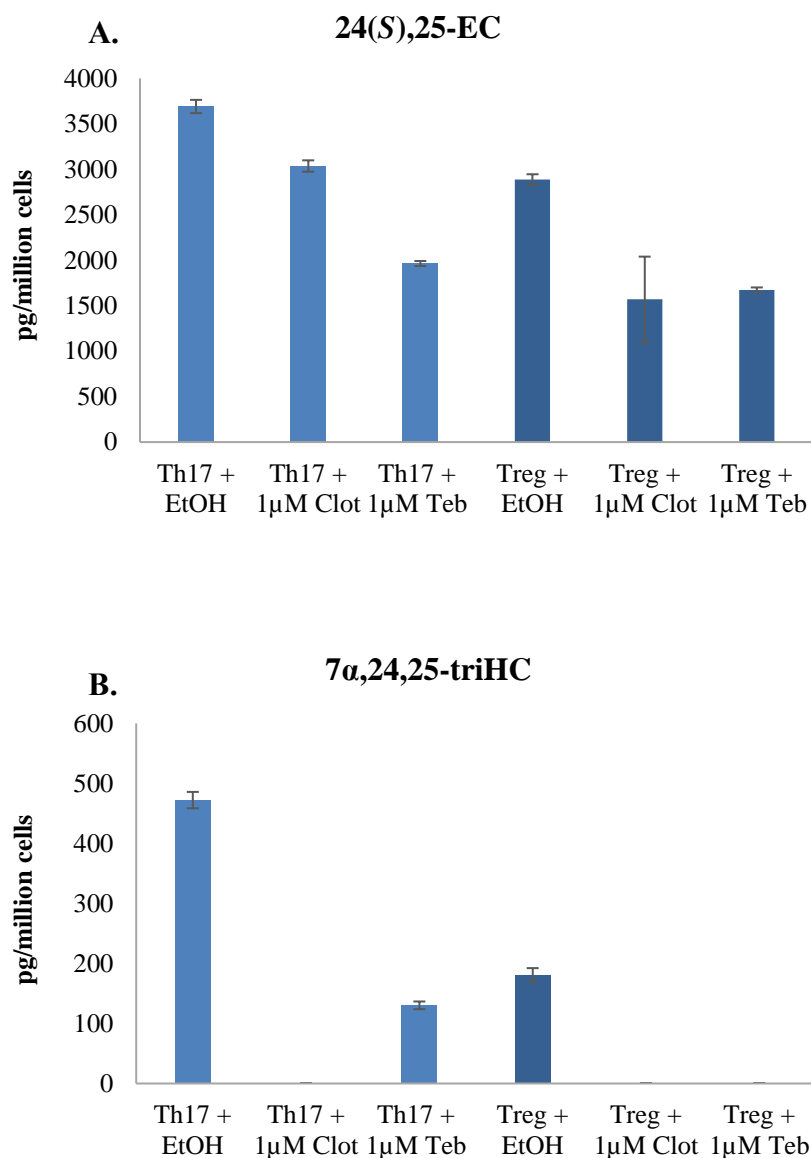


Figure 4.31 Normalised LC-MSⁿ quantification of upstream and downstream oxysterols of CYP7B1 activity reveal inhibition of CYP7B1 with clotrimazole and tebuconazole treatment from Donor 2 activated Th17 and Treg polarised naïve CD4⁺ T cell culture media. (A) High 24(S),25-EC concentration were detected in Th17 and Treg polarised cells with or without clotrimazole treatment. (B) 7α,24,25-triHC concentrations were considerably reduced in Th17 and Treg polarised cells with clotrimazole and tebuconazole treatment. Data normalised to the number of cells initially seeded. Error bars represent S.D. of triplicate LC-MSⁿ injections, n=1.

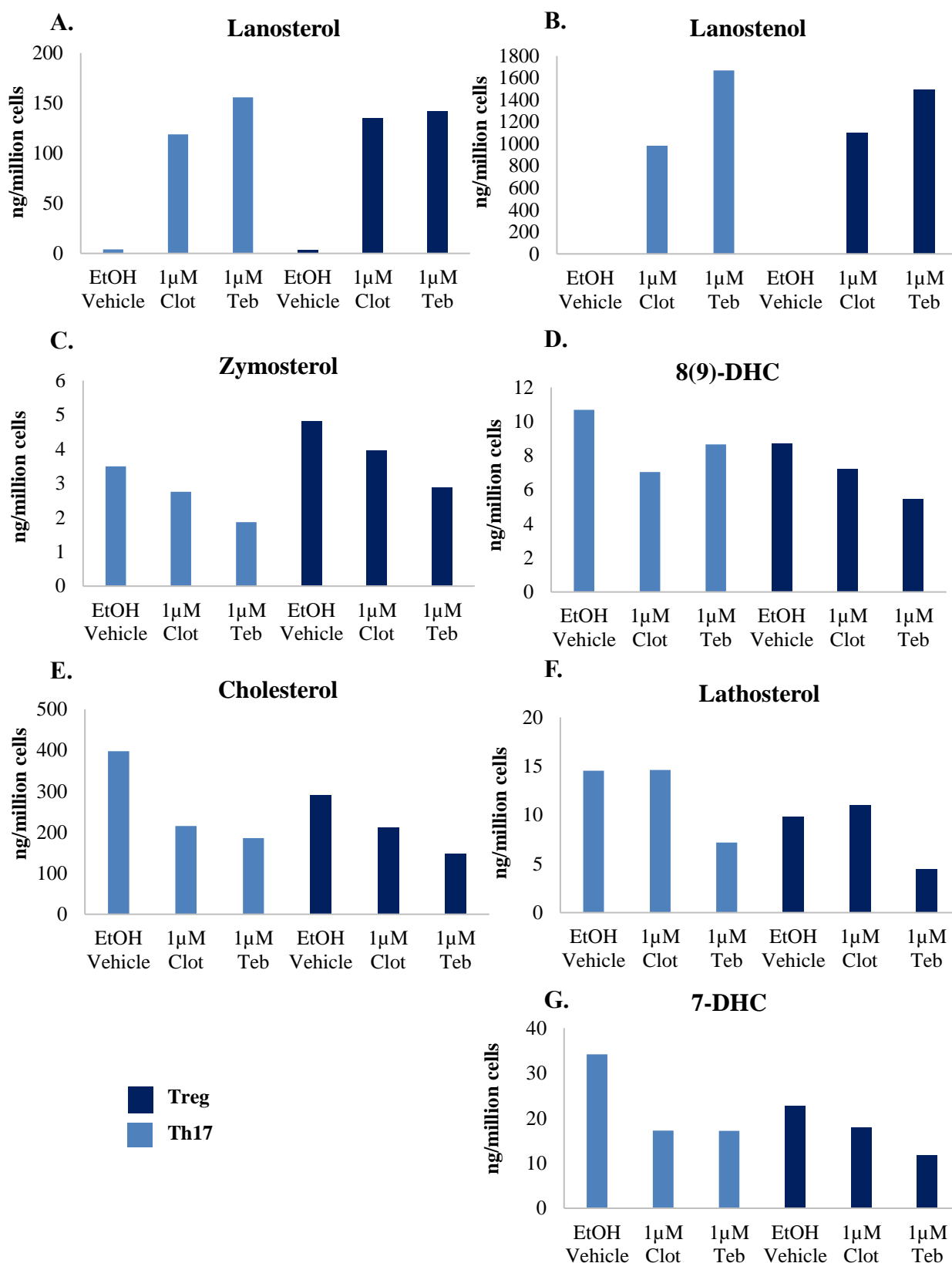


Figure 4.32 Normalised GC-MS quantification of upstream and downstream sterols of CYP51 in Donor 2 activated Th17 and Treg polarised naïve CD4⁺ T cells. Azole compounds clotrimazole and tebuconazole inhibit CYP51 activity in the Bloch and Kandutsch-Russell pathways in Th17 and Treg polarised cells. A) Increased concentrations of lanosterol were detected in Th17 and Treg polarised cells with clotrimazole and tebuconazole treatment. B) Increased lanostenol concentrations were observed in Th17 and Treg polarised cells with clotrimazole and tebuconazole treatment. Reduced concentrations of (C) zymosterol, (D) 8(9)-DC, (E) cholesterol, (F) lathosterol and (G) 7-DHC were observed with azole treatments. Data normalised to cell number. n=1. GC-MS analysis performed by Alison Dickson.

Oxysterol analysis of cell culture media from Donor 3 Th17 and Treg polarised cells with and without 0.5 to 1 μ M clotrimazole or tebuconazole treatment is summarised in Table 4.7. As with Donors 1 and 2, the most abundant oxysterol in Th17 and Treg polarised cells was 24(*S*),25-EC. Concentrations of 24(*S*),25-EC increased up to four fold in Th17 cells with 0.5 μ M clotrimazole or tebuconazole treatments shown in Figure 4.33A, while 24(*S*),25-EC concentrations in Treg cells increased two fold with clotrimazole treatment. Downstream metabolite 7 α ,24,25-triHC concentrations showed inhibition of CYP7B1 activity in a dose dependant manner, a six fold reduction was observed with 0.5 μ M clotrimazole treatments and forty fold with 1 μ M clotrimazole treatment shown in Figure 4.33B. Similar concentrations of 7 α ,24,25-triHC were detected with 0.5 to 1 μ M tebuconazole treatments. GC-MS analysis of cholesterol precursors upstream and downstream of CYP51 was performed on Donor 3 Th17 and Treg polarised cells by Alison Dickson. In concurrence with Donor 2, GC-MS analysis showed clotrimazole and tebuconazole inhibit CYP51 activity with increased concentrations of upstream substrates lanosterol and lanostenol in both Th17 and Treg polarised cells (Figure 4.34A and Figure 4.34B respectively). This inhibitory effect was not observed in further downstream cholesterol precursors (Figure 4.34). Tebuconazole treatment of Th17 and Treg polarised cells in both Donor 2 and Donor 3 was shown to have a greater inhibitory effect towards CYP51 while clotrimazole showed a greater inhibitory effect towards CYP7B1.

Table 4.7 Quantified oxysterols in media fraction of Donor 3 activated naïve CD4⁺ T cells cultured under Th17 or Treg polarised conditions with and without azole treatments. ND = not detected

Sterols in conditioned media	Activated naïve CD4 ⁺ T cells (pg/million cells)									
	Th17 polarised cells	Th17polarised cells with 0.5µM clotrimazole	Th17polarised cells with 1µM clotrimazole	Th17polarised Cells with 0.5µM Tebuconazole	Th17polarised cells with 1µM Tebuconazole	Treg polarised cells	Treg polarised cells with 0.5µM clotrimazole	Treg polarised cells with 1µM clotrimazole	Treg polarised cells with 0.5µM Tebuconazole	Treg polarised cells with 1µM Tebuconazole
24(S)-HC	76.26	83.83	85.75	82.02	76.77	84.77	88.62	71.35	58.25	68.99
24(R)-HC	14.25	20.52	18.70	12.92	11.53	20.31	14.97	25.78	13.54	15.94
25-HC	18.64	51.49	49.03	41.82	49.28	116.18	161.36	175.02	157.28	150.11
27-HC	17.98	16.83	24.45	17.17	18.49	18.15	20.41	27.32	22.33	28.59
24(S),25-EC	824.12	3294.57	3305.61	1356.66	1853.72	1195.54	2402.07	2399.88	1428.04	1461.11
7α,24,25-triHC	720.54	108.37	20.66	605.47	457.90	359.20	7.04	ND	137.16	122.84

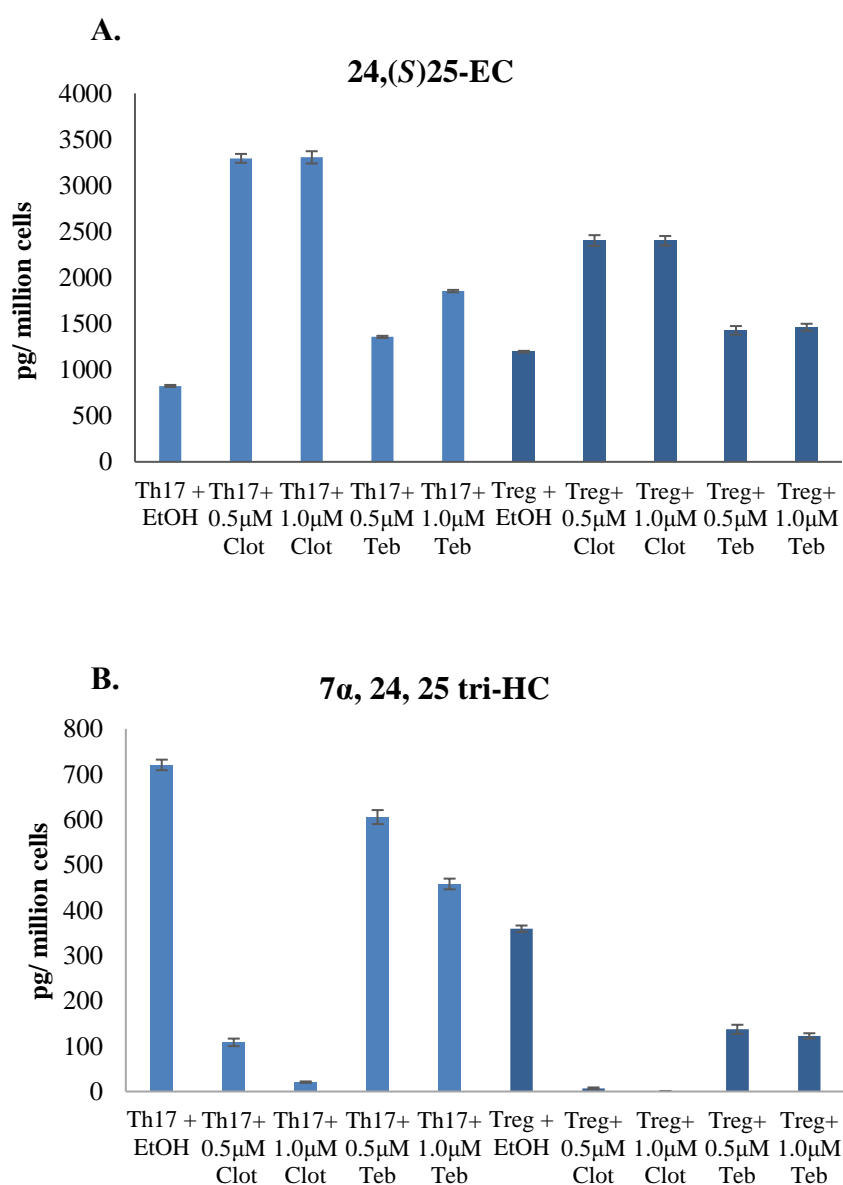


Figure 4.33 Normalised LC-MSⁿ quantification of upstream and downstream oxysterols of CYP7B1 activity in Donor 3 activated Th17 and Treg polarised naïve CD4⁺ T cell culture media. (A) High 24(S),25-EC concentration were detected in Th17 and Treg polarised cells with or without azole treatment. (B) 7α,24,25-triHC concentrations were considerably reduced in Th17 and Treg polarised cells with clotrimazole and tebuconazole treatment in a dose dependant manner. Data normalised to the number of cells initially seeded. Error bars represent S.D. of triplicate LC-MSⁿ injections, n=1.

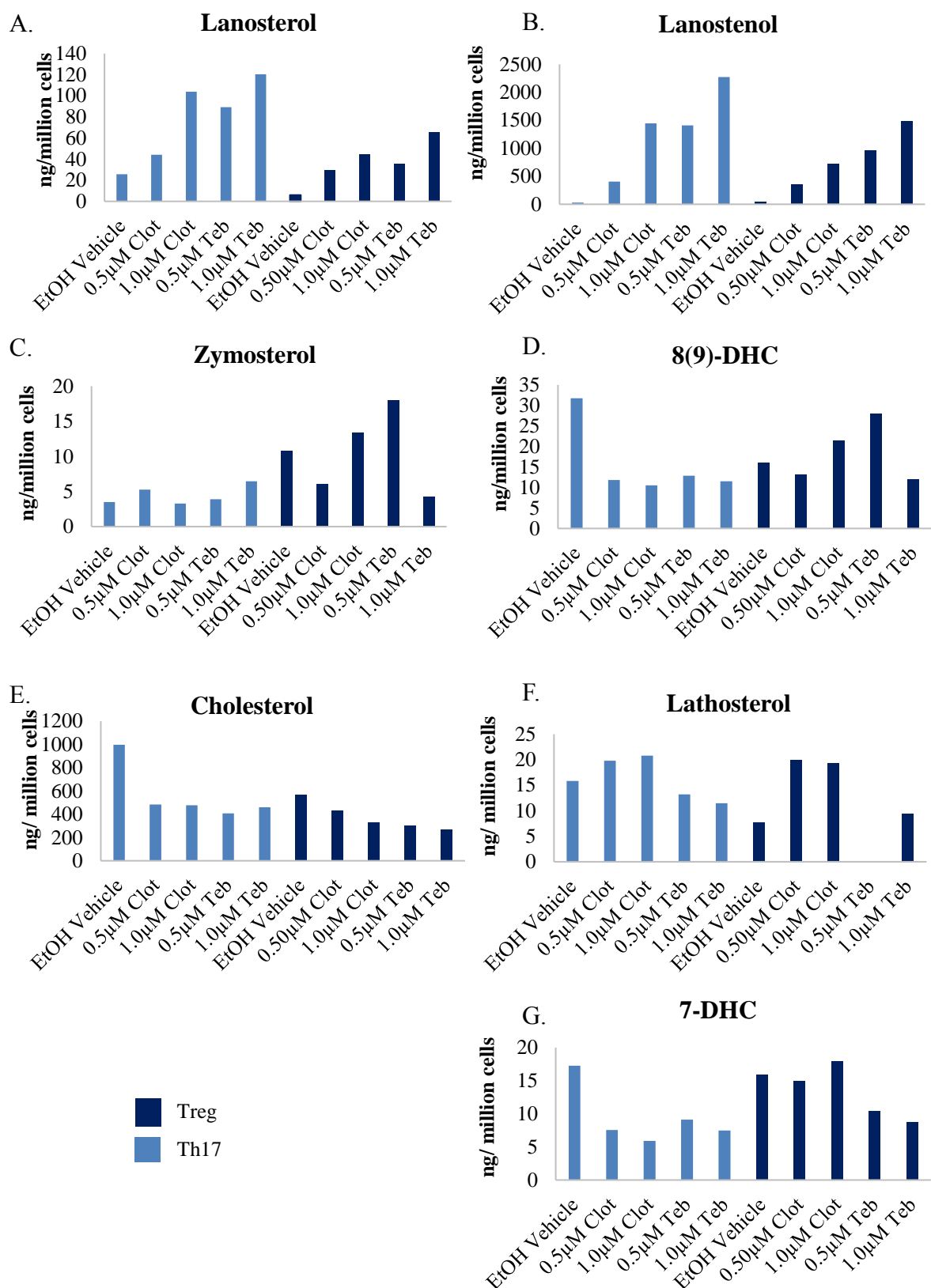


Figure 4.34 Normalised GC-MS quantification of upstream and downstream sterols of CYP51 in Donor 3 activated Th17 and Treg polarised naïve CD4⁺ T cells. Azole compounds clotrimazole and tebuconazole inhibit CYP51 activity in the Bloch and Kandutsch-Russell pathways in Th17 and Treg polarised cells. Increased concentrations of (A) lanosterol and (B) lanostenol were detected in Th17 and Treg polarised cells with clotrimazole and tebuconazole treatments in a dose dependant manner. Partial rescue was observed in (C) zymosterol, (D) 8(9)-DC, (E) cholesterol, (F) lathosterol and (G) 7-DHC concentrations. Data normalised to cell number. n=1. GC-MS analysis performed by Alison Dickson.

Quantification of Donor 4 Th0 and Th17 polarised cell culture media is summarised in Table 4.8. Non-polarised, Th0, activated nCD4⁺ T cells produced detectable concentrations of 24(*S*)-HC, 25-HC and 24(*S*),25-EC in cell culture media however these oxysterols were present at lower concentrations than activated Th17 polarised cell culture media. Inhibition of CYP7B1 activity was observed in Th17polarised cells with 0.5 μ M clotrimazole treatment, downstream metabolite 7 α ,24,25-triHC was forty fold lower than Th17 polarised with vehicle control (Figure 4.35B), while 24(*S*),25-EC concentrations increased two fold with 0.5 μ M clotrimazole treatment shown in Figure 4.35A.

Table 4.8 Quantified oxysterols in the media fraction of Donor 4 activated naïve CD4⁺ T cells cultured under non-polarised, Th0 or Th17 polarised conditions with and without 0.5 μ M clotrimazole treatments. ND = not detected

Sterols in conditioned media	Activated naïve CD4 ⁺ T cells (pg/million cells)			
	Th0 Non-polarised cells	Th0 Non-polarised cells with 0.5 μ M clotrimazole	Th17 polarised cells	Th17polarised cells with 0.5 μ M clotrimazole
24(<i>S</i>)-HC	20.71	6.62	120.62	111.63
24(<i>R</i>)-HC	ND	ND	33.06	29.38
25-HC	5.81	7.45	16.75	24.62
27-HC	63.43	43.00	3.93	4.64
24(<i>S</i>),25-EC	325.50	88.80	818.76	1764.50
7α,24,25-triHC	ND	ND	369.84	9.64

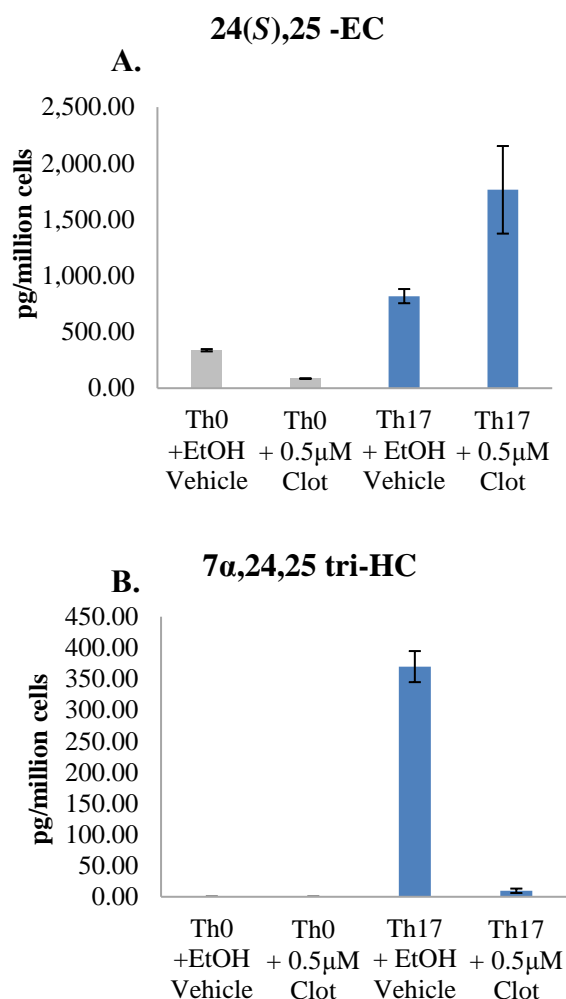


Figure 4.35 Normalised LC-MSⁿ quantification of upstream and downstream oxysterols of CYP7B1 activity in Donor 4 activated non-polarised Th0 and Th17 polarised naïve CD4⁺ T cell culture media. (A) High 24(*S*),25-EC concentration were detected in Th17 polarised cells with increased concentrations in 0.5 μM clotrimazole treated cells. (B) 7α,24,25-triHC concentrations were considerably reduced in Th17 polarised cells with clotrimazole treatment. Data normalised to the number of cells initially seeded. Error bars represent S.D. of triplicate LC-MSⁿ injections for Th0 non-polarised cells and S.D. of duplicate technical replicates of Th17 polarised cells, n=1.

Oxysterols 24(*S*)-HC, 24(*R*)-HC,25-HC and 24(*S*),25-EC were detected in the cell culture media of Donor 5 Th0 non- polarised cells, while 7 α ,24,25-triHC was also quantified in Th17 polarised cell culture media, summarised in Table 4.9. Treatment of Th17 polarised cells with 0.0625 to 0.5 μ M clotrimazole was shown to inhibit CYP7B1 activity in a dose dependant manner (Figure 4.36). 7 α ,24,25-triHC concentrations were fivefold lower with 0.0625 μ M clotrimazole, tenfold lower with 0.125 μ M clotrimazole and fortyfold lower with 0.5 μ M clotrimazole treatments. Similar concentrations of upstream metabolite 24(*S*),25-EC were detected in Th17 polarised cells with vehicle treatment and Th17 polarised cells with clotrimazole treatments as seen with Donors 1 and 2 (Figure 4.36A).

Table 4.9 Quantified oxysterols in media fraction of Donor 5 activated naïve CD4⁺ T cells cultured under non-polarised, Th0 or Th17 polarised conditions with and without 0.0625 to 0.5 μ M clotrimazole treatments. ND = not detected

Sterols in conditioned media	Activated naïve CD4 ⁺ T cells (pg/million cells)				
	Th0 Non-polarised cells	Th17 polarised cells	Th17polarised cells with 0.0625 μ M clotrimazole	Th17polarised cells with 0.125 μ M clotrimazole	Th17polarised cells with 0.5 μ M clotrimazole
24(<i>S</i>)-HC	11.08	56.93	42.32	63.36	54.65
24(<i>R</i>)-HC	3.40	19.68	13.60	16.82	12.18
25-HC	7.79	15.87	11.03	14.82	16.54
27-HC	13.69	7.34	4.47	6.79	7.79
24(<i>S</i>),25-EC	366.13	1700.95	1357.07	1789.12	1658.35
7α,24,25-triHC	ND	191.02	36.00	17.90	4.70

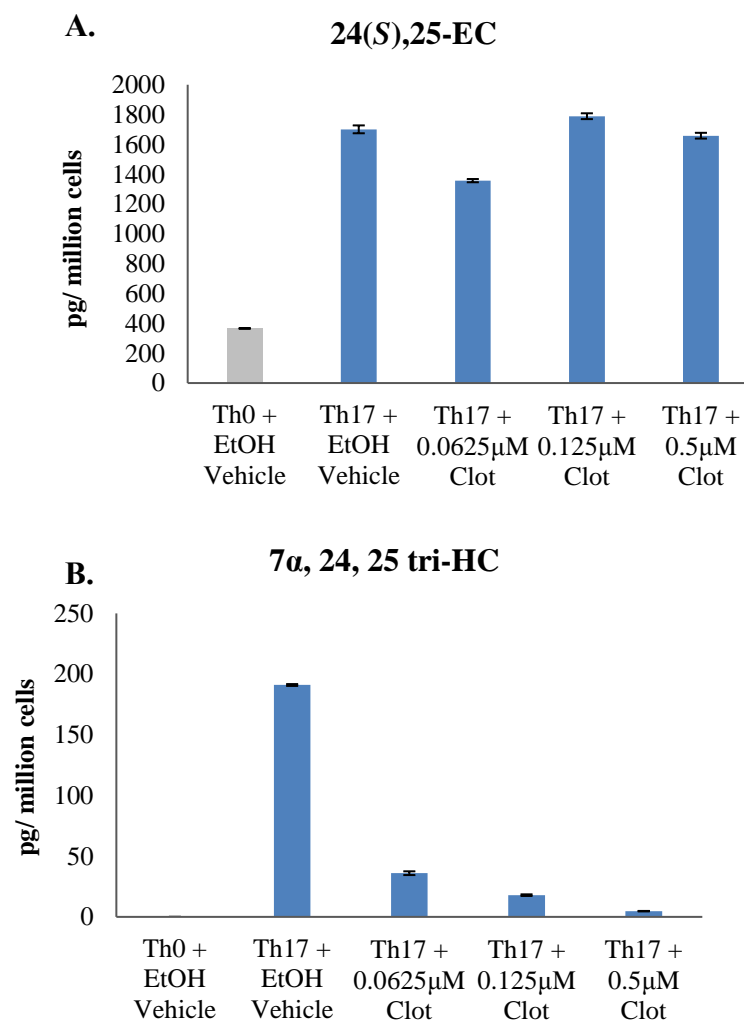


Figure 4.36 Normalised LC-MSⁿ quantification of upstream and downstream oxysterols of CYP7B1 activity in Donor 5 activated non-polarised Th0 and Th17 polarised naïve CD4⁺ T cell culture media. (A) High 24(S),25-EC concentration were detected in Th17 polarised cells with and without clotrimazole treatments. (B) 7 α ,24,25-triHC concentrations were considerably reduced in Th17 polarised cells with clotrimazole treatments in a dose dependant manner. Data normalised to the number of cells initially seeded. Error bars represent S.D. of triplicate LC-MSⁿ injections for Th0 non-polarised cells and S.D. of duplicate technical replicates of Th17 polarised cells, n=1.

Quantification of oxysterols in the cell culture media of Donor 6 non-polarised Th0 and Th17 polarised cells is summarised in Table 4.10. In contrast to the previous Donors, similar concentrations of 24(*S*),25-EC were detected in activated non-polarised cell culture media and Th17-polarised cell culture media (Figure 4.37A) Inhibition of CYP7B1 activity was seen to a lesser extent in Donor 6 Th17 polarised cell culture media with 0.5 μ M clotrimazole treatment. 7 α ,24,25-triHC concentrations were reduced thirteen fold in Th17 polarised cell culture media with 0.5 μ M clotrimazole treatment shown in Figure 4.37B.

Table 4.10 Quantified oxysterols in media fraction of Donor 6 activated naïve CD4⁺ T cells cultured under non-polarised, Th0 or Th17 polarised conditions with and without 0.5 μ M clotrimazole treatments.

Sterols in conditioned media	Activated naïve CD4 ⁺ T cells (pg/million cells)		
	Th0 Non-polarised cells	Th17 polarised cells	Th17polarised cells with 0.5 μ M clotrimazole
24(<i>S</i>)-HC	77.03	71.92	77.90
24(<i>R</i>)-HC	7.86	15.58	14.64
25-HC	3.57	7.93	18.13
27-HC	24.46	7.84	15.12
24(<i>S</i>),25-EC	2727.60	1881.83	3123.97
7α,24,25-triHC	61.05	575.45	44.09

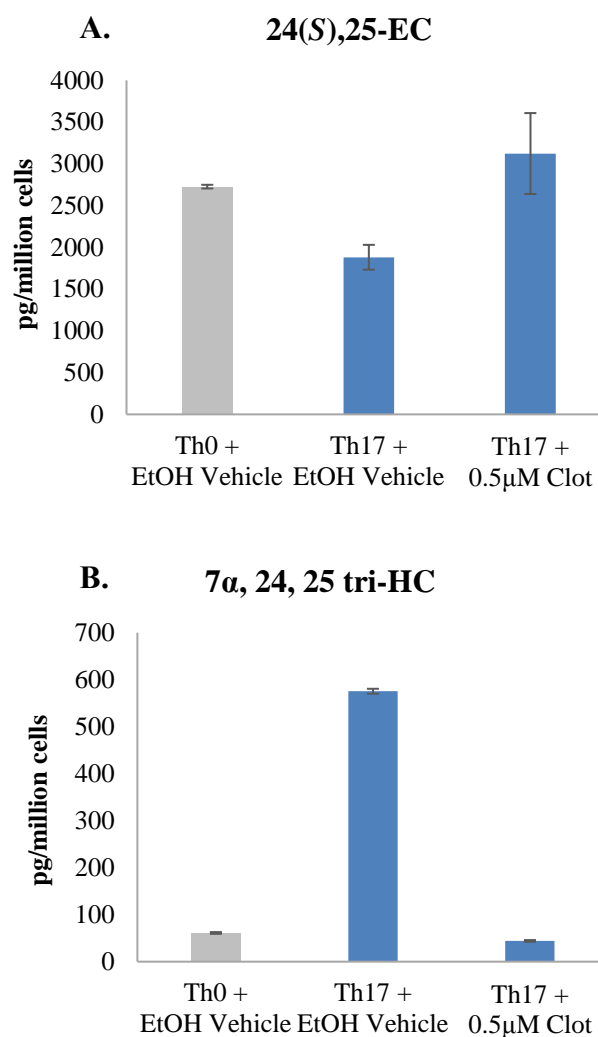


Figure 4.37 Normalised LC-MSⁿ quantification of upstream and downstream oxysterols of CYP7B1 activity in Donor 6 activated non-polarised Th0 and Th17 polarised naïve CD4⁺ T cell culture media. (A) High 24(S),25-EC concentration were detected in Th17 polarised cells with increased concentrations in clotrimazole treated cells. (B) 7 α ,24,25-triHC concentrations were considerably reduced in Th17 polarised cells with clotrimazole treatment. Data normalised to the number of cells initially seeded. Error bars represent S.D. of triplicate LC-MSⁿ injections for Th0 non-polarised cells and S.D. of duplicate technical replicates of Th17 polarised cells, n=1.

Quantification of oxysterols in the cell media of Donor 7 Th17 polarised cells is summarised in Table 4.11. Inhibition of CYP7B1 activity was seen with day 0 clotrimazole treatment of Donor 7 Th17 polarised cells at 0.0625 μ M. While only a small increase of upstream oxysterol 24(*S*),25-EC was detected in cell culture media with 0.0625 μ M clotrimazole treatments (Figure 4.38A), the concentration of downstream oxysterol 7 α ,24,25-triHC detected in cell culture media was fourfold lower shown in Figure 4.38B.

Table 4.11 Quantified oxysterols in media fraction of Donor 7 activated naïve CD4⁺ T cells cultured under Th17 polarised conditions with and without day 0 clotrimazole treatments

Sterols in conditioned media	Activated naïve CD4 ⁺ T cells (pg/million cells)	
	Th17 polarised cells	Th17polarised cells with 0.0625 μ M clotrimazole
24(<i>S</i>)-HC	411.61	515.25
24(<i>R</i>)-HC	56.79	55.42
25-HC	58.20	98.99
27-HC	26.41	35.26
24(<i>S</i>),25-EC	1320.48	2167.59
7 α ,24,25-triHC	293.90	67.80

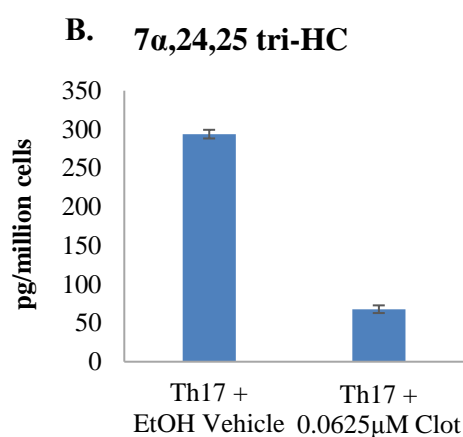
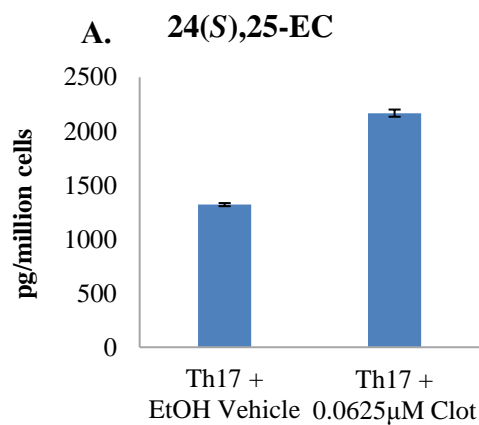


Figure 4.38 Normalised LC-MSⁿ quantification of upstream and downstream oxysterols of CYP7B1 activity in Donor 7 activated Th17 polarised naïve CD4⁺ T cell culture media with day 0 clotrimazole treatment. (A) High 24(S),25-EC concentration were detected in Th17 polarised cells with increased concentrations in clotrimazole treated cells. (B) Reduced 7 α ,24,25-triHC concentrations were detected in Th17 polarised cells with clotrimazole treatment. Data normalised to the number of cells initially seeded. Error bars represent S.D. of triplicate LC-MSⁿ injections, n=1.

Oxysterol concentrations detected in the cell media of Donor 8 activated Th17 polarised cells is summarised in Table 4.12. As with previous Donors, similar concentrations of 24(*S*)-HC, 24(*R*)-HC and 25-HC were quantified in Th17 polarised cell culture media with and without clotrimazole treatments. Inhibition of CYP7B1 activity in Th17 polarised cells was seen with day 0 clotrimazole treatment in a dose dependant manner. Increased concentrations of upstream oxysterol 24(*S*),25-EC was detected in cell culture media with 0.125 μ M and 0.5 μ M clotrimazole treatments (Figure 4.39A) while a fourfold decrease in the concentration of downstream oxysterol 7 α ,24,25-triHC was detected in cell culture media of Th17 polarised cells with 0.125 μ M clotrimazole treatment and twenty fourfold decrease was detected with 0.5 μ M clotrimazole treatment shown in Figure 4.39B.

Table 4.12 Quantified oxysterols in media fraction of Donor 8 activated naïve CD4⁺ T cells cultured under Th17 polarised conditions with and without day 0 0.125 to 0.5 μ M clotrimazole treatments.

Sterols in conditioned media	Activated naïve CD4 ⁺ T cells (pg/million cells)		
	Th17 polarised cells	Th17polarised cells with 0.125 μ M clotrimazole	Th17polarised cells with 0.5 μ M clotrimazole
24(<i>S</i>)-HC	310.15	345.42	430.64
24(<i>R</i>)-HC	41.70	35.78	39.36
25-HC	24.35	26.55	45.98
27-HC	17.33	22.46	39.53
24(<i>S</i>),25-EC	3663.48	4723.62	6239.24
7α,24,25-triHC	728.60	161.54	30.28

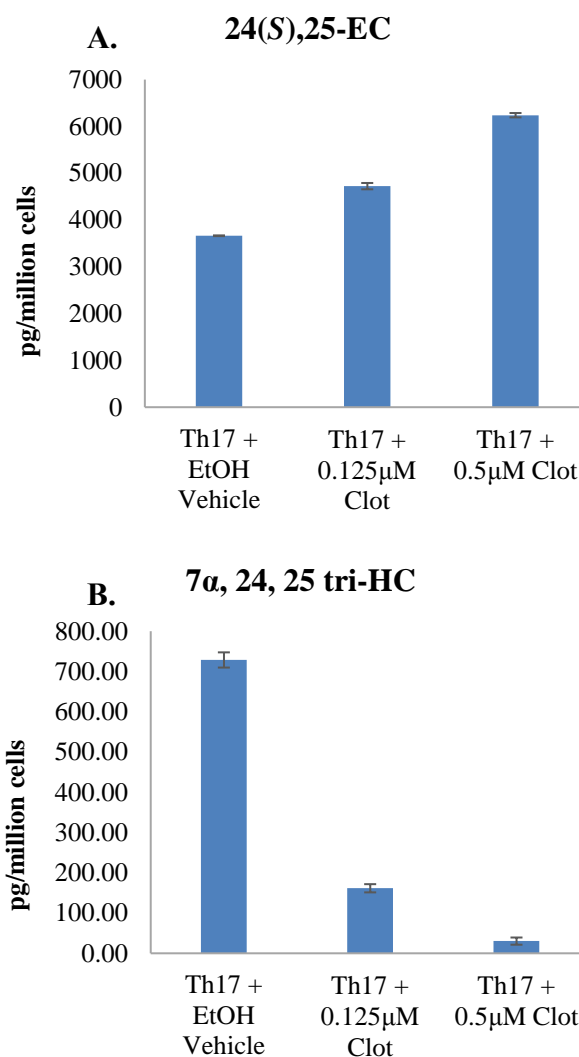


Figure 4.39 Normalised LC-MSⁿ quantification of upstream and downstream oxysterols of CYP7B1 activity in Donor 8 activated Th17 polarised naïve CD4⁺ T cell culture media with day 0 clotrimazole treatments. (A) Increased 24(*S*),25-EC concentrations were detected in Th17 polarised cells with increased concentrations of clotrimazole treatments. (B) Reduced 7α,24,25-triHC concentrations were detected in Th17 polarised cells with clotrimazole treatment. Data normalised to the number of cells initially seeded. Error bars represent S.D. of triplicate LC-MSⁿ injections, n=1.

Oxysterol concentrations detected in the cell media of Donor 9 activated Th17 polarised cells is summarised in Table 4.13. Monohydroxycholesterols 24(*S*)-HC, 24(*R*)-HC and 25-HC were quantified in non-polarised Th0 and Th 17 polarised cell culture media with the highest concentrations detected in Th17 polarised conditions. As previously seen, the most abundant oxysterol of Th17 polarised cells detected was 24(*S*),25-EC, high levels of 24(*S*),25-EC was also detected in Th0 cell culture media. Inhibition of CYP7B1 activity in Th17 polarised cells was seen with day 0 clotrimazole treatment in a dose dependant manner. Increased concentrations of upstream oxysterol 24(*S*),25-EC was detected in cell culture media with 0.125 μ M and 0.25 μ M clotrimazole treatments (Figure 4.40A). Downstream oxysterol 7 α ,24,25-triHC was fourfold lower in the cell culture media of Th17 polarised cells with 0.125 μ M clotrimazole treatment and tenfold lower with 0.25 μ M clotrimazole treatment shown in Figure 4.40B.

Table 4.13 Quantified oxysterols in media fraction of Donor 9 activated naïve CD4⁺ T cells cultured under non-polarised, Th0 or Th17 polarised conditions with and without day 0 0.125 to 0.25 μ M clotrimazole treatments.

Sterols in conditioned media	Activated naïve CD4⁺ T cells (pg/million cells)			
	Th0 non-polarised cells	Th17 polarised cells	Th17polarised cells with 0.125 μ M clotrimazole	Th17polarised cells with 0.25 μ M clotrimazole
24(<i>S</i>)-HC	106.74	272.27	347.34	412.24
24(<i>R</i>)-HC	56.53	98.58	92.26	111.30
25-HC	61.55	59.87	131.37	194.28
27-HC	75.57	22.00	46.71	65.60
24(<i>S</i>),25-EC	4387.55	2870.93	7555.39	8919.86
7α,24,25-triHC	164.81	2181.340	578.14	203.22

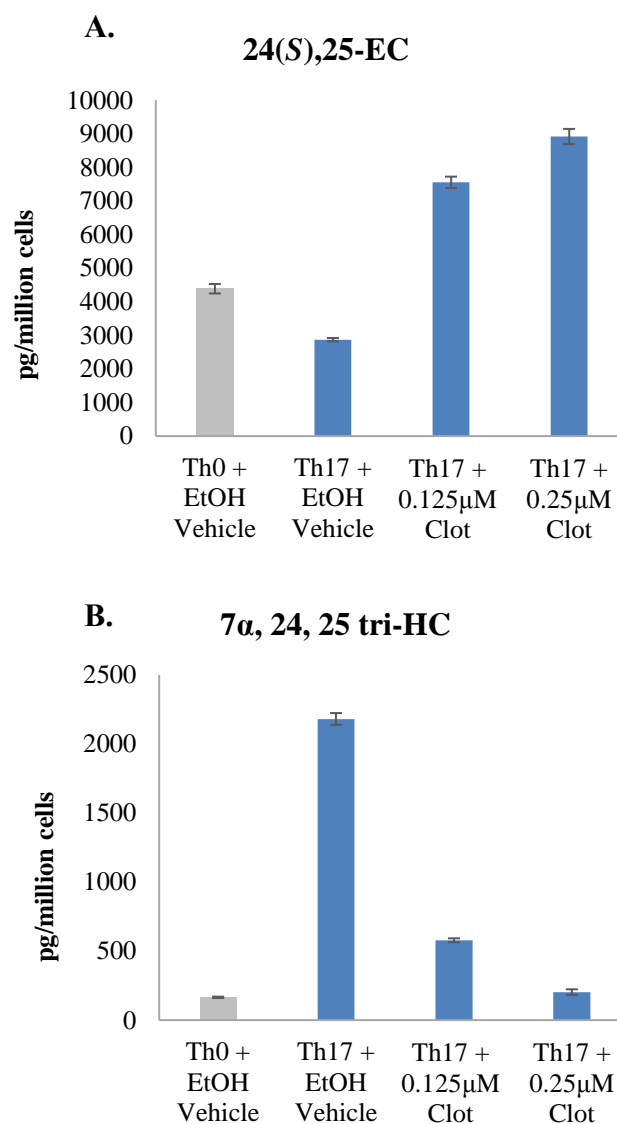


Figure 4.40 Normalised LC-MSⁿ quantification of upstream and downstream oxysterols of CYP7B1 activity in Donor 9 activated non-polarised Th0 or Th17 polarised naïve CD4⁺ T cell culture media with day 0 clotrimazole treatments. (A) Increased 24(S),25-EC concentrations were detected in Th17 polarised cells with increased concentrations of clotrimazole treatments. (B) Reduced 7 α ,24,25-triHC concentrations were detected in Th17 polarised cells with clotrimazole treatments. Data normalised to the number of cells initially seeded. Error bars represent S.D. of triplicate LC-MSⁿ injections, n=1.

Quantification of oxysterols upstream and downstream of CYP7B1 activity in these experiments confirms the inhibitory effect of azole compounds towards CYP7B1. While both clotrimazole and tebuconazole showed inhibition of CYP7B1, LC-MS analysis showed clotrimazole had a greater inhibitory effect than tebuconazole towards CYP7B1 whereas GC-MS analysis of cholesterol precursors and products of primary azole target CYP51, performed by Alison Dickson, showed tebuconazole had a greater inhibitory effect towards CYP51. The inhibitory effect of clotrimazole was seen in a dose dependant manner from 0.0625 μM treatment on the third or first day of Th17 polarised cell culture. Combined experimental data for day 3 clotrimazole treatments showed a significant decrease in CYP7B1 downstream metabolite $7\alpha,24,25\text{-triHC}$ concentrations with clotrimazole treatments at 0.5 μM and 1.0 μM shown in Figure 4.41B.

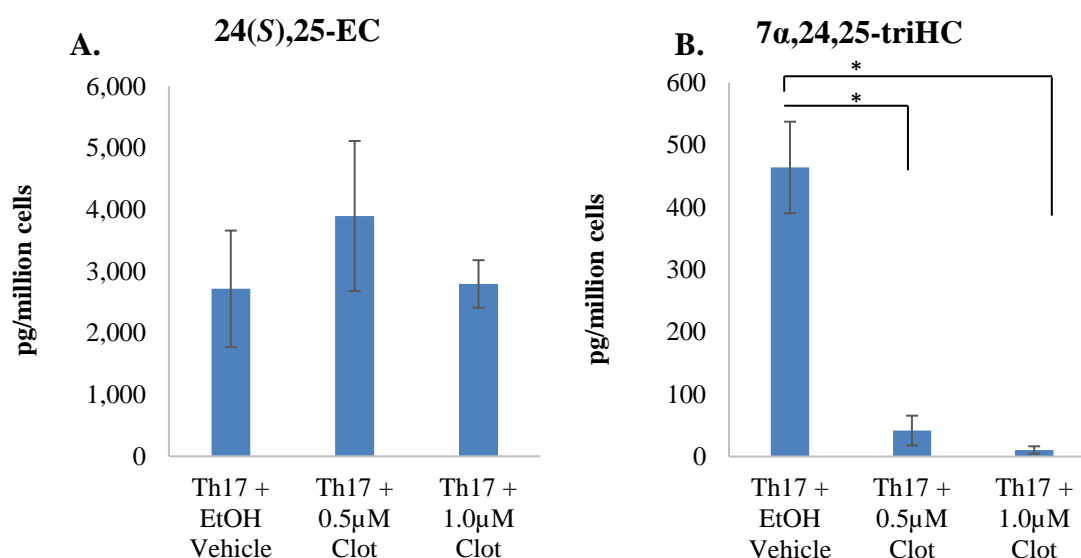


Figure 4.41 Normalised LC-MSⁿ quantification of upstream and downstream oxysterols of CYP7B1 activity in activated Th17 polarised naïve CD4⁺ T cell culture media with day 3 clotrimazole treatments. (A) No significant change was detected in upstream substrate 24(S),25-EC in Th17 polarised cells with clotrimazole treatments. (B) $7\alpha,24,25\text{-triHC}$ concentrations were significantly reduced in Th17 polarised cells with clotrimazole treatments. Data normalised to the number of cells initially seeded. Error bars represent SEM, $n \geq 3$, * $p \leq 0.05$.

4.4 Discussion

This chapter investigated the role of oxysterol 7 α -hydroxylase, CYP7B1, in Th17 cells and IL-17 production. Azole compounds have previously been reported to inhibit IL-17 production in Th17 cells ⁽¹⁶⁾. Analysis of *IL17* mRNA expression by qRT-PCR showed downregulation of *IL17* expression with 1 μ M clotrimazole and tebuconazole treatments although donor variation was observed at lower concentrations of clotrimazole and the relative change was small. IL-17 concentrations detected in the cell culture media of Th17 polarised cells with and without azole treatment was shown to correlate with the expression levels of *IL17* mRNA.

While downregulation of *IL17* expression was seen with azole treatments of Th17 polarised cells on the third day of cell culture, flow cytometry analysis revealed varying effect on CD25 activation, proliferation and viability of cells with azole treatments between donors. However, the greatest effect on CD25 activation and cell proliferation was seen when azole treatment was added on the first day of cell culture. High purity of isolated nCD4⁺ T cells was achieved prior to cell culture and qRT-PCR analysis revealed successful polarisation of Th17 and Treg cells however a small percentage of isolated cells cultured under polarising conditions do not differentiate which may contribute to the variation observed between donors.

Although these experiments confirm azole treatment can change the expression of *IL17* in Th17 cells, it is difficult to determine the true affect due to the variation in experimental conditions and limited replicates for all concentrations used. A range of treatment concentrations was used to determine an optimum concentration, however a preferable donor strategy which focussed on technical and biological replicates at a set number of concentrations would have provided a greater understanding of the affect of azole treatment on *IL17* expression in Th17 cells.

Recent studies have shown azoles including ketoconazole and clotrimazole suppress IL-17A production in both mouse and human Th17 differentiated cells; this was attributed to the inhibition of lanosterol 14 α -demethylase cytochrome P450 enzyme, CYP51A1 in the cholesterol biosynthesis pathway ⁽²⁰⁾. It was therefore suggested that cholesterol precursors downstream of CYP51A1 act as endogenous ROR γ t ligands, desmosterol was proposed to be a strong candidate for an endogenous

ROR γ t agonist. However, azole drugs have also been reported to interact with other cytochrome P450 enzymes including CYP7B1⁽²¹⁻²³⁾.

While GC-MS analysis of Th17 polarised cells cultured with azole treatments confirmed the inhibition of CYP51A1 activity, LC-MS analysis of oxysterols extracted from cell culture media revealed azoles also inhibited CYP7B1 activity. High concentrations of 24(S),25-EC and downstream metabolite 7 α ,24,25-triHC were detected in Th17 polarised cells which was greatly reduced with azole treatment. Clotrimazole treatment was shown to have a greater inhibitory effect on *IL17* expression which correlated to a greater inhibition of CYP7B1 activity, while tebuconazole showed greater inhibition of CYP51A1 activity but a smaller inhibitory effect on *IL17* expression. As CYP7B1 is induced in Th17 cells and greater inhibition of CYP7B1 resulted in greater inhibition of *IL17* expression, downstream metabolites of CYP7B1 activity in the cholesterol metabolism pathway may be endogenous ROR γ t ligands.

4.5 References

1. Ouyang, W., Kolls, J. K., & Zheng, Y. (2008). The Biological Functions of T Helper 17 Cell Effector Cytokines in Inflammation. *Immunity*, 28(4), 454–467. <https://doi.org/10.1016/j.immuni.2008.03.004>
2. Ye, P., Rodriguez, F. H., Kanaly, S., Stocking, K. L., Schurr, J., Schwarzenberger, P., ... Kolls, J. K. (2001). Requirement of Interleukin 17 Receptor Signaling for Lung CXC Chemokine and Granulocyte Colony-stimulating Factor Expression , Neutrophil Recruitment , and Host Defense. *J. Exp. Med.*, 194(4), 519–527.
3. Conti, H. R., Shen, F., Nayyar, N., Stocum, E., Sun, J. N., Lindemann, M. J., ... Gaff, S. L. (2009). Th17 cells and IL-17 receptor signaling are essential for mucosal host defense against oral candidiasis. *The Journal of Experimental Medicine*, 206(2), 299–311. <https://doi.org/10.1084/jem.20081463>
4. Harrington, L. E., Hatton, R. D., Mangan, P. R., Turner, H., Murphy, T. L., Murphy, K. M., & Weaver, C. T. (2005). Interleukin 17 – producing CD4 + effector T cells develop via a lineage distinct from the T helper type 1 and 2 lineages. *Nature Immunology*, 6(11), 1123–1132. <https://doi.org/10.1038/ni1254>
5. Park, H., Li, Z., Yang, X. O., Chang, S. H., Nurieva, R., Wang, Y., ... Dong, C. (2005). A distinct lineage of CD4 T cells regulates tissue inflammation by producing interleukin 17. *Nature Immunology*, 6(11), 1133–1141.
6. Bettelli, E., Korn, T., Oukka, M., & Kuchroo, V. K. (2008). Induction and effector functions of TH17 cells. *Nature*. <https://doi.org/10.1038/nature07036>
7. Langrish, C. L., Chen, Y., Blumenschein, W. M., Mattson, J., Basham, B., Sedgwick, J. D., ... Cua, D. J. (2005). IL-23 drives a pathogenic T cell population that induces autoimmune inflammation. *The Journal of Experimental Medicine JEM*, 00(2), 233–240. <https://doi.org/10.1084/jem.20041257>
8. Ivanov, I. I., McKenzie, B. S., Zhou, L., Tadokoro, C. E., Lepelley, A., Lafaille, J. J., ... Littman, D. R. (2006). The Orphan Nuclear Receptor ROR γ t Directs the Differentiation Program of Proinflammatory IL-17+ T Helper Cells. *Cell*, 126(6), 1121–1133. <https://doi.org/10.1016/j.cell.2006.07.035>
9. Manel, N., Unutmaz, D., & Littman, D. R. (2008). The differentiation of human TH-17 cells requires transforming growth factor- β and induction of the nuclear receptor ROR γ t. *Nature Immunology*, 9(6), 641–649. <https://doi.org/10.1038/ni.1610>

10. Ghilardi, N., & Ouyang, W. (2007). Targeting the development and effector functions of TH17 cells. *Seminars in Immunology*, 19, 383–393.
<https://doi.org/10.1016/j.smim.2007.10.016>
11. Acosta-rodriguez, E. V, Napolitani, G., Lanzavecchia, A., & Sallusto, F. (2007). Interleukins 1 b and 6 but not transforming growth factor- b are essential for the differentiation of interleukin 17 – producing human T helper cells. *Nature Immunology*, 8(9), 942–949. <https://doi.org/10.1038/ni1496>
12. Sakaguchi, S. (2004) Naturally arising CD4+ regulatory T cells for immunologic self tolerance and negative control of immune responses, *Annu. Rev. Immunol* , 22,,531-562
13. Santori, F. R., Huang, P., van de Pavert, S. A., Douglass, E. F., Leaver, D. J., Haubrich, B. A., ... Littman, D. R. (2015). Identification of Natural ROR γ Ligands that Regulate the Development of Lymphoid Cells. *Cell Metabolism*, 21(2), 286–297. <https://doi.org/10.1016/j.cmet.2015.01.004>
14. Wang, Y., Kumar, N., Solt, L. A., Richardson, T. I., Helvering, L. M., Crumbley, C., ... Burris, T. P. (2010). Modulation of Retinoic Acid Receptor-related Orphan Receptor α and γ Activity by 7-Oxygenated Sterol Ligands. *Journal of Biological Chemistry*, 285(7), 5013–5025. <https://doi.org/10.1074/jbc.M109.080614>
15. Fu, S., Zhang, N., Yopp, A. C., Chen, D., Mao, M., Chen, D., ... Bromberg, S. (2004). TGF- b Induces Foxp3 + T-Regulatory Cells from CD4 + CD25 – Precursors. *American Journal of Transplantation*, 4, 1641–1627.
<https://doi.org/10.1111/j.1600-6143.2004.00566.x>
16. Kojima, H., Muromoto, R., Takahashi, M., Takeuchi, S., Takeda, Y., Jetten, A. M., & Matsuda, T. (2012). Inhibitory effects of azole-type fungicides on interleukin-17 gene expression via retinoic acid receptor-related orphan receptors α and γ . *Toxicology and Applied Pharmacology*, 259(3), 338–345.
<https://doi.org/10.1016/j.taap.2012.01.011>
17. Heusinkveld, H. J., Molendijk, J., Berg, M. Van Den, & Westerink, R. H. S. (2013). Azole Fungicides Disturb Intracellular Ca²⁺ in an Additive Manner in Dopaminergic PC12 Cells. *Toxicological Sciences*, 134(2), 374–381.
<https://doi.org/10.1093/toxsci/kft119>
18. Sung, D., Kim, J., Won, K. J., Kim, B., Shin, C., Park, J., & Bae, Y. M. (2012). Blockade of K⁺ and Ca²⁺ Channels by Azole Antifungal Agents in Neonatal Rat Ventricular Myocytes. *Biological and Pharmaceutical Bulletin*, 35(9), 1469–1475.

19. Livak, K. J., & Schmittgen, T. D. (2001). Analysis of Relative Gene Expression Data Using Real-Time Quantitative PCR and the $2^{-\Delta\Delta CT}$ Method. *Methods*, 25(4), 402–408. <https://doi.org/10.1006/meth.2001.1262>
20. Hu, X., Wang, Y., Hao, L.-Y., Liu, X., Lesch, C. A., Sanchez, B. M., ... Glick, G. D. (2015). sterol metabolism controls TH17 differentiation by generationg endogenous ROR γ agonists. *Nature Chemical Biology*, 11, 141–148.
21. Yantsevich, A. V., Dichenko, Y. V., Mackenzie, F., Mukha, D. V., Baranovsky, A. V., Gilep, A. A., ... Strushkevich, N. V. (2014). Human steroid and oxysterol 7 α -hydroxylase CYP7B1: Substrate specificity, azole binding and misfolding of clinically relevant mutants. *FEBS Journal*. <https://doi.org/10.1111/febs.12733>
22. Goetz, A. K., & Dix, D. J. (2009). Mode of Action for Reproductive and Hepatic Toxicity Inferred from a Genomic Study of Triazole Antifungals. *Toxicologicaol Sciences*, 110(2), 449–462. <https://doi.org/10.1093/toxsci/kfp098>
23. Martin, M. T., Dix, D. J., Judson, R. S., Kavlock, R. J., Reif, D. M., Richard, A. M., ... Houck, K. A. (2010). Impact of Environmental Chemicals on Key Transcription Regulators and Correlation to Toxicity End Points within EPA ' s ToxCast Program. *Chem. Res. Toxicol*, 23, 578–590.

Chapter 5. Investigating the role of CYP7B1 in the expression on IL17 in primary murine CD4⁺ T cells and the potential of murine cell line EL4 for the study of IL-17 production

5.1 Introduction

The previous Chapter looked to investigate the role of CYP7B1 in Th17 cell differentiation and IL-17 production by small molecule inhibitors, while inhibition of CYP7B1 activity was confirmed the effects on IL-17 production was inconclusive. In this chapter a murine model is used to investigate the effect of *Cyp7b1* KO in primary murine naïve CD4⁺ T cells. The oxysterol 7 α hydroxylase enzyme CYP7B1 is ubiquitously expressed in murine cells with a role in the cholesterol metabolism pathway by hydroxylating oxysterols including 25-HC and 27-HC at the 7 α position ^(1,2). Extracellular detection of 25-HC, 27-HC and 24-HC has been reported in the majority of murine primary CD4⁺ T cell subsets with increased 25-HC reported in the Treg subset ⁽³⁾. Intracellular detection of 25-HC was also reported in Th0, Th1, Th2 and Treg cells but not the Th17 subset. The previous chapter showed CYP7B1 could also act on 24(*S*),25-EC to produce 7 α ,24(*S*),25-EC. The objective of this section of the chapter is to determine whether CYP7B1 affects the levels of endogenous ROR γ t ligands by determining the effect of *Cyp7b1* KO on *Il17* expression.

The subsequent section of this chapter looks at the potential of the murine T cell thymoma cell line, EL4, for the investigation of the role of oxysterols in the ROR γ t/IL-17 pathway. EL4 cells have previously been used to study the potential of synthetic ROR γ t ligands as they endogenously express ROR γ t and IL-17A ⁽⁴⁾. EL4 cells were used to investigate the effect of synthetic ROR α and ROR γ ligand SR1001 on endogenous gene expression in EL4 cells. The effect of further synthetic ligands including SR1555 and SR2211 has also been investigated by determining the effect on *Il17a* mRNA in EL4 cells ^(5,6). The novel allosteric ligand of ROR γ t, MRL-871 has also been reported with cellular activity confirmed through treatment of EL4 cells ⁽⁷⁾. Recently, a novel allosteric ligand of ROR γ t, FM26 was identified through in silico guided pharmacophore screening and optimisation with the EL4 cell line used to determine the cellular activity of ROR γ t inverse agonists by measuring

reduction in *Il17* mRNA expression ⁽⁸⁾. Publications have also been reported on the inhibitory effect of FoxP2 on *Il17* mRNA expression in EL4 cells through direct interaction with ROR γ t ⁽⁹⁾.

Aims:

1. Investigate the effect of *Cyp7b1* knockout in primary murine naïve CD4⁺ T cells.
2. Determine the suitability of murine EL4 lymphocyte cell line for the study of the *Il17* expression using known inhibitors of ROR γ t.

5.2 Materials and Methods

5.2.1 Isolation of naïve CD4⁺ T cells from murine splenocytes

Splenocytes of *Cyp7b1* knockout (KO) mice and wild type (WT) littermates were harvested by collaborator Tina Raselli, University Hospital Zurich, by homogenising spleens with a 70 μ M filter and syringe with 10 mL PBS. The homogenate was transferred to a 50 mL falcon tube with a further 40 mL PBS and centrifuged at 350 x g, 4°C for 5 minutes. The supernatant was discarded, cells were resuspended in 3 mL ACK buffer and incubated on ice for 5 minutes for lysis of red blood cells. Subsequently, 8 mL RPMI FCS medium was added and cell suspension centrifuged at 450 x g, 4°C for 5 minutes. The supernatant was discarded and cells were resuspended in 50 mL RPMI FCS for transfer to our laboratory. The splenocyte suspension received on dry ice was centrifuged at 300 x g, 4°C for 5 minutes. The supernatant was discarded, cells were resuspended in 6 mL X-Vivo-20 and transferred to a 15 mL falcon tube. A further 4 mL X-Vivo-20 was added to the 50 mL falcon tube to rinse and transferred to the 15 mL falcon tube. The cell suspension was centrifuged at 300 x g, 4°C for 5 minutes. The supernatant was discarded and cells resuspended in 10 mL PBS. The cell number and viability was determined with trypan blue and a C-chip haemocytometer as described in *section 2.1.11.1*. Naïve CD4⁺ T cells were isolated by density gradient centrifugation and negative selection with MACS® technology as described in *section 2.1.7* and *2.1.7.1*.

5.2.2 Purity and activation analysis of naïve CD4⁺ T cells by flow cytometry

Following isolation of naïve CD4⁺ T cells, aliquots of cells were stained with anti-CD4, anti-CD44 or anti-CD62L antibodies and analysed by flow cytometry as described in *section 2.1.12.4*. The activation of cells following cell culture was determined by staining an aliquot of cells with anti-CD25 antibodies and analysed by flow cytometry.

5.2.3 Culture conditions for unstimulated murine naïve CD4⁺ T cells in X-Vivo-20 media

Isolated murine naïve CD4⁺ T cells were seeded at 0.9 to 1 x 10⁶ cells in 1 mL X-Vivo-20 media and cultured for 6 days in a 24-well plate at 37°C and 5% CO₂. A mock X-Vivo-20 media was also seeded and processed in parallel with cell samples.

5.2.4 Culture conditions for CD3 and CD28 activated Th17 or Treg polarised naïve CD4⁺ T cells in X-Vivo-20 media

Activation and polarisation cell culture methods were adapted from Manel et al. 2008⁽¹⁰⁾. Isolated murine naïve CD4⁺ T cells were seeded at 0.9 to 1 x 10⁶ cells in 1 mL X-Vivo-20 media with anti-CD3 and anti-CD28 loaded microbeads in non-polarising (Th0), Th17 or Treg polarising conditions listed in Table 5.1 and cultured for 6 days in a 24 well plate at 37°C, 5% CO₂. A mock X-Vivo-20 media was also seeded and processed in parallel with cell samples. On culture day 3, cells were split equally in two wells and topped up with fresh media for the relevant polarised conditions. After 6 days of culture, cells were harvested by resuspending in the culture media and transferring to 2 mL Eppendorf tubes. Cell suspensions were centrifuged at 300 x g for 5 minutes and supernatants were transferred to fresh tubes for oxysterol analysis. Cell pellets were resuspended in PBS and counted using the method described in *section 2.1.11* and aliquots taken for flow cytometry. Subsequently cell suspensions were divided equally into two tubes and centrifuged at 300 x g for 5 minutes and cell pellets were stored for RNA extraction and oxysterol analysis.

Table 5.1 Th17, Treg and non-polarising cell culture conditions for murine naïve CD4⁺ T cells in X-Vivo-20 media

Treatment	Non-polarising Th0 conditions	Th-17 polarised conditions	Treg polarised conditions	Non- activated
Anti-CD3 and anti-CD28 microbeads	1.5:1 Bead to cell ratio	1.5:1 Bead to cell ratio	1.5:1 Bead to cell ratio	-
Mouse IL-2	-	-	10 ng/mL	-
Mouse IL-23	-	20 ng/mL	-	-
Mouse TGF-β	-	5 ng/mL	5 ng/mL	-
Mouse anti-IL4	10 μ g/mL	10 μ g/mL	-	-
Mouse anti-IFNγ	10 μ g/mL	10 μ g/mL	-	-

5.2.5 Culture conditions for PMA and ionomycin stimulated EL4 cell line

The murine lymphoblast cell line, EL4, was purchased from SIGMA and maintained at 0.2 to 1x10⁶ cells/mL in Corning® T-25 flasks at 37°C, 5% CO₂. For initial stimulation experiments 1.125 to 2.5x10⁶ EL4 cells were seeded in serum free DMEM (Gibco, Cat. no. 41966-029), X-Vivo-20 (Lonza, Cat. no. LZBE04-448Q) or 10% FBS DMEM media in 24 or 12 well plate and incubated overnight at 37°C, 5% CO₂. Subsequently, EL4 cells were stimulated with 50 ng/mL PMA and 1 μ g/mL ionomycin as described in *section 2.1.9.2* and incubated for 5 hours at 37°C, 5% CO₂.

5.2.6 Oxysterol treatment and inhibition of EL4 cell line

A preliminary experiment with oxysterol treatments was performed with 1.25x10⁶ EL4 cells seeded in 1.5 mL X-Vivo-20 media in a 24-well plate in two sets. 24(S),25-EC (Avanti, Cat no. 700039P) and 25-HC (Avanti, Cat no. 700019P) treatments were prepared at 4 μ M in X-Vivo-20 from stock while ursolic acid was prepared at 8 μ M in X-Vivo-20 from stock concentration (Sigma-Aldrich, Cat no. 89797). Then, 500 μ L 24(S),25-EC, 25-HC or ursolic acid treatments were added to

set 1 of seeded cells and mixed by pipette to give a final concentration of 1 μ M 24(S),25-EC, 1 μ M 25-HC or 2 μ M ursolic acid. This set was incubated overnight at 37°C, 5% CO₂. Subsequently, 100 μ L of 20X PMA and ionomycin stock was added to wells while 100 μ L of X-Vivo-20 media was added to a non-activated control well and incubated at 37°C, 5% CO₂ for 5 hours. To the second set of cells 500 μ L of X-Vivo-20 media was added to wells and incubated overnight at 37°C, 5% CO₂. Subsequently, 500 μ L of media was gently removed from wells and 500 μ L 24(S),25-EC, 25-HC or ursolic acid treatments were added to wells and mixed by pipette to give a final concentration of 1 μ M 24(S),25-EC, 1 μ M 25-HC or 2 μ M ursolic acid. Cells were incubated at 37°C, 5% CO₂ for 1 hour prior to the addition of 100 μ L of 20X PMA and ionomycin to wells or 100 μ L of X-Vivo-20 media to a non-activated control and a further incubation at 37°C, 5% CO₂ for 5 hours. Following the 5 hour incubation both sets of cells were harvested by resuspending cells in culture media and transferring to centrifuge tubes. Cell suspensions were centrifuged at 300 x g for 10 minutes and the supernatant was transferred to 2 mL EppendorfTM tubes. Cell pellets were washed with PBS and centrifuged at 300 x g for 10 minutes and supernatant discarded. Media was stored at -20°C and cell pellets at -80°C.

This experiment was repeated with 0.9×10^6 cells seeded in 2.5 mL X-Vivo-20 media in a 12-well plate. Subsequently, 500 μ L 6X ursolic acid treatments were added to seeded cells in duplicate and mixed by pipette to give a final concentration of 2 μ M ursolic acid. The first treatment of ursolic acid was prepared from an original stock while the second ursolic acid treatment was prepared from a fresh stock. Cells were incubated overnight at 37°C, 5% CO₂ prior to the addition of 150 μ L of 20X PMA and ionomycin stock to wells while 150 μ L of X-Vivo-20 media was added to a non-activated control well and incubated at 37°C, 5% CO₂ for 5 hours before harvesting.

Further experiments with reported ROR γ t inhibitors ursolic acid and T0901317 were performed with EL4 cells seeded in X-Vivo-20 or DMEM 10% FBS media. Firstly, 0.9×10^6 EL4 cells were seeded 2.5 mL media in a 12-well plate. Then, 500 μ L 6X ursolic acid or T0901317 treatments were added to wells and gently mixed by pipette to give final concentrations of 2 μ M ursolic acid, 1 μ M T0901317 or 10 μ M T0901317. Cells were incubated overnight at 37°C, 5% CO₂. Following incubation

150 μ L 20X PMA and ionomycin was added to wells or 150 μ L media was added to a non-activated control and cells were incubated at 37°C, 5% CO₂ for 5 hours. In parallel, a further 0.9×10^6 EL4 cells were seeded in 3 mL media and incubated overnight at 37°C, 5% CO₂. Subsequently, 500 μ L of media was gently removed from untreated cells and 500 μ L 6X T0901317 treatment was added to give 1 μ M T0901317. Cells were incubated at 37°C, 5% CO₂ for 1 hour prior to the addition on 150 μ L of 20X PMA and ionomycin followed by a further incubation at 37°C, 5% CO₂ for 5 hours. This was to determine the optimum period of time for inhibition without detrimental effects on cells. Following the 5 hour incubation both sets of cells were harvested and cell pellets analysed.

Further experiments were performed on EL4 cells with 1 μ M to 30 μ M clotrimazole treatments in DMEM 10% FBS. EL4 cells were seeded at 1.0×10^6 in a 12-well plate and incubated overnight at 37°C, 5% CO₂. Subsequently, 500 μ L of media was removed from wells and 500 μ L 4X clotrimazole treatments were added to wells and mixed well by pipetting. Cells were incubated at 37°C, 5% CO₂ prior to stimulation with 100 μ L of 20X PMA and ionomycin followed by a further incubation at 37°C, 5% CO₂ for 5 hours before harvesting for analysis.

5.2.7 Flow cytometry analysis of CD25 activation and cell viability of EL4 cultures

CD25 and 7AAD staining and flow cytometry analysis of cell aliquots taken during harvesting of cell cultures was performed as described in *section 2.1.12.4* and *2.1.11.2* respectively.

5.2.8 Sample processing for qRT-PCR analysis

mRNA was extracted from cell pellets following the extraction method in *section 2.2.2.1* mRNA expression levels of genes of interest were determined using a two-step quantitative reverse transcription PCR (qRT-PCR) as described in *section 2.2.2* and *2.2.2.5* mRNA expression levels were analysed using the $2^{-\Delta\Delta Ct}$ method ⁽¹¹⁾.

5.2.9 Sample processing for oxysterol analysis

Oxysterols were extracted from media supernatant fractions in Ethanol containing internal sterol standards as described in *section 2.3.2*. Oxysterol analysis was performed by LC-ESI-MSⁿ. Identification and quantification of enzymatically

derived oxysterols was achieved with the method described in *section 2.3.4.4*.

Autoxidation products of the cholesterol B-ring which can be produced during sample preparation and sterols in the mock media were considered artefacts and were not included in the analysis.

5.3 Results

5.3.1 Naïve CD4⁺ T cells isolated from murine splenocytes by MACs showed > 98% CD4⁺ purity

Single stain flow cytometry analysis of MACs isolated cells from *Cyp7b1* KO mice showed 99% CD4⁺ purity while isolated cells from WT littermates showed CD4 purity between 98 to 99%. Surface staining of marker CD62L (L-Selectin) showed purity >95% and >93% for *Cyp7b1* KO and WT mice respectively. Aliquots were also stained for memory T cell marker CD44, 70 to 84% of *Cyp7b1* KO cells were CD44⁺, while 74 to 86% of WT cells were CD44⁺. The level of activation of isolated cells monitored by CD25 (IL-2 receptor α) expression revealed 19 to 40% of *Cyp7b1* KO cells were CD25⁺ and 25 to 38% of WT cells isolated were CD25⁺. Figure 5.1 shows a representation of the gating strategy used to identify cells. The purity of each of *Cyp7b1* KO and WT naïve CD4⁺ cells analysed by flow cytometry prior to culture is represented in Figure 5.2.

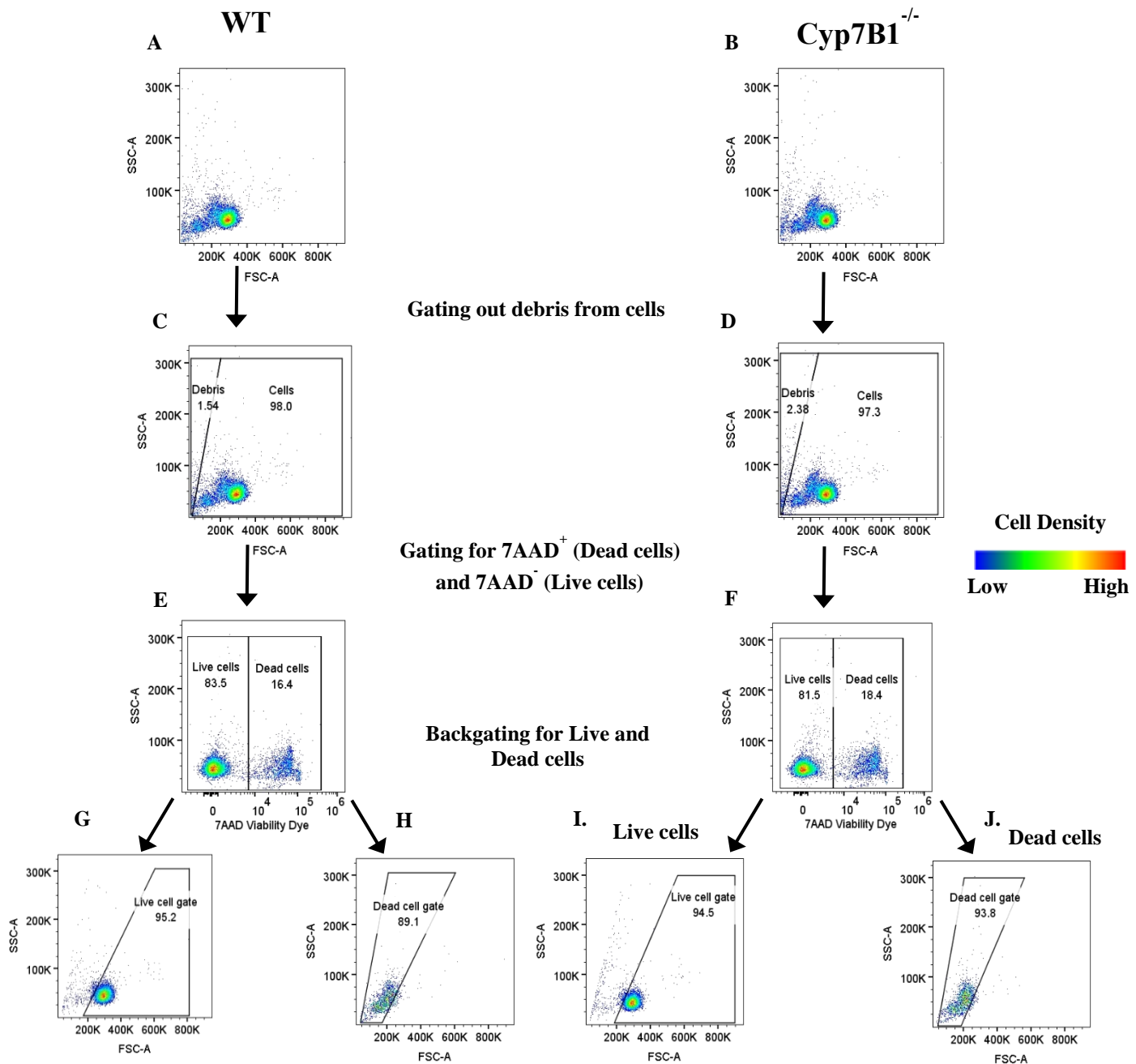


Figure 5.1 Gating strategy applied to *Cyp7b1* KO and WT isolated naïve CD4⁺ T cells to identify live cells and exclude dead cells using 7AAD Viability dye staining. Sample aliquots were single stained with 7AAD viability stain and not fixed prior to processing with ACEA Bioscience Novocyte. Analysis was performed with FlowJo software. Events were plotted on FSC/SSC for both WT (A) and *Cyp7b1* KO (B) isolated cells to gate only cells and exclude debris WT (C), *Cyp7b1* KO, (D). Cells were plotted with 7AAD/SSC to identify the dead/ apoptotic cells which have incorporated the 7AAD stain that was able to penetrate compromised cell membranes and bind to the double stranded DNA (E, F). An FSC/SSC plot was applied to the identified cells to create the Live cell gate and Dead cell gates for WT (G,H) and *Cyp7b1* KO cells (I,J). The Live cell gate was then applied to other single stained aliquots of the same sample.

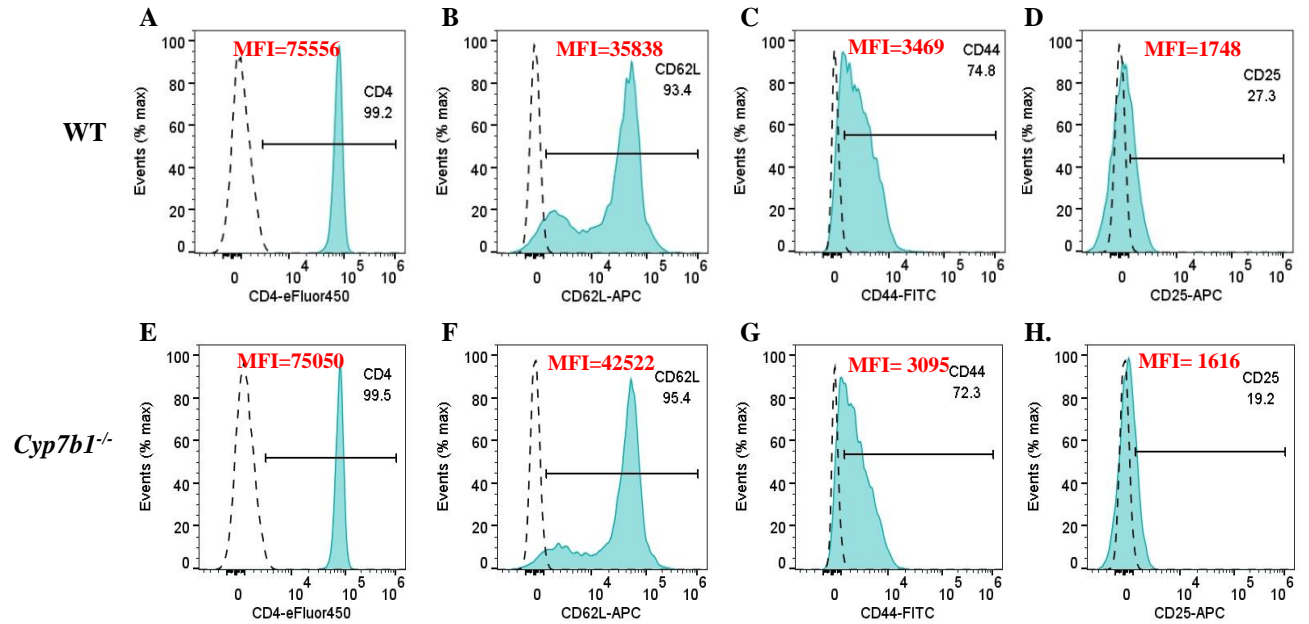


Figure 5.2 Representative flow cytometry analysis of isolated murine naïve CD4⁺ T cells from the splenocytes of set 1 *Cyp7b1* KO and WT littermate. Both WT (A) and *Cyp7b1* KO (E) mice showed good purity with 99% CD4⁺. 93% of isolated WT cells were CD62L⁺ cells (B) and 95% of isolated *Cyp7b1* KO cells were CD62L⁺ cells (F). 74% of WT cells were CD44⁺ (C), 72% of KO cells isolated were CD44⁺ (G). Low CD25 expression was seen in both isolated WT and *Cyp7b1* KO cells. 27% of WT cells were CD25⁺ (D) and 19% of *Cyp7b1* KO cells were CD25⁺ cells. Filled histograms represent the fluorochrome conjugated antibody stained cells. Gates were determined using background fluorescence of unstained samples (1%) indicated by the dashed histogram. The Median Fluorescence intensities (MFI) are indicated in red.

5.3.2 *Cyp7b1* KO in murine CD4⁺ T cells has little effect on CD25 expression and cell viability of activated naïve CD4⁺ cells

Both Non-activated WT and *Cyp7b1* KO cultured cells showed little change in IL-2 receptor alpha (IL-2R α), CD25 expression on the T cell surface after 6 days of culture (Figure 5.3). The CD25 expression of Th0 WT cultured cells was 95% and 89% for *Cyp7b1* KO cells indicating good activation. Lower CD25 expression was seen in both Th17 WT cells and Th17 *Cyp7b1* KO cells with 60% and 51% CD25⁺ respectively. While Treg expression of CD25⁺ also showed good activation with 92% CD25⁺ for both WT and *Cyp7b1* KO. A small reduction of CD25 expression was seen in *Cyp7b1* KO cells compared with WT polarised equivalents in all polarising conditions excluding Treg conditions which showed no difference between the WT and *Cyp7b1* KO as seen in the overlaid histograms in Figure 5.3. Flow cytometry analysis of cell viability through 7AAD incorporation was used to determine the viability of cells harvested after 6 days of culture. WT and *Cyp7b1* KO non-activated nCD4⁺ T cells showed a higher proportion of cell death in comparison to activated Th0, Th17 and Treg polarised cells which had considerably reduced 7AAD incorporation shown in Figure 5.4. *Cyp7b1* KO activated Th0 cells showed no difference in cell viability to the WT equivalent (Figure 5.4C and Figure 5.4D respectively). Th17 polarised cells showed slightly lower cell death in *Cyp7b1* KO cells in comparison to their WT equivalent shown in Figure 5.4E and Figure 5.4F respectively. This was also seen with Treg WT and *Cyp7b1* KO cells (Figure 5.4G and Figure 5.4H respectively).

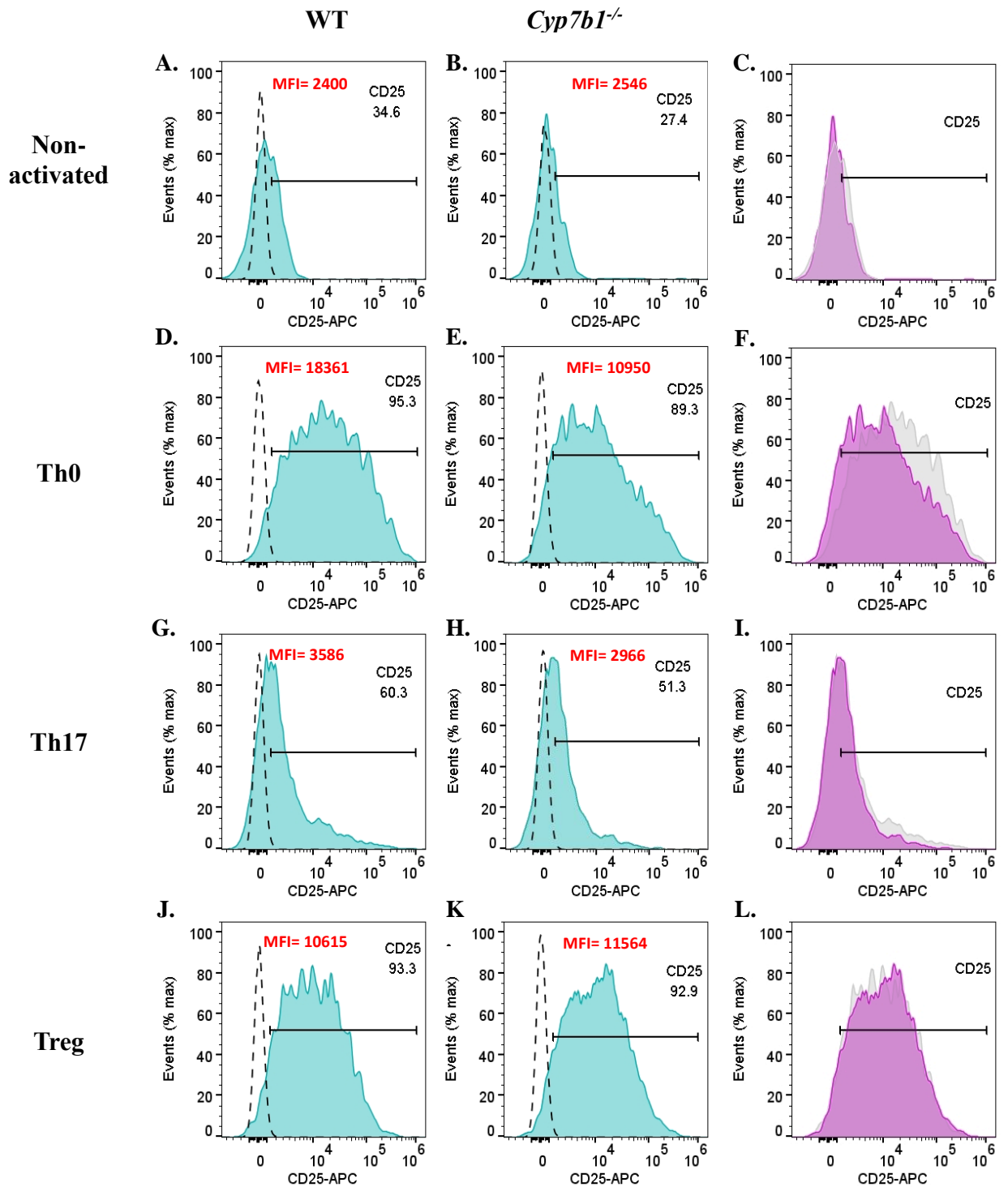


Figure 5.3 Flow cytometry analysis of CD25 expression of murine naïve CD4⁺ T cells after 6 days of culture under Th0, Th17 or Treg polarising conditions. Filled blue histograms represent the fluorochrome conjugated antibody stained cells. Gates were determined using background fluorescence of unstained samples (1%) indicated by the dashed histogram. The Median Fluorescence intensities (MFI) are indicated in red. Filled purple and grey histogram overlays represent *Cyp7b1* KO cells (purple) with WT cells (grey) for Non-activated (C), Th0 (F), Th17 (I) and Treg (L).

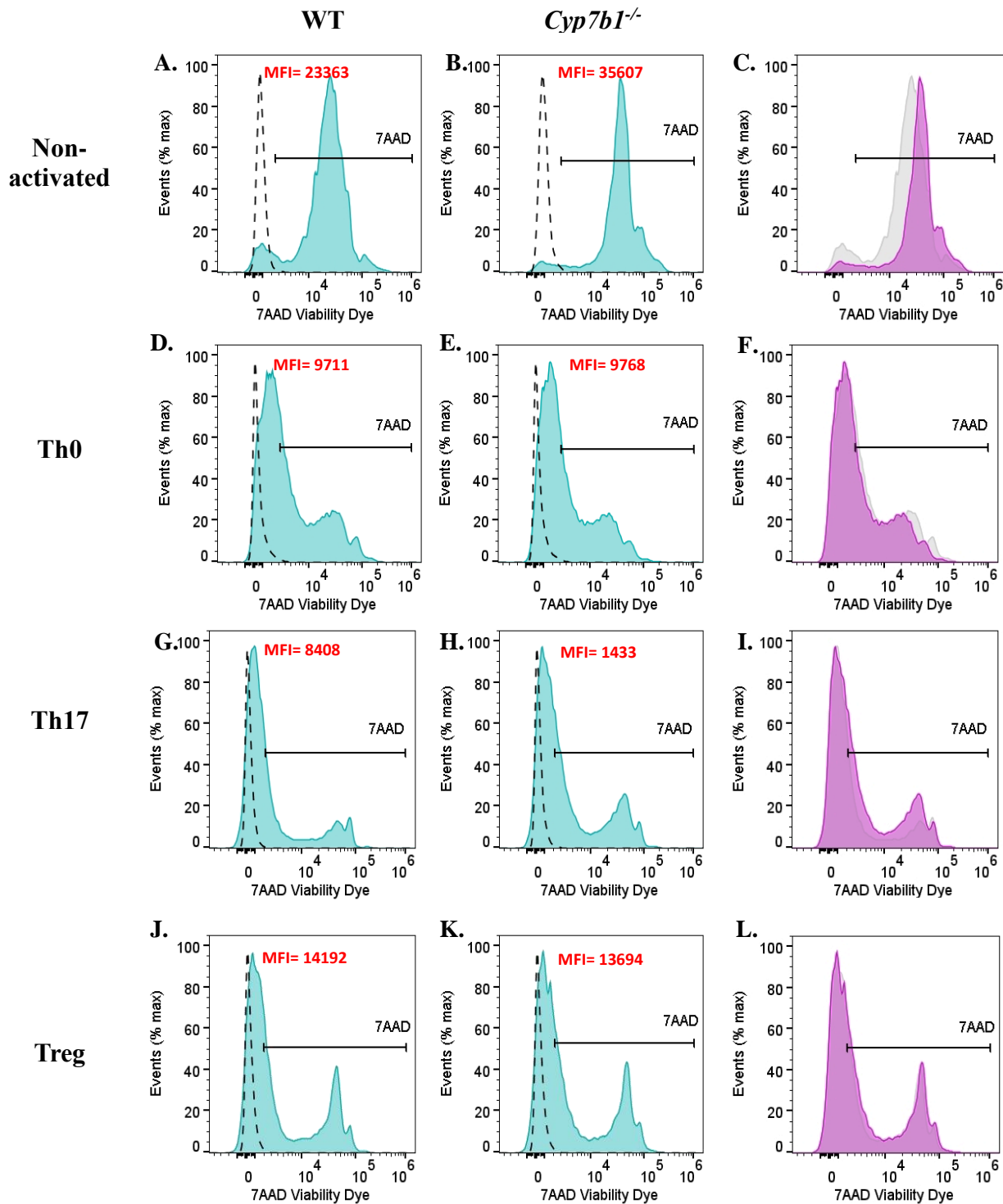


Figure 5.4 Flow cytometry analysis of incorporated 7AAD staining, gated from all isolated murine naïve CD4⁺ T cells after 6 days of culture under Th0, Th17 or Treg polarising conditions. . Filled blue histograms represent the fluorochrome conjugated antibody stained cells. Gates were determined using background fluorescence of unstained samples (1%). The Median Fluorescence intensities (MFI) are indicated in red. Greatest 7AAD staining was observed in Non-activated (A) WT and (B) *Cyp7b1* KO. Filled purple and grey histograms overlays represent *Cyp7b1* KO cells (purple) with WT cells (grey) for Non-activated (C), Th0 (F), Th17 (I) and Treg (L).

5.3.3 *Il17* mRNA expression was downregulated in *Cyp7b1* KO mice

In order to determine the effect of *Cyp7b1* KO on the expression of IL-17, *Il17a* mRNA expression of Th0, Th17 and Treg cells was analysed by qRT-PCR. Th17 polarised cells were the only subset to express *Il17a* mRNA as shown in Figure 5.5 confirming successful polarisation of the CD4⁺ T cell subsets. It was also revealed that *Il17a* mRNA expression was downregulated in *Cyp7b1* KO Th17 cells from expression seen in the WT equivalent. Interestingly, when the expression of *Cyp7b1* mRNA was analysed by qRT-PCR *Cyp7b1* expression was not detected in Th0, Th17 or Treg polarised *Cyp7b1* KO or WT cells.

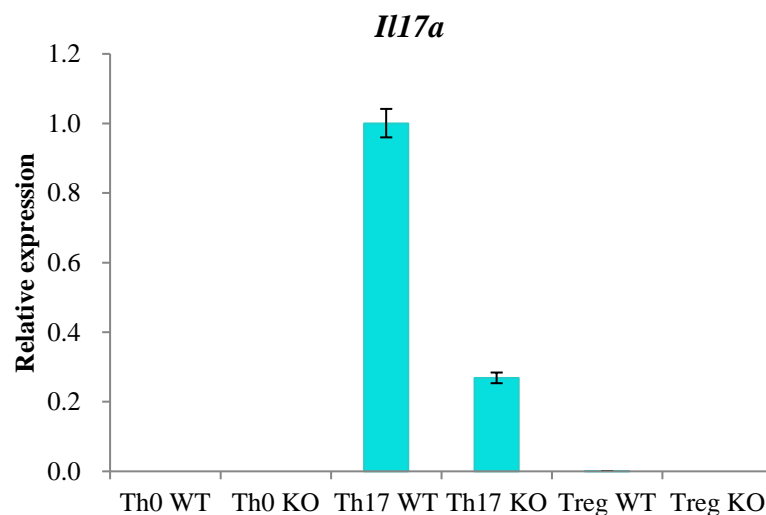


Figure 5.5 qRT-PCR analysis of *Il17a* mRNA expression of murine *Cyp7b1* KO and WT naïve CD4⁺ non-polarised Th0, Th17 polarised or Treg polarised cells. *Il17a* mRNA expression was normalised to *Rp18s* expression and fold change relative to Th17 WT sample. Error bars indicate S.D of technical replicates, n=1

5.3.4 Oxysterol profiling of murine CD4⁺ T cells

Oxysterols analysis performed on supernatant from primary mouse naïve CD4⁺ T cells cultured under activated non-polarised (Th0) or Th17 and Treg polarised conditions showed production of enzymatically-derived side-chain oxidised monohydroxycholesterol 25-HC and low levels of 24(*R*)-HC at 534.4054 *m/z* seen in the RIC in Figure 5.7. These oxysterols were not detected in non-activated conditions and were not found to be present in the X-Vivo-20 mock media (Figure 5.9). Oxysterol 24(*S*),25-EC was detected as hydrolysed 24,25-DiHC at 550.4003 *m/z* (Figure 5.8) however downstream metabolite 7 α ,24,25-EC was not detected in WT or KO cells of any subtype. No dihydroxycholsterols were detected in the X-Vivo-20 mock media (Figure 5.10). The quantified oxysterols for each culture condition are summaries in Figures 5.6A-C.

Due to the labile nature of the 24(*S*),25-EC epoxide group in acidic solvent used in the EADSA derivatisation process, 24(*S*),25-EC can be detected as isomer 24-KC, hydrolysed to 24,25-diHC or methanolysed to 24-hydroxycholesterol-25-methylether and 25-hydroxycholesterol-24-methylether⁽¹²⁾. In this study however, only hydrolysed 24,25-diHC was detected.

CA, 7 β -CA and 7 α -CA are naturally present in X-Vivo-20 media and no considerable change in levels was detected between X-Vivo-20 and cell culture media. In addition, 27-HC and cholesterol B-ring autoxidised sterols 7-KC and 6 β -HC were excluded from analysis as they were also detected in X-Vivo-20 mock media.

Th17 polarised cells showed the highest levels of 25-HC at 37.58 pg/ million cells and 50.57 pg/ million cells in WT and *Cyp7b1* KO supernatant samples respectively shown in Figure 5.6A, while 24(*R*)-HC was greatest in non-polarised Th0 culture conditions at 27.01 pg/ million cells and 26.72 pg/million cells in WT and *Cyp7b1* KO supernatant samples respectively (Figure 5.6B). The levels of 24,25-diHC were greater in Th17 and Treg culture conditions at 237.66 pg/ million cells and 227.99 pg/ million cells in WT supernatant samples in comparison to non-polarised Th0 samples at 126.5 pg/ million cells in the WT supernatant sample presented in Figure 5.6C, However the level of 24,25-diHC detected was considerably lower than

previously seen in human naïve CD4⁺ T cell experiments. Low levels of 25-HC were detected in Th0 conditions of KO mice and no notable change was seen in Treg conditions, however a slight increase was seen under Th17 KO conditions. No substantial change in 24(*R*)-HC detection was seen between WT and *Cyp7b1* KO samples under all polarised conditions, while 24(*S*),25-diHC levels were slightly lower in all KO conditions.

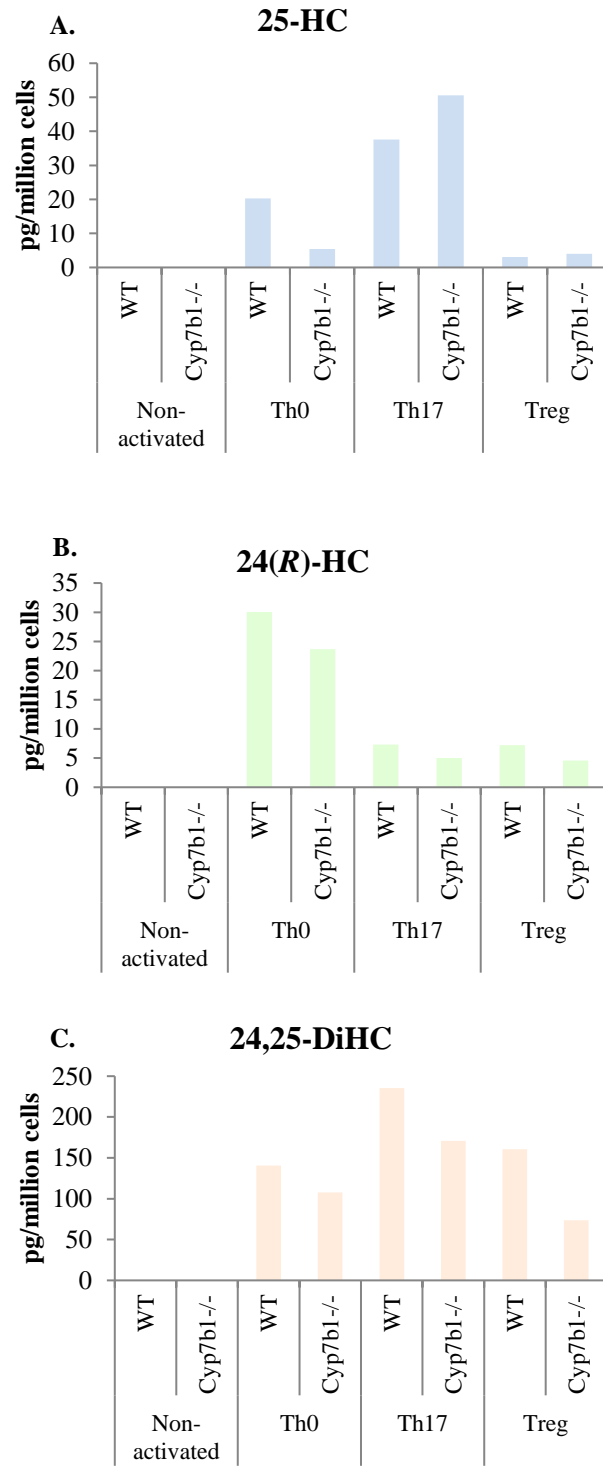


Figure 5.6 Oxysterol analysis of polarised primary murine naïve CD4⁺ T cell culture media. (A) Highest levels of 25-HC was detected in *Cyp7b1* KO Th17 cell culture media. (B) 24(R)-HC concentrations were highest in WT and *Cyp7b1* KO Th17 cell culture media. (C) 24,25-DiHC was detected in Th0, Th17 and Treg polarised WT and KO cells. n=1

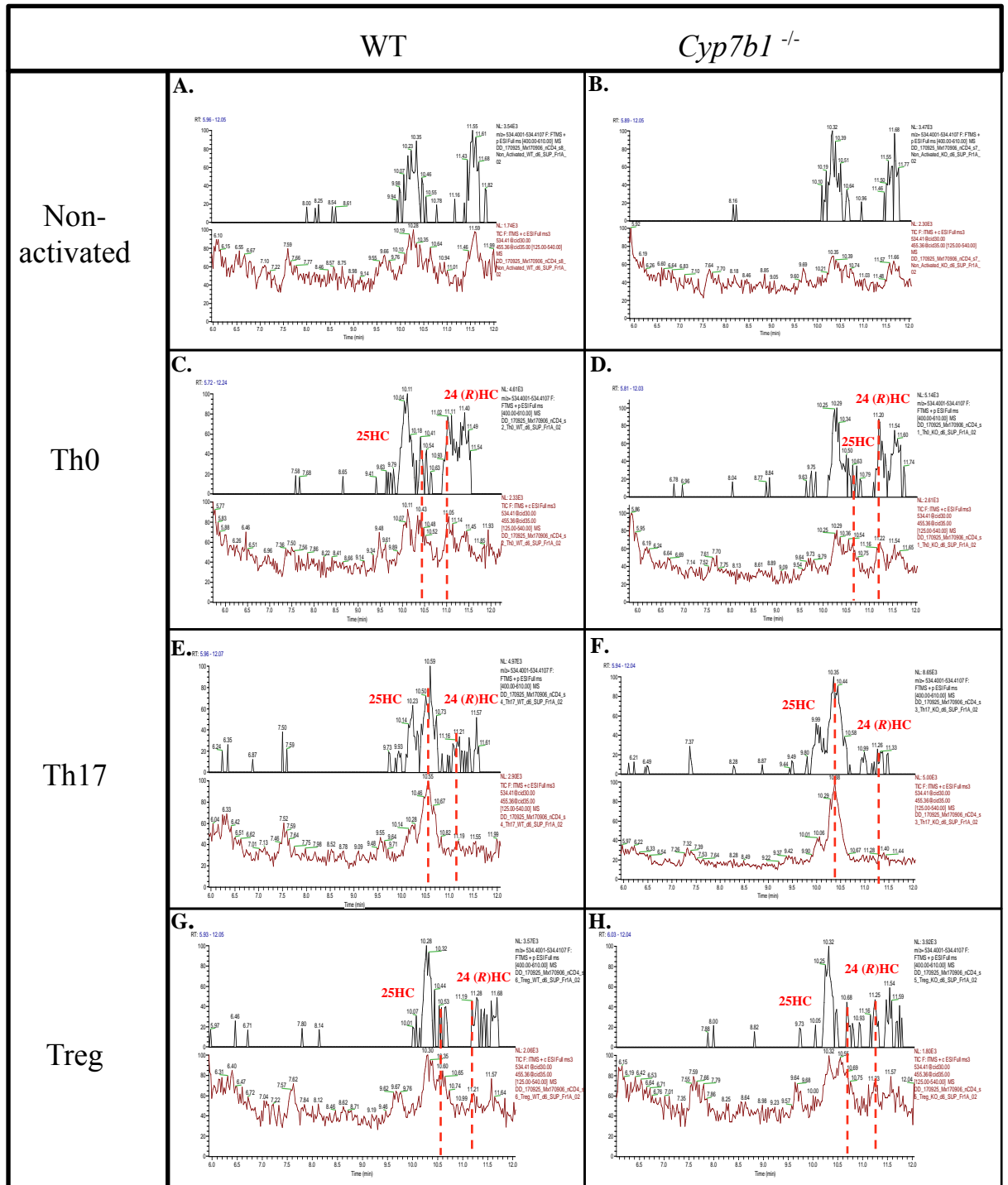


Figure 5.7 Reconstructed ion chromatogram (RIC) of monohydroxycholesterols at 534.4054 ± 10 ppm detected in Fraction 1A non-activated and activated polarised WT or *Cyp7b1* KO murine CD4⁺ T cell culture supernatants after 6 days. No detectable levels of enzymatically derived monohydroxycholesterols were identified in non-activated WT murine naïve CD4⁺ T cell supernatant (A) or *Cyp7b1* KO murine naïve CD4⁺ T cell supernatant (B). 25-HC and 24(R)-HC was detectable at ~10.5 mins and ~11.2 mins respectively in WT Th0, Th17 and Treg polarised conditions (C, E and G respectively). *Cyp7b1* KO Th0, Th17 and Treg also showed detectable levels of 25-HC and 24(R)-HC (D, F and H respectively).

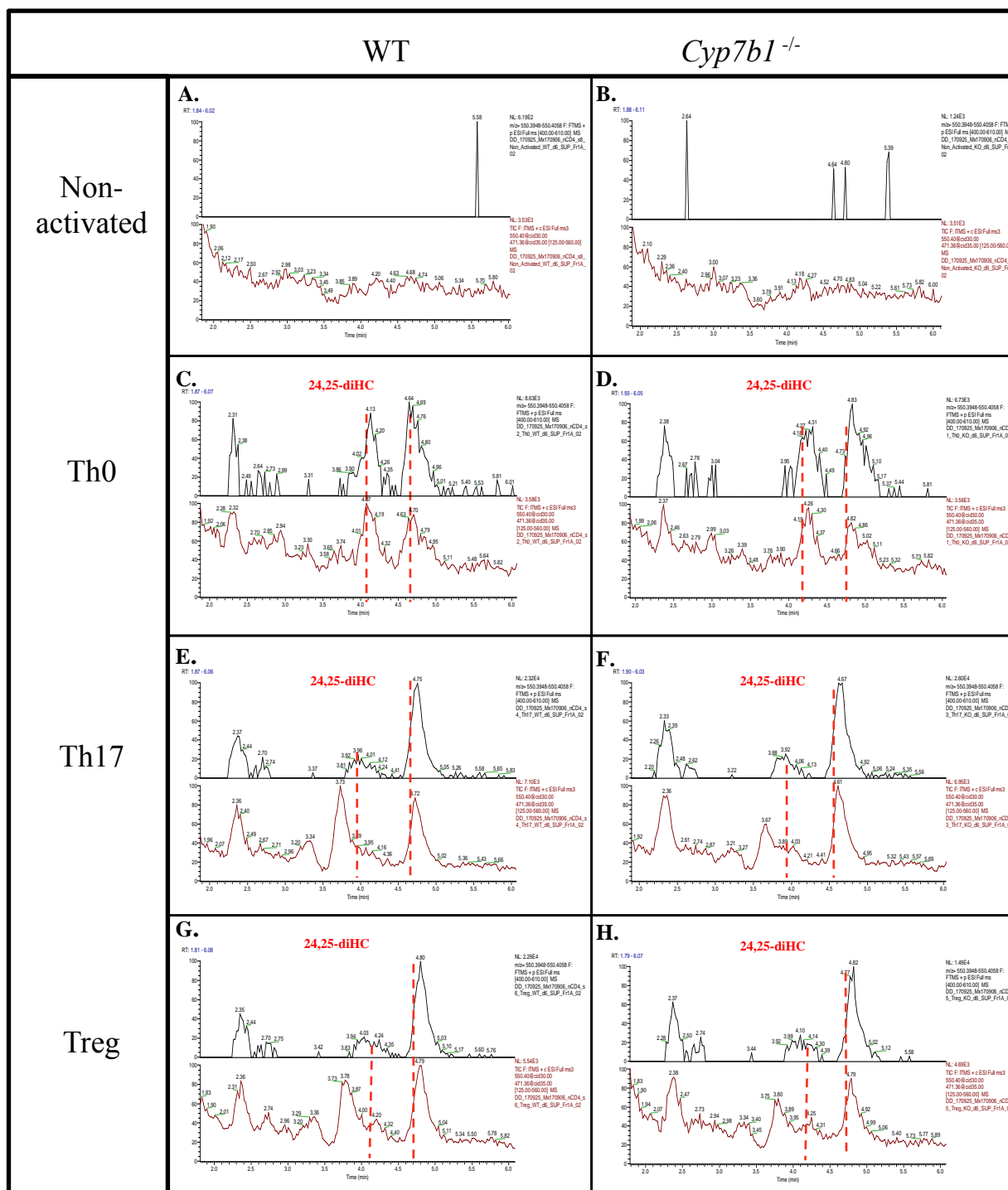


Figure 5.8 Reconstructed ion chromatogram (RIC) of dihydroxycholesterols at 550.4003 ± 10 ppm detected in Fraction 1A non-activated and activated polarised WT or *Cyp7b1* KO murine $CD4^+$ T cell culture supernatants after 6 days. No detectable levels of dihydroxycholesterols were identified in non-activated WT murine naïve $CD4^+$ T cell supernatant (A) or *Cyp7b1* KO murine naïve $CD4^+$ T cell supernatant (B). 24, 25-diHC was detectable at ~3.8 and ~4.1 mins in WT Th0, Th17 and Treg polarised conditions (C, E and G respectively). *Cyp7b1* KO Th0, Th17 and Treg also showed detectable levels of 24, 25-diHC (D, F and H respectively).

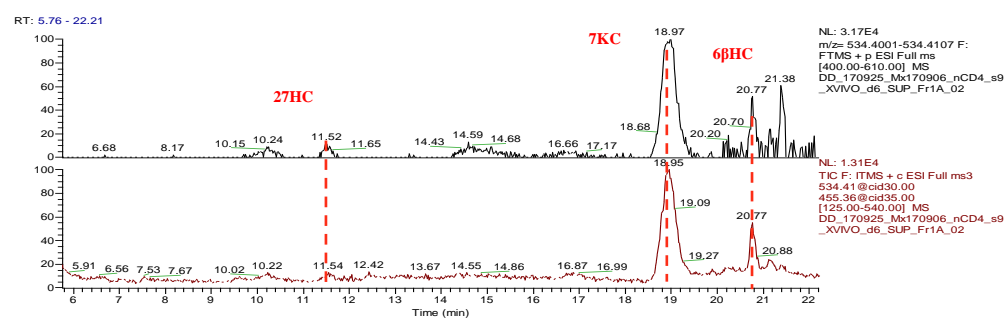


Figure 5.9 Reconstructed ion chromatogram (RIC) at 534.4054 ± 10 ppm of reference mock X-Vivo-20 media. A peak at 10.24 min was detected but the MS³ spectra showed this was not 24(S)-HC. The peak at 11.52 min was identified as 27-HC, naturally present in X-Vivo-20 media.

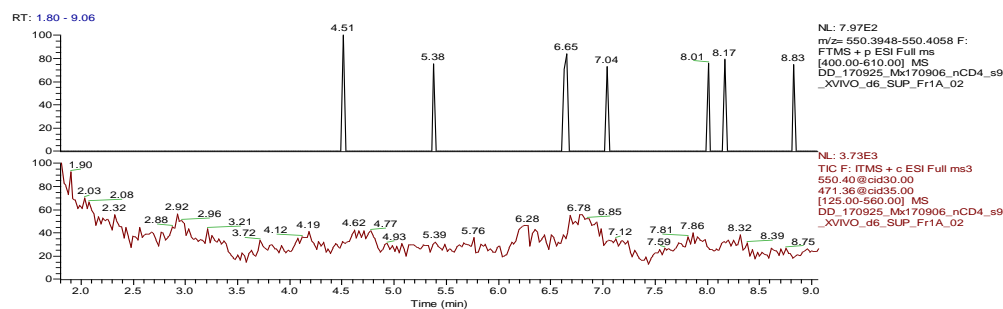


Figure 5.10 Reconstructed ion chromatogram (RIC) at 550.4003 ± 10 ppm of reference mock X-Vivo-20 media. No identifiable dihydroxycholesterol peaks were detected in the mock X-Vivo-20 fraction.

5.3.5 Stimulation of murine cell line EL4 induces *Il17a* mRNA expression

Initial EL4 experiments were performed with serum-free DMEM, serum-free X-Vivo-20 and 10% FBS DMEM to establish the optimum media for investigating ROR γ t activation and *Il17a* expression in EL4 cells. FBS is often used in cell culture as a source of growth factors and minerals however FBS naturally contains some oxysterols therefore a serum-free media is preferable to determine the endogenous levels from EL4 cells. EL4 cells were cultured in serum-free DMEM, X-Vivo-20 or 10% FBS DMEM and stimulated with PMA and ionomycin alongside non-activated control samples. Similar morphology was observed in for activated and non-activated cells in both media (Figure 5.13). *Il17a* mRNA expression was determined by qRT-PCR which confirmed *Il17a* expression in EL4. *Il17a* mRNA expression was upregulated in EL4 cells seeded in serum free X-Vivo-20 and 10% FBS DMEM media upon stimulation with PMA and ionomycin, however cells seeded in serum-free DMEM did not show upregulation when stimulated in comparison with the non-activated control sample and was actually significantly reduced in activated conditions (Figure 5.11). Further experiments were therefore performed with X-Vivo-20 media or 10% FBS DMEM when indicated.

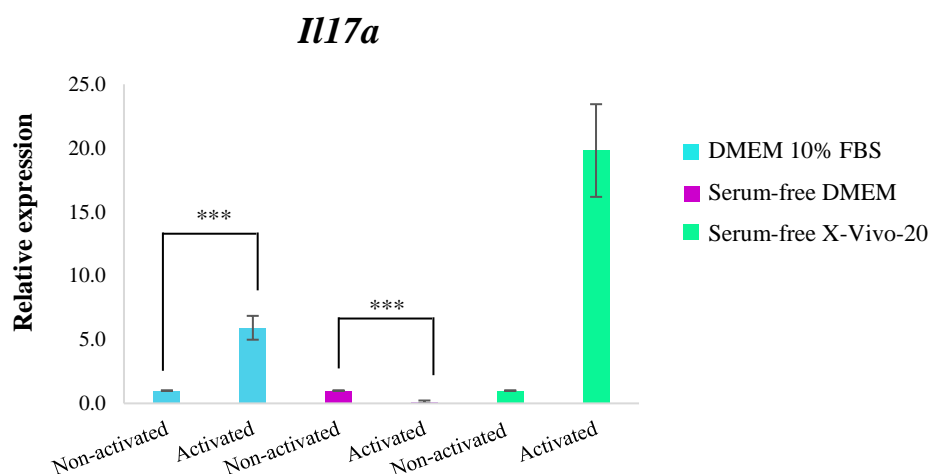


Figure 5.11 qRT-PCR analysis of *Il17a* mRNA expression of murine cell line EL4 cells stimulated in DMEM 10% FBS (blue), serum-free DMEM (purple) or serum-free X-Vivo-20 (green). DMEM 10% FBS $p = 0.000921$, Serum-free DMEM $p = 0.00079$, X-Vivo-20 $p = 0.010295$. *Il17a* mRNA expression was normalised to *Rp18s* expression and fold change relative to the non-activated control sample seeded in the corresponding media. Error bars indicate S.D. of replicates, $n = 3$

5.3.6 Stimulation of murine cell line EL4 induces *Ifng* and *Il4* mRNA expression

EL4 cells cultured in 10% FBS DMEM or serum-free X-Vivo-20 media and stimulated with PMA and ionomycin (Figure 5.12) showed induced expression of cytokines *Ifng* and *Il4* mRNA. A significant increase in *Il4* expression was seen in activated cells with DMEM 10% FBS and X-Vivo-20 media however upregulation of *Ifng* showed a wide variation between replicates and was only significant in DMEM 10% FBS media (Figure 5.12A). qRT-PCR analysis of *Il10* mRNA expression showed a significant increase in expression between non-activated control samples and activated samples with DMEM 10% media but no significant difference was seen with X-Vivo-20 media Figure 5.12B).

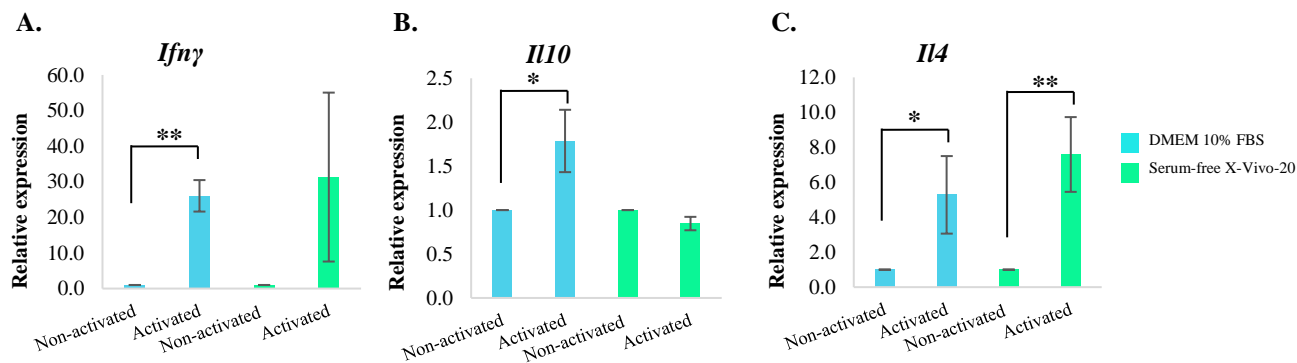


Figure 5.12 qRT-PCR analysis of cytokine mRNA expression of murine EL4 cells stimulated in DMEM 10% FBS (blue) and serum-free X-Vivo-20 (green). (A) *Ifng* mRNA was upregulated in Activated samples DMEM 10%FBS $p = 0.000298$, X-Vivo-20 $p = 0.146963$ (B) no considerable change in *Il10* mRNA expression was seen with activation, DMEM 10%FBS $p = 0.030937$, X-Vivo-20 $p = 0.340157$. (C) *Il4* mRNA was upregulated in Activated samples DMEM 10%FBS $p = 0.021797$, X-Vivo-20 $p = 0.005726$. mRNA expression was normalised to *Rp18s* and *ACTB* expression and fold change relative to the non-activated control sample seeded in the corresponding media. Error bars indicate S.D. of replicates, $n = 3$.

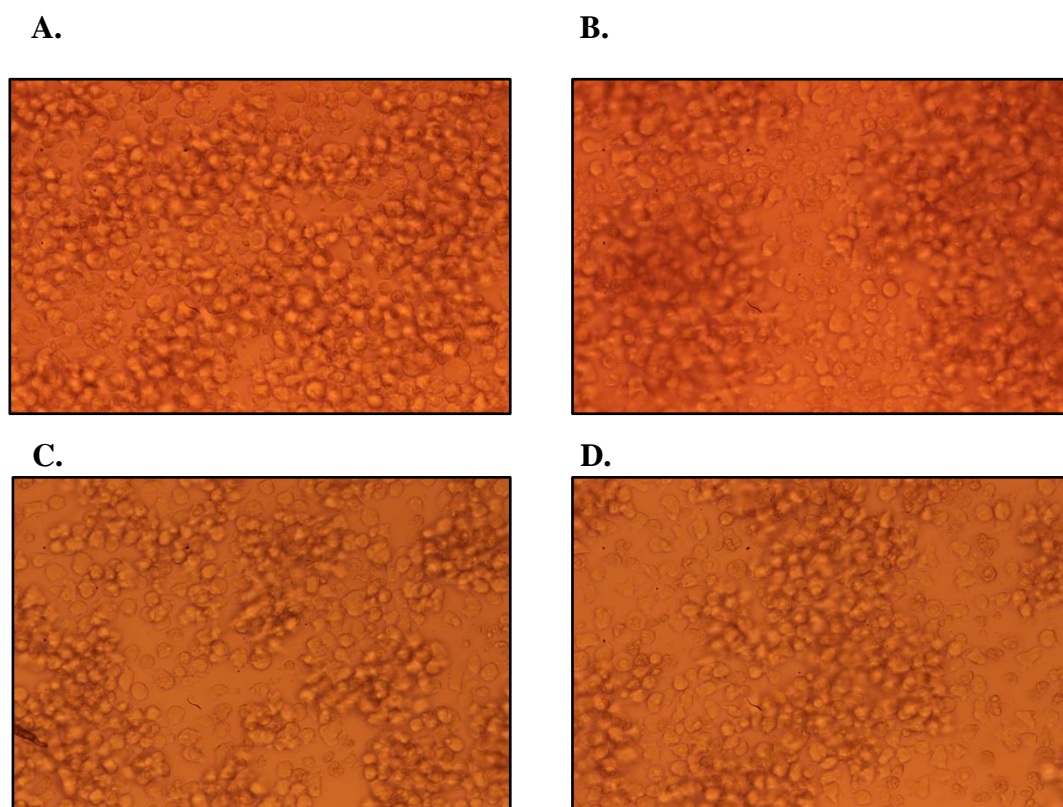


Figure 5.13 EL4 cells (A) Non-activated EL4 cells seeded in DMEM 10% FBS. (B) Activated EL4 cells seeded in DMEM 10% FBS 5hrs post stimulation. (C) Non-activated EL4 cells seeded in serum-free X-Vivo-20. (D) Activated EL4 cells seeded in serum-free X-Vivo-20 5hrs post stimulation. X20 magnifications.

5.3.7 EL4 cell experiments with oxysterols and known inhibitor treatments

To determine the effects of oxysterols 24(S),25-EC and 25-HC on the expression of *Il17* mRNA in EL4 cells an inhibitory control was sought. EL4 cells were shown to express *Il17* at low levels without activation, if a suitable inhibitor could be identified it would be possible to investigate whether oxysterols of interest could rescue *Il17* expression. Ursolic acid has previously been reported to inhibit *Il17* expression in Th17 cells at 2 μ M and was therefore included as an inhibitory control in an EL4 experiment with 1 μ M 24(S),25-EC and 1 μ M 25-HC treatments⁽¹³⁾. qRT-PCR analysis of mRNA extracted from cell pellets confirmed *Il17* expression is upregulated in EL4 cells upon stimulation (Figure 5.14A and Figure 5.14B). Both cells with overnight treatment or cells with 6 hour incubation showed further

upregulation of *Il17* with 25-HC treatments and 24(*S*),25-EC treatments. Contrary to published work, Set 1 cells treated with 2 μ M ursolic acid and incubated overnight prior to stimulation showed no inhibition of *Il17* expression. Set 2 cells treated with 2 μ M ursolic acid for 6 hours showed upregulation of *Il17* expression relative to the non-activated control sample however expression was lower than the activated control sample and oxysterol treated cells.

Set 1 24(*S*),25-EC overnight treatment of EL4 cells led to almost twofold reduction of *Lxr β* mRNA expression in stimulated cells while 25-HC overnight treatment showed *Lxr β* mRNA expression was downregulated tenfold from control samples (Figure 5.14C). Set 2 EL4 cells with 6 hour treatments showed no considerable difference of mRNA expression between the activated sample and treated cells (Figure 5.14D). *Abcg1* mRNA expression was also downregulated with 24(*S*),25-EC and greater downregulation was seen with 25-HC for set 1 samples (Figure 5.14E). As seen with *Lxr β* no considerable difference of *Abcg1* mRNA expression was seen with set 2 samples (Figure 5.14F).

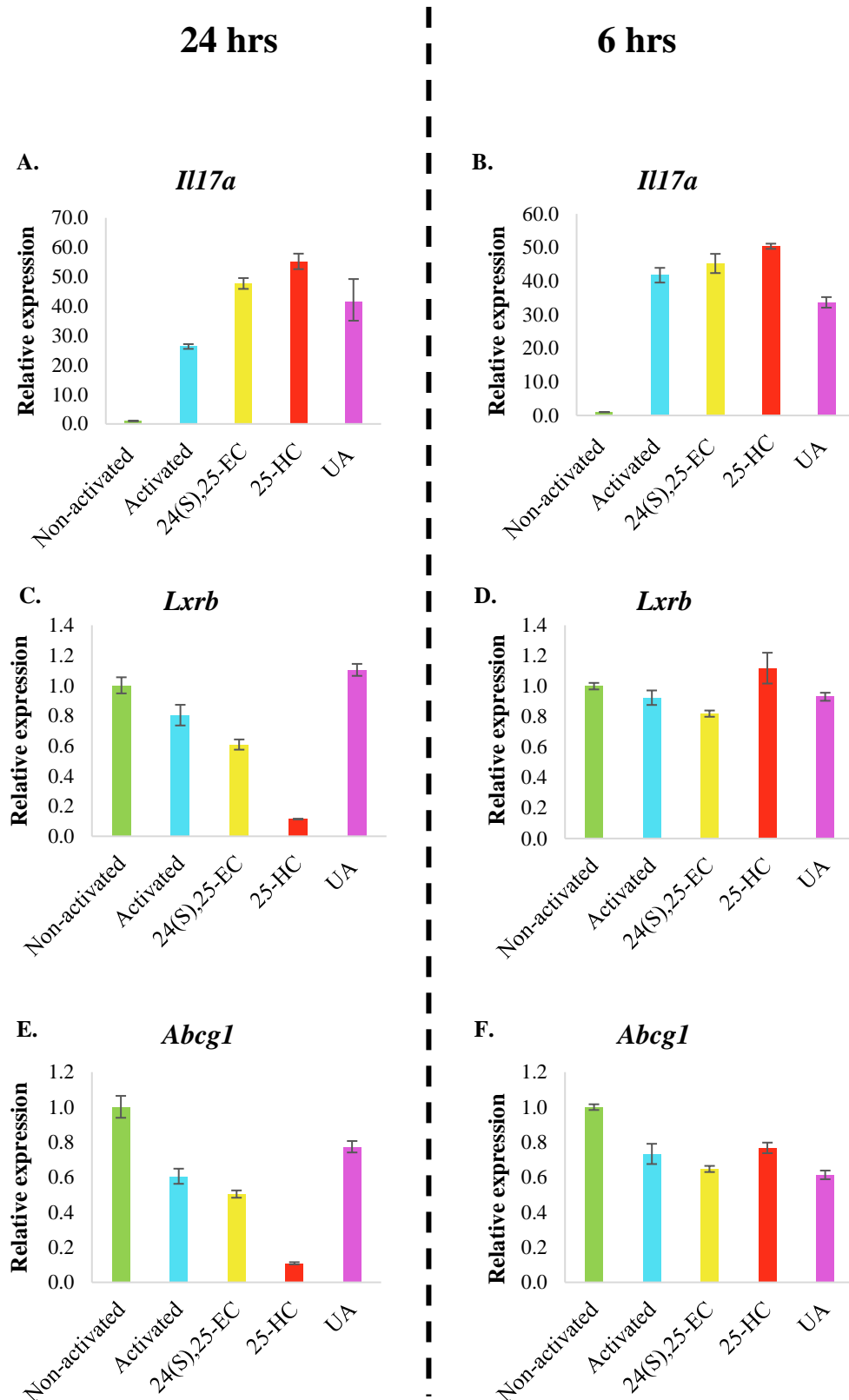


Figure 5.14 qRT-PCR analysis of murine activated EL4 cells cultured in X-Vivo-20 with 24(S),25-EC and 25-HC or ursolic acid (UA) treatments for 24 or 6 hrs. (A) *Il17* mRNA expression of cells after 24 hr treatment. (B) *Il17* mRNA expression of cells after 6 hr treatment. (C) *Lxrb* mRNA expression of cells after 24 hr treatment. (D) *Lxrb* mRNA expression of cells after 6 hr treatment. (E) *Abcg1* mRNA expression of cells after 24 hr treatment. (F) *Abcg1* mRNA expression of cells after 6 hr treatment. mRNA expression was normalised to *Rp18s* expression and fold change relative to the non-activated control sample. Error bars indicate S.D. of technical replicates, n =1

To further investigate the inhibition of *Il17*, additional EL4 experiments were performed with 5 μ M ursolic acid and an alternative reported inhibitor T0901317 at 1 μ M or 10 μ M^(14, 15). T0901317 is a known LXR β agonist however no change in *Abcg1* mRNA expression was observed in stimulated EL4 (Figure 5.15B). No inhibition of *Il17* mRNA expression was seen with 1 μ M T0901317 or 5 μ M ursolic acid treatments after 24 hrs (Figure 5.15A). These experimental conditions were repeated with EL4 seeded in DMEM 10% FBS with qRT-PCR analysis of *Il17* mRNA. Inhibition of *Il17* expression was not seen with 5 μ M ursolic acid or T0901317 at 1 μ M or 10 μ M with DMEM 10% FBS media (Figure 5.16).

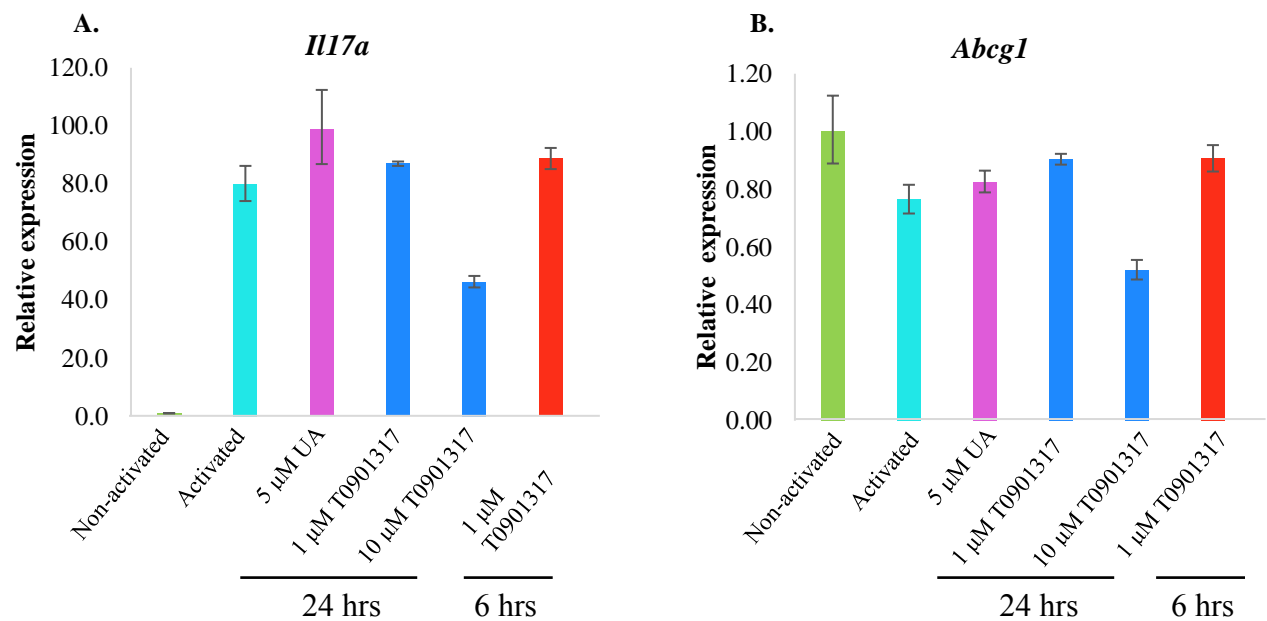


Figure 5.15 qRT-PCR analysis of murine EL4 cells with ursolic acid (UA) or T0901317 treatments for 24 or 6 hrs in X-Vivo-20 media. (A) *Il17* mRNA expression of EL4 cells after treatment. (B) *Abcg1* mRNA expression of EL4 cells after treatment. mRNA expression was normalised to *Rp18s* and *Actb* expression and fold change relative to the non-activated control. Error bars indicate S.D. of technical replicates, n = 1

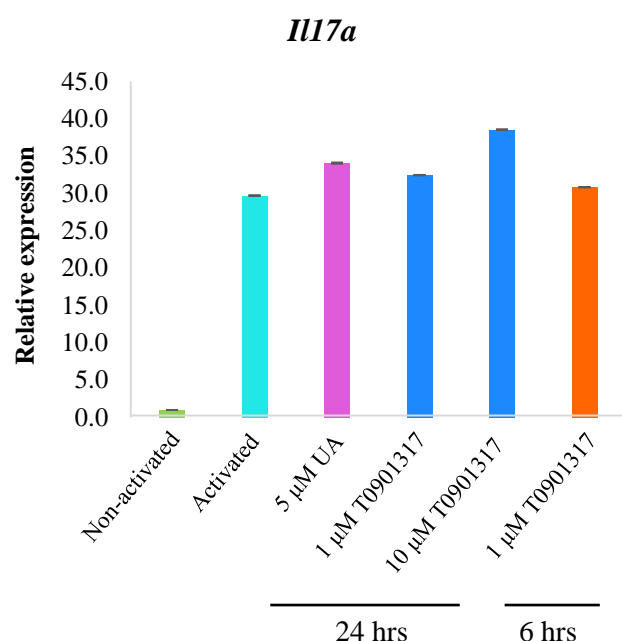


Figure 5.16 qRT-PCR analysis of murine EL4 cells with ursolic acid (UA) or T0901317 treatments for 24 or 6 hrs in DMEM 10% FBS media. *Il17a* mRNA expression of EL4 cells after treatment. mRNA expression was normalised to *Rp18s* and *Actb* expression and fold change relative to the non-activated control. Error bars indicate S.D. of technical replicates, n =1

Flow cytometry analysis of EL4 cells following 5 μ M ursolic acid and 1 μ M T0901317 treatments in X-Vivo-20 media showed no effect on CD25 activation and 7AAD cell viability staining relative to the activated control sample with 76.3 to 81.9% CD25⁺ cells and 17.6 to 23.2% 7AAD⁺ cells (Figure 5.17). However, treatment of EL4 cells with 10 μ M T0901317 resulted in a decreased activation of cells with only 45.6% CD25⁺ cells and reduced cell viability with 73.2% 7AAD⁺ staining showing T0901317 has a detrimental effect on EL4 cells at 10 μ M in X-Vivo-20 media. 6 hr treatment of EL4 cells with 1 μ M T0901317 showed no difference in CD25⁺ and 7AAD staining in comparison to the activated control sample. EL4 cells with 5 μ M ursolic acid and 1 μ M T0901317 treatments in DMEM 10% FBS media also showed no effect on CD25 activation and 7AAD cell viability staining relative to the activated control sample with 81.5 to 86.2% CD25⁺

cells and 21.7 to 23.2% 7AAD⁺ cells (Figure 5.18). In contrast to EL4 treatment of 10 μ M T0901317 in X-Vivo-20 media, 10 μ M T0901317 treatments in DMEM 10% FBS media showed minimal effect on the activation and cell viability with 79.6% CD25⁺ and 18.9% 7AAD⁺ cells. As seen in X-Vivo-20 media 6 hr treatment of EL4 cells with 1 μ M T0901317 showed little effect on CD25⁺ and 7AAD staining.

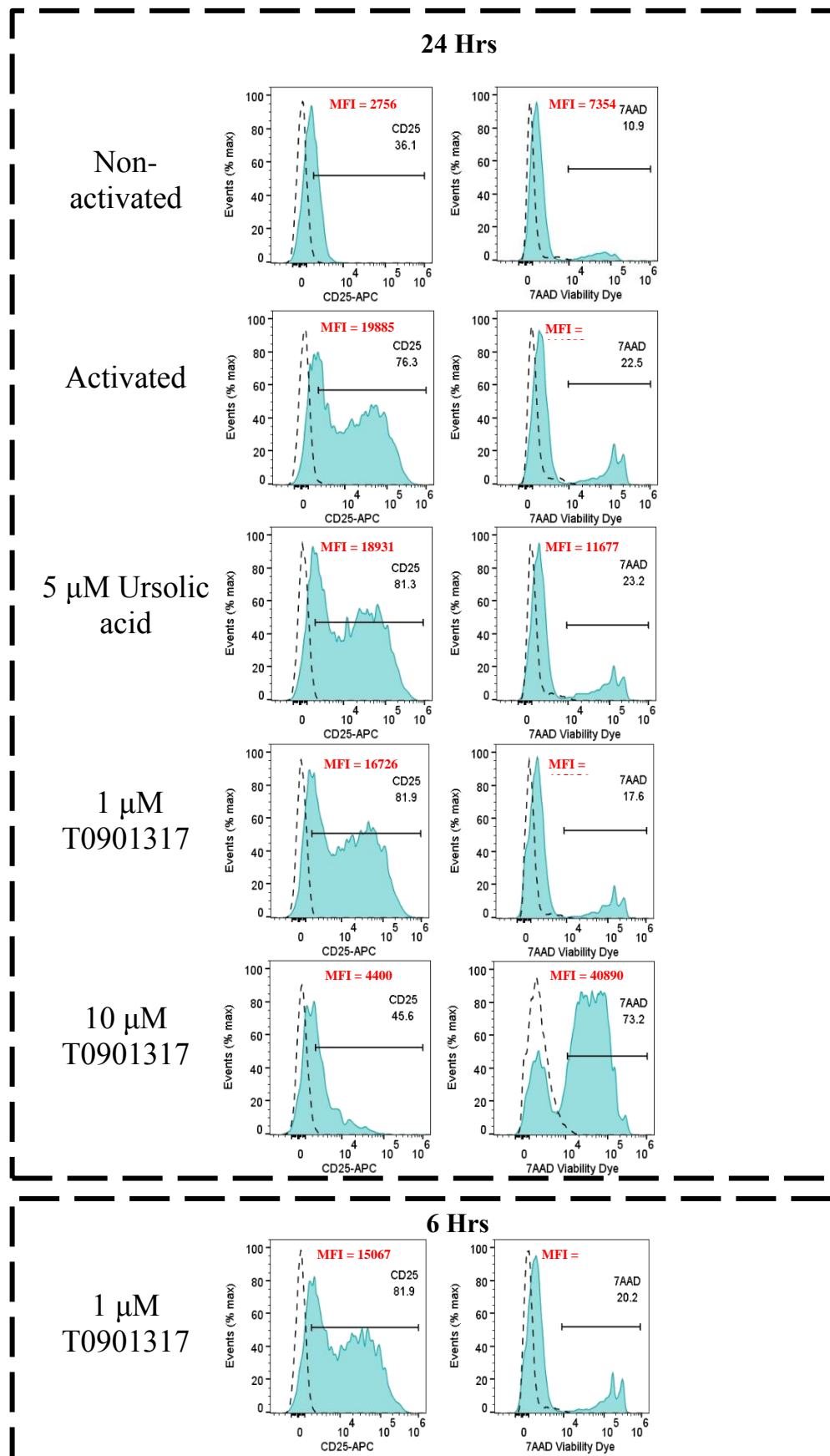


Figure 5.17 Flow cytometry analysis of CD25 expression and 7AAD viability dye staining of stimulated EL4 cells after 24hr or 6 hr treatments with T0901317 or ursolic acid in X-Vivo-20 media. Filled blue histograms represent the fluorochrome conjugated antibody stained cells. Gates were determined using background fluorescence of unstained samples (1%) indicated by the dashed histogram. Median fluorescence intensities (MFI) are indicated in red.

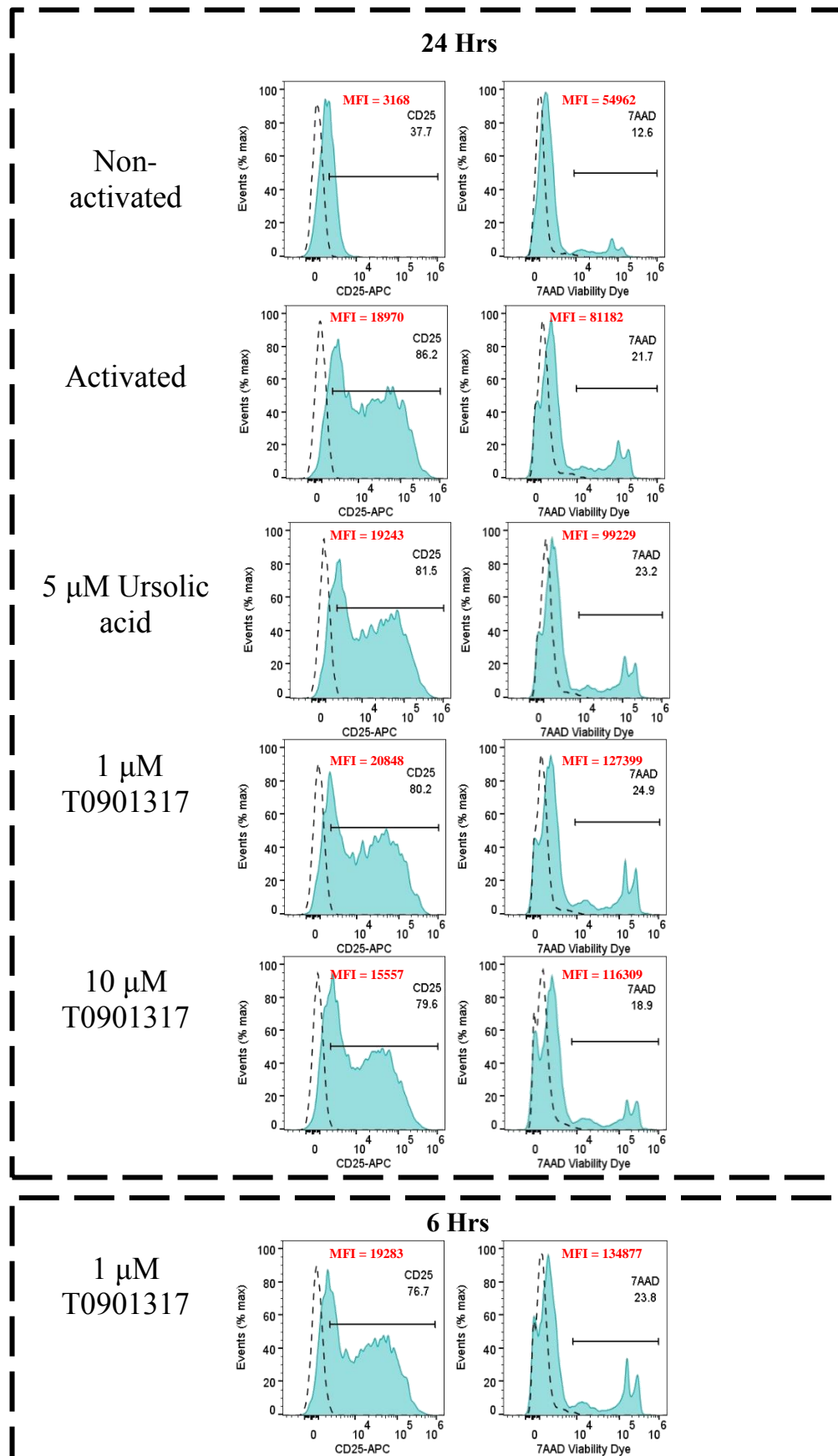


Figure 5.18 Flow cytometry analysis of CD25 expression and 7AAD viability dye staining of stimulated EL4 cells after 24hr or 6 hr treatments with T0901317 or ursolic acid in DMEM 10% FBS. Filled blue histograms represent the fluorochrome conjugated antibody stained cells. Gates were determined using background fluorescence of unstained samples (1%) indicated by the dashed histogram. Median fluorescence intensities (MFI) are indicated in red.

Finally, the effect of clotrimazole treatment on the expression of *Il17* was investigated in stimulated EL4 cells. An initial experiment with 3 μ M clotrimazole in DMEM 10% FBS and X-Vivo-20 media showed no effect on *Il17a* mRNA expression compared with the activated control samples (Figure 5.19). Clotrimazole is a non-specific CYP enzyme inhibitor which reduces *Il17* expression. In order to determine whether IL-17 inhibition could be achieved with higher clotrimazole concentrations further experiments were performed with clotrimazole treatments ranging from 1 to 30 μ M in DMEM 10% FBS media. qRT-PCR analysis of *Il17a* mRNA expression revealed clotrimazole had no inhibitory effect on *Il17* expression at 1 to 10 μ M (Figure 5.20). *Il17a* mRNA expression was to some extent downregulated with 30 μ M clotrimazole treatment however flow cytometry analysis revealed increase 7AAD incorporation in harvested cells at 30 μ M suggesting a detrimental effect on cells at this concentration (Figure 5.21 and Figure 5.22).

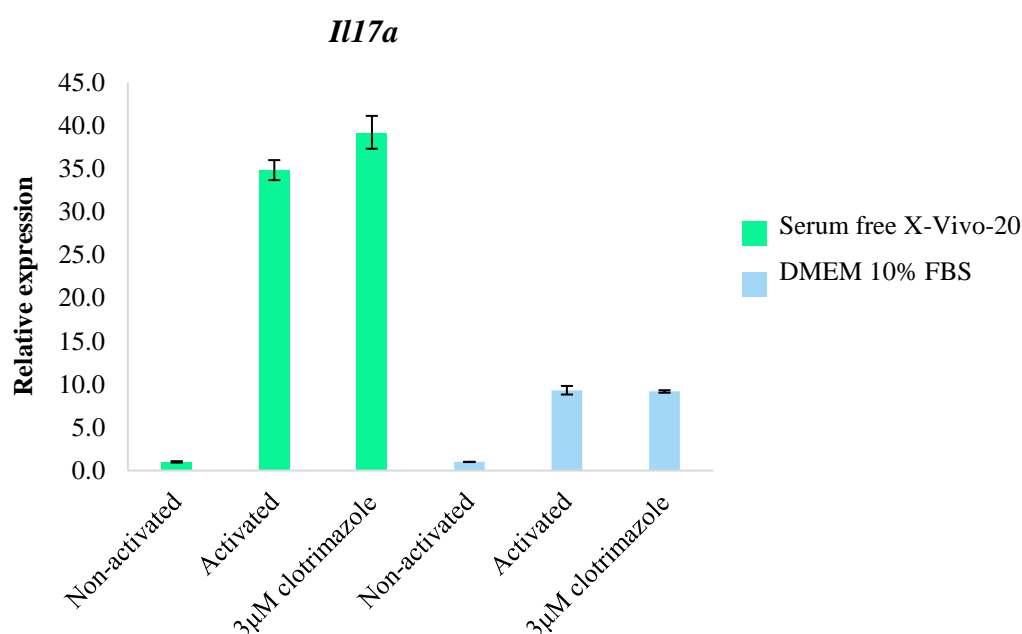


Figure 5.19 qRT-PCR analysis of *Il17a* mRNA expression in stimulated EL4 cells with 3 μ M clotrimazole treatment after 6 hrs in DMEM 10% FBS or serum-free X-Vivo-20 media. mRNA expression was normalised to *Rp18s* and *Actb* expression and fold change relative to the relevant non-activated control sample. Error bars indicate S.D. of technical replicates, n =1

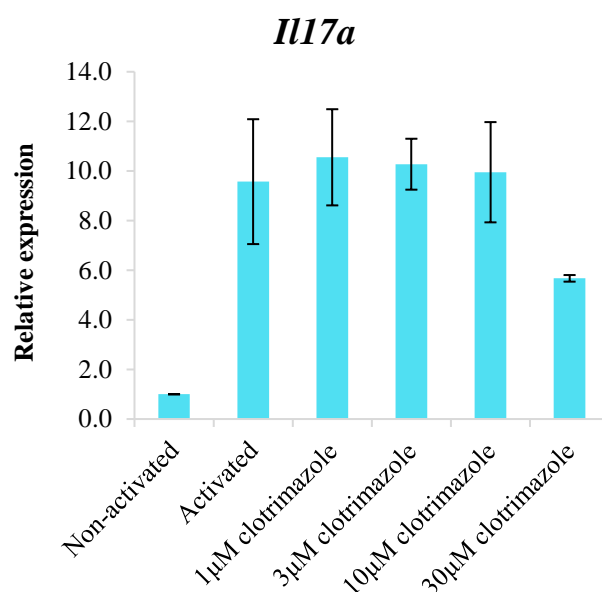


Figure 5.20 qRT-PCR analysis of *Il17a* mRNA expression in stimulated EL4 cells with 1 to 30 μ M clotrimazole treatment after 6 hrs in DMEM 10% FBS media. mRNA expression was normalised to *Rp18s* and *Actb* expression and fold change relative to the non-activated control. Error bars indicate S.D, n = 2

Flow cytometry analysis of CD25 activation and cell viability analysis with 7AAD staining of the initial experiment with 3 μ M clotrimazole showed no considerable difference between the activated control sample and 3 μ M clotrimazole treatments in both X-Vivo-20 and DMEM 10% FBS media (Figure 5.21). The non-activated samples showed a higher proportion of CD25⁺ cells than previous experiments however qRT-PCR analysis showed upregulation of *Il17* mRNA expression with ionomycin and PMA stimulation of activated samples when compared to the non-activated samples (Figure 5.19). Flow cytometry analysis of further clotrimazole experiments revealed no considerable difference in CD25 activation and 7AAD incorporation with 1 to 10 μ M clotrimazole (Figure 5.23 and Figure 5.24). Treatment with 30 μ M clotrimazole did result in a slight reduction in CD25⁺ cells and increased 7AAD incorporation which suggests clotrimazole has a damaging effect on EL4 at 30 μ M, therefore inhibition of *Il27* expression at 30 μ M may be contributed to the toxicity at this concentration.

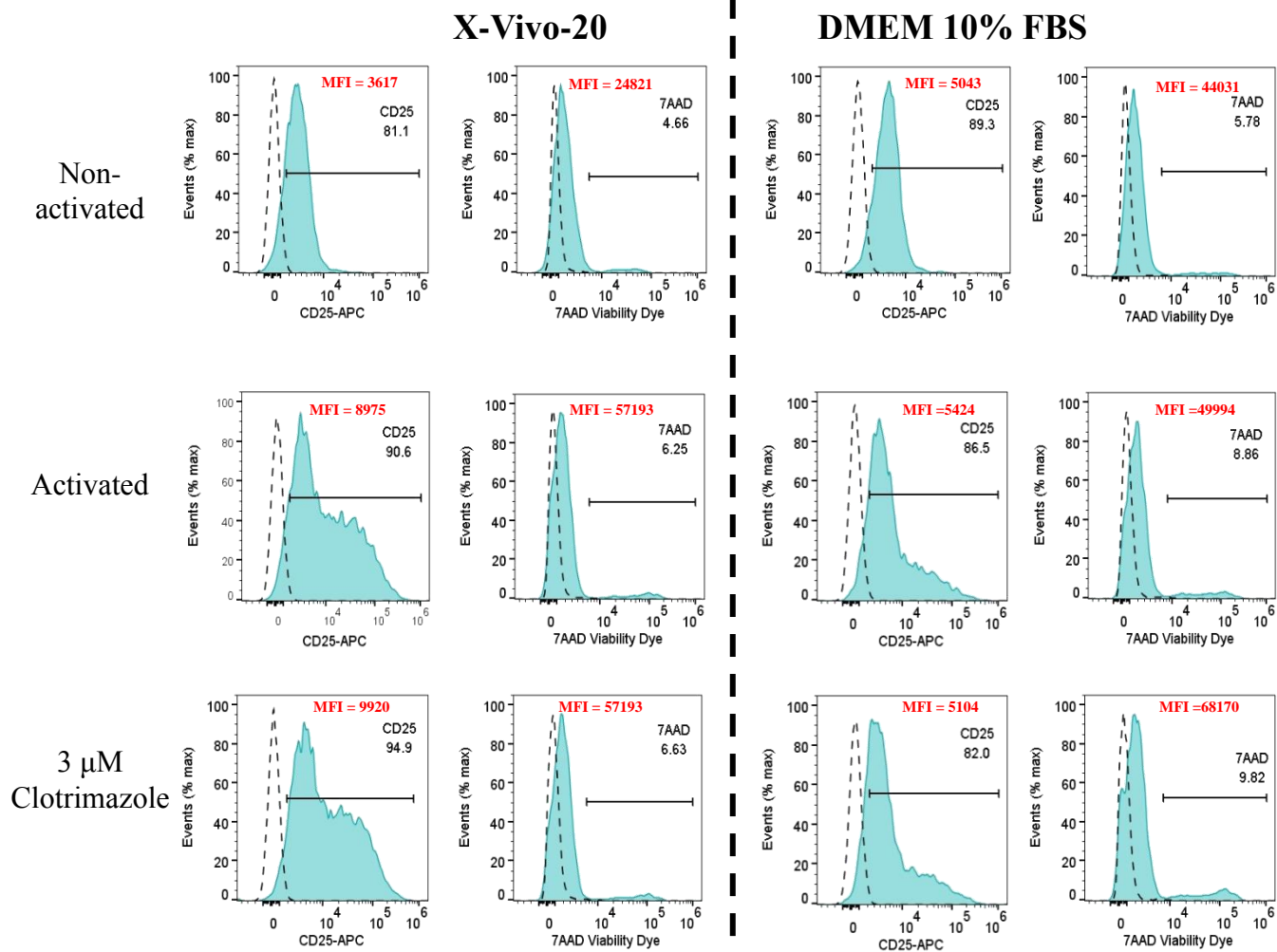
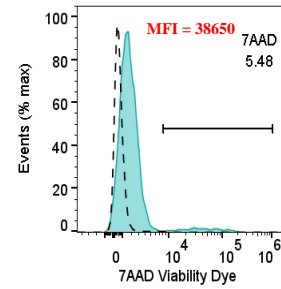
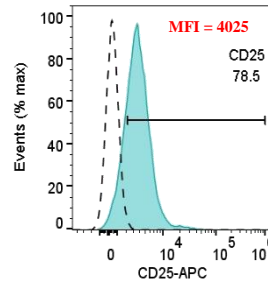
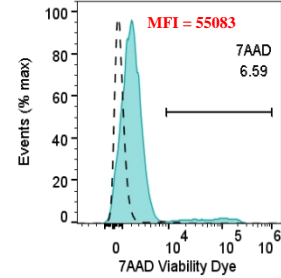
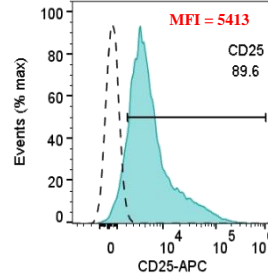


Figure 5.21 Flow cytometry analysis of CD25 expression and 7AAD viability dye staining of stimulated EL4 cells after 6 hr treatments with 3 μ M clotrimazole in DMEM 10% FBS. Filled blue histograms represent the fluorochrome conjugated antibody stained cells. Gates were determined using background fluorescence of unstained samples (1%) indicated by the dashed histogram. Median fluorescence intensities (MFI) are indicated in red.

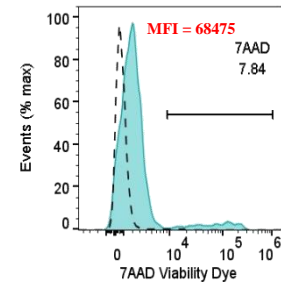
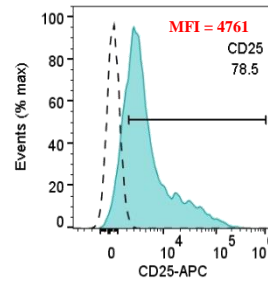
Non-activated



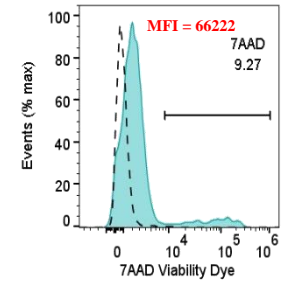
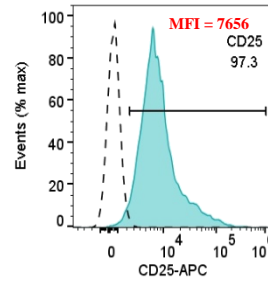
Activated



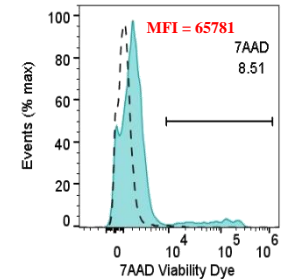
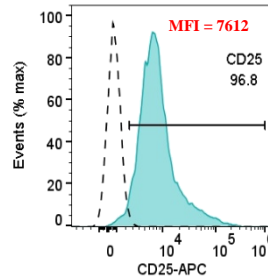
1 μ M
Clotrimazole



3 μ M
Clotrimazole



10 μ M
Clotrimazole



30 μ M
Clotrimazole

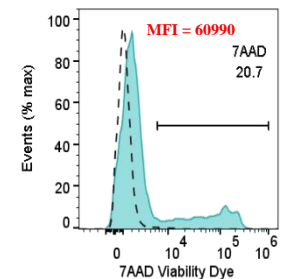
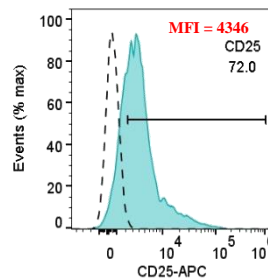


Figure 5.22 Flow cytometry analysis of CD25 expression and 7AAD viability dye staining of stimulated EL4 cells after 6 hrs clotrimazole treatments in DMEM 10% FBS, experiment 1. Filled blue histograms represent the fluorochrome conjugated antibody stained cells. Gates were determined using background fluorescence of unstained samples (1%) indicated by the dashed histogram. Median fluorescence intensities (MFI) are indicated in red.

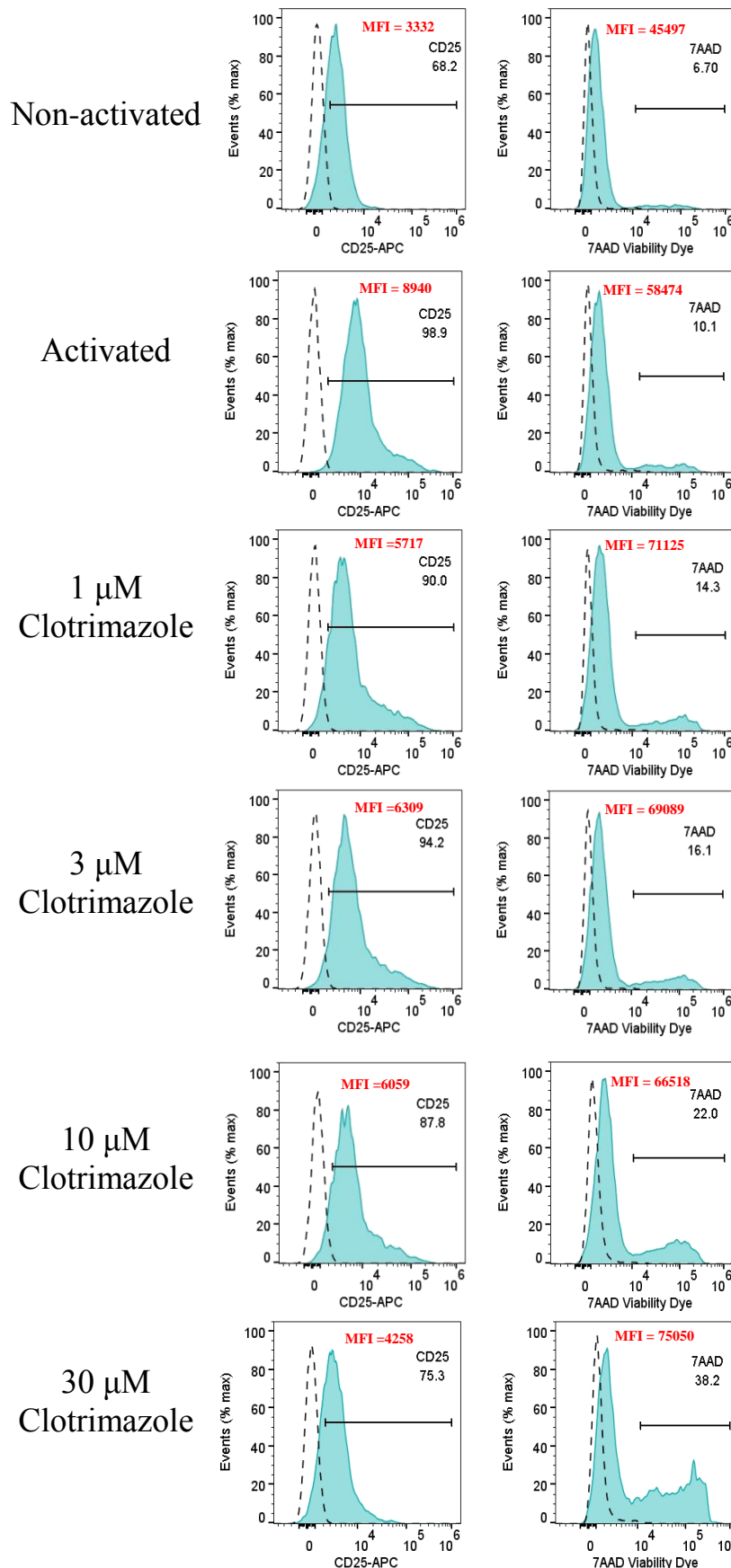


Figure 5.23 Flow cytometry analysis of CD25 expression and 7AAD viability dye staining of stimulated EL4 cells after 6 hrs clotrimazole treatments in DMEM 10% FBS, experiment 2. Filled blue histograms represent the fluorochrome conjugated antibody stained cells. Gates were determined using background fluorescence of unstained samples (1%) indicated by the dashed histogram. Median fluorescence intensities (MFI) are indicated in red.

5.3.8 Oxysterol profile of EL4 cells

Oxysterols were extracted from EL4 cell pellets and cell culture supernatants and processed by LC-MS to identify endogenous oxysterols present in EL4 cell pellets or excreted in cell culture supernatants under non-activated and activated conditions. Enzymatically derived monohydroxycholesterols 22(*R*)-HC, 25-HC and 24(*R*)-HC were detected at 534.4054 *m/z* in both non-activated and activated EL4 cell pellets and supernatant samples (Figure 5.24, Figure 5.25), these monohydroxycholesterols were not detected in mock X-Vivo-20 media (Figure 5.26).

Monohydroxycholesterol 24(*S*)-HC was also detected in both non-activated and activated cell pellets but no detectable levels were seen in cell culture supernatants for either non-activated or activated conditions. Fraction 1B analysis confirms these enzymatically derived monohydroxycholesterols were 3 β hydroxy forms as opposed to the 3-oxo forms.

24(*S*),25-EC, hydrolysed as 24,25-diHC was detected in non-activated and activated cell pellet and cell culture supernatants at 550.4003 *m/z* (Figure 5.27 and Figure 5.28 respectively) however downstream metabolite 7 α ,24,25-EC was not detected in either non-activated or activated cell pellets or cell culture media. During Girard's reagent P derivatisation geometric isomers of oxysterols including 24(*S*)-HC, 24(*R*)-HC and 24,25-diHC form resulting in slightly different retention times and two peaks are seen in chromatograms (Figure 5.24 and Figure 5.27).

Similar oxysterol levels were quantified in both cell pellets and cell culture media. The detected level of oxysterols 25-HC and 24(*R*)-HC showed little change between non-activated and activated conditions. However, a significant difference in concentrations of 22(*R*)-HC, showing an increase of approximately twofold in activated conditions (Figure 5.29 and Figure 5.30). A significant increase in 24,25-diHC levels were also detected in activated cell pellets and 24(*S*)-HC was only found in cell pellet samples (Figure 5.29). Interestingly, the concentration of 24,25-diHC is low in comparison to the concentrations seen with human nCD4⁺ T cell experiments in the previous chapter.

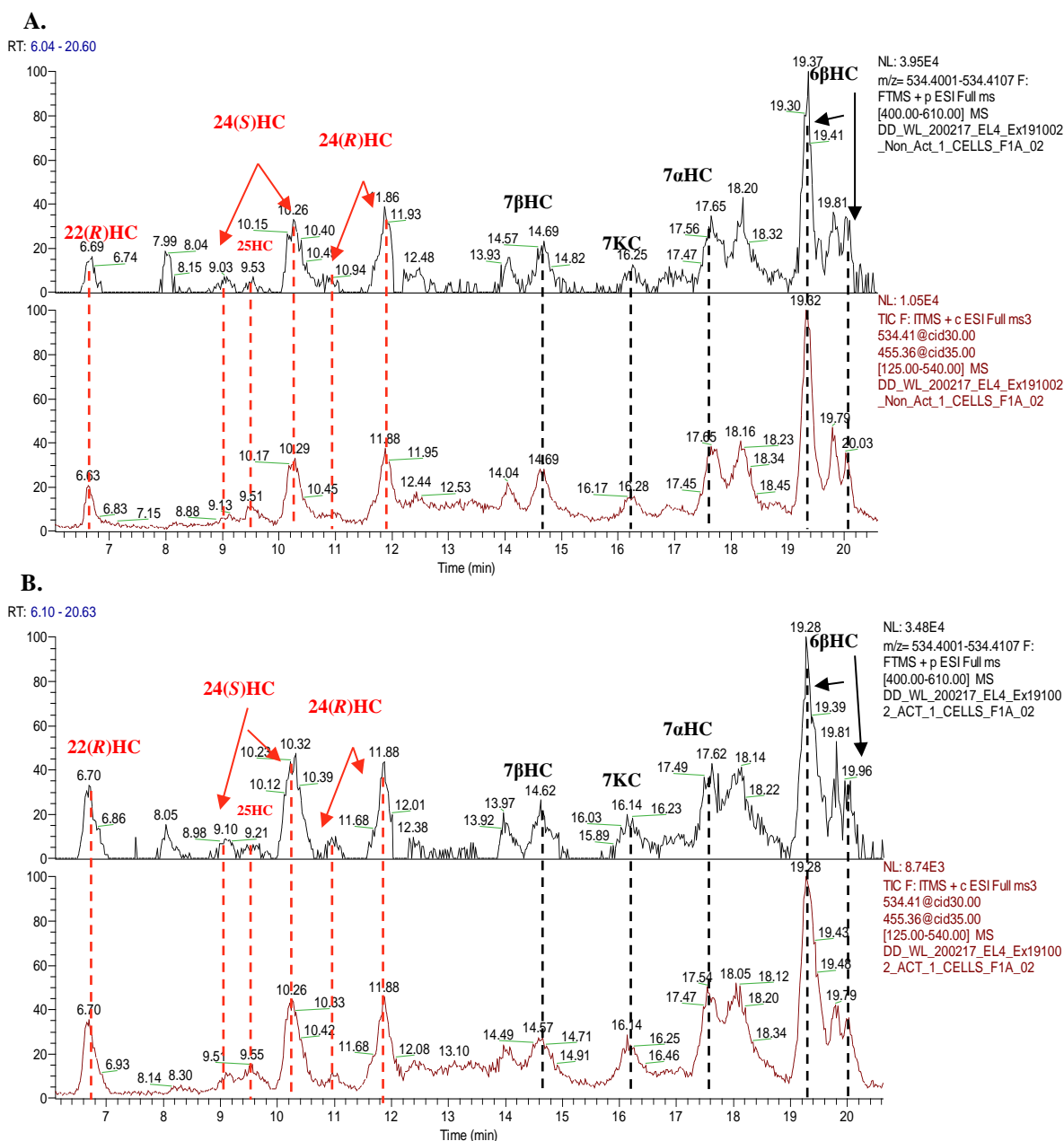


Figure 5.24 Reconstructed ion chromatogram (RIC) of monohydroxycholesterols at 534.4054 ± 10 ppm in Fraction 1A of (A) non-activated and (B) activated EL4 cell pellets following cell culture. Enzymatically derived monohydroxycholesterols 22(R)-HC, 24(S)-HC, 25-HC and 24(R)-HC peaks detected are indicated by the dashed red lines. The peak which elutes at ~6.7 min was identified as 22(R)-HC. Peaks eluting at ~9.1 min and ~10.3 min were identified as 24(S)-HC, ~9.5 min as 25-HC, ~10.3 min and ~11.9 min as 24(R)-HC based on exact mass and MS³ fragmentation spectra. Later eluting peaks identified were cholesterol autoxidation products 7β-HC, 7-KC, 7α-HC and 6β-HC indicated by the dashed black lines.

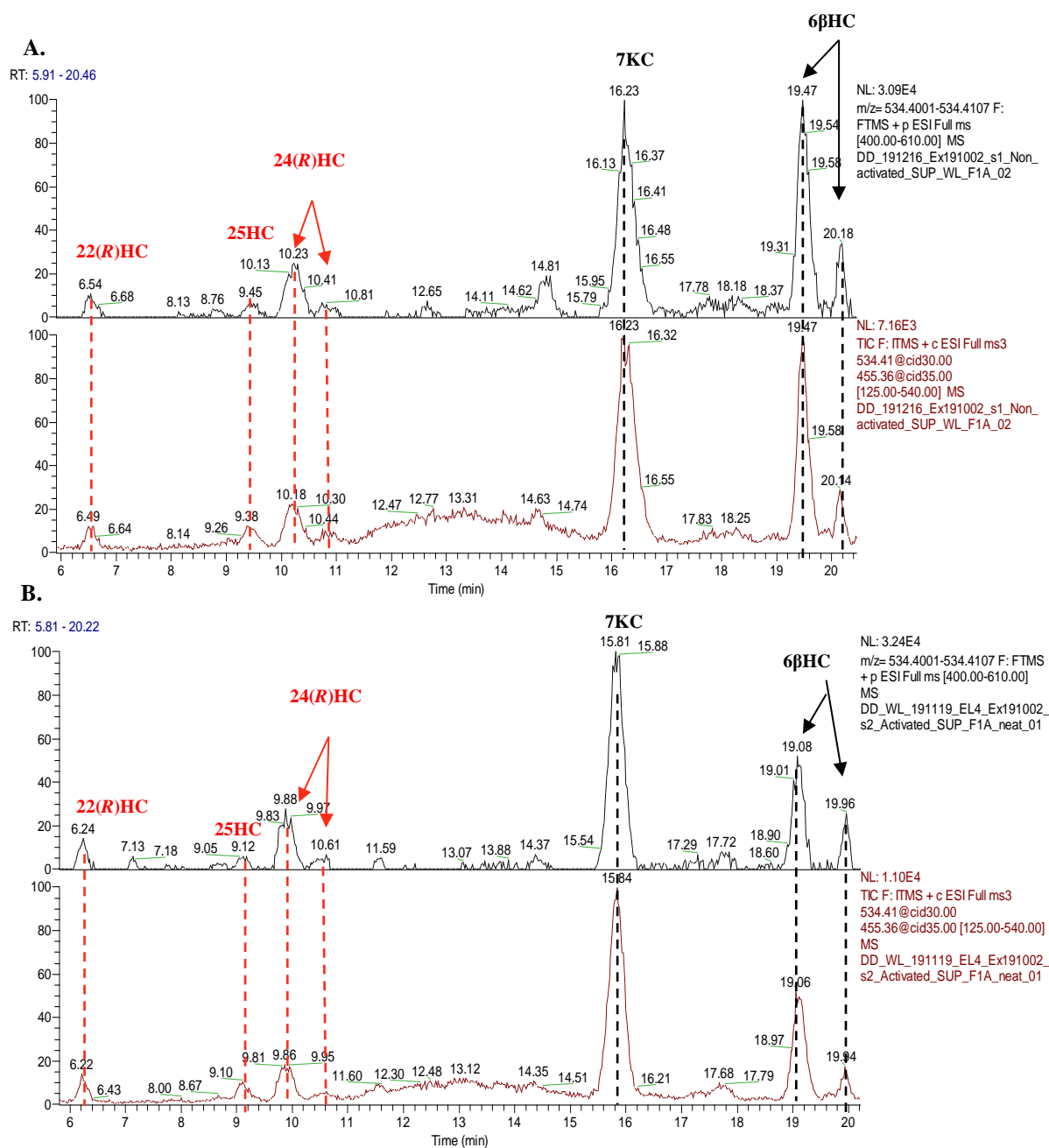


Figure 5.25 Reconstructed ion chromatogram (RIC) of monohydroxycholesterols at 534.4054 ± 10 ppm in Fraction 1A of (A) non-activated and (B) activated EL4 cell culture supernatant. Enzymatically derived monohydroxycholesterols 22(R)-HC, 25-HC and 24(R)-HC peaks detected are indicated by the dashed red lines. The peak which elutes at ~6.5 min was identified as 22(R)-HC. Peaks eluting at ~9.2 min were identified as 25-HC, ~10.0 min and ~10.6 min as 24(R)-HC based on exact mass and MS³ fragmentation spectra. Later eluting peaks identified were cholesterol autooxidation products 7-KC and 6β-HC indicated by the dashed black lines.

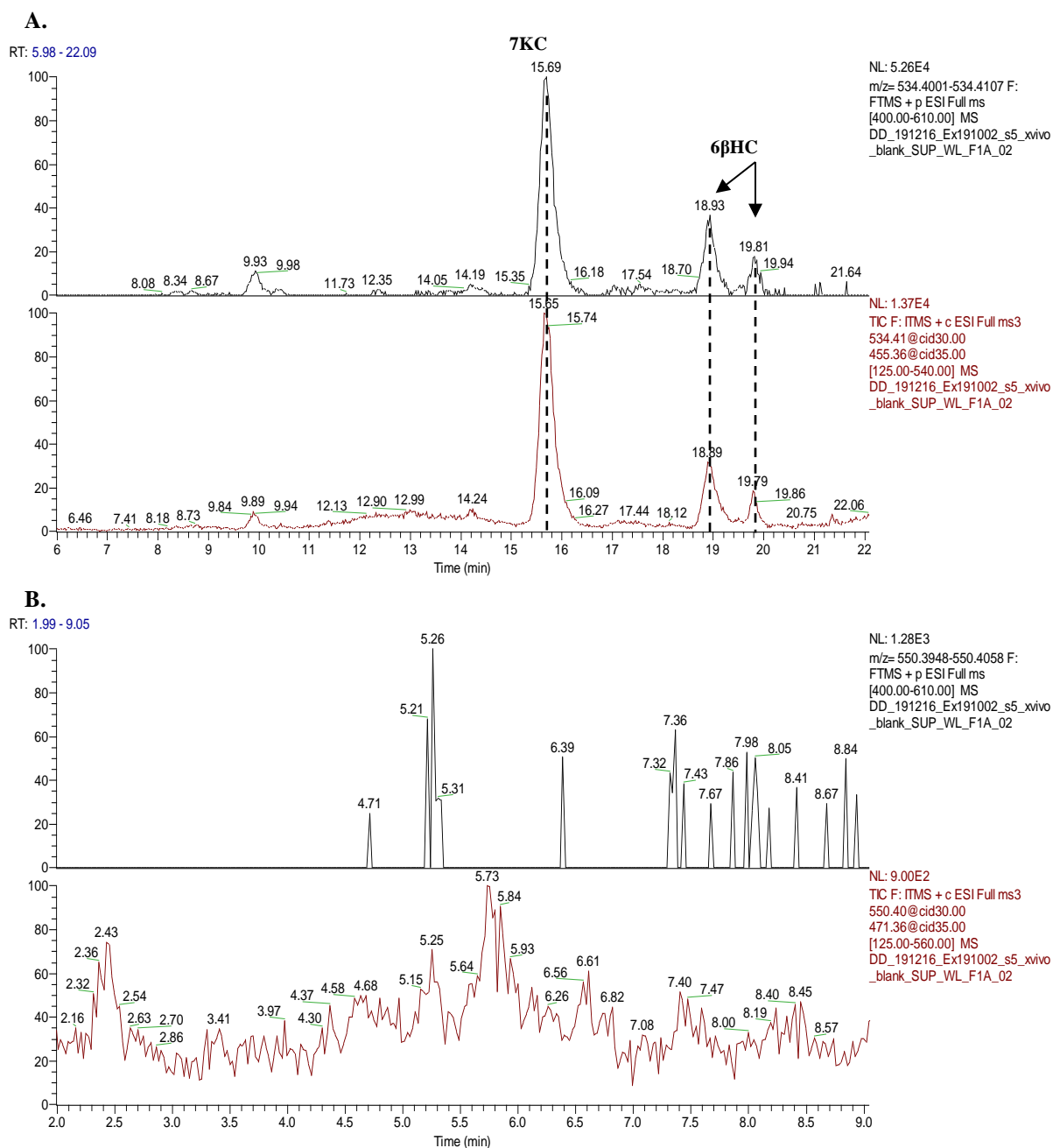


Figure 5.26 Reconstructed ion chromatogram (RIC) of hydroxycholesterols at 534.4054 ± 10 ppm and 550.4003 ± 10 ppm in Fraction 1A of X-Vivo-20 mock media. (A) Cholesterol autoxidation products 7-KC and 6 β -HC detected at 534.4054 ± 10 ppm indicated by the dashed black lines. (B) RIC at 550.4003 ± 10 ppm showed no detectable dihydroxycholesterols.

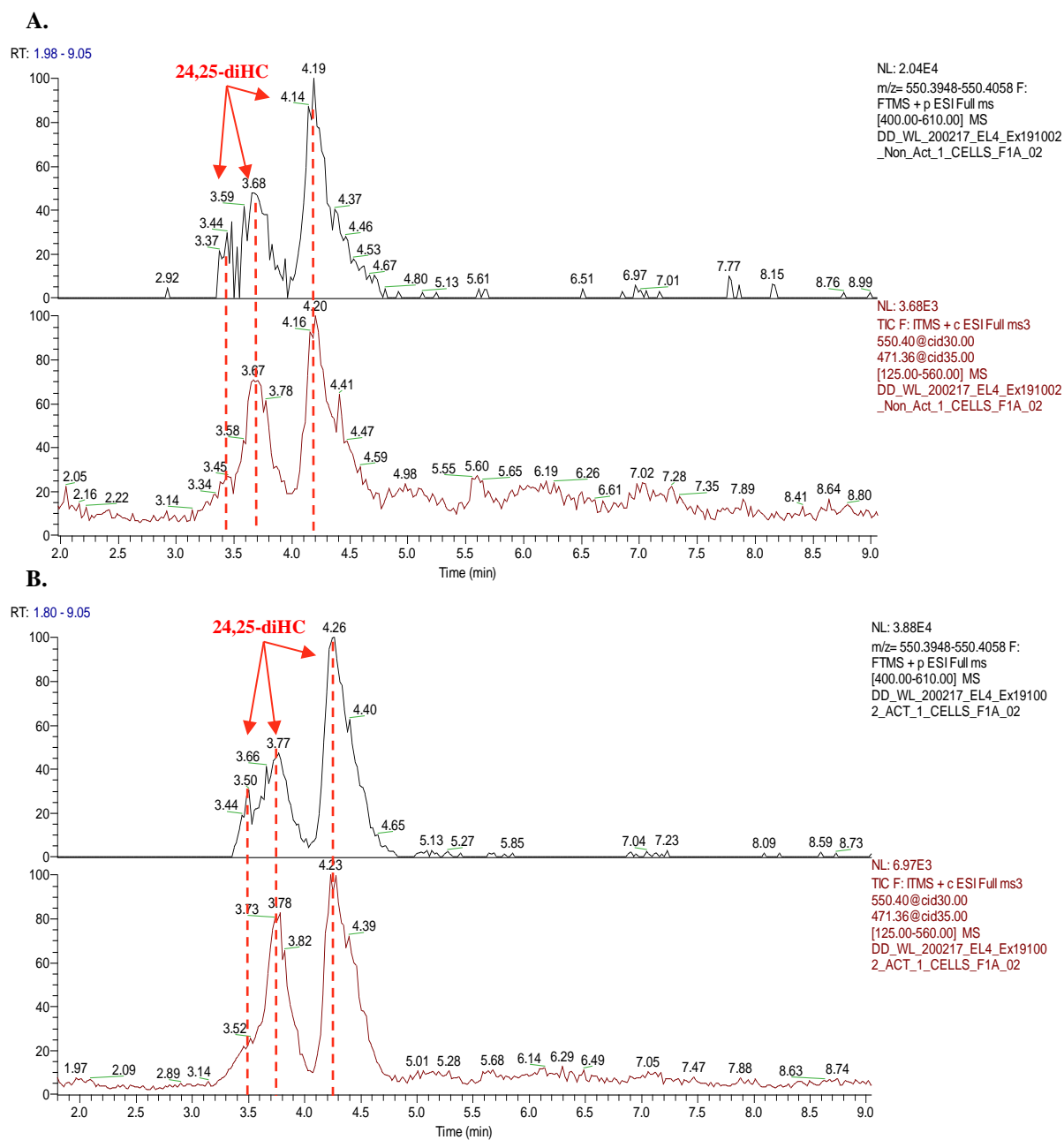


Figure 5.27 Reconstructed ion chromatogram (RIC) of dihydroxycholesterols at 550.4003 ± 10 ppm in Fraction 1A of (A) non-activated and (B) activated EL4 cell pellets following cell culture. The peaks which elutes at ~3.5 min, ~3.8 min and ~4.2 min were identified as 24,25-diHC based on exact mass and MS³ fragmentation spectra, indicated by the dashed red lines.

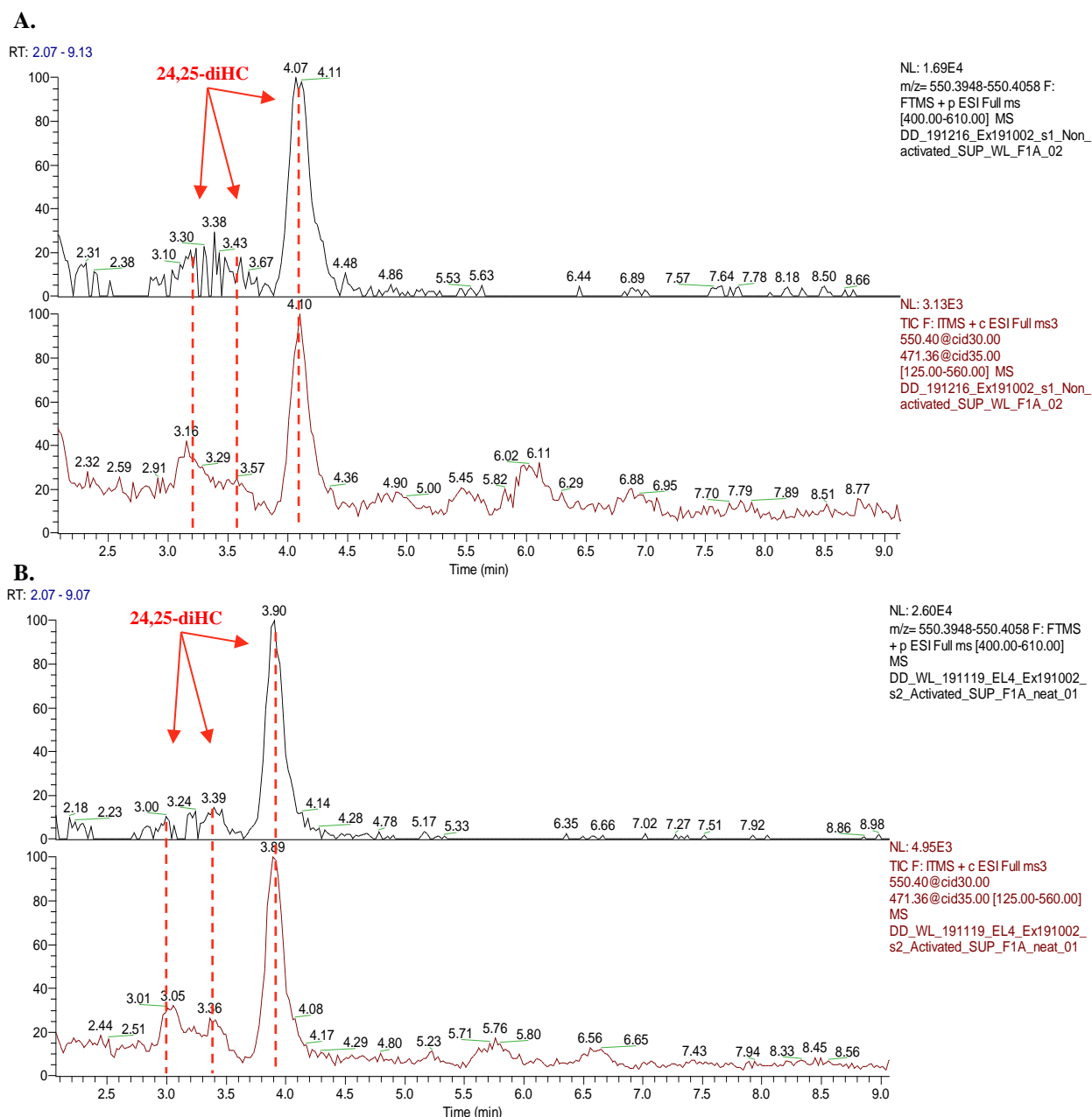


Figure 5.28 Reconstructed ion chromatogram (RIC) of dihydroxycholesterols at 550.4003 ± 10 ppm in Fraction 1A of (A) non-activated and (B) activated EL4 cell culture media. The peaks which elutes at ~3.0 min, ~3.4 min and ~3.9 min were identified as 24,25-diHC based on exact mass and MS³ fragmentation spectra, indicated by the dashed red lines.

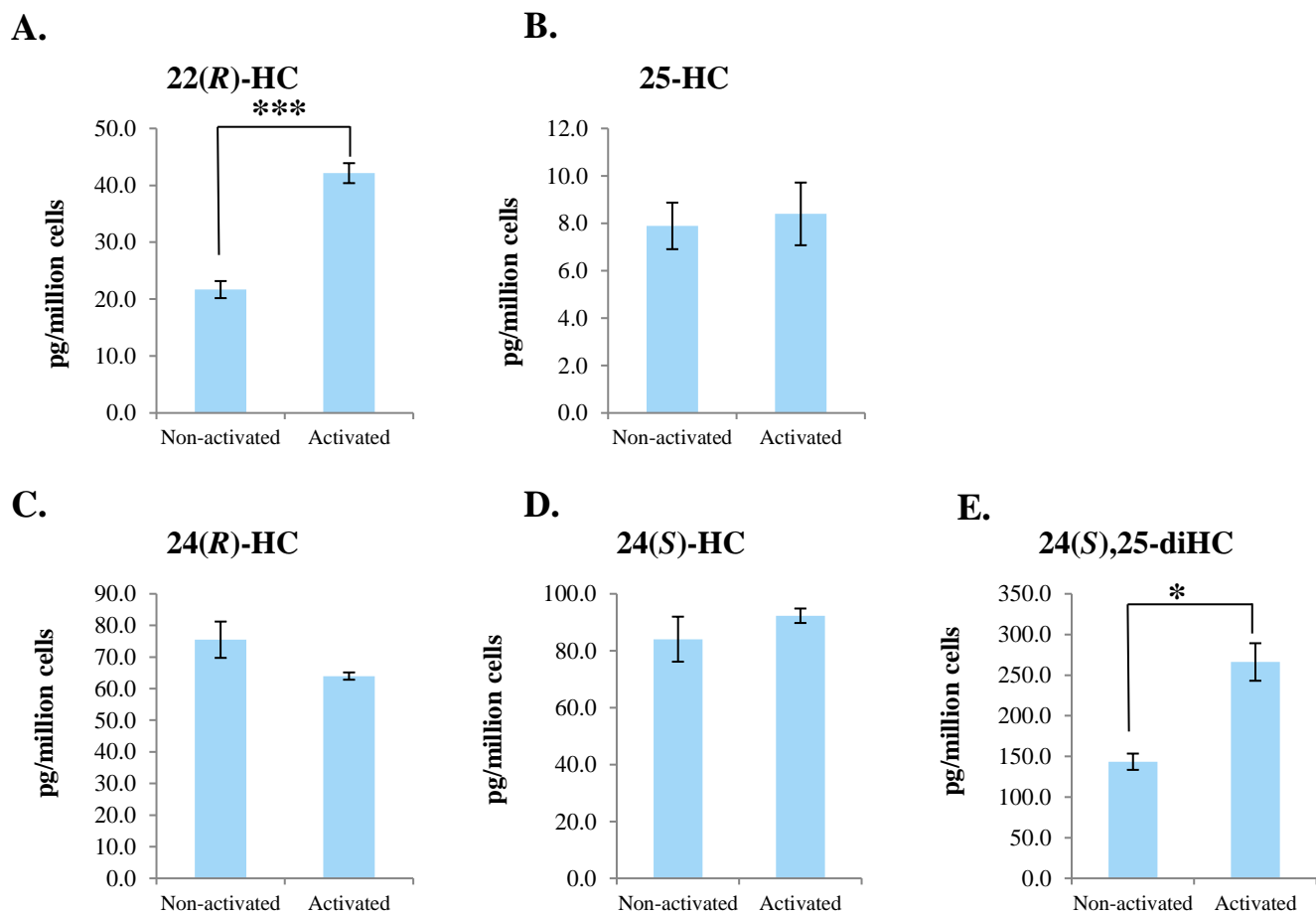


Figure 5.29 Oxysterols detected in cell pellets of non-activated and activated EL4 cells after cell culture. (A) 22(R)-HC $p=0.000635$ (B) 25-HC $p=0.739$ (C) 24(R)-HC $p=0.0507$ (D) 24(S)-HC $p=0.133$ (E) 24(S),25-diHC $p=0.0146$. Quantified values were normalised to the number of cells initially seeded. Error bars indicate SD of replicates, $n=3$.

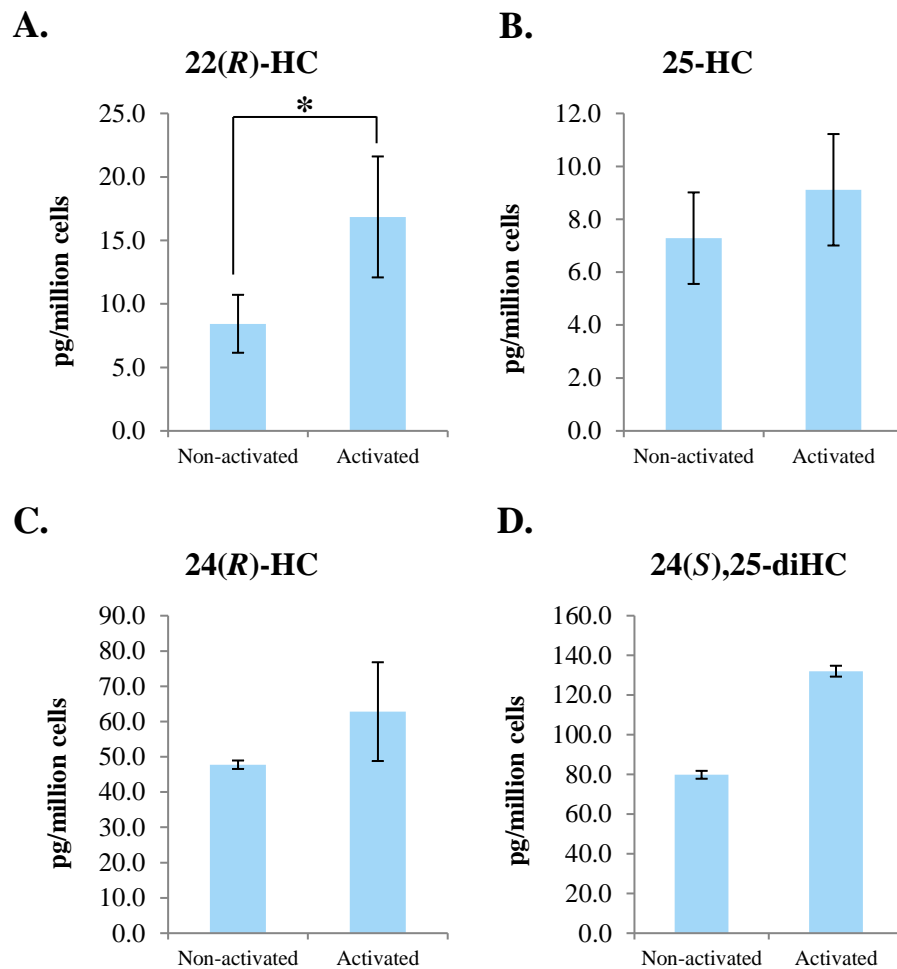


Figure 5.30 Oxysterols detected in cell culture media of non-activated and activated EL4 cells after cell culture. (A) 22(*R*)-HC $p = 0.04$ (B) 25-HC $p = 0.0729$ (C) 24(*R*)-HC $p = 0.182$ (D) 24(*S*),25-diHC $p = 0.116$. Quantified values were normalised to the number of cells initially seeded. Error bars indicate SD of replicates, $n=3$.

5.4 Discussion

The role of oxysterol 7 α -hydroxylase, CYP7B1, in Th17 production and IL-17 expression was investigated in this chapter with primary murine WT and *Cyp7b1* KO nCD4⁺ cells isolated from splenocytes and polarised under Th0, Th17 or Treg conditions. *Il17a* mRNA expression analysis by qRT-PCR confirmed successful Th17 polarisation of WT Th17 polarised cells, although lower activation was achieved with Th17 polarisation in comparison with non-polarised Th0 or Treg polarised cells. The KO Th17 polarised cells however showed a fourfold downregulation of *Il17* mRNA which suggest loss of CYP7B1 activity has an adverse effect on IL-17 production. Although downregulation of *Il17a* was seen in the KO Th17 polarised cells relative to the WT Th17 polarised cells there was no *Cyp7b1* mRNA detected in either WT or KO cells. The gender of littermates may also contribute to the expression levels of *Cyp7b1* seen as sexually dimorphic expression of CYP7B1 has been reported in murine tissue with higher expression seen in males⁽¹⁾.

Analysis of oxysterols extracted from cell culture media revealed the level of oxysterol 25-HC detected in *Cyp7b1* KO murine Th17 polarised cells was increased somewhat relative to the WT Th17 polarised cells, while no difference in 24(R)HC was seen. This concurs with published studies of *Cyp7b1* KO mice which showed increase 25-HC and 27-HC in murine cells⁽¹⁶⁾. Similarly to results seen with human naïve CD4⁺ T cell experiments in the previous chapters, 24(S),25-EC is produced in activated murine nCD4⁺ T cells under Th17 and Treg polarised conditions and excreted into cell culture media. Interesting, while 25-HC was shown to be higher in the *Cyp7b1* KO, the detectable levels of 24(S),25-diHC corresponding to 24(S),25-EC was lower in *Cyp7b1* KO. This correlates with the downregulation of *Il17* mRNA in Th17 subset of *Cyp7b1* KO cells and suggest CYP7B1 may be require for the expression of endogenous ligands of ROR γ t. The detectable levels of 24(S),25-diHC was however considerable lower than the levels seen in activated human nCD4⁺ cells under Th17 polarised conditions.

The potential of murine Thymoma cell line EL4 in the study of ROR γ t and IL-17 was also explored in this chapter. Both DMEM 10% FBS and Serum-free hematopoietic X-Vivo-20 were found to be suitable culture media for EL4 cells

however X-Vivo-20 was found to be an optimum media for determining the endogenous oxysterol concentrations in EL4 cells and cell culture media.

qRT-PCR analysis confirmed expression of *Il17* mRNA in EL4 cells and upregulation of *Il17* mRNA expression upon stimulation of EL4 cells with PMA and ionomycin. *Ifn γ* and *Il4* was also shown to be upregulated with PMA and ionomycin stimulation. Flow cytometry analysis showed rapid upregulation of CD25 within 6 hrs of stimulation.

An initial experiment with 24(S),25-EC and 25-HC oxysterol treatments showed increase *Il17* mRNA expression after 6 hrs while downregulation of *Lxr β* and *Abcg1* mRNA expression was seen after 24hrs. However, treatment of cells with ursolic acid showed no inhibition of *Il17* mRNA which has been previously reported ⁽¹³⁾. Further experiments performed with higher concentrations of ursolic acid also showed no inhibition of *Il17* mRNA expression. Addition of LXR β agonist and reported ROR γ t inverse agonist T0901317 showed no effect on *Il17* or *Abcg1* mRNA expression at 1 μ M after 24hrs ^(15,17). Downregulation of *Il17* and *Abcg1* mRNA was only achieved with T0901317 at 10 μ M, however flow cytometry analysis revealed reduced CD25 expression and increase 7AAD incorporation with 10 μ M T0901317 treatments suggesting cell viability is reduced with high concentrations of T0901317.

Azole compounds have also previously been reported to effect IL-17 production of Th17 cells, imibenconazole was reported to inhibit *Il17* mRNA expression in EL4 cells in a dose dependant manner however cytotoxic effects were noted with treatments at 30 μ M ⁽¹⁷⁾. In the previous chapter, it was revealed azole compound clotrimazole may reduce *IL17* expression in human primary nCD4⁺ under Th17 polarising conditions, although variation was seen between donors. Therefore, EL4 experiments were performed with 1 to 30 μ M clotrimazole treatments. No effect on *Il17* mRNA expression was seen with lower concentrations of clotrimazole. 30 μ M clotrimazole treatment did show reduced expression of *Il17* relative to the activated EL4 cells but expression was still greater than the non-activated control sample. CD25 expression was slightly reduced and higher 7AAD incorporation was seen with 30 μ M clotrimazole treatment which suggests cell viability is affected by high clotrimazole concentration as reported for imibenconazole.

Sterol analysis of non-activated and activated EL4 cell culture media revealed differences in oxysterols levels compared with primary human and murine nCD4⁺ T cells. Oxysterol 22(*R*)-HC was detected intracellularly from cell pellets and extracellularly in cell culture media which was not seen in either human or murine primary nCD4⁺ T cells. Interestingly, increased 22(*R*)-HC levels were detected upon stimulation of cells with PMA and ionomycin. The levels of 24,25-diHC were also higher in activated cells while 24(*R*)-HC, 24(*S*)-HC and 25-HC showed no considerable difference between non-activated and activated conditions. Similar levels of 24,25-diHC were detected in EL4 cell culture supernatant to those seen in primary mouse nCD4⁺ T cell culture supernatant which contrasts to the reasonably higher levels seen in primary human nCD4⁺ T cell culture polarised supernatants. This suggests that there is a possible difference in the roles of oxysterols in the adaptive immune response of human and mouse T cells and therefore experiments with human primary cells or cell lines are preferable for the study of the endogenous oxysterol ligands for RORγt in humans.

5.5 References

1. Li-Hawkins, J., Lund, E. G., Turley, S. D., & Russell, D. W. (2000). Disruption of the oxysterol 7 α -hydroxylase gene in mice. *Journal of Biological Chemistry*, 275(22), 16536–16542. <https://doi.org/10.1074/jbc.M001811200>.
2. Russell, D. W. (2003). The Enzymes, Regulation, and Genetics of Bile Acid Synthesis. *Annual Review of Biochemistry*, 72(1), 137–174. <https://doi.org/10.1146/annurev.biochem.72.121801.161712>
3. Vigne, S., Chalmin, F., Duc, D., Clottu, A. S., Apetoh, L., & Pot, C. (2017). IL-27-Induced Type 1 Regulatory T-Cells Produce Oxysterols that Constrain IL-10 Production, 8(September), 1–13. <https://doi.org/10.3389/fimmu.2017.01184>.
4. Solt LA, Kumar N, Nuhant P, Wang Y, Lauer JL, Liu J, Istrate MA, Kamenecka TM, Roush WR, Vidovic D, Schurer SC, Xu J, Wagoner G, Drew PD, Griffin PR, Burris TP. Suppression of TH17 differentiation and autoimmunity by a synthetic ROR ligand. *Nature*. 2011;472:491–494.
5. Solt LA, Kumar N, He Y, Kamenecka TM, Griffin PR, Burris TP. Identification of a selective ROR γ ligand that suppresses T(H)17 cells and stimulates T regulatory cells. *ACS Chem Biol*. 2012;7(9):1515-1519. doi:10.1021/cb300264.
6. Kumar N, Lyda B, Chang MR, et al. Identification of SR2211: a potent synthetic ROR γ -selective modulator. *ACS Chemical Biology*. 2012 Apr;7(4):672-677. DOI: 10.1021/cb200496y.
7. Scheepstra, M., Leysen, S., van Almen, G. *et al.* Identification of an allosteric binding site for ROR γ t inhibition. *Nat Commun* 6, 8833 (2015). <https://doi.org/10.1038/ncomms9833>.
8. Femke A. Meijer, Richard G. Doveston, Rens M.J.M. de Vries, Gaël M. Vos, Alex A.A. Vos, Seppe Leysen, Marcel Scheepstra, Christian Ottmann, Lech-Gustav Milroy, and Luc Brunsveld. Ligand-Based Design of Allosteric Retinoic Acid Receptor-Related Orphan Receptor γ t (ROR γ t) Inverse Agonists. *Journal of Medicinal Chemistry* 2020 63 (1), 241-259. DOI: 10.1021/acs.jmedchem.9b01372.
9. Ichiyama K, Yoshida H, Wakabayashi Y, Chinen T, Saeki K, Nakaya M, Takaesu G, Hori S, Yoshimura A, Kobayashi T. Foxp3 inhibits ROR γ mat-

- mediated IL-17A mRNA transcription through direct interaction with ROR γ t. *J Biol Chem*. 2008 Jun 20;283(25):17003-8. doi: 10.1074/jbc.M801286200. Epub 2008 Apr 23. PMID: 18434325.
10. Manel, N., Unutmaz, D., & Littman, D. R. (2008). The differentiation of human TH-17 cells requires transforming growth factor- β and induction of the nuclear receptor ROR γ t. *Nature Immunology*, 9(6), 641–649. <https://doi.org/10.1038/ni.1610>
 11. Livak, K. J., & Schmittgen, T. D. (2001). Analysis of Relative Gene Expression Data Using Real-Time Quantitative PCR and the 2- $\Delta\Delta$ CT Method. *Methods*, 25(4), 402–408. <https://doi.org/10.1006/meth.2001.1262>
 12. Griffiths, W. J., Crick, P. J., Wang, Y., Ogundare, M., Tuschl, K., Morris, A. A., ... Wang, Y. (2013). Analytical strategies for characterization of oxysterol lipidomes: Liver X receptor ligands in plasma. *Free Radical Biology and Medicine*, 59, 69–84. <https://doi.org/10.1016/j.freeradbiomed.2012.07.027>.
 13. Nurieva, R. I., Wang, X., Dong, C., Ding, S., Zhong, B., & Xu, T. (2011). Ursolic Acid Suppresses Interleukin-17 (IL-17) Production by Selectively Antagonizing the Function of ROR γ t Protein. *Journal of Biological Chemistry*, 286(26), 22707–22710. <https://doi.org/10.1074/jbc.c111.250407>.
 14. Kojima, H., Muromoto, R., Takahashi, M., Takeuchi, S., Takeda, Y., Jetten, A. M., & Matsuda, T. (2012). Inhibitory effects of azole-type fungicides on interleukin-17 gene expression via retinoic acid receptor-related orphan receptors α and γ . *Toxicology and Applied Pharmacology*, 259(3), 338–345. <https://doi.org/10.1016/j.taap.2012.01.011>.
 15. Kumar, N., Solt, L. A., Conkright, J. J., Wang, Y., Istrate, M. A., Busby, S. A., ... Griffin, P. R. (2010). The Benzenesulfoamide T0901317 [N- (2 , 2 , 2-Trifluoroethyl) -N- benzenesulfonamide] Is a Novel Retinoic Acid Receptor- Related Orphan Receptor-Inverse Agonist. *Molecular Pharmacology*, 77(2), 228–236. <https://doi.org/10.1124/mol.109.060905.cholesterol>.
 16. Heverin, M., Ali, Z., Olin, M., Tillander, V., Joibari, M. M., Makoveichuk, E., ... Björkhem, I. (2017). On the regulatory importance of 27-hydroxycholesterol in mouse liver. *Journal of Steroid Biochemistry and Molecular Biology*, 169, 10–21. <https://doi.org/10.1016/j.jsbmb.2016.02.001>.

17. Kojima, H., Muromoto, R., Takahashi, M., Takeuchi, S., Takeda, Y., Jetten, A. M., & Matsuda, T. (2012). Inhibitory effects of azole-type fungicides on interleukin-17 gene expression via retinoic acid receptor-related orphan receptors α and γ . *Toxicology and Applied Pharmacology*, 259(3), 338–345. <https://doi.org/10.1016/j.taap.2012.01.011>.

Chapter 6. Investigating oxysterol pathways in total CD4⁺ T helper cells

6.1 Introduction

The differentiation of Th17 cells is driven at the transcriptional level by the ligand-activated nuclear receptor ROR γ t⁽¹⁾. TGF- β is an upstream regulator for this process in common with the differentiation of immunosuppressive regulatory T cells (Treg)⁽²⁻³⁾. Cholesterol derivatives including both oxysterols and cholesterol precursors including desmosterol have been reported to act as agonists and inverse agonists of ROR γ t but the endogenous ligand of ROR γ t is yet to be determined^(4, 5). In chapter four it was shown that azole compound clotrimazole inhibited oxysterol 7 α -hydroxylase, CYP7B1, activity in activated Th17 polarised cells which generally resulted in downregulation of *IL17* expression. Oxysterols which are 7-substituted through the activity of CYP7B1 have been reported to bind to the LBD of ROR γ however these oxysterols were not detected in Th17 differentiated CD4⁺ T cells in the previous chapters⁽⁵⁾. Oxysterol 24(*S*),25-epoxycholesterol (24(*S*),25-EC), a known substrate of CYP7B1 is produced abundantly in activated T cells through a shunt pathway during cholesterol biosynthesis. It is a potent selective agonist of the nuclear receptor Liver X receptor (LXR) and is a reported inverse agonist of ROR γ t⁽⁶⁻⁷⁾. The focus of this chapter was to investigate the effect of oxysterols downstream of 24(*S*),25-EC and CYP7B1 activity on cytokine expression and expression of LXR target genes in CD4⁺ T cells.

Aims:

1. Investigate the effect of oxysterols downstream of 24(*S*),25-EC and CYP7B1 activity on CD4⁺ T cells cytokine expression.
2. Investigate the effect of oxysterols downstream of 24(*S*),25-EC and CYP7B1 activity on LXR activity in activated CD4⁺ T cells.

6.2 Materials and Methods

6.2.1 Preparation of oxysterols for cell culture treatment

Oxysterols and EtOH vehicle controls used for cell culture treatment were prepared as described in *section 2.1.2*.

6.2.2 Isolation of human CD4⁺ T cells from peripheral blood

CD4⁺ T cells were isolated from human peripheral blood by density gradient centrifugation with MACS[®] technology as described in *section 2.1.4* and *section 2.1.5.2* respectively.

6.2.3 Purity and activation analysis of CD4⁺ T cells by flow cytometry

Following isolation, the purity of isolated cells from each donor was determined by flow cytometry. Aliquots of CD4⁺ T cells were stained with anti-CD4 antibodies and analysed by flow cytometry as described in *section 2.1.12*. The activation of cells following cell culture was determined by staining an aliquot of cells with anti-CD25 antibodies and analysed by flow cytometry.

6.2.4 Culture conditions for CD3/CD28 activated CD4⁺ T cells in X-Vivo-20 media

CD4⁺ T cells were isolated from healthy human donors and purity of isolated cells was assessed by flow cytometry prior to cell culture. Isolated CD4⁺ T cells were cultured at 2.5×10^6 cells/mL/cm². Isolated cells from Donors 1 to 6 were activated with anti-human CD3 and anti-human CD28 microbeads as described in *section 2.1.6.2* and isolated cells from Donors 7 to 9 were activated with LEAFTM purified anti-human CD3 coated wells and LEAFTM purified anti-human CD28 antibodies as described in *section 2.1.6.2.3*. Cells were cultured in X-Vivo-20 haematopoietic media at 37°C, 5% CO₂ with oxysterol treatments summarised in Table 6.1.

24(S),25-EC and downstream epoxycholesterol metabolites can undergo hydroxylation within cells therefore treatments with dihydroxycholesterol and trihydroxycholesterol equivalent oxysterols were also performed. Oxysterols have a short half-life due to the addition of oxygen which enables rapid degradation and redistribution therefore cell cultures were harvested after 24 hrs ⁽⁸⁾. Cells were

collected for RNA extraction and gene expression analysis. Donor 2 and Donor 4 experiments and analysis were performed by Tom Hearn.

Table 6.1 Experiment conditions and end point analysis for CD4⁺T cell cultures in X-Vivo-20 with oxysterol treatments.

Donor	Activation	Treatments	Analysis
1	Anti-human CD3 and anit-human CD28 MACiBeads	24(S),25-EC 7 α ,24(S),25-EC	Cells for RNA extraction
2	Anti-human CD3 and anit-human CD28 MACiBeads	24(S),25-EC 7 α ,24(S),25-EC	Cells for RNA extraction
3	Anti-human CD3 and anit-human CD28 MACiBeads	7 α ,24(S),25-EC 7 α ,24(S),25-EC-3- one	Cells for RNA extraction
4	Anti-human CD3 and anit-human CD28 MACiBeads	7 α ,24(S),25-EC 7 α ,24(S),25-EC-3- one	Cells for RNA extraction
5	Anti-human CD3 and anit-human CD28 MACiBeads	7 α ,24(S),25-EC 7 α ,24(S),25-EC-3- one 7 α ,24,25-triHC 7 α ,24,25-triHC-3- one 24,25-diHC	Cells for RNA extraction
6	Anti-human CD3 and anit-human CD28 MACiBeads	7 α ,24,25-triHC 7 α ,24,25-triHC-3- one 24,25-diHC 24(S),25-EC	Cells for RNA extraction
7	LEAF TM purified anti-human coated wells and LEAF TM purified anti-human CD28	7 α ,24,25-triHC 7 α ,24,25-triHC-3- one 24,25-diHC 24(S),25-EC	Cells for RNA extraction
8	LEAF TM purified anti-human coated wells and LEAF TM purified anti-human CD28	7 α ,24,25-triHC 7 α ,24,25-triHC-3- one 24,25-diHC 24(S),25-EC	Cells for RNA extraction
9	LEAF TM purified anti-human coated wells and LEAF TM purified anti-human CD28	7 α ,24,25-triHC 7 α ,24,25-triHC-3- one 24,25-diHC 24(S),25-EC	Cells for RNA extraction

6.2.5 Gene expression analysis

Messenger RNA expression of CD4⁺ T cell cytokines and LXR target genes were analysed by qRT-PCR as described in *section 2.2.2*. Raw Ct values normalised against *RP18S* and *ACTB* were used to calculate the relative expression levels of cultured cells using the $2^{-\Delta\Delta C_t}$ method ⁽⁹⁾.

6.2.6 Statistical analysis

When indicated, the statistical significance of differences in mRNA expression was determined using a Mann-Whitney rank test with Microsoft Excel, where p values ≤ 0.05 were considered statistically significant.

6.3 Results

6.3.1 CD4⁺ T cells isolated from human PBMCs by MACs showed > 96% CD4⁺ purity

Single stain flow cytometry analysis of MACs isolated cells from human PBMCs showed 96.1 to 98.8% CD4⁺ purity. Figure 6.1 shows a representation of the gating strategy used to identify cells. The level of activation of isolated cells monitored by CD25 (IL-2 receptor α) expression showed 29.1 to 42.5% of isolated cells were CD25⁺ cells. Figure 6.2 shows a representation of day 0 flow analysis of CD4⁺ T cells isolated from Donor 1.

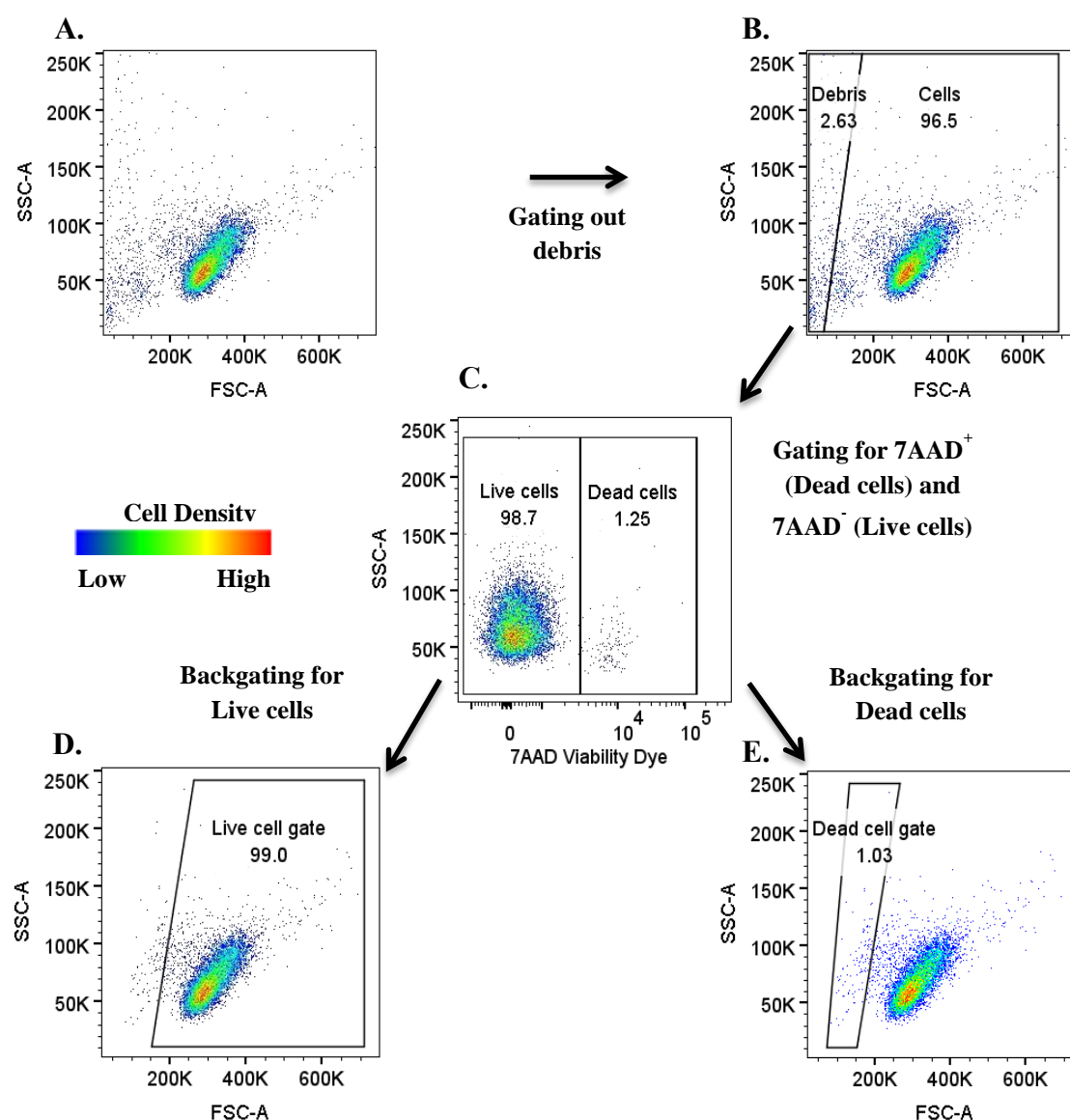


Figure 6.1 Representative Gating strategy applied to isolated CD4⁺ T cells to identify live cells and exclude dead cells using 7AAD Viability dye staining. Sample aliquots were single stained with 7AAD viability dye and not fixed prior to processing with ACEA Bioscience Novocyte. Analysis was performed with FlowJo software. Events were plotted on FSC/SSC for (A) ungated, (B) isolated cells excluding debris. (C) Cells were plotted with 7AAD/SSC to identify the dead/ apoptotic cells which have incorporated the 7AAD stain that was able to penetrate compromised cell membranes and bind to the double stranded DNA. An FSC/SSC plot was applied to the identified cells to create the (D) live cell gate and (E) dead cell gate. The Live cell gate was then applied to other single stained aliquots of the same sample.

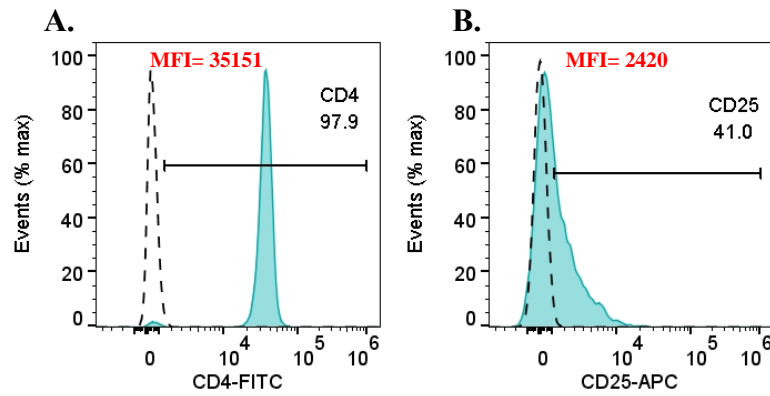


Figure 6.2 Representative flow cytometry analysis of isolated CD4⁺ T cells from Donor 1 prior to cell culture. (A) 97.9% CD4⁺ purity was achieved with MACs separation. (B) 41.0% of isolated CD4⁺ T cells expressed CD25. Filled histograms represent the fluorochrome conjugated antibody stained cells. Gates were determined using background fluorescence of unstained samples (1%) indicated by the dashed histogram. The Median Fluorescence intensities (MFI) are indicated in red.

6.3.2 Oxysterol treatments showed little effect on CD25 expression or cell viability of activated CD4⁺ T helper cells after 24 hours

Donor 1 and 2 CD4⁺ isolated cells treated with 24(*S*),25-EC and 7 α ,24,25-EC showed little variation in CD25 expression from the vehicle control (EtOH) represented in Figure 6.3. CD4⁺ isolated T cells from Donor 1 showed 76.8% CD25 expression after 24hrs activation with vehicle control. Similar CD25 expression was observed with 24(*S*),25-EC treatments from 75.5 to 73.4% with 0.1 to 1.0 μ M treatments respectively, shown in Figure 6.3A. Treatment with 7 α ,24,25-EC also showed little effect with 73.8 to 68.9% CD25⁺ cells from 0.1 to 1.0 μ M 7 α ,24,25-EC treatments respectively, shown in Figure 6.3C. No change in 7AAD viability staining was observed with 24(*S*),25-EC and 7 α ,24,25-EC treatments shown in Figure 5.3B and Figure 5.3D respectively.

As with 24(*S*),25-EC and 7 α ,24,25-EC treatments of Donor 1 and 2, treatment of activated CD4⁺ T cells with 7 α ,24,25-EC and downstream metabolite 7 α ,24,25-EC-3-one of Donors 3 and 4 isolated cells had little effect on CD25 expression after 24hrs, represented in Figure 6.3 and Figure 6.4 respectively. CD4⁺ isolated T cells from Donor 3 showed 85% CD25 expression with vehicle control (EtOH). No considerable change in CD25 expression was seen with 7 α ,24,25-EC treatments of Donor 3 isolated cells with 82.3 to 79.1% CD25 expression observed at 0.1 to 1.0 μ M respectively. As seen with Donors 1 and 2, 7 α ,24,25-EC treatments had no effect on the viability of cells shown in Figure 5.4D. Activated CD4⁺ T cells with 7 α ,24,25-EC-3-one treatments also showed little change in CD25 expression with 82.1 to 81.1% CD25⁺ cells seen with 0.1 to 1.0 μ M treatments shown in Figure 6.4A. As with 24(*S*),25-EC and 7 α ,24,25-EC treatments, there was no effect on cell viability with 7 α ,24,25-EC-3-one.

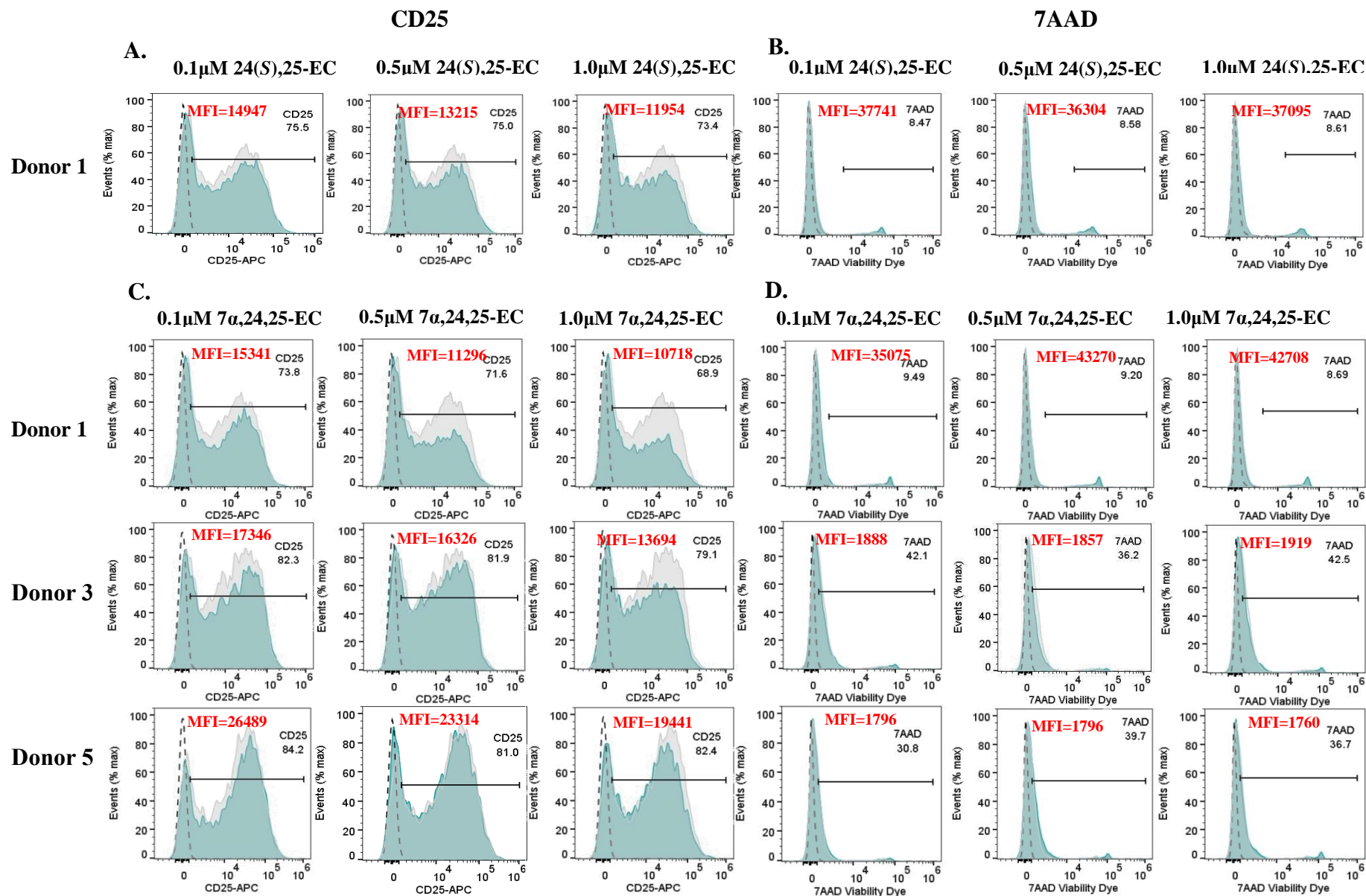


Figure 6.3 Flow cytometry analysis of activated CD4⁺ T cells from Donors 1, 3 and 5 cultured with 24(S),25-EC or 7α,24,25-EC treatments at 0.1μM, 0.5μM and 1.0μM concentrations harvested after 24hrs of cell culture. Top panel: (A) CD25 expression with 24(S),25-EC treatments. (B) 7AAD viability staining with 24(S),25-EC treatments. (C) CD25 expression with 7α,24,25-EC treatments, (D) 7AAD viability staining with 7α,24,25-EC treatments. Filled blue histograms represent the fluorochrome conjugated antibody stained activated CD4⁺ cells with oxysterol treatments overlaid with vehicle control (grey). Gates were determined using background fluorescence of unstained samples (1%) indicated by the dashed histogram. The Median Fluorescence intensities (MFI) are indicated in red.

Donor 5 isolated CD4⁺ T cells also showed similar CD25 expression with vehicle control (85.3%) and 7 α ,24,25-EC or 7 α ,24,25-EC-3-one treatments. Treatment with 7 α ,24,25-EC at 0.1 to 1.0 μ M showed 84.2 to 82.4% CD25⁺ cells respectively, shown in Figure 6.3. 7 α ,24,25-EC-3-one treated cells with 0.1 to 1.0 μ M showed 84.0 to 82.0% CD25⁺ cells (Figure 6.4). At 1 μ M 24,25-diHC was also shown to have no effect on CD25 expression of Donor 5 isolated CD4⁺ T cells shown in Figure 6.5. Viability staining with 7AAD revealed oxysterol treatments of Donor 5 isolated cells had little effect on cell viability with the greatest difference seen with 1 μ M treatments.

Activated CD4⁺ T cells isolated from Donor 6 revealed high CD25 expression with vehicle treatment (93.5%) and oxysterol treatments presented in Figure 6.5. As seen with the previous donors, 1 μ M 24(S),25-EC and the hydroxyl form 24,25-diHC showed little effect on CD25 activation with 88.6% and 90.2% CD25 expression respectively (Figure 6.6). The effect of the hydroxyl forms of 7 α ,24,25-EC and 7 α ,24,25-EC-3-one, 7 α ,24,25-triHC and 7 α ,24,25-triHC-3-one were also investigated with Donor 6 isolated CD4⁺ T cells. No considerable change in CD25 expression was observed with 1 μ M treatments of 7 α ,24,25-triHC (92.6%) or 7 α ,24,25-triHC-3-one (91.7%). Oxysterol treatments of Donor 6 isolated cells also showed similar 7AAD staining to the vehicle control revealing no effect on cell viability.

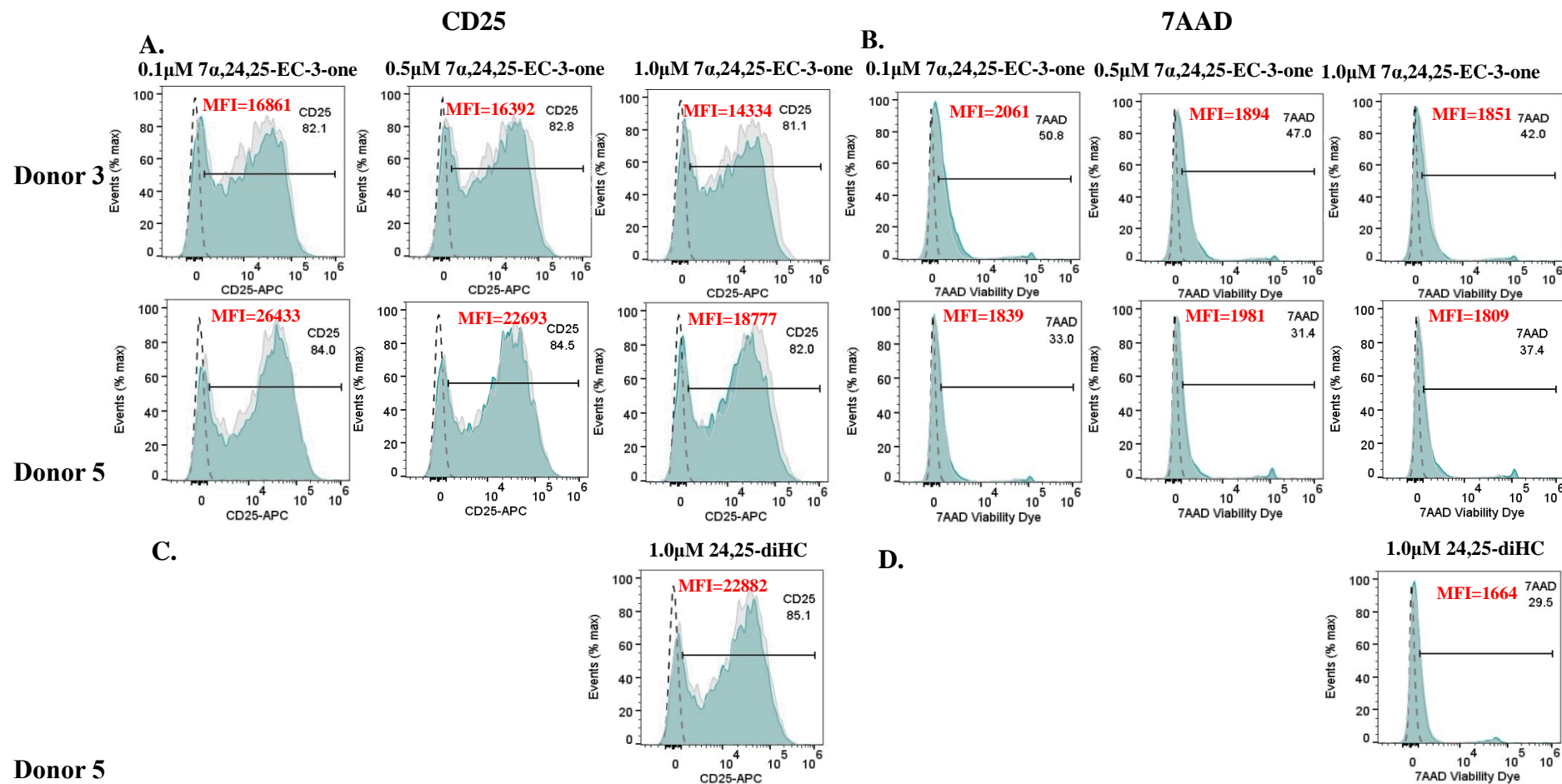


Figure 6.4 Flow cytometry analysis of activated CD4⁺ T cells from Donors 3 and 5 cultured with 7 α ,24,25-EC-3-one or 24,25-diHC treatments at 0.1 μ M, 0.5 μ M and 1.0 μ M concentrations harvested after 24hrs of cell culture. Top panel: (A) CD25 expression with 7 α ,24,25-EC-3-one treatments. (B) 7AAD viability staining with 7 α ,24,25-EC-3-one treatments. (C) CD25 expression with 1.0 μ M 24,25-diHC treatments, (D) 7AAD viability staining with 1.0 μ M 24,25-diHC treatments. Filled blue histograms represent the fluorochrome conjugated antibody stained activated CD4⁺ cells with oxysterol treatments overlaid with vehicle control (grey). Gates were determined using background fluorescence of unstained samples (1%) indicated by the dashed histogram. The Median Fluorescence intensities (MFI) are indicated in red.

24(*S*),25-EC, 24,25-diHC, 7 α ,24,25-triHC and 7 α ,24,25-triHC-3-one treatments were also shown to have no effect on the activation of CD4⁺ T cells isolated from Donors 7, 8 and 9. 80.6% of Donor 7 isolated cells with vehicle control expressed CD25 and little change was seen with oxysterol treatments with 78.3 to 81.8% of cells expressing CD25 as shown in Figure 6.5. High CD25 expression was achieved with activated CD4⁺ T cells with vehicle and oxysterol treatments isolated from Donor 8. 97.2% of activated cells with vehicle treatment from Donor 8 expressed CD25. Figure 6.5 shows oxysterol treatments of Donor 8 activated CD4⁺ T cells did not affect activation of cells with 97.0 to 97.7% of cells expressing CD25. As seen with Donors 6 to 8, the activation of Donor 9 isolated CD4⁺ T cells was unaffected with 1 μ M 24(*S*),25-EC, 24,25-diHC, 7 α ,24,25-triHC and 7 α ,24,25-triHC-3-one treatments. High CD25 expression was observed with vehicle control and all oxysterol culture conditions shown in Figure 6.5 and Figure 6.6. Little change in 7AAD staining was also seen with oxysterol treatments of Donor 7 to 9. 7AAD staining of Donor 7 and Donor 8 cultured cells was highest with 1 μ M 24(*S*),25-EC treatments although this was not a great difference from the EtOH control. No considerable change in cell viability was shown with oxysterol treatments of Donor 9 cultured CD4⁺ T cells.

These experiments confirm oxysterol treatments of 24(*S*)25-EC, downstream metabolites and their hydroxyl forms have no negative impact on the viability of CD4⁺ T cells and no considerable change in the activation of CD4⁺ T cells was seen.

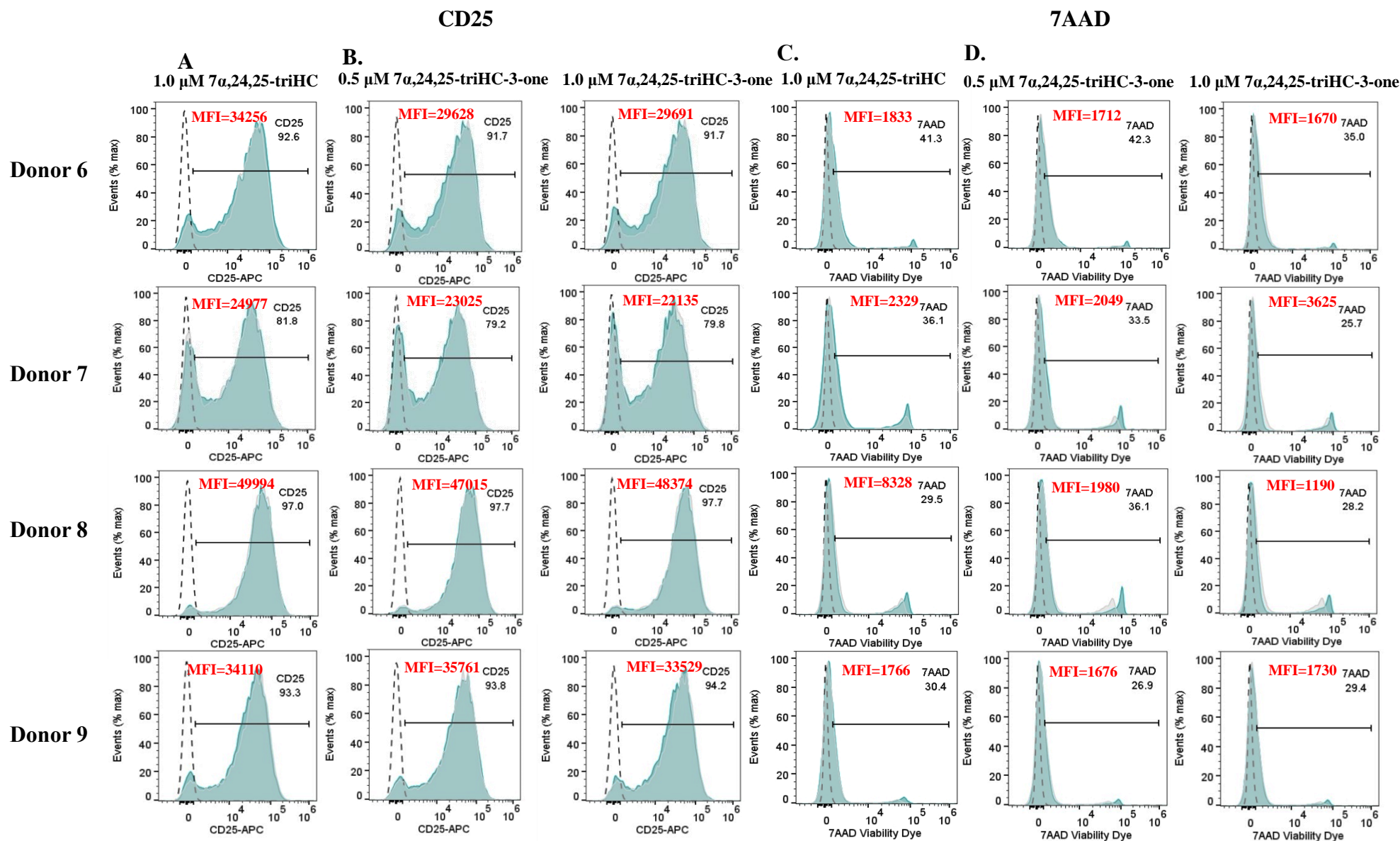


Figure 6.5 Flow cytometry analysis of activated CD4⁺ T cells from Donors 6 to 9 cultured with 7α,24,25-triHC or 7α,24,25-triHC-3-one treatments at 0.5μM or 1.0μM concentrations harvested after 24hrs of cell culture. Top panel: (A) CD25 expression with 7α,24,25-triHC treatments. (B) CD25 expression with 7α,24,25-triHC-3-one treatments. (C) 7AAD viability staining with 7α,24,25-triHC treatments. (D) 7AAD viability staining with 1.0μM 7α,24,25-triHC-3-one treatments. Filled blue histograms represent the fluorochrome conjugated antibody stained activated CD4⁺ cells with oxysterol treatments overlaid with vehicle control (grey). Gates were determined using background fluorescence of unstained samples (1%) indicated by the dashed histogram. The Median Fluorescence intensities (MFI) are indicated in red.

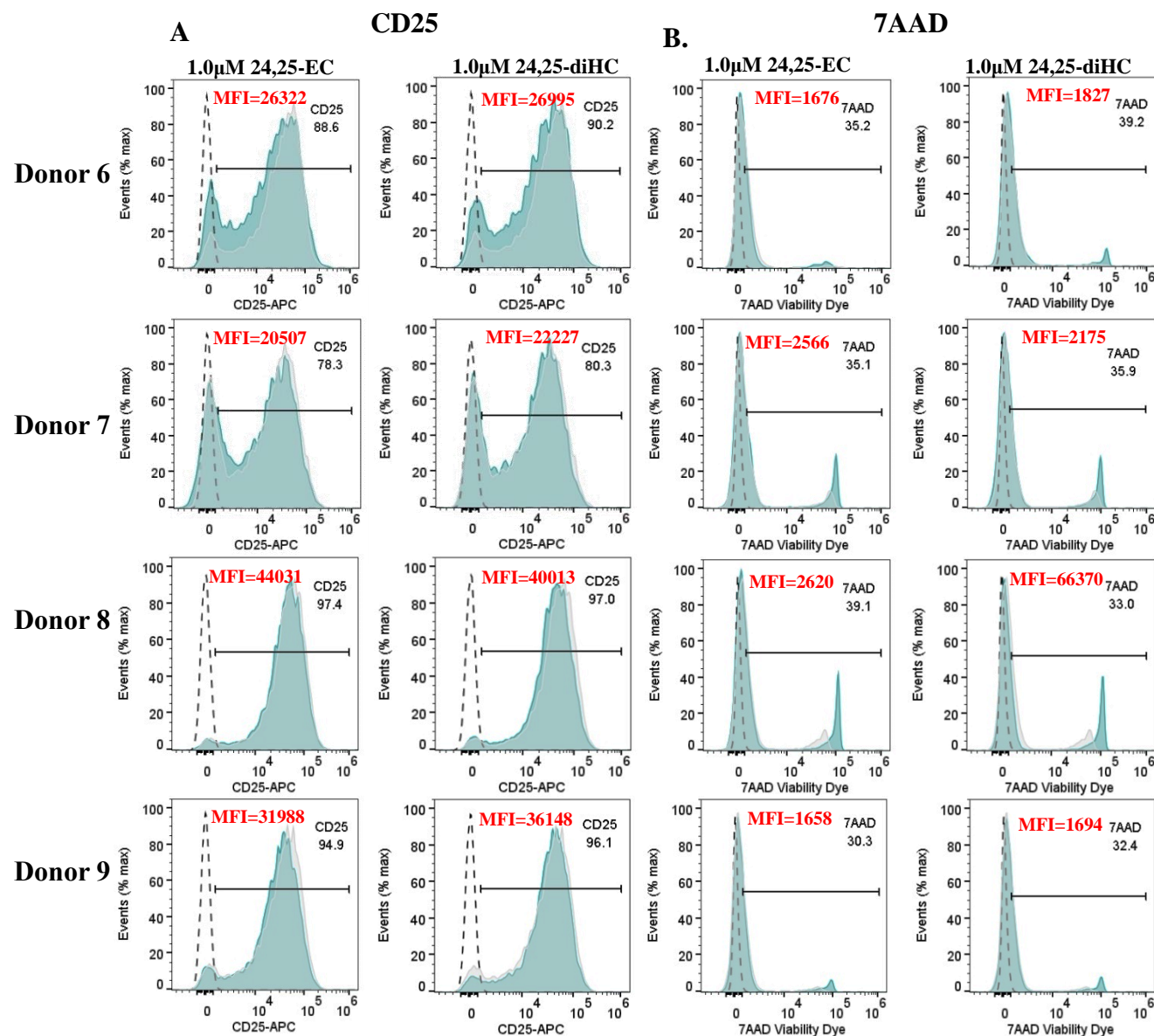


Figure 6.6 Flow cytometry analysis of activated CD4⁺ T cells from Donors 6 to 9 cultured with 24(S),25-EC or 24,25-diHC treatments at 1.0μM concentrations harvested after 24hrs of cell culture. Top panel: (A) CD25 expression with 24(S),25-EC and 24,25-diHC treatments. (B) 7AAD viability staining with 24(S),25-EC and 24,25-diHC treatments. Filled blue histograms represent the fluorochrome conjugated antibody stained activated CD4⁺ cells with oxysterol treatments overlaid with vehicle control (grey). Gates were determined using background fluorescence of unstained samples (1%) indicated by the dashed histogram. The Median Fluorescence intensities (MFI) are indicated in red.

6.3.3 Downstream metabolites of 24(S),25-EC reveal a potential pathway of deactivation in CD4⁺ T cells

The activity of LXR agonist and reported ROR γ t inverse agonist, 24(S),25-EC and downstream metabolites (Figure 6.7) towards the mRNA expression of signature CD4⁺ T cell cytokines and LXR target genes were investigated in activated total CD4⁺ T cells isolated from Donors 1 to 9. As expected, significant upregulation of LXR target gene *ABCG1* was seen with a twenty fourfold increase with 1 μ M 24(S),25-EC treatments of activated CD4⁺ T cells (Figure 6.8A). Significant increase in *ABCG1* expression was also shown with the hydroxyl equivalent 24,25-diHC. Downregulation of *ABCG1* expression would be expected if these oxysterols were antagonist of LXR. Downstream metabolite 7 α ,24,25-EC was also revealed to act as an LXR agonist with a tenfold increase in *ABCG1* expression. The hydroxyl equivalent, 7 α ,24,25-triHC, increased *ABCG1* expression to a lesser extent. This agonist activity was not seen with further downstream metabolite 7 α ,24,25-EC-3-one and the hydroxyl form 7 α ,24,25-triHC-3-one. Upregulation of LXR target gene *ABCG1* mRNA expression was seen in a dose dependent manner with 0.1 to 1.0 μ M 24(S),25-EC and 7 α ,24,25-EC treatments shown in Figure 6.9. Treatments with 24(S),25-EC, 24,25-diHC and 7 α ,24,25-EC also showed reduced *HMCGR* expression shown in Figure 6.8B although this was not a significant decrease. No significant change in *IL10* expression was seen with oxysterol treatments with the exception of 7 α ,24,25-EC which was revealed to downregulate *IL10* expression threefold, shown in Figure 6.8C. 24(S),25-EC and downstream metabolites had no significant affect towards the expression of *IL17*, *IL4* or *IFNG* shown in Figure 6.8D, Figure 6.8E and Figure 6.8F respectively.

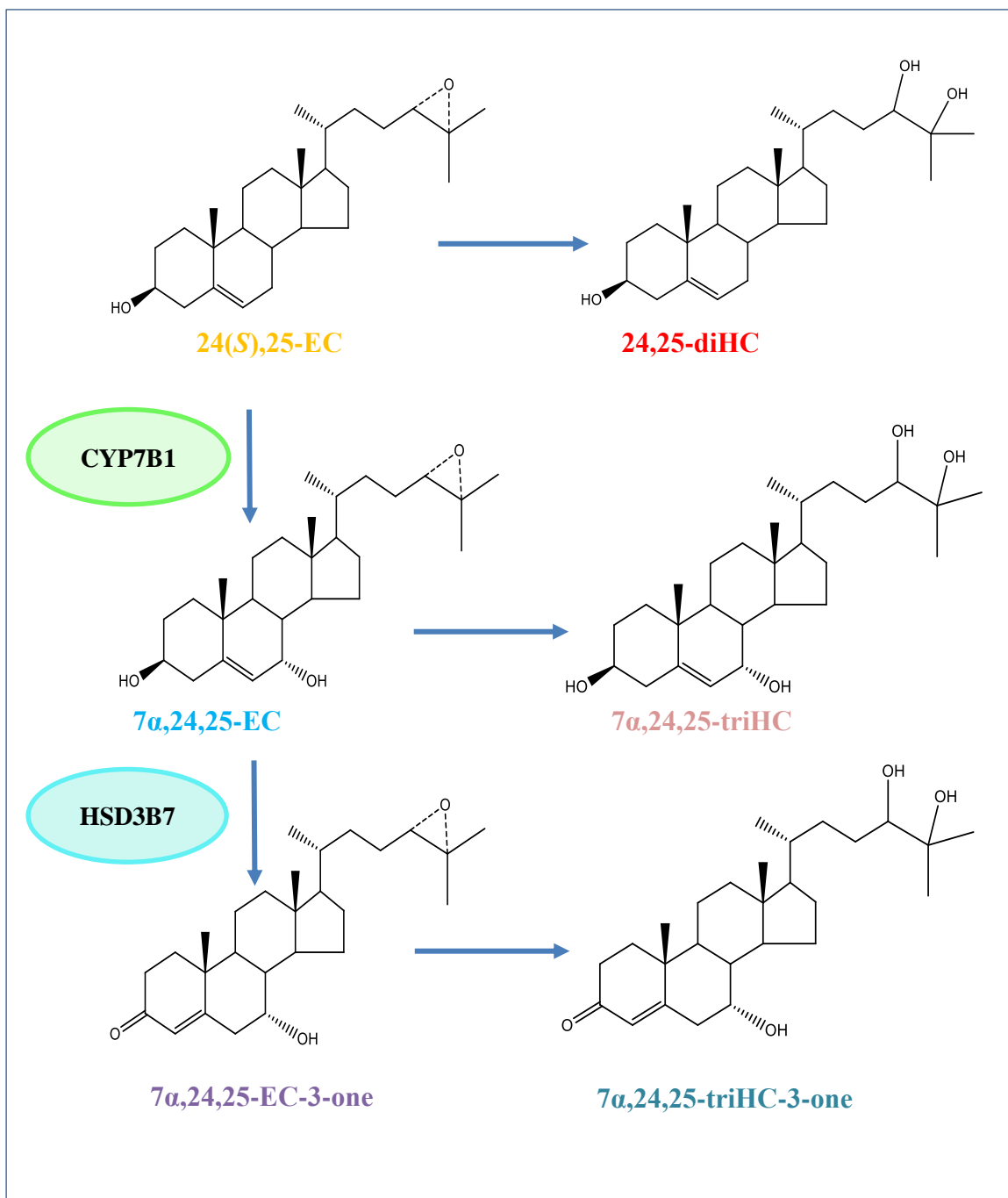


Figure 6.7 Schematic of 24(*S*),25-EC metabolism through CYP7B1 and HSD3B7 activity in the Kandutsch-Russell pathway and their hydroxyl equivalents.

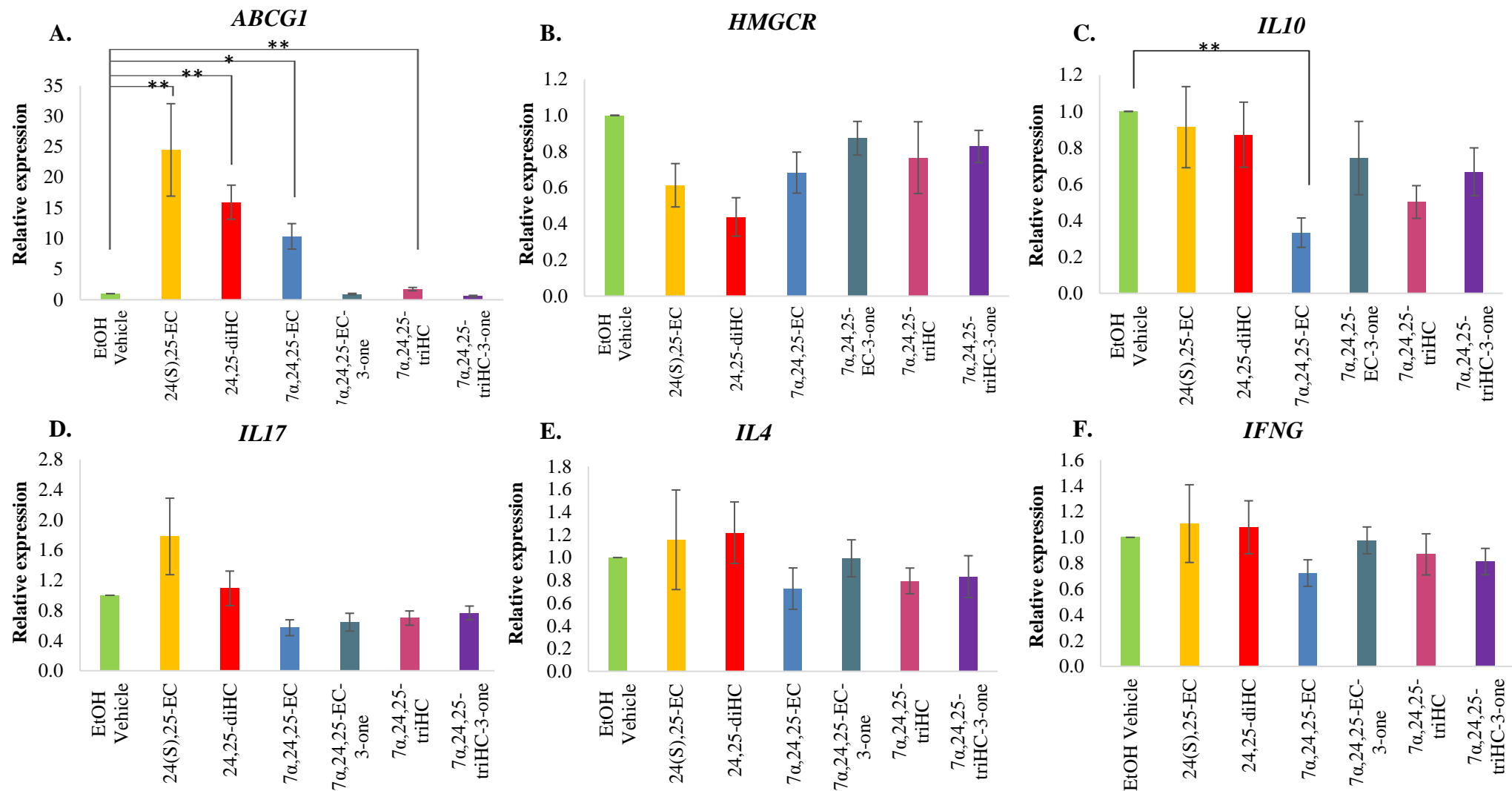


Figure 6.8 qRT-PCR analysis of mRNA expression of activated CD4⁺ cells with 1μM 24(S),25-EC and downstream metabolites treatments. (A) *ABCG1* expression was upregulated with 24(S),25-EC (p=0.0015), 24,25-diHC (p=0.003), 7α,24,25-EC (p=0.016) and 7α,24,25-triHC (p=0.004). (B) *HMGCR* downregulation was seen with 24(S),25-EC, 24,25-diHC and 7α,24,25-EC. (C) *IL10* expression was downregulated with 7α,24,25-EC treatment (p=0.004). (D) no significant difference in *IL17* expression was observed with oxysterol treatments. (E) *IL4* expression was not affected by oxysterol treatments. (F) no change in *IFNG* expression was seen with oxysterol treatments. mRNA expression was normalised to *RP18S* and *ACTB*. Fold change is relative to the EtOH vehicle sample. ± SEM of biological replicates. n≥3

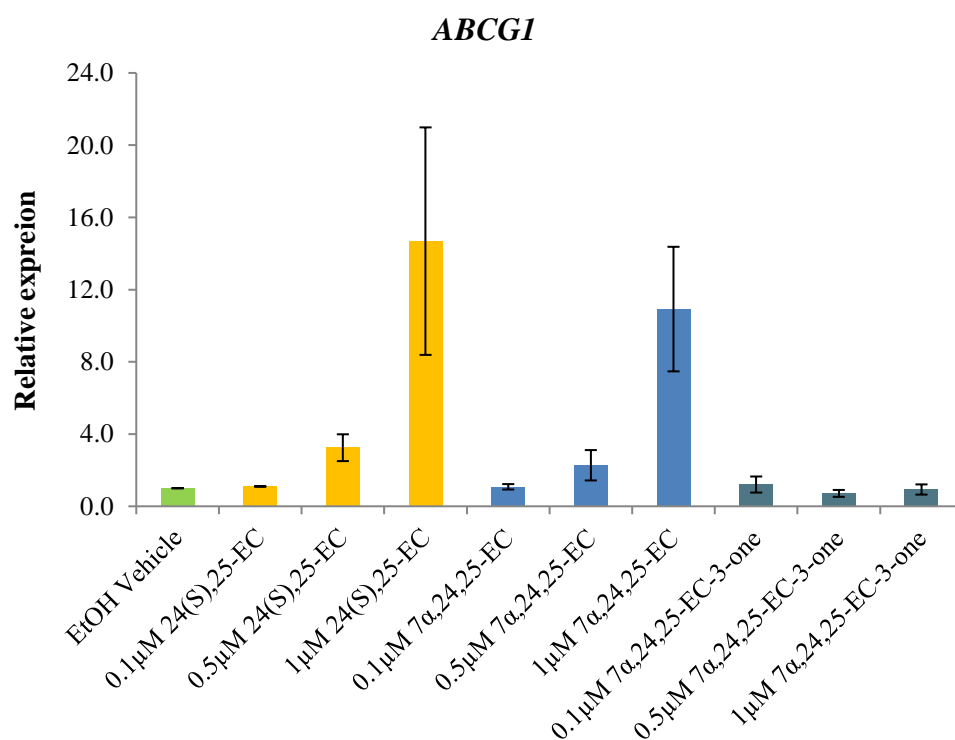


Figure 6.9 qRT-PCR analysis of *ABCG1* mRNA expression in activated CD4⁺ T cells with increasing concentration of 24(*S*),25-EC and downstream metabolites. *ABCG1* expression of activated CD4⁺ T cells was upregulated with 24(*S*),25-EC and 7α,24,25-EC treatments in a dose-dependent manner. mRNA expression was normalised to *RPI8S* and *ACTB*. Fold change is relative to the EtOH vehicle sample. ± SD of biological replicates. n≥2

6.4 Discussion

This chapter investigated the 24(*S*),25-EC metabolism pathway in total CD4⁺ T cells. Flow cytometry analysis showed treatment of CD4⁺ T cells with 24(*S*),25-EC and further downstream metabolites had no effect on the activation of CD4⁺ T cells and did not affect the viability of cells. Analysis of LXR target gene *ABCG1* through qRT-PCR analysis revealed a potential pathway of deactivation for the endogenous LXR agonist 24(*S*),25-EC through the combined activity of CYP7B1 and ubiquitously expressed 3 β -hydroxysteroid dehydrogenase type 7 (HSD3B7) which requires a 7 α -hydroxyl group in the substrate to be oxidised to their 3-oxo equivalent^(10, 11). Conversion of 24(*S*),25-EC to 7 α ,24,25-EC revealed 7 α ,24,25-EC retains LXR agonistic activity, although mRNA expression of *ABCG1* was highest with 24(*S*),25-EC treatments. Further downstream metabolite 7 α ,24,25-EC-3-one revealed loss of LXR agonist activity. These results suggest the activity of both CYP7B1 and HSD3B7 is necessary to deactivate 24(*S*),25-EC in CD4⁺ T cells.

Deactivation of LXR ligands through HSD3B7 has previously been proposed in the study of sterols in cerebrospinal fluid (CSF) in which intermediates of the bile acid biosynthesis pathway, which act as LXR ligands, are metabolised by HSD3B7 before secretion into the CSF⁽¹²⁾. HSD3B7 activity has also been shown to inactivate EBI2 ligand 7 α ,25-diHC in stromal cells⁽¹³⁾. As previously mentioned, 7 α ,27-diHC an endogenous agonist of EBI2, is reported to act as an agonist of ROR γ t along with 7 β ,27-diHC, although these oxysterols were not detected in Th17 cell culture media in this study⁽¹⁴⁻¹⁵⁾. It has been proposed that 7 β ,27-diHC undergoes metabolic regulation through the combined action of 11BHSD1 and 11BHSD2 through stereospecific oxoreduction and reverse oxidation of 7K,27-HC and 7 β ,27-HC respectively however deactivation can also occur through the activity of HSD3B7^(11, 16). The deactivation pathway of 24(*S*),25-EC shown in this study could be involved in the production of endogenous agonists of ROR γ t. Although no significant change in *IL17A* mRNA expression was observed with oxysterol treatments of total CD4⁺ T cells, treatments of Th17 polarised cells with these oxysterols may reveal a possible pathway in which the inverse agonist activity of 24(*S*),25-EC towards ROR γ t is deactivated.

6.5 References

1. Ivanov, I. I., McKenzie, B. S., Zhou, L., Tadokoro, C. E., Lepelley, A., Lafaille, J. J., ... Littman, D. R. (2006). The Orphan Nuclear Receptor ROR γ t Directs the Differentiation Program of Proinflammatory IL-17+ T Helper Cells. *Cell*, 126(6), 1121–1133.
<https://doi.org/10.1016/j.cell.2006.07.035>
2. Manel, N., Unutmaz, D., & Littman, D. R. (2008). The differentiation of human TH-17 cells requires transforming growth factor- β and induction of the nuclear receptor ROR γ t. *Nature Immunology*, 9(6), 641–649.
<https://doi.org/10.1038/ni.1610>
3. Fu, S., Zhang, N., Yopp, A. C., Chen, D., Mao, M., Chen, D., ... Bromberg, S. (2004). TGF- β Induces Foxp3 + T-Regulatory Cells from CD4 + CD25 – Precursors. *American Journal of Transplantation*, 4, 1641–1627.
<https://doi.org/10.1111/j.1600-6143.2004.00566.x>
4. Santori, F. R., Huang, P., van de Pavert, S. A., Douglass, E. F., Leaver, D. J., Haubrich, B. A., ... Littman, D. R. (2015). Identification of Natural ROR γ Ligands that Regulate the Development of Lymphoid Cells. *Cell Metabolism*, 21(2), 286–297. <https://doi.org/10.1016/j.cmet.2015.01.004>
5. Wang, Y., Kumar, N., Solt, L. A., Richardson, T. I., Helvering, L. M., Crumbley, C., ... Burris, T. P. (2010). Modulation of Retinoic Acid Receptor-related Orphan Receptor α and γ Activity by 7-Oxygenated Sterol Ligands. *Journal of Biological Chemistry*, 285(7), 5013–5025.
<https://doi.org/10.1074/jbc.M109.080614>
6. Lehmann, M., Kliewer, S. A., Moore, L. B., Smith-oliver, T. A., Oliver, B. B., Su, J., ... Willson, T. M. (1996). Activation of the Nuclear Receptor LXR by Oxysterols Defines a New Hormone Response Pathway. *Journal of Biological Chemistry*, 272(6), 3137–3140.
<https://doi.org/10.1074/jbc.272.6.3137>
7. Wang, Y., Kumar, N., Crumbley, C., Griffin, P. R., & Burris, T. P. (2010). A second class of nuclear receptors for oxysterols: Regulation of ROR α and ROR γ activity by 24S-hydroxycholesterol (cerebrosterol). *Biochimica et Biophysica Acta - Molecular and Cell Biology of Lipids*, 917–923.
<https://doi.org/10.1016/j.bbalip.2010.02.012>

8. Björkhem, I., & Diczfalussy, U. (2002). Friends, Foes, or Just Fellow Passengers? *Arterioscler Thromb Vasc Biol*, 22(5), 734–742.
<https://doi.org/10.1161/01.ATV.0000013312.32196.49>
9. Livak, K. J., & Schmittgen, T. D. (2001). Analysis of Relative Gene Expression Data Using Real-Time Quantitative PCR and the 2- $\Delta\Delta$ CT Method. *Methods*, 25(4), 402–408. <https://doi.org/10.1006/meth.2001.1262>
10. Russell, D. W. (2003). The Enzymes, Regulation, and Genetics of Bile Acid Synthesis. *Annual Review of Biochemistry*, 72(1), 137–174.
<https://doi.org/10.1146/annurev.biochem.72.121801.161712>
11. Griffiths, W. J., & Wang, Y. (2020). Oxysterols as lipid mediators : Their biosynthetic genes , enzymes and metabolites. *Prostaglandins and Other Lipid Mediators*, 147, 1–14.
<https://doi.org/10.1016/j.prostaglandins.2019.106381>
12. Ogundare, M., Theofilopoulos, S., Lockhart, A., Hall, L. J., Arenas, E., Sjo, J., ... Griffiths, W. J. (2010). Cerebrospinal Fluid Steroidomics : Are Bioactive Bile Acids Present in Brain ? *Journal of Biological Chemistry*, 285(7), 4666–4679. <https://doi.org/10.1074/jbc.M109.086678>
13. Yi, T., Wang, X., Kelly, L. M., An, J., Xu, Y., Saller, A. W., ... Cyster, J. G. (2012). Oxysterol gradient generation by lymphoid stromal cells guides activated B cell movement during humoral responses. *Immunity*, 37(21), 535–548. <https://doi.org/10.1038/jid.2014.371>
14. Liu, C., Yang, X. V, Wu, J., Kuei, C., Mani, N. S., Zhang, L., ... Lovenberg, T. W. (2011). Oxysterols direct B-cell migration through EBI2. *Nature*, 3–9.
<https://doi.org/10.1038/nature10226>
15. Soroosh, P., Wu, J., Xue, X., Song, J., Sutton, S. W., Sablad, M., ... Dandridge, R. A. (2014). Oxysterols are agonist ligands of ROR t and drive Th17 cell differentiation. *Proceedings of the National Academy of Sciences*, 111(33), 12163–12168. <https://doi.org/10.1073/pnas.1322807111>
16. Beck, K. R., Inderbinen, S. G., Kanagaratnam, S., Kratschmar, D. V., Jetten, A. M., Yamaguchi, H., & Odermatt, A. (2019). 11 β -Hydroxysteroid dehydrogenases control access of 7 β ,27-dihydroxycholesterol to retinoid-related orphan receptor γ . *Journal of Lipid Research*, 60(9), 1535–1546.
<https://doi.org/10.1194/jlr.m092908>

Chapter 7. *In silico* modelling of the interaction between potential endogenous oxysterol ligands and nuclear hormone transcription factors ROR γ t and LXR β

7.1 Introduction

ROR γ t is the master transcription factor required for Th17 differentiation from naive CD4⁺ T cells and IL-17 production ⁽¹⁾. The endogenous ligand of ROR γ t has yet to be identified; cholesterol derivatives have been reported to have agonistic activity towards ROR γ t but the endogenous ligand is still unclear ⁽²⁻⁵⁾. ROR γ t is a member of the nuclear hormone receptor family of transcription factors which also includes ubiquitously expressed Liver X Receptor beta (LXR β). Several oxysterols have been identified as LXR β ligands and it has been proposed that potent LXR β agonist 24(S),25-EC has inverse agonist activity towards ROR γ t ⁽⁶⁾. Inverse agonists bind to receptor binding domains and exert the opposing effect of an agonist suppressing the ligand activity.

In collaboration with Jonathan Mullins and Karl Austin-Muttitt of the Genome and Structural Bioinformatics Research Group, the potential of oxysterols as ROR γ t and LXR β ligands was investigated through *In silico* 3D modelling and protein-ligand docking simulations.

Atomic resolution homology models of proteins of interest are constructed from the amino acid sequence and an experimental 3D structure of the protein or a related homologous protein. Alignment of identical sequences from the query amino acid sequence and the 3D protein structure maps residues of homology between the amino acid sequence and the 3D structure and are combined into a single predicted structure. This homology method relies on highly similar amino acid sequences adopting similar secondary and tertiary structures since residues involved in protein folding are known to be highly conserved due to evolutionary pressure ⁽⁷⁾.

The position and orientation of a ligand when bound to a protein can be predicted by protein-ligand docking simulations. A search algorithm recursively positions the ligand into different poses to find the position which results in the minimum energy

conformation is ⁽⁸⁾. Scoring functions predict the most stable pose for the ligand within the proteins ligand binding domain (LBD) and the binding affinity is determined as the sum of electrostatic and Van der Waals forces.

This Chapter employs *In silico* homology modelling and protein-ligand docking analysis to stimulate oxysterol interactions within the binding pocket of nuclear hormone receptors ROR γ t and LXR β LBD.

7.2 Methods

7.2.1 *In silico* modelling of protein and ligand structures

7.2.1.1 Homology modelling of protein structures with Modeller

Modeller software was used to build homology models of mouse ROR γ ligand binding domains (LBD) in the active conformation using the corresponding amino acid sequences obtained from UniProt with a template x-ray crystal structure of ROR γ with bound putative agonist 22(R)-HC (PDB:3L0J) or 25-HC (PDB:3L0L) from the RCSB Protein Data Bank (PDB)^(2, 9-11). Modeller produces a 3D model from the alignment of the sequence of interest with a known related structure by satisfaction of spatial restraints. To maintain the relative orientation of amino acids in the binding pocket co-crystallised ligands were co-modelled. Water molecules of interest were also co-modelled with the protein and treated as part of the protein for docking simulations. This method was also used to produce a homology model of LXR β LBD in the active conformation. Human LXR β amino acid sequence was obtained from UniProt and x-ray crystal structure of LXR β with bound agonist 24(S),25-EC (PDB: 1P8D) from the RCSB PDB⁽¹²⁾.

7.2.1.2 Modelling ligand structures

3D structures of the sterol ligands of interest shown in Figure 7.1 and Figure 7.2 were produced with Chem3D software (PerkinElmer). Unusual ring geometries of bound sterols can be observed *in vitro* in x-ray crystal structures. These were not well modelled with *ab initio* generation of 3D structures therefore the structures of ligands were created with Chem3D using 25-Hydroxycholesterol (25-HC) extracted from an x-ray crystal structure, PDB:3L0L to obtain the ring structure base⁽²⁾. Ligands were then relaxed in a full-atom molecular mechanics simulation to correct any inaccuracies from x-ray crystallisation or Chem3D modifications.

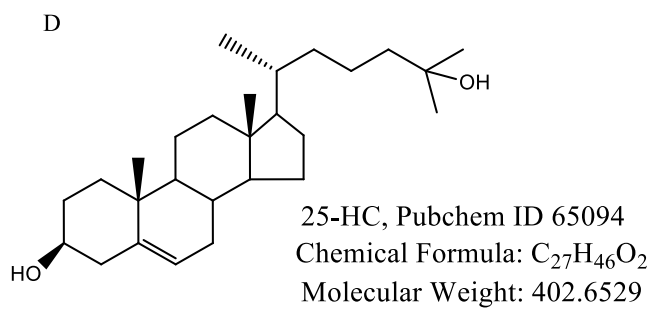
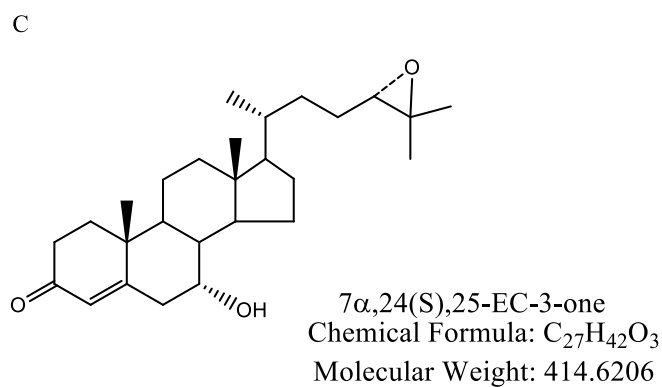
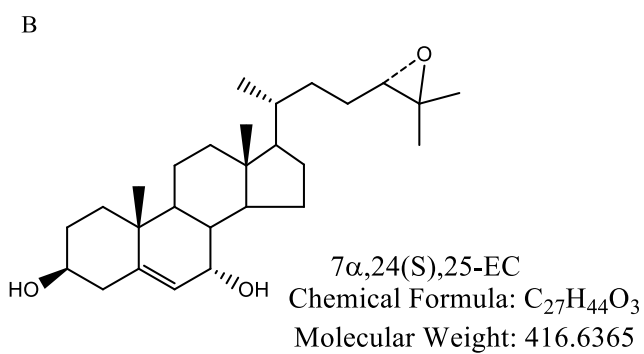
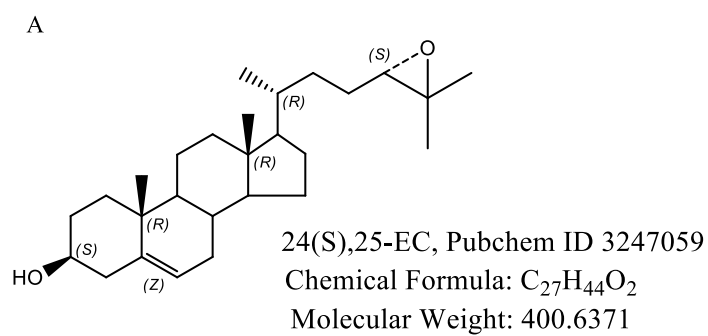


Figure 7.1 Initial oxysterol structures for *in silico* study. (A) 24(S),25-EC (B) 7α,24(S),25-EC (C) 7α,24(S),25-EC-3-one (D) 25-HC.

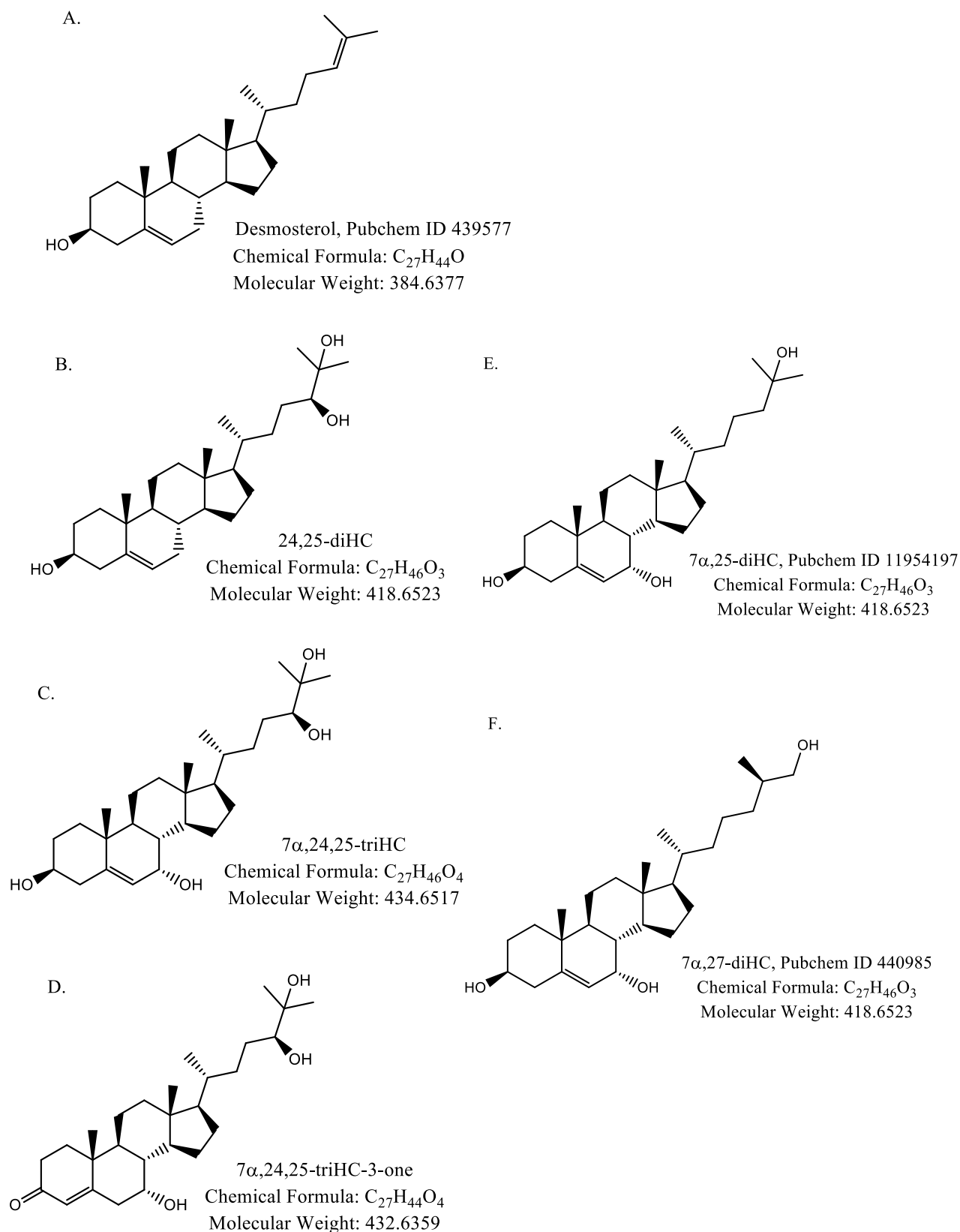


Figure 7.2 Further sterol structures for *in silico* study. (A) Desmosterol (B) 24,25-diHC (C) 7 α ,24,25-triHC (D) 7 α ,24,25-triHC-3-one (E) 7 α ,25-diHC (F) 7 α ,27-diHC

7.2.2 Protein-ligand docking simulations

7.2.2.1 Pre-docking preparation

Prior to performing docking simulations ligands from crystal structures were removed from homology models and partial charge of atoms calculated. The Electronegativity Equalization Method (EEM) was applied to structures to determine the partial charge of atoms in respect to the molecules 3D structure ⁽¹³⁻¹⁵⁾.

7.2.2.2 FKCOMBU pre-docking preparations

An initial ligand fit in the LBD was established with FKCOMBU (Flexible ‘K’emical structure ‘COM’parison using Build Up algorithm) program. FKCOMBU performs a pairwise comparison and flexible molecular alignment superposition of ligands with an example binding from the reference ligands to create an initial ligand fit in the ligand binding domain ⁽¹⁶⁾.

7.2.2.3 Protein-ligand docking simulations with PLANTS

Homology models were modified at residue HIS479 for ROR γ (Figure 7.3) and HIS435 for LXR β (Figure 7.4) to produce various initial histidine rotamer poses selected from the Richardson rotamer library for optimisation.

Initial predicted docking complexes produced with FKCOMBU described in *section 7.2.2.2* were refined with a flexible protein-ligand docking algorithms PLANTS (Protein-Ligand ANT System) as describes in *section 2.4.2.2* ⁽¹⁷⁾. PLANTS is a swarm based docking method that uses Ant Colony Optimisation (ACO), a class of stochastic optimisation algorithms, to generate the lowest energy conformations ⁽¹⁸⁾. PLANTS finds the minimum energy conformation of the ligand in the binding site by marking low energy ligand conformations which are modified in subsequent iterations to generate low energy conformations with a higher probability. The most energetically favourable pose of the ligand in the binding site is determined using PLANTS scoring functions to determine the strongest binding affinity (Table 7.1). In the PLANTS simulations the sterol B and C rings were fixed in their pre-docked position while the remaining ligand structure was able to flex freely. The protein sidechain residues were also able to flex freely during docking simulations to obtain the optimum sidechain residue pose which gave the greatest probability. PLANTS software was initially designed with kinase structures which have numerous CHO (carbon-oxygen hydrogen) interactions involved in ligand binding, CHO interactions

are of less significance in the protein structures in this study therefore CHO interactions were disabled. Simulation search parameters were increased, $N = 80$, $\sigma = 64$, to account for the high degrees of freedom in a system with side-chain flexibility, ligand flexibility and the addition of water molecules. Molecular graphics and analysis were performed with UCSF Chimera ⁽¹⁹⁾.

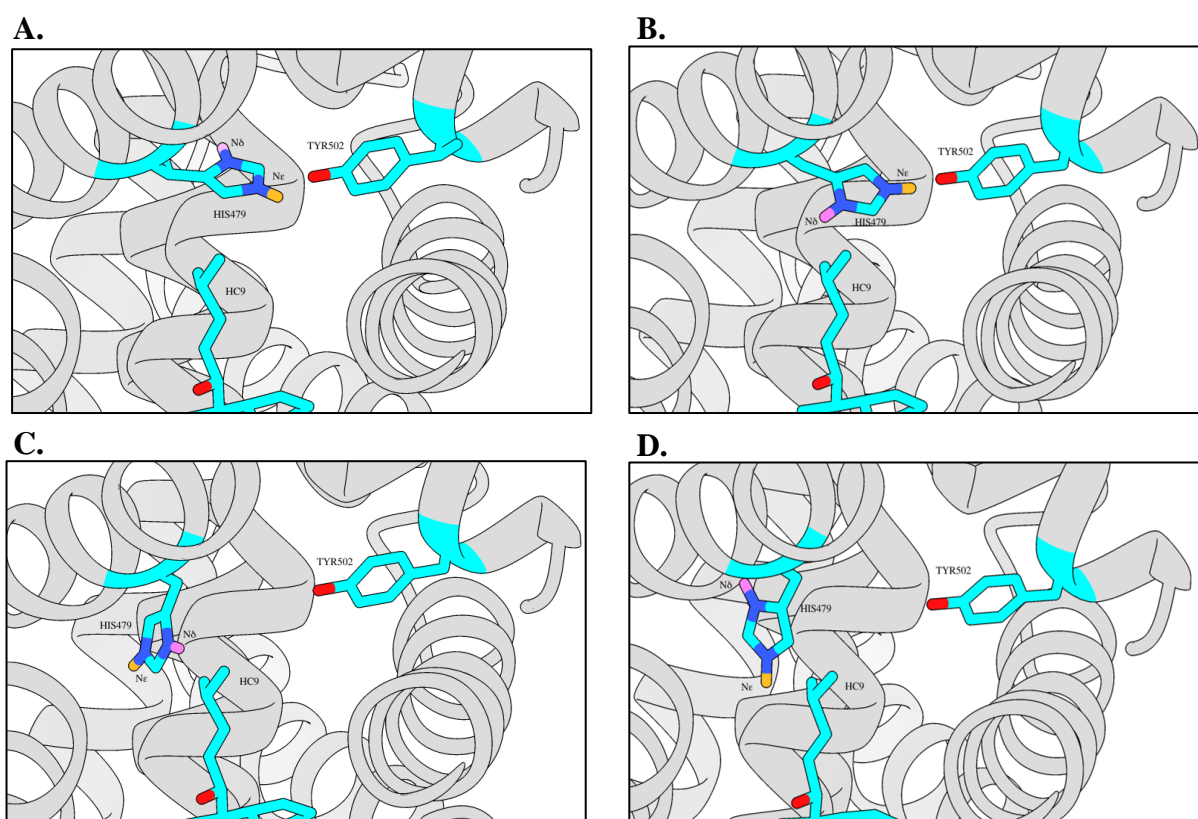


Figure 7.3 Initial HIS479 rotomer, tautomer poses for protein-ligand docking simulations with PLANTS. (A) Native ‘HC9’ pose (B) Flipped native pose (C) Oriented away from TYR502 (D) Flipped oriented away from TYR502. The pink hydrogen is present in the N δ protonated HID tautomer only and the orange hydrogen is only present in the N ϵ protonated HIE tautomer.

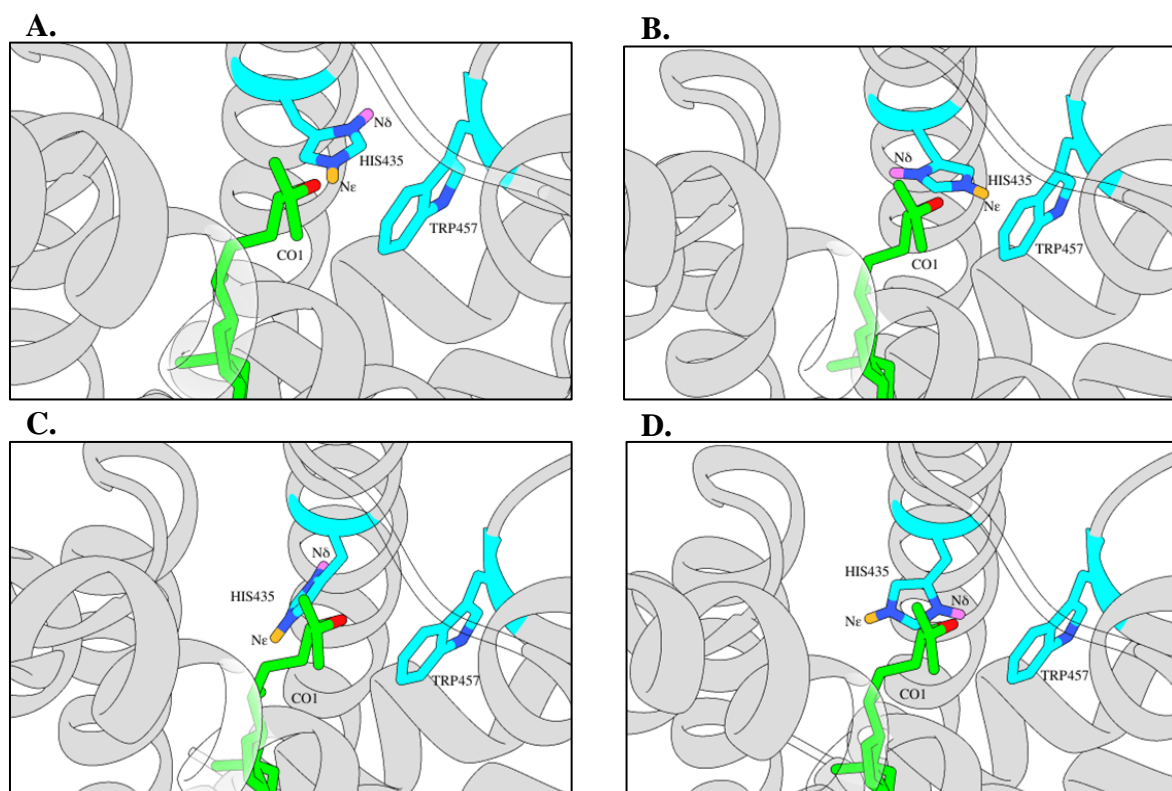


Figure 7.4 Initial HIS435 rotomer, tautomer poses for protein-ligand docking simulations with PLANTS. (A) Native 'CO1' pose (B) Flipped native pose (C) Oriented away from TRP457 (D) Flipped oriented away from TRP457. The pink hydrogen is present in the Nδ protonated HID tautomer only and the orange hydrogen is only present in the Ne protonated HIE tautomer.

Table 7.1 PLANTS scoring functions.

Types of interactions	Scoring function terms
Van Der Waals effects	plp steric
Atom-atom clashes	ligand intra score chemplp clash plp repulsive
Hydrophilic and hydrophobic interactions	plp buried polar chemplp lipohilic
Hydrogen bonding	plp h bond chemplp weak cho chemplp charged hb chemplp cho
Metal co-ordination	plp meta chemplp charged metal chemplp metal
Sulphur interactions	Sulphur acceptors
Ligand entropy	plp torsion chemplp torsion

7.3 Results

7.3.1 ROR γ t protein-ligand docking simulations

It has previously been reported that the AF2 alpha helix H12 is stabilised to give an active conformation via a hydrogen bond network between HIS479 of helix 11 (H11) and TYR502 of H12 referred to as the HIS-TYR lock which enables coactivator peptides to bind to a pocket of the LBD ⁽²⁰⁾. Putative agonist 25-HC has been shown to stabilise H12 through a hydrogen bond network with a solvent bridge (Figure 7.5). The hydroxyl tail is orientated towards H11 while the oxysterol A ring is positioned towards H1 and H2. HIS479 residue has a deprotonated N δ atom orientated towards the binding pocket resulting in N ϵ misalignment with TYR502. The side chain hydroxyl group of 25-HC forms a direct hydrogen bond with HIS479, a solvent bridge with TYR502 is also formed stabilising the protein by a network of three hydrogen bonds ⁽²⁾. The 3 β hydroxyl group (3 β -OH) of the sterol ring structure coordinates the ligand binding by direct hydrogen binding with GLN286 and a solvent bridge to ARG367.

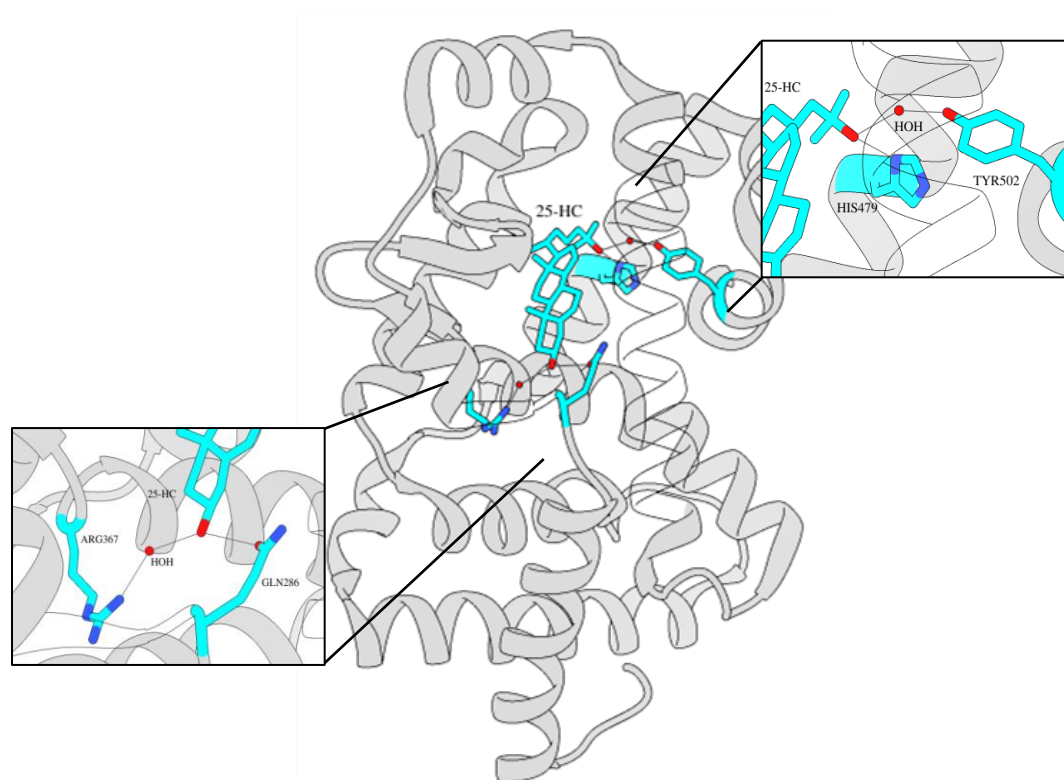


Figure 7.5 A network of three hydrogen bonds (black) including a solvent bridge fixes TYR502 in the active conformation with 25-HC (cyan) bound ROR γ . From PBD:3L0L.

Another proposed agonist of ROR γ t, 22(*R*)-HC was reported to show typical binding with the 3 β -OH of 22(*R*)-HC ring structure coordinating the sterol binding by direct hydrogen binding with GLN286 and a solvent bridge to ARG367 (Figure 7.6) ⁽²⁾.

When 22(*R*)-HC is bound to ROR γ , TYR502 is stabilised by a hydrogen bond with HIS479 in which the protonated N ϵ atom of the histidine donates a hydrogen atom to the hydroxyl group of tyrosine.

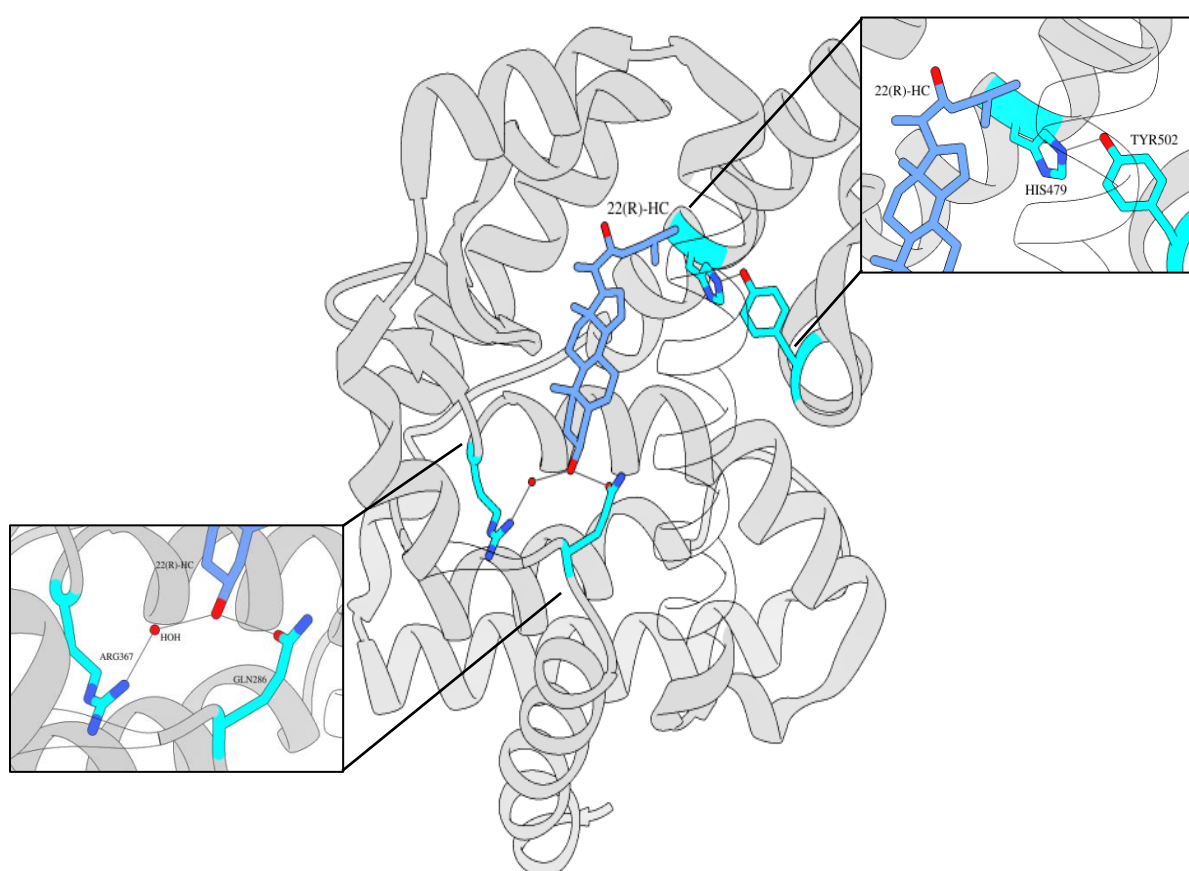


Figure 7.6 Hydrogen bonding (black) between HIS479 and TYR502 hold H12 in the active conformation with 22(*R*)-HC (blue) bound ROR γ . From PBD:3L0J. .

When TYR502 is not fixed H12 is destabilised and unravels losing the binding pocket. Compounds with strong binding affinity to ROR γ which destabilise TYR502 are inverse agonists. Many inverse agonists identified have a short-long switch

mechanism of action in which compounds are either longer than the binding pocket and push TYR502 away from the binding pocket or are too short to reach TYR502⁽²¹⁾.

In this Chapter, protein-ligand dockings of putative agonist 25-HC, proposed inverse agonist 24(*S*),25-EC and downstream metabolites were investigated. Histidine has an imidazole side-chain ring, which is partially protonated. Histidine is therefore able to function as a hydrogen bond donor or acceptor by changing tautomer. Therefore protein-ligand dockings were performed with multiple rotamer and tautomer (HIE or HID) positions and poses with the minimum energy requirement determined. A control model (HC3 model) was created from PDB:3L0L to confirm docking simulations were able to reproduce the known 25-HC binding in ROR γ seen in co-crystallised structures. 25-HC-ROR γ docking simulations successfully reproduced the HIS479 hydrogen bond network with a solvent bridge and the 3 β -OH hydrogen bond network with GLN286 and solvent bridge to ARG367 (Figure 7.7) validating the *in silico* models produced. An alternative tautomeric state was revealed which resulted in the same positioning and orientation of HIS479 but also allowed a direct hydrogen bond between HIS479 and TYR502 similar to that seen in co-crystallised structures of other oxysterols. The energy scores for the ligand and HIS479 residue therefore provided a point of reference for binding for stabilised side-chain residues (Table 7.2). As the unique mechanism of hydrogen bonds is seen in 25-HC bound ROR γ crystal structure further docking stimulations were performed with a homology model (HC9 model) derived from the crystal structure of ROR γ in complex with 22(*R*)-HC (PDB:3L0J)⁽²⁾.

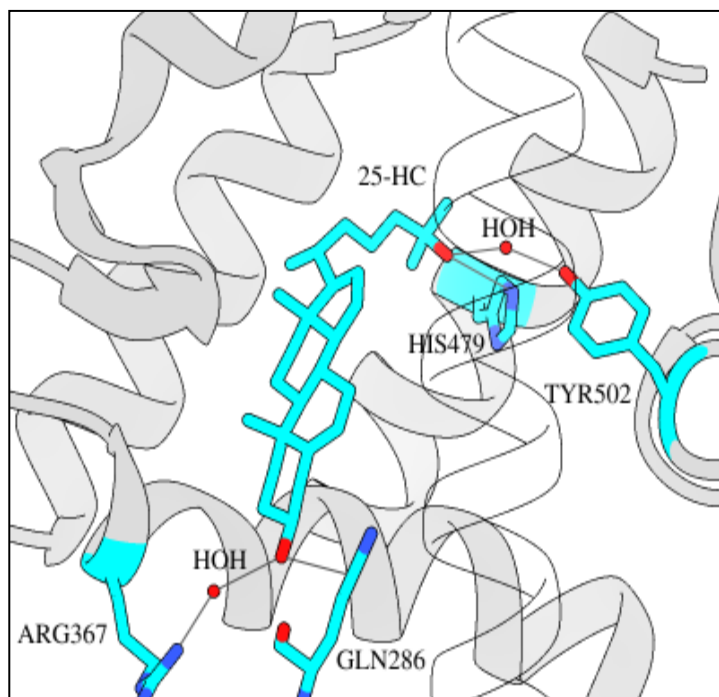


Figure 7.7 25-HC-ROR γ docking simulations with HC3 model reproduces binding seen in co-crystallised structure PDB:3L0L. A hydrogen bond network is seen with a direct hydrogen bond (black) between 25-HC (cyan) and HIS479 and solvent bridge to TYR502. The 3 β -OH group forms a direct hydrogen bond with GLN286 and a solvent bridge to ARG367.

Table 7.2 25-HC in the ROR γ control model ‘HC3’. Strong binding affinity for the ligand is achieved with a high histidine stability score.

Ligand	HIS479 score	Ligand score
25-HC	-10.271	-107.678

Protein-ligand docking simulation of 25-HC with the HC9 homology model revealed a strong binding affinity with stabilisation of ROR γ in the active conformation even without the water molecule required for the solvent bridge to TYR502. The simulation identifies a direct hydrogen bonding between the C25 side-chain hydroxyl

group and HIS479, HIS479 also directly binds with TYR502 in this simulation stabilising the AF2 helix (Figure 7.8).

Protein-ligand docking simulations of proposed inverse agonist 24(*S*),25-EC and downstream metabolite 7 α ,24(*S*),25-EC revealed a strong binding affinity, however a reduced histidine stability score was observed (Table 7.3). The side chain tail of these ligands pushes the histidine residue into a position where it can no longer form a hydrogen bond with TYR502 and is therefore unable to stabilise the AF2 helix (Figure 7.9 and Figure 7.10).

The hydrogen bond network between the ligand structure and side-chain residue GLN286 and solvent bridge to ARG367 seen in crystal structures with co-crystallised ligands was reproduced in all docking simulations excluding 7 α ,24(*S*),25-EC-3-one⁽²²⁾. 7 α ,24(*S*),25-EC-3-one has a 3-oxo group in place of the 3 β -OH group and is therefore unable to donate a hydrogen to GLN286. This results in the loss of the hydrogen bond network (Figure 7.11). Consequently a considerably reduced binding affinity is seen which suggests the loss of the ARG367-GLN286 hydrogen bond network prevents efficient binding of the ligand within the LBD.

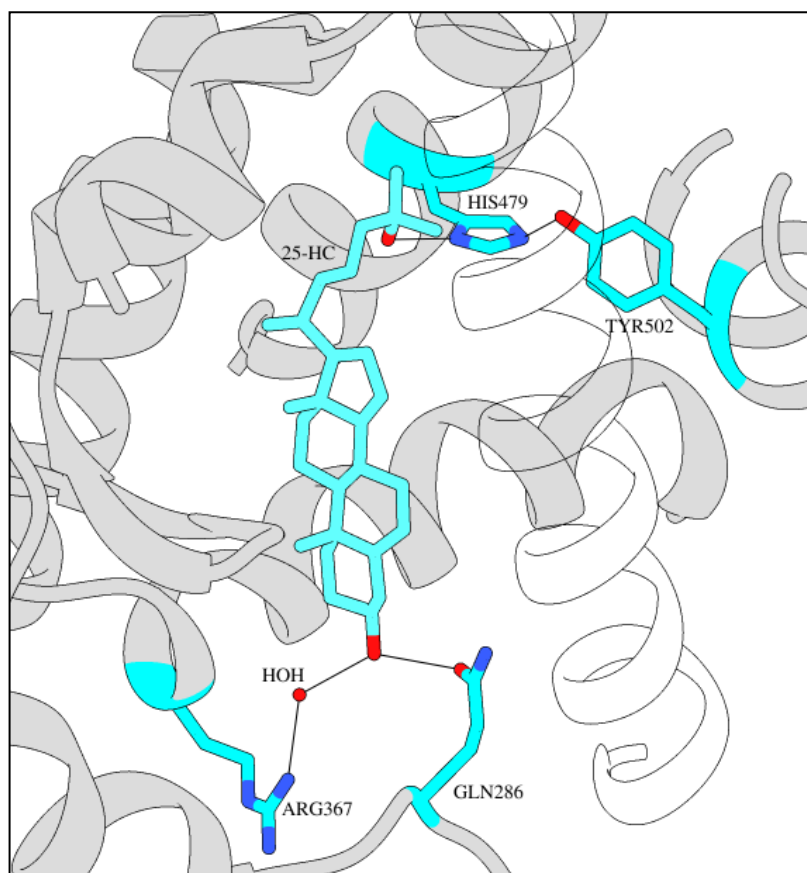


Figure 7.8 25-HC-ROR γ docking simulations with HC9 model. Hydrogen bonding (black) between 25-HC (cyan), HIS479 and TYR502 stabilises H12 in the active confirmation. The 3 β -OH group forms a direct hydrogen bond with GLN286 and a solvent bridge to ARG367.

Table 7.3 Binding affinities of sterol ligands for ROR γ

Ligand	HIS479 score	Ligand score
25-HC	-7.397	-104.985
24(<i>S</i>),25-EC	-5.152	-100.765
7 α ,24(<i>S</i>),25-EC	-5.113	-96.556
7 α ,24(<i>S</i>),25-EC-3-one	-4.950	-43.731
24,25-diHC	-6.378	-102.798
7 α ,24,25-triHC	-10.919	-98.312
7 α ,24,25-triHC-3-one	-10.313	-44.180
7 α ,25-diHC	-8.456	-100.867
7 α ,27-diHC	-6.903	-103.366
Desmosterol	-2.243	-102.443

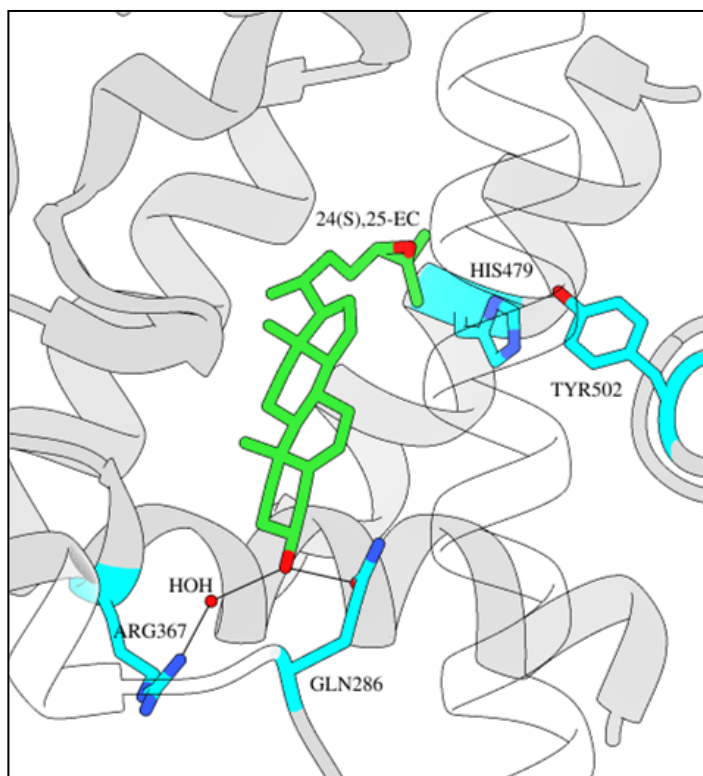


Figure 7.9 24(S),25-EC-ROR γ docking simulation with HC9 model. The 3 β -OH group of 24(S),25-EC (green) forms a direct hydrogen bond (black) with GLN286 and a solvent bridge to ARG367 however HIS479 and TYR502 stabilisation is not established.

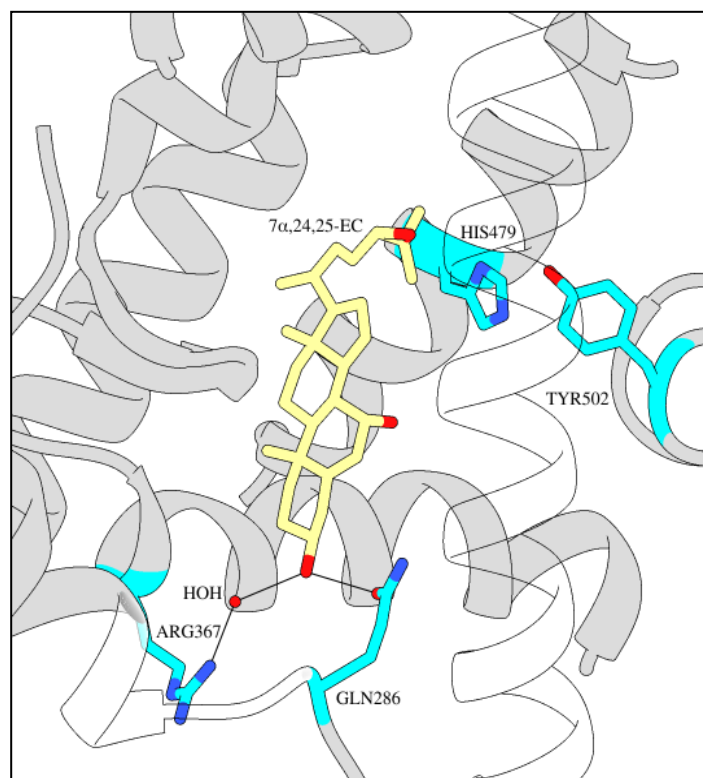


Figure 7.10 7 α ,24(S),25-EC-ROR γ docking simulation with HC9 model. The 3 β -OH group of 7 α ,24(S),25-EC (yellow) forms a direct hydrogen bond (black) with GLN286 and a solvent bridge to ARG367 however HIS479 and TYR502 stabilisation is not established.

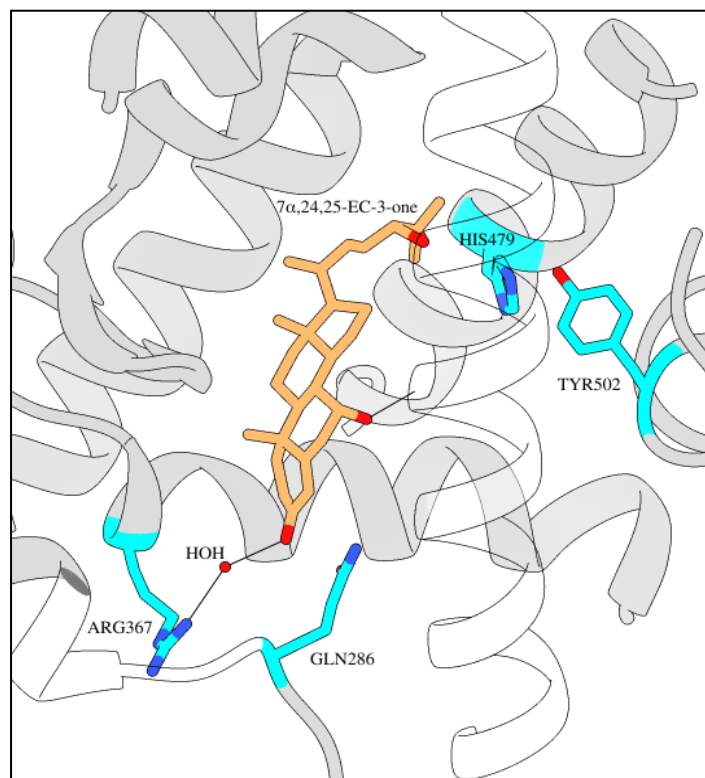


Figure 7.11 7 α ,24(*S*),25-EC-3-one-ROR γ docking simulation with HC9 model. The 3-oxo group of 7 α ,24(*S*),25-EC-3-one (orange) is unable to donate a hydrogen to GLN286. HIS479 and TYR502 stabilisation is also not established.

Due to the labile nature of the epoxy group, 24(*S*),25-EC and metabolites can be hydrolysed converting the epoxy group to hydroxyl groups therefore additional docking simulations were performed with the hydroxyl forms of these oxysterols. Docking simulations with additional CYP7B1 metabolites 7 α ,25-diHC and 7 α ,27-diHC and cholesterol precursor, desmosterol were also performed. The corresponding hydroxyl oxysterols showed similar binding affinities to the epoxy oxysterols (Table 7.3) however docking simulations predict 24,25-diHC is able to stabilise H12 in the active formation through hydrogen bonding of the hydroxyl group at C25 and side chain residue HIS479 suggesting agonist activity towards ROR γ t (Figure 7.12). 7 α ,24,25-triHC docking simulations reveal possible hydrogen bonds with HIS479 and the hydroxyl groups at C24 and C25 which appears to position HIS479 away from TYR502 and is therefore unable to stabilise H12 (Figure

7.13). $7\alpha,24,25$ -triHC-3-one has a reduced binding affinity, the 3-oxo group of $7\alpha,24,25$ -triHC-3-one is unable to donate a hydrogen to GLN286 which results in the loss of the hydrogen bond network (Figure 7.14) as seen with $7\alpha,24,25$ -EC-3-one (Figure 7.11). Both $7\alpha,25$ -diHC and $7\alpha,27$ -diHC were able to stabilise H12 in the active conformation via hydrogen bonding with HIS479 and the hydroxyl group at C25 or C27 respectively enabling HIS479 to form a hydrogen bond with TYR502 (Figure 7.15 and Figure 7.16). Desmosterol docking simulations also predicted agonist activity towards ROR γ t (Figure 7.17). Electrostatic forces between Desmosterol and side chain residues in the LBD positions HIS479 so as to enable a hydrogen bond between HIS479 and TYR502 (Figure 7.18).

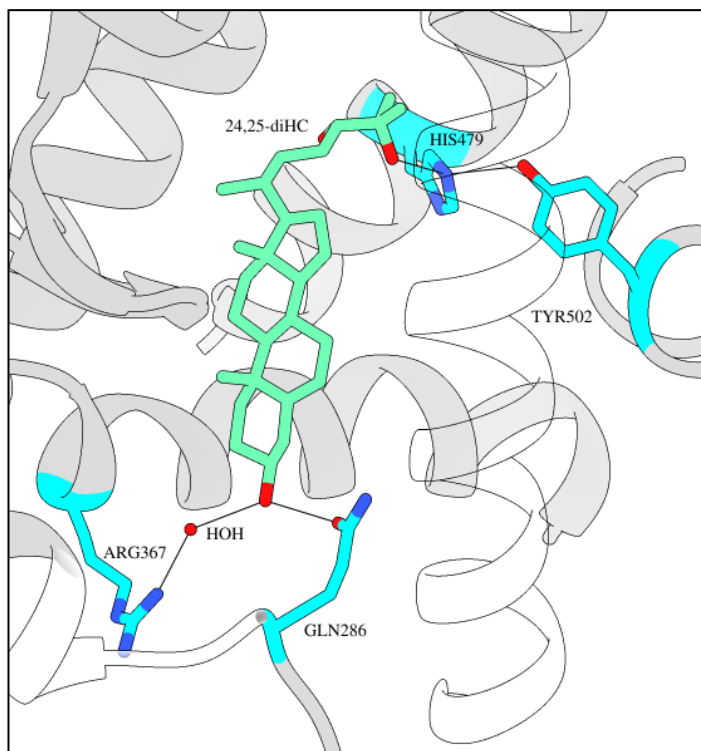


Figure 7.12 24,25-diHC-ROR γ docking simulation with HC9 model. Hydrogen bonding (black) between the 24,25-diHC (green) hydroxyl group at C25, HIS479 and TYR502 stabilises H12 in the active conformation. The 3β -OH group forms a direct hydrogen bond with GLN286 and a solvent bridge to ARG367.

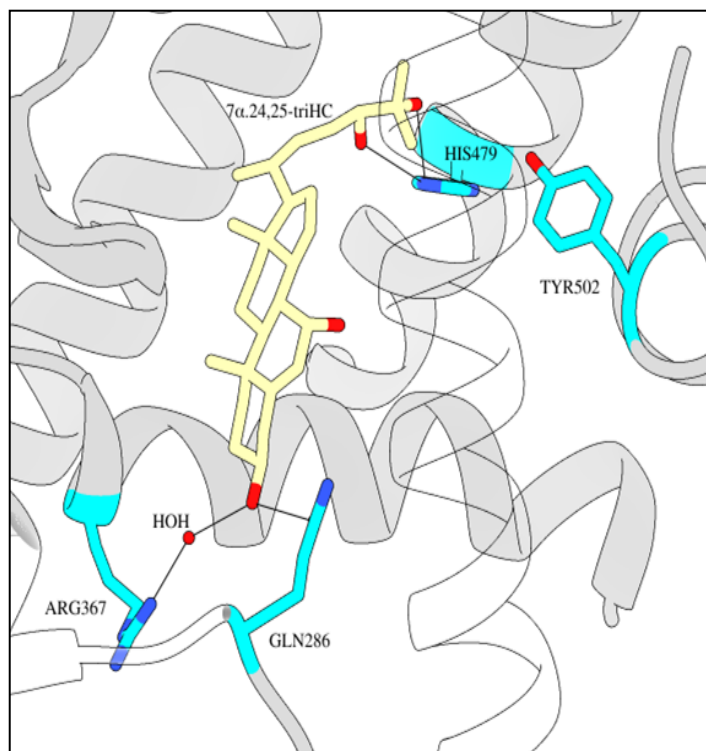


Figure 7.13 $7\alpha,24,25$ -triHC-ROR γ docking simulation with HC9 model. Hydrogen bonding (black) between the $7\alpha,24,25$ -triHC (yellow) hydroxyl group at C25 or C24 with HIS479 positions HIS479 away from TYR502 causing a loss of hydrogen bonding between HIS479 and TYR502. The 3β -OH group forms a direct hydrogen bond with GLN286 and a solvent bridge to ARG367.

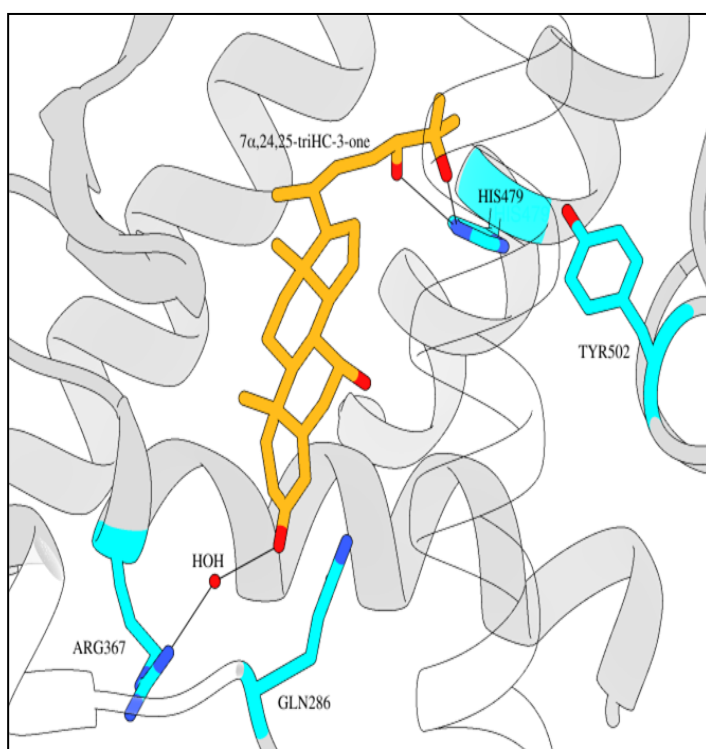


Figure 7.14 $7\alpha,24,25$ -triHC-3-one-ROR γ docking simulation with HC9 model. Hydrogen bonding (black) between the $7\alpha,24,25$ -triHC-3-one (orange) hydroxyl group at C25 or C24 with HIS479 positions HIS479 away from TYR502 causing a loss of hydrogen bonding between HIS479 and TYR502. The 3-oxo group can form a solvent bridge to ARG367 but no hydrogen bond can be formed with GLN286 affecting the position of $7\alpha,24,25$ -triHC-3-one in the LBD .

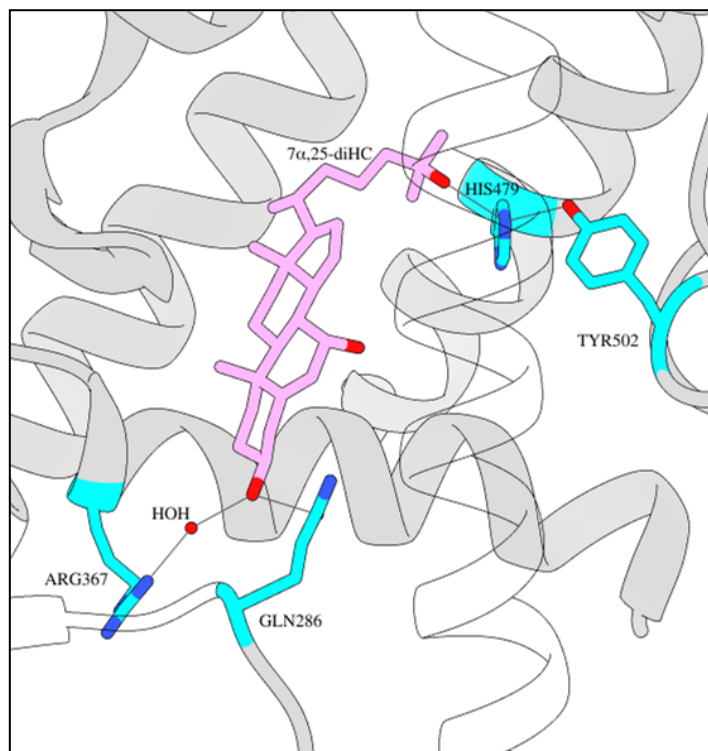


Figure 7.15 $7\alpha,25$ -diHC-ROR γ docking simulation with HC9 model. Hydrogen bonding (black) between the $7\alpha,25$ -diHC (fuchsia) hydroxyl group at C25 with HIS479 and TYR502 stabilises H12 in the active confirmation. The 3β -OH group forms a direct hydrogen bond with GLN286 and a solvent bridge to ARG367.

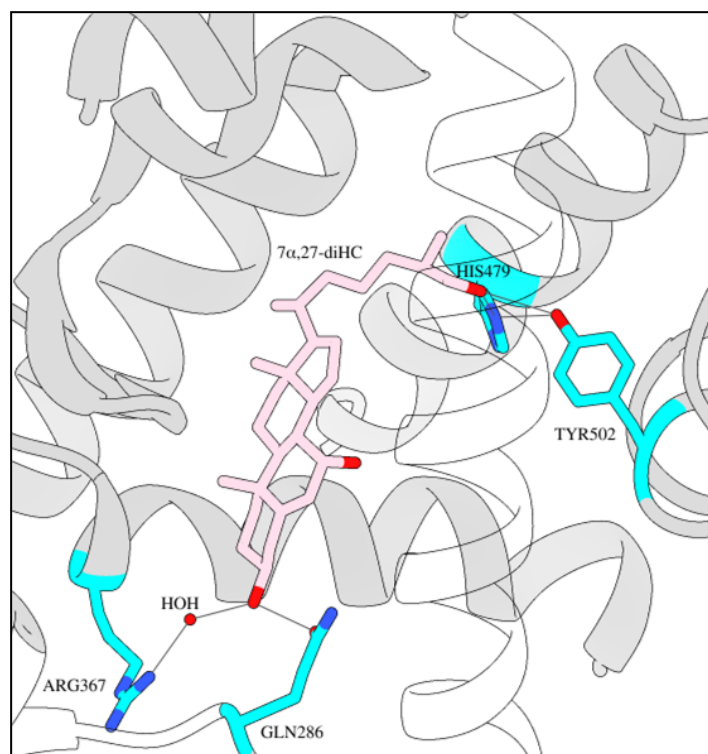


Figure 7.16 $7\alpha,27$ -diHC-ROR γ docking simulation with HC9 model. Hydrogen bonding (black) between the $7\alpha,27$ -diHC (pink) hydroxyl group at C27 with HIS479 or TYR502 stabilises H12 in the active confirmation. The 3β -OH group forms a direct hydrogen bond with GLN286 and a solvent bridge to ARG367.

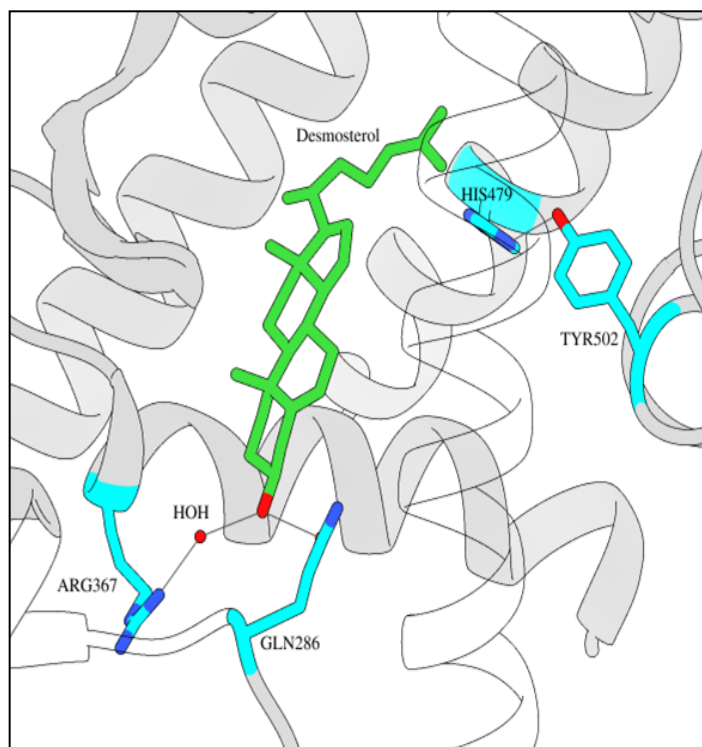


Figure 7.17 Desmosterol-ROR γ docking simulation with HC9 model. When Desmosterol (green) is bound HIS479 is oriented towards TYR502 forming a hydrogen bond (black) which stabilises H12 in the active confirmation. The 3 β -OH group forms a direct hydrogen bond with GLN286 and a solvent bridge to ARG367.

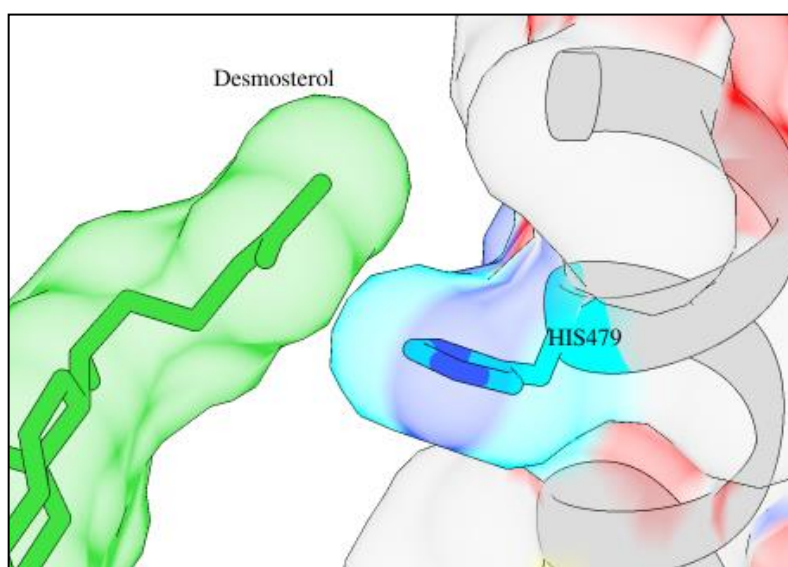


Figure 7.18 Desmosterol-ROR γ docking simulations show the Desmosterol side chain tail is orientated in close proximity towards HIS479 and electrostatic forces positions HIS479 in a favourable pose for H12 stabilisation.

7.3.2 LXR β protein-ligand docking simulations

Previously, crystal structure analysis of the LXR β LBD has revealed a histidine-tryptophan (HIS-TRP) switch in which hydrogen bonds are formed between residues HIS435 and TRP457 to stabilise the AF2 helix within the LBD in the active conformation ⁽¹²⁾. In the crystal structure, 1P8D, HIS435 donates a hydrogen bond to the potent ligand 24(*S*),25-EC enabling the AF2 helix to be stabilised in the active conformation (Figure 7.19). The A-ring of 24(*S*),25-EC orientates towards helix 1 (H1) while the D-ring epoxide tail is positioned towards the C-terminal end of helix 10 (H10) close to the HIS-TRP switch.

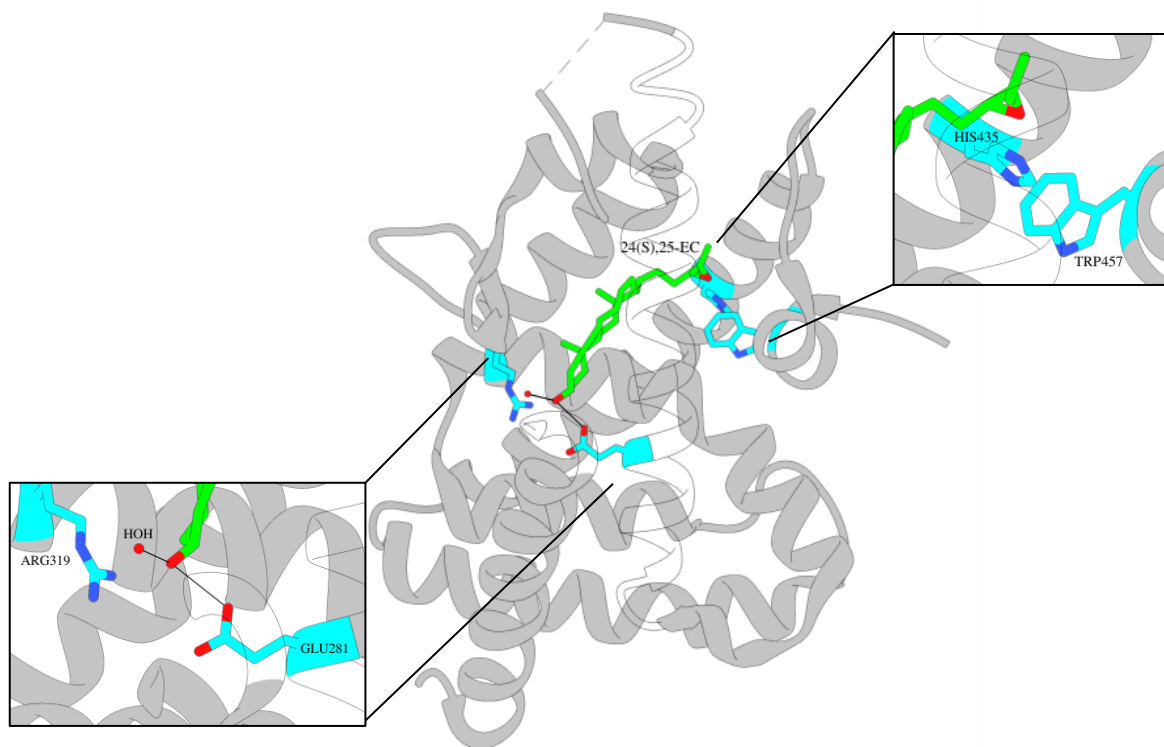


Figure 7.19 LXR β is fixed in an active conformation with 24(*S*),25-EC (green) by stabilisation of the HIS-TRP switch. Electrostatic forces between 24(*S*),25-EC and HIS435 positions HIS435 towards TRP457 and stabilises H12. A hydrogen bond (black) between the 3 β -OH group of 24(*S*),25-EC and GLU281 directs the positioning of 24(*S*),25-EC in the LBD directly or via a solvent bridge. From PDB:1P8D.

Simulations of 24(*S*),25-EC position the hydroxyl group of the sterol A-ring toward H1 forming a hydrogen bond with GLU281 and a hydrogen bond with a water molecule presence in crystal structure (Figure 7.21). These hydrogen bonds and water interaction were also predicted with 7 α ,24(*S*),25-EC and 25-HC docking simulations (Figure 7.22 and Figure 7.20 respectively). This hydrogen bond network is lost with the 3 β -OH conversion to a 3-oxo group in metabolite 7 α ,24(*S*),25-EC-3-one (Figure 7.23) and a considerably reduced binding affinity is reported with the 3-oxo group as predicted in ROR γ docking simulations suggesting this oxysterol is not able to bind with the LBD to give an active conformation (Table 7.4). A hydrogen bond is predicted between HIS435 and the epoxy group of 24(*S*),25-EC fixing the HIS-TRP switch in the active conformation, 7 α ,24(*S*),25-EC docking simulations also predicts stabilisation of the LBD in the active conformation with a hydrogen bond between HIS435 and the epoxy group of 7 α ,24(*S*),25-EC. The 25-HC docking simulation also predicts hydrogen bonding between the hydroxyl group at C25 and HIS435 (Figure 7.20). A possible hydrogen bond with the sidechain residue GLN438 was also predicted providing a strong binding affinity (Table 7.4).

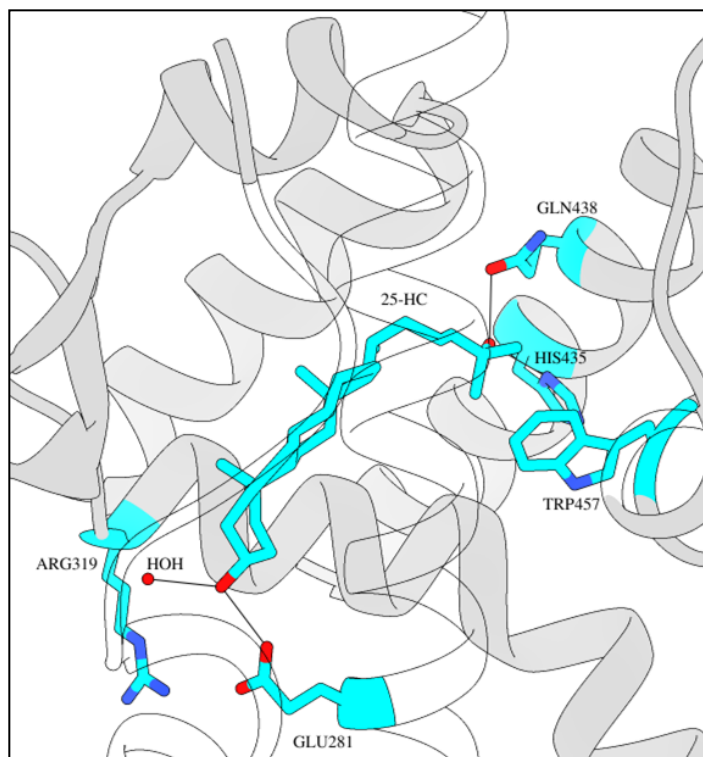


Figure 7.20 25-HC-LXR β docking simulation with CO1 model. The hydroxyl group at C25 of 25-HC (cyan) can form a hydrogen bond with HIS435 or GLN438 stabilising the HIS-TRP switch. A hydrogen bond (black) between the 3 β hydroxyl group of 25-HC and GLU281 directs the positioning of 25-HC in the LBD directly or via a solvent bridge.

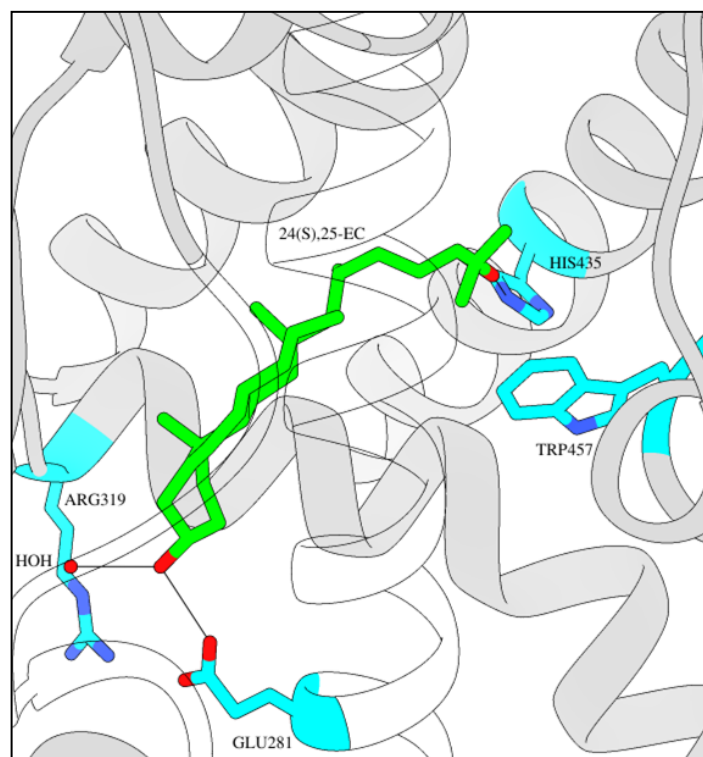


Figure 7.21 24(*S*),25-EC-LXR β docking simulation with CO1 model. LXR β is fixed in an active conformation with 24(*S*),25-EC (green) by stabilisation of the HIS-TRP switch. A hydrogen bond (black) is found between the epoxy group and HIS435 positioning HIS435 towards TRP457 to stabilise H12. A hydrogen bond (black) between the 3 β -OH group of 24(*S*),25-EC and GLU281 directs the positioning of 24(*S*),25-EC in the LBD directly or via a solvent bridge.

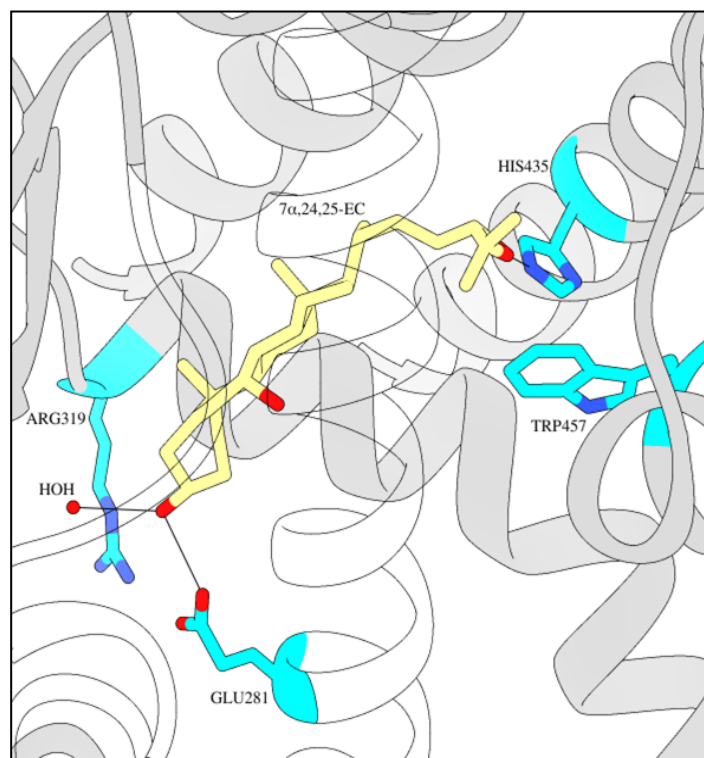


Figure 7.22 $7\alpha,24(S),25\text{-EC-LXR}\beta$ docking simulation with CO1 model. LXR β is fixed in an active conformation with $7\alpha,24(S),25\text{-EC}$ (yellow) by stabilisation of the HIS-TRP switch. A hydrogen bond (black) is found between the epoxy group and HIS435 positioning HIS435 towards TRP457 to stabilise H12. A hydrogen bond (black) between the $3\beta\text{-OH}$ group of $7\alpha,24(S),25\text{-EC}$ and GLU281 directs the positioning of $7\alpha,24(S),25\text{-EC}$ in the LBD directly or via a solvent bridge.

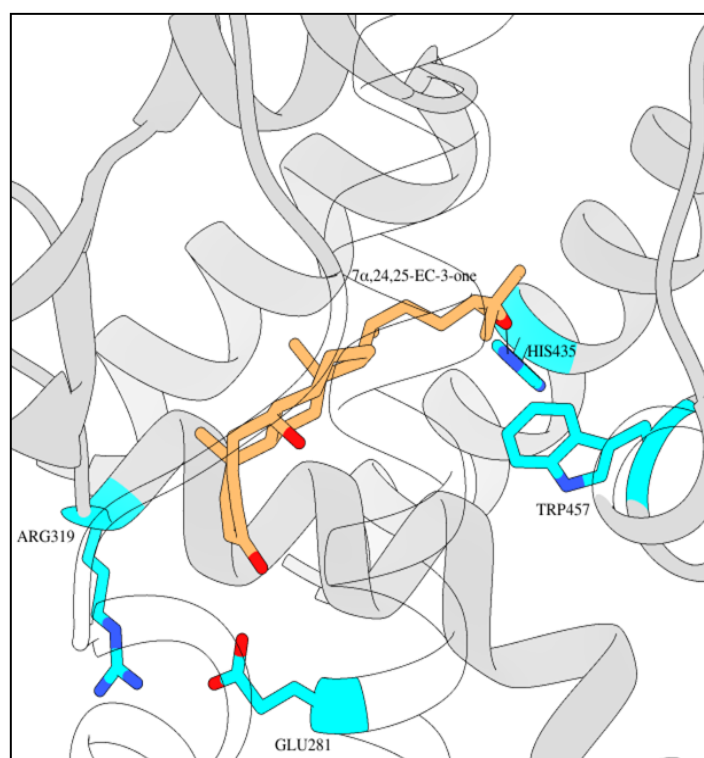


Figure 7.23 $7\alpha,24(S),25\text{-EC-3-one-LXR}\beta$ docking simulation with CO1 model. The epoxy group of $7\alpha,24(S),25\text{-EC-3-one}$ (orange) can form a hydrogen bond with HIS435 but no hydrogen bond can be formed between GLU281 and the 3-oxo group and $7\alpha,24(S),25\text{-EC-3-one}$ cannot stabilise the HIS-TRP switch.

As with the ROR γ model further docking simulations were performed with the hydroxyl forms of these oxysterols 24,25-diHC, 7 α ,24,25-triHC and 7 α ,24,25-triHC-3-one in addition to CYP7B1 metabolites 7 α ,25-diHC and 7 α ,27-diHC and cholesterol precursor, desmosterol. 24,25-diHC bound LXR β simulations predict the stabilisation of H12 through the HIS-TRP switch (Figure 7.24). The sterol 3 β -OH of 24,25-diHC forms a hydrogen bond with GLU281 typically seen with oxysterol dockings. A solvent bridge is predicted through hydrogen bonds between the 3 β -OH and a water molecule, present in the crystal structure of LXR β LBD hydrogen bonded with ARG319 on helix 5 (H5). The hydroxyl group at C24 is predicted to hydrogen bond with HIS435 however a hydrogen bond is also possible with side chain residue GL438 on helix 11 (H11) which results in a strong binding affinity (Table 7.4). The 7 α ,24,25-triHC docking simulations predicted the same binding mechanism as 24,25-diHC (Figure 7.25) however when 3 β -OH is converted to a 3-oxo group as with 7 α ,24,25-triHC-3-one, hydrogen bonding cannot be formed with GLU281 resulting in a reduced binding affinity (Figure 7.26). Although hydrogen bonding between the hydroxyl group at C24 with HIS435 or GLN438 could be possible it is anticipated that the 3-oxo group prevents 7 α ,24,25-triHC-3-one binding within the LXR β LBD as predicted with ROR γ .

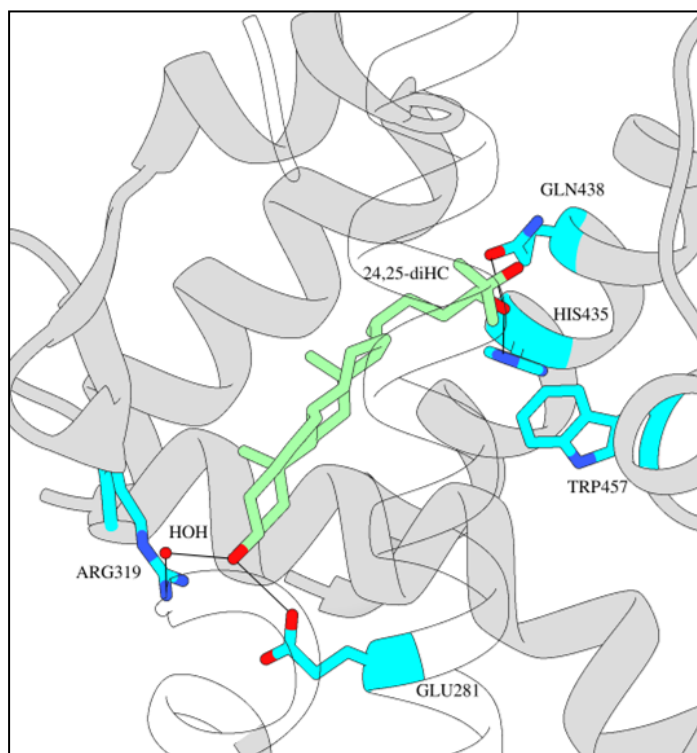


Figure 7.24 24,25-diHC-LXR β docking simulation with CO1 model. LXR β is fixed in an active conformation with 24,25-diHC (green) by stabilisation of the HIS-TRP switch. A hydrogen bond (black) is found between the hydroxyl group at C24 and GLN438 or HIS435 which positions HIS435 towards TRP457 stabilising H12. A hydrogen bond (black) between the 3 β -OH group of 24,25-diHC and GLU281 directs the positioning of 24,25-diHC in the LBD directly or via a solvent bridge to ARG319.

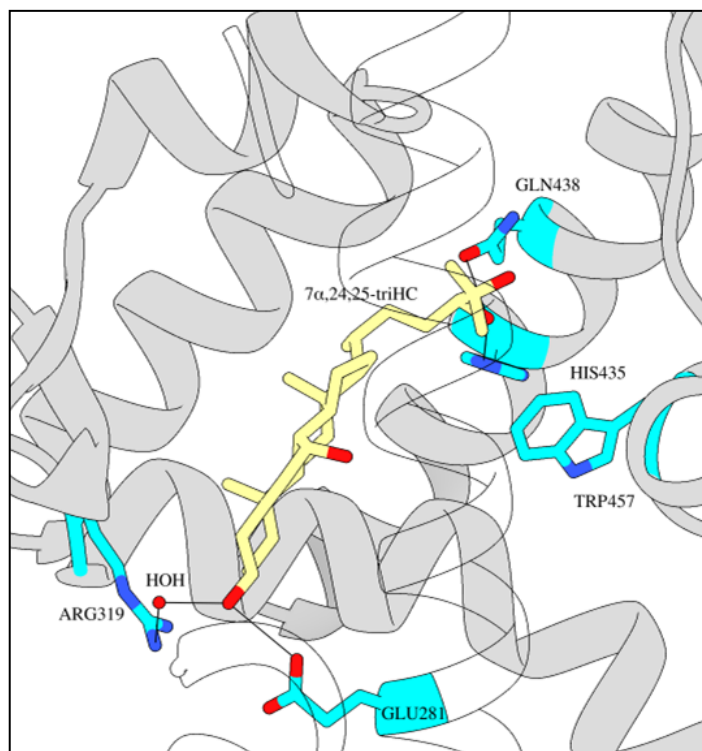


Figure 7.25 7 α ,24,25-triHC-LXR β docking simulation with CO1 model. LXR β is fixed in an active conformation with 7 α ,24,25-triHC (yellow) by stabilisation of the HIS-TRP switch. A hydrogen bond (black) is found between the hydroxyl group at C24 and GLN438 or HIS435 which positions HIS435 towards TRP457 stabilising H12. A hydrogen bond (black) between the 3 β -OH group of 7 α ,24,25-triHC and GLU281 directs the positioning of 7 α ,24,25-triHC in the LBD directly or via a solvent bridge to ARG319.

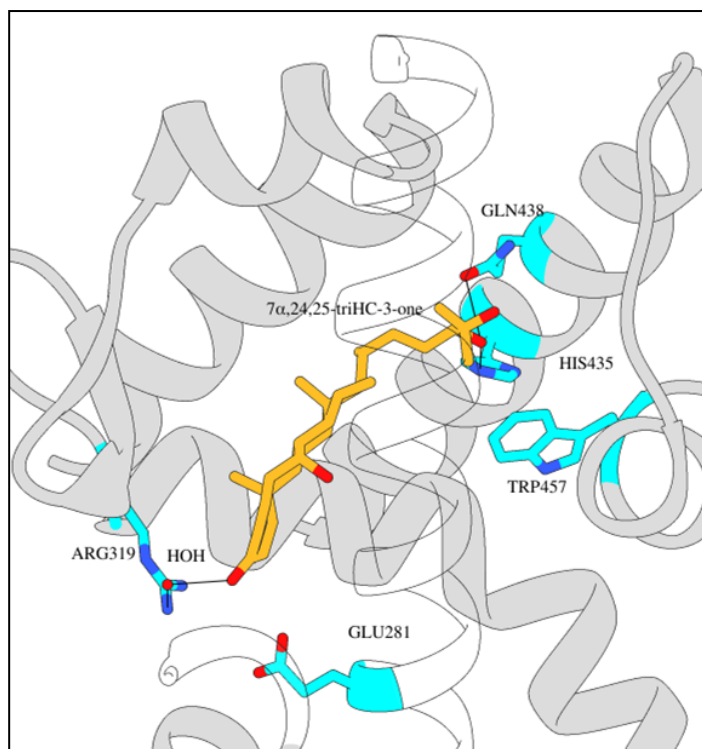


Figure 7.26 7 α ,24,25-triHC-3-one-LXR β docking simulation with CO1 model. A hydrogen bond (black) is found between the 7 α ,24,25-triHC-3-one (orange) hydroxyl group at C24 and GLN438 or HIS435 which positions HIS435 towards TRP457. The 3-oxo group can form a solvent bridge to ARG319 but no hydrogen bond can be formed with GLN281 affecting the position of 7 α ,24,25-triHC-3-one in the LBD and the HIS-TRP switch cannot be stabilised.

CYP7B1 metabolites $7\alpha,25$ -diHC and $7\alpha,27$ -diHC were also predicted to stabilise H12 in the active conformation. The C25 hydroxyl group of $7\alpha,25$ -diHC has the potential to hydrogen bond with GLN438 while HIS435 is positioned towards TRP457 with electrostatic forces stabilising the HIS-TRP switch (Figure 7.27). $7\alpha,27$ -diHC like $7\alpha,25$ -diHC can form a hydrogen bond between GLN438 and the hydroxyl group at C27 (Figure 7.28). Hydrogen bonding of the C27 hydroxyl group with HIS435 is also possible with $7\alpha,27$ -diHC.

Docking simulations with cholesterol precursor Desmosterol predict agonist activity towards LXR β with similar binding affinity to oxysterols in this study but reduced histidine stability (Table 7.4). Although desmosterol has no sidechain tail hydroxyl group it is predicted to stabilise the HIS-TRP switch of LXR β (Figure 7.29). As with the ROR γ model, when desmosterol is bound the histidine residue is positioned in the agonist pose so as to enable HIS435 and TRP457 interaction and stabilisation of H12.

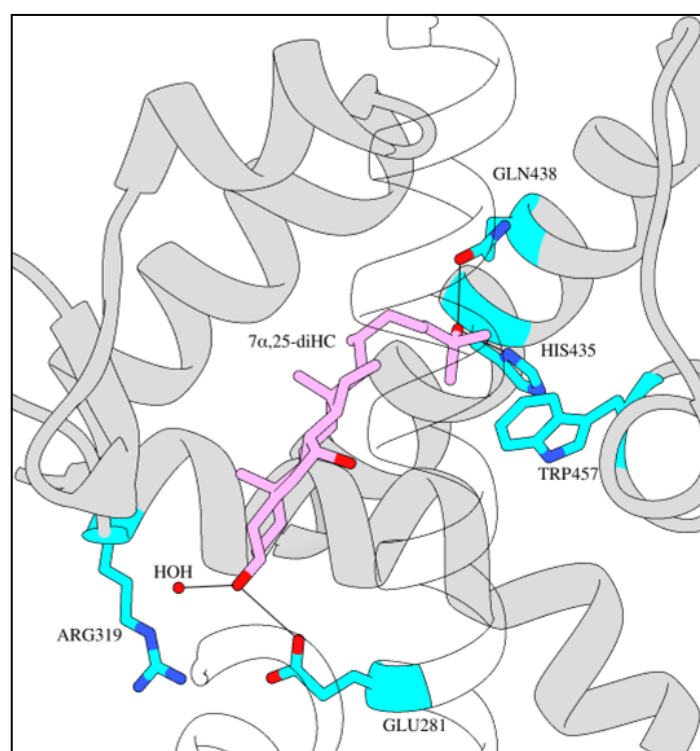


Figure 7.27 $7\alpha,25$ -diHC-LXR β docking simulation with CO1 model. LXR β is fixed in an active conformation with $7\alpha,25$ -diHC (fuchsia) by stabilisation of the HIS-TRP switch. A hydrogen bond (black) is found between the hydroxyl group at C25 and GLN438, HIS435 is positioned towards TRP457 stabilising H12. A hydrogen bond (black) between the 3β hydroxyl group of $7\alpha,25$ -diHC and GLU281 directs the positioning of $7\alpha,25$ -diHC in the LBD.

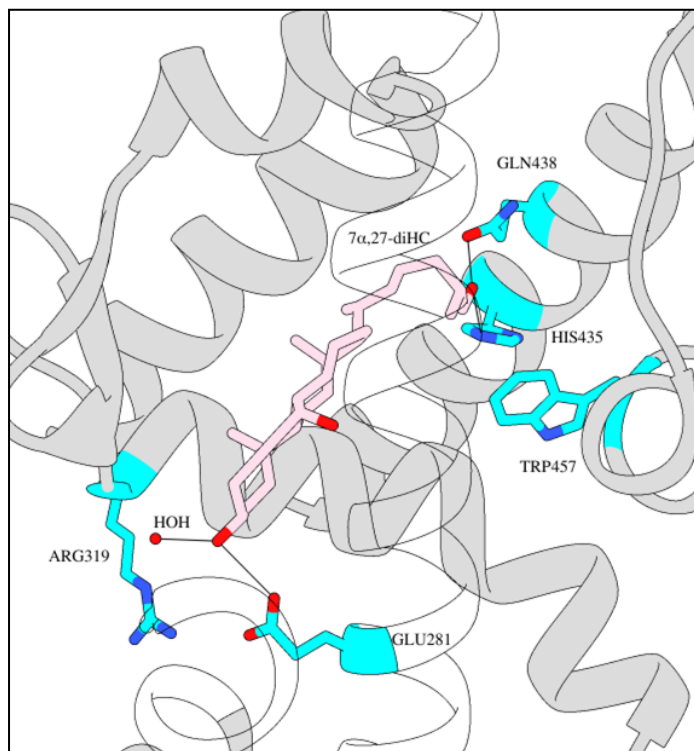


Figure 7.28 $7\alpha,27$ -diHC-LXR β docking simulation with CO1 model. LXR β is fixed in an active conformation with $7\alpha,27$ -diHC (pink) by stabilisation of the HIS-TRP switch. A hydrogen bond (black) is found between the hydroxyl group at C27 and GLN438 or HIS435, positioning HIS435 towards TRP457 stabilising H12. A hydrogen bond (black) between the 3β hydroxyl group of $7\alpha,27$ -diHC and GLU281 directs the positioning of $7\alpha,27$ -diHC in the LBD.

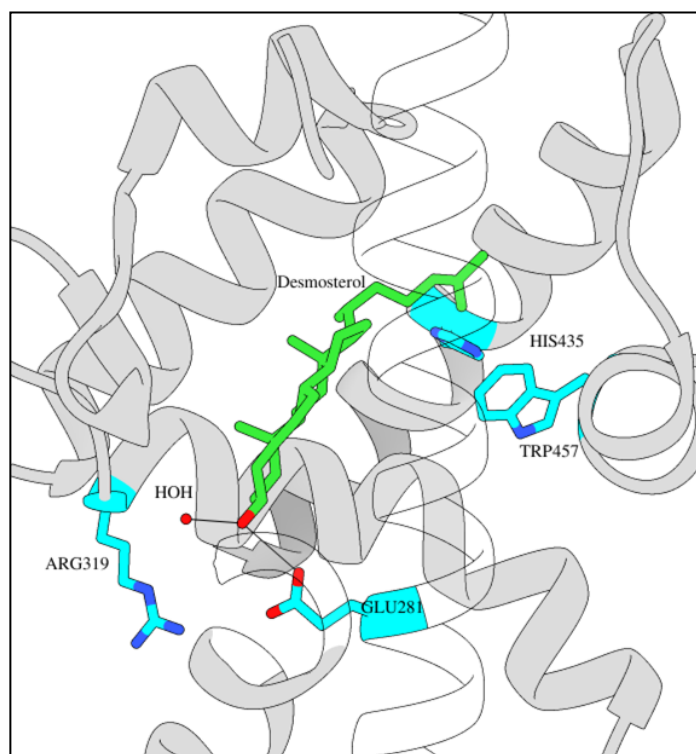


Figure 7.29 Desmosterol-LXR β docking simulation with CO1 model. When desmosterol (green) is bound HIS435 is oriented towards TRP457 and stabilises H12 in the active confirmation. The 3 β -OH group forms a direct hydrogen bond with GLU281 and solvent interaction.

Table 7.4 Binding affinities of sterol ligands for LXR β LBD.

Ligand	HIS435 score	Ligand score
25-HC	-7.2585	-65.1445
24(<i>S</i>),25-EC	-5.8336	-64.2133
7 α ,24(<i>S</i>),25-EC	-5.8265	-63.8526
7 α ,24(<i>S</i>),25-EC-3-one	-6.0368	-40.1113
24,25-diHC	-5.746	-121.759
7 α ,24,25-triHC	-5.722	-119.847
7 α ,24,25triHC-3-one	-5.684	-66.776
7 α ,25-diHC	-7.295	-117.032
7 α ,27-diHC	-5.221	-115.278
Desmosterol	-1.286	-115.755

7.4 Discussion

Oxysterols have previously been identified as ROR γ t ligands with agonist and inverse agonist activity ^(2,6). These oxysterols are structurally similar including structural isomers but can have opposing activity towards ROR γ , therefore the focus of this chapter was to investigate the mechanism by which an oxysterol can stabilise the LBD of ROR γ t in an active conformation.

20 α -HC, 22(*R*)-HC and 25-HC have been reported to act as ROR γ t agonist ⁽²⁾. The binding mode of these oxysterols in the ROR γ pocket was established through crystal structures which revealed hydrogen bonding between important side chain residues HIS479 and TYR502 within the LBD which stabilised the AF2 helix (H12) in the active conformation. The co-crystallised structures of 25-HC bound ROR γ (PDB:3L0L) and 22(*R*)-HC bound ROR γ PDB:3L0J also revealed a water molecule present in the crystal structures which interacts with the sterol A ring to form a solvent bridge with side chain residues GLN286 and ARG367. Docking simulations of 25-HC were able to reproduce the hydrogen bond network seen in the crystal structure of 25-HC bound ROR γ validating the model produced in this chapter.

Cholesterol precursor desmosterol has previously been identified as a potential ROR γ t agonist ⁽⁴⁾. Docking simulation in this study predict agonist activity for desmosterol with a strong binding affinity however it showed the weakest histidine stability score of -2.243 (Table 7.3). 7 α ,27-diHC and 7 β ,27-diHC have been reported to increase IL-17 producing cells in mice studies while 7 α ,25-diHC is an endogenous ligand of the G-protein coupled receptor EB12 ^(3,23-24). Docking simulations with 7 α ,27-diHC and 7 α ,25-HC predict agonist activity with strong binding affinity and histidine stability however while these oxysterols have been reported to act as ROR γ ligands, mass spectrometry analysis revealed no detectable levels of these oxysterols in nCD4⁺ T cell cultures under Th17 polarising conditions (*Chapter 4*).

Known LXR β agonist 24(*S*),25-EC has reported inverse agonist activity towards ROR γ ⁽⁶⁾. 24(*S*),25-EC and downstream metabolite 7 α ,24(*S*),25-EC can be detected by mass spectrometry as 24,25-diHC and 7 α ,24,25-triHC respectively from *in vitro* nCD4⁺ T cell cultures under Th17 polarising conditions (*Chapter 4*). Chapter 6 discussed the possibility of a pathway in which the activity of 24(*S*),25-EC is

deactivated through the combined activity of CYP7B1 and HSD3B7. This Chapter demonstrates the mechanism in which sterol interaction in a hydrogen network coordinates the binding of sterols in the LBD and orientates the sterols towards key side chain residues important for the stabilisation of the AF2 helix.

ROR γ docking simulations show the interaction of sterols in a hydrogen network through the 3 β -OH group with GLN286 and ARG367 provides a strong binding affinity. Oxysterols which have a 3-oxo group in place of the 3 β -OH group lose the ability to coordinate this network which results in a reduced binding affinity. This supports the hypothesis that metabolism of oxysterol 24(S),25-EC through CYP7B1 and HSD3B7 leads to the loss of activity towards ROR γ t. This has been demonstrated with G-protein coupled receptor (GPCR) EBI2 with oxysterol ligands ⁽²⁵⁾. 7 α ,25-diHC and 7 α ,27-diHC are reported to bind to EBI2 with the 3 β -OH group interacting with side chain residue GLU183 in the LBD but inactivity was reported with 7 α ,27-diHC-3-one in which the 3 β -OH group is replaced with a 3-oxo group which suggests the 3 β -OH group is important for agonist activity.

Stabilisation of the AF2 helix is reached through hydrogen bonding between hydroxyl groups on the oxysterol tail with HIS479 which orientates HIS479 in an optimal pose for hydrogen bonding with TYR502 on H12. 24(S),25-EC is unable to position HIS479 so as to enable hydrogen bonding with TYR502 which destabilises H12, however docking simulations show 24,25-diHC is able to stabilise H12 in the active conformation. Chapter 6 investigates the effect of oxysterols including 24(S),25-EC on CD4⁺ T cells *in vitro*. 24(S),25-EC showed no inverse agonist activity towards ROR γ with no downregulation of *IL17* mRNA detected however due to the labile nature of the epoxy group it is possible that conversion to 24,25-diHC occurred during cell culture which is not predicted to be an inverse agonist.

The LXR β model predicts a similar binding mechanism of sterols within the LBD. As expected known LXR β ligand 24(S),25-EC was shown to have agonist activity towards LXR β . Downstream metabolite 7 α ,24(S),25-EC was also shown to be an LXR β agonist however this activity was lost with further metabolised oxysterol 7 α ,24(S),25-EC-3-one in which the 3 β hydroxyl group is converted to a 3-oxo group. *In silico* modelling of these ligand-protein interactions reveal the mechanism in which these oxysterols bind to the LBD and holds the protein in an active

conformation. 24(*S*),25-EC and 7 α ,24(*S*),25-EC are able to create a hydrogen bond with side chain residue HIS435 positioning HIS435 towards TRP457 enabling electrostatic forces to stabilise the HIS-TRP switch. As seen with ROR γ and other oxysterol receptors, when the oxysterols are metabolised by HSD3B7 the 3 β -OH group conversion to a 3-oxo group leads to a loss of activity of these oxysterols ⁽²⁴⁾. *In silico* modelling of these interactions shows the 3 β -OH group is important for positioning the ligand in the LBD. The 3 β -OH group forms a hydrogen bond with side chain residue GLU218 which holds the ligand in a position which allows the ligand sidechain interaction with HIS435. When the 3-oxo group is present no hydrogen bond is formed and therefore the ligand is unable to bind in an active conformation.

24,25-diHC and 7 α ,24,25-triHC were predicted to have agonist activity towards LXR β with strong binding affinity and histidine stability score (Table 7.4). Hydrogen bonding between the hydroxyl group at C24 is predicted with side chain residues GLN438 and HIS435 contributes to the relative stronger binding affinity scores. 7 α ,25-diHC and 7 α ,27-diHC were also predicted to bind to LXR β in the agonist conformation with similar binding affinities. Desmosterol docking simulations demonstrated agonist binding in LXR β with a reduced histidine stability score as seen with the ROR γ model.

7.5 References

1. Ivanov I. I., McKenzie B. S., Zhou L., Tadokoro C. E., Lepelley A., Lafaille J. J., et al. (2006). The orphan nuclear receptor ROR γ t directs the differentiation program of proinflammatory IL-17+ T helper cells. *Cell* 126, 1121–1133. doi: 10.1016/j.cell.2006.07.035
2. Jin L., Martynowski D., Zheng S., Wada T., Xie W., Li Y. (2010) Structural Basis for Hydroxycholesterols as Natural Ligands of Orphan Nuclear Receptor ROR γ . *Molecular Endocrinology*, 24(5), 923-929. Doi:10.1210/me.2009-0507
3. Soroosh P., Wu J., Xue X., Song J., Sutton S. W., Sablad M., Yu J., Nelen M. I., Liu X., Castro G., Luna R., Crawford S., Banie H., Dandridge R. A., Deng X., Bittner A., Kuei C., Tootoonchi M., Rozenkrants N., Herman K., Gao J., Yang X. V., Sachen K., Ngo K., Fung-Leung W. P., Nguyen S., de Leon-Tabaldo A., Blevitt J., Zhang Y., Cummings M. D., Rao T., Mani N. S., Liu C., McKinnon M., Milla M. E., Fourie A. M., Sun S. (2014) Oxysterols are agonist ligands of ROR γ t and drive Th17 cell differentiation. *Proc. Natl. Acad. Sci. U. S. A.* 111, 12163–12168.
4. Hu X., Wang Y., Hao L.-Y., Liu X., Lesch C. A., Sanchez B. M., Wendling J. M., Morgan R. W., Aicher, T. D., Carter L. L., Toogood P. L., Glick G. D. (2015) Sterol metabolism controls TH17 differentiation by generating endogenous ROR γ agonists. *Nat. Chem. Biol.* 11, 141–147.
5. Solt, L. A., Garcia-Ordóñez, R. D., Helvering, L. M., Burris, T. P., Wang, Y., Kumar, N., ... Zhang, X. (2009). Modulation of Retinoic Acid Receptor-related Orphan Receptor α and γ Activity by 7-Oxygenated Sterol Ligands. *Journal of Biological Chemistry*, 285(7), 5013–5025. <https://doi.org/10.1074/jbc.m109.080614>
6. Wang, Y., Kumar, N., Crumbley, C., Griffin, P. R., & Burris, T. P. (2010). A second class of nuclear receptors for oxysterols: Regulation of ROR α and ROR γ activity by 24S-hydroxycholesterol (cerebrosterol). *Biochimica et Biophysica Acta - Molecular and Cell Biology of Lipids*. <https://doi.org/10.1016/j.bbalip.2010.02.012>
7. Hamill SJ, Cota E, Chothia C, Clarke J. Conservation of folding and stability within a protein family: the tyrosine corner as an evolutionary cul-de-sac. *J Mol Biol.* 2000 Jan 21;295(3):641-9. doi: 10.1006/jmbi.1999.3360. PMID: 10623553.

8. Pagadala, N. S., Syed, K., & Tuszynski, J. (2017). Software for molecular docking: a review. *Biophysical Reviews*, 9(2), 91–102.
<http://doi.org/10.1007/s12551-016-0247-1>
9. Consortium, T. U. (2019). UniProt : a worldwide hub of protein knowledge, 47(November 2018), 506–515. <https://doi.org/10.1093/nar/gky1049>.
10. Berman, H. M., Westbrook, J., Feng, Z., Gilliland, G., Bhat, T. N., Weissig, H., ... Bourne, P. E. (2000). The Protein Data Bank Helen. *Nucleic Acids Research*, 28(1), 235–242. <https://doi.org/10.1093/nar/28.1.235>
11. Katoh, K., Misawa, K., Kuma, K., & Miyata, T. (2002). MAFFT: a novel method for rapid multiple sequence alignment based on fast Fourier transform, 30(14), 3059–3066. <https://doi.org/10.1093/nar/gkf436>
12. Williams, S., Bledsoe, R. K., Collins, J. L., Boggs, S., Lambert, M. H., Miller, A. B., ... Willson, T. M. (2003). X-ray crystal structure of the liver X receptor β ligand binding domain: Regulation by a histidine-tryptophan switch. *Journal of Biological Chemistry*, 278(29), 27138–27143.
<http://doi.org/10.1074/jbc.M302260200>
13. Mortier, W. J.; Ghosh, S. K.; Shankar, S. J. Electronegativity Equalization Method for the Calculation of Atomic Charges in Molecules. *Am. Chem. Soc.* **1986**, 108, 4315-4320.
14. Ionescu, Crina-Maria; Geidl, Stanislav; Svobodová Vařeková, Radka; Koča, Jaroslav J. Rapid Calculation of Accurate Atomic Charges for Proteins via the Electronegativity Equalization Method. *Chem. Inf. Model* **2013**, 53, 2548-2558.
15. Ionescu, Crina-Maria; Sehnal, David; Falginella, Francesco L.; Pant, Purbaj; Pravda, Lukáš Bouchal, Tomáš Svobodová Vařeková, Radka; Geidl, Stanislav; Koča, Jaroslav J. Atomic Charge Calculator: interactive web-based calculation of atomic charges in large biomolecular complexes and drug-like molecules. *Cheminform* **2015**, 7, 50-62.
16. Kawabata, T., & Nakamura, H. (2014). 3D Flexible Alignment Using 2D Maximum Common Substructure: Dependence of Prediction Accuracy on Target-Reference Chemical Similarity. <https://doi.org/10.1021/ci500006d>
17. Korb O., Stützle T., Exner T.E. (2006) PLANTS: Application of Ant Colony Optimization to Structure-Based Drug Design. In: Dorigo M., Gambardella L.M., Birattari M., Martinoli A., Poli R., Stützle T. (eds) Ant Colony Optimization and

Swarm Intelligence. ANTS 2006. Lecture Notes in Computer Science, vol 4150. Springer, Berlin, Heidelberg.

18. Korb, O., Stützle, T., & Exner, T. E. (2009). Empirical scoring functions for advanced Protein-Ligand docking with PLANTS. *Journal of Chemical Information and Modeling*, 49(1), 84–96. <https://doi.org/10.1021/ci800298z>
19. Pettersen, E. F., Goddard, T. D., Huang, C. C., Couch, G. S., Greenblatt, D. M., Meng, E. C., & Ferrin, T. E. (2004). UCSF Chimera - A visualization system for exploratory research and analysis. *Journal of Computational Chemistry*, 25(13), 1605–1612. <https://doi.org/10.1002/jcc.20084>
20. Jetten, A. M., Takeda, Y., Slominski, A., Kang, H. S., Section, B., Sciences, E. H., ... Program, C. (2018). Retinoic acid-related Orphan Receptor γ (ROR γ): connecting sterol metabolism to regulation of the immune system and autoimmune disease. *Curr Opin Toxicol*, 8, 66–80.
<https://doi.org/10.1016/j.cotox.2018.01.005> Retinoic
21. Sun, N., Yuan, C., Ma, X., Wang, Y., Gu, X., & Fu, W. (2018). Molecular Mechanism of Action of ROR γ t Agonists and Inverse Agonists : Insights from Molecular Dynamics Simulation. *Molecules*, 23(12), 3181.
<https://doi.org/10.3390/molecules23123181>
22. Li, Y., Lambert, M. H., & Xu, H. E. (2003). Activation of Nuclear Receptors: A Perspective from Structural Genomics. *Structure*, 11(7), 741–746.
[https://doi.org/10.1016/s0969-2126\(03\)00133-3](https://doi.org/10.1016/s0969-2126(03)00133-3)
23. Hannedouche, S., Zhang, J., Yi, T., Shen, W., Nguyen, D., Pereira, J. P., ... Sailer, A. W. (2011). Oxysterols direct immune cell migration via EBI2. *Nature*, 475(7357), 524–527. <https://doi.org/10.1038/nature10280>
24. Liu, C., Yang, X. V, Wu, J., Kuei, C., Mani, N. S., Zhang, L., ... Lovenberg, T. W. (2011). Oxysterols direct B-cell migration through EBI2. *Nature*, 3–9.
<https://doi.org/10.1038/nature10226>
25. Zhang, L., Shih, A. Y., Yang, X. V, Kuei, C., Wu, J., Deng, X., ... Lovenberg, T. W. (2012). Identification of Structural Motifs Critical for Epstein-Barr Virus- Induced Molecule 2 Function and Homology Modeling of the Ligand Docking Site □. *Molecular Pharmacology*, 82(6), 1094–1103.
<https://doi.org/10.1124/mol.112.080275>

Chapter 8. General Discussion

The role of T helper cell subset Th17 and the Th17 signature cytokine IL-17 in autoimmune diseases such as rheumatoid arthritis (RA), multiple sclerosis (MS) and psoriasis is becoming increasingly evident⁽¹⁻⁴⁾. Previous studies have identified intermediates of cholesterol biosynthesis and oxysterol metabolites as potential ligands of Th17 cells master transcription factor ROR γ t however there is still uncertainty over the endogenous ligand which drives ROR γ t activity^(5,6). The studies described here investigated 24(S),25-EC and downstream metabolites which are endogenously present in CD4⁺ T cells, specifically focussing on the Th17 subset and their potential role as ROR γ t ligands.

Chapter 3 focussed on method development for free and total oxysterol analysis of cell pellet and cell culture media through alkaline hydrolysis with enzyme-assisted derivatisation and high performance liquid chromatography coupled mass spectrometry. This enabled analysis of total sterols present in the cell pellets and cell culture media of neonatal naïve CD4⁺ T cells for comparison of free and sterol sterols.

Enzyme-assisted derivatisation with high performance liquid chromatography coupled with mass spectrometry was utilised to investigate the inhibitory effect of azole compounds, specifically clotrimazole, towards CYP7B1 in activated Th17 cell culture media in Chapter 4. The study of IL-17 inhibition with clotrimazole confirmed inhibition of CYP7B1 activity in Th17 polarised CD4⁺ T cells. This has previously been contributed to the inhibition of CYP51 with cholesterol precursors upstream of CYP51 proposed as potential ligands of ROR γ t⁽⁸⁾. However further technical and biological replicates would be required to determine the true mechanism in which azole drugs inhibit IL-17 expression in Th17 cells.

Chapter 5 investigated the effect of CYP7B1 inhibition in murine nCD4⁺ T cells through *Cyp7b1*^{-/-} mice. This revealed loss of CYP7B1 activity reduced *Il17a* expression in KO mice, however qRT-PCR analysis revealed no detectable expression of *Cyp7b1* mRNA. The potential of the EL4 cell line in the study of ROR γ and IL-17 expression was also investigated in this chapter. While activated EL4 cells resulted in upregulation of *Il17* expression it was not possible to reproduce previous results with known ROR γ t inhibitions with these cells. LC-MS analysis

revealed quantifiable levels of 22(*R*)-HC which has also been reported to have agonistic activity towards ROR γ t but is not detected in human CD4⁺ T cells⁽⁷⁾. LC-MS analysis also showed lower levels of 24(*S*),25-EC in the primary murine CD4⁺ T cells which suggest there are possible differences in the roles of oxysterol in human and murine immune responses. Therefore, a human cell line would be a more advantageous for the study of oxysterol ligands of ROR γ t.

Chapter 6 investigated the role of LXR agonist and proposed ROR γ t inverse agonist 24(*S*),25-EC and downstream metabolites in CD4⁺ T cells⁽⁵⁾. These studies expands the understanding of the deactivation pathway of 24(*S*),25-EC in CD4⁺ T cells in which the activity of both CYP7B1 and HSD3B7 is required to deactivate 24(*S*),25-EC.

Chapter 7 *in silico* modelling was utilised to investigate the mechanism by which oxysterols may be agonists or inverse agonists of nuclear hormone transcription factors ROR γ t and LXR β . Protein-ligand docking simulations revealed the importance of histidine stabilisation for active conformation of the LBD of these transcription factors and shows how oxysterol isomers can have differing ligand activity within the binding domains of nuclear receptors LXR β and ROR γ t. This has provided a greater understanding of the important moieties for ROR γ t and LXR β binding in an active conformation. A complementary study with a ROR γ t reporter assay would provide confirmation of agonist and inverse agonist ligand activity for these oxysterols.

To further advance understanding of oxysterol ligands for ROR γ t in Th17 cells and IL-17 production, a future study of the affect of oxysterol treatments to CD4⁺ T cells from patients with an autoimmune diseases in which IL-17 expression is elevated would be advantageous. Oxysterol analysis of the endogenous oxysterol presents in these CD4⁺ T cells may also identify oxysterols with a role in the pathogenesis of these autoimmune diseases.

References

1. Ferber, I. A., Brocke, S., Taylor-Edwards, C., Ridgway, W., Dinisco, C., Steinman, L., Dalton, D., Farhman, C. G. (1996). Mice with a disrupted IFN-gamma gene are susceptible to the induction of experimental autoimmune encephalomyelitis (EAE). *J Immunol.* 156(1): 5-7
2. Komiyama Y., Nakae S., Matsuki T., et al. (2006) IL-17 plays an important role in the development of experimental autoimmune encephalomyelitis. *Journal of Immunology.* 177(1):566–573
3. Tang, L., Yang, X., Liang, Y., Xie, H., Dai, Z., & Zheng, G. (2018). Transcription factor retinoid-related orphan receptor γ t: A promising target for the treatment of psoriasis. *Frontiers in Immunology*, 9(MAY).
<https://doi.org/10.3389/fimmu.2018.01210>
4. Kotake, S., Udagawa, N., Takahashi, N., Matsuzaki, K., Itoh, K., Ishiyama, S., ... Suda, T. (1999). IL-17 in synovial fluids from patients with rheumatoid arthritis is a potent stimulator of osteoclastogenesis. *Journal of Clinical Investigation*, 103(9), 1345–1352.
5. Wang, Y., Kumar, N., Crumbley, C., Griffin, P. R., & Burris, T. P. (2010). A second class of nuclear receptors for oxysterols: Regulation of ROR α and ROR γ activity by 24S-hydroxycholesterol (cerebrosterol). *Biochimica et Biophysica Acta - Molecular and Cell Biology of Lipids*, 917–923.
<https://doi.org/10.1016/j.bbalip.2010.02.012>
6. Jin, L., Martynowski, D., Zheng, S., Wada, T., Xie, W., & Li, Y. (2010). Structural Basis for Hydroxycholesterols as Natural Ligands of Orphan Nuclear Receptor ROR γ . *Molecular Endocrinology*, 24(5), 923–929.
<https://doi.org/10.1210/me.2009-0507>
7. Jin L., Martynowski D., Zheng S., Wada T., Xie W., Li Y. (2010) Structural Basis for Hydroxycholesterols as Natural Ligands of Orphan Nuclear Receptor ROR γ . *Molecular Endocrinology*, 24(5), 923-929.
Doi:10.1210/me.2009-0507
8. Kojima, H., Muromoto, R., Takahashi, M., Takeuchi, S., Takeda, Y., Jetten, A. M., & Matsuda, T. (2012). Inhibitory effects of azole-type fungicides on interleukin-17 gene expression via retinoic acid receptor-related orphan

receptors α and γ . *Toxicology and Applied Pharmacology*, 259(3), 338–345.
<https://doi.org/10.1016/j.taap.2012.01.01>